The Crystallisation History of Normal Mid-Ocean Ridge Basalts from the Eastern Pacific Ocean and Implications for the Composition of Primary Mid-Ocean Ridge Magmas: Evidence from Mineralogy, Pillow-Rim Glasses and Melt Inclusion Studies.

by

Andrew W. McNeill, B.Sc.(Hons.)

UNIVERSITY OF TASMANIA

Geology

submitted in fulfilment of the requirements
for the degree of Doctor of Philosophy
University of Tasmania

November, 1997

Statement of Previous Publication

This thesis contains the results of research carried out at the Geology Department, University of Tasmania between 1991 and 1997.

Part of the material presented in Chapter 3 was published as:

McNeill A. W. and Danyushevsky, L.V.(1996) Composition and crystallisation temperatures of primary melts from Hole 896A basalts: evidence from melt inclusion studies. In *Proc. ODP Sci. Results,* Vol. 148 (ed. J. Alt, H. Kinoshita, L. Stokking, and P. J. Michael), pp. 21-35. Ocean Drilling Program.

Fisk M. R., McNeill A. W., Teagle D. A., Furnes H., and Bach W. (1996) Major element chemistry of Leg 148, Hole 896A glass: data report. In *Proc. ODP Sci. Results*, Vol. 148 (ed. J. Alt, H. Kinoshita, L. Stokking, and P. J. Michael), pp. 483-487. Ocean Drilling Program.

Part of the material presented in Chapter 5 was published as:

McNeill A. W. (1995) Petrology of chilled dike margins recovered from Hole 504B, Leg 140. In *Proc. ODP Sci. Results*, Vol. 137/140 (ed. J. Erzinger, H. J. B. Dick, and L. B. Stokking), pp. 35-42. Ocean Drilling Program.

This thesis contains no material which has been accepted for the award of any other degree or diploma in any tertiary institution and to the best of my knowledge and belief, contains no material previously published or written by another person, except where due reference is made in the text of the thesis.

Date: 26/7/98

Signature: 

Authority of Access

This thesis may be made available for loan and limited copying in accordance with the Copyright Act 1968.

Date: 26/7/97

Signature: 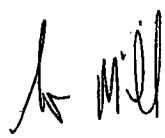

Abstract

An understanding of MORB petrogenesis requires compositional data on primary melts, as these provide direct information on the PT-conditions and mechanisms of mantle melting and melt segregation beneath mid-ocean ridges. The reconstruction of primary melts from the compositions of erupted liquids (pillow-rim glasses) requires an understanding of the early crystallisation history of the primary melts. As recent models of MORB petrogenesis imply that not only early crystallisation, but, also extensive mixing of primary melts occurs, information on the early stages of evolution of the primary melts is even more crucial. Such information may be preserved by early formed phenocrysts and can be obtained by studying these phenocrysts and their melt inclusions. However, the ability of melt inclusions to preserve the compositions of trapped liquids needs to be examined (e.g., homogenised melt inclusions in cotectic phenocrysts should have the same compositions, and those trapped during a period of fractionation, as recorded by the pillow-rim glasses, should have compositions similar to the glasses).

The three MORB suites described in this thesis are from ODP/DSDP Holes 896A and 504B, Costa Rica Rift, and Sample D9-1 from the Gorda Ridge, in the east Pacific Ocean. Compositional and textural variations of phenocrysts (olivine, plagioclase and spinel) have been used to interpret the crystallisation history for each suite and, together with pillow-rim glass compositions, form the basis for interpreting the compositional variations of melt inclusions.

Samples from the Costa Rica Rift and the Gorda Ridge have phenocryst assemblages dominated by calcic plagioclase (>An_{88}) with lesser olivine (<$Fo_{91.6}$) and Cr-Al spinel. The magmatic histories of samples from both ridge segments are dominated by low pressure (<2 kb) fractionation (both crystal and in-situ), magma mixing and minor crustal assimilation. The high pressure fractionation of phases other than olivine is not an important process in the history of these suites.

The Hole 896A and 504B samples are strongly LREE-depleted, and record cotectic olivine+plagioclase crystallisation at <9.5 wt.% MgO. However, melt inclusions and phenocrysts record an initial period of olivine-only crystallisation from 1340°C, ~15 wt.% MgO and $Fo_{91.6}$ to ~1215°C, 9.5 wt.% MgO and Fo_{87}, followed by

cotectic olivine (<Fo_{87})+plagioclase (<An_{94}) crystallisation as recorded by the pillow-rim glasses.

In contrast, the Gorda Ridge sample is less LREE-depleted, and melt inclusions and phenocrysts recorded cotectic olivine (<Fo_{90}) and plagioclase(<An_{94}) crystallisation from ~1230°C, 10.5 wt.% MgO. The melt inclusions and phenocrysts are related to the host pillow-rim glasses (MgO<8.5 wt.%) by mixing and in-situ fractionation processes.

Melt inclusions in primitive phenocrysts do not preserve evidence for diverse melt fractions produced in a polybaric melting column. Crystallisation, therefore, commenced after aggregation of these liquids, or the trapped liquids are the result of fractionation from isobaric batch melts.

Olivine-addition calculations for Costa Rica Rift (Hole 896A) and Gorda Ridge samples indicate primary batch melts were in equilibrium with a mantle source (MORB pyrolite-90) at 18-20 Kb and this is confirmed by preliminary results of basalt-peridotite sandwich experiments on a potential Hole 896A primary liquid (T. J. Falloon pers. comm., 1997).

Melting parameters (P_o, P_f, F_{max}) were estimated using published polybaric melting models. The major element (FeO* and Na_2O) compositions of possible aggregate liquids for the studied suites are consistent with both equilibrium and fractional melting, with P_o=20-27 kb, P_f=5-18 kb and F_{max}=12-24%. For the Costa Rica Rift and Gorda Ridge samples currently available models cannot differentiate between these alternative origins as aggregates of equilibrium or fractional melts, or by fractionation from an isobaric batch melt, .

The results of heating stage experiments indicate that if the magmatic liquids were fluid-saturated and the kinetics of melting during reheating are taken into consideration, then melt inclusions in plagioclase and olivine can be successfully homogenised and yield trapping, or crystallisation temperatures. However, these homogenisation temperatures are up to 50°C lower than trapping temperatures inferred from published vertical furnace experiments (e.g., Nielsen et al., 1995). The melt inclusions in vertical furnace experiments are here interpreted to have been overheated (and possibly poorly quenched), and consequently, their compositions are not representative of the liquids trapped to form the melt inclusions. As such, they cannot be used to infer aspects of the petrogenesis of a given suite of samples.

A comparison of the compositions of melt inclusions in cotectic (plagioclase, olivine and spinel) phenocrysts, and in phenocrysts interpreted to have crystallised

from liquids similar to the pillow-rim glasses, has identified compositional variations, particularly for TiO_2 and FeO* in plagioclase-hosted inclusions, that are not related to trapped liquid compositions. These compositional variations, found in all phenocryst phases, are thought to be caused by post-trapping re-equilibration. However, the melt inclusions do partially recover trapped liquid compositions and can, with care, be used to interpret the magmatic history of a sample, or suite of samples.

Acknowledgments

This thesis bears no resemblance to what was planned when I first started my studies. Through all the mishaps I have enjoyed the friendship and help of many people, without which I would have given up in despair years ago. I would particularly like to thank:

My 'associate' supervisor Dr. Leonid Danyushevsky, who has patiently guided me into the world of melt inclusion studies, and persisted with a slow-learner.

Dr. Tony Crawford, for convincing me to do a PhD and for encouraging me to participate in the ODP. I should also thank Tony for assuming overall supervision of this project, when Prof. D.H. Green left the department, and for never allowing me to leave a meeting more depressed than when I went in (well nearly never!).

Those who invested their time in parts of my PhD study which did not see the light of day; Dr. Ron Berry, Dr. Rick Varne, and especially Keith Harris, who taught me the arcane rituals of the high-pressure lab. I hope this work will be written up some day!

For technical assistance; Wis Jablonski (electron microprobe), Graham Rowbottom (FTIR), Phil Robinson (XRF), Keith Harris (heating stage), and Simon Stevens and Naomi Deards (lapidary). Also, Jeanette Harris and Peter Cornish who guided me through the bureaucracy, and June Pongratz for advice on matters of computing.

Drs. Jon Blundy and Steve Eggins, for doing the ion-probe and laser ablation ICP-MS analyses respectively, of my samples.

Shipboard Scientists on ODP Legs 140 and 148, in particular Marty Fisk, Dave Vanko, Kevin Johnson, Damon Teagle, Phillipe Pezard, Simon Allerton and Laura Stokking, who made these cruises a wonderful experience.

All my fellow students in the Geology department and CODES, both past and present, but in particular the (ex-)residents of room C461; Andrew Tunks, Matt White, and Dave Selley. Thank you all for making the last few years very enjoyable.

The post-doctoral and visiting Fellows who worked in the department over the last few years, especially Trevor Falloon, Dima Kamenetsky, John Sinton, Bob Musgrave, Wayne Taylor, and Steve Eggins.

And last, but not least, my partner (accomplice?) Tess, and my parents Pat and David. Thank you very much for your love and support, it has been, and will always be, very important to me.

Contents

Chapter 3 The Crystallisation History of Primitive Hole 896A, Leg 148, Basalts: Evidence from Phenocryst Compositions and Melt Inclusion Studies

List of Figures

List of Tables

Chapter 1

Introduction

1.1 The petrogenesis of mid-ocean ridge basalts

A better understanding of mid-ocean ridge basalt (MORB) petrogenesis requires compositional data on primary melts, as these can provide direct information on the PT-conditions and mechanisms of mantle melting and melt segregation beneath mid-ocean ridges (Green and Ringwood, 1967; Klein and Langmuir, 1987; Thompson, 1987; Falloon et al., 1988; Elthon, 1990; Niu and Batiza, 1991b; Kinzler and Grove, 1992b; Langmuir et al., 1992). However, the compositions of primary melts are known to be modified prior to eruption, by crystallisation, mixing, and assimilation, and consequently the erupted liquids (represented by pillow-rim glasses) do not represent primary melts (O'Hara, 1968a; O'Hara, 1968b; Grove et al., 1992). Thus it is important to obtain information on the early stages of primary melt evolution and to recover the early crystallisation history of these magmas. This information may be preserved by early formed phenocrysts, and can be obtained by studying these phenocrysts and their melt inclusions. Although in many cases such phenocrysts are not delivered to the surface, examples of MORB with primitive mineralogy are numerous (e.g., Donaldson and Brown, 1977; Humler and Whitechurch, 1988; Natland, 1989).

1.1.1 Models of MORB petrogenesis

MORB are the product of partial melting of peridotite, the result of upwelling and adiabatic decompression of mantle material beneath mid-ocean ridges. The genesis of MORB can be described by four end-member processes, batch or fractional melting, to describe the melting process, and passive or dynamic flow, to describe mantle upwelling (Shen and Forsyth, 1995). Early models, based on experimental melting studies, invoked isobaric batch melting and diapiric (dynamic) upwelling to produce MORB. However, the work of McKenzie (1984) and other researchers suggesting that basaltic liquids could separate from the mantle at low degrees (<1%) of melting, led to widespread acceptance of polybaric fractional, or continuous, melting, although the relative importance of passive and dynamic mantle flow mechanisms in this melting process is still a matter of debate (see Forsyth (1992) and Scott (1992)).

In the following sections, both fractional and batch melting are described, as in reality melting is probably a combination of the two processes. The implications of these different melting mechanisms, and processes of post-segregation modification, for the compositions of erupted MORB glasses are discussed below.

Batch melting

Experimental studies of the melting of postulated MORB mantle source compositions (such as MORB pyrolite, and Tinaquillo lherzolite; Ringwood (1975) and Falloon et al. (1988)) at high pressure have been used to establish the compositions of equilibrium liquids (primary melts) produced under geophysically reasonable conditions (1250-1450°C, 8-30 kb, and 5-25% melting). Early experimental work led to debate as to whether primary melts are generated at 8-11 kb, and ~1280°C (Fuji and Bougalt, 1983; Presnall and Hoover, 1984; Fuji and Scarfe, 1985; Fuji, 1989), and have compositions similar to the most primitive MORB glasses known (with MgO >9.5 wt.%, and(or) Mg' (100 x Mg/(Mg + Fe^{2+})) values of >70), or are produced at higher pressures (15-30 kb) and temperatures and are related to primitive MORB by olivine fractionation (O'Hara, 1968a; Stolper, 1980; Elthon and Scarfe, 1984; Falloon and Green, 1987). Arguments for these two models were summarised by Wilkinson (1982), Thompson (1987), and Elthon (1990). Falloon and Green (1988) resolved the debate by showing that primary MORB melts segregate at pressures of 8-25 kb, temperatures of 1350-1550°C, and have compositions with 10-17 wt.% MgO, that can be related to primitive MORB by varying amounts of olivine fractionation. A conclusion that has been supported by more recent experimental studies (Baker and Stolper, 1994; Kushiro, 1996).

The melting process implicit in these models is called batch, or equilibrium, partial melting (Schilling, 1966; Gast, 1968), as it requires that the liquid produced by melting continually reacts and re-equilibrates with its solid residue at the site of melting, until mechanical conditions allow it to escape as a single batch of magma. The experimental results summarised above form the basis of models that predict the major element composition of liquids produced by melting at a given pressure and temperature, or degree of melting (Jaques and Green, 1980; Falloon et al., 1988; McKenzie and Bickle, 1988; Niu and Batiza, 1991b; Kinzler and Grove, 1992a; Kinzler and Grove, 1992b). Equations to describe the incompatible element contents of liquids produced by this process have been presented by Gast (1968), Shaw (1970), and Hertogen and Gijbels (1976). From these equations and the incompatible element contents of primitive MORB glasses, it was inferred that MORB may result from 5-20% melting of postulated mantle sources (Green and Ringwood, 1967; Schilling, 1971; Richter, 1986). A conflicting viewpoint has been given by O'Hara (1977) and O'Hara (1985) who considered that the trace element signature is so confused by magma

chamber processes that it cannot be inverted to give information on melting processes. However, the incompatible element-based estimates of degree of melting for incompatible element-enriched MORB (E- or P-MORB) may be lower than estimates based on major element compositions (Schilling, 1975; Frey et al., 1978), implying that the incompatible element signature of the source region for such melts may have been modified by assimilation-contamination processes.

Fractional melting

Geophysical considerations of mantle porosity and permeability (McKenzie, 1984; McKenzie, 1985a), experimental data on peridotite partial melt geometry (Waff and Bulau, 1979; Kohlstedt, 1992), the trace element compositions of clinopyroxene from abyssal peridotites (Johnson et al., 1990; Johnson and Dick, 1992), inversion of rare-earth element data (Richter, 1986; McKenzie and O'Nions, 1991), and some isotopic data (McKenzie, 1985b; Salters and Hart, 1989), have been used to argue that polybaric fractional or continuous, and not batch, processes best describe MORB mantle melting. Fractional, or Rayleigh, melting, involves the generation of infinitesimally small melt fractions that instantaneously separate from their residue. However, true fractional melting probably does not occur in nature and incremental, critical or continuous melting processes are considered more likely (Langmuir et al., 1992). In these processes, essentially equilibrium partial melting occurs until the melt fraction exceeds a critical value, governed by the permeability of the mantle host, (generally considered to be <1-3% (Ahern and Turcotte, 1979; Maaloe, 1982; McKenzie, 1985b; Riley and Kohlstedt, 1991; Kohlstedt, 1992)). Above this threshold, the excess melt is continuously lost, but the mantle residue always retains a critical amount of melt.

Estimates of the major element composition of liquids produced by fractional-continuous melting are currently hampered by the absence of reliable experimental data on low degree partial melts (although see; Johnson and Kushiro (1992) and Baker et al. (1995)), and current models predicting the major element compositions of such liquids (McKenzie and Bickle, 1988; Niu and Batiza, 1991b; Kinzler and Grove, 1992b; Kinzler and Grove, 1992a) are based on extrapolation from batch melting experiments, as summarised above, at higher degrees of melting (generally >10%). However, the trace element signature of fractional-continuous melts can be derived, given estimates of mantle compositions and mineralogy, using the equations of Gast (1968), Maaloe (1982), Johnson and Dick (1992), and Sobolev and Shimizu (1993) and are expected to be significantly different to those produced by batch melting. The first melt fractions to separate must be strongly enriched in incompatible elements, whereas melt fractions produced at total degrees of melting greater than 10% are expected to be extremely depleted in incompatible elements (Sobolev and Shimizu, 1993). Some melt inclusions

in early formed, primitive, MORB phenocrysts, (e.g., in olivine (Sobolev and Shimizu, 1993; Shimizu, 1994), plagioclase (K. Johnson et al., 1995; Nielsen et al., 1995) and spinel (Kamenetsky, 1996)), have a wide range of incompatible element contents, varying from enriched to extremely depleted ("ultra-depleted melts"; Sobolev and Shimizu, 1993) and are interpreted to indicate that the trapped liquids represent partial melt fractions that were produced by fractional or continuous melting.

It has been argued that, as none of the analysed MORB glasses which have major element compositions consistent with high degrees of melting, have "ultra-depleted" incompatible element contents, then the initial melt fractions were mixed, or aggregated prior to eruption. Shaw (1970), Maaloe (1982) and Langmuir et al. (1992) have demonstrated that if the small melt fractions produced by fractional-continuous melting mix soon after segregation from their source, then the incompatible element geochemical signature of these liquids will be indistinguishable from that of equilibrium, or batch, partial melts.

In fractional-continuous melting models, erupted MORB glasses are generally not representative of mantle melting processes, and are at best a rather complicated weighted average of the melt produced at depth (O'Hara, 1985). Continuous melting allows for low degree partial melts to be produced over a range of pressures in the melting column (McKenzie and Bickle, 1988; Johnson et al., 1990) with each melt fraction having a major and trace element signature related to the depth and extent of melting. However, in some models of MORB evolution these melt fractions may then be mixed and(or) fractionated repeatedly at different levels in the melting column and crust (e.g., Figure 1 of Grove et al., 1992). These processes would result in erupted glasses that in the majority, if not all cases, have compositions that should not retain any signature of the melting process.

In addition to mixing and fractionation, the process of melt migration may also lead to compositional modification of primary melts. Traditional batch meting models invoke diapiric ascent (e.g., Green and Ringwood, 1967; Crane, 1985) in which the melt is isolated from interaction with the mantle by a mechanical boundary layer (Schmelling et al., 1988; Cruden, 1990). However, fractional-continuous models with low degree melts require two-phase flow, or diffuse porous melt migration (McKenzie, 1984; Richter and McKenzie, 1984; McKenzie, 1985a), in which the rate of liquid migration is governed by the melting rate (Maaloe and Scheie, 1982; Spiegelman and McKenzie, 1987). There has been debate as to whether large scale melt migration is diffuse (Ahern and Turcotte, 1979; Spiegelman and McKenzie, 1987) or whether melts are rapidly channelled into conduits (Nicolas, 1986; Morgan, 1987). If flow is dominantly porous, then melt-mantle interaction, re-equilibration affecting major element (Kelemen, 1990),

trace element (Navon and Stolper, 1987) and isotope systematics (Lundstrom et al., 1995) is likely. However, much geochemical evidence (Klein and Langmuir, 1987; Bedard, 1989; Salters and Hart, 1989) can be interpreted to indicate that re-equilibration has not occurred and that melt ascent was rapid, possibly focussed in highly permeable conduits (Richardson et al., 1996). Such melt pathways, preserved as replacive dunite bodies, have been identified in ophiolites (Takahashi, 1992; Kelemen et al., 1995), and from in-situ upper mantle drilled at the Hess Deep (Arai and Matsukage, 1996; Dick and Natland, 1996). These dunite pathways show convincing evidence for extensive melt-mantle interaction (Kelemen et al., 1992; Takazawa et al., 1992; Arai and Matsukage, 1996), which may result in the production of high-Al, high-Ca MORB (Dick and Natland, 1996). However, once conduits are formed and armoured by dunite margins, then minimal melt modification, apart from fractional crystallisation, should occur.

1.1.2 The importance of primitive MORB phenocrysts in understanding MORB petrogenesis.

Olivine and plagioclase phenocrysts that are more primitive (i.e., have higher Fo and An contents) than can crystallise from erupted glasses are commonly found in many MORB suites, and are often described as megacrysts (e.g., Donaldson and Brown, 1977). Studies of these primitive phenocrysts can provide information on two aspects of the petrogenesis of MORB:

1. Their early crystallisation history, i.e., when cotectic crystallisation began, the compositions of co-crystallising phases, and the possibility of mixing between primitive melts. An important tool in understanding this aspect of MORB petrogenesis is the textural and compositional relationship between phenocrysts and their silicate and(or) oxide solid inclusions. Of particular use are the Cr- and Al-rich spinels, commonly found included in both olivine and plagioclase megacrysts, as their compositional variations may indicate cotectic crystallisation (Allan et al., 1988; Roeder, 1994), the effects of magma mixing (Roeder and Reynolds, 1991), and the temperature (Irvine, 1967; Ballhaus et al., 1991), oxidation state (Danyushevsky and Sobolev, 1996) and composition, Mg#, of the liquid from which they crystallised (Allan, 1992).

Studies of the early crystallisation history of MORB led Dmitriev et al. (1984) to suggest that for the slow-spreading Mid-Atlantic Ridge there are two end-member types of MORB. The most common type (MORB-2) is produced from primary melts that were olivine (Fo_{90}-$Fo_{90.5}$) + plagioclase (An_{86}-$An_{94.5}$) + Cr-spinel cotectic from the onset of crystallisation. Melts of this type were thought to separate from the

mantle at pressures of ~10 kb (Dmitriev et al., 1984; Dmitriev et al., 1985). The second magma type (MORB-1) was affected by a period of olivine ($Fo_{91.5}$)+ Cr-spinel crystallisation prior to cotectic olivine-plagioclase crystallisation, and was believed to have separated from the mantle at higher pressures (>15 kb).

2. Primary melt compositions. The primary melts for a given suite of MORB should have compositions that would allow them to crystallise the most primitive phenocrysts sampled (highest Fo, for olivine only, and highest Fo and An for initially cotectic crystallisation). The compositions, Mg#, of liquids from which primitive olivines crystallise are easily determined as mineral-melt exchange coefficients (K_d) are well known (Roeder and Emslie, 1970; Ford et al., 1983; Ulmer, 1989). However, this is not the case for plagioclase, and existing plagioclase-melt equilibria models give different results (e.g., Drake, 1976; Ariskin and Barmina, 1990; Weaver and Langmuir, 1990; Grove et al., 1992; Panjasawatwong et al., 1995). Of course, it cannot be guaranteed that the most primitive phenocrysts of a given suite have been sampled (they may not be present in the samples studied, or may not have been delivered to the surface at all), and thus the compositions of primary melts derived by these means are considered to be 'minimum' compositional estimates. However, these estimates may be further constrained by indirect evidence such as the mineralogy of abyssal peridotites.

Abyssal peridotites have typically been sampled from fracture zones at slow spreading ridges (e.g., Dick, 1989; Johnson et al., 1990) and are rare in dredge suites from intermediate-fast spreading ridges, although data from the East Pacific Rise (Niu and Hekinian, 1997a; Niu and Hekinian, 1997b) and Hess Deep (Francheteau et al., 1990; Dick and Natland, 1996), have recently been published. The mineralogy of these samples, normally variable proportions of olivine + orthopyroxene ± spinel ± clinopyroxene, is interpreted to represent the residue of variable amounts of partial melting (Elthon, 1990), and therefore should be in equilibrium with the primary melt generated from an individual peridotite sample. In practice orthopyroxene, clinopyroxene, and spinel may have variable compositions and modal abundances, the result of sub-solidus re-equilibration (spinel and orthopyroxene, (Elthon, 1990)), sub-solidus recrystallisation (exsolution of clinopyroxene from orthopyroxene, (Fuji, 1989; Elthon, 1990)), the pressure and degree of melting (orthopyroxene (Elthon, 1990), and clinopyroxene (Johnson et al., 1990)), and infiltration and impregnation by basaltic melts, that crystallise plagioclase and clinopyroxene (Johnson et al., 1990). Given these constraints, the compositions of orthopyroxene, clinopyroxene and spinel may be difficult to interpret with confidence. However, residual olivines are unlikely to be compositionally modified and have an average composition in sampled abyssal peridotites of $Fo_{90.5}$, with a range of Fo_{89}-Fo_{92} (Elthon, 1990). Primary melts must

therefore be in equilibrium, at their pressure of separation, with a mantle assemblage of orthopyroxene + clinopyroxene + spinel and olivine of Fo_{89}-Fo_{92}.

Primitive phenocrysts in erupted MORB lavas also typically contain melt inclusions, samples of the liquid from which the host phenocryst crystallised, which may provide some additional constraints on the nature of primitive or near-primary liquids.

1.1.3 Melt inclusions in primitive phenocrysts as a source of information on MORB petrogenesis

Melt inclusions, comprising silicate and(or) sulphide melt, and(or) co-crystallising minerals, are trapped by irregularities in the growth of a crystal and are interpreted to be samples of the liquid from which the crystal was growing (Roedder, 1984). Theoretical and experimental considerations (discussed in Chapter 2) suggest that two pieces of petrological data may be obtained from melt inclusions; the temperature of trapping and the composition of the liquid trapped in the melt inclusion.

Melt inclusions from MORB phenocrysts formed at different stages of magmatic evolution can be used to interpret the liquid line of descent and temperature interval of crystallisation (Roedder, 1979). However, before using compositional data, it is necessary to demonstrate that the compositions of the melt inclusions are not modified by re-equilibration with their host or other post-trapping processes, but are representative of the liquid composition at the moment of trapping. This has been attempted in one study, Sobolev et al. (1989), in which experimentally homogenised melt inclusions hosted by cotectic olivine, plagioclase, and clinopyroxene, in primitive MORB from the mid-Atlantic ridge, have been compared. Sobolev et al. (1989) found that melt inclusions trapped at the same temperature by different phases have similar MgO, Al_2O_3, CaO, and FeO contents, but variable TiO_2, and Na_2O.

Melt inclusions in primitive MORB phenocrysts have received considerable attention in recent years, with interest stimulated by the development of fractional-continuous models of mantle melting. Indeed, if the liquids produced by fractional-continuous melting crystallise prior to mixing/aggregation, then the melt fractions may be trapped as melt inclusions in primitive phenocryst phases, and such melt inclusions may be the only way of directly sampling these liquids.

Several studies have found that plagioclase-, spinel-, and olivine-hosted melt inclusions with major element compositions more primitive than pillow-rim glasses from the same area, also have two common incompatible-element compositional features: rare earth element (REE) patterns that range from depleted to enriched, often

in a single sample, (e.g., Shimizu and Hassler, 1993; Nielsen et al., 1994), and variable, but low, Ti contents in plagioclase hosted melt inclusions, that were interpreted to be related to the degree of geochemical depletion, as indicated by Zr and $(La/Sm)_n$ values (K. Johnson et al., 1995; Nielsen et al., 1995). This compositional range has been interpreted to indicate the sampling of liquids produced by fractional-continuous melting at various depths in the mantle melting column (Sobolev and Shimizu, 1994), and has been used to infer the mechanisms of upwelling and focussing of melt extraction (Nielsen et al., 1995). However, several important questions concerning the reliability of melt inclusion data from MORB phenocrysts have, to date, not been investigated in sufficient detail. These are:

1. The compositions of melt inclusions in phenocrysts which crystallised from more evolved liquids, i.e., liquids represented by pillow-rim glasses, must be identical to the compositions of those pillow-rim glasses, and cannot have the unusual incompatible element characteristics found in melt inclusions from more primitive phenocrysts. Detailed comparisons of melt inclusions in primitive and more evolved phenocrysts have not been done.

2. Melts produced at different depths in the melting column should not only have different trace element contents, but should also have variable major element contents. In particular, experimental studies of mantle melting (Jaques and Green, 1980; Fuji and Bougalt, 1983; Falloon and Green, 1988) have convincingly established that SiO_2 decreases and FeO increases with increasing depth of melting. Also, the Mg' value of melts that segregated at shallow levels should be higher than those generated at higher pressure, as the mantle is interpreted to become more refractory with decreasing depth. The expected correlations between incompatible trace elements and major elements in melt inclusions have not been addressed.

3. Melt inclusions in cotectic phases, i.e., in minerals that crystallised together from the same magmatic liquid, should have the same composition. Published studies of primitive MORB samples have, with the exception of (Sobolev et al., 1989), generally used melt inclusions in olivine and(or) spinel (e.g., Sobolev and Shimizu, 1992; Sobolev and Shimizu, 1993), or plagioclase (e.g., Sinton et al., 1993; K. Johnson et al., 1995; Nielsen et al., 1995). A detailed comparison of melt inclusions in all early formed phenocryst phases (i.e., olivine, plagioclase, and spinel) has not been done.

With these questions unresolved, it is not clear if it is possible to use melt inclusion compositions to derive information on primitive or primary melts and mantle melting processes. Instead, variations in melt inclusion compositions may reflect

anomalies during trapping, re-equilibration with the host after trapping, the effects of experimental reheating, or some other process.

1.2. Aims of this study

The major aims of this thesis are to:

1. Investigate in detail, using large numbers of analyses of individual phenocryst phases, the mineralogy of primitive MORB. As discussed previously, the compositional and textural relationships between phenocryst phases and their inclusions can be used to infer crystallisation sequences and pressures, provide evidence for magma mixing and melt oxidation state, and by using mineral-melt equilibria calculations, can be used to partially recover the composition of the liquid from which the phenocrysts formed. Data from early formed phenocrysts can therefore provide direct evidence for the nature of primitive or primary melts, and can be used to interpret their evolution. In addition, these data may be used to provide a framework for the interpretation of results from melt inclusions, and to act as an internal check on the consistency of these results.

2. Based on the phenocryst data, investigate in detail, using large datasets, variations in melt inclusion compositions in cotectic phenocryst phases, to resolve the possible problems with interpreting the significance of melt inclusion compositions, as discussed above, and to assess the applicability of these data in interpreting the petrogenesis of MORB.

3. To use petrological information obtained from both early formed phenocrysts, and the melt inclusions that they host, to address problems of MORB primary melt compositions, conditions of melt generation and segregation, and models of MORB petrogenesis.

1.3 Thesis structure

Chapter 2 is a review of the theoretical and practical aspects of the study of melt inclusions, including current methods used to recover trapping temperatures and trapped liquid compositions. A detailed description of the experimental equipment, techniques, kinetic experiments, and data treatment used in the present study are also presented. This review is included to provide the background for a discussion and comparison of data obtained from melt inclusions in the present study, and results from the literature.

Chapter 3 reports a study of depleted primitive N-MORB basalts from Ocean Drilling Program (ODP) Hole 896A, Cost Rica Rift, eastern Pacific Ocean. These

samples are characterised by the presence of both highly anorthitic plagioclase (to $An_{94.5}$) and forsteritic olivine (to $Fo_{91.6}$) phenocrysts. Compositional and textural relationships between phenocryst phases are described, and used as a basis to discuss magma chamber processes and their effect on sampled liquids and phenocrysts. The phenocryst data are then used to aid in interpreting the compositions of both naturally quenched melt inclusions, and those produced by heating stage experiments on melt inclusions in olivine and plagioclase.

Chapter 4 reports a study of a single high-An plagioclase-rich dredge sample, KK2-83-NP-D9-1, from the central Gorda Ridge, north eastern Pacific Ocean. Textural and compositional variations of phenocryst phases are used to deduce the crystallisation sequence of this sample. These results are then used to constrain interpretations of the composition of naturally quenched and experimentally reheated melt inclusions in both primitive and evolved cotectic phases (olivine, plagioclase and spinel).

In Chapter 5, the petrology of samples from the sheeted dyke complex of DSDP/ODP Hole 504B, situated approximately 1 km north of Hole 896A, are described, together with the results of heating stage experiments, used to determine the trapping temperature and compositions of melt inclusions in plagioclase. These results are compared with those from Hole 896A (Chapter 3).

The second aim of the present study is addressed in Chapter 6, by summarising the results of melt inclusion studies from Chapters 3, 4, and 5, and the literature. The question of which data from, in particular plagioclase-hosted, melt inclusions can be used in petrogenetic interpretations is addressed, and the implications of variations of TiO_2 and FeO* abundances in plagioclase-hosted melt inclusions discussed. A comparison is made between the experimental results of the present study, using a visually controlled heating stage, and the technique adopted in published studies that uses a 1 atm vertical quench furnace. Data from Hole 504B (K. Johnson et al., 1995) and the Gorda Ridge (Nielsen et al., 1995) are used for this comparison.

In Chapter 7, the compositions of primary melts for the suites described in Chapters 3, 4, and 5 are estimated. These primary melts are compared with each other, and with published results, and implications of these results for models of mantle melting, and conditions of magma segregation are then discussed. Some comments are offered on the long standing problem of the petrogenetic significance of high-An (An_{88}-$An_{94.5}$) plagioclase in MORB.

The main results of the present study are summarised in Chapter 8.

Chapter 2

Methods of Studying Melt Inclusions

2.1 Introduction

Melt inclusions have had a long history of study (Roedder, 1979), however, their usefulness as indicators of the early crystallisation history of magmas has only recently become evident following the development of microbeam analytical techniques and equipment suitable for reliable heating (homogenisation) experiments. The efforts of Russian and French workers in this field have been summarised by Sobolev and Kostyuk (1975) and Clocchiatti (1975), respectively, and reviews of the more recent literature have been compiled by Roedder (1979, 1984). Since these reviews, the study of melt inclusions has become more popular and a number of studies have been published (e.g., Sobolev et al., 1989; Sobolev and Shimizu, 1993; Sobolev and Danyushevsky, 1994; Nielsen et al., 1995).

In this chapter, aspects of the origin and post-trapping modification of melt inclusions, including the assumptions used in experimental studies, are summarised as an introduction to a discussion of current techniques used to study melt inclusions. This section focuses in particular on the heating stage currently in use at the University of Tasmania, which was designed and developed by A.V. Sobolev and colleagues at the Vernadsky Institute of Geochemistry, Moscow (Sobolev et al., 1980; Sobolev, 1983).

As the present study deals with melt inclusions from phenocrysts in MORB lavas (which are CO_2-saturated; Dixon et al., 1995), the following discussion relates largely to melt inclusions trapped in the early crystallising phases of primitive mantle-derived magmas that were fluid-saturated at the time of crystallisation. Although in general processes may be similar, some of the following discussion and comments are not necessarily applicable, or relevant, to melt inclusions from more evolved, or fluid-undersaturated magmas.

2.2 Melt inclusions

At room temperature, melt inclusions in MORB are composed of partly- to completely recrystallised glass, with or without a shrinkage bubble, accidentally

trapped co-crystallising phases, and(or) an immiscible sulphide globule. Melt inclusions may be divided into three classes, based on mode of formation; primary, secondary, and pseudo-secondary. Secondary melt inclusions are the result of healing of late-stage fractures after crystal growth, whereas pseudo-secondary melt inclusions result from healing of fractures formed during crystal growth (Roedder, 1984). Primary melt inclusions, however, are trapped by irregularities in crystal growth, the result of processes such as rapid dendritic crystallisation, resorption and regrowth, or from irregularities caused by the trapping of solid inclusions, e.g., spinel attached to the growth surface of phenocrysts crystallised from primitive mantle melts (Roedder, 1979; Sobolev and Danyushevsky, 1994). Both pseudo-secondary and primary melt inclusions may have trapped samples of the liquid from which the host crystal grew. However, in practice primary melt inclusions are of most interest; they may be differentiated from both secondary and pseudo-secondary inclusions, which may have similar appearance, on the basis of inclusion shape and distribution using the criteria listed by Roedder (1984). In the present study primary melt inclusions were identified largely on the basis of their random three-dimensional distribution, regular or negative crystal shape (although see Roedder (1984)), concentration in growth zones, and often large size relative to that of the host crystal. Secondary melt inclusions occur on, or are linked by fractures, typically have more irregular shapes, and may form planes of inclusions with orientations un-related to growth zones or crystallographic axes.

The liquid initially trapped in primary melt inclusions is generally assumed to be representative of the bulk liquid from which the host mineral grew. This has been demonstrated to be the case by comparing melt inclusion compositions from co-crystallising phases in MORB (Sobolev et al., 1989), boninites (Danyushevsky et al., 1992), and hawaiites (Sobolev et al., 1991). However, Roedder (1984) discussed several processes that could lead to non-representative melt inclusion compositions, and concluded that boundary layer effects are likely to be important. Compositional gradients around a growing crystal, the result of variable diffusion rates of elements away from, or toward, the crystal, may be sampled by melt inclusions, and could produce non-representative compositions, particularly in smaller inclusions. However, it can be shown that these compositional gradients generally have a minimal effect on melt inclusion compositions (Roedder, 1984; Lu et al., 1995).

A prerequisite of many melt inclusion studies is that inclusions are both primary and homogeneously trapped. These 'normal' melt inclusions result from trapping of a homogeneous liquid and are composed of at least two phases at room temperature, i.e., glass and daughter crystals on the wall of the host, ± a shrinkage bubble and daughter crystals in the inclusion volume. In contrast, heterogeneously trapped melt inclusions

are the result of trapping a non-homogeneous liquid, either melt + fluid or melt + solid. These two modes of trapping are differentiated on the basis of phase proportions, or ratios, observed in a range of melt inclusions from a given sample. Homogeneously trapped melt inclusions should all have similar phase proportions, whereas heterogeneously trapped inclusions will have variable phase proportions (Roedder, 1984).

2.3 Post-trapping processes

After a melt inclusion is trapped, decreasing temperature leads to the formation of daughter crystals on the walls of the inclusion (Roedder, 1979). If the trapped liquid was in equilibrium with more than one crystallising phase, then daughter crystals of other phases may also form in the volume of the melt inclusion, although kinetic barriers to crystallisation may prevent this. Crystallisation results in a decrease in both total melt inclusion volume and trapped melt volume, and differences in thermal expansion coefficients between melt and solid, together with decreasing pressure, leads to the formation of a shrinkage bubble. As fluid solubility is mainly dependent on pressure (Burnham, 1979), the pressure drop inside an inclusion will cause fluid from the trapped, fluid-saturated, melt to exsolve into the shrinkage bubble as it nucleates.

Sorby (1858) observed the formation of shrinkage bubbles in melt inclusions and suggested that by reheating the melt inclusion and reversing post-trapping crystallisation until the shrinkage bubble dissolved, the temperature of trapping could be estimated. This process is called homogenisation and forms the basis of modern experimental melt inclusion studies. Homogenisation is defined as the moment of dissolution of the last phase inside a melt inclusion, normally a shrinkage gas bubble, resulting in a homogeneous melt (Roedder, 1984). The shrinkage bubble will disappear when the pressure inside the melt inclusion is equal to the pressure of trapping, and this corresponds to the point at which all daughter crystals, both on the walls and in the volume of the inclusion, have melted. In a homogeneously trapped and fluid-saturated system the composition of the melt inclusion at the moment of homogenisation is equal to that of the trapped melt, and the temperature of homogenisation (T_h) matches the temperature of trapping.

In natural systems, fluid oversaturation is required to overcome kinetic energy barriers to bubble nucleation. As the majority of MORB magmas are CO_2-supersaturated (Johnson et al., 1994; Dixon and Stolper, 1995; Dixon et al., 1995), shrinkage bubbles would be expected in melt inclusions hosted by phenocrysts in MORB lavas. This is not the case, however, and many melt inclusions, particularly

those in olivine, do not have shrinkage bubbles at room temperature. Factors such as fast quench rate (Clocchiatti, 1980), small melt inclusion size and(or), composition (i.e., melt viscosity) may inhibit the nucleation of a shrinkage bubble and produce a metastable glassy inclusion (Roedder, 1984). The lack of a shrinkage bubble is therefore likely to be the result of metastability, and is not an indication that crystallisation of daughter phases has not occurred (some crystallisation will always occur on the melt inclusion walls, as there are no kinetic barriers to nucleation).

Additional processes that may affect melt inclusion composition after trapping include diffusive exchange between the melt inclusion and host mineral and(or) melt (Roedder, 1979; Danyushevsky et al., 1992; Qin et al., 1992), and leakage, or decrepitation, of the inclusion. These processes may affect the composition, and homogenisation temperatures of melt inclusions, and are discussed in more detail below (sections 2.5.3, and 2.6.2).

2.4 Methods of studying melt inclusions

In recent years, two main approaches have been adopted in the study of melt inclusions:

2.4.1 Naturally quenched melt inclusions

In the present study, naturally quenched melt inclusions are defined as those melt inclusions that were quenched during eruption as silicate glass, a shrinkage bubble, silicate daughter crystals on the walls of the inclusion, and(or) immiscible sulphides. Major element (e.g., Watson, 1976; Falloon and Green, 1988; Sichel and Sigurdsson, 1993), trace element (Ireland and McDonough, 1993; Sobolev and Shimizu, 1993; Gurenko and Chaussidon, 1994; Shimizu, 1994) and volatile (Sisson and Layne, 1992; Czabo and Bodnar, 1993; Lowenstern, 1994) contents have been used to infer the nature of liquids quenched inside melt inclusions. The simplest approach to melt inclusion studies is to acknowledge that absolute major element contents have been variably modified by post-entrapment crystallisation but that ratios of elements not incorporated into overgrowths on the host mineral are not altered and thus preserve some of the chemical signature of the parental melt. The majority of trace elements may be considered to be incompatible in post-trapping crystallisation, particularly in olivine (Gurenko and Chaussidon, 1995), and only a correction for post-trapping enrichment is required.

More sophisticated attempts to recover trapped melt compositions have used three approaches in correcting for post-trapping crystallisation. Anderson (1974) used shrinkage bubble/glass volume ratios, optical haloes around melt inclusions and the

zonation of host minerals to calculate the amount of post-trapping crystallisation of the host. Watson (1976) commented that uncertainties of up to 200% may occur in estimating bubble volumes, and the assumption that the initial trapped void was spherical makes large errors in these calculations likely.

The second approach requires that melt inclusions are analysed from co-precipitating phenocryst phases, and magmatic liquid compositions are calculated by determining the intersection point of control, or fractionation, lines for melt inclusions in each phase (Watson, 1976). Two of the assumptions used in this approach may not be valid in many cases. First, the requirement that melt inclusions in different crystal types have sampled the same melt at the same time may not be met if, for example, magma mixing has occurred. Second, the assumption that diffusion through the host crystal is unimportant in altering the composition of the trapped melt may be invalid, as discussed below, and by Sobolev and Danyushevsky (1994).

The third recalculation technique uses experimentally determined mineral-melt distribution coefficients to add back small increments of host mineral until the composition of the melt inclusion is in equilibrium with the host phenocryst (Dungan and Rhodes, 1978; Danyushevsky et al., 1988; Gurenko and Chaussidon, 1995). The compositions of melt inclusions in olivine are most commonly recalculated in this way. In addition, these calculations can be used to estimate trapping temperatures, although the reliability of these estimates depends on the calibration of the mineral-melt thermometer used, the H_2O content of the trapped melt (most thermometers are calibrated on 'dry' systems), the melt inclusion remaining a closed system after trapping, and whether fractional or equilibrium crystallisation controlled formation of daughter phases on the walls of the inclusion.

In the present study, homogenisation experiments are the preferred method of recovering initial trapped melt compositions. However, the compositions of naturally quenched melt inclusions are used to aid in interpreting post-trapping processes and to estimate trapped melt compositions when reliable homogenisation experiments are not possible, for example, when the melt was fluid under-saturated or heterogeneously trapped.

2.4.2 Experimental approach

The experimental re-heating of melt inclusions, as described above, allows determination of both the trapping, or crystallisation, temperature and melt composition. Two techniques have been used in recent studies. One involves heating a small sample of melt inclusion-bearing phenocrysts in a one-atmosphere furnace, under controlled

oxygen fugacity. The other relies on a visually-controlled heating stage with a pure Ar or He atmosphere.

The one-atmosphere furnace method has been used by Sinton et al. (1993), Nielsen et al. (1994), and K. Johnson et al. (1995). The general procedure for this technique is to heat batches of crystals, suspended from platinum wires or in a Pt bucket, in a vertical gas-mixing furnace with a CO_2+H_2 atmosphere (producing fO_2 conditions approximating QFM), for periods of 1-6 hours and to then drop-quench the phenocrysts in water.

A detailed description of the technique used for Gorda Ridge samples (discussed in Chapter 6) has been provided by R. Nielsen (pers. comm., 1997): the furnace was kept at 1000°C so that when the experimental assembly was lowered into position the crystals reached this temperature in several seconds. The temperature was held at 1000°C for 15 minutes, then increased at 60°C/min to approximately 50°C below the inferred trapping temperature at which point the heating rate was decreased to 15°C/min to avoid overshooting the desired temperature. The phenocrysts were then held at run temperature for 2 hours before quenching, by passing a current through and vaporising, the 0.03" diameter Pt supporting wire thus dropping the crystal out of the furnace, with a quench time of <0.2 sec.

Experiments are run at a series of temperatures bracketing the inferred trapping temperature. The quenched melt inclusions are then examined using an optical microscope and melt inclusion-host pairs analysed for experiments at each temperature. The criteria used to establish trapping temperature are: the disappearance of daughter crystals and shrinkage bubble, inflections in trends of the major element compositions of melt inclusions, and(or) comparison of melt inclusion compositions with predicted fractionation trends. The advantages of vertical furnace experiments are considered to be superior temperature control and fast quench times (Nielsen et al., 1995). However, the major drawbacks of the published studies using this technique is the lack of consideration of kinetic processes, discussed in detail in section 2.5.3, and the inability to directly observe the homogenisation of melt inclusions.

Three types of heating stage have been used in recent published studies, commercial models, e.g., the Linkam TH1500 stage (Hansteen, 1991) or a modified Leitz 1350 stage (Schiano et al., 1992; Vaggelli et al., 1992; Belkin and De Vivo, 1993), and the custom-made stage designed and described by Sobolev et al. (1980). In addition, several studies have used a combination of heating stage and vertical furnace, whereby homogenisation temperature (T_h) was determined from heating stage experiments, and

this temperature then used as a guide for heating batches of crystals in a furnace (Clocchiatti and Massare, 1985; Hansteen, 1991).

An important advantage that heating stages have over 1 atm furnaces is that processes occurring during re-heating can be observed directly under the microscope, and the melt inclusions can be quenched at the exact moment of bubble/crystal disappearance, thus providing a direct estimate of homogenisation temperature (T_h) and allowing trapping temperature to be estimated to within 10-20°C (Sobolev and Danyushevsky, 1994). A disadvantage of the heating stage technique is that thin wafers of crystal, rather than whole phenocrysts, are used. This places a practical limit on the size of melt inclusions used in heating stage experiments, as larger (>50-100 μm) inclusions often leak, a result of melting back the melt inclusion walls and(or) the lower mechanical strength of the host crystal.

As stated previously, the heating stage used at the University of Tasmania is the same as that designed by Sobolev et al. (1980). This type of stage was used, as it is considered to provide much faster quenching and more precise temperature estimates than the commercially available stages. For example, temperature corrections based on the melting point of Au were <10°C using the Sobolev et al. stage, but have been reported as 30-40°C (Vaggelli et al., 1992) and 50-90°C (Roedder, 1984) for the Leitz 1350 stage.

The stage is water-cooled, with a $Pt_{90}Rh_{10}$ foil heater in the form of a 6 mm-long by 2 mm-diameter vertical tube. The thin walls (0.15 mm) of this heating tube are designed to promote fast quenching at the end of an experiment. A 1 mm-diameter Pt sample holder ring is situated in the centre of the heater and $Pt/Pt_{90}Rh_{10}$ thermocouple wires are welded to this ring to allow temperature to be monitored. Temperature gradients in the working area have been shown to be <10°C in both horizontal and vertical planes (Sigurdsson, 1994). Temperature is manually controlled using a variable voltage transformer, or variac.

Ultra-pure helium (99.999% He) is used as an atmosphere for all experiments. The gas is passed through a Supelco® high capacity gas purifier at 580-590°C, removing O_2, H_2O, and CO_2, and is cooled through Cu tube coils before passing through the heating stage. Helium is used as it has a very low thermal conductivity, providing a low thermal inertia in the sample heater, and thus rapid quenching when heating power is switched off.

2.5 Experimental technique

2.5.1 Sample selection and preparation

As the present study is concerned with primitive MORB melts, samples from each suite were selected on the basis of high glass or whole rock MgO contents and(or) high phenocryst abundance. Both glassy pillow-rims and the chilled margins and interiors of dolerite dykes were sampled. Plagioclase was the most abundant phenocryst in all three suites studied, with lesser olivine and spinel. Rare clinopyroxene phenocrysts were found in only two of the three suites studied.

Mineral separates were prepared by careful crushing and sieving. Phenocrysts were hand picked from the 0.3-1.0 mm size fraction, mounted in epoxy and polished. These grain mounts were then examined optically, any melt and solid inclusions described, and a search made for grains with primary fluid inclusions. The few grains with fluid inclusions were removed from the mounts for low temperature heating stage experiments to determine primary fluid composition and pressure of trapping.

All phenocrystal plagioclase, olivine, spinel, and where present clinopyroxene, were analysed by electron microprobe to establish the range of phenocryst compositions for each sample and to check for homogeneity of individual phenocrysts. These data, and descriptions of mineral-inclusion relationships, were used to determine the order of crystallisation, information needed to interpret results where melt inclusions in more than one phenocryst phase were examined. Where exposed, glassy naturally quenched melt inclusions were also analysed. The grain mounts were cut and polished to 250-350 μm thickness and the plagioclase, and where present, olivine grains hosting primary melt inclusions suitable for microthermometry were extracted from the epoxy mounts.

2.5.2 Experimental procedure

The sample phenocryst was placed on a 200-300 μm thick plate of transparent, refractory mantle olivine, and a small piece of Au placed on the sample grain as close as possible to the melt inclusions of interest. The melting point of this Au was used to calibrate temperature during each run. The sample was then placed on the sample holder, the heating stage sealed, and then flushed with He for 5-6 minutes before heating commenced.

Both plagioclase and olivine were heated rapidly to 1150°C. The initial heating rate used was dependent on the presence or absence of a shrinkage bubble in a melt inclusion at room temperature; slower heating rates were required to nucleate a bubble in, and to fully recrystallise, inclusions that had quenched to glass only. Above

1150°C, temperature was increased at a rate determined from a series of kinetic experiments, as discussed below. After homogenisation, the experiment was quenched by turning off power to the heater and simultaneously increasing the flow of He gas through the stage. Quench times are estimated to be <1 second for the first 300°C.

After an experiment, each phenocryst was mounted in epoxy in a Cu tube and examined using an optical microscope to locate melt inclusions suitable for analysis. The sample was then polished until the selected melt inclusions were exposed, and both melt inclusions and adjacent host mineral analysed by electron-, and in some instances ion-microprobe.

2.5.3 Kinetic experiments

In an ideal case, where cotectic crystallisation has occurred, both the shrinkage bubble and any daughter crystals in the volume of a melt inclusion, as distinct from those on the walls, will disappear simultaneously at the point of homogenisation. This may not happen in normal experiments, and typically bubble disappearance is 10-15°C higher than crystal disappearance. The reasons for this relate to the kinetics of melting material from the host walls, including factors such as the presence of a thermal gradient during heating and volumes or areas of daughter crystals available for melting. If a melt inclusion is heated too fast, these kinetic effects will lead to homogenisation at a much higher temperature than the true trapping temperature (overheating). However, if the melt inclusion is quenched immediately the bubble disappears, then the melt composition should still be the same as at the time of trapping. The relationship between increasing heating rate and higher T_h has been demonstrated experimentally by Bakumenko (1975). As heating rates are slowed, T_h decreases asymptotically to what is interpreted to be the true T_h (Sobolev and Danyushevsky, 1994).

The ideal case, described above, assumes that the melt inclusions are closed systems; however, in nature this is not the case, and two further processes may occur at high temperature:

Chemical diffusion. Diffusion of both hydrogen and oxygen out of melt inclusions has been described or inferred by Pasteris and Wanamaker (1988) and Sobolev and Danyushevsky (1994). Diffusion of H through the host crystal will occur if $a_{H(incl.)} > a_{H(environment)}$. Hydrogen is provided by dissociation of H_2O in the melt inclusion, which reduces the volume of melt (anhydrous melt is more dense than hydrous melt at low pressure) and thus melting of more host crystal is required to dissolve the shrinkage bubble. This is in addition to the effect of increased melting temperature for "dry" magma, and may lead to an increase in T_h of up to 15-25°C for

melt inclusions in MORB-hosted crystals (Sobolev et al., 1989). A further effect of H_2O dissociation is the oxidation of melt in the inclusion to produce magnetite, a process most commonly observed in more hydrous melts (Roedder, 1979; Sobolev and Danyushevsky, 1994).

Pressure. At the time of trapping, pressure inside a melt inclusion is equal to the external confining pressure. However, on arrival at the Earth's surface the internal pressure of a melt inclusion is much greater than that of the external environment, typically 80-90% of the source pressure (Tait, 1992). This may lead to brittle or ductile deformation of the host crystal, either during eruption, or during re-heating experiments. Brittle fracturing leads to cracks, and extreme overheating is required to dissolve the shrinkage bubble, if it will dissolve at all. Ductile deformation involves modification of the crystal lattice and will increase the size of the melt inclusion, lowering internal pressure and resulting in homogenisation at higher temperatures (the "stretched inclusions" of Roedder, 1984).

All the factors discussed above can be combined into two main questions that must be answered to be confident of experimental homogenisations:

What is the heating rate at high temperature (>1100°C) that will produce homogenisation at the minimum achievable temperature (i.e., trapping temperature)?

How long can a melt inclusion be kept at a temperature near T_h (e.g., >1150°C) without causing an increase in T_h and(or) a change in composition?

To attempt to answer these questions, a series of kinetic experiments were done for each of the three suites used in the present study. Plagioclase phenocrysts from all three suites were used for experiments, but too few olivines hosting melt inclusions were recovered from Holes 504B and 896A for kinetic experiments. Three types of experiment were done:

1. Experiments to determine variability of T_h with time at high (>1150°C) temperature.

These experiments provided information on melt inclusion behaviour associated with both high temperature and repeated homogenisation of an individual inclusion. Samples were selected with a range of melt inclusion sizes and number of inclusions. Melt inclusions of varying size were kept at 1150 or 1190°C and homogenised, using a heating rate of 50 °C/min, several times over a period of 2-3 hours.

Observations of melt inclusion behaviour in plagioclase were restricted to inclusions of <30 μm diameter in Hole 896A samples and <50 μm in Gorda Ridge and

Hole 504B samples, as larger inclusions leaked in all experiments. Three main types of behaviour were seen (Fig. 2.1):

A. Homogenisation temperature was initially constant, within obtainable accuracy, for 27-55 minutes (2-4 homogenisations) and then increased continuously over several homogenisations until the end of the experiment. This behaviour is interpreted to indicate that the melt inclusions had leaked, or decrepitated, after the first 2-4 homogenisations (Fig. 2.1A).

B. Homogenisation temperature was constant for the first 50-60 minutes (2-3 homogenisations) then increased over the next 60-100 minutes (2-3 homogenisations). The increase in T_h ranged from 15-55°C, with T_h increasing more in larger melt inclusions than in smaller melt inclusions (e.g., 55°C for a 40x15 μm inclusion and 30°C for a 20x10 μm inclusion). After this time, T_h was stable and did not vary during 2-3 further homogenisations (e.g., Fig. 2.1B). Internal pressure and the dissociation of H_2O may both produce this type of behaviour; however, the low H_2O content of these melt inclusions (section 3.4.5 and 5.2) and the lack of magnetite crystallisation, can be interpreted to indicate that stretching of melt inclusions due to pressure is the main cause of increased T_h.

C. Homogenisation temperature remained constant throughout the experiment. This happened in the olivines from the Gorda Ridge and in the slowly cooled, and thus largely crystalline, melt inclusions in plagioclase from the sheeted dykes of Hole 504B. However, one melt inclusion from hole 504B showed an initial drop in T_h that was followed by constant to slightly increasing T_h over the remainder of the experiment (Fig. 2.1C). This behaviour suggests some re-setting of melting kinetics in the inclusion such that T_h at a high heating rate is similar to that expected from a much lower heating rate, as discussed below. A further important observation was that fine black minerals (magnetite?) formed after a minimum of 20 minutes at high temperature in olivine-hosted inclusions.

2. Experiments to determine the effect of heating rate on T_h (Fig. 2.2).

The experiments of Danyushevsky et al. (1992) have shown that heating rates of 1-60°C/min are optimum for basaltic to ultramafic melt compositions. Therefore, starting at a temperature of 1150°C, melt inclusions were homogenised at heating rates of 50, 25, 10, 5, 2, and 1°C/min. After each homogenisation, inclusions were recrystallised at temperatures of less than 1000°C and then kept for 1 minute at 1150°C before the next homogenisation. Faster heating rates were used initially. Total times above 1150°C were approximately 60 minutes.

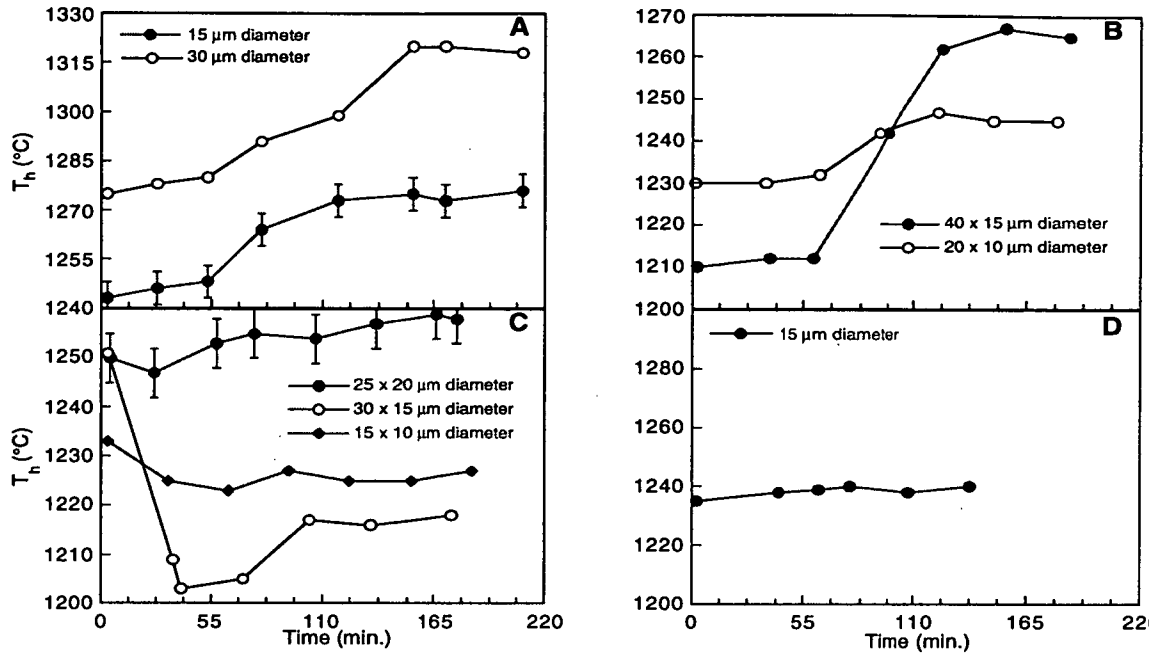

Figure 2.1: Variation of homogenisation temperature (T_h) with time at T >1150°C. Melt inclusions in plagioclase from **A**. Hole 896A. **B**. Gorda Ridge. **C**. Hole 504B. **D.** Melt inclusions in olivine from the Gorda Ridge. Error bars show estimated precision of ±5°C. See text for discussion.

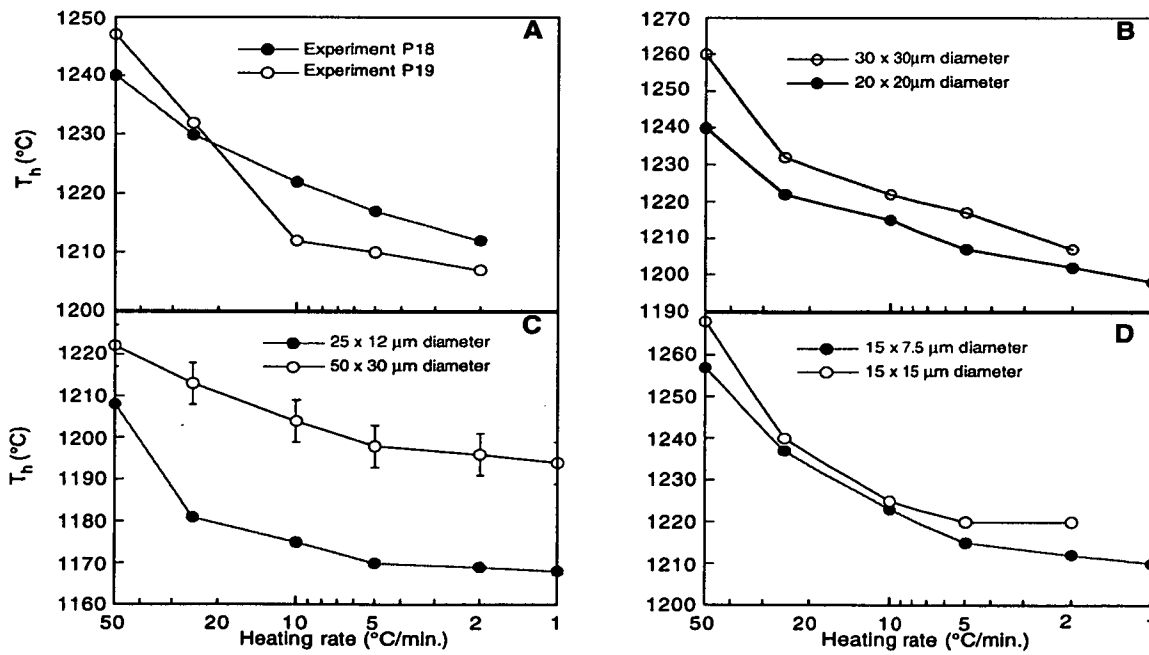

Figure 2.2: Dependence of homogenisation temperature (T_h) on heating rate. Melt inclusions in plagioclase from **A**. Hole 896A. **B**. Gorda Ridge. **C**. Hole 504B. **D**. Melt inclusions in olivine from the Gorda Ridge. Error bars give estimated experimental precision of ±5°C. See text for discussion.

In these experiments, a large decrease in T_h was observed at heating rates above 10°C/min but at lower rates T_h remained relatively constant, decreasing by only a few degrees. In experiments on samples from Hole 896A and the Gorda Ridge, the lower heating rate results may have been affected by increased T_h due to the length of time at high temperature and(or) number of homogenisations.

3. Experiments to determine the time to homogenisation at a given temperature (Fig. 2.3).

Temperature was increased rapidly (50-100°C/min) to a chosen temperature, then held at that temperature until the inclusion homogenised. The first temperature was chosen to achieve homogenisation in less than 1 minute, and then decreased by 10°C for each successive homogenisation. Between homogenisations, inclusions were recrystallised at temperatures of <1000°C. Times above 1150°C were 1 to 1.25 hours.

Figure 2.3 shows that smaller melt inclusions homogenised faster than large melt inclusions at a given temperature, and that smaller inclusions could also be homogenised at lower temperatures than larger inclusions. If a melt inclusion was not homogeneous at a given temperature within 5-5.5 min for samples from Hole 896A, 7.5-10.0 min for samples from the Gorda Ridge, or 6 min for samples from Hole 504B, then it would not homogenise within 20-25 minutes. However, results from melt inclusions in samples from Hole 504B also suggest a further complication (size effect?), with small (<20 μm) melt inclusions having maximum homogenisation times of <1 minute at a given temperature (Fig. 2.3C). If Hole 896A or Gorda samples, were homogenised more than once at a given temperature, then the time to homogenisation often increased in successive reheatings. Also, if a melt inclusion was homogenised initially at a low temperature, then at a higher temperature, homogenisation could not be repeated at the initial temperature. The significance of these behaviours are not clear, but suggest that increased time at high temperature (>1150°C) may result in irreversible stretching of inclusions.

The data from kinetic experiments, combined with general observations of melt inclusion behaviour recorded during experiments and summarised in sections 3.4.4, 4.4.4, and 5.6.3, were used to produce a set of guidelines for the re-heating of melt inclusions from each of the studied suites.

In practice, melt inclusions of 10-50 μm diameter in plagioclase, and 10-100 μm in olivine, proved most useful for experiments. The majority of melt inclusions with larger diameter were found to leak during re-heating, whereas those of <10 μm diameter were too small both to observe melting, and for analysis by electron-probe. Small

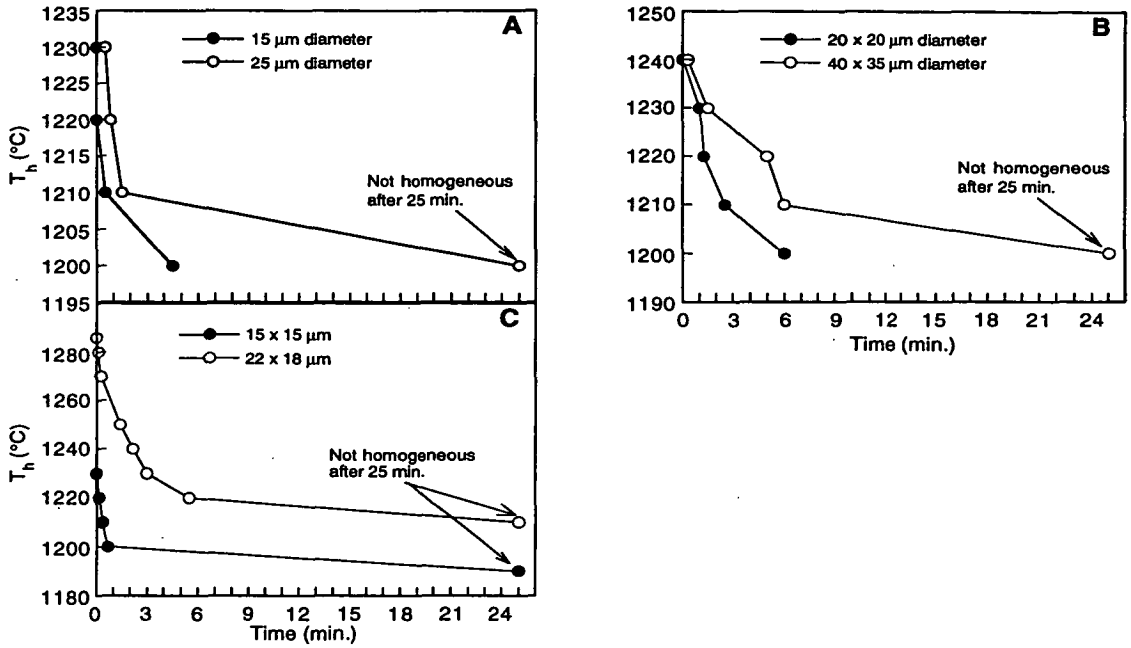

Figure 2.3: Time taken for a melt inclusion to homogenise at a range of temperatures. Melt inclusions in plagioclase from **A**. Hole 896A. **B**. Gorda Ridge. **C**. Hole 504B.

diameter (10-15 µm) melt inclusions often homogenised more rapidly at a given temperature than large inclusions, as described above, and were used as indicators of approach to homogenisation.

Melt inclusions in plagioclase from Hole 896A and the Gorda Ridge can withstand 2-3 homogenisations or 50-60 minutes at above 1150°C before an increase in T_h occurs. Experiments using samples from these suites were therefore limited to under 1 hour at high temperature. In contrast, the stability of T_h with time and number of homogenisations for Hole 504B samples indicate that longer heating times, and thus lower heating rates, can be used. The formation of magnetite in olivine after approximately 20 minutes indicates experiments should be limited to less than this time at high (>1100°C) temperature.

Experiments on heating rate suggest that rates of below 5°C/min will yield the lowest T_h for all three suites studied, and although lower heating rates will lead to slightly lower temperatures, this must be balanced against the potential effects of increased time at high temperature. The heating regimen used for melt inclusions in plagioclase from Hole 896A and the Gorda Ridge was therefore to fully recrystallise (and thus nucleate a bubble in) all inclusions below 1100°C, then increase temperature to 1150°C and wait for at least 1 minute before increasing temperature at 5°C/min until the small melt inclusions were close to homogenisation. Temperature was then held at

this point, or increased at approximately 2°C/min, until the melt inclusions of interest were homogenised. Similar initial heating rates were used for plagioclase from Hole 504B, but when strong melting of daughter phases occurred, the heating rate was decreased to <1°C/min until melt inclusions were homogeneous.

The heating rates interpreted to be appropriate for Hole 896A and Gorda Ridge plagioclase-hosted inclusions are much faster than required for Hole 504B, and faster than would be suggested by the results of previous studies, i.e., the Vema fracture zone (Sobolev et al., 1989) and the Australia-Antarctica Discordance (Sigurdsson, 1994). Higher heating rates increase the potential for overheating but appear to be necessary, as inclusions exhibit behaviour that indicates they cannot be kept at high temperatures (>1150°C) for long periods of time, and which are consistent with stretching of inclusions due to pressure differences, as discussed above.

Most melt inclusions in olivine lack shrinkage bubbles at room temperature, and repeated heating and cooling between 500°C and 1000°C was required to nucleate a bubble. Once the inclusion was recrystallised and a bubble had nucleated, the temperature was increased to 1150°C. Above this temperature, olivines from Hole 896A were heated using the same rates as for plagioclase from that Hole as, although no kinetic experiments were done on olivine, inclusions in differing phenocryst types from the same sample may be homogenised at similar rates (Sobolev et al., 1989). Olivines from the Gorda Ridge were heated at 5°C/min until approximately 1210°C, or strong melting was seen, then at 2°C/min until homogenisation.

The differences in melting behaviour of melt inclusions from extrusive and intrusive suites, and additional implications of results from these kinetic experiments, are discussed with respect to a comparison of the heating stage and vertical furnace experimental techniques in Chapter 6.

2.6 Analysis of results

2.6.1 Assessment of data quality

After analysing the homogenised melt inclusion and its host mineral, it is necessary to assess the quality of each experiment. The first stage is to evaluate if the melt is saturated in the host mineral (i.e., melt liquidus temperature equals T_h, and the host mineral is on the liquidus) by applying mineral-melt thermometers (Ford et al., 1983; Ariskin et al., 1986; Ariskin and Barmina, 1990; Weaver and Langmuir, 1990; Danyushevsky et al., 1996) which allow calculation of liquidus temperatures of the mineral(s) of interest by using the composition of the melt inclusion. Calculated

temperatures are plotted against T_h, and in dry systems, the T_h should be within 10-20°C, the accuracy of the thermometers used, of the calculated temperature. If results are outside this range, then the melt inclusion is not saturated.

To produce a calculated temperature higher than T_h, the composition of the melt inclusion must be oversaturated with a component from the host mineral, and this may result from analytical overlap with the host, due to the uncontrolled thickness (depth) of inclusions being analysed.

Low calculated temperatures may result from either overheating or poor quenching. If a melt inclusion is overheated, i.e., homogenisation is obtained at higher temperature than the temperature of trapping, and quenched immediately homogenisation is achieved, then the inclusion composition will be equal to that at the time of trapping. The calculated temperature, based on the inclusion composition, will therefore be lower than the experimental temperature. Poor quenching, particularly common in smaller melt inclusions such as those used in the present study, results in the crystallisation of the host mineral on the walls of the inclusion. In a dry system it is therefore impossible to differentiate between the effects of overheating and quench modification. However, the use of kinetic experiments to determine optimal heating rates should preclude overheating and low calculated temperatures in the present study are interpreted largely to be due to poor quenching.

In the present study a calibration developed by (Danyushevsky et al., 1996) was used to estimate the olivine-plagioclase cotectic, and is based on the olivine-melt geothermometer of Ford et al. (1983) and the plagioclase-melt geothermometer of Weaver and Langmuir (1990). A correction may be introduced to the latter to obtain a best fit for the olivine-plagioclase cotectic over the MORB compositional spectrum (Danyushevsky et al., 1996). Two points should be made with respect to the Weaver and Langmuir (1990) thermometer:

1. The thermometer was calibrated using plagioclase less anorthitic than An_{83}. Using Weaver and Langmuir (1990) the calculated liquidus plagioclases for the samples examined in the present study are $<An_{82}$, more sodic than the plagioclase ($>An_{90}$) interpreted (from mineralogical and melt inclusion data) to be equilibrium with these samples. These more sodic calculated plagioclase compositions will affect liquid line of descent calculations, as discussed in detail in section 3.5.1. Although the Weaver and Langmuir calibration is not successful in predicting liquidus plagioclase compositions it is successful in predicting the appearance of plagioclase on the liquidus and in reproducing the MORB olivine-plagioclase cotectic, as demonstrated by Danyushevsky et al. (1996).

2. The correction to obtain a best fit to the olivine-plagioclase cotectic, as defined by Danyushevsky et al. (1996);

$$T_{WLC} = T_{WL} + (0.239 \times T_{FD} - 279.6)$$

(where T_{WLC} and T_{WL} are the corrected and original Weaver and Langmuir plagioclase temperatures, respectively, and T_{FD} is the Ford et al. (1983) olivine temperature) is based on the assumption that the liquid of interest is cotectic and is reliant on the results of the olivine melt thermometer of Ford et al. (1983). Given that a melt inclusion affected by, e.g., poor quenching will not have a cotectic composition and thus non-cotectic calculated plagioclase and olivine temperatures, then the correction must be applied with care, in the interpretation of homogenised melt inclusions, and its use is discussed further in Chapters 4 and 5.

The results of mineral-melt thermometers are, however, insufficient to demonstrate that the trapping temperature has been correctly established, and further independent criteria are required to guard against compositional over- or underheating and the possibility of post-trapping re-equilibration of melt inclusion and host. Sobolev et al. (1989) have suggested three further tests to evaluate the quality of experimental data; correspondence between trends in natural glass compositions and the experimentally re-heated melt inclusions, correlation between host mineral composition and T_h, and similarity of melt inclusion compositions homogenised at the same temperature in different host minerals. These criteria are generally only applicable if magma mixing has not occurred, and they will be discussed in more detail in Chapters 3, 4, and 5 with respect to the experimental data presented in each chapter.

Chapter 3 has been removed for copyright or proprietary reasons.

Part of the material presented in Chapter 3 was published as:
McNeill A. W. and Danyushevsky, L.V.(1996) Composition and crystallisation temperatures of primary melts from Hole 896A basalts: evidence from melt inclusion studies. In Proc. ODP ScL Results, Vol. 148 (ed. J. Alt, H. Kinoshita, L. Stokking, and P. J. Michael), pp. 21-35. Ocean Drilling Program.
Fisk M. R., McNeill A. W., Teagle D. A., Fumes H., and Bach W. (1996) Major element chemistry of Leg 148, Hole 896A glass: data report. In Proc. ODP ScL Results, Vol. 148 (ed. J. Alt, H. Kinoshita, L. Stoklcing, and P. J. Michael), pp. 483-487. Ocean Drilling Program.

Chapter 4

The Crystallisation History of Sample KK2-83-NP-D9-1, Gorda Ridge: Evidence from Phenocryst Compositions and Melt Inclusion Studies

4.1 Introduction

The Gorda Ridge is a 300 km long spreading segment, situated off the Oregon-northern California coast, in the northeast Pacific Ocean (Fig. 4.1). It is bounded to the south by the Mendocino Fracture Zone and to the north by the Blanco Fracture Zone, and is itself divided into three segments by small scale (18-20 km) ridge offsets at 42.3°N and 41.6°N. The northernmost offset also marks a change in spreading rate, from a full rate of 5.5 cm/yr to the north (Riddihough, 1980) decreasing to 2.3 cm/yr at the southern end of the ridge (Wilson, 1989).

Samples of basaltic glass dredged from along the length of the Gorda Ridge were described by Davis and Clague (1987) who reported abundant megacrysts of highly anorthitic plagioclase (up to An_{92}) in two dredge samples from the Central Gorda Ridge. More detailed studies of the petrology of basalts from the Escanaba Trough, at the southern end of the ridge (Davis et al., 1994), and of gabbroic xenoliths and their host basalts from the northern segment of the ridge (Davis and Clague, 1990), have found only plagioclase of $<An_{88}$, suggesting that the highly anorthitic compositions are restricted to the central ridge segment. This study focuses on a highly porphyritic dredge sample (KK2-83-NP-D9-1; 42°14.9'N, 127°04.6'W, water depth 3048 m) from the Central Gorda Ridge, collected in 1983 during a United States Geological Survey cruise, and kindly provided by Roger Nielsen, Oregon State University. This sample was selected on the basis of abundant high-An plagioclase phenocrysts, hosting melt inclusions suitable for reheating experiments, and the availability of results of reheating experiments using a 1 atm furnace (Nielsen et al. 1994; Nielsen et al., 1995) which allow a direct comparison with the heating stage technique (in Chapter 6).

In this chapter, variations in the composition of plagioclase and olivine phenocrysts, and spinel included in these phases, are described, and these data are used

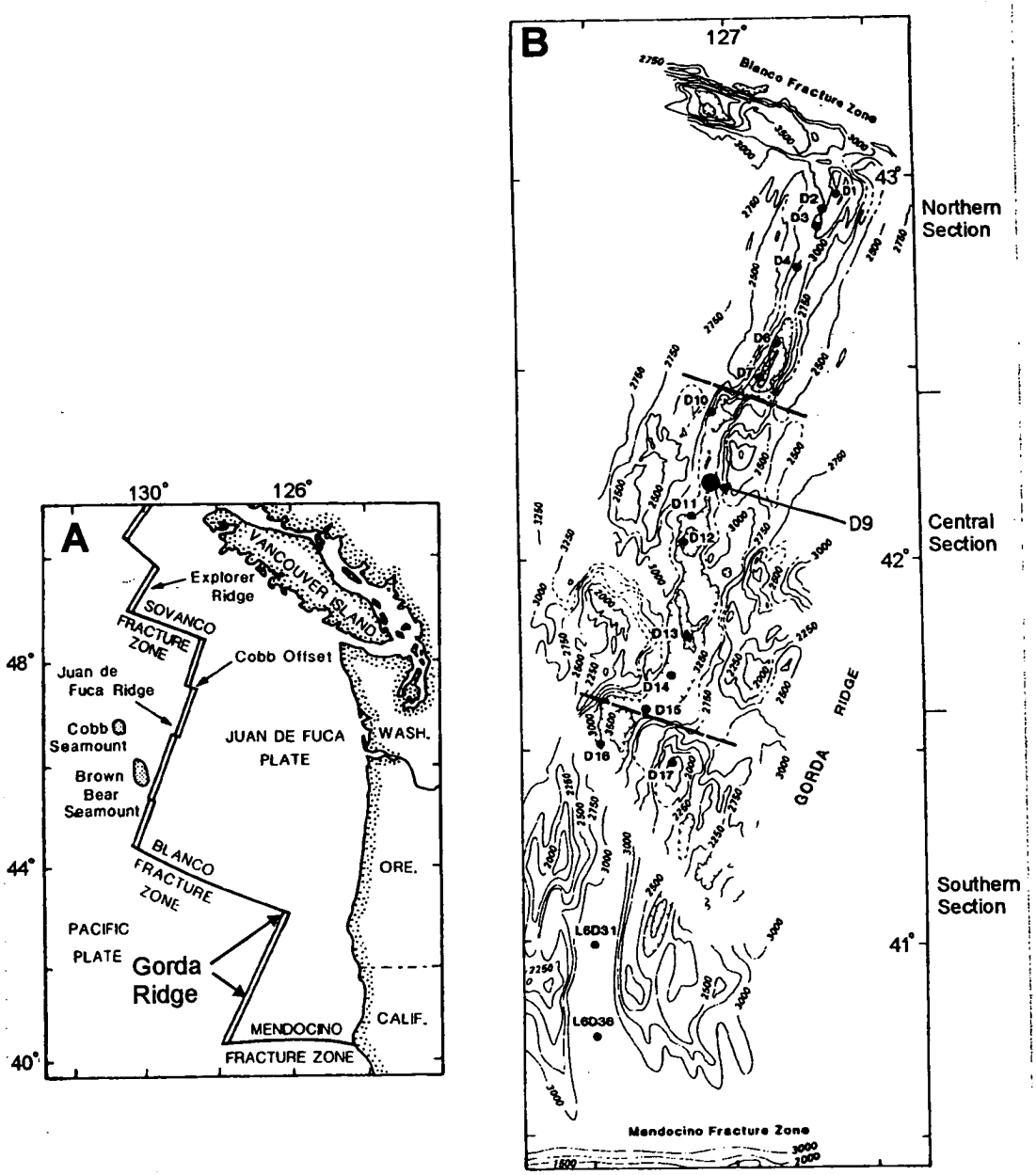

Figure 4.1: Tectonic setting of the Gorda Ridge in the northeast Pacific Ocean (A) and the location of Dredge site D9-1 on the Central Gorda Ridge (B). After Davis and Clague (1987)

to establish the crystallisation history of Sample KK2-83-NP-D9-1 (hereafter abbreviated to Sample D9-1). These results are used as the basis for interpreting the compositions of naturally quenched melt inclusions in plagioclase, olivine and spinel, and the results of heating stage experiments on plagioclase- and olivine-hosted melt inclusions. These data are then used to define the crystallisation history, and constrain the composition and crystallisation temperatures of parental liquids for Sample D9-1.

4.2 Pillow-rim glass chemistry

Three analyses of pillow-rim glass samples from D9-1 are given in Table 4.1. These analyses, from different laboratories, show discrepancies in some elements (e.g., MgO and CaO) that are discussed in Appendix 1. The composition of Sample D9-1 (from the present study) is compared with that of other glasses from the Central Gorda Ridge and Sample D4-15, the most primitive glass recovered from the northern ridge segment, in Figure 4.2. Note that the pillow-rim glass analyses of Davis and Clague (1987) have been recalculated, to remove inter-laboratory bias, as discussed in Appendix 1.

Sample D9-1 is a moderately evolved N-MORB whose composition, according to Davis and Clague (1987) is consistent with derivation from the most primitive Gorda Ridge glass by olivine and plagioclase fractionation. Indeed the pillow-rim glasses form a single trend of decreasing Al_2O_3 with decreasing MgO content, consistent with olivine-plagioclase co-crystallisation. However, the glasses define a trend for TiO_2 and CaO, that has a steeper slope than the Hole 896A cotectic, suggesting an effect from clinopyroxene crystallisation (Figs. 4.2B and E). At a given MgO, the Gorda Ridge glasses have higher TiO_2, K_2O and Na_2O, and lower CaO/Na_2O, than the majority of the Hole 896A and 504B (as discussed in Chapter 5) pillow-rim glasses, i.e., they are less depleted, and have compositions similar to the 'enriched' group T and M samples from Hole 504B (section 5.2.1), and fall in the field of Pacific MORB (Fig. 4.3).

Trace element analyses of Gorda Ridge glasses are presented in Davis and Clague (1987). Samples D9-1, and the primitive D4-15 are LREE-depleted, with $(La/Sm)_n$ values of 0.44 and 0.4 respectively, but both are less depleted than the Hole 896A glasses, which have $(La/Sm)_n$ <0.38. The low $(La/Sm)_n$ of D9-1 is largely due to a low La content (Fig. 4.4), and normalised Ce and Sm abundances are very similar to those of the average N-MORB of Sun and McDonough (1989).

The H_2O content of the D9-1 glass was determined by FTIR, at the University of Tasmania, and found to be 0.11 wt.%, in agreement with the results of Michael and Nielsen (1995), who analysed the same glass. This water content is also consistent

Table 4.1. Analyses of KK2-83-NP-D9-1 pillow-rim glass.

[a]Analysis	1	2	3
SiO_2	50.20	50.42 ±0.13[b]	50.69 ±0.24
TiO_2	1.40	1.28 ±0.02	1.25 ±0.04
Al_2O_3	15.70	15.30 ±0.04	15.35 ±0.06
FeO*	9.54	9.41 ±0.04	9.48 ±0.08
MnO	0.18	0.20 ±0.02	0.13 ±0.04
MgO	8.40	8.70 ±0.06	8.13 ±0.07
CaO	11.50	12.34 ±0.09	12.09 ±0.14
Na_2O	2.47	2.29 ±0.06	2.30 ±0.05
K_2O	0.10	0.06 ±0.01	0.06 ±0.01
P_2O_5	0.12	0.11 ±0.01	0.08 ±0.03
Cr_2O_3			0.03
total	99.61	100.17	99.59
CaO/ Na_2O	4.7	5.4	5.3
Mg#	61.2	62.4	60.6
[c]No.	6	10	9

[a]1, from Davis and Clague (1987); 2, from Nielsen et al. (1995); 3, the present study.
[b]mean analysis and standard deviation.
[c]Number of analyses.

with analyses of Pacific MORB glasses of similar Mg# and K_2O content (Byers et al., 1986; Michael, 1988). At the same MgO, glasses from Hole 896A have lower H_2O contents (<0.09 wt.%), consistent with their more depleted chemistry. If K_2O and H_2O are compared, the D9-1 glass lies well off the extension of the trend defined by Hole 896A glasses, with much higher K_2O at a given H_2O. Michael and Nielsen (1995) also report a CO_2 content of 80±80 ppm for Sample D9-1, close to the solubility limit for glasses erupted at a water depth of approximately 3000 m (Dixon et al., 1995), suggesting that Sample D9-1 was saturated with a CO_2-rich fluid at the time of eruption.

4.3 Petrography and mineral chemistry

The petrography of Sample D9-1 has been described by Davis and Clague (1987). The sample contains, calculated on a vesicle-free basis, approximately 38 vol.% plagioclase phenocrysts and xenocrysts, with lesser olivine phenocrysts (0.8 vol.%); spinel occurs only as inclusions in olivine and plagioclase. Clinopyroxene phenocrysts have not been found in Sample D9-1, or any other samples from the Central Gorda Ridge. Rare sulphide globules occur in the host glass, in plagioclase phenocrysts. Plagioclase and olivine have a wide range of size and shape, varying from euhedral microphenocrysts

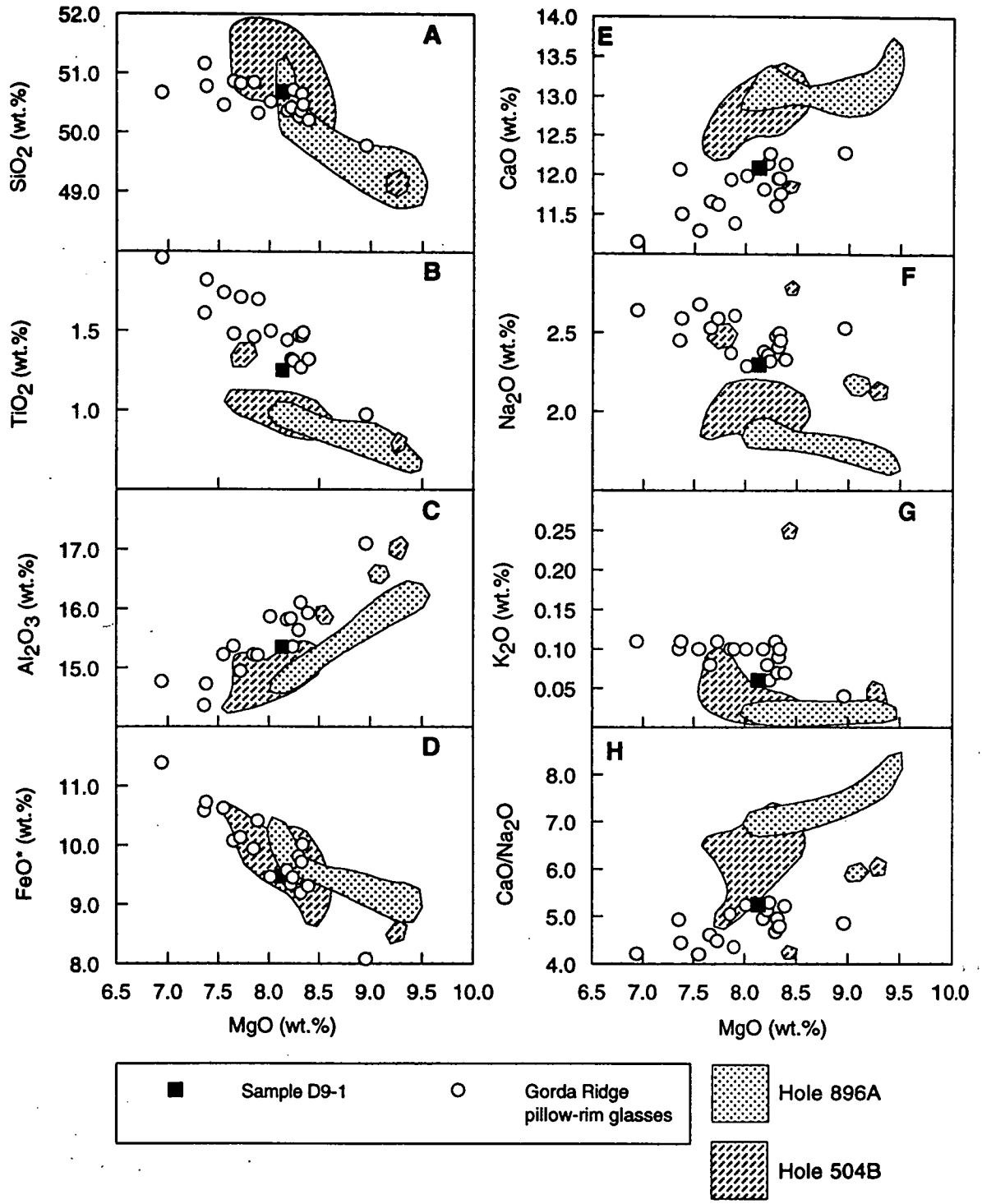

Figure 4.2: Major element variations of Central Gorda Ridge pillow-rim glasses from Davis and Clague (1987). The most primitive Gorda Ridge pillow-rim glass, D4-15, and the fields of Hole 896A (Chapter 3) and Hole 504B (Chapter 5) pillow-rim glasses are included for comparison. Note that all analyses from Davis and Clague (1987) have been corrected, for inter-laboratory bias, as discussed in Appendix 1. FeO*- all Fe as FeO. See text for discussion.

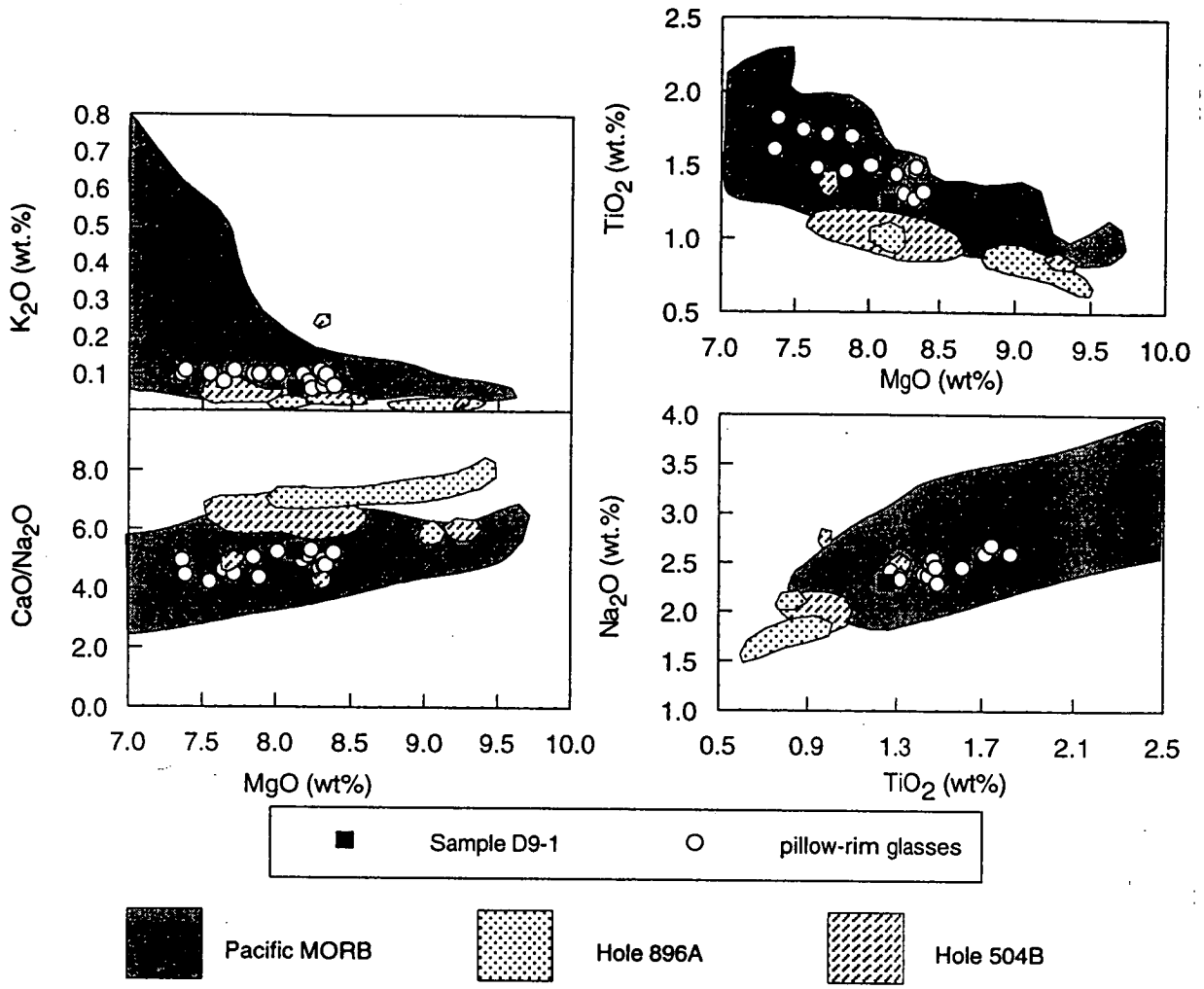

Figure 4.3: Comparison of compositional variations in Central Gorda Ridge pillow-rim glasses. The fields of Hole 896A (the present study), Hole 504B (Natland et al., 1983), and Pacific MORB (Tighe, 1988; Melson and O'Hearn, 1990) are included for comparison. The Pacific compositional field is defined by a dataset of >1100 glass analyses from active ridge segments.

and microlites, <0.1-1 mm diameter, to anhedral or subhedral (and in the case of olivine typically embayed) phenocrysts and megacrysts, up to 4 and 15 mm diameter for olivine and plagioclase respectively.

4.3.1 Plagioclase

Compositions of plagioclase phenocrysts and megacrysts are given in Appendix 4.1. Core compositions range from An_{82}-$An_{94.5}$ (Fig. 4.5), a similar range to that found in Hole 896A samples (Fig. 3.7). Phenocrysts have homogeneous cores with finely oscillatory zoned rims, and may be either normally or reverse zoned, with overall variations from core to rim of generally <3-5% An (Nielsen et al., 1995), but up to 12% An in some phenocrysts (Davis and Clague, 1987). In contrast to Hole 896A, for which histograms of plagioclase core compositions have a single well defined peak (Fig. 3.7), Sample D9-1 has an apparently bimodal distribution of phenocryst compositions, with peaks at $An_{85.5}$ and $An_{91.5}$ (Fig. 4.5).

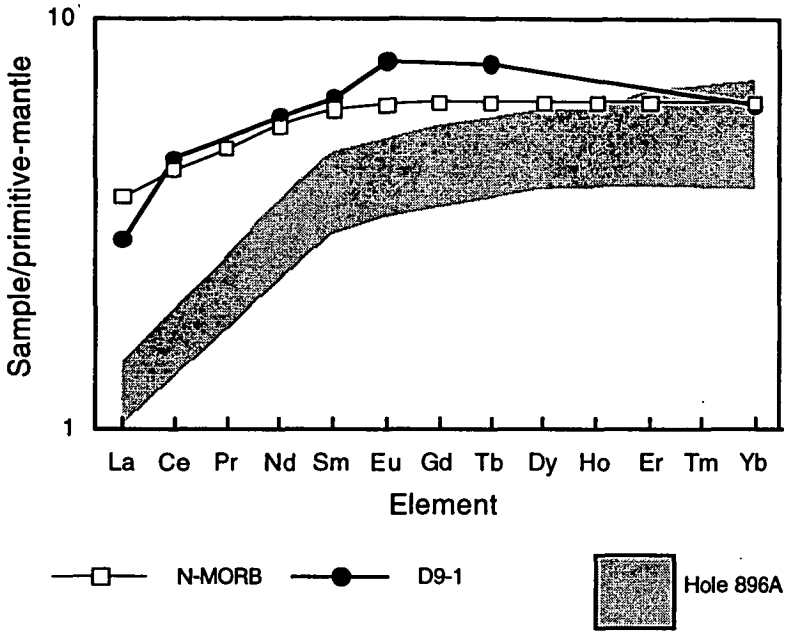

Figure 4.4: Primitive mantle-normalised rare earth element patterns of Sample D9-1 pillow-rim glass (from Davis and Clague (1987)). A typical N-MORB pattern (Sun and McDonough, 1989) and the range of Hole 896A pillow-rim glasses analysed in the present study (section 3.2.2) are shown for comparison.

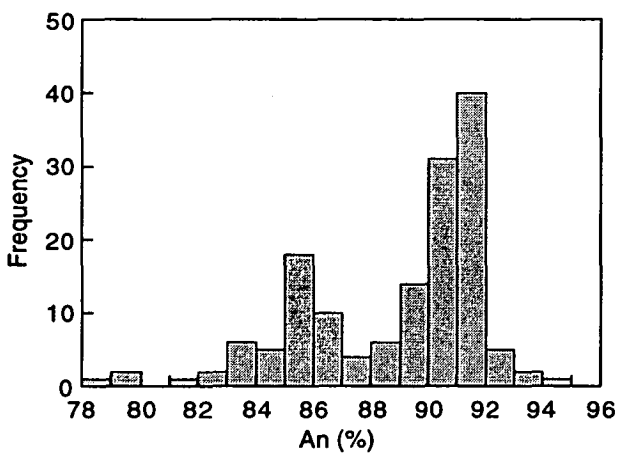

Figure 4.5: Plagioclase phenocryst 'core' compositions from Sample KK2-83-NP-D9-1. The bimodal distribution is interpreted to result from xenocrystal (>An_{88}) and equilibrium (<An_{87}) phenocryst populations.

The composition of plagioclase in equilibrium with the D9-1 pillow-rim glass was calculated using published calibrations of plagioclase-liquid equilibria. Results from the calibrations of Panjasawatwong et al. (1995; assuming a crystallisation temperature of 1230°C and pressure of 1 atm), Grove et al. (1992), Ariskin and Barmina (1990) and Weaver and Langmuir (1990) are shown in Figure 4.6. The calculated compositions of Grove et al. (1992) and Panjasawatwong et al. (1995) fall on the extension of the trend defined by Hole 896A glasses, whereas the calibrations of Ariskin and Barmina (1990) and Weaver and Langmuir (1990) yield considerably lower equilibrium anorthite compositions, that lie off this trend. The results of Grove et al. (1992) and Panjasawatwong et al. (1995), $An_{82.6}$ and $An_{84.6}$ respectively, overlap with the least anorthitic phenocryst population, and it is interpreted that phenocrysts of this composition crystallised from liquids similar to the D9-1 glass, whereas phenocrysts of $>An_{85}$ may have crystallised from liquids with higher CaO/Na_2O values. The highly anorthitic phenocrysts, with a mode of $An_{91.5}$, are therefore interpreted to be xenocrysts. Both the high- and low-An phenocrysts host inclusions of spinel, sulphide, and glass but no inclusions of olivine were found.

4.3.2 Olivine

Olivine phenocrysts are much less abundant than plagioclase phenocrysts, and all grains separated were analysed. Results are included in Appendix 4.2. Core compositions vary from $Fo_{83.2}$ to $Fo_{90.1}$ (Fig. 4.7). The olivines analysed in the present study are generally unzoned, with variations of <1 Fo unit from core to rim, although rare normally zoned phenocrysts have variations of up to 2 Fo units. However, both normally and reverse zoned phenocrysts, with variations of up to 4 Fo units were reported from Gorda Ridge samples by Davis and Clague (1987). Using the melt Fe^{2+}/Fe^{3+} derived from spinel compositions (see below) and an olivine-melt Fe^{2+}-Mg exchange coefficient of 0.3 (Roeder and Emslie, 1970; Ulmer, 1989), the calculated olivine in equilibrium with the D9-1 glass is Fo_{84}. As with plagioclase from this sample this suggests that the majority of olivine phenocrysts are not in equilibrium with the host glass, and crystallised from more primitive liquids, i.e., with higher MgO contents, as was the case for olivines sampled from Hole 896A.

Despite the evidence indicating that olivine $Fo_{87.6}$ should have crystallised from liquids more primitive than represented by D9-1, one phenocryst of this composition hosts an inclusion of plagioclase, An_{82}, that should be in equilibrium with Sample D9-1 glass. A similar relationship was described from Hole 896A samples, and will be discussed further in section 4.5.1.

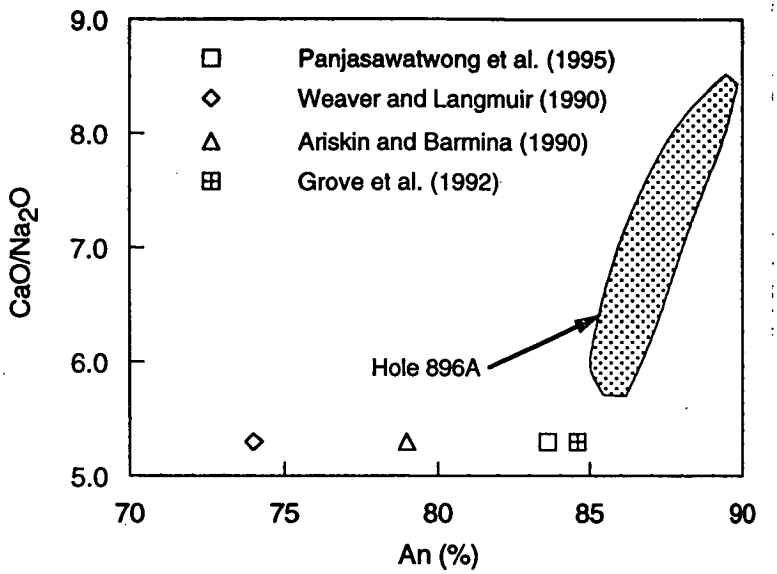

Figure 4.6: Relationship between host glass CaO/Na_2O and calculated equilibrium plagioclase compositions for Sample KK2-83-NP-D9-1, and the field of interpreted equilibrium plagioclase from Hole 896A samples. The calibrations of Panjasawatwong et al. (1995) and Grove et al. (1992) yield results consistent with the Hole 896A trend.

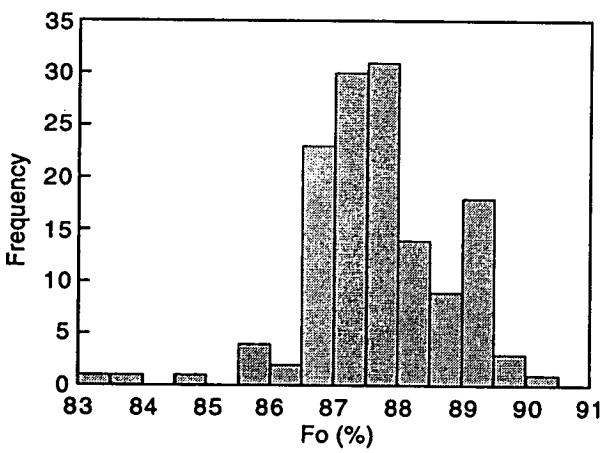

Figure 4.7: Histogram of olivine phenocryst 'core' compositions from Sample KK2-83-NP-D9-1.

4.3.3 Spinel

Spinel crystals occur included in, or attached to, phenocrysts of both plagioclase and olivine. The spinels are subhedral to anhedral, 100-150 μm diameter, and occur as either isolated solid inclusions, as clusters (with up to 5 joined spinels in an individual plagioclase phenocryst) and in rare combined melt-spinel inclusions in both plagioclase and olivine. The spinels host inclusions of glass, plagioclase, and combined glass +

plagioclase (although it is difficult to determine if the plagioclase was accidentally trapped or is a daughter phase). Spinels with solid inclusions of plagioclase were found in several plagioclase phenocrysts. The plagioclase inclusions have compositions ($An_{94.5}$-An_{91}) that are consistent with the plagioclase (An)-spinel (Cr# and Mg') compositional relationships shown in Figures 4.8B and C, and are similar to, or up to approximately 1% An higher, than the plagioclase that hosts the spinel.

Analyses of spinels are presented in Appendix 4.3, and are summarised in Figure 4.8. Compositionally they can be classified as both chromium spinels and magnesiochromites using the terminology of Sigurdsson and Schilling (1976). The spinels are generally unzoned but may have higher Cr# and lower Mg' cores than rims, with variations of up to approximately 0.5 Mg' and 0.2 Cr#.

The co-variation of Cr# and Mg' (Fig. 4.8A) indicates that spinel crystallisation accompanied olivine and plagioclase fractionation (Allan et al., 1988). The compositional similarity, in terms of Cr# and Mg', between spinels in olivine and those included in plagioclase of $<An_{87}$ (Figs. 4.8A, B and C), could be interpreted to indicate that the olivine and plagioclase ($<An_{87}$) crystallised at the same time. However, spinels included in olivines $Fo_{86.6}$-$Fo_{88.5}$, have a generally constant Mg' and Cr# (Figs. 4.8D and E) in contrast to spinels in olivine from other MORB suites, which generally show well defined trends of decreasing Mg' with host Fo content (Fig. 4.9A). The Cr# of MORB spinels have less well defined trends (Fig. 4.9B) and some suites (e.g., the Vema Fracture Zone) are like Sample D9-1 in that there is no obvious correlation between Cr# and host composition.

Equilibration temperatures calculated for spinel inclusions in olivine, using the olivine-spinel Fe^{2+}-Mg exchange thermometer of Ballhaus et al. (1991), are lower, 1001-1104°C, than inferred magmatic temperatures for this sample, 1230-1260°C (Nielsen et al., 1995). These temperatures indicate that the spinel inclusions have re-equilibrated with their host olivine and(or) magmatic liquid, a process discussed by Scowen et al. (1991). Whether this process has also affected spinels in plagioclase is unclear, due to a lack of data on plagioclase-spinel equilibria; however, the correlation between decreasing host An content and increasing Cr# and decreasing Mg' of spinel inclusions (Figs. 4.8B and C) suggest that only minimal re-equilibration has occurred.

The correlation between Cr# and Mg' and host An content of spinels from Sample D9-1, contrasts with the complex relationships between spinel and host plagioclase composition described from Hole 896A samples (section 3.3.3 and Fig. 3.10), and may indicate that a simpler magmatic history, possibly the result of

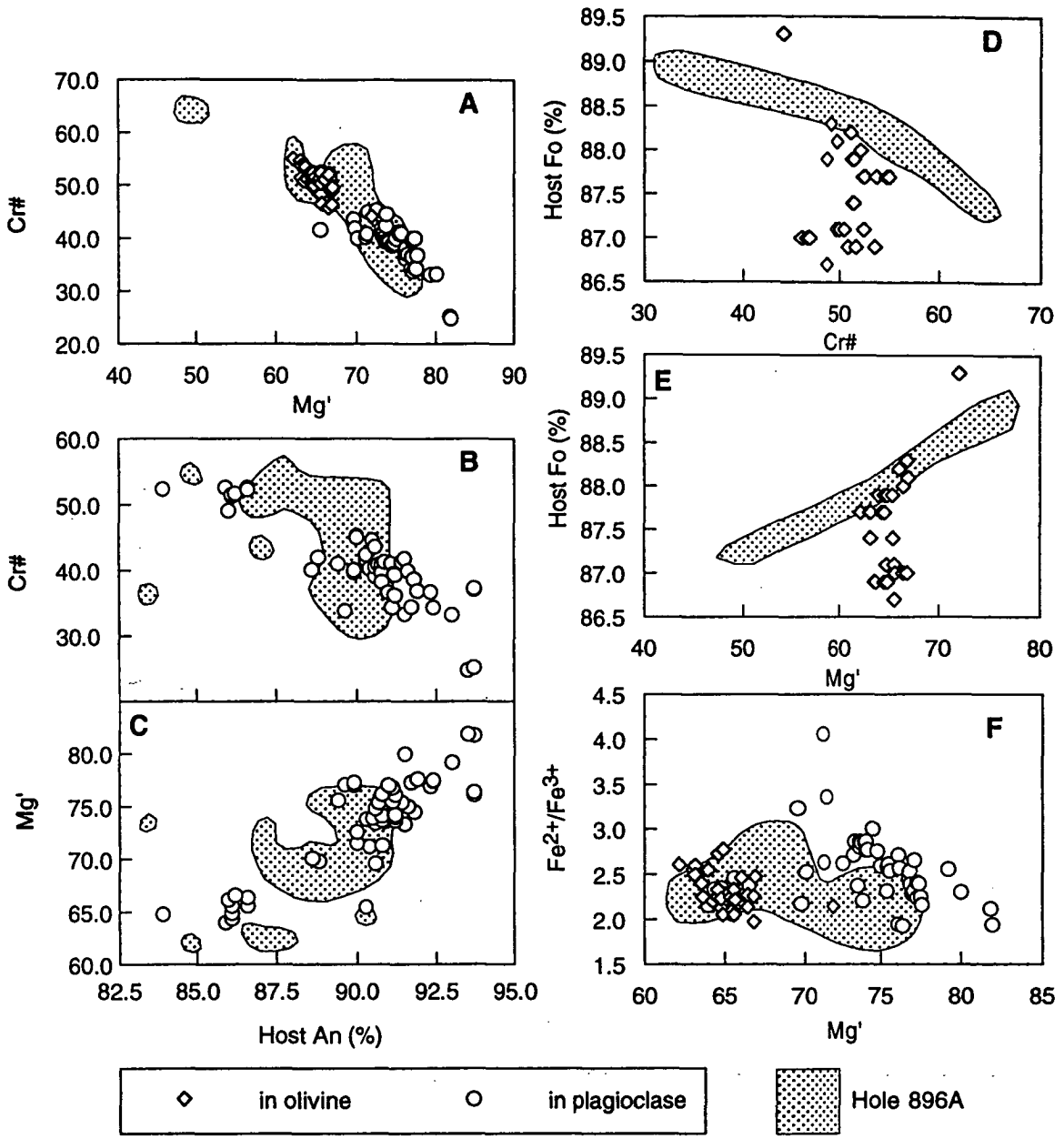

Figure 4.8: Compositional variation of spinels. **A.** Cr# (100 x (Cr/(Cr + Al)) vs. Mg' (100 x (Mg/Mg + Fe2+)) for all spinels from Sample KK2-83-NP-D9-1. Host anorthite content vs. Cr# (**B**) and Mg' (**C**) of included spinels. Host forsterite content vs Cr# (**D**) and Mg' (**E**) of included spinels. **F**, calculated Fe^{2+}/Fe^{3+} for all spinels. Fields on all plots are those of Hole 896A spinels. See text for discussion.

fractionation of a single parental liquid, produced the observed compositional range of spinels. However, the range in Cr# (24.8 to 52.6) of spinels included in plagioclase from D9-1, is greater than that of spinels found in any Hole 896A sample, and covers most of the range of spinel compositions from all MORB samples (Roeder, 1994). A similar range of Cr# values was found for spinels in Sample F-2-1 from the Lamont Seamounts, which were also included in highly anorthitic plagioclase (Allan et al., 1989). An experimental study of this sample, designed to determine factors controlling spinel

composition, led Roeder and Reynolds (1991) to conclude that both magma mixing and fractionation of plagioclase were important controls in producing highly variable Cr# in spinels from a single sample.

If the composition and crystallisation temperature of a spinel are known, then the Mg' of the liquid in equilibrium with the spinel can be estimated using the spinel-liquid Fe^{2+}-Mg exchange relationship developed by Allan (1992) and Allan (1994);

$$\left(\frac{Mg^{2+}}{Fe^{2+}}\right)_{liquid} = \left(\frac{Mg^{2+}}{Fe^{2+}}\right)_{spinel} \times e^{\left(\frac{-\Delta G^{o}_{ex}+\Delta\mu^{o}_{23}(X_3)+\Delta\mu^{o}_{24}(X_4)+\Delta\mu^{o}_{25}(X_5)}{RT}\right)}$$

where the values of $\Delta\mu^{o}_{23}$, $\Delta\mu^{o}_{24}$ and $\Delta\mu^{o}_{25}$ were determined to be 4.80, 3.5561+(0.0015698x$T°K$) and 6.39 Kcal/gfmw respectively (Hill and Sack, 1987); X_3, X_4 and X_5 are derived from the number of cations in a formula unit (based on 3 cations) of Cr^{3+}, Ti^{4+} and Fe^{3+} respectively, and ΔG^{o}_{ex} is derived from the experimentally determined spinel-olivine (Hill and Sack, 1987) and olivine-liquid (Roeder and Emslie, 1970) Fe^{2+}-Mg exchange coefficients.

As the compositions of spinels included in Sample D9-1 plagioclase are apparently unaffected by post-trapping re-equilibration, they may be suitable for these calculations. Given a crystallisation temperature of 1210°C (see section 4.4.4 and discussion in section 4.5.2), the spinels included in low-An plagioclase ($An_{83.9}$-$An_{86.1}$) are calculated to have crystallised from liquids with Mg' values of 62-64.5, i.e., similar to the D9-1 glass (Mg' =63.2; calculated using melt Fe^{2+}/Fe^{3+} = 7.9, as described below). This result supports the interpretation of equilibrium between host glass and low-An (<87) plagioclase discussed in section 4.3.1. The most magnesian spinel sampled (Mg'=81.9) occurs in a plagioclase of $An_{93.5}$. This phenocryst hosts a second spinel (Mg'=81.8) that, in turn, has an inclusion of $An_{94.5}$ plagioclase. The compositions of these spinels indicate that, using the equations of Allan (1994), the most anorthitic plagioclase analysed was in equilibrium with liquids of Mg' = 73. Such liquids would also be in equilibrium with olivine of Fo_{90} (using an olivine-liquid Fe^{2+}-Mg exchange coefficient of 0.3 (Roeder and Emslie, 1970; Ulmer, 1989)), which matches the composition of the most primitive olivine recovered from Sample D9-1 ($Fo_{90.1}$). To confirm this result, the spinel-olivine equilibration temperature was estimated for the most magnesian spinel (Mg' = 81.9), and olivine of Fo_{90}, using the geothermometer of Ballhaus et al. (1991). The calculated temperature, 1245°C, is consistent with the results of Nielsen et al. (1995), and of the present study (section 4.4.4), from the reheating of melt inclusions in olivine and plagioclase. These results suggest that plagioclase joined the cotectic early in the history of this magma, and was crystallising

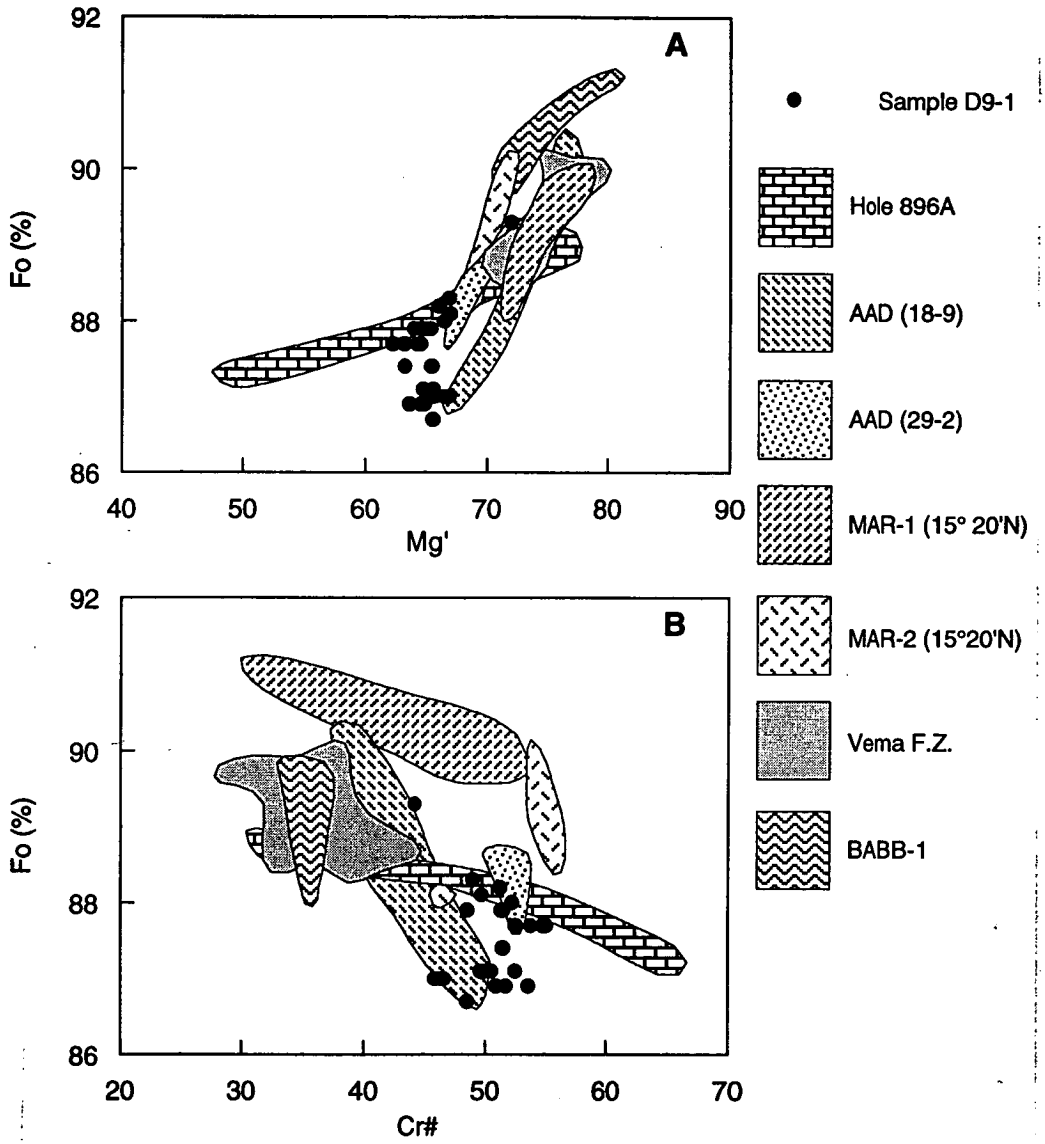

Figure 4.9: Compositional variation of spinels included in olivine from available MORB and BABB suites. Mg' (**A**) and Cr# (**B**) vs. host olivine composition. The Mg' of spinels generally correlate with host olivine composition, whereas Cr# is not as well correlated. See text for further discussion. Data sources are; AAD(18-9), AAD(29-2) and BABB1 from Sigurdsson (1994); Vema, MAR-1 and MAR-2 from Sobolev, et al. (1989) and Hole 896A from the present study (Appendix 2.2.3).

with olivine that could be in equilibrium with a mantle assemblage.

The Fe^{2+}/Fe^{3+} values of analysed spinels are shown in Figure 4.8F. The range in Fe^{2+}/Fe^{3+} of all spinels (1.9-4.0) is similar to that of Hole 896A samples, and is consistent with analyses of spinels from Sample D9-1 by Davis and Clague (1987) and Nielsen et al. (1995). There may be trends of varying Fe^{2+}/Fe^{3+} in more primitive spinels, however, the spinels in plagioclase interpreted to be in equilibrium with the host glass have a range in Fe^{2+}/Fe^{3+} of 2.15 to 2.3. Assuming that Fe^{2+}/Fe^{3+}=2.2 is

representative of spinels that crystallised from the host glass, then the Fe^{2+}/Fe^{3+} of the glass can be calculated using the method of Danyushevsky and Sobolev (1996), as outlined in section 3.3.3. These calculations yield a Fe^{2+}/Fe^{3+} value of 7.9 (i.e., $Fe^{3+}/\sum Fe = 0.11$) identical to the value for Hole 896A glasses, and higher, i.e., more oxidised, than for typical N-MORB, which have $Fe^{3+}/\sum Fe$ values of 0.07±0.03 (Christie et al., 1986).

4.3.4 Sulphides

Fe-Ni-Cu sulphide globules up to 75 μm diameter are found as inclusions in plagioclase, in melt inclusions and in the host glass. Analyses are given in Appendix 4.6. The globules in olivine-hosted melt inclusions have exsolved into two phases, Ni-rich and Ni-poor, whereas those in plagioclase appear to be homogeneous. These globules suggest that magmatic liquids parental to Sample D9-1 were sulphur saturated, and this is consistent with the appearance of sulphides in melt inclusions during reheating.

4.3.5 Synthesis: glass and phenocryst chemistry

Plagioclase phenocryst core compositions define a bimodal population; a low-An grouping ($<An_{87}$, mode $An_{85.5}$) which are interpreted to be in equilibrium with liquids that range in composition from that of the D9-1 glass to more magnesian compositions, and a more anorthitic population ($>An_{88}$, mode $An_{91.5}$), that are interpreted to have crystallised from liquids more primitive than the Central Gorda Ridge pillow-rim glasses.

The majority of olivine phenocrysts have compositions of $>Fo_{87}$ and are also interpreted to have crystallised from more primitive liquids than that represented by the D9-1 glass, which is calculated to be in equilibrium with olivine of Fo_{84}.

The overall trend of the Central Gorda Ridge pillow-rim glasses, in particular the decreasing CaO, suggests that clinopyroxene crystallisation may have been important. However, the lack of clinopyroxene in Sample D9-1 and the compositional trend, in terms of Cr# and Mg', of spinels, suggest that the phenocryst phases from this sample are related by olivine-plagioclase-spinel cotectic crystallisation.

The spinel inclusions in olivine have re-equilibrated with their hosts, however, those in plagioclase have compositions which suggest that the most anorthitic plagioclase crystallised from liquids that were in equilibrium with the most magnesian olivine sampled. Crystallisation is therefore interpreted to have been cotectic from early in the evolution of these liquids (type 2 MORB as discussed in section 1.1.2; Dmitriev et al., 1985), in contrast to the Hole 896A liquids, which underwent a period of olivine-only crystallisation prior to cotectic olivine-plagioclase fractionation (type 1 MORB; Dmitriev et al., 1985).

The early cotectic crystallisation of liquids parental to D9-1 implies that melt inclusions in plagioclase, olivine and spinel should have identical compositions at the same stage of fractionation, and should lie on an olivine-plagioclase cotectic from Sample D9-1, i.e., melt inclusions in evolved phenocrysts, Fo_{84} and $<An_{85}$, and their included spinels, should have compositions similar to that of the host D9-1 pillow-rim glass. Phenocrysts and their melt inclusions from Sample D9-1, therefore, provide an opportunity to further assess whether melt inclusions in plagioclase can be used as indicators of trapped liquid compositions, or are affected by trapping processes which lead to variations in TiO_2, FeO* and SiO_2 as was the case with melt inclusions from Hole 896A samples.

4.4 Melt inclusions

Primary melt inclusions occur in all phenocryst phases. Those in plagioclase and olivine were used for heating stage experiments and are described in detail below, and illustrated in Figure 4.10.

4.4.1 Occurrence

Melt inclusions in plagioclase are numerous, with 10 to >100 inclusions in a single phenocryst. They range in size from 2-240 μm diameter, although the majority are 20-40 μm diameter. The smaller melt inclusions generally have a better defined negative crystal shape and more strongly crystallographically controlled orientation than the larger inclusions. The form and arrangement of melt inclusions in a phenocryst are generally very similar to those from Hole 896A, although concentrically arranged inclusions are more common in phenocrysts from Sample D9-1. The melt inclusions also range from clear light brown and glassy, typically without a shrinkage bubble (Fig. 4.10A), to darker brown and partially recrystallised, with a shrinkage bubble (Figs. 4.10B and C). These variations are consistent with phenocrysts sampled from both the outermost chilled margin and the weakly crystallised zone of a pillow, as has been described from the lavas of DSDP Hole 417D by Clocchiatti (1980). When exposed in grain mounts, and viewed in reflected light, the partially recrystallised inclusions have a core of homogeneous glass and rim of finely crystalline material around their walls (Fig. 4.10D). This material is a quench intergrowth of plagioclase and glass, and is distinct from the border of cognate substance which is optically continuous with the host plagioclase (Nielsen et al., 1995).

Approximately 70% of olivine phenocrysts host melt inclusions; of these, 30% have just one inclusion and 30% host more than five inclusions. The melt inclusions are generally dark brown, lack shrinkage bubbles and only rarely have daughter crystals.

Figure 4.10: Photomicrographs of melt inclusions from sample KK2-83-NP-D9-1.

A. Glassy naturally quenched primary melt inclusions in a densely included plagioclase. Note that the majority of these melt inclusions lack shrinkage bubbles. Plane light.

B. Glassy naturally quenched melt inclusions in a densely included plagioclase. These primary melt inclusions generally have shrinkage bubbles, negative crystal forms, and have a strong crystallographic control on their orientation. Plane light.

C and **D**. A large partially crystallised primary melt inclusion in plagioclase. The dark colour of this inclusion contrasts with the smaller clear glassy inclusion indicated with an arrow (plane light; **C**). In reflected light (**D**) a margin of finely crystalline lighter coloured daughter crystals cover the walls of the large melt inclusion, with a darker glassy centre. Nielsen et al. (1995) report anomalously low Na_2O contents in analyses that overlap with this crystalline zone. Note that the smaller glassy inclusion, indicated with an arrow, lacks the crystalline margin.

E and **F**. A large heterogeneously trapped melt inclusion in olivine. In reflected light (**E**) this large glassy melt inclusion hosts a large (35 μm diameter) sulphide globule. In plane light the sulphide lies above two buried spinels, also interpreted to be in the volume of the melt inclusion.

G. A glassy primary melt inclusion in olivine. The melt inclusion has a negative crystal form and lacks a shrinkage bubble. Note the two smaller melt inclusions deeper in the phenocryst. Plane light.

H. Melt inclusions in spinel hosted by a plagioclase phenocryst. The rounded spinel (cream coloured) hosts three apparently glassy melt inclusions. The largest irregularly shaped melt inclusion also hosts a plagioclase (An_{93}) crystal (indicated by the arrow). It is thought that the plagioclase was accidentally trapped. Reflected light.

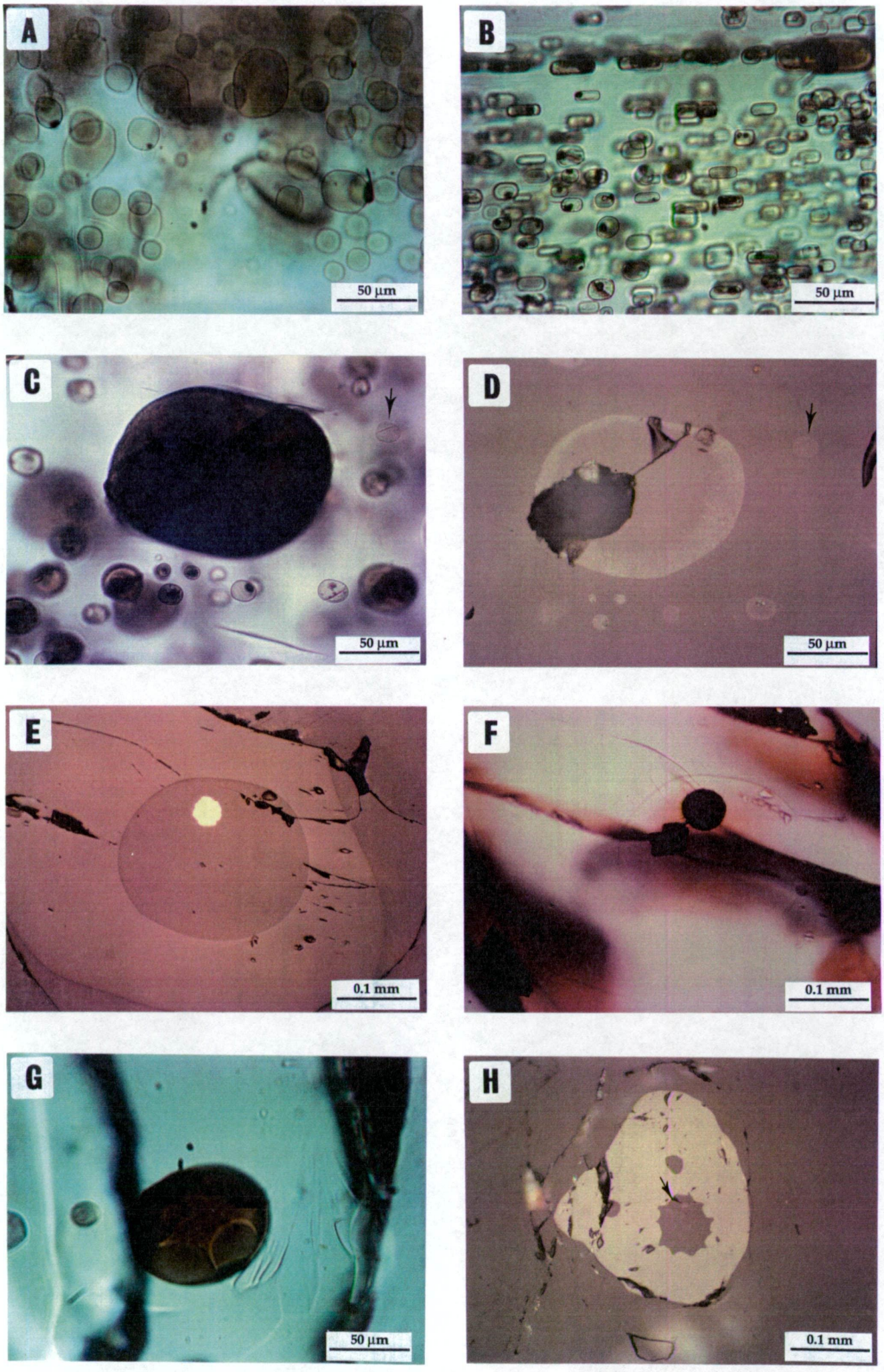
A
50 µm
B
50 µm
C
50 µm
D
50 µm
E
0.1 mm
F
0.1 mm
G
50 µm
H
0.1 mm

They range in size from <5 to 650 μm diameter, with most in the range 10-320 μm, and have variable shape, from elongate-tubular to rounded and negative crystal forms (Fig. 4.10G). Combined spinel-glass inclusions are present but uncommon, and a single combined spinel-sulphide-glass inclusion was found (Figs. 4.10E and F).

4.4.2 Compositions of naturally quenched melt inclusions

The compositions of naturally quenched melt inclusions in plagioclase, spinel and olivine are given in Appendix 4.4 and compositional variations are shown in Figures 4.11 to 4.17. During analysis of melt inclusions in plagioclase, care was taken to avoid the finely crystalline rim of some inclusions, as analyses from this zone may be affected by extreme Na_2O depletion (Nielsen et al., 1995).

Figure 4.11 shows that the melt inclusions in plagioclase and olivine have a much wider range of compositions, in terms of TiO_2, Al_2O_3, MgO, CaO and Na_2O, than the Central Gorda Ridge pillow-rim glasses. This scatter is a function both of variable amounts of post-trapping modification, and the trapping of a variety of liquids, including some more primitive than the pillow-rim glasses (cf. Hole 896A where melt inclusions were trapped from liquids similar in composition to the pillow-rim glasses). The effects of post-trapping modification are best illustrated in Figure 4.11A, where melt inclusions from olivine and plagioclase define trends at a high angle to that of the pillow-rim glasses. Similar trends were obvious in the Hole 896A data (Figs. 4.12 and 3.13) and are attributed to the formation of post-trapping overgrowths on the walls of melt inclusions during cooling. The melt inclusions from Sample D9-1 have a more restricted range of MgO and Al_2O_3 compositions than inclusions from Hole 896A (Fig. 4.12C), and this is attributed to less modification by post-trapping crystallisation, consistent with the glassy, rapidly quenched, nature of many of the D9-1 inclusions.

An indication of trapped liquid compositions can be obtained from naturally quenched melt inclusions by assuming that post-trapping compositional modification is dominated by quench overgrowths. The effects of these overgrowths can be reversed by projecting naturally quenched melt inclusion compositions along plagioclase or olivine control lines (Fig. 4.11A). When the compositions of low-An hosted melt inclusions are reversed along plagioclase control lines they intersect the pillow-rim glass defined trend at MgO contents ranging from that of the D9-1 glass to more magnesian values, approximating that of the most magnesian Central Gorda Ridge glass (Fig. 4.11A). Additionally there is a correlation between host An content and melt inclusion composition, with the majority of inclusions in plagioclase <An_{85} having lower 'reversed' MgO contents than inclusions in plagioclase of An_{86}. This correlation is consistent with mineralogical data indicating that the more evolved plagioclase, <An_{85},

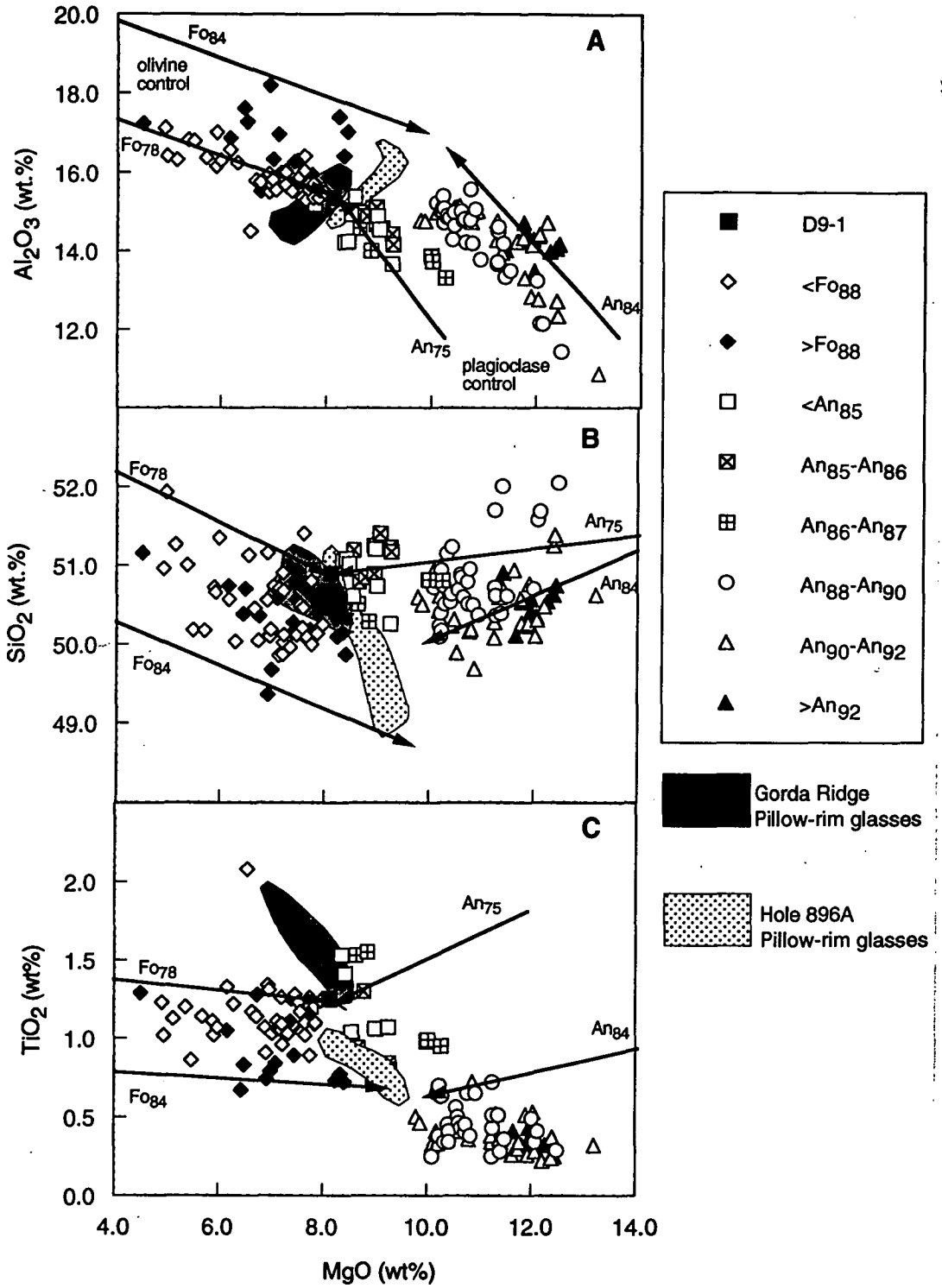

Figure 4.11: Variations in major element composition of naturally quenched melt inclusions in plagioclase and olivine phenocrysts from Sample D9-1. The field of Central Gorda Ridge and Hole 896A pillow-rim glasses are shown for comparison. Olivine and plagioclase control lines link melt inclusion or glass compositions and their host phenocrysts. *Continued*

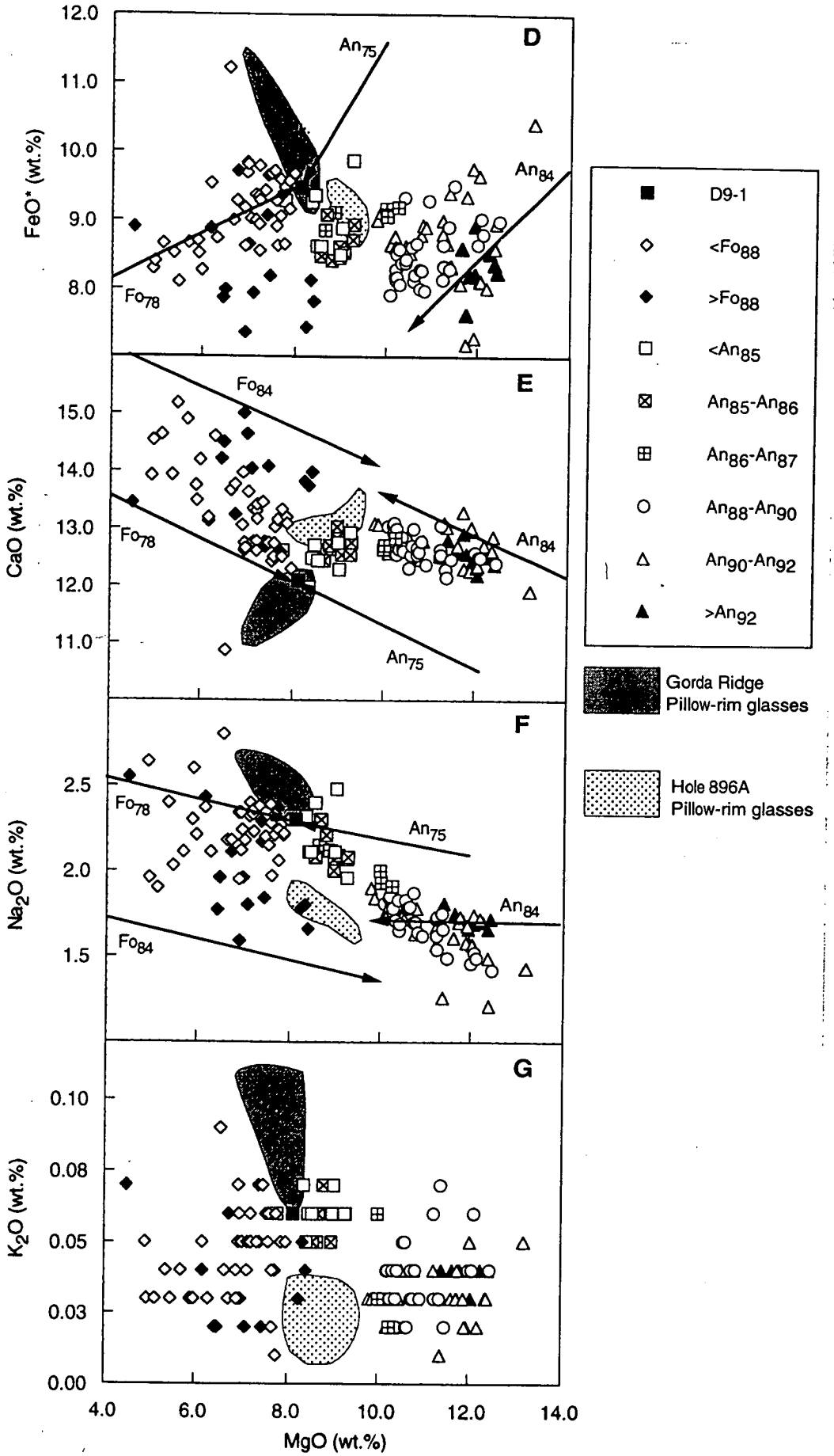

Figure 4.11: *continued*

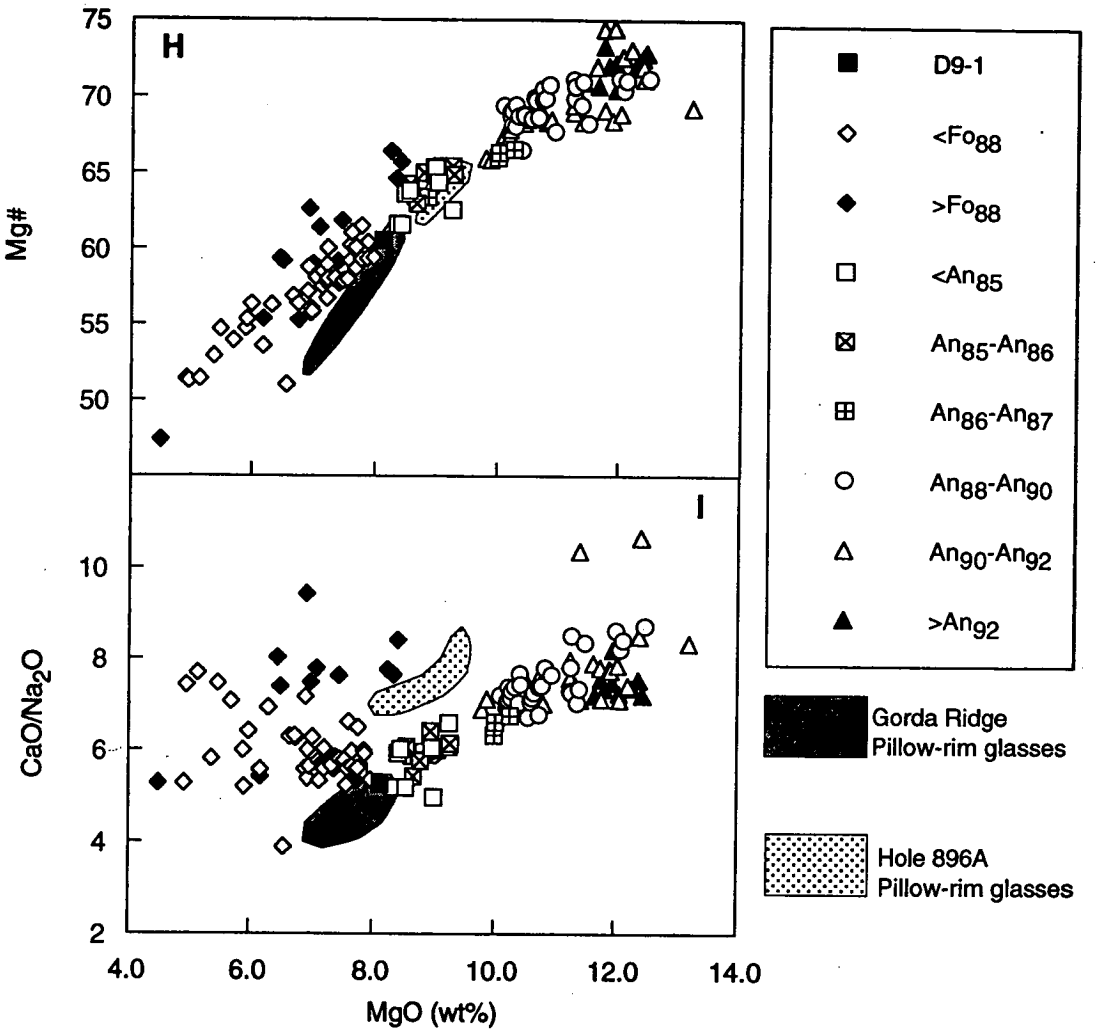

Figure 4.11: *continued* These lines are calculated using estimates of the composition of quench overgrowths form inclusions, and define the direction of compositional change produced by reversing post-trapping crystallisation of melt inclusions. See text for discussion. Melt inclusions in olivine and plagioclase phenocrysts are subdivided on the basis of host composition, e.g., $<An_{85}$, as indicated. The Sample D9-1 pillow-rim glass is also shown for comparison.

crystallised from liquids similar to the D9-1 glass, whereas inclusions in plagioclase An_{85}-An_{87} crystallised from more magnesian liquids. In contrast melt inclusions in high-An ($>An_{88}$) phenocrysts all lie on plagioclase control lines from more primitive compositions than the pillow-rim glasses, as predicted from mineralogical evidence, and melt inclusions in plagioclase $>An_{92}$ trend toward more primitive, MgO- and Al_2O_3-rich, compositions than those in plagioclase of $<An_{90}$ (Fig. 4.11A).

The MgO and Al_2O_3 contents of naturally quenched melt inclusions in plagioclase therefore confirm interpretations of phenocryst compositions (section 4.3.5) and are consistent with varying degrees of post-trapping modification of liquids that, in

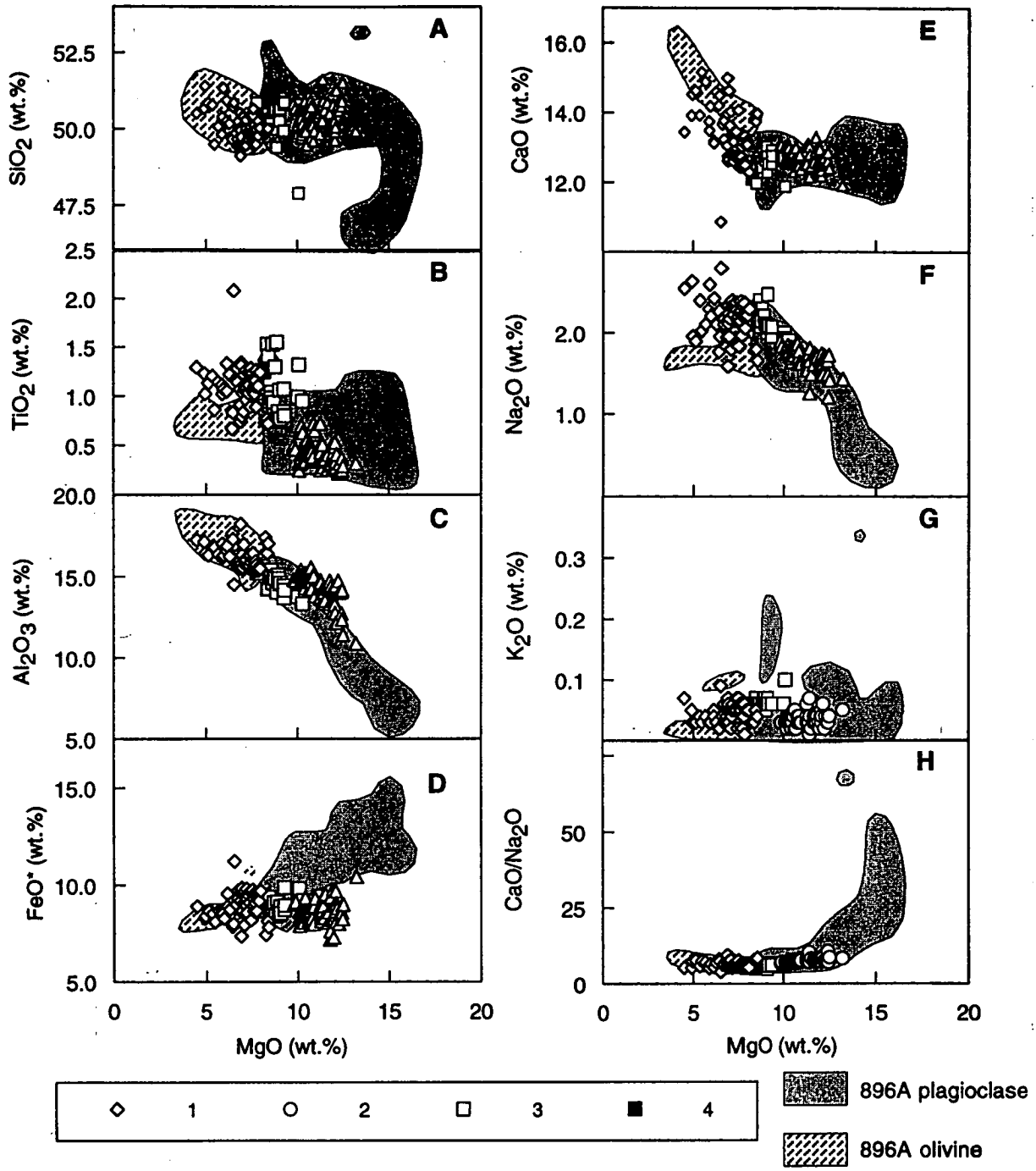

Figure 4.12: Major element compositional variations of naturally quenched melt inclusions in olivine and plagioclase phenocrysts from Sample D9-1, compared with those of naturally quenched melt inclusions from Holes 896A (fields shown). Symbols; 1- melt inclusions in olivine; 2- melt inclusions in high-An (>An_{88}) plagioclase; 3- melt inclusions in low-An (<An_{87}) plagioclase; 4- Sample D9-1 pillow-rim glass.

the case of low-An plagioclase, lie on the pillow-rim glass defined trend and have compositions similar to the D9-1 glass, in terms of MgO and Al_2O_3. Given this result, it would be expected that, if compositions of low-An plagioclase-hosted melt inclusions are representative of trapped liquids, the variations in other major elements should also be related to the pillow-rim glasses on plagioclase control lines. This is not the case; SiO_2 contents project to a range of compositions that extend to higher values (Fig. 4.11B), and TiO_2 contents extend to lower values (0.5 wt.%) than any of the pillow-rim glasses (Fig. 4.11C). The FeO* contents of the majority of melt inclusions (8.2-9.8 wt.%) are generally lower than that of the D9-1 glass and fall on the trend of the pillow-rim glasses, but when corrected for post-trapping modification along plagioclase control lines, have lower FeO* contents than the glass trend (Fig. 4.11D). The low FeO* contents result in calculated Mg# values for plagioclase-hosted melt inclusions (Fig. 4.11H) that may be higher than for the pillow-rim glasses (i.e., Mg# values of 59.9-66.5 and 52.2-61.9 for the melt inclusions and glasses respectively). These variations, in SiO_2, TiO_2 and FeO*, are all consistent with those seen in both naturally quenched and homogenised melt inclusions from Hole 896A. However, the melt inclusions in low-An plagioclase from D9-1 have high CaO contents (12.4-13.0 wt.%, and thus CaO/Na_2O; Figs. 4.11E and I), relative to the pillow-rim glasses (11.3-12.3 wt.% CaO). Higher CaO contents were not found in melt inclusions from Hole 896A samples, where melt inclusion CaO contents were consistent with those of the pillow-rim glasses.

The compositions of melt inclusions hosted by olivine Fo_{83}-Fo_{90} generally define trends in Figure 4.11 that result from the trapping of liquids with compositions ranging from those of the pillow-rim glasses to more primitive compositions, consistent with mineralogical evidence. However, in detail the relationships are less clear; melt inclusions in olivine $<Fo_{88}$ generally project to more evolved liquid compositions than inclusions in $>Fo_{88}$, but some inclusions in $>Fo_{88}$ project to compositions similar to, and in some cases more evolved than, the D9-1 glass. This is particularly obvious for FeO* and Al_2O_3 (Figs. 4.11A and D) and is inconsistent with mineralogical evidence suggesting the D9-1 glass is in equilibrium with less primitive olivine (Fo_{84}).

Three olivine phenocrysts, grains A31-OL58, A31-OL80 and A31-OL19, host melt inclusions in which TiO_2 and CaO/Na_2O may vary by up to 0.7 wt.% (~50 rel.%) and 2.5 respectively. These phenocrysts are compositionally zoned (up to 2 Fo units) and there is a strong correlation between melt inclusion TiO_2 content and CaO/Na_2O, and host olivine composition in each phenocryst (Fig. 4.13). These compositional variations are interpreted to result from the trapping of liquids at different stages along the liquid line of descent, including one melt inclusion (A31-OL80-GL2) that appears to be more evolved than the host glass, and similar to the most evolved Gorda Ridge glass

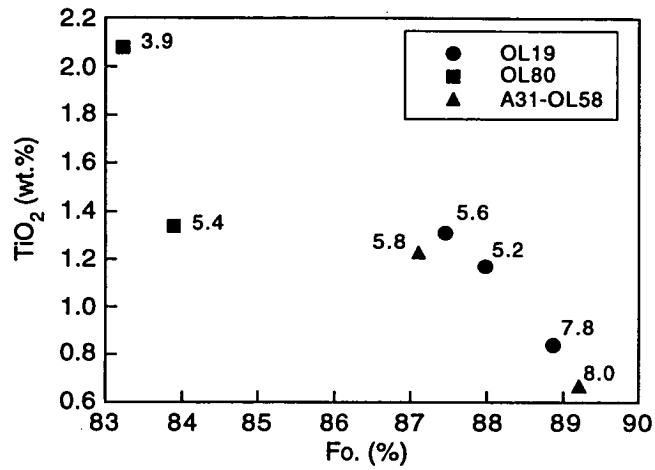

Figure 4.13: Compositional variation of naturally quenched melt inclusions trapped in zoned olivines. There is a good correlation between TiO_2 and host composition for individual phenocrysts. Numbers adjacent to points are CaO/Na_2O values for melt inclusions. CaO/Na_2O is a good indicator of trapped liquid composition as both Ca and Na are incompatible in the olivine that is inferred to have crystallised on the walls of the inclusion after trapping. Note that despite a good correlation within each phenocryst, melt inclusions in different phenocrysts, Fo_{88}-Fo_{84} have constant TiO_2 and CaO/Na_2O, inconsistent with the effects of fractional crystallisation. See text for discussion.

(Fig. 4.11). However, the TiO_2 contents of melt inclusions in different phenocrysts of Fo_{84}-Fo_{88} are virtually constant, allowing for the minor effects of post-trapping enrichment (Fig. 4.11C), and do not increase as would be expected from crystallisation on the olivine-plagioclase(±clinopyroxene) cotectic. Similarly, CaO/Na_2O of melt inclusions should decrease with decreasing host Fo content during cotectic plagioclase-olivine crystallisation. This is not the case, with olivines of Fo_{84}-Fo_{88} hosting melt inclusions of similar CaO/Na_2O (Fig. 4.13). If all analysed melt inclusions in olivine are considered (Fig. 4.14), there is generally a good correlation between inclusion, and host olivine composition for inclusions in olivines more magnesian than Fo_{88}. However, at lower Fo contents (86-88) considerable scatter of CaO/Na_2O is evident, from 5.2 (similar to D9-1) to ~8 (Fig. 4.14C), a range much larger than would be expected from analytical error. Similar variations occur in the ratios of other elements that are incompatible in olivine, e.g., Al_2O_3 and TiO_2 (Fig. 4.14A) and CaO/Al_2O_3 (Fig. 4.14B). The overall range of CaO/Al_2O_3 values in olivine Fo_{87}-Fo_{88}, 0.77 to 0.92, is much larger than for all Central Gorda Ridge pillow-rim glasses, and covers much of the range of primitive MORB glasses, with CaO/Al_2O_3 values of 0.66-0.88 (T. J. Falloon pers. comm., 1996). The high FeO* contents (>9.4 wt.%) of many inclusions in olivine of Fo_{86}-Fo_{88} (Figs. 4.11D and 4.14D), are similar to that of the D9-1 glass, and are not consistent with either post-trapping crystallisation of olivine (which should force

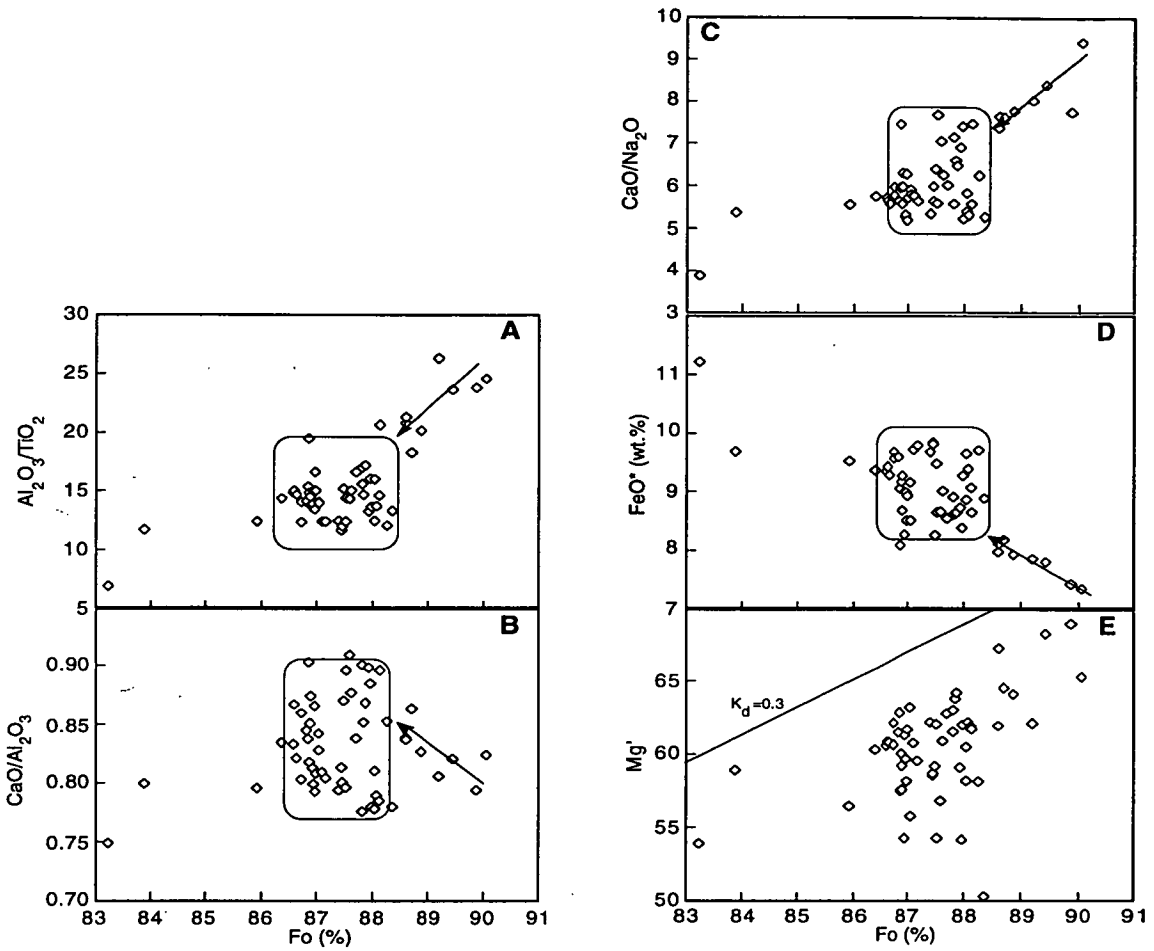

Figure 4.14: Compositions of naturally quenched melt inclusions hosted by olivine. Variations in ratios of major elements incompatible in olivine, FeO* and Mg' (= 100 x (Mg/(Mg + Fe^{2+})); where Fe^{2+} = 0.89xFeO*) with host forsterite content. Lines on **A-D** give the trend of compositions of melt inclusions in >Fo_{88} and the fields indicate the range of compositions of melt inclusions in Fo_{86}-Fo_{88}. Line on (E) shows the equilibrium relationship between olivine and liquid (calculated assuming an olivine-melt Fe^{2+}-Mg exchange coefficient of 0.3). See text for discussion. FeO* = all Fe as FeO.

compositions along the control lines shown on Fig. 4.11D), or the more primitive nature of the host olivines, both of which should lead to lower FeO* contents.

As discussed previously, all naturally quenched melt inclusions in olivine have been affected by post-trapping crystallisation of olivine, as evidenced by the trend of increasing Al_2O_3 with decreasing MgO (Fig. 4.11A). This is confirmed by calculated olivine-melt Fe^{2+}-Mg exchange coefficients (calculated using $Fe^{3+}/\sum Fe$=0.11, see section 4.3.3) that range from 0.13 to 0.28 (Fig. 4.14E), and are lower than the accepted value of 0.3 (Roeder and Emslie, 1970; Ulmer, 1989). It should be noted that these calculations are minimally affected by the $Fe^{3+}/\sum Fe$ used; if a value of 0.15 is used, derived from the

most primitive spinel sampled in the present study and consistent with analyses from Davis and Clague (1987) and Nielsen et al. (1995), then calculated exchange coefficients are increased by only 0.01.

To remove the effects of post-trapping crystallisation the composition of selected melt inclusions in olivine (Fo_{83} to $Fo_{90.1}$) were recalculated by simulating the reverse of olivine crystallisation until the inclusions were in equilibrium with their host phenocryst. This was done with the Petrolog computer program of Danyushevsky et al. (1990) and using the olivine-melt model of Ford et al. (1983). Calculations required removal of 3-10.5 wt.% olivine and yield equilibrium temperatures of 1195-1270°C. The resulting melt inclusion compositions do not correlate with host olivine composition; most inclusions from olivine ($Fo_{86.6}$-$Fo_{90.1}$) have MgO contents of 10-11 wt.% (Fig. 4.15A). In addition, the majority of these compositions do not follow the olivine-plagioclase cotectic, as would be expected from mineralogical evidence. Some of the melt inclusions fall on an olivine-only crystallisation path from Sample D9-1 in terms of Al_2O_3 and FeO*, however, the majority of melt inclusions are too CaO-rich to be related to the D9-1 glass by either olivine-only or plagioclase-olivine crystallisation (Fig. 4.15). Variations can also be seen in a single zoned phenocryst (Fig. 4.15); a melt inclusion from olivine of Fo_{84} has an equilibrium temperature of 1195°C and a composition very similar to that of the D9-1 glass (Fig. 4.15). A second melt inclusion from this phenocryst (A31-OL80; Fo_{83} in Fig. 4.15) was interpreted to have crystallised from more evolved liquids than the D9-1 glass, based on high TiO_2 and low CaO/Na_2O (see above) but has a recalculated composition with ~9.3 wt.% MgO, and an equilibration temperature of 1240°C. The discrepancies in calculated composition and temperature are the result of the high FeO* content of some naturally quenched melt inclusions, as discussed above (Figs. 4.11D and 4.14D), which lead to high re-calculated MgO contents, and thus high calculated equilibration temperatures.

The high FeO* contents of olivine-hosted naturally quenched melt inclusions have not previously been described from other MORB suites, and were found in only one inclusion from Hole 896A (Fig. 3.25 and section 3.4.4), where re-calculated inclusion compositions generally lie on olivine-only fractionation trends extending from the most magnesian pillow-rim glasses. The reason for the high FeO* may be related to; (1) the kinetics of quench processes leading to the non-equilibrium crystallisation of more MgO-rich olivine on melt inclusion walls, (2) the modification of melt inclusion compositions by leakage after trapping, or (3) post-trapping crystallisation of clinopyroxene, rather than olivine, on the walls of inclusions. Processes 1 and 3 may be reversed during the experimental reheating of melt inclusions and further discussion of high-FeO* contents is best done by comparison with the results of homogenisation

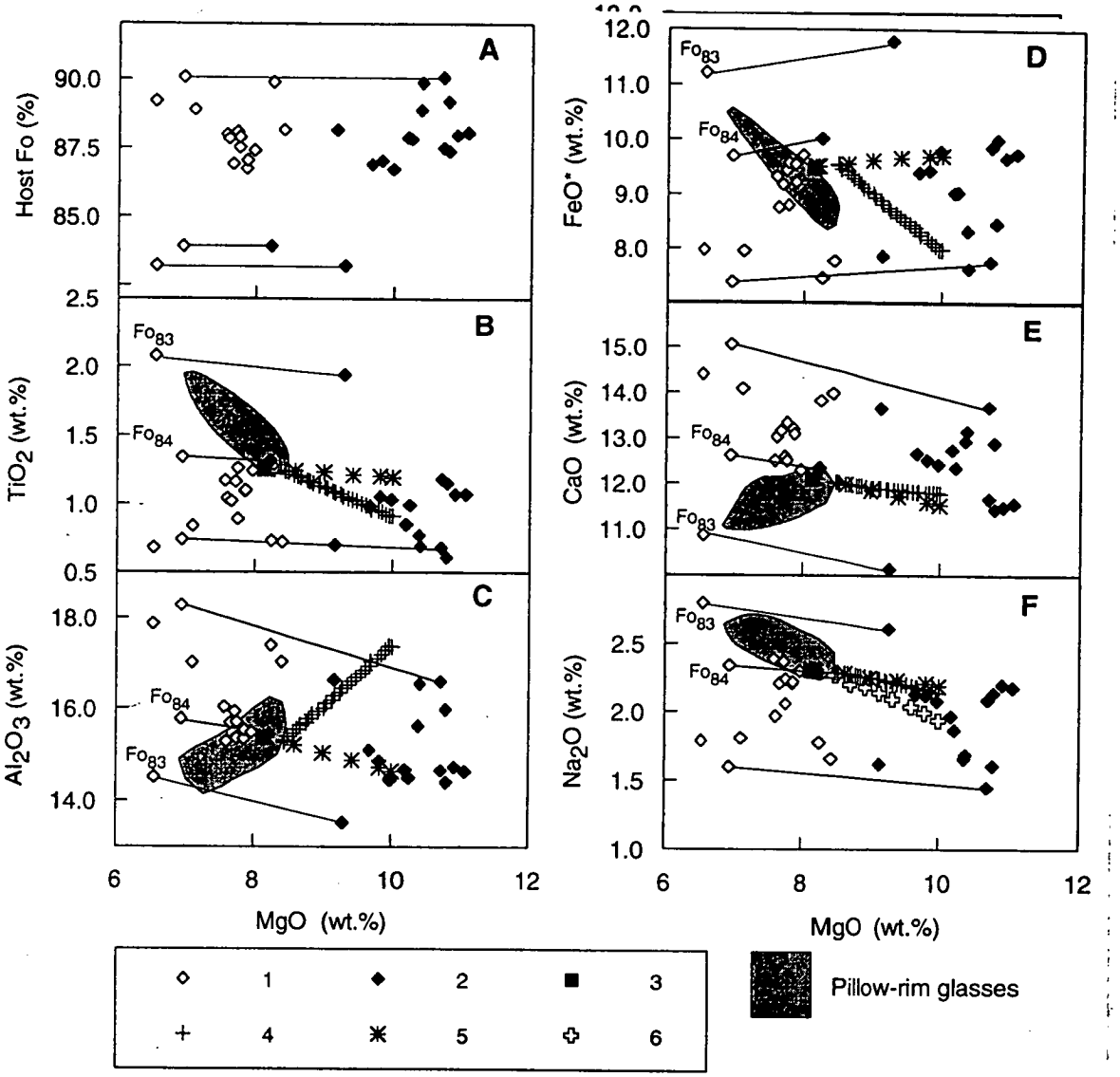

Figure 4.15: A. Host olivine composition vs MgO, and **B-F** major element vs. MgO variations of naturally quenched melt inclusions in olivine that were recalculated to be in equilibrium with their host phenocrysts (see text for description of calculations). Lines connecting points indicate the compositional changes resulting from recalculation for selected inclusions. The field of Central Gorda Ridge pillow-rim glasses is shown for comparison. See text for discussion. Symbols; 1- naturally quenched melt inclusions; 2- recalculated naturally quenched melt inclusions; 3- Sample D9-1 pillow-rim glass; 4- olivine-plagioclase cotectic calculated from Sample D9-1 using the models of Ford et al. (1983) for olivine and the modified (Danyushevsky et al., 1996) Weaver and Langmuir (1990) models for plagioclase. Individual crosses indicate 1% fractionation; 5- An olivine-only crystallisation trend calculated, using Ford et al. (1983), from Sample D9-1; 6- an empirically corrected plagioclase-olivine cotectic to account for the low-An content (more sodic) of plagioclase calculated by the Weaver and Langmuir (1990) calibration (hereafter W+L). The correction was derived (see section 3.5.1) by comparing the results of W+L with the Hole 896A group 1 pillow-rim glasses.

experiments (section 4.4.4). It is, however, significant that the olivines from Sample D9-1, typically <Fo_{88}, which host high-FeO* melt inclusions, also host spinels with constant Mg' and Cr# (section 4.3.3; Fig. 4.8E) whereas olivines from Hole 896A, where high-FeO* melt inclusions are rare, host spinels with variations of Mg' and Cr# that are more typical of other MORB suites (Fig. 4.9).

The high K_2O contents (>0.1 wt.%) found in some olivine- and plagioclase-hosted melt inclusions from Hole 896A, were not recorded in analyses of naturally quenched melt inclusions, in all phenocryst types, from Sample D9-1 (Fig. 4.12G). The naturally quenched melt inclusions in olivine from Sample D9-1 generally have a similar range of compositions and compositional trends to inclusions from Hole 896A (Fig. 4.12). However, the trends for plagioclase may be different; a correlation exists between increasing host-An content (and thus melt inclusion MgO content) with decreasing TiO_2 content of melt inclusions from Sample D9-1, and this is not seen in the inclusions from Hole 896A, which have a wide range of TiO_2 at a given MgO (Fig. 4.12B). There is no apparent variation in FeO* content with increasing MgO for Sample D9-1 melt inclusions (Fig. 4.12D), compared with a trend of increasing FeO*, with increasing MgO in Hole 896A melt inclusions. Melt inclusions from Sample D9-1 do not have compositions that extend to high CaO/Na_2O, as do some of the more modified melt inclusions from Hole 896A (Fig. 4.12H).

Compositions of naturally quenched, spinel-hosted melt inclusions are shown in Figure 4.16 (note that these compositions have been recalculated to 0.1 wt.% Cr_2O_3 to remove the effects of variable analytical overlap with the host spinel). All spinels in plagioclase are wholly included within phenocrysts, in contrast to those from olivine which are attached to phenocrysts. The spinels are interpreted to be attached to the olivines as they occur in the thin rinds of glass which typically enclose olivine phenocrysts separated from Sample D9-1. The compositions of the melt inclusions in spinel (Mg'=63.2-64.9) attached to olivine ($Fo_{87.4}$-$Fo_{87.9}$) are very similar to that of the host glass and not more magnesian as would be expected if the spinel and olivine had crystallised together. I interpret this to indicate that the spinels crystallised from liquids of the composition of the host glass and became attached to the olivines, either in the magma chamber or during eruption.

Despite the interpretation that the compositions of melt inclusions in spinel are typically little modified by post-trapping crystallisation (Le Roex et al., 1981; Kamenetsky, 1996), the compositions of melt inclusions in plagioclase-hosted spinel show considerable variation. Figure 4.16 shows that although the inclusions appear to have cotectic TiO_2 contents, variations in SiO_2, Al_2O_3 and CaO contents, in particular,

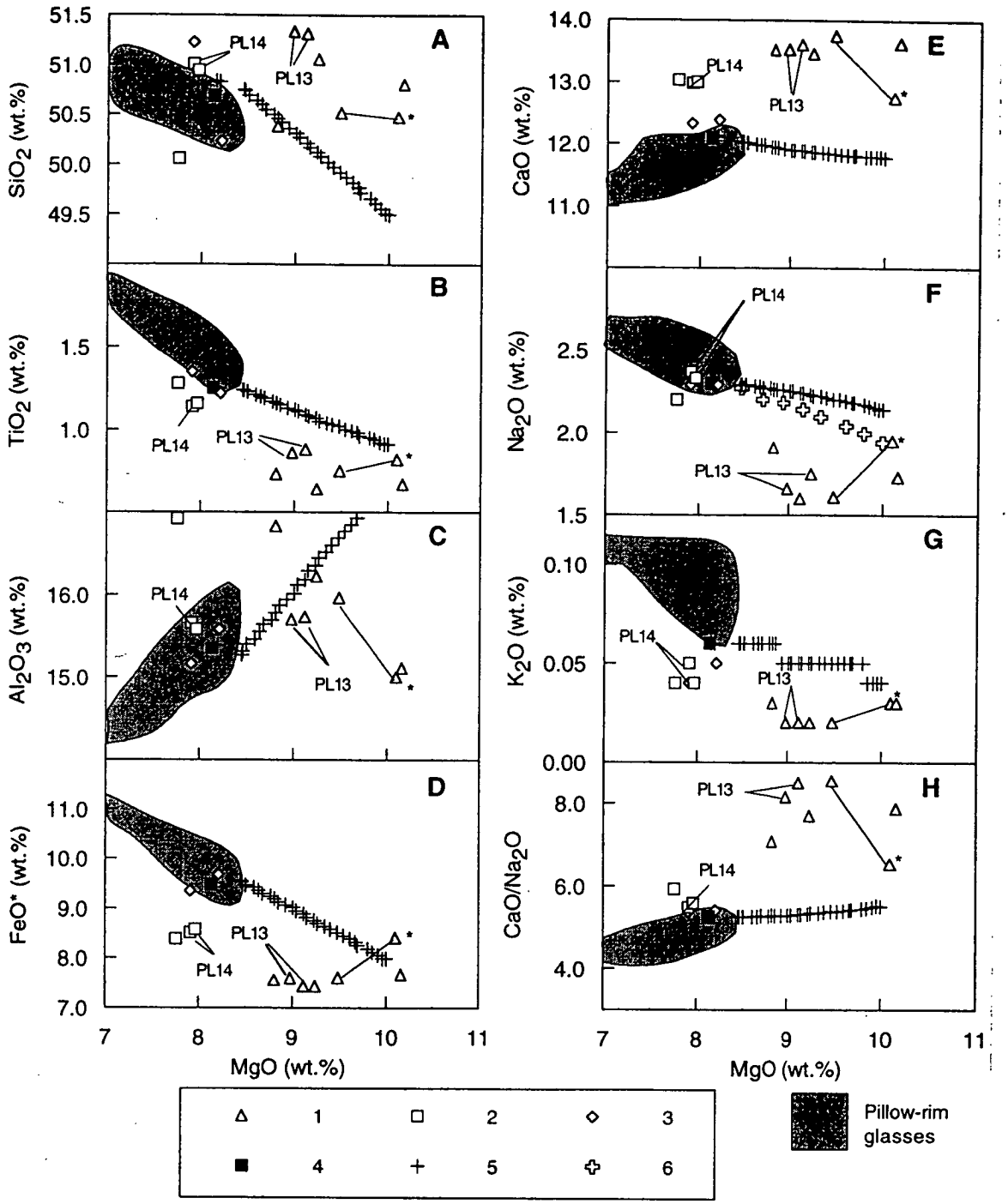

Figure 4.16: Compositional variations of naturally quenched melt inclusions in spinel. Note that analyses have been recalculated to 0.1 wt.% Cr_2O_3 to remove the effects of ?analytical overlap with their host spinel. Symbols; 1- melt inclusions in spinel from high-An (>An_{88}) plagioclase; 2- melt inclusions in spinel from low-An (<An_{87}) plagioclase; 3- melt inclusions in spinel attached to olivines; 4- Sample D9-1 pillow-rim glass; 5- plagioclase-olivine cotectic from Sample D9-1; 6- corrected plagioclase-olivine cotectic. The cotectics were calculated as described in Figure 4.15. The field of Central Gorda Ridge pillow-rim glasses, with MgO >7.0 wt.%, is shown for comparison. Two melt inclusions from a single spinel in plagioclase grain A31-PL8 are joined by a tie line. The indicated inclusion (*) hosts an accidentally trapped (or daughter?) plagioclase crystal, and compositional differences between the two melt inclusions may be related to post-trapping crystallisation of plagioclase on this crystal. See text for discussion.

do not follow the pillow-rim glass-defined compositional trend or the plagioclase-olivine cotectic from Sample D9-1. In addition, the melt inclusions in spinel in low-An plagioclase, which should have compositions similar to, or slightly more primitive than, the D9-1 glass, have compositions that range to higher Al_2O_3 and CaO, and lower FeO* and MgO contents, although TiO_2, Na_2O and K_2O contents are similar to D9-1 (Fig. 4.16). The high CaO of these melt inclusions, ~13%, is consistent with the CaO content of melt inclusions in plagioclase, 12.4-13% (Fig. 4.17F), and this similarity suggests that high CaO contents are a primary feature related to trapped liquid composition. Melt inclusions in spinel from high-An plagioclase, are more magnesian than those in low-An plagioclase, consistent with mineralogical evidence, but, have higher SiO_2 and CaO, and lower FeO* and Na_2O and range to lower Al_2O_3 than would be expected from the calculated plagioclase-olivine cotectic (Fig. 4.16). Compositions of melt inclusions in individual spinels are similar (Fig. 4.16) and the variability of inclusion compositions therefore results from variations between spinel grains.

Summary

Variations in the MgO and Al_2O_3 contents of the naturally quenched melt inclusions can be used to demonstrate that the low-An plagioclase-hosted melt inclusions were trapped from liquids with compositions ranging from similar, in terms of MgO, to that of D9-1 to slightly more magnesian compositions, similar to the most magnesian Central Gorda Ridge pillow-rim glasses, and that the high-An plagioclase crystallised from more primitive liquids, as inferred from textural and compositional variations of phenocryst phases. However variations of other elements, in low-An hosted inclusions, most notably SiO_2, TiO_2, FeO* and CaO, do not reproduce the pillow-rim glass compositions, when corrected for post-trapping crystallisation. The high SiO_2 and low FeO* (and thus high Mg#) and TiO_2 contents of Sample D9-1 melt inclusions are consistent with trends seen in samples from Hole 896A, but the high CaO contents were not recorded previously. The high CaO, relative to the pillow-rim glasses, were also recorded from melt inclusions in spinel hosted by low-An plagioclase and this suggests that the trapped liquids had higher CaO contents than the Sample D9-1 pillow-rim glass.

These results further emphasise the problems of using supposedly incompatible element contents and ratios, i.e., TiO_2 and Mg#, of naturally quenched melt inclusions in plagioclase to interpret the petrogenesis of MORB, as has been done previously (e.g., Humler and Whitechurch, 1988; Natland, 1989; Sichel and Sigurdsson, 1993).

The compositions of naturally quenched melt inclusions in spinel show considerable scatter; those in low-An plagioclase have lower FeO*, and MgO contents

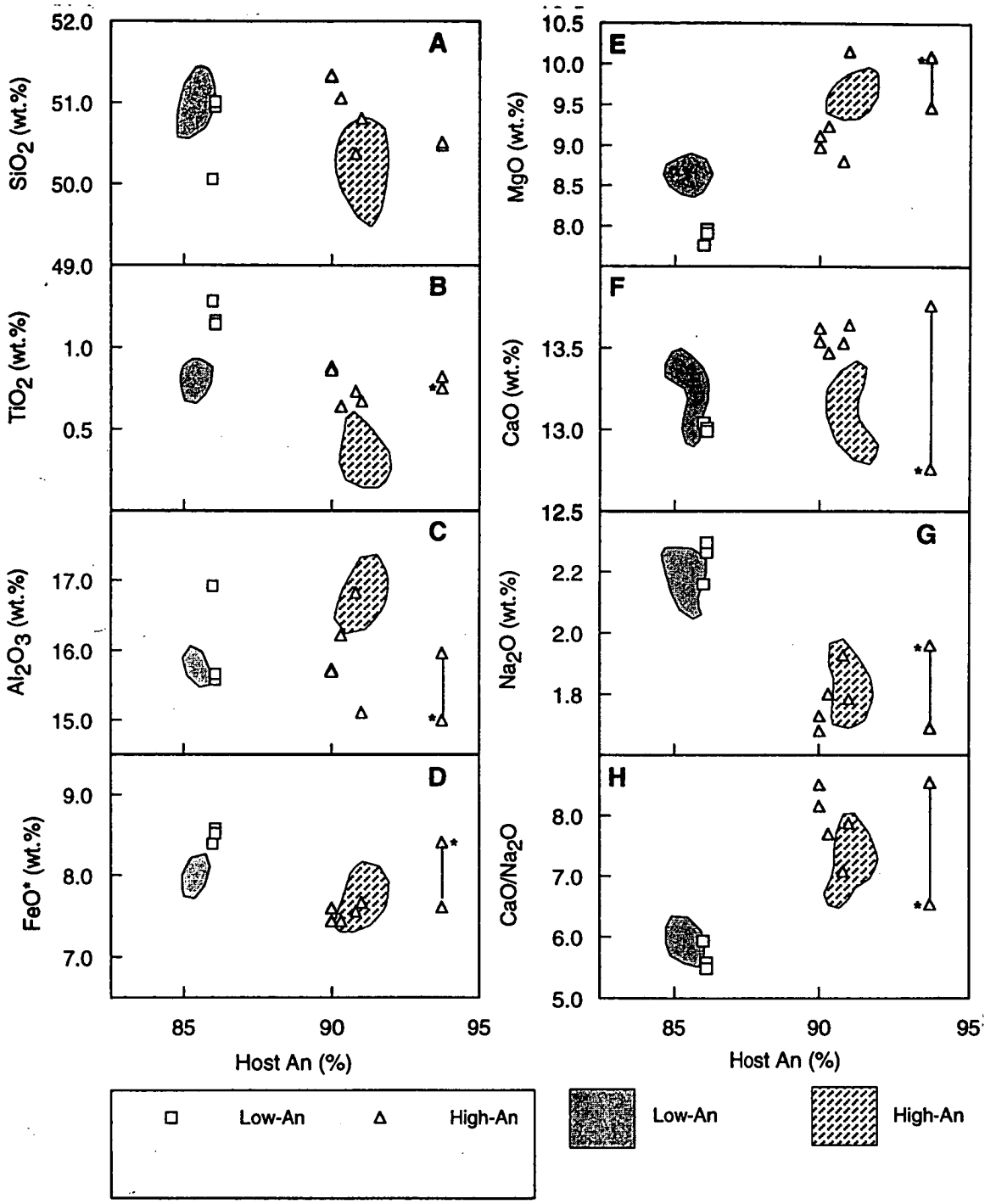

Figure 4.17: Compositional variations of naturally quenched melt inclusions in spinel included in plagioclase phenocrysts. Melt inclusions are divided on the basis of host phenocryst composition, and the fields for homogenised melt inclusions from high- and low-An plagioclase are shown for comparison. Analyses joined by tie line are as for Figure 4.16. See text for discussion.

(and in one case higher Al_2O_3) than would be expected, if they had crystallised from the pillow-rim glasses, possibly a result of re-equilibration. The interpretation that the

high-An plagioclase crystallised from more primitive liquids is supported by the composition of melt inclusions in spinel in these plagioclase, which indicate that the liquids had lower TiO_2, and higher MgO, and CaO/Na_2O than the pillow-rim glasses. However, these inclusions have a wide range of compositions, and their Na_2O, CaO, SiO_2 contents do not fall on the plagioclase-olivine cotectic from Sample D9-1.

Many of the analysed melt inclusions from olivine have high-FeO* contents, resulting in compositions which are not consistent with either a plagioclase-olivine or olivine-only crystallisation history for Sample D9-1. The reasons for the variations in olivine-hosted melt inclusions, which were observed in one inclusion from Hole 896A, but, have not been reported from other MORB suites, are not clear but may be clarified by the results of heating stage experiments.

4.4.3 Fluid inclusions

Primary fluid inclusions were found in both olivine and high (>An_{88}) anorthite plagioclase phenocrysts indicating the magmatic liquid was fluid saturated during crystallisation of these phenocrysts. No fluid inclusions were found in low-An (<87) plagioclase. This is most likely a function of sampling, due to the rarity of fluid inclusions, as the CO_2 measurements of Michael and Nielsen (1995; see section 4.2) on Sample D9-1, and the CO_2-H_2O measurements on Gorda Ridge pillow-rim glasses of Dixon and Stolper (1995), indicate that more evolved liquids, that could have crystallised the low-An plagioclase, were fluid saturated at their depth of eruption.

4.4.4 Melt inclusion experiments

Plagioclase

All melt inclusions used in experiments were 15-30 μm diameter, glassy with no obvious coarse grained daughter crystals, and the majority lacked fluid bubbles. The melt inclusions were heated at rates of 5°C/min. from 1150°C to approximately 1200-1210°C and then at 1-2°C/min. until homogenisation was achieved (from the kinetic experiments described in section 2.5.3). The sequence of phase changes within an inclusion during a typical experiment are shown in Figure 4.18. The illustrated melt inclusions lacked shrinkage bubbles at room temperature, and their behaviour during heating contrasts with those inclusions which had bubbles at room temperature. Melt inclusions with shrinkage bubbles started recrystallising at higher temperatures (>850-900°C) and then darkened progressively. Slow heating at low temperatures (<1100°C) was required to recrystallise all melt inclusions, and it was found that if inclusions were not fully recrystallised then they would homogenise at lower temperatures than the fully recrystallised inclusions; only results from fully recrystallised melt inclusions are used in the present study. Closer to T_h, generally >1200°C, the majority of clear silicate

Figure 4.18: Photomicrographs of the phase changes during reheating of naturally quenched melt inclusions.

These photomicrographs document the changes that occurred in experiment P156 (an overheated but not equilibrated run) that used melt inclusions in plagioclase, An_{85}, from sample KK2-83-NP-D9-1.

At room temperature the melt inclusions were glassy and a light brown colour (**A**). Two types of melt inclusions can be seen; square to rounded rectangular primary melt inclusions (one of which is indicated with an arrow) and a band of lozenge shaped secondary melt inclusions that are connected by a partially healed fracture (above the arrowed melt inclusion). At 700°C (**B**) the melt inclusions had started to recrystallise and shrinkage bubbles nucleated in some inclusions. By 820°C (**C**) shrinkage bubbles had nucleated in all melt inclusions and crystallisation was progressing. By 1000°C (**D**) the melt inclusions were black and completely crystallised and there were no obvious changes over the next 150°C. At 1190°C (**E**) the daughter crystals in the melt inclusions were melting to produce a mixture of melt + crystals + shrinkage bubble. Melting continued through 1210°C (**F**) at which temperature only shrinkage bubbles and small crystals remained. Some of the smaller melt inclusions were virtually homogeneous, i.e., the shrinkage bubble had dissolved and the heating rate was decreased to 1-2°C/minute. By 1222°C (**G**) many primary melt inclusions appeared to be homogeneous, but, the secondary melt inclusions had leaked causing a dramatic increase in the size of their shrinkage bubbles. At this point the experiment was quenched. At room temperature the secondary melt inclusions have large shrinkage bubbles, whereas the majority of primary melt inclusions are glassy, and without shrinkage bubbles (**H**).

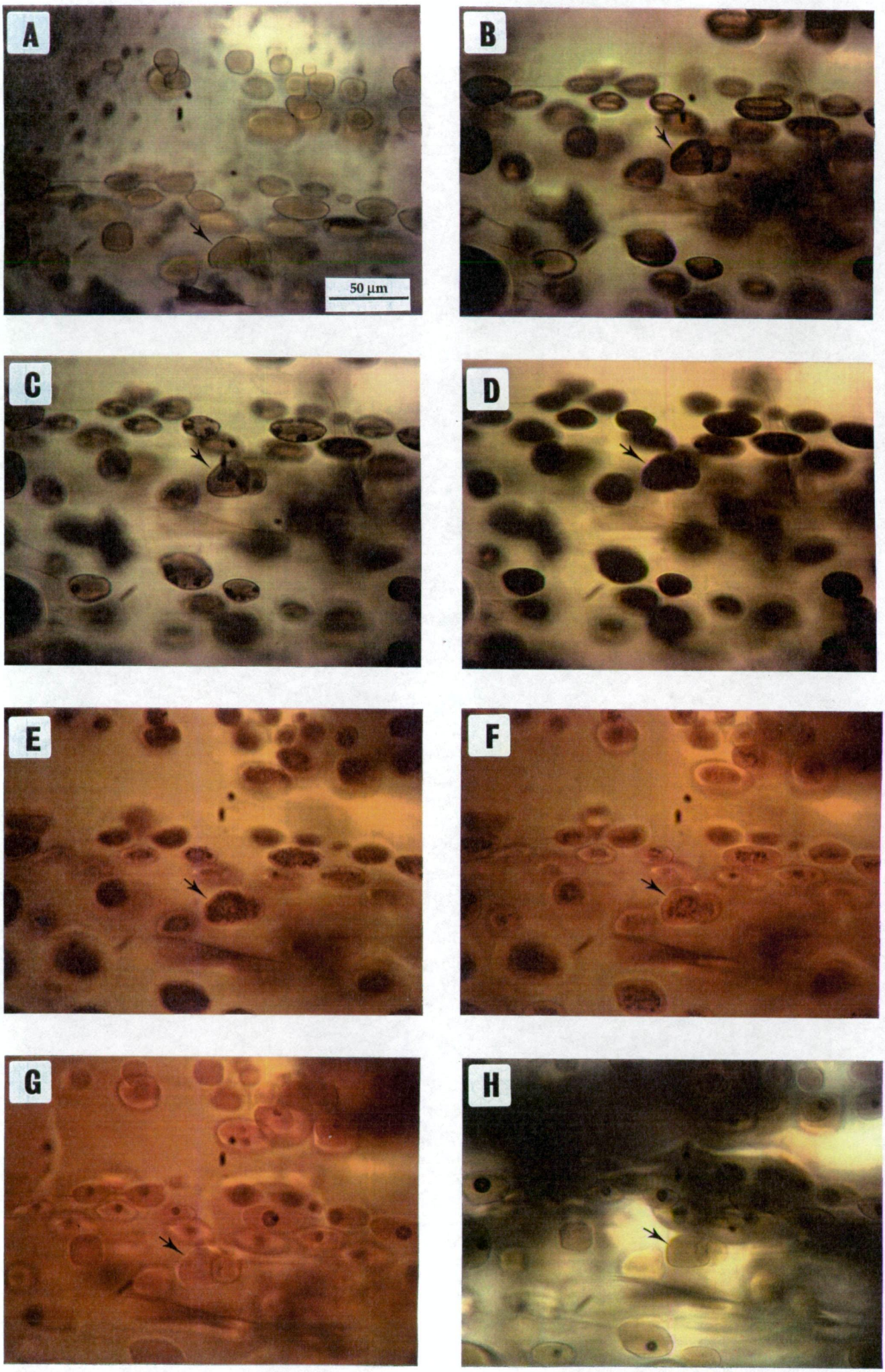
A
50 µm
B
C
D
E
F
G
H

daughter crystals had melted, leaving a shrinkage bubble and rare, opaque, ~1-3 μm Fe-Cu-Ni sulphide globules. The sulphides often decreased in size with time, and typically merged with the shrinkage bubble, as happened in plagioclase from Hole 896A, making determination of the exact moment of bubble disappearance difficult. The relative timing of bubble disappearance and melting of daughter crystals inside an inclusion was dependent both on heating rate and size of daughter crystals. For finely recrystallised melt inclusions, and slow heating rates (<1-2°C/min.) the crystals and bubble disappeared simultaneously, indicating cotectic crystallisation (see section 2.5.3). However, at faster heating rates (2-5°C/min.) homogenisation occurred 10-30°C higher than the melting of daughter crystals within the volume of the inclusion. During slow heating, the initially fine grained daughter phases commonly recrystallised to form a single, 1-3 μm diameter olivine crystal. In some experiments where this occurred, the shrinkage bubble disappeared before the olivine melted, and typically the olivine did not melt when inclusions were kept at the temperature of bubble disappearance for up to 10 minutes.

Melt inclusions in 16 high-An, and 7 low-An phenocrysts were successfully homogenised at temperatures of 1195-1234°C, and 1220-1230°C respectively. As the magmatic liquids which crystallised these phenocrysts are interpreted to have been fluid saturated (section 4.4.3) the T_h, determined by the disappearance of the shrinkage bubble in melt inclusions, should equal the trapping temperature (Sobolev and Danyushevsky, 1994).

The compositions of 129 homogenised melt inclusions from these experiments are given in Appendices 4.8 and 4.9 and are shown in Figure 4.19. On the basis of mineralogical evidence (section 4.3) the melt inclusions should have compositions that lie on the olivine-plagioclase cotectic. However, the melt inclusions define trends at an angle to the cotectic (Fig. 4.19C) that, assuming no chemical exchange occurred between host and inclusion after trapping, are consistent with compositional modification by poor quenching, analytical overlap, and over-, or more rarely, underheating.

As discussed previously, in sections 2.6.1 and 3.4.4, a comparison of plagioclase and olivine saturation temperatures (calculated using the geothermometers of Ford et al. (1983) and Weaver and Langmuir (1990)) and experimental homogenisation temperatures can be used to define the compositional variations that result from processes such as overheating and poor quenching, as calculated olivine and plagioclase temperatures are largely a function of liquid MgO, and Al_2O_3 content respectively. To illustrate how variations in calculated saturation temperatures are interpreted the results of several reheating experiments are shown in Figure 4.20.

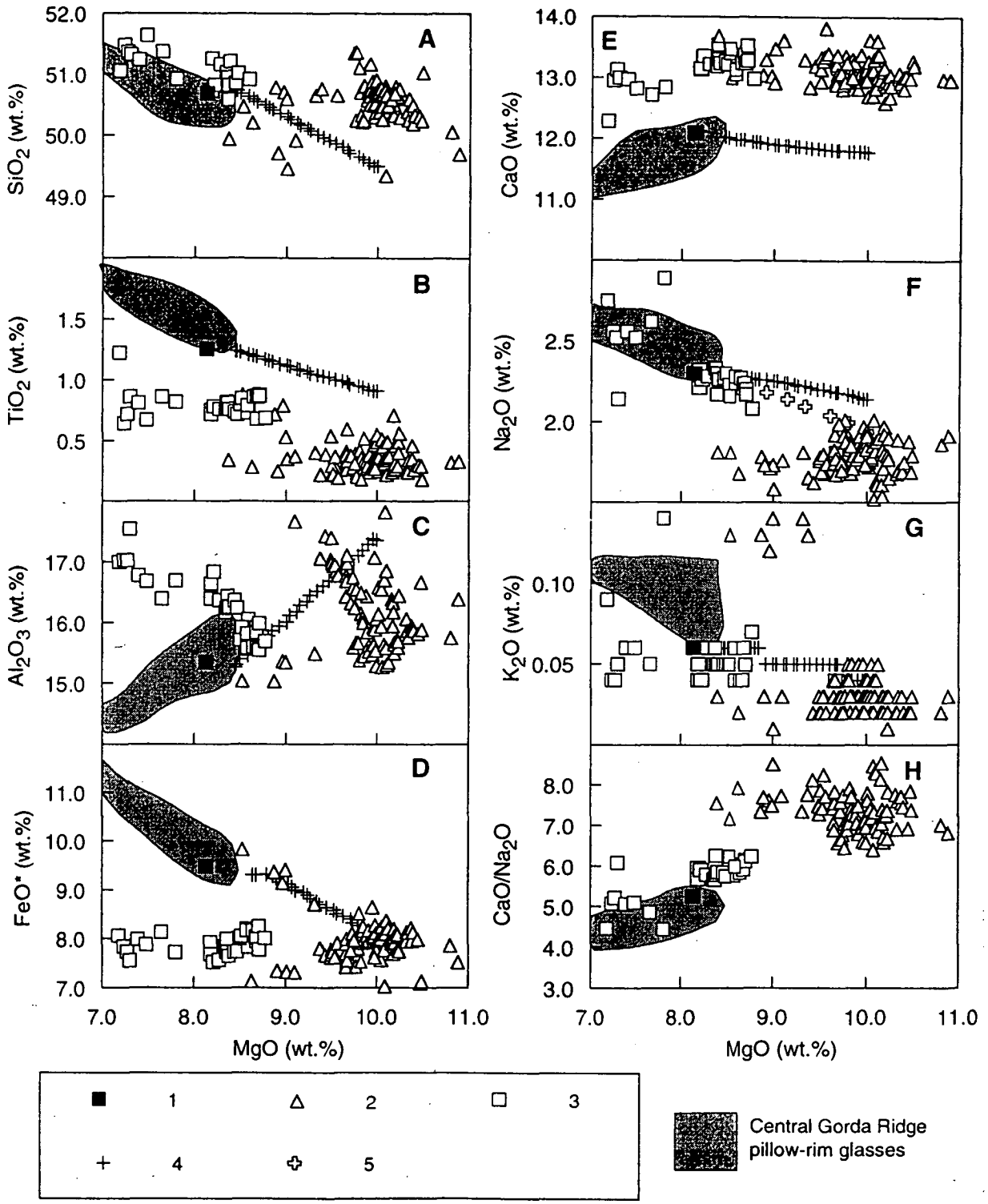

Figure 4.19: Compositional variation of all experimentally homogenised inclusions in plagioclase. Pillow-rim glasses, with >7.0 wt.% MgO, are plotted for comparison. See text for discussion. Symbols; 1- Sample D9-1 pillow-rim glass; 2- melt inclusions in high-An, >An_{88}, plagioclase; 3- melt inclusions in low-An, <An_{87}, plagioclase; 4- calculated plagioclase-olivine cotectic for Sample D9-1; 5- corrected plagioclase-olivine cotectic for Sample D9-1. Cotectics were calculated as discussed in Figure 4.15. See text for discussion.

Melt inclusion 3 (Fig. 4.20) is considered to be a successful experiment; run temperature (T_h) is interpreted to equal the trapping temperature and the inclusion composition is thought to be representative of the trapped liquid. The melt inclusion has calculated plagioclase and olivine saturation temperatures that are similar (i.e., the inclusion composition is cotectic; Fig. 4.20C), and the calculated saturation temperatures are, within the error of the experimental calibrations, the same as the experimental run temperature (Figs. 4.20A and B).

Kinetic experiments (section 2.5.3) indicated that, as with plagioclase-hosted melt inclusions from Hole 896A, the Sample D9-1 melt inclusions could not be kept at high temperatures for long periods, and the heating rates used for these inclusions were therefore faster than for other suites (e.g., Sobolev et al. (1989) and Hole 504B (section 2.5.3)). However, as was discussed in section 2.5.3, faster heating rates increase the potential for overheating (i.e., homogenisation at a higher temperature than the trapping temperature). In addition to the high T_h, overheating may affect the composition of a melt inclusion; if a melt inclusion is overheated and left at T_h, then some of the host mineral may be melted, as the liquid in the melt inclusion becomes saturated with its host phenocryst at the higher temperature. Melt inclusion 6 (Fig. 4.20) is overheated and equilibrated; melting of the plagioclase host decreases the MgO, and increases the Al_2O_3 content of the inclusion, leading to a lower calculated olivine temperature ($T_{olivine}$) than run temperature (T_{run}), and a plagioclase temperature ($T_{plagioclase}$) that is similar to the run temperature (the inclusion is saturated in plagioclase component but undersaturated in terms of olivine). However, if a melt inclusion is overheated, but, quenched immediately homogenisation occurs, its composition should be the same as the trapped liquid as melting of extra host plagioclase will not have occurred, i.e., the rate of melting of post-trapping overgrowths on the inclusion walls did not keep pace with heating rate. In this case (inclusion 5; Fig. 4.20) $T_{olivine}$ and $T_{plagioclase}$ are less than T_{run} (the melt inclusion is undersaturated in both olivine and plagioclase at the run temperature), but are similar, and close to being cotectic. Although the melt inclusions composition is cotectic, the temperature of homogenisation is too high, and the trapping temperature can be estimated from the calculated olivine and(or) plagioclase saturation temperatures.

As discussed previously (section 2.6.1) the generally small size, 15-30 μm, of melt inclusions used in these experiments increase the likelihood of poor quenching (i.e., the quench rate was too slow and allowed crystallisation on the walls of the inclusion during cooling) and also analytical overlap with the host mineral (generally a result of the unknown thickness of an inclusion and penetration of the electron beam into the underlying host phenocryst). Poor quenching and overlap produce opposite

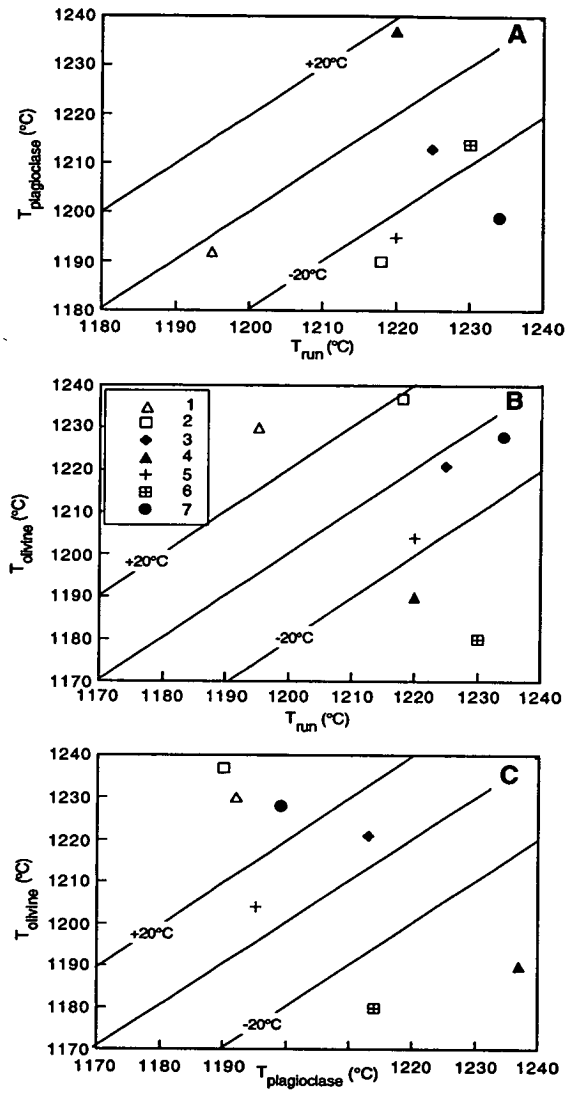

Figure 4.20: **A**, Calculated plagioclase temperatures (using the plagioclase-melt geothermometer of Weaver and Langmuir (1990)), and **B**, calculated olivine temperature (using the calibration of Ford, et al. (1983)) versus run temperature for representative homogenised inclusions in plagioclase. **C**, Calculated plagioclase versus calculated olivine temperatures for representative homogenised inclusions in plagioclase. Points shown are discussed in the text and show temperature variations that indicate inclusions have been affected by poor quenching (points 2 and 7), analytical overlap (point 4), and over- (points 5 and 6) or underheating (point 1). Point 3 represents a 'good', i.e., cotectic composition. See text for discussion.

compositional changes; poor quenching leads to a depletion in Al_2O_3 and an enrichment in MgO, i.e., a high $T_{olivine}$ and low $T_{plagioclase}$ relative to T_{run} (Fig. 4.20; melt inclusion 2), whereas analytical overlap produces low MgO and high-Al_2O_3 contents, and thus low $T_{olivine}$ and high $T_{plagioclase}$ for a given run temperature (Fig. 4.20; melt inclusion 4). Analytical overlap leads to compositional variations that are similar to the effects of overheating. However, overheating should affect all melt inclusions in a phenocryst whereas overlap may only affect some inclusions. Additionally, the T_{run} of overheated melt inclusions will be higher than that of inclusions affected by analytical overlap, which should have T_{run} similar to the 'good' experiments.

One unexpected feature of these experiments was the underheating of melt inclusions (not all of the host mineral that crystallised on the wall of the inclusion after trapping was re-melted during an experiment). Melt inclusion 1 (Fig. 4.20) is interpreted to be underheated. The high $T_{olivine}$, with $T_{plagioclase}$ close to run temperature, suggest that the inclusion has equilibrated, in terms of Al_2O_3 at the run temperature but, the high MgO content indicates insufficient re-melting of overgrowths on the walls of the inclusion. Underheating may occur if the melt inclusions were fluid undersaturated (as was the case with inclusions in olivine from Hole 896A, section 3.4.4), however, if this were the case then all experiments would be expected to be affected by underheating. Fluid undersaturation is also discounted as all evidence points to liquids that were fluid saturated at the time of trapping (section 4.4.3). A more likely explanation for the underheating comes from the observation that if melt inclusions were not completely crystallised during reheating then they would homogenise at a lower temperature than the completely crystallised melt inclusions. Slow reheating at low temperatures was used to try and avoid this effect, however, the underheated melt inclusions from Sample D9-1 are interpreted to result from incomplete crystallisation during reheating.

Calculated plagioclase temperatures for the low-An melt inclusions indicate that, given the error of the calibration, most inclusions are saturated with plagioclase. However, the systematic shift towards low calculated temperatures of these melt inclusions, relative to T_{run}, suggest that poor quenching and(or) overheating without re-equilibration has occurred (Fig. 4.21A). Poor quenching should lead to calculated olivine temperatures that are higher than T_{run}, but this is not the case (Fig. 4.21B) and overheating is therefore considered to be the major factor. When calculated plagioclase and olivine temperatures are compared (Fig. 4.21C) it can be interpreted that runs with T_h of 1230°C are overheated and saturated, with experiment P155 also affected by poor quenching (pushing calculated temperatures back toward the cotectic). The other runs are interpreted to be overheated but melting had not progressed to the stage that the

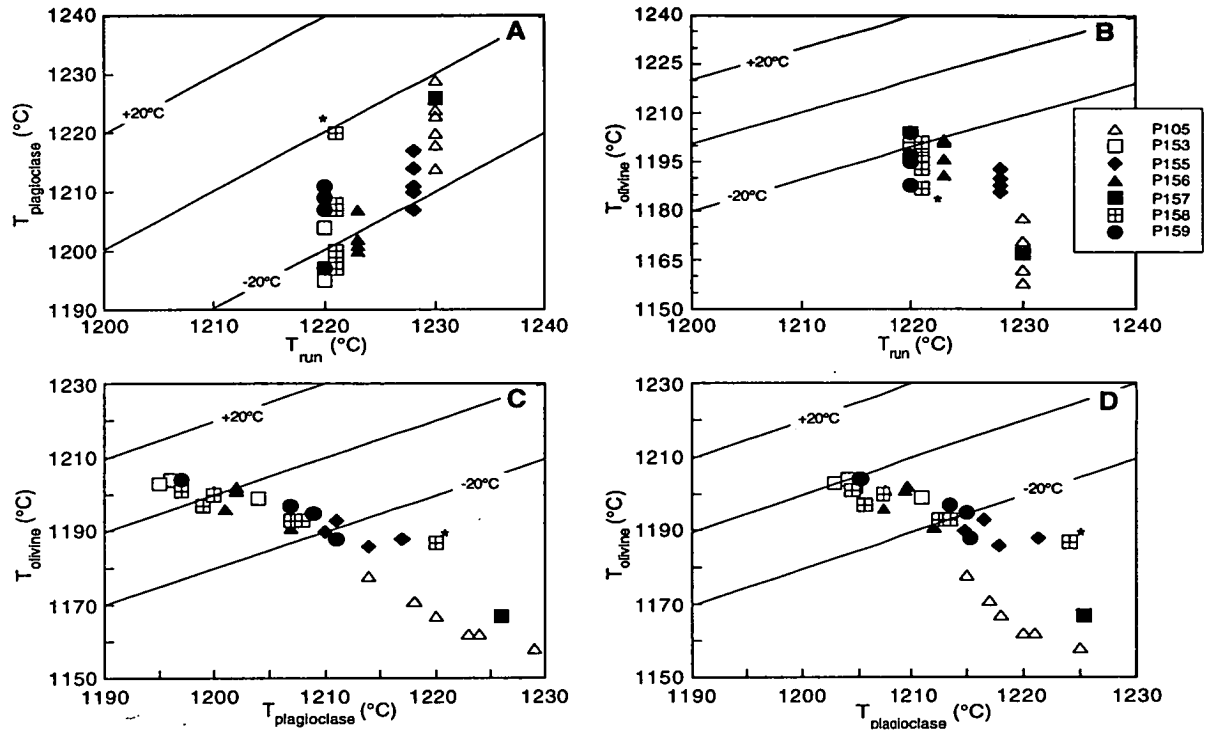

Figure 4.21: A. Calculated plagioclase temperatures (using the plagioclase-melt geothermometer of Weaver and Langmuir (1990)) versus run temperature for all experimentally homogenised melt inclusions in low-An plagioclase. **B.** Calculated olivine temperatures (using the geothermometer of Ford, et al. (1983)) versus run temperature for all experimentally homogenised melt inclusions in low-An plagioclase. **C.** Calculated olivine temperature versus calculated plagioclase temperature for all homogenised melt inclusions in low-An plagioclase. **D.** As for **C** but the plagioclase temperature has been adjusted to produce a best fit for the MORB olivine-plagioclase cotectic using the correction of Danyushevsky et al. (1996). Melt inclusions from each experiment have the same symbol. A single high-K_2O melt inclusion in experiment P158 is indicated (*). See text for discussion.

host plagioclase had been melted, i.e., the melt inclusions had not become saturated with plagioclase at the run temperature, and compositions are therefore close to cotectic. All melt inclusions from an individual phenocryst have calculated temperature variations consistent with overheating, and the spread in temperatures toward lower $T_{olivine}$, and higher $T_{plagioclase}$ for inclusions in some phenocrysts is interpreted to reflect analytical overlap with the host plagioclase. Melt inclusion P158-5 lies well off the cotectic, and in contrast to other inclusions from this phenocryst has high K_2O, and will be discussed separately below. Melt inclusions interpreted to have compositions representative of trapped liquids are those closest to the cotectic as indicated in Figure 4.21.

The overheating of low-An plagioclase results from heating rates that were too fast for the kinetics of melting of daughter crystals. The heating rates used for low-An melt inclusions were the same as for the high-An inclusions, and were based on kinetic experiments which probably used high-An inclusions (as these were much more

common than low-An phenocrysts with inclusions). A series of kinetic experiments should therefore have been run specifically using the low-An plagioclase, and this result stresses the importance of kinetic experiments in preventing overheating. However, those inclusions that were less overheated, with T_h of 1220-1223°C, have quenched compositions that are consistent with the calculated plagioclase-olivine cotectic (Figs. 4.20 and 4.21), indicating that the kinetics of melting were slow enough that the host crystal was not melted. The trapping temperature of these inclusions is therefore estimated from the calculated olivine and plagioclase saturation temperatures, 1196-1204°C and 1203-1210°C respectively (calculated using Ford et al. (1983) and the modified Weaver and Langmuir (1990) calibration of Danyushevsky et al. (1996), as discussed in section 2.6.1).

Data for the high-An inclusions are interpreted to indicate the effects of underheating, poor-quenching, analytical overlap, and overheating (Fig. 4.22). Generally low $T_{plagioclase}$, relative to T_{run} (Fig. 4.22B), is interpreted to indicate poor quenching, a result of the small inclusion size in many phenocrysts. All melt inclusions from an over-, or underheated phenocryst have the same compositional/temperature trends, although some scatter may be introduced where poor quenching or analytical overlap have affected individual inclusions from these experiments (e.g., melt inclusion P89; Fig. 4.22C). Melt inclusions interpreted to have compositions that are not significantly affected by analytical overlap, poor quenching or over/underheating are closest to the cotectic on Figure 4.22C. Experiments P112, and P108 have been affected by overheating but their melt inclusion compositions are interpreted not to have equilibrated at higher temperatures. Trapping temperatures for these two experiments were therefore estimated from calculated olivine and plagioclase saturation temperatures, as discussed above. The origin of high-K_2O, >0.11 wt.%, melt inclusions, including one 'good' inclusion (P112-R3), are discussed below.

On the basis of the preceding discussion a total of 31 analysed melt inclusions from 6 high-An, and 4 low-An experiments, with trapping temperatures, both experimental and calculated, of 1215-1227°C and 1196-1204°C respectively, are interpreted to have compositions on the plagioclase-olivine cotectic (Fig. 4.23). There is a good correlation between host An content and inferred trapping temperature (Fig. 4.24B), with higher trapping temperatures for high-An hosted melt inclusions than for low-An, although within these groupings there is no obvious correlation between host mineral and melt inclusion composition, a result of the narrow range of compositions, <1.3% An, of the host plagioclase. There is also a correlation between host An content and the CaO/Na_2O of homogenised melt inclusions, consistent with results from Hole 896A and low pressure experimental results on plagioclase-melt equilibria (Figs. 4.24A

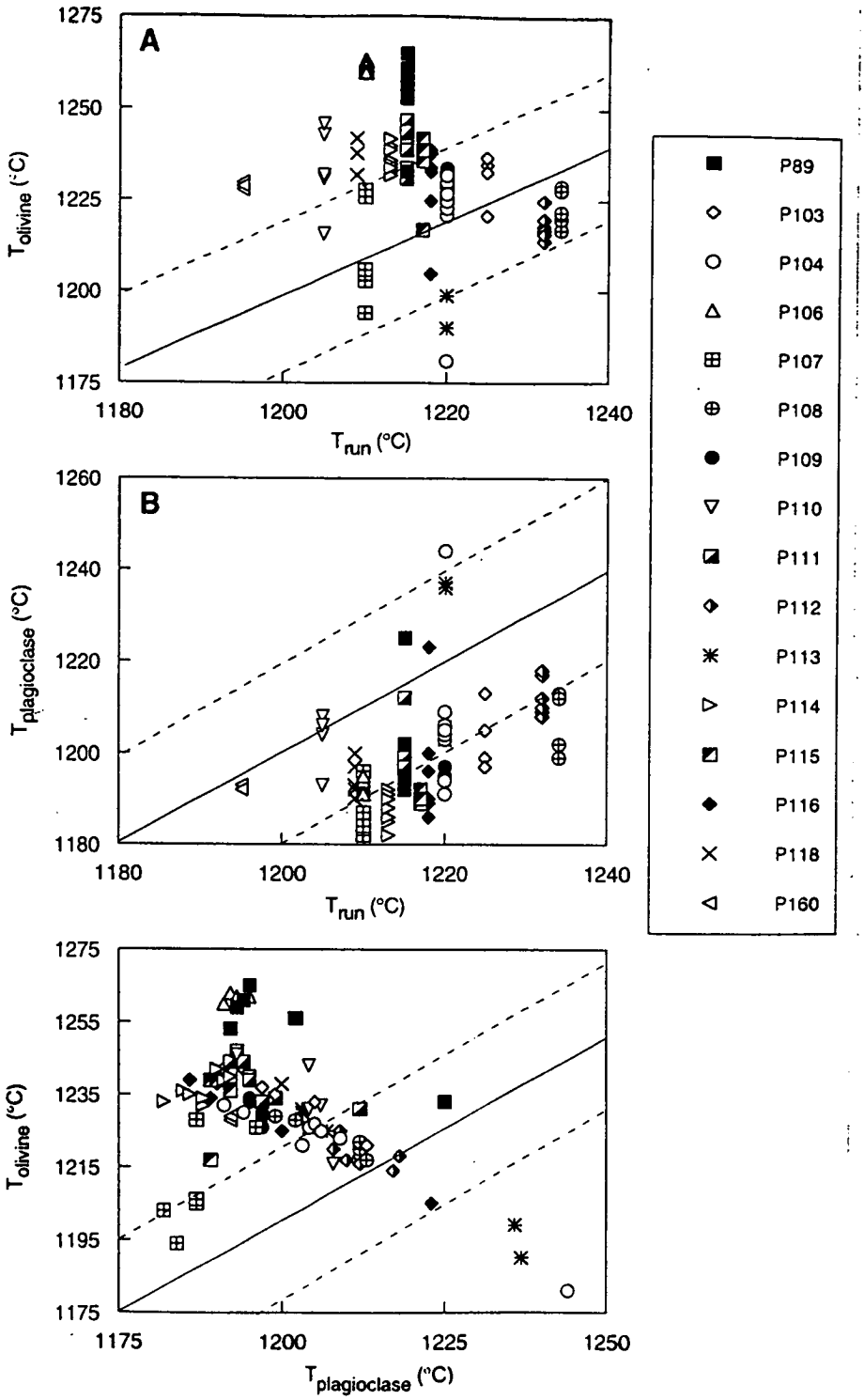

Figure 4.22: A. Calculated plagioclase temperatures (using the plagioclase-melt geothermometer of Weaver and Langmuir, 1990) versus run temperature for all experimentally homogenised inclusions in high-An plagioclase. **B.** Calculated olivine temperatures (using the geothermometer of Ford et al., 1983) versus run temperature for all experimentally homogenised inclusions in high-An plagioclase. **C.** Calculated olivine temperature versus calculated plagioclase temperature for all homogenised inclusions in high-An plagioclase. Inclusions from each experiment have the same symbol. Solid line is 1:1 line for temperature, dashed lines gives accuracy of ±20°C. See text for discussion.

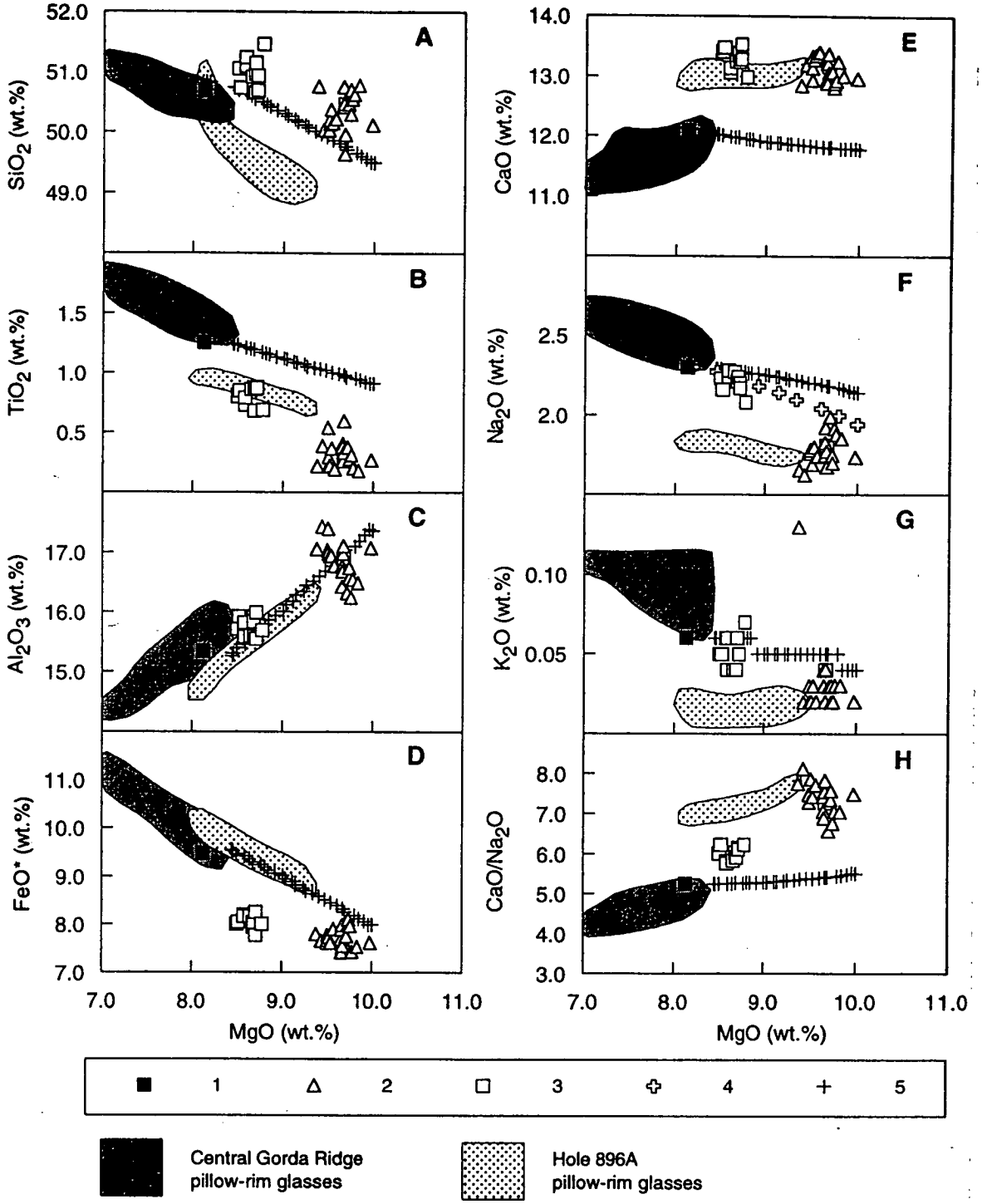

Figure 4.23: Compositional variations of homogenised melt inclusions in plagioclase unaffected by under- and overheating, poor quenching, and(or) analytical overlap with host plagioclase. The fields of pillow-rim glasses from the Central Gorda Ridge and Hole 896A (Groups 1 and 4) are shown for comparison. See text for discussion. Symbols; 1- Sample D9-1 pillow-rim glass; 2- melt inclusions from high-An, >An_{88}, plagioclase; 3- melt inclusions from low-An, <An_{87}, plagioclase; 4- corrected olivine-plagioclase cotectic for Sample D9-1; 5- calculated olivine-plagioclase cotectic for Sample D9-1. The cotectics were calculated as described in Figure 4.15.

and 3.8), indicating that the melt inclusions were trapped from liquids that were in equilibrium, in terms of CaO/Na_2O, with their host plagioclase.

The effects of excluding melt inclusions interpreted to be affected by poor quenching, analytical overlap and under- or overheating can be seen in Figure 4.25. MgO and Al_2O_3 variations (Fig. 4.25C) indicate that the excluded melt inclusions from low-An plagioclase were affected by overheating, whereas those in high-An plagioclase were affected by underheating and(or) bad quenching, as suggested by overlap with the field of naturally quenched inclusions. The selection of melt inclusions using calculated saturation temperatures has been successful in reproducing the cotectic, however, are non-cotectic liquid trends obscured by this procedure? The similarity in the range of the TiO_2, FeO*, CaO, K_2O and Na_2O (Fig. 4.25) contents of 'good' and 'bad' homogenised melt inclusions suggest that geochemically different types of liquids have not been excluded.

Melt inclusions in low-An plagioclase (An_{85}-An_{86}) have MgO, Al_2O_3, Na_2O and K_2O contents that lie at the high-MgO end of the pillow-rim glass defined trend, and are consistent with crystallisation from liquids with higher MgO contents than the D9-1 glass (8.5-8.8 wt.% vs. 8.1 wt.% MgO; Fig. 4.23). However, the CaO, CaO/Na_2O and SiO_2 contents are higher, and the TiO_2 and FeO* contents of melt inclusions are lower at a given MgO than the pillow-rim glass trend. The range of TiO_2, FeO*, and SiO_2 contents, relative to the cotectic, are consistent with melt inclusion compositions in plagioclase from Hole 896A and are not interpreted to be primary features. However, the higher than cotectic CaO contents were also found in the naturally quenched spinel-hosted melt inclusions and are interpreted to be a primary feature (section 4.4.2). The CaO contents of the low-An melt inclusions are similar to those of melt inclusions in spinel and high-An plagioclase (13.0-13.5 wt.% and 12.8-13.4 wt.% CaO respectively).

Melt inclusions from high-An plagioclase have MgO >9.4 wt.%, and Al_2O_3, Na_2O, and K_2O contents that all lie close to the plagioclase-olivine cotectic from Sample D9-1, whereas SiO_2 contents are generally higher, and TiO_2 lower than this trend. Melt inclusions have FeO* contents, 7.4-8.1 wt.%, that lie below the cotectic, but, there is no clear difference between melt inclusion and cotectic FeO* abundances as was seen in the Hole 896A samples or the low-An inclusions Fig. 4.23D). The Mg' values of the homogenised high-An melt inclusions (70.6-72.5) have a narrower range than in the naturally quenched inclusions (Mg' values of 68.5-76.6). The Mg' values of melt inclusions in high-An plagioclase may therefore be more representative of trapped liquid compositions than those in low-An plagioclase. The (CaO/Na_2O values of high-An melt inclusions, 6.6-8.1, have a narrower range than, and are consistent with,

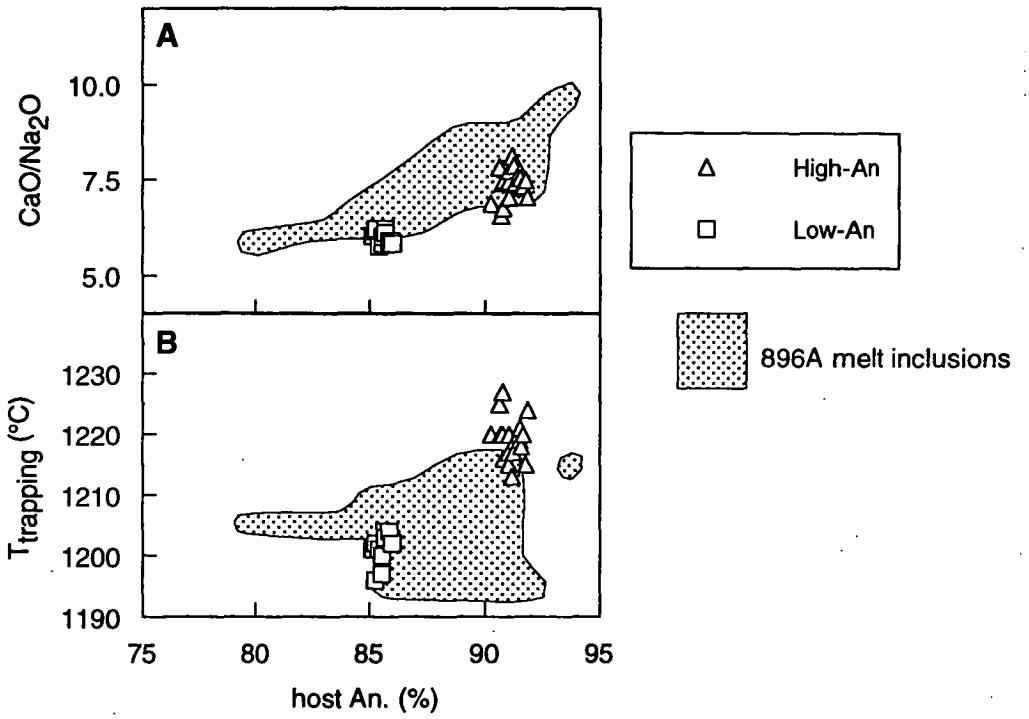

Figure 4.24: Host anorthite content versus melt inclusion CaO/Na_2O (**A**) and trapping temperature (**B**) for all inclusions interpreted to be unaffected by under or overheating, poor quenching, and(or) analytical overlap. Trapping temperatures are from homogenisation temperatures and calculated equilibration temperatures for overheated, but not equilibrated, melt inclusions. The field of homogenised melt inclusions from Hole 896A are included for comparison. See text for discussion.

inclusions of the same An content from Hole 896A (An_{90}-An_{92}; Fig. 4.23).

Seven melt inclusions from both high- (experiments P107, P112, and P115) and low-An (experiment P158) plagioclase have higher K_2O contents, >0.12 wt.%, than the majority of analysed inclusions, and the pillow-rim glasses (with <0.11 wt.% K_2O; Fig. 4.25). The two most likely causes of high-K_2O in melt inclusions are; the trapping of more enriched melts, or, as a result of alteration, as was interpreted for high-K_2O inclusions from Hole 896A (section 3.4.5). The compositions of all but one of the high-K_2O melt inclusions are affected by under- or overheating making comparisons between melt inclusions in different phenocrysts difficult. However, in all phenocrysts with high-K_2O melt inclusions there were also inclusions with normal K_2O contents. When these are compared the only consistent difference is that high-K_2O inclusions have lower MgO contents (Fig. 4.26A). There is no obvious correlation of high-K_2O with high Na_2O contents, as found for Hole 896A melt inclusions (Fig. 4.26D; section 3.4.5), but this may be a function of lower K_2O enrichment than in the Hole 896A samples. Without additional trace element data it is impossible to satisfactorily determine the origin of the high K_2O contents, but an origin as a result of hydrothermal alteration is considered most likely by comparison with the Hole 896A samples.

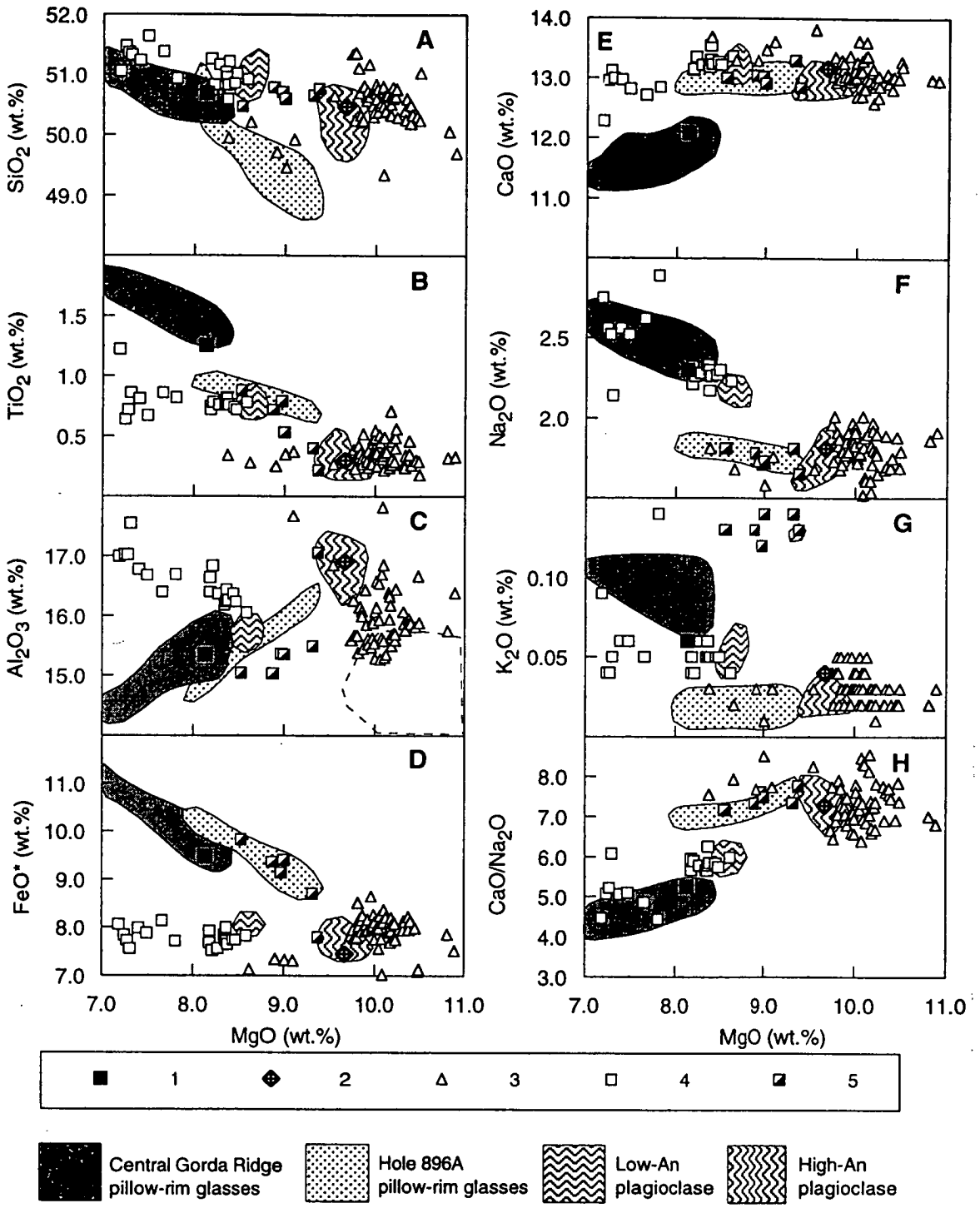

Figure 4.25: Comparison of the compositional range of homogenised melt inclusions in plagioclase unaffected by poor quenching, analytical overlap and under- or overheating (fields for high-An and low-An hosted inclusions shown separately), with that of inclusions affected by these processes. the fields of pillow-rim glasses, as for Figure 4.23, are shown for comparison. The dashed line on (**C**) encloses part of the field of naturally quenched inclusion compositions. See text for discussion. Symbols; 1- Sample D9-1 pillow-rim glass; 2- Average composition of inclusions homogenised at 1250°C from Nielsen, et al. (1995); 3 and 4- compositions of inclusions affected by poor quenching, analytical overlap and(or) over- or underheating from high-An and low-An plagioclase respectively; 5- homogenised inclusions with high, >0.1 wt.%, K_2O contents.

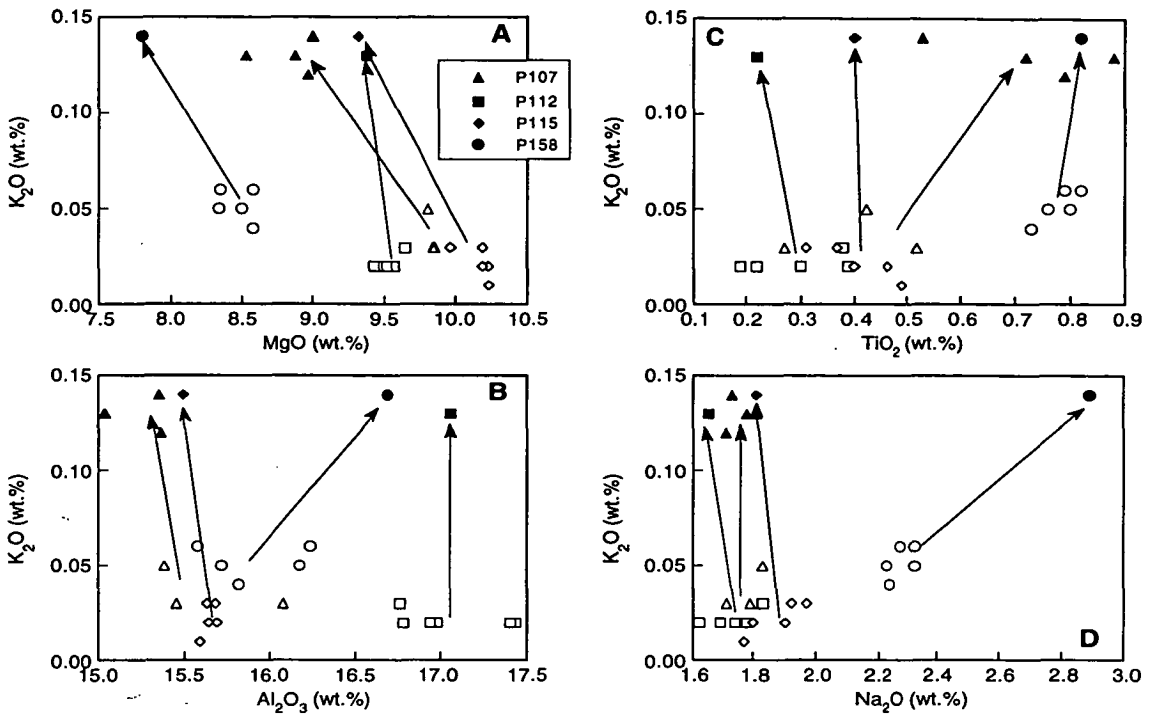

Figure 4.26: Compositions of homogenised high-K_2O melt inclusions in plagioclase (filled symbols) from experiments, as shown, compared with normal-K_2O melt inclusions from the same phenocryst (open symbols). Lines link melt inclusions in the same crystal. See text for discussion.

The results of homogenisation experiments on Sample D9-1 plagioclase, using a vertical quench furnace, were reported by Nielsen et al. (1994) and Nielsen et al. (1995). A trapping temperature of 1250°C was inferred, and the average composition of all analysed inclusions from high-An plagioclase (Fig. 4.25) is similar to that of high-An plagioclase homogenised at approximately 1220°C in the present study (Table 4.2). The results of the heating stage experiments described above, indicate that reheating melt inclusions to 1250°C should produce compositional changes consistent with strong overheating, particularly as inclusions were left at this temperature for up to 8 hours and should have re-equilibrated. A detailed discussion of the results of Nielsen et al. (1994) and Nielsen et al. (1995) will be presented in Chapter 6.

Olivine

Glassy melt inclusions, lacking shrinkage bubbles, and with diameters of up to approximately 100 μm were used in experiments. Slow heating rates, and repeated heating and cooling from 500-1000°C were required to nucleate a fluid bubble in all inclusions at 770-860°C. The melt inclusions darkened and were fully recrystallised by 1060-1070°C; with obvious re-melting starting at 1160-1170°C. Heating rates above

Table 4.2. Average homogenised melt inclusion compositions from high-An plagioclase.

[a]Analysis	Nielsen et al. (1995)	The present study
SiO_2	50.48 (±0.43)[b]	50.34 (±0.31)
TiO_2	0.30 (±0.08)	0.31 (±0.11)
Al_2O_3	16.91 (±0.33)	16.83 (±0.33)
FeO*	7.45 (±0.26)	7.74 (±0.19)
MnO	0.14 (±0.02)	0.14 (±0.04)
MgO	9.67 (±0.28)	9.64 (±0.15)
CaO	13.17 (±0.23)	13.10 (±0.19)
Na_2O	1.81 (±0.08)	1.78 (±0.09)
K_2O	0.04 (±0.01)	0.03 (±0.02)
P_2O_5	0.03 (±0.04)	0.03 (±0.03)
Cr_2O_3		0.07 (±0.03)
Total	100.00	100.00
CaO/Na_2O	7.28	7.36
Mg#	69.8	68.9

[a]Analyses from Nielsen et al. (1995) have been corrected for inter-laboratory bias (as discussed in Appendix 1) and re-calculated to 100 wt.%

[b]mean analysis and standard deviation

1150°C were 5°C/min until strong melting was observed, then 2°C/min until small (<20-30 μm) melt inclusions were homogeneous (from kinetic experiments, section 2.5.3). This temperature was taken to be T_h and a further 10-25 min was then required to homogenise larger melt inclusions. Despite appearing homogeneous the larger inclusions often nucleated shrinkage bubbles on quenching, indicating that complete homogenisation had not been achieved. Fine grained, <1-2 μm, black minerals (?magnetite, see discussion in section 2.5.3) formed after 12-25 min in some experiments, although abundances, <1 vol.%, were lower than in melt inclusions from Hole 896A samples.

Homogenisation was achieved in only 9 of 12 experiments, as many of the larger melt inclusions leaked during reheating. The T_h of the successful experiments, in olivine hosts of $Fo_{86.5}$-$Fo_{89.5}$, was 1205-1240°C. As the trapped liquid is interpreted to be fluid saturated (section 4.4.3) these temperatures represent trapping temperatures, and are consistent, given the error of the homogenisation technique (±15°C; Sobolev and Danyushevsky (1994)), with the range of trapping temperatures for plagioclase-hosted

inclusions, 1196-1227°C. The similarity of trapping temperatures in plagioclase and olivine supports the conclusion, from mineralogical evidence, of early cotectic crystallisation.

Seventeen inclusions were analysed from the olivine experiments and results are presented in Appendix 4.10. Olivine saturation temperatures (calculated using the geothermometer of Ford et al. (1983)) suggest that 9 of the 17 analysed melt inclusions were saturated with olivine at their run temperature (Fig. 4.27A).

Host olivine composition does not correlate with T_h for the 'saturated' melt inclusions (Fig. 4.27B). Experiment OL20 has a very high T_h, 1237°C, for its host composition, suggesting that it was overheated. The calculated Fe^{2+}-Mg mineral-liquid exchange coefficients (K_d) for the two melt inclusions from this experiment are quite different; 0.26 and 0.31 for OL20-1 and OL20-2 respectively. The MgO contents of these melt inclusions are similar, 9.5 vs 9.7 wt.%, and the differences in exchange coefficient appear to be related to differing FeO* contents, 1.3 wt.% higher in OL20-1 than in OL20-2. The low K_d of OL20-1 is therefore interpreted to be a manifestation of the high-FeO* problem described from the naturally quenched melt inclusions (section 4.4.2). The effect of the elevated FeO* can be seen in the composition of OL20-1 when recalculated to be in equilibrium with its host olivine (using the procedures described for the naturally quenched inclusions in section 4.4.2); its MgO content is higher (11.6 wt.%) with lower Al_2O_3 and CaO (13.41 wt.% and 11.43 wt.%) than inclusion OL20-2 (9.7, 14.5, and 12.3 wt.% MgO, Al_2O_3, and CaO respectively) at an equilibration temperature of 1280°C (whereas T_h was 1237°C and the melt inclusion was probably overheated at this temperature). Given these results, it would appear that the high-FeO* contents recorded in many naturally quenched melt inclusions are not eliminated by the homogenisation process. Variations in calculated saturation temperatures of olivine-hosted melt inclusions from Sample D9-1, may therefore result from variable FeO* contents and may not reflect the effects of overheating, analytical overlap or poor quenching.

The most primitive Central Gorda Ridge pillow-rim glasses, with FeO* contents of 9.1-9.3 wt.%, are calculated to be in equilibrium with olivine of Fo_{86}. All homogenised inclusions, in olivine of Fo_{87}-$Fo_{89.5}$, should therefore have crystallised from more magnesian, and less FeO*-rich, liquids than the glasses. This does not appear to be the case with the majority of homogenised inclusions having FeO* contents that are >9.2 wt.% (Fig. 4.28). Homogenised melt inclusions with low FeO* contents are all hosted by olivine >Fo_{89}, supporting the observation, based on analyses of naturally quenched melt inclusions (section 4.4.2), that the high-FeO* contents are associated with olivines of mainly Fo_{86}-Fo_{88}. As indicated previously (section 4.4.2),

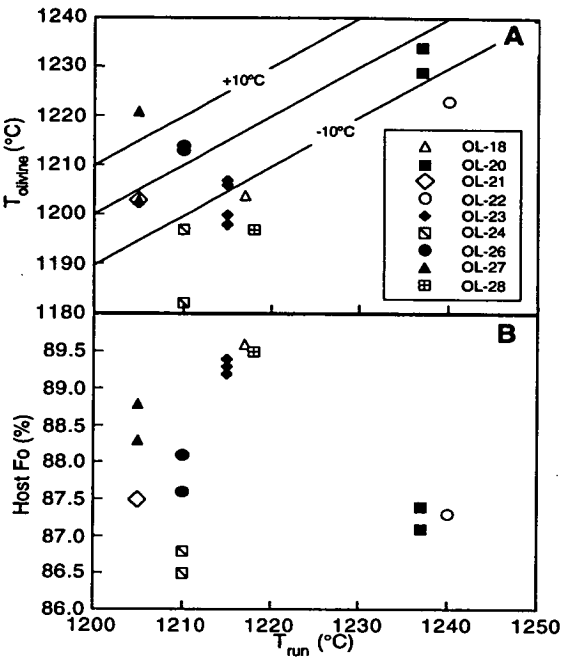

Figure 4.27: A. Comparison of calculated olivine temperature, using the geothermometer of Ford et al. (1983), and run temperature for all homogenised olivine-hosted melt inclusions. Melt inclusions from each experiment have the same symbol. Melt inclusions interpreted to be unaffected by analytical overlap or poor quenching are within ±10°C of the line shown on **A. B.** Comparison of run temperature and host olivine composition for all homogenised melt inclusions; inclusions in Fo_{87} olivine with high run temperatures are interpreted to be overheated. See text for discussion.

spinel inclusions in these olivines have compositions that do not correlate with their host and this suggests some form of re-equilibration in these inclusions.

Homogenised melt inclusions with low FeO* contents, <9.0 wt.%, have mineral-melt exchange coefficients, 0.25-0.28 (calculated assuming a melt Fe^{2+}/Fe^{3+} of 7.9, as calculated from spinel composition). These values are lower than would be expected if there was equilibrium between the melt inclusions and their host olivines (assuming an olivine-melt Mg-Fe^{2+} K_d of 0.3 (Roeder and Emslie, 1970; Ulmer, 1989)). Low exchange coefficients may indicate that the melt inclusions are affected by poor quenching and(or) high FeO* contents.

To evaluate if the low exchange coefficients result from poor quenching, a calculation was done (using the Petrolog program of Danyushevsky et al. (1990)) by assuming that a melt inclusion trapped in olivine, $Fo_{87.8}$, was in equilibrium with an olivine of $Fo_{87.3}$ after quenching. The calculation yields a saturation temperature that is 12°C lower, and an olivine-melt Mg-Fe^{2+} exchange coefficient of 0.295, i.e., 0.014 lower than would be expected for equilibrium. This result suggests that the effects of poor

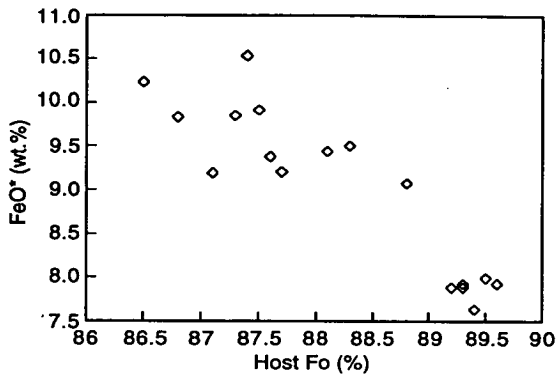

Figure 4.28: Variations in FeO* content of homogenised melt inclusions with host olivine composition. Inclusions in olivine of Fo_{86}-Fo_{88} have high FeO* contents, similar to, or higher than the most primitive Central Gorda Ridge pillow-rim glass. See text for discussion.

quenching would not be sufficient to produce the low exchange coefficients (<0.28) of some melt inclusions.

To evaluate if the selected 'low-FeO*' melt inclusions actually have high-FeO* contents, their compositions were recalculated to be in equilibrium with their host olivine (see section 3.4.4). The recalculated homogenised and naturally quenched melt inclusions in olivine Fo_{89}-Fo_{90} generally have more primitive compositions than the homogenised melt inclusions in plagioclase An_{90}-An_{92} (Fig. 4.29) but, have similar FeO*, CaO, Na_2O, and K_2O contents, with higher TiO_2, and lower Al_2O_3. The FeO* contents of the most MgO-rich melt inclusions are higher than the calculated cotectic (Fig. 4.29D), and this suggests that even the 'low-FeO*' melt inclusions may have high-FeO* contents. When compared with host olivine compositions the recalculated low-FeO* melt inclusion compositions show a good correlation for MgO and FeO*, but for other elements there is a range of compositions at a given host composition; also a function of the high-FeO* contents (Fig. 4.30). The compositions of many olivine-hosted melt inclusions are therefore unreliable as indicators of trapped liquid compositions, however, trapping temperatures, may be inferred for the recalculated low-FeO* naturally quenched inclusions (1195°C, for Fo_{84}) and the successfully homogenised melt inclusions (1205-1218°C for $Fo_{86.5}$-$Fo_{89.5}$).

The composition of a single melt inclusion, in olivine Fo_{88}, homogenised at 1250°C using a vertical quench furnace was reported by Nielsen et al. (1995). The melt inclusion has high MgO, 10.8 wt.% (corrected for inter-laboratory bias in microprobe analyses, see Appendix 1), and low Al_2O_3 (15.6 wt.%) and does not lie on the pillow-rim glass defined cotectic (Fig. 4.29). Calculated olivine and plagioclase saturation

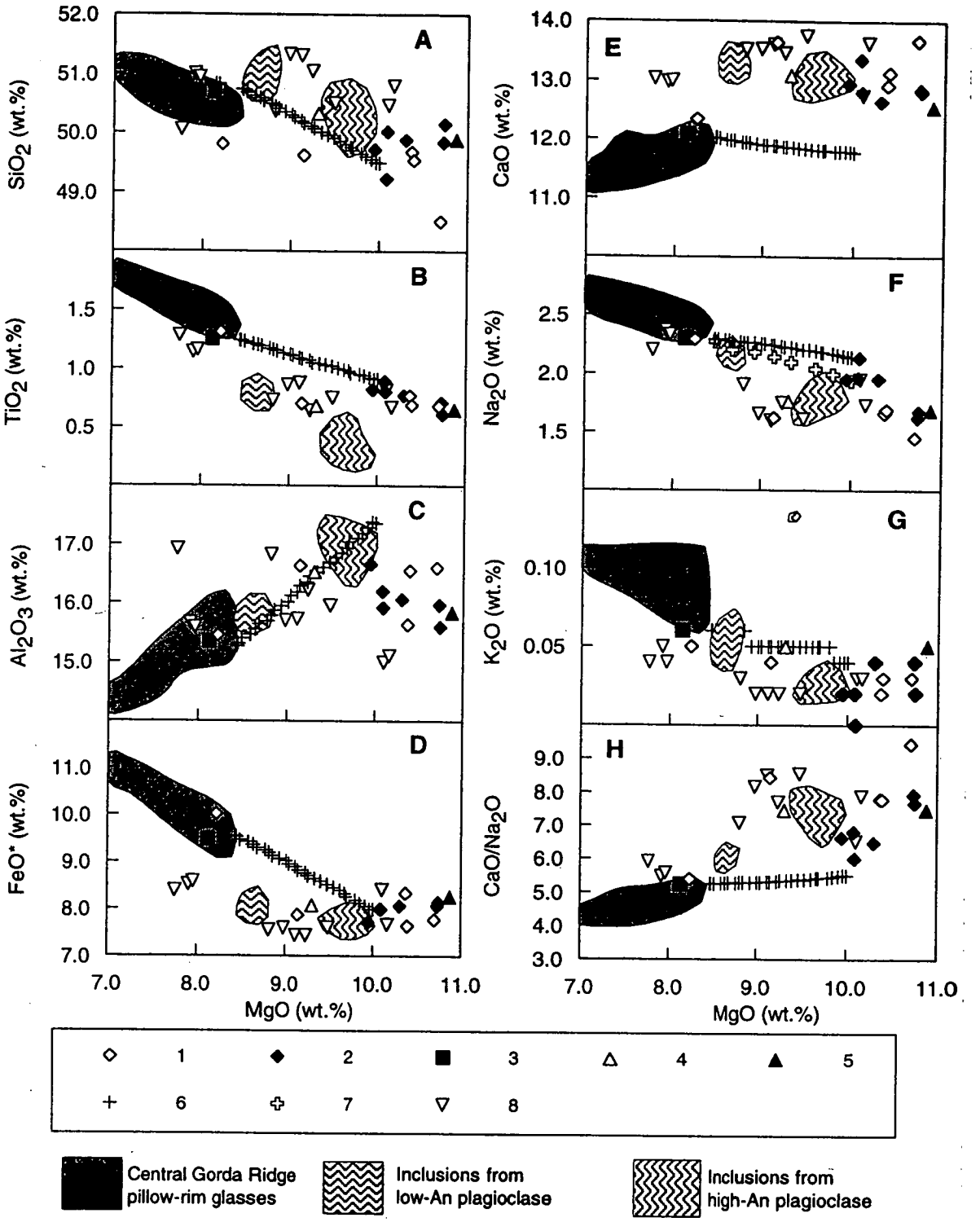

Figure 4.29: Compositional variations of homogenised and naturally quenched melt inclusions in olivine compared with melt inclusions in plagioclase and spinel. The melt inclusions in olivine have been selected on the basis that they have low FeO* contents and have been recalculated to be in equilibrium with their host olivine. See text for calculation procedures. Symbols; 1 - naturally quenched melt inclusions; 2 - homogenised melt inclusions; 3 - Sample D9-1 pillow-rim glass; 4 and 5 - melt inclusion in olivine reheated to 1250°C (Nielsen et al., 1995), the reported composition of this inclusion is interpreted to result from overheating (5) and it has therefore been recalculated to be in equilibrium with its host olivine, to reverse the effects of overheating (4). See text for recalculation procedures; 6 and 7 - calculated plagioclase-olivine and corrected cotectics for Sample D9-1, see Figure 4.15 for calculation methods; 8 - naturally quenched melt inclusions in spinels from plagioclase.

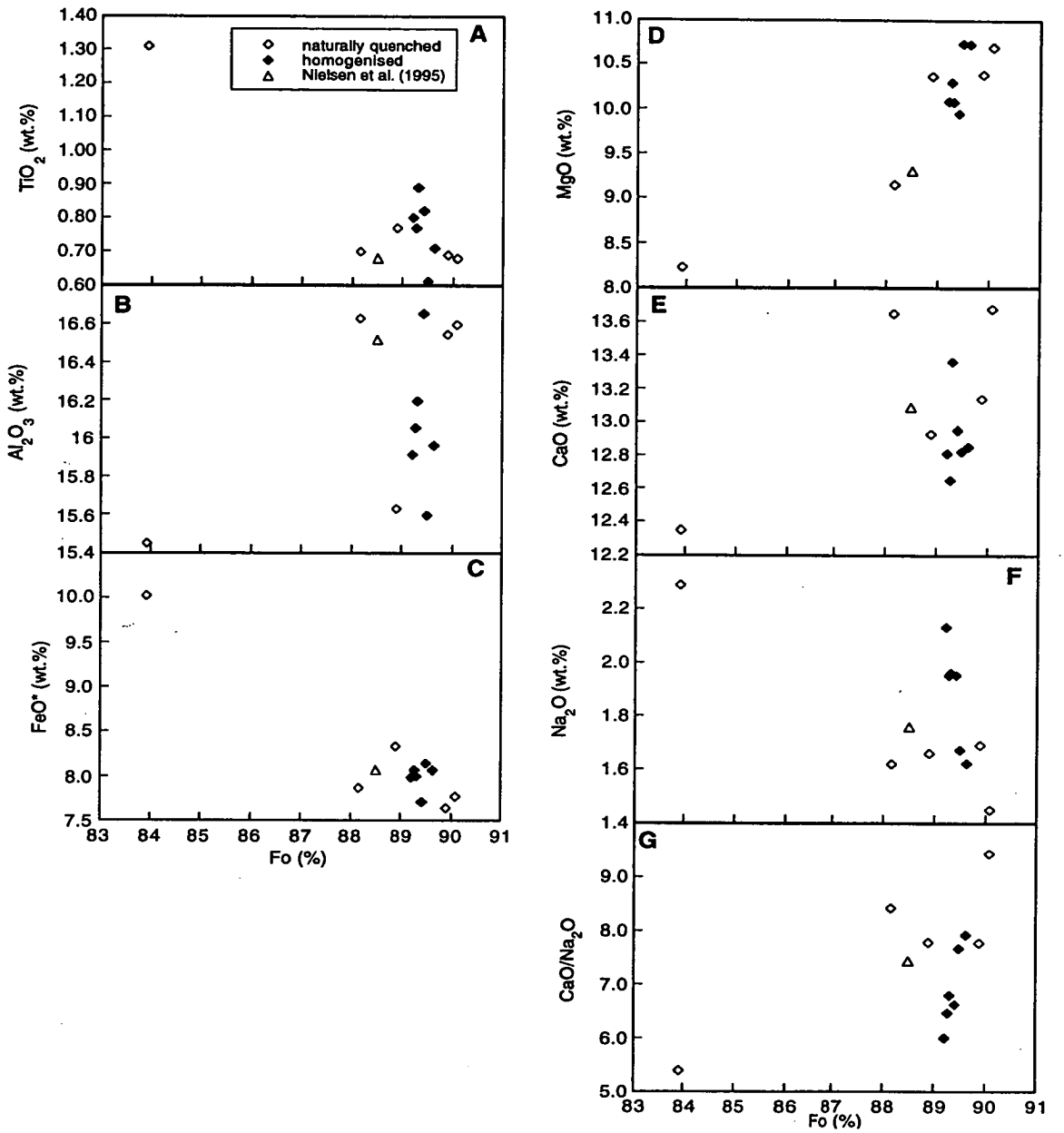

Figure 4.30: Host phenocryst composition vs. melt inclusion composition for melt inclusions in olivine. Homogenised and naturally quenched melt inclusions in olivine were recalculated to be in equilibrium with their host. The melt inclusion from Nielsen et al. (1995) was homogenised but overheated. Its composition was therefore recalculated to be in equilibrium with its host olivine. See text for discussion and description of recalculation methods.

temperatures of 1250°C, and 1190°C respectively suggest that the melt inclusion has been overheated. Although the melt inclusion has a composition that is saturated in olivine at the run temperature, it is not in equilibrium with its host olivine (as indicated by a calculated mineral-melt Fe^{2+}-Mg exchange coefficient of 0.36) but rather, is in equilibrium with olivine of $Fo_{89.9}$. Calculations to remove the effects of overheating, by adding back olivine of the host composition until the melt inclusion is in equilibrium with its host phenocryst indicate that about 4 wt.% of the host has been melted. The calculated equilibrium composition (with 9.3 wt.% MgO and 16.5 wt.% Al_2O_3) is similar to that of a recalculated naturally quenched melt inclusion in olivine Fo_{88}, analysed as part of the present study (Fig. 4.29). The calculated liquidus temperature (1212°C) of the melt inclusion is also consistent with the homogenisation temperatures of melt inclusions in olivine Fo_{88}-$Fo_{88.5}$ (1205-1210°C) from the present study.

Summary

The trapping temperatures of successfully homogenised melt inclusions in plagioclase are 1196-1204°C for low-An and 1215-1227°C, for high-An hosted inclusions. The high-An hosted melt inclusions were trapped from more primitive, MgO-rich, liquids than the low-An hosted inclusions, which have MgO contents similar to the most magnesian Central Gorda Ridge glasses. All melt inclusions have MgO, Al_2O_3, Na_2O, and K_2O abundances which lie on, or are close to, the calculated olivine-plagioclase cotectic from Sample D9-1. Low TiO_2, and high SiO_2 contents in plagioclase-hosted melt inclusions, relative to the pillow-rim glasses, are consistent with trends of melt inclusion compositions in plagioclase from Hole 896A and are not interpreted to be primary features. The low FeO* contents of low-An hosted melt inclusions, relative to the pillow-rim glasses, are also consistent with results from Hole 896A, but contrast with the FeO* contents of inclusions in high-An plagioclase which lie close to the calculated plagioclase-olivine cotectic. The high CaO contents of melt inclusions in low-An plagioclase, relative to the pillow-rim glasses, were also found in naturally quenched inclusions from spinel, and are interpreted to be a primary feature of the trapped liquids. The CaO contents of melt inclusions in low-An plagioclase are similar to those in high-An plagioclase, and define a trend that has a much shallower slope, more like the Hole 896A pillow-rim glass defined plagioclase-olivine cotectic than the trend of Central Gorda Ridge glasses.

Melt inclusions in olivine, $Fo_{86.5}$-$Fo_{89.5}$, homogenised at similar temperatures to those in plagioclase, but differ in composition, and do not form a trend that is related either to the cotectic, or to olivine-only crystallisation. These differences in composition relate largely to the high FeO* contents of the olivine-hosted melt inclusions. When recalculated to be in equilibrium with their hosts, the homogenised

melt inclusions have a similar range of compositions to the recalculated naturally quenched inclusions. The high FeO* contents of many olivine-hosted melt inclusions, also described from the naturally quenched inclusions, were not eliminated by reheating.

4.5 Discussion

4.5.1 Evidence for crystallisation history and magma chamber processes

In this section, evidence from pillow-rim glass compositions, textural and compositional relationships of phenocrysts and their mineral and melt inclusions are discussed with the aim of defining the crystallisation history for Sample D9-1, and the nature of its parental liquids.

Crystallisation history

The textural and compositional relationships of phenocrysts, and the trapping temperatures and compositions of melt inclusions in plagioclase of up to An_{91}-An_{92} and olivine of Fo_{88}, indicate that early cotectic plagioclase-olivine crystallisation occurred. More primitive plagioclase, up to An_{94}, hosts spinel inclusions that were in equilibrium, in terms of MgO and FeO*, with olivine Fo_{90}, suggesting cotectic crystallisation with the most primitive olivine sampled in the present study.

Olivine-plagioclase-spinel fractionation is supported by the compositions of high-An and low-An (An_{90}-An_{92} and $<An_{86}$ respectively), hosted melt inclusions which have virtually constant to slightly increasing, CaO contents, similar to the Hole 896A cotectic (Fig. 4.23) and increasing CaO/Al_2O_3 (Fig. 4.31). However, The CaO contents of melt inclusions in plagioclase, olivine and spinel are all higher than in the D9-1 glass, suggesting that either mixing or clinopyroxene crystallisation is required to link the melt inclusion compositions and their host pillow-rim glass.

Evidence for mixing

The mineralogy and pillow-rim glass chemistry of samples from the Central Gorda Ridge, are similar to a suite of basalts from a slow spreading (35 mm/yr) ridge segment at 26°S on the Mid-Atlantic Ridge (M.A.R.), that were studied by Niu and Batiza (1994). Two types of basalt were described from the 26°S suite. Type 1 basalts were interpreted to have undergone early cotectic olivine-plagioclase (up to An_{93}) crystallisation and pillow-rim glasses from these samples formed a well defined coherent fractionation trend. In contrast the type 2 basalts crystallised olivine prior to plagioclase, and their pillow-rim glasses had lower CaO contents, and defined a less coherent trend, the result of a range of parental melt compositions. The type 1 basalts

may be compared with the liquids trapped in melt inclusions from Sample D9-1, whereas the type 2 basalts have similarities to the Central Gorda Ridge pillow-rim glass samples. Niu and Batiza (1994) concluded that the two basalt types were the result of differing parental liquids, produced at differing depths and extents of melting, whose composition was broadly related to location on the ridge segment relative to the bounding offsets. Following this interpretation, the characteristics of Sample D9-1 could be interpreted to result from mixing of two parental liquids; type 1 and type 2, represented by the melt inclusions and pillow-rim glasses respectively, produced at different depths and by different extents of melting. However, an alternate explanation is that the melt inclusions from Sample D9-1 are related to the pillow-rim glass by clinopyroxene crystallisation.

Evidence for clinopyroxene crystallisation

No clinopyroxene has been recovered from Sample D9-1 or any other Central Gorda Ridge samples (Davis and Clague, 1987). However, the pillow-rim glass trend, with decreasing CaO and CaO/Al_2O_3 with decreasing MgO (Fig. 4.2E), and the mass balance calculations of Davis and Clague (1987) support crystallisation of clinopyroxene during the evolution of these liquids. If this is the case, could the pillow-rim glasses, and in particular Sample D9-1, be produced by olivine-plagioclase-clinopyroxene fractionation from the liquids trapped by low-An plagioclase? Calculated LLDs (Fig. 4.31) indicate that at low pressures, <2 kb, the low-An plagioclase can be linked to the Sample D9-1 pillow-rim glass by olivine-plagioclase-clinopyroxene crystallisation (although there is not such a good fit for CaO/Al_2O_3, the differences are within the error of typical glass analyses; see Table 4.1). This result has two implications. Firstly it confirms that the high-An and low-An plagioclase phenocrysts are related by plagioclase-olivine fractionation, and can be related to the Sample D9-1 pillow-rim glass by olivine-plagioclase-clinopyroxene crystallisation. Secondly, variations in melt inclusion and pillow-rim glass composition indicate that pyroxene crystallisation occurred, but, pyroxene is not a liquidus phase. The 'pyroxene paradox', is a feature previously described from many MORB suites (e.g., Rhodes et al., 1979; Francis, 1986).

Magma chamber processes: clinopyroxene crystallisation

The 'pyroxene paradox' in Gorda Ridge samples contrasts with the situation of Hole 896A samples where glass trends did not strongly indicate crystallisation of clinopyroxene, but clinopyroxene was present as an, albeit minor, phenocryst phase. The presence of pyroxene in the latter case was attributed to crystallisation as a result of undercooling during magma mixing in a periodically replenished, periodically tapped and continuously fractionated (RTF; O'Hara, 1977; O'Hara and Matthews, 1981) magma chamber. In the case of the Gorda Ridge samples the 'pyroxene paradox' can be

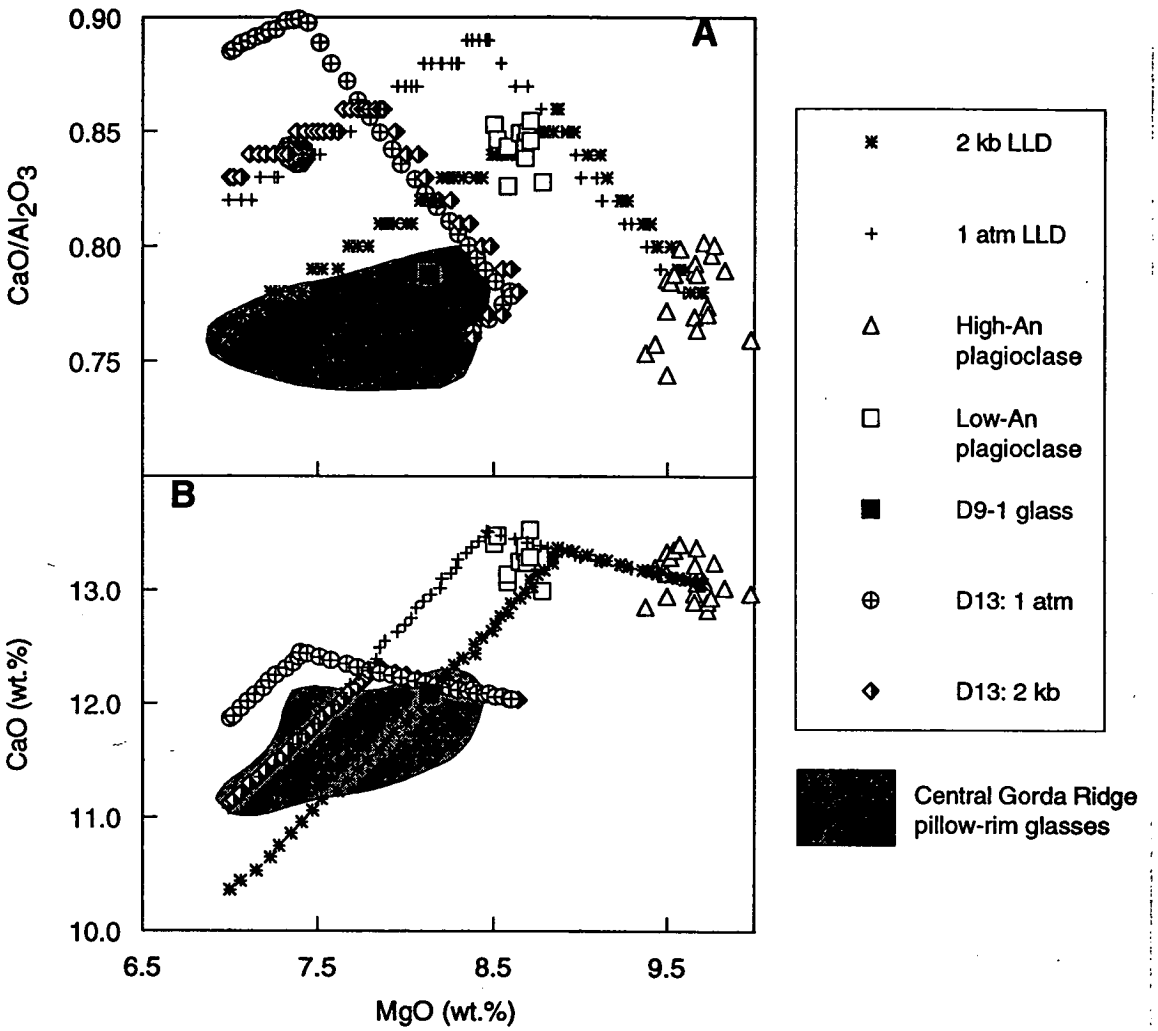

Figure 4.31: Liquid lines of descent for the average homogenised melt inclusion in high-An plagioclase, and the most primitive Central Gorda Ridge pillow-rim glass (D13-3). The compositions of melt inclusions from low-An plagioclase, the D9-1 pillow-rim glass and the Central Gorda Ridge pillow-rim glass analyses of Davis and Clague (1987) are shown for comparison. Liquid lines of descent were calculated for 1 atm and 2 kb pressure using the Petrolog program (Danyushevsky et al., 1990) with the models of Ford et al. (1983) for olivine, Weaver and Langmuir (1990; modified after Danyushevsky et al., 1996) for plagioclase, and Ariskin et al. (1986) for clinopyroxene. These models were selected on the basis that they produce the best fit for the 1 atm MORB olivine-plagioclase±clinopyroxene cotectic (Danyushevsky et al., 1996). See text for discussion.

resolved by including the process of in-situ crystallisation in an RTF magma chamber model. In-situ crystallisation (Campbell, 1978; Langmuir, 1989; Nielsen and De Long, 1992), also described as small packet crystallisation by O'Hara and Fry (1996), is a process whereby fractional crystallisation occurs in a boundary layer, or solidification front, where cooling is occurring at the margins of a magma chamber (Marsh, 1996). The evolved liquids produced in the solidification zone are then returned to, and mix with, the main magma body, a result of compaction, diffusive exchange and(or) convective exchange (McBirney, 1995). Some of the phases that crystallised in the solidification front will not be liquidus phases in the less evolved magma lens, and this

results in mixed magmas that may show compositional control by a phase, such as clinopyroxene, that is not present in the phenocryst population of the main magma body.

Evidence of in-situ, or interstitial crystallisation has been reported from oceanic gabbros, interpreted to be the crystallisation products of crystal mush zones (Bloomer et al., 1989; Meyer et al., 1989; Dick et al., 1992), and in all these cases clinopyroxene is a ubiquitous phase. Although no gabbroic samples have been recovered from the Central Gorda Ridge, Davis and Clague (1990) have described abundant olivine-plagioclase-clinopyroxene gabbro xenoliths from the Northern Gorda Ridge. The sampled clinopyroxenes include magnesian, Mg#=89, and Cr-rich, 0.5-1.5 wt.% oikocrysts that have compositional trends, in terms of Cr_2O_3 and TiO_2 vs MgO, that are similar to the clinopyroxenes from Hole 896A.

Davis and Clague (1987) suggested that the overall trend in Central Gorda Ridge pillow-rim glasses results from olivine-plagioclase-clinopyroxene crystallisation, however, 1 atm and 2 kb LLDs calculated for the most primitive pillow-rim glass, suggest that clinopyroxene would not appear on the liquidus until MgO <7.3-7.5 wt.%, i.e., clinopyroxene should not crystallise from the majority of pillow-rim glasses. However, as these samples come from an ~75 km long ridge segment it is unlikely that they represent a single liquid line of descent and variations in pillow-rim glass compositions may therefore result from; fractionation of a range of parental liquids (cf. 26°S M.A.R.; Niu and Batiza, 1994), mixing of liquids produced by fractionation of a single parental liquid (see Figure C2 of Langmuir et al., 1992), in-situ crystallisation, as discussed above, or high pressure fractionation.

Magma chamber processes: mixing

Both interpretations discussed in the previous sections imply that magma mixing was a major process in the evolution of Sample D9-1, and other Gorda Ridge basalts. Magma mixing is also indicated by the compositions, relative abundances, and textural relationships of sampled phenocrysts:

1. Plagioclase, An_{82}, interpreted to have crystallised from liquids more evolved than the host glass, included in olivine, $Fo_{87.6}$, that crystallised from liquids more primitive than the D9-1 glass.

2. The compositional range of spinel included in plagioclase. Similar variations in spinel compositions from high-An plagioclase have been interpreted on the basis of mixing primitive and more evolved liquids (Allan et al., 1988; Roeder and Reynolds, 1991).

2. The compositional range of spinel included in plagioclase. Similar variations in spinel compositions from high-An plagioclase have been interpreted on the basis of mixing primitive and more evolved liquids (Allan et al., 1988; Roeder and Reynolds, 1991).

3. Compositional zoning, both normal and reverse of plagioclase and olivine. Particularly the strong zoning in olivine, up to 2 Fo units found in the present study, but up to 4 Fo units reported by Davis and Clague (1987).

4. Variations of melt inclusion composition in zoned phenocrysts. Phenocryst OL80 is zoned and hosts two melt inclusions, one of which has a composition, in terms of TiO_2, and CaO/Na_2O, that is more evolved than the D9-1 glass.

5. The phenocryst-rich nature of Sample D9-1. This sample is typical of a class of MORB, <6% of all MORB samples, that are characterised by >20 vol.% phenocrysts, of which the majority (80-100%) are plagioclase (Bryan, 1983), leading to, in the case of D9-1, a plagioclase-olivine ratio of 46:1, well above the cotectic proportions of 3:1 for typical N-MORB (Grove and Bryan, 1983; Tormey et al., 1987). Such basalts are found mostly at slow spreading centres (Bougalt and Hekinian, 1974; Hekinian et al., 1976; Flower, 1980; Le Roex et al., 1996) and have only rarely been recovered from intermediate to fast spreading centres (Hekinian and Walker, 1987). The high crystallinity of Sample D9-1, is interpreted to represent part of the crystal mush zone, 25-50% crystalline, in the solidification front of a magma chamber (Marsh, 1996), although enrichment in phenocrysts may also occur during transport, by flow differentiation in the centres of dykes (Komar, 1976), and eruption (Staudigal and Bryan, 1981). The accumulation of excess plagioclase in the solidification front has been attributed to simple flotation, and settling of denser olivine and spinel, during magma mixing (Kuo and Kirkpatrick, 1982; Cullen et al., 1989). A more complex model for excess plagioclase accumulation was presented by Elthon (1984) who argued that magma mixing was an important process, but in addition, the temperature difference between primitive and more evolved plagioclase-bearing magma would lead to melting of plagioclase in the evolved magma, and re-precipitation from the mixed melt that was enriched in plagioclase.

4.5.2 Variations and implications of melt inclusion compositions.

As discussed above, the compositional trends of high-An and low-An hosted melt inclusions are consistent with olivine-plagioclase cotectic crystallisation, and differ from the trend of the pillow-rim glasses that require clinopyroxene crystallisation. The compositions of melt inclusions in spinels hosted by plagioclase, particularly their CaO contents, support this interpretation, however, what are the implications of the

compositions of olivine-hosted melt inclusions? The most primitive Central Gorda Rdige pillow-rim glass sampled was in equilibrium with olivine, Fo_{86}. Only one, low-FeO* melt inclusion hosted by more evolved olivine, Fo_{84}, was analysed, and has a composition similar to that of the D9-1 pillow-rim glass. The compositions of low-FeO* melt inclusions in more primitive olivine, (Fo_{88}-Fo_{90}) range from less to more magnesian than homogenised melt inclusions in high-An plagioclase (probably a function of variable FeO* contents), and most significantly have CaO contents that are similar to these melt inclusions. Olivine phenocrysts are therefore from two populations; evolved phenocrysts that crystallised from liquids similar to the erupted pillow-rim glasses, and more primitive phenocrysts that crystallised from the same liquids as the plagioclase and spinel.

If plagioclase, olivine and spinel crystallised together then their melt inclusions should have similar compositions. This is not the case for some major element oxides (Figs. 4.17 and 4.29). The TiO_2 contents of many plagioclase-hosted melt inclusions are lower than for inclusions in spinel or olivine (which do not fit the calculated cotectic; Fig. 4.29B) and this is best demonstrated by the compositions of naturally quenched melt inclusions in plagioclase phenocryst A27-PL8; a spinel included in this phenocryst hosts two melt inclusions with 0.73-0.81 wt.% TiO_2, whereas melt inclusions in the host plagioclase have TiO_2 contents of 0.2-0.5 wt.%. The SiO_2 contents of plagioclase-hosted melt inclusions are generally higher than in olivine-hosted inclusions, but have a similar range to that of spinel-hosted melt inclusions (Fig. 4.29A). As stated previously, these differences are not attributed to variations in trapped liquid composition, but may result from trapping or post-trapping processes. The Al_2O_3 contents of melt inclusions in olivine and spinel are generally lower than those in plagioclase. However, the CaO, Na_2O and K_2O contents of melt inclusions in all phenocryst types are similar (Figs. 4.29 E, F and G). Variations in CaO/Na_2O values, 6-9 in olivine-hosted, and 6.6-8.2 in plagioclase- and spinel-hosted melt inclusions, are less than for primitive melt inclusions in plagioclase from Hole 896A and suggest that parental liquids to Sample D9-1 had a more restricted compositional range.

4.5.3 Synthesis of crystallisation history

Based on the constraints discussed above the crystallisation history of Sample D9-1 is interpreted to be dominated by the assemblage olivine+spinel+plagioclase. The abundance of plagioclase phenocrysts in this sample requires that plagioclase accumulation and gravitational or hydraulic separation, of olivine and spinel occurred during transit through the crust and possibly in an axial melt lens. Frequent recharge and mixing with primitive liquids may have buffered the temperature and composition of the melt lens allowing formation of the large relatively compositionally homogeneous

I would suggest that the lack of clinopyroxene in any Central Gorda Ridge samples, indicates that crystallisation of clinopyroxene did not commence in the melt lens but that mixing of phenocryst-poor liquids resulting from in-situ crystallisation in the solidification front of the magma chamber and liquids with more primitive compositions in the melt lens, or in the case of Sample D9-1 the solidification front, occurred just prior to eruption. In this scenario processes are dominated by fractionation and mixing in the shallow crust and, as with the Hole 896A samples, high-pressure fractionation is not considered to have been a significant process. There is no evidence to suggest that distinctly different parental liquids contributed to the genesis of Sample D9-1, as has been suggested for the 26°S M.A.R. samples studied by Niu and Batiza (1994), although there are similarities in the mineralogy and compositional variations of melt inclusions and pillow-rim glasses, of these suites.

4.6 Summary and conclusions

Sample KK2-83-NP-D9-1 is a moderately evolved N-MORB with a more 'enriched' chemistry, i.e., higher TiO_2, K_2O, Na_2O and H_2O content and $(La/Sm)_n$, at a given MgO, than the samples from Hole 896A analysed in the present study. Sample D9-1 is typical of a class of MORB lavas which has a high phenocryst abundance, ~40% phenocrysts, with the phenocryst assemblage dominated by anorthitic plagioclase (>90% of phenocrysts) with lesser olivine, Fo_{83}-$Fo_{90.1}$ and Cr-Al spinel.

Plagioclase phenocrysts have a bimodal compositional distribution; a low An grouping, interpreted to have crystallised from liquids slightly more primitive than represented by the D9-1 glass, and a more anorthitic population, interpreted to have crystallised from more primitive liquids. Compositional and textural relationships between spinels and their host plagioclase phenocrysts are interpreted to indicate that the most anorthitic plagioclase, An_{94}, crystallised from a liquid that was in equilibrium with the most primitive olivine sampled, $Fo_{90.1}$, and that cotectic olivine-spinel-plagioclase crystallisation commenced early in the history of this sample.

The trapping temperatures of homogenised melt inclusions in high-An plagioclase (1215-1227°C) and olivine ($Fo_{86.5}$-$Fo_{89.5}$; 1205-1218°C) support the interpretation, based on mineralogy, of early cotectic plagioclase-olivine crystallisation. However, the compositions of melt inclusions in the high-An and olivine phenocrysts are different, a result of the high-FeO* contents of many naturally quenched and homogenised olivine-hosted inclusions. The homogenised melt inclusions in high-An plagioclase phenocrysts have compositions that are more primitive than the D9-1 pillow-rim glass and appear to lie on a plagioclase-olivine cotectic from Sample D9-1, in

terms of Al_2O_3, MgO, Na_2O and K_2O. However, in detail the high- and low-An hosted melt inclusions are related by olivine-plagioclase fractionation and the D9-1 glass can be derived from the low-An hosted inclusions by clinopyroxene crystallisation, or more likely as clinopyroxene phenocrysts are absent, mixing with in-situ fractionated liquids.

As with melt inclusions from Hole 896A the TiO_2 content of melt inclusions in plagioclase are lower than those of melt inclusions in olivine and spinel, at a similar stage of fractionation.

Chapter 5 has been removed for copyright or proprietary reasons.

Part of the material presented in Chapter 5 was published as:
McNeill A. W. (1995) Petrology of chilled dike margins recovered from Hole 504B, Leg 140. In Proc. ODP ScL Results, Vol. 137/140 (ed. J. Erzinger, H. J. B. Dick, and L. B. Stolcking), pp. 35-42. Ocean Drilling Program.

Chapter 6

The Interpretation of Data from Melt Inclusions in MORB Phenocrysts

6.1 Introduction

In this chapter I address the second aim of the present study, i.e., to assess the usefulness and reliability of melt inclusion data from MORB phenocrysts, by summarising the results of melt inclusion studies from Chapters 3, 4, and 5, and the literature. Variations in compositions and trapping temperatures of olivine-, spinel- and plagioclase-hosted melt inclusions are summarised, and possible reasons for, and the petrogenetic implications of, variations in the TiO_2 and FeO* contents of plagioclase-hosted inclusions are discussed in detail.

Differences in inferred trapping temperatures, from the visually controlled heating stage experiments of the present study, and published vertical quench furnace experiments, were noted for samples from the Costa Rica Rift (Hole 504B; section 5.6.3) and the Gorda Ridge (Sample D9-1; section 4.4.4). In this chapter I attempt to explain these different inferred trapping temperatures, using observations of melt inclusion behaviour and data from mineral-melt geothermometers; I also highlight potential problems with the vertical quench furnace technique.

6.2 Melt inclusion compositions

6.2.1 Melt inclusions in olivine

Homogenisation experiments were done using olivine phenocrysts from both Hole 896A and Sample D9-1 from the Costa Rica Rift and the Gorda Ridge. The Hole 896A melt inclusions (section 3.4.4; Fig. 3.25) homogenised at lower temperatures than the majority of plagioclase-hosted inclusions, and had compositions that were not consistent with the pillow-rim glass-defined cotectic. This was interpreted to be a result of fluid undersaturation of the primitive liquids trapped in these melt inclusions, and trapped liquid compositions were therefore recovered by recalculation of naturally quenched compositions (see sections 2.4.1 and 3.4.4).

In contrast, the homogenisation temperatures of Sample D9-1 olivine-hosted

melt inclusions are interpreted to represent trapping temperatures, but, the compositions of the homogenised melt inclusions have low olivine-liquid Fe^{2+}-Mg exchange coefficients, a result of high-FeO* contents. Variations in the FeO* content of olivine-hosted melt inclusions are known to result from:

1. Analytical overlap with magnetite. The occurrence of high-FeO* contents in both homogenised and naturally quenched melt inclusions indicates that analytical overlap with the magnetite formed during homogenisation experiments (sections 2.5.3, 3.4.4 and 4.4.4) is not the cause of high-FeO* contents in Sample D9-1 melt inclusions.

2. Re-equilibration with host olivine. In some studies of melt inclusions in olivine, compositions of homogenised inclusions have systematically lower FeO* when compared with natural glass compositions of the same MgO, and higher olivine-melt Fe^{2+}-Mg exchange coefficients than would be expected from experimental studies (Gurenko et al., 1991; Sigurdsson, 1994; Sobolev and Danyushevsky, 1994). These variations are explained by Fe^{2+}-Mg exchange between the melt inclusion, daughter olivine on the walls of the inclusion and the host olivine, with Fe^{2+} diffusing from both the melt inclusion and daughter minerals into the more MgO-rich host olivine. As stated above, re-equilibration of this type produces lower, not higher, FeO* contents.

The cause of the high-FeO* contents in melt inclusions, found in only one melt inclusion from Hole 896A (section 3.4.4) and not previously reported in studies of MORB phenocrysts (e.g., Sobolev et al., 1989), is therefore unknown.

In both suites, problems with results from olivine-hosted melt inclusions, underheating and high-FeO* contents, were identified only as a result of detailed comparison of mineralogy, melt inclusion data from all cotectic phases and(or) the host pillow-rim glass compositions. If melt inclusion compositions and trapping temperatures were determined for olivine only, in isolation from all other petrographic data, then errors in the petrogenetic interpretation of the melt inclusions could result.

6.2.2 Melt inclusions in spinel

Naturally quenched melt inclusions in spinel were analysed from Hole 896A samples (section 3.4.2; Fig. 3.17) and from Sample D9-1 (section 4.4.2; Figs. 4.16 and 4.17). A feature of all these analyses are high Cr_2O_3-contents, 0.2-1.7 wt.%, that have been reported in other electron-microprobe analyses of melt inclusions in MORB spinel (V. Kamenetsky and L. V. Danyushevsky pers. comm., 1997). The Cr_2O_3 contents were corrected to 0.1 wt.% by subtraction of the host spinel from the melt inclusion composition, and all the following discussions refer to these corrected analyses. The major element compositions of melt inclusions in spinel, in terms of TiO_2, CaO, Na_2O,

and K_2O are generally consistent with those of the host pillow-rim glasses and melt inclusions in cotectic phases, although TiO_2 contents are higher than in plagioclase-hosted melt inclusions. However, Al_2O_3, FeO, MgO and SiO_2 contents may be variable, and although FeO* contents are generally lower than in host pillow-rim glasses, there are no consistent patterns to these variations. The origin of these variations is not known but they may result from some form of re-equilibration between the melt inclusions and their host spinel and(or) host liquid.

Kamenetsky (1996) concluded, based on a detailed study of melt inclusions in spinel from the FAMOUS area, Mid-Atlantic Ridge, that naturally quenched and experimentally reheated spinel-hosted melt inclusions could recover trapped liquid compositions. As the spinels were opaque, and thus homogenisation could not be seen, Kamenetsky used a sequence of heating experiments, from 1240-1330°C, to demonstrate that overheating did not significantly affect melt inclusion composition. One sample used in Kamenetsky's study (Sample B) hosted spinels that were interpreted to have crystallised from the liquid that was erupted and quenched to form the host pillow-rim glass. The average compositions of melt inclusions, in terms of TiO_2, CaO, Na_2O, and K_2O, from Sample B are consistent with trapping of liquids identical to the host pillow-rim glass (Table 6.1). However, as with the melt inclusions analysed in the present study, the Al_2O_3, FeO* MgO and SiO_2 contents of the melt inclusions differ from those of the pillow-rim glasses by ~1.0-0.8, 0.5-0.3, 0.1-0.8 and 0.7 wt.% respectively. Variations in FeO* and MgO contents may also contribute, in addition to analytical uncertainty, to the range, 0.25-0.31, of calculated olivine-liquid exchange coefficients for equilibrium olivines discussed by Kamenetsky (1996). The re-equilibration of spinels, in terms of FeO and MgO content, with their host liquids, or host olivine phenocrysts, has been discussed in section 4.3.3 and by Scowen et al. (1991), and it is therefore likely that the spinels would also re-equilibrate with their melt inclusions. The results of Kamenetsky (1996) also suggest that reheating of spinel-hosted melt inclusions does not completely reverse any post-trapping compositional modification, as reheated Sample B melt inclusions have very similar compositions to the naturally quenched melt inclusions (Table 6.1).

Another potential problem with spinel-, and other largely opaque mineral-, hosted melt inclusions is the presence of accidentally trapped phases that may not be visible (heterogeneously trapped melt inclusions). Accidentally trapped phases (e.g., Fig. 4.10H) may affect the compositions of both naturally quenched and homogenised melt inclusions:

In naturally quenched melt inclusions, post-trapping crystallisation may occur

Table 6.1. Compositions of melt inclusions in spinel from Sample B of Kamentetsky (1996)

	[a]1	2	3
[b]No.	13	9	10
SiO_2	50.80	50.43	49.65
TiO_2	0.58	0.61	0.68
Al_2O_3	16.04	15.66	16.70
[c]FeO*	7.58	7.72	8.00
MnO	0.10	0.16	0.08
MgO	9.59	10.41	9.63
CaO	13.47	13.16	13.48
Na_2O	1.68	1.68	1.69
K_2O	0.07	0.12	0.07
P_2O_5	0.08	0.06	0.03
	100.00	100.00	100.00
[d]Mg#	69.4	70.7	68.3
CaO/Na_2O	8.0	7.8	8.0

[a]1=Melt inclusions homogenised at 1320°C; 2=naturally quenched melt inclusions; 3=host pillow-rim glass.

[b]Number of analyses used to calculate mean.

[c]All Fe as FeO.

[d]Mg#=100 x (Mg/(Mg+Fe))

on the accidentally trapped phases, e.g., the melt inclusion shown in Figures 4.16 and 4.17 which has a composition consistent with modification by interaction with an accidentally trapped plagioclase crystal (the plagioclase was not visible in plane light, and was found under reflected light only after electron microprobe analyses indicated its presence; Fig. 4.10H).

Any accidentally trapped crystal would most likely be melted at the temperatures (1300-1330°C) suggested for use in homogenisation experiments by Kamenetsky (1996). The composition of the quenched melt inclusion would not, therefore, be representative of trapped liquid composition and could lead to erroneous petrogenetic conclusions.

These considerations all indicate that, in contrast the conclusions of Kamenetsky (1996), the compositions of melt inclusions in spinel, either as phenocrysts or included in olivine and(or) plagioclase, may not act as completely closed systems, and therefore do not completely preserve the composition of trapped magmatic liquids. However, results from the present study and the literature suggest that the TiO_2, CaO, Na_2O and K_2O contents of homogeneously trapped spinel-hosted melt inclusions do approximate trapped liquid compositions and can be used in petrogenetic interpretation of a given MORB suite.

6.2.3 Melt inclusions in plagioclase

In the preceding chapters, plagioclase-hosted melt inclusions have been described from suites where the plagioclase phenocrysts crystallised from liquids with a similar compositional range to the host pillow-rim glasses (Holes 896A and 504B), and where the plagioclase crystallised from liquids that were not obviously related to the pillow-rim glasses, by processes such as simple fractional crystallisation, but where melt inclusion-bearing cotectic phases, olivine and spinel, were present (Sample D9-1). Experimental results have been used to demonstrate that, if the magmatic liquids were fluid-saturated and careful consideration is given to the kinetics of reheating, both glassy rapidly quenched and slowly cooled crystalline melt inclusions can be successfully homogenised. These experiments were shown to provide two petrologically useful pieces of information:

1. Crystallisation temperature. Trapping temperatures, inferred from the homogenisation temperature (T_h), of melt inclusions in plagioclase are consistent with calculated liquidus temperatures of host pillow-rim glasses (for Hole 896A and 504B samples) and the T_h of cotectic olivine-hosted melt inclusions (Sample D9-1) and are considered to represent crystallisation temperatures for the host plagioclase.

2. Trapped liquid compositions. A comparison of host pillow-rim glasses and melt inclusions in cotectic minerals indicates that homogenised melt inclusions in plagioclase can recover trapped liquid compositions in terms of Al_2O_3, MgO, CaO and Na_2O contents. Rare high K_2O contents, associated with high Na_2O and possibly H_2O, are interpreted to result from alteration by hydrothermal fluids (Hole 896A; section 3.5.2), and in general K_2O contents reflect those of trapped liquids. However, variations in the SiO_2, TiO_2, and in most cases FeO*, contents of melt inclusions, not seen in the pillow-rim glasses or melt inclusions from cotectic phases, are interpreted not to be related to variations in trapped liquid compositions. It is the variations of these elements, particularly Ti and Fe, considered to be incompatible in post trapping crystallisation of plagioclase on the walls of melt inclusions, that are interpreted to make the composition of naturally quenched melt inclusions unreliable indicators of trapped liquid compositions and the reasons for this are discussed below.

Low TiO_2 and FeO in plagioclase-hosted melt inclusions*

The results of studies for which the compositions of melt inclusions in plagioclase and co-existing phases have been reported are summarised in Table 6.2. In the majority of these studies melt inclusions in plagioclase have lower TiO_2 contents than inclusions in co-existing phases and their host pillow-rim glasses. In addition, low TiO_2 contents have been reported in plagioclase-hosted melt inclusions from DSDP Hole 417D (Sinton

Table 6.2. TiO_2 contents of melt inclusions and pillow-rim glasses

Source (location)	TiO_2 (wt.%) plagioclase	olivine/spinel	clinopyroxene	Host glass
Sobolev et al. (1989) (MAR)	**0.58-0.80**	**0.87-0.93**		
Watson (1978)[1] (MAR)	0.70-0.80	1.0-1.30	1.0	
Price et al. (1986)	0.24-0.54[2]	0.88		
(SEIR)	0.60-1.60[3]	0.88-1.15		
Humler and Whitechurch (CIR)	0.30-0.74	0.50-0.70		
Natland (1989) (EPR)	0.18-0.88	0.69-1.25		
Clocchiatti (1980)[5] (MAR)	0.22-0.91		1.29-1.41	
Davis and Clague (1990) (Gorda)	1.20-1.60	1.10-1.30	1.50-1.60	
Dungan and Rhodes (MAR)	0.80-1.02			1.40-1.44
This Study-896A	**0.13-0.87**	**0.54-0.74/**		0.64-1.03
(CRR)		0.64-0.93[7]		
This Study-504B (CRR)	**0.29-0.75**			0.83-1.38
This Study-D9-1	**0.18-0.59**	**0.61-0.89/**		
(Gorda)		0.64-0.88[7]		

Locations: MAR - Mid-Atlantic Ridge; EPR - East Pacific Rise; Gorda - Gorda Ridge; CIR - Central Indian Ridge; SEIR - Southeast Indian Ridge; CRR - Costa Rica Rift.

Values in bold type are from homogenised melt inclusions. The remainder are from naturally quenched inclusionns.

[1]recalculated at 9.0 wt.% MgO

[2]In high-An plagioclase

[3]In low-An plagioclase

[4]Olivine recalculated to remove post-trapping effects; An_{89} and Fo_{90}

[5]Exact timing of plagioclase and clinopyroxene crystallisation is unclear, but, probably crystallised together.

[6]In plagioclase An_{75}-An_{78} interpreted to be in equilibrium with host glass on the basis of 1 atm. crystallisation experiments.

[7]TiO_2 content in olivine/spinel.

and Byerly, 1980), the Galapagos Platform (Sinton et al., 1993), the Mid-Atlantic Ridge (Langmuir, 1980, in Elthon and Casey, 1985), and from the Juan De Fuca Ridge (R. Nielsen pers. comm., 1995). In contrast, analyses of melt inclusions in plagioclase phenocrysts from continental settings, suggest that low TiO_2 contents are not a feature in these suites, although data is available from only two studies (Clocchiatti and Massare, 1985; J. Johnson et al., 1995).

The identification of low FeO* contents, and thus high Mg# values, in plagioclase-hosted melt inclusions requires a detailed comparison with coexisting phases

and host pillow-rim glasses, and is most obvious when the Mg# of plagioclase-hosted melt inclusions is greater than that of the most primitive olivine-hosted melt inclusion, or pillow-rim glass for a particular suite. Published studies, largely using naturally quenched melt inclusion compositions, generally do not provide sufficient data to evaluate if low-FeO* melt inclusions are present. However, as an example, low FeO* as indicated by high Mg#, can be inferred in the results of Humler and Whitechurch (1988) who report the compositions of naturally quenched melt inclusions in primitive olivine and plagioclase. The olivine, Fo_{90}, hosts melt inclusions with recalculated equilibrium Mg# values of 72.5, whereas a single plagioclase megacryst, An_{89}, hosts melt inclusions with Mg# values of 68.4-77, i.e., extending to more primitive compositions than melt inclusions in the most primitive olivine sampled.

The low FeO* and TiO_2 contents of plagioclase-hosted melt inclusions may be interpreted in two ways:

1. Variations are not related to trapped liquid compositions and are related to interaction with the host plagioclase during, or after, trapping. The evidence for this mode of origin is largely from the lack of low-FeO* and TiO_2 contents in melt inclusions from cotectic phenocryst phases, or host pillow-rim glasses. The differences between the TiO_2 content of plagioclase-hosted melt inclusions, and those in olivine and spinel are best illustrated by grain A27-PL8, from the Gorda Ridge. A spinel included in this phenocryst hosts two melt inclusions with 0.73-0.81 wt.% TiO_2, whereas melt inclusions in the host plagioclase have TiO_2 contents of 0.2-0.5 wt.%. In this example the host plagioclase is unzoned, $An_{90.3}$-$An_{90.4}$, and there are no differences in the abundances of other moderately incompatible major elements between the melt inclusions in spinel (1.6-1.9 wt.% Na_2O and 0.02-0.03 wt.% K_2O) and those in plagioclase (1.6-1.8 wt.% Na_2O and 0.02-0.04 wt.% K_2O). I consider such observations, when coupled with textural and compositional evidence that plagioclase, olivine and spinel crystallised together, to indicate that variations in the TiO_2 content of plagioclase-hosted melt inclusions are not related to trapped liquid compositions.

2. Variations result from trapped liquids with a range of compositions. In this interpretation the variable TiO_2 (and possibly FeO* and SiO_2) contents of melt inclusions result from the trapping of individual melt fractions produced by fractional-continuous melting at different depths in the mantle melting column (K. Johnson et al., 1995; Nielsen et al., 1995). As discussed in section 1.1, the FeO* and SiO_2 contents of MORB mantle melts are largely a function of the depth of melting, whereas TiO_2 contents may be related to the degree of incompatible element depletion, in turn a function of either the extent of melting or source mantle heterogeneity. The salient points of this model are:

A. The low-TiO_2 contents of plagioclase-hosted melt inclusions are interpreted to correlate with the degree of geochemical depletion and the chondrite-normalised spidergrams of low-TiO_2 melt inclusions typically have negative Ti and Zr anomalies. Additionally, variations in Ti and Zr with $(La/Sm)_n$ are consistent with calculated fractional-continuous melting models and both enriched and depleted melt inclusions may be found in a single sample.

B. Low-TiO_2 melt inclusions are not found in olivine or spinels and these must not have sampled the depleted melt fractions and therefore did not crystallise from the same liquids as the plagioclase phenocrysts. The plagioclase phenocrysts are also not genetically related to their host pillow-rim glasses, which have 'normal' TiO_2 contents.

C. Low TiO_2 contents are not coupled with variations in other major elements (e.g., FeO*, Na_2O, K_2O) as they are buffered by reactions with wall-rocks, in the crust or upper mantle, to the olivine-plagioclase-spinel cotectic (Sinton et al., 1993; Nielsen et al., 1995). Pyroxene must be absent in this system as it would act as a reservoir for trace elements and could affect the trace element composition of the buffered liquid.

Below, I address these points, using data obtained in the present study, to demonstrate that variations in the composition of plagioclase-hosted melt inclusions are not the result of trapping individual melt fractions:

A. No substantially more enriched or depleted melt inclusion compositions were analysed from Hole 896A samples (the only suite for which I have trace element data). The $(La/Sm)_n$ of melt inclusions in both olivine and plagioclase ranges from 0.29 to 0.44, excluding one high-K_2O inclusion (9-1-24/PL15). There is no correlation between $(La/Sm)_n$ or $(La/Yb)_n$ and Ti or Ti/Zr, with a range of Ti at a given La/Sm or La/Yb (Fig. 6.1). If melt inclusion 9-1-24/PL15 is excluded, one inclusion, with the highest Ti content, plots away from the other melt inclusions. Negative Ti and Zr anomalies, such as those described by K. Johnson et al. (1995) and Nielsen et al. (1995), are not seen (Fig. 3.27), and it would appear that Ti contents are not strongly related to the degree of depletion, as has been reported by Nielsen et al. (1994, 1995). It should be noted that the range of Ti contents of the melt inclusions analysed in the present study, is considerably less than the overall range from all plagioclase-hosted melt inclusions, but is approximately that of Ti in olivine- and spinel-hosted melt inclusions.

To determine if the range of Ti contents seen in Hole 896A melt inclusions is a result of variable degrees of the mantle melting, an open system melting path was calculated using the method of Johnson et al. (1990), Johnson and Dick (1992) and Johnson and Kong (1992). Variations in Ti and Ti/Zr describe a steeper trend than that

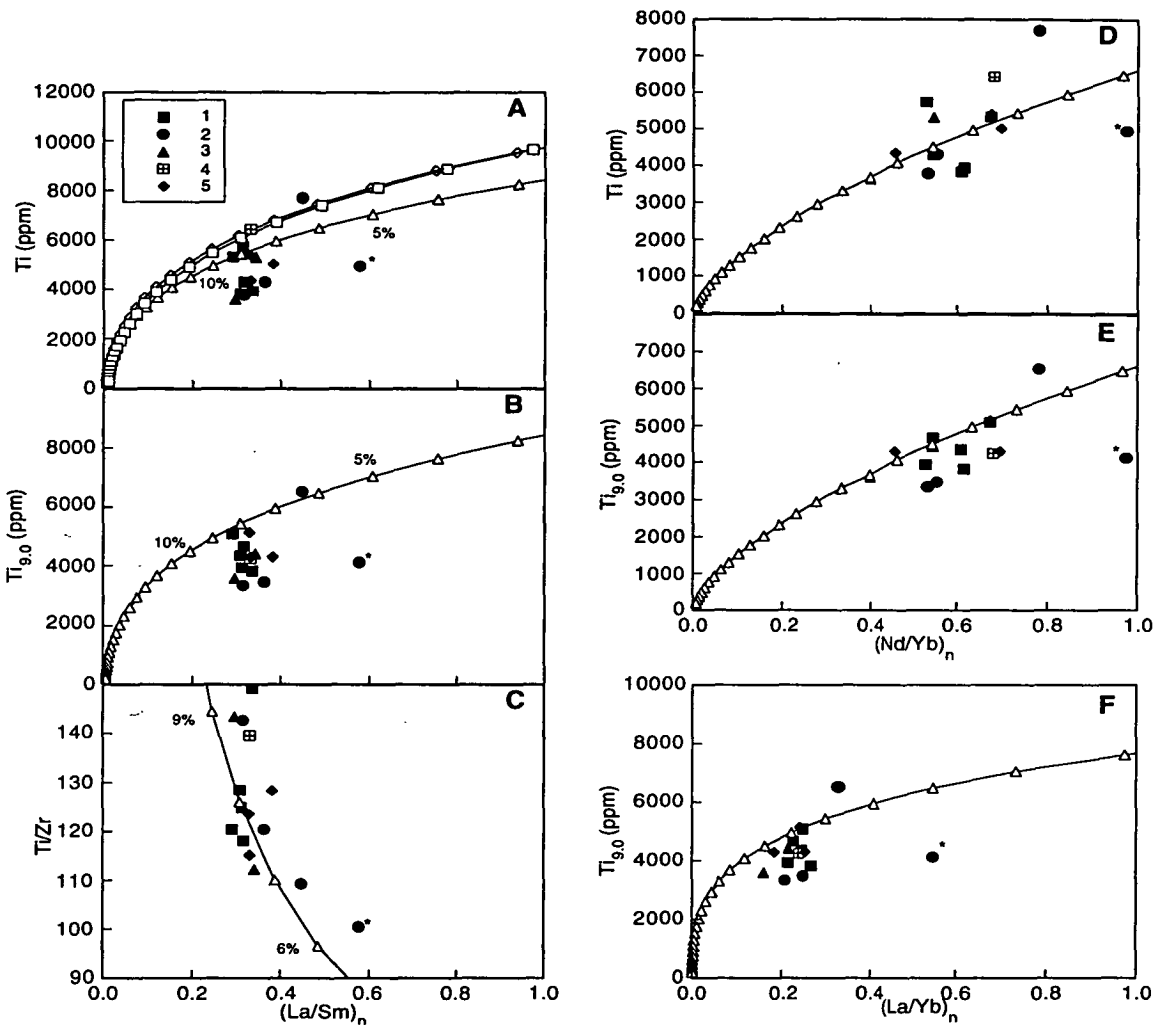

Figure 6.1: Variation in degree of REE fractionation. Ti (**A**), $Ti_{9.0}$ (**B**), and Ti/Zr (**C**) vs. $(La/Sm)_n$. Ti (**D**), and $Ti_{9.0}$ (**E**) vs. $(Nd/Yb)_n$, and $Ti_{9.0}$ versus $(La/Yb)_n$ (**F**). Where $Ti_{9.0}$ = Ti content recalculated to 9.0 wt.% MgO to minimise the effects of fractionation. Curves are from an open-system melting model (see below). Symbols; 1 - pillow-rim glass (ICP-MS); 2 - naturally quenched melt inclusions in plagioclase; 3 - Pillow rim glass (SIMS); 4 - naturally quenched melt inclusion in olivine; 5 - homogenised melt inclusions in plagioclase. The high-K melt inclusion, 9-1-24/Pl15, is indicated with a *.

Calculation of $Ti_{9.0}$: Calculations were done using the Petrolog program and the models of Ford et al. (1983) for olivine, and Weaver and Langmuir (1990) for plagioclase. Melt inclusion compositions were first recalculated, by modelling the reverse of fractionation until both olivine and plagioclase are on the liquidus (i.e., the composition is on the plagioclase-olivine cotectic). Both melt inclusions and pillow-rim glasses were then recalculated, by either crystallisation (if MgO >9.0 wt.%) or addition (when MgO <9.0 wt.%) of olivine and plagioclase, along the cotectic until the calculated liquids had 9.0 wt.% MgO.

Melting Model: The melting model was calculated using the open system model of Johnson and Dick (1992) and Johnson and Kong (1992), assuming a constant 2% porosity, and with the partition coefficients, starting composition, and melting modes as used by K. Johnson et al. (1995). Open triangles indicate 1% melting intervals. Additional curves on **A** are melting models for the depleted mantle of Gurenko and Chaussidon (1995; open squares) and the primitive mantle of Sun and McDonough (1989; open diamonds).

produced at low $(La/Sm)_n$ and $(La/Yb)_n$ by the model (Fig. 6.1), and variations in the source composition are unlikely to produce a melting path that will parallel these trends. For example, if less depleted sources, i.e., with higher $(La/Sm)_n$ and Ti content, such as the depleted mantle of Gurenko and Chaussidon (1995) or primitive mantle of Sun and McDonough (1989) are used, then the calculated melting curve will have higher Ti or Ti/Zr at a given $(La/Sm)_n$, but will still approach an asymptotic curve at $(La/Sm)_n$ <0.1 (Fig. 6.1A). Variations of HFSE elements, and Ti in particular, in Hole 896A melt inclusions and pillow-rim glasses are therefore not directly related to the melting process.

Low TiO_2 contents, generally >0.29 wt.% and up to 0.5 wt.%, have been reported in primitive olivine phenocrysts from Iceland and the Mid-Atlantic Ridge (Gurenko et al., 1991; Sobolev and Shimizu, 1992; Sobolev and Shimizu, 1993). In the case of the melt inclusions from Iceland, the TiO_2 contents of the inclusions, 0.41-0.43 wt.%, are similar to those of the host pillow-rim glasses, 0.46 wt.%, and are consistent with their primitive and depleted nature (Gurenko and Chaussidon, 1995). The 'ultra-depleted' melt inclusion in olivine, with 0.29 wt.% TiO_2, described by Sobolev and Shimizu (1992), is more primitive, 10.5 wt.% MgO, and depleted, CaO/Na_2O value of 11, Al_2O_3 content of 15.5 wt.%, and $(La/Sm)_n$ of 0.04, than for example, the Hole 896A plagioclase-hosted melt inclusions analysed in the present study (with CaO/Na_2O <10, Al_2O_3 up to 16.4 wt.%, and $(La/Sm)_n$ of >0.29). The rare low TiO_2 melt inclusions found in olivine phenocrysts are therefore consistent with the primitive and depleted nature of the trapped liquids, unlike the low TiO_2 contents in plagioclase-hosted melt inclusions that were trapped from evolved and considerably less depleted liquids.

Nielsen and co-workers did not recognise the variations in FeO* and SiO_2 contents of melt inclusions documented in the present study, but variations in these elements may provide support for their interpretation. It has been suggested that, if the effects of fractionation are removed, then Fe and Si contents of a MORB liquid are largely a function of the depth of melting, and Na, and to a certain extent Ti, contents vary with the extent of melting (Klein and Langmuir, 1987; Falloon and Green, 1988; Niu and Batiza, 1991b). Variations of these elements, and in particular the correlation between FeO* and Na_2O normalised to 8 wt.% MgO to remove the effects of fractionation, have been used in many recent interpretations of MORB petrogenesis (Brodholt and Batiza, 1989; Klein and Langmuir, 1989; Niu and Batiza, 1991b; Langmuir et al., 1992; Shen and Forsyth, 1995). Mantle heterogeneity (Shen and Forsyth, 1995), and the extent of melting (Kinzler and Grove, 1992a), may affect Fe contents, but there should be, at least on a local scale, a correlation between Fe, Si, and Na related to the pressure and extent of melting in a mantle melting column.

Variations in Fe, Ti, Na, and Si contents of melt inclusions with >9.0 wt.% MgO, from all suites used in the present study, are shown in Figures 6.2 and 6.3. High-MgO melt inclusions were used to avoid the necessity for correction to a reference MgO content and the attendant variations in normalised values, resulting from uncertainties in estimated liquid lines of descent, as discussed by Albarede (1992) and Shen and Forsyth (1995). If the liquids trapped to form the melt inclusions were produced by melting and segregation at different depths in a melting column, then a positive correlation between FeO* and Na_2O would be expected, i.e., low-Na_2O and low FeO* liquids resulting from shallow high degree melting and high-Na_2O, high-FeO* liquids from deep low degree melting (Klein and Langmuir, 1989). The sampling of melts produced in this way would also lead to a negative correlation between SiO_2 and Na_2O (ibid). However, more recent melting parameterisations (Langmuir et al., 1992) suggest that the situation is more complex, and that FeO* contents will remain virtually constant in a given melting column, and that only Na_2O will vary (predicted SiO_2 contents for this model are not described).

There is no well defined correlation between elements that should indicate the extent and pressure of melting (Figs. 6.2A, B and 6.3A, B) with constant Na_2O contents and variable FeO*. Nor is there any correlation between elements which should reflect the pressure of melting, i.e., SiO_2 and FeO* (Figs. 6.2C and 6.3C) or between Na_2O and TiO_2 which may reflect the extent of melting (Figs. 6.2D and 6.3D). Variations in FeO*, TiO_2 and SiO_2 contents are not the result of polybaric melting in a single melting column.

B. In the studies of Sinton et al. (1993), K. Johnson et al. (1995) and Nielsen et al. (1995) the plagioclase-hosted melt inclusions have compositions that are interpreted to be more primitive than the host glasses (although see section 6.3.1), and it is possible that they may have trapped individual melt fractions. However, the liquids trapped in Hole 896A and 504B, and Sample D9-1 low-An plagioclase are not more primitive than the pillow-rim glasses of these suites (Figs. 3.22, and 5.13), and this precludes the possibility of trapping individual melt fractions that mixed to form the pillow-rim glasses. In the Hole 896A and 504B samples, low Ti contents are found in melt inclusions with a range of MgO contents. It could be argued that, if the phenocrysts are considered not to have crystallised from their host glasses, the melt inclusions with 8-9 wt.% MgO could represent melts prior to aggregation. However, the trends in melt inclusion compositions parallel the host glasses and are compatible with crystallisation along the olivine-plagioclase cotectic and this is not consistent with fractionation of low

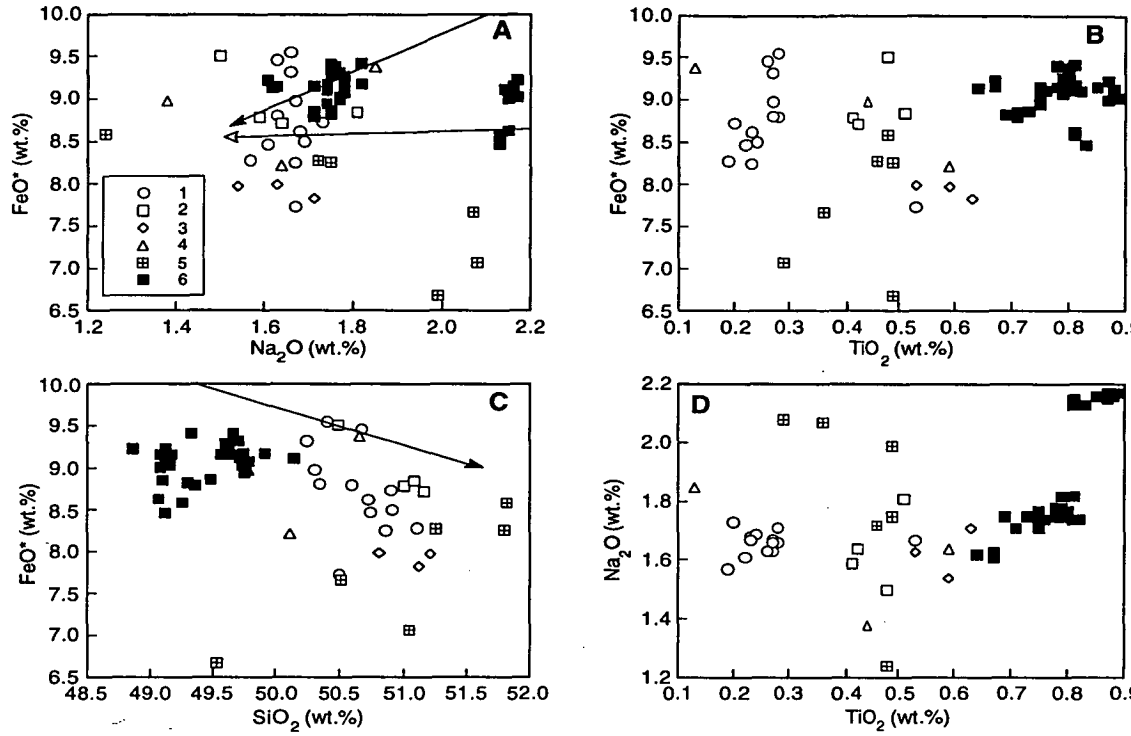

Figure 6.2: Variations in FeO* (all Fe as FeO) vs Na_2O (**A**), TiO_2 (**B**), and SiO_2 (**C**), and Na_2O vs TiO_2 (**D**) for homogenised melt inclusions in plagioclase from Hole 896A and 504B. To minimise the effects of fractionation only inclusions with >9.0 wt.% MgO are plotted. Pillow-rim glasses are included for comparison. Symbols; 1 to 4 - inclusions from Hole 896A samples 27R-1, Piece 13, 27R-1, Piece 15, 4R-1, Piece 2, and 9R-1, Piece 24 respectively; 5 - melt inclusions from Hole 504B; 6 - pillow-rim glasses from Holes 504B and 896A. The heavy line on **A** and **C** is the intra-column trend, for polybaric melting commencing at 40 kb from Klein and Langmuir (1989). The light line on A is the intra-column trend for polybaric fractional melting commencing at 20 kb using the model of Langmuir et al. (1992).

degree melts with a range of compositions. The range of MgO contents of pillow-rim glasses and melt inclusions from these suites indicates that liquids were evolved, as discussed in section 3.5.1, and have been affected by both a period of olivine(±spinel) fractionation, and magma mixing, and it is difficult to see how the signature of individual melt fractions would be preserved through these processes.

In all three suites examined in the present study, there is abundant evidence to suggest that the sampled plagioclase, olivine and spinel phenocrysts were crystallising from the same liquid, and the compositions of melt inclusions in these phases should therefore be similar. However, if the low TiO_2 contents of plagioclase-hosted melt reflect trapped liquid compositions, then the plagioclase must have crystallised from different liquids to the olivine and spinel. This implies that there must be efficient separation of phenocryst phases, such that spinel or olivine, with low-TiO_2 melt inclusions are not sampled by the magma chamber or that all sampled olivine and spinel,

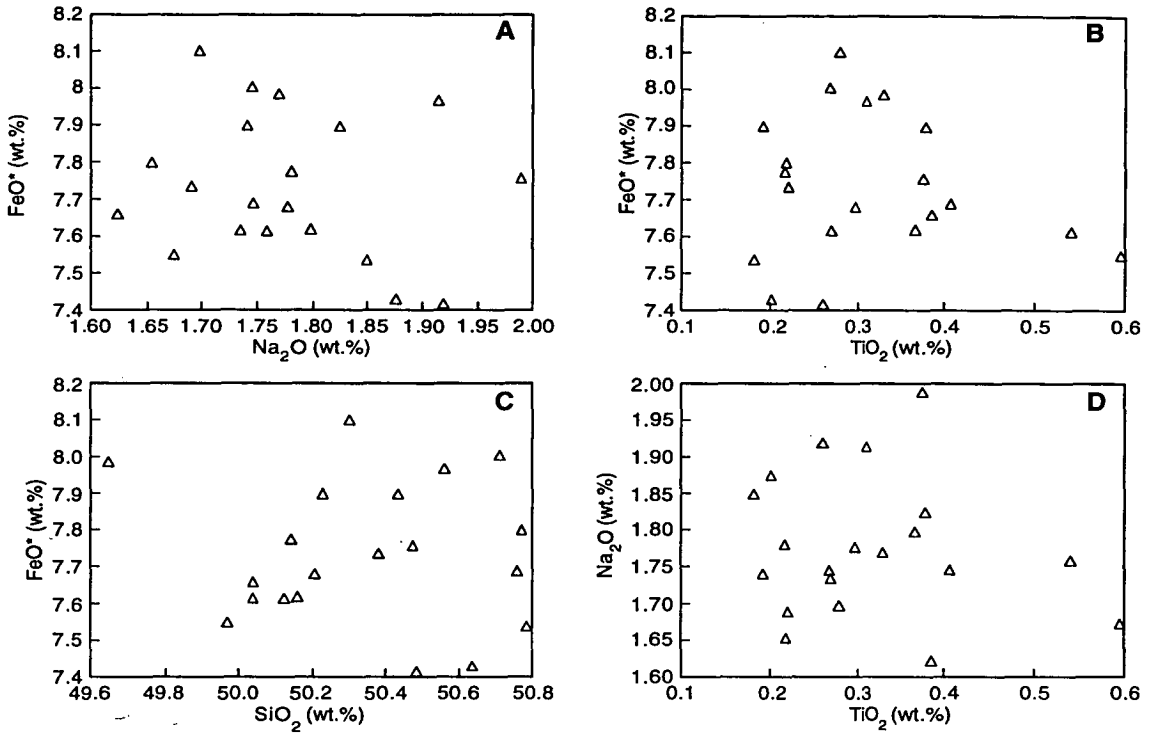

Figure 6.3: Variations in FeO* (all Fe as FeO) vs Na_2O (**A**), TiO_2 (**B**), and SiO_2 (**C**), and Na_2O vs TiO_2 (**D**) for homogenised melt inclusions in high-An plagioclase from Sample D9-1. All inclusions have MgO contents in the range 9.4-9.9 wt.%. See text for discussion.

some of which could be in equilibrium with a mantle source, must come from liquids that were not geochemically depleted. Additionally 'high'-TiO_2 melt inclusions in spinel hosted by plagioclase must not have crystallised from the same liquids as the plagioclase. Mixing of liquids must also be efficient, to prevent eruption of liquids with low TiO_2 contents, however, the occurrence of low-TiO_2 melt inclusions with MgO contents similar to erupted pillow-rim glasses in low-An plagioclase, require that these liquids remained un-mixed during fractionation in the magma supply system.

C. Mechanisms to preserve the trace element signature of low degree melts, by reactions in the lower crust or upper mantle, were discussed by Sinton et al. (1993) and Nielsen et al. (1995). In these scenarios the major element compositions of low degree partial melts are buffered by the mineralogy of the crystal mush zone, or reactions such as the melting of spinel-lherzolite to produce anorthitic plagioclase, olivine and liquid from the assemblage clinopyroxene, orthopyroxene and spinel (Kinzler and Grove, 1992). These reactions are interpreted to force the major element compositions of liquids toward the olivine-plagioclase-spinel cotectic, but their trace element signature

may vary according to local heterogeneities in mineralogy and(or) the compositions of primitive melts (Sinton et al., 1993). Evidence for such a process, from the shallow mantle section at the Hess Deep, has been presented by Dick and Natland (1996), and is largely based on the occurrence of very calcic (up to $An_{98.7}$) plagioclase in gabbroic segregations from dunites. However, it is unclear whether these plagioclases are primary or are the result of pervasive alteration, which leads to a range of plagioclase contents from An_{85} in the least altered to An_{98} in the most altered gabbros (Früh-Green et al., 1996), and as such this evidence is not conclusive. Additionally, the buffering process should work to remove the low FeO* and high SiO_2 contents of many melt inclusions. That these elements differ from cotectic abundances suggests that the proposed buffering process does not occur, or if it occurs is highly inefficient.

If the proposed buffering reactions occur in the crystal mush zone, then they must occur in a pyroxene-free system, as pyroxene will act as a reservoir for trace elements (Nielsen et al., 1995); however, there is evidence that clinopyroxene was an important phase in the evolution of all the studied suites. On the basis of these observations, I suggest that the crustal reaction process, described by Sinton et al. (1993) and Nielsen et al. (1995), is unlikely to have preserved the low TiO_2 contents individual melt fractions, resulting in the variable and low TiO_2 abundances in plagioclase-hosted melt inclusions.

Possible causes of low TiO_2 and FeO contents in plagioclase-hosted melt inclusions*

The low TiO_2 and FeO* contents of many plagioclase-hosted melt inclusions from MORB, typically not seen in melt inclusions from coexisting phenocryst phases, or host pillow-rim glasses, are therefore unlikely to result from variations in trapped liquid composition and must result from some process during or after trapping. If this is the case, is there any evidence from inter-, or intra-phenocryst variations in the TiO_2 and FeO* contents of inclusions that indicates the nature of these processes? The following discussion of variations of melt inclusion TiO_2 and FeO* contents, both within a single phenocryst, and between the phenocrysts of a suite of samples, is based on the results of the present study and those of Sinton et al. (1993) and Nielsen et al. (1995).

Generally, the TiO_2 content of re-heated plagioclase-hosted melt inclusions ranges from being consistent with that of cotectic phases or the host pillow-rim glass suite, to much lower values (<0.2 wt.%; Figs. 5.20 and 3.19), although melt inclusions from Hole 504B (Fig. 5.13B and K. Johnson et al. (1995)), mostly have lower TiO_2 than those in cotectic phenocrysts or the pillow-rim glasses. The degree of correlation between melt inclusion TiO_2 content and host-An content or degree of fractionation varies between suites. Melt inclusions from Hole 504B define a trend parallel to the

pillow-rim glasses (Fig. 5.13B), however, there is a less strong correlation for Sample D9-1 (Fig. 4.23B), and inclusions from Hole 896A show no correlation between TiO_2 and MgO content (Fig. 3.19B). Variations in the degree of correlation between host-An content and melt inclusion TiO_2 content are also seen; Gorda Ridge and Hole 504B samples show a correlation of decreasing TiO_2 with decreasing An (Figs. 4.23B and 5.15B respectively), but, this correlation is not as obvious for Hole 896A (Fig. 3.23A) samples. However, melt inclusions from Hole 896A, Group 2 plagioclase have higher TiO_2 than plagioclase from other groups, consistent with the high TiO_2 content of their host glasses (section 3.5.2).

The TiO_2 contents of melt inclusions in individual phenocrysts from Holes 896A and 504B are relatively constant, with variations of generally <0.1 wt.% but up to 0.2 wt.%. In contrast, the TiO_2 content of melt inclusions hosted by plagioclase from Sample D9-1 may vary by a factor of 2-3 (e.g., <0.3-0.9 wt.% TiO_2) in a single phenocryst (Fig. 6.4B, and Nielsen et al. (1995)), and a similar range of TiO_2 contents has also been reported in melt inclusions from the Galapagos Platform (Sinton et al., 1993). These variations in TiO_2 content may be related to the distribution of melt inclusions in a phenocryst; much of the variation reported by Sinton et al. (1993) and Nielsen et al. (1995) occurs between bands of concentrically arranged inclusions, with TiO_2 both increasing and decreasing, between bands from core to rim (e.g., Fig. 7A of Nielsen et al., 1995). These variations do not correlate with host-An content or other major element variations in a melt inclusion. In contrast, the majority of spinel- and olivine-hosted melt inclusions have constant TiO_2 contents in a given phenocryst, and where significant variations in TiO_2 content are recorded, these may be related to trapping of liquids at different stages of fractionation (e.g., Fig. 4.13). There is no apparent correlation between the size of a melt inclusion and its TiO_2 content, both within, and between phenocrysts, in results from the present study (Fig. 6.4) and Sinton et al. (1993) and Nielsen et al. (1995).

Variations in FeO* content are less well described. However, there is no apparent relationship between FeO* content and melt inclusion size (Fig. 6.4) or TiO_2 content (Figs. 6.2B and 6.3B).

Any plausible explanation for the low TiO_2 and FeO* contents of plagioclase-hosted melt inclusions must account for the variations described above. Processes which may affect melt inclusion compositions include:

1. Boundary layer effects. As discussed in section 2.2 the trapping of compositional gradients around growing crystals may result in non-representative melt

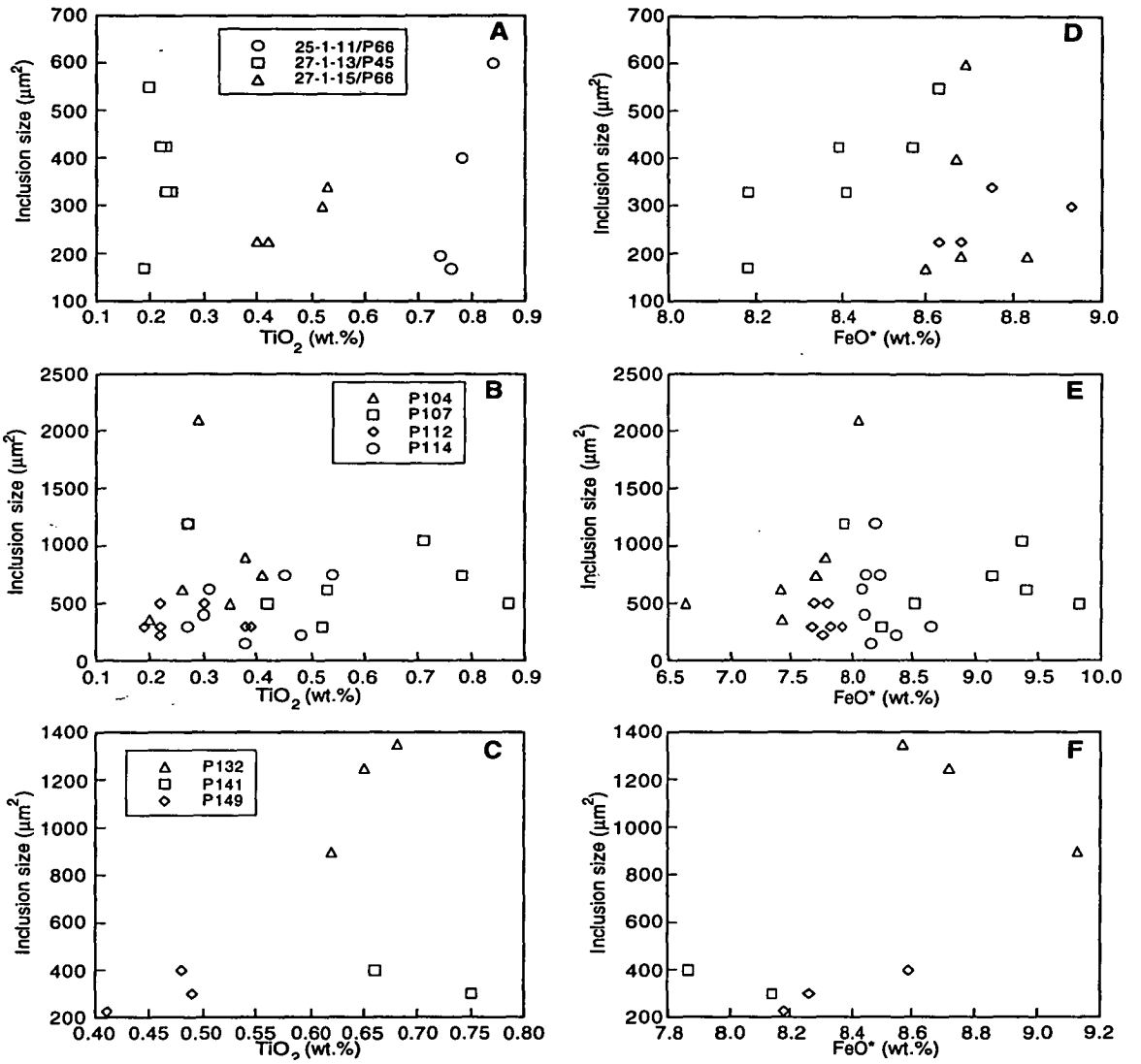

Figure 6.4: Variations of TiO_2 and FeO* content with melt inclusion size for experimentally homogenised plagioclase phenocrysts from Hole 896A (**A** and **D**), sample D9-1 (**B** and **E**) and Hole 504B (**C** and **F**). Inclusion size is calculated as the product of length and width of the inclusion. The TiO_2 and FeO* contents of homogenised melt inclusions are largely independent of inclusion size.

inclusion compositions. If this were the case then a relationship between composition and melt inclusion size would be expected. No consistent relationship has been found, as discussed above (Fig. 6.4).

2. Crystallisation of 'hidden' magnetite. The crystallisation of opaque minerals, interpreted to be magnetite occurred in olivine-hosted melt inclusions during heating stage experiments (sections 3.4.4 and 4.4.4) and is interpreted to result from dissociation of H_2O and oxidation of the melt (section 2.5.3). In experiments using

plagioclase-hosted melt inclusions from the Mid-Atlantic Ridge, magnetite was found to crystallise in many inclusions (Sobolev et al. (1989) and L. V. Danyushevsky, pers. comm. 1997), and in these samples low FeO* contents are correlated with low TiO_2 contents. However, this explanation is not consistent with the presence of low-FeO* and TiO_2 in naturally quenched melt inclusions where magnetite is not present.

3. Re-equilibration between melt inclusion and host plagioclase or liquid. The presence of low TiO_2 and FeO* in naturally-quenched melt inclusions implies that this process, if it occurs, must take place in the magmatic transport and storage system prior to eruption and cooling, and is not a result of (although it may be enhanced by) reheating during homogenisation experiments.

Re-equilibration may be consistent with the enhanced FeO* and TiO_2 depletion, relative to pillow-rim glasses, in the more slowly cooled Hole 504B melt inclusions (Fig. 5.13B) but, it is unclear how it would account for the 'cyclic' variations of TiO_2 across an individual phenocryst, as shown in Figure 7A of Nielsen et al. (1995). TiO_2 is interpreted to substitute for SiO_2 in the plagioclase structure (Peters et al., 1995); and this coupled substitution may provide a mechanism for producing higher SiO_2 and lower TiO_2 contents in melt inclusions. The TiO_2 contents of plagioclase are generally low (0.01-0.03 wt.% (Sato, 1989; Phinney and Morrison, 1990)), but highly variable TiO_2 contents, coupled with LREE variations, in plagioclase of otherwise homogeneous composition have been reported from gabbros at the Mid-Cayman Rise (Keen and Elthon, 1996).

Plagioclase may incorporate significant Fe into its structure, typically <1 wt.% FeO* in MORB phenocrysts, in both the tetrahedral ($Fe^{2+}Si$ or $Fe^{3+}Si$ substituting for AlAl) and the M-sites (Fe^{2+} substituting for Ca or Na) (Longhi et al., 1976; Sato, 1989; Xue and Morse, 1994). However, the FeO* content of plagioclase may be controlled by oxidation state (Sato, 1989; Phinney and Morrison, 1990; Phinney, 1992), crystallisation kinetics (Longhi et al., 1976), FeO* content of the crystallising magma (Tegner, 1997) and(or) anorthite composition (Kempton et al., 1985; Sato, 1989; Tegner, 1997). It is difficult, if not impossible to resolve which of these processes may be responsible for exchange of Fe between melt inclusion and host plagioclase.

Both TiO_2 and FeO* can therefore be incorporated into the plagioclase structure, however, these elements are relatively incompatible, with mineral-liquid partition coefficients of ~0.04 and ~0.05 respectively (Sato, 1989; Phinney, 1992; Peters et al., 1995).

Of the three processes listed above, I believe that some form of re-equilibration is the most likely cause of low TiO_2 and FeO* contents in both naturally quenched and

experimentally homogenised melt inclusions in plagioclase, although the exact mechanism is unclear. Detailed trace element analyses of host plagioclase and melt inclusions are required to resolve this problem, but, unfortunately such analyses are presently not available.

6.3 A comparison of homogenisation techniques; the heating stage and the vertical quench furnace

6.3.1 Hole 504B, Costa Rica Rift

As discussed in section 5.6.3, the composition and trapping temperatures of melt inclusions in plagioclase of An_{81}-$An_{94.8}$ from the sheeted dykes of Hole 504B were determined using a one atmosphere vertical quench furnace (K. Johnson et al., 1995). Trapping temperatures of 1260-1270°C were inferred from the presence of olivine daughter crystals in runs at 1260° (the significance of these daughter olivines are discussed in section 6.3.2) but not in those heated to 1270-1280°C, which were glassy with or without a shrinkage bubble. Detailed descriptions of the melt inclusions, either before or after reheating, were not provided. Variations in SiO_2, Al_2O_3 and trace element contents of melt inclusions were used to suggest that the host plagioclase had not been remelted, i.e., the melt inclusions were not overheated. It was also concluded that a correlation between the Ca# (=Ca/(Ca + Na)) of the melt inclusions and host plagioclase, paralleling the trend of experimental data on MORB compositions, indicated equilibrium had been obtained. The major and trace element data were then used to infer that many of the melt inclusions were samples of primary melts produced by polybaric near-fractional melting.

As discussed previously, the trapping temperatures quoted by K. Johnson et al. (1995), are ~50°C higher than those obtained for plagioclase of similar composition in the present study(1188-1218°C). Also, the compositions of homogenised melt inclusions reported by K. Johnson et al. (1995) show considerably more scatter than those of melt inclusions homogenised in the present study. The differences in melt inclusion compositions are best illustrated by a comparison of Al_2O_3 and MgO contents (Figs. 5.18 and 6.5). The majority of the reheated melt inclusions analysed by K. Johnson et al. (1995) form a trend with constant Al_2O_3 (17.8-18.0 wt.%) over the range 5.6-9.3 wt.% MgO, that is at an angle to the plagioclase-olivine cotectic as defined by the Hole 504B and 896A pillow-rim glasses. The differing trends are most likely the result of the overheating in the vertical quench furnace experiments, and this can be demonstrated from the results of mineral-melt geothermometry (sections 2.6.1 and 4.4.4). Calculated olivine saturation temperatures are lower than run temperatures, suggesting overheating or analytical overlap (Fig. 6.6B). If the melt inclusions were

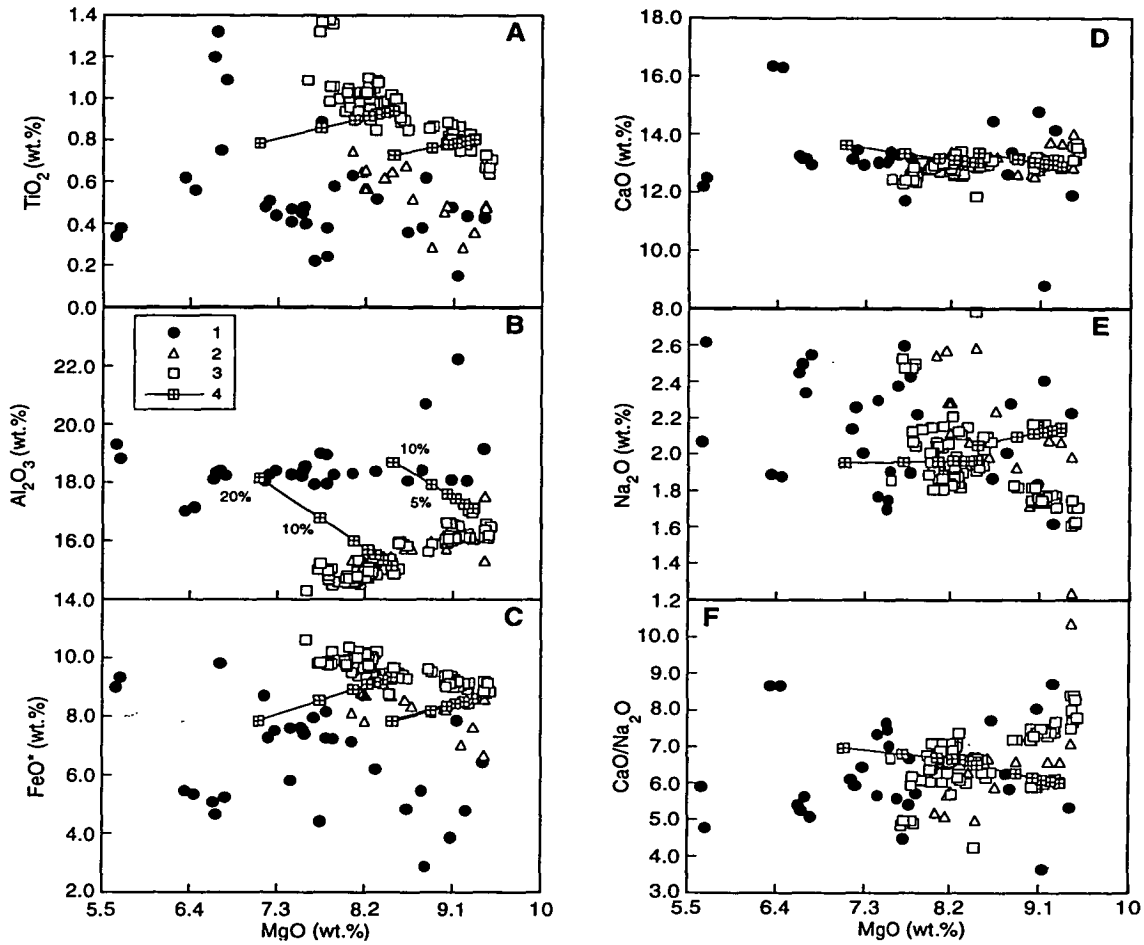

Figure 6.5: Variations in major element composition of homogenised melt inclusions in plagioclase from Hole 504B. The melt inclusions were homogenised in a vertical quench furnace by K. Johnson et al. (1995). Note that only analyses with totals >98.0 wt.% are plotted (some reported inclusion analyses have totals as low as 95.2 wt.% suggesting analytical problems). These analyses have also been corrected for inter-laboratory bias, as discussed in Appendix 1. The compositions of Hole 896A and 504B pillow-rim glasses, and homogenised melt inclusions in plagioclase from this study are shown for comparison. Plagioclase control lines show the effect of overheating inclusions with compositions similar to the Hole 504B pillow-rim glasses. See text for discussion. Symbols; 1- melt inclusions from K. Johnson et al. (1995); 2- melt inclusions from this study; 3- Hole 504B and 896A pillow-rim glasses; 4 - plagioclase control lines produced by adding variable amounts of plagioclase, An_{83} and An_{90}, to moderately evolved, 8.4 wt.% MgO, and primitive, 9.3 wt.% MgO respectively, Hole 504B pillow-rim glasses.

overheated and kept at high temperature (for up to 4 hours in the vertical furnace experiments), then they will have melted some of their host plagioclase. If this were the case, the melt inclusions would become saturated in plagioclase at the run temperature and so would have calculated plagioclase saturation temperatures that were similar to their trapping temperatures ($T_{trapping}$). However, the majority of melt inclusions have calculated temperatures that are lower than $T_{trapping}$, suggesting that the overheated compositions have been further modified by poor quenching (Figure 6.6A). Two of the melt inclusions have calculated temperatures that are higher than $T_{trapping}$, indicating analytical overlap, and this is consistent with the high, >20 wt.%, Al_2O_3 contents of these melt inclusions.

The effects of overheating a melt inclusion with a cotectic composition similar to those of the Hole 504B and 896A pillow-rim glasses can be simulated by the addition of a plagioclase component to the pillow-rim glasses (Fig. 6.5). Note that these calculations assume that the added plagioclase has a constant composition and that no diffusive exchange has occurred between the melt inclusion and its host. The addition of varying amounts of plagioclase define plagioclase control lines that link the pillow-rim glasses and the majority of melt inclusions from K. Johnson et al. (1995). An important feature to note is that although the addition of plagioclase causes major changes in Al_2O_3 and MgO contents (Fig. 6.5B), it has only a minor effect on CaO/Na_2O (Fig. 6.5F) or Ca#, i.e., the addition of 20% An_{83} increases the Ca# of the liquid by only 2 rel.%, and would therefore not affect the apparent equilibrium relationship between plagioclase and their melt inclusions cited by K. Johnson et al. (1995) and shown in Figure 6.7. An additional factor in the apparently unaffected CaO/Na_2O values may be re-equilibration with the host plagioclase; the time (4 hours) at high temperature may have been sufficient for the melt inclusions to equilibrate with their host plagioclase in terms of CaO and Na_2O.

Not all melt inclusion compositions can be related to the Hole 504B and 896A pillow-rim glasses by reasonable amounts of plagioclase addition or subtraction. Some melt inclusions have high, ~16.3 wt.%, or low, 8.8 wt.%, CaO contents (Fig. 6.5D), that may indicate the leakage, or decrepitation, of inclusions. Leakage of melt inclusions from Hole 504B may be enhanced by; fracturing (as described in section 5.6.3), or the size of the melt inclusions relative to that of the host crystal used in homogenisation experiments. The phenocrysts used by K. Johnson et al. were 0.7-1 mm diameter, similar to the size used in the present study, but, the analysed melt inclusions were larger (50-250 μm; in Figure 2 of K. Johnson et al. (1995)) than those used in the present study (<30 μm); melt inclusions >50 μm leaked in the majority of heating stage experiments. The presence of shrinkage bubbles in some reheated melt inclusions also

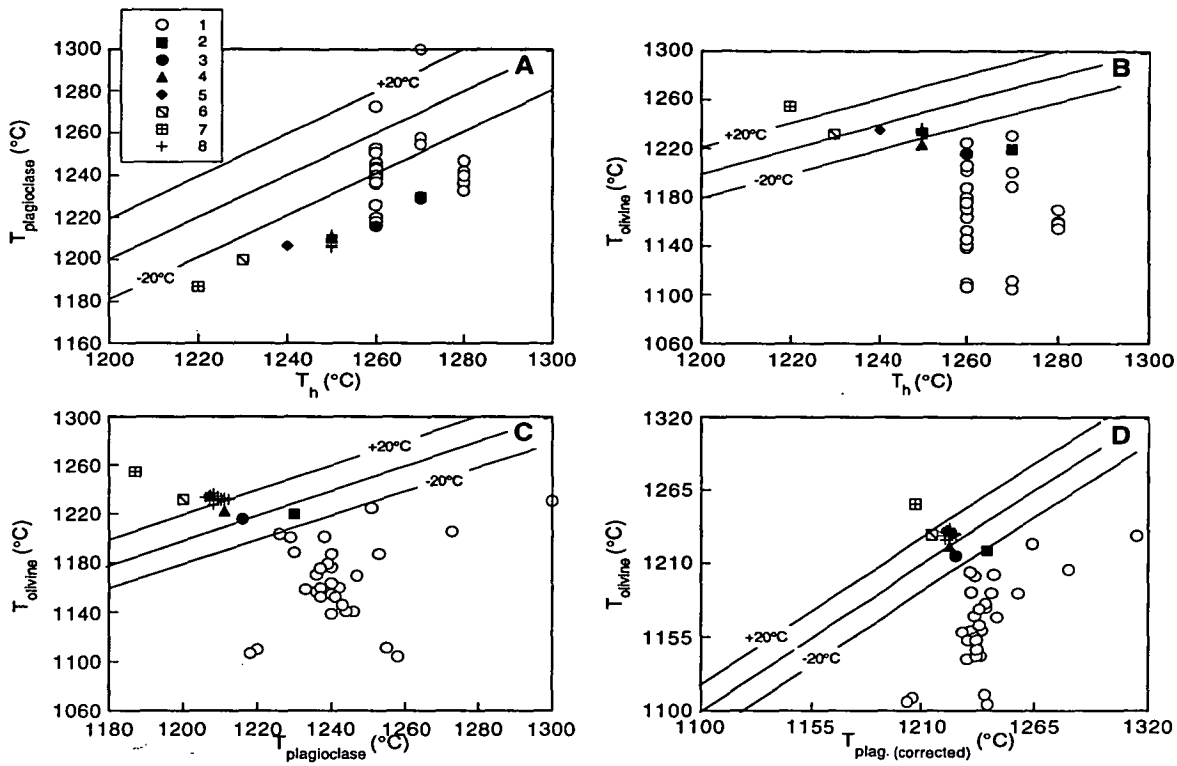

Figure 6.6: **A**, calculated plagioclase temperatures (using the plagioclase-melt thermometer of Weaver and Langmuir (1990)), and **B**, calculated olivine temperature (using the calibration of Ford et al. (1983)) versus run temperatures for melt inclusions in plagioclase homogenised in vertical quench furnace experiments. Data is from Hole 504B (K. Johnson et al., 1995) and the Gorda Ridge (Nielsen et al., 1995; R. Nielsen pers. comm., 1995). Calculated olivine temperature versus **C**, calculated plagioclase temperature, and **D**, corrected plagioclase temperature, using the correction of Danyushevsky et al. (1996). See text for discussion. Symbols; 1- melt inclusions from Hole 504B samples (K. Johnson et al., 1995); 2 to 7- Average melt inclusions from Gorda Ridge samples reheated to 1270, 1260, 1250, 1240, 1230, and 1220°C respectively (Nielsen et al., 1995); 8- Melt inclusions from a single An_{90} Gorda Ridge plagioclase reheated to 1250°C.

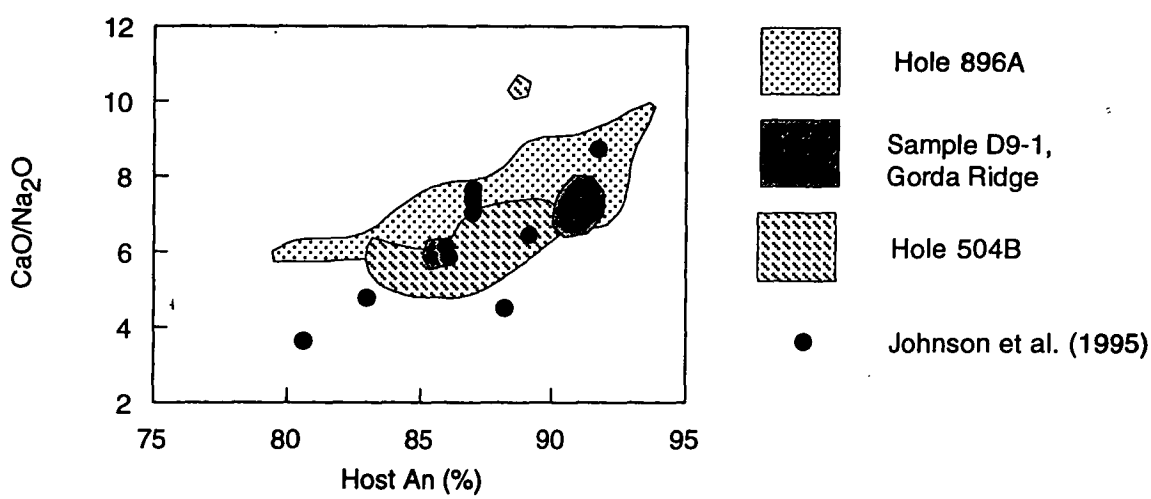

Figure 6.7: Host anorthite content versus melt inclusion CaO/Na_2O for inclusions from Hole 504B homogenised in a vertical quench furnace by Johnson et al. (1995). The fields of inclusions, homogenised in a heating stage as part of the present study, are shown for comparison. Note that the inclusions from Johnson et al. are interpreted to be overheated, and that this has not obviously affected CaO/Na_2O values, which are consistent with results from the present study.

suggest that leakage may have occurred.

The majority of melt inclusions have low FeO* and TiO_2 contents relative to the pillow-rim glasses (Figs. 6.5B and C) and at low MgO contents, FeO* and TiO_2 contents extend to much lower abundances than recorded for Hole 504B melt inclusions analysed in the present study. These lower abundances may indicate that the 'enhanced' depletion of these oxides, results from a combination of slow cooling and crystallisation, and re-equilibration during reheating at high temperatures (as discussed above).

In addition to the major element data, K. Johnson et al. (1995) report trace element compositions for selected reheated melt inclusions. These data were used to argue that, based on Sr/Sr* and Eu/Eu* values, there was little evidence for analytical overlap, and by implication overheating, in all but two melt inclusions (Fig. 6.8). These authors suggested that if the melt inclusions had been affected by analytical overlap or overheating, then both positive Sr/Sr* and Eu/Eu* anomalies should be evident. This is not necessarily the case; positive Sr/Sr* anomalies may also result from the assimilation of crustal material or mixing processes, as discussed in section 3.4.4, whereas the lack of positive Eu/Eu* anomalies may result from:

1. Analytical uncertainty, which is quoted to be >20 rel.% for Eu (K. Johnson et al., 1995). When this uncertainty is considered (Fig. 6.8), more melt inclusions may have positive Eu anomalies, particularly if analyses generally underestimate Eu contents.

2. Differences in relative abundances of Eu in plagioclase and melt inclusions. K. Johnson et al. (1995) do not present trace element analyses of the host plagioclase; however, this data was obtained for plagioclase of a similar composition from Hole 896A (J. Blundy, pers. comm., 1995) where Eu and Sm average 0.1 and 0.05 ppm respectively. As data for Dy is unavailable the ratio Eu/Sm is used as a proxy for Eu/Eu* as there is a strong correlation, between these ratios (Fig. 6.9). Results of calculations, simulating the overheating and addition of 20 wt.% plagioclase to melt inclusions HRN10/13 and HRN3/2, suggest that the Eu/Eu* values of melt inclusions with low Eu and Sm contents are most affected, increasing by 6 rel.% in this example, whereas those with high Eu and Sm contents are virtually unaffected, with Eu/Eu* increasing by 1 rel.%, well within analytical uncertainty as discussed above (Fig. 6.9).

3. Re-equilibration between host plagioclase and melt inclusion. This process should remove any Eu/Eu* anomaly and will be enhanced by the high temperatures, and times at elevated temperature, experienced by the melt inclusions in the vertical furnace experiments. Evidence for re-equilibration may be obtained from the compositional variations of plagioclase adjacent to the melt inclusions; however this data is not

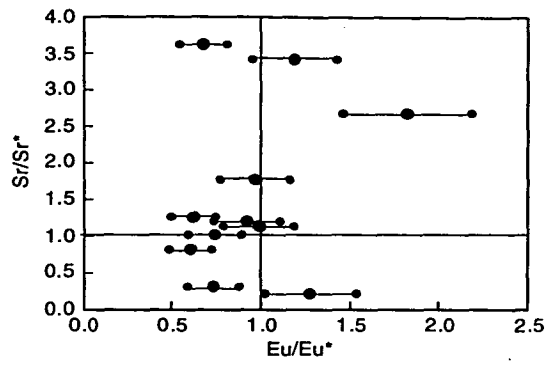

Figure 6.8: Sr/Sr* vs Eu/Eu* of homogenised melt inclusions in plagioclase from Johnson et al. (1995). These ratios were used by K. Jonhson et al. (op cit.) to infer that analyses with Eu/Eu* and Sr/Sr* values >1 were affected by ion beam overlap on samples or melting of plagioclase (overheating). Error bars give uncertainty in Eu/Eu* values given a 20 rel.% uncertainty in Eu analyses. See text for further discussion.

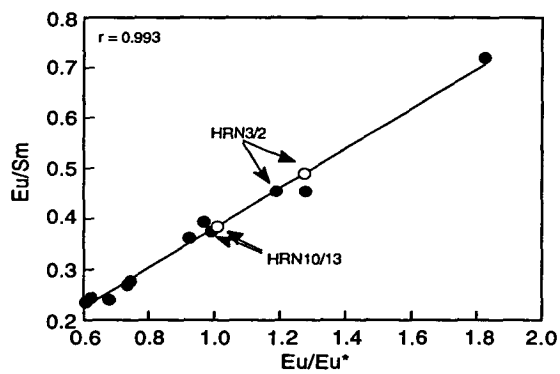

Figure 6.9: Eu/Sm vs Eu/Eu* for homogenised melt inclusions in plagioclase from K. Johnson et al. (1995). There is a good corelation between these two ratios. The effects of overheating on the Eu/Sm values of two melt inclusions (HRN3/2 and HRN10/13 with low and high Eu and Sm abundances respectively) were simulated by the addition of 20 wt.% plagioclase. 'Overheated' Eu/Eu* values were then calculated from the linear relationship between Eu/Sm and Eu/Eu* (the correlation coefficient for the straight line fit is 0.993). The 'overheated' melt inclusions are shown as open circles. See text for discussion.

reported. Re-equilibration between a melt inclusion and its host may also be enhanced by the movement of inclusions, i.e., slight temperature gradients in a phenocryst during experiments may lead to precipitation at the cold edge, and melting of the host mineral, at the hot edge of a melt inclusion, a phenomena that has been observed occasionally in high temperature experiments (L. V. Danyushevsky pers. comm., 1996).

In conclusion, the tests of major and trace element compositions of melt inclusions in plagioclase used by K. Johnson et al. (1995) are inadequate to demonstrate that their compositions do not result from overheating, poor quenching, and(or) analytical overlap. When the vertical furnace experimental data are interpreted using the procedures applied to data from the present study, it is apparent that the major element compositions of the majority of the melt inclusions are affected by overheating and probably poor quenching. The reported melt inclusion compositions, therefore, do not represent the composition of the trapped liquids and cannot be used to support interpretations of the petrogenesis of Hole 504B basalts.

This comparison highlights one of the main differences between the heating stage and vertical furnace experiments; in heating stage experiments fast heating can lead to homogenisation at a higher temperature than the trapping temperature (overheating), but, melt inclusion compositions, if quenched on homogenisation, should still correspond to that of the trapped liquid (see sections 2.6.3 and 4.4.4 for discussion). However, overheating in the furnace experiments where the inclusion is kept at a temperature $>T_{trapping}$ for some period of time, in this case 4 hours, allows time for the liquid in a melt inclusion to resorb the host crystal until they reach equilibrium, i.e., the inclusion becomes saturated with the host at the experimental temperature.

6.3.2 Sample D9-1, the Gorda Ridge

As stated in section 4.4.4, melt inclusions in plagioclase and olivine from Sample D9-1 were reheated at 1220-1270°C in a vertical quench furnace and results were reported by Nielsen et al. (1994, 1995). The intersection of the calculated olivine-plagioclase cotectic for the host glass and the compositional trend of the reheated melt inclusions, and the presence or absence of olivine daughter crystals, were used to infer a trapping temperature of 1250°C.

The composition of a single homogenised olivine-hosted melt inclusion, reported by Nielsen et al. (1995), was discussed in section 4.4.4, and on the basis of a high olivine-liquid Fe-Mg distribution coefficient, 0.36, and calculated olivine and plagioclase saturation temperatures, was interpreted to be overheated. This conclusion is consistent with trapping temperatures of 1205-1218°C obtained for olivines of $Fo_{86.5}$-$Fo_{89.5}$ using the heating stage (section 4.4.4).

The average composition of melt inclusions in plagioclase, reheated to 1250°C by Nielsen et al. (1995) and the average composition of inclusions in high-An plagioclase, from the present study are virtually identical (Fig. 6.10; Table 4.2). The similarity of these results poses two important questions:

1. Why do the two experimental techniques produce the same liquid composition at 1250°C (Nielsen et al., 1995) as at 1215-1227°C (the present study)? Such a temperature difference should lead to compositional variations, the result of overheating if the temperature estimates from the present study are correct, or underheating if the temperatures of Nielsen et al. (1995) are correct, as was seen for melt inclusions homogenised by these two techniques from Hole 504B (section 6.3.1) or the olivine-hosted inclusion discussed above. Two possible causes are problems with temperature control, and(or) poor quenching or analytical overlap with the host plagioclase.

The temperature calibration techniques for the heating stage experiments are detailed in section 2.4.2, and involve the use of Au grains, placed as close as possible (<300 μm) to the inclusions of interest, to calibrate temperature in each run, and to demonstrate that temperature differences in the working area are <10°C. Temperatures in the vertical quench furnace experiments are controlled using a Pt/Rh thermocouple placed ~10 mm from the sample. The hotspot in a vertical furnace is approximately 25 mm long and shows temperature variations of <2-3°C (K. L. Harris, pers. comm., 1997). Temperature control in both homogenisation techniques should therefore be sufficient to prevent the ~25-30°C discrepancy in estimated trapping temperatures.

If the true trapping temperature is 1250°C, as inferred by Nielsen et al. (1995), then the melt inclusions that were heated to 1215-1227°C in the present study should be underheated, i.e., homogenisation occurred at a lower temperature than trapping. Some plagioclase-hosted melt inclusions were interpreted to be underheated (as discussed in section 4.4.4), the result of incomplete crystallisation during reheating, but the compositions of the majority of melt inclusions were not affected by underheating. Underheating will result in incomplete melting of plagioclase that crystallised on the walls of the inclusion after trapping, and the inclusions will therefore be depleted in Al_2O_3, and enriched in MgO relative to the trapped liquid composition (see section 4.4.4 for discussion). For the melt inclusion compositions from the two studies to be similar it is necessary to infer that there was analytical overlap, and incorporation of a plagioclase component, in **all** analyses of melt inclusions in the present study. I consider such widespread analytical overlap to be unlikely and suggest that, based on Figures 4.21 and 4.22, the composition of melt inclusions is more likely to have been affected by poor quenching, common in relatively small inclusions such as those

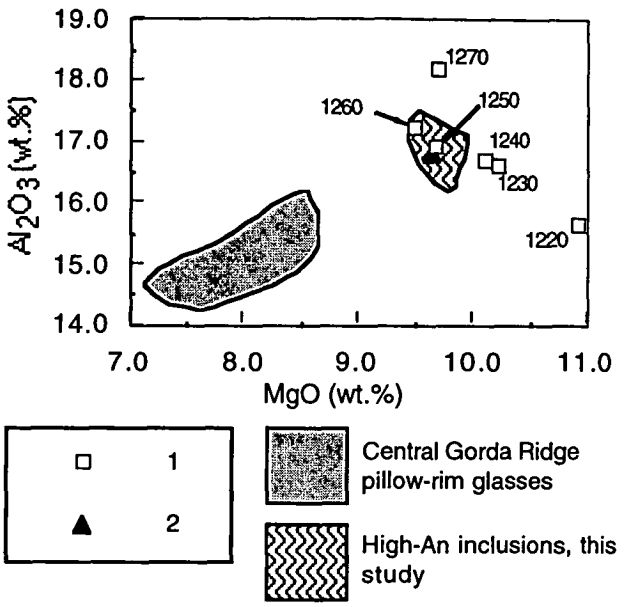

Figure 6.10: Compositions of homogenised melt inclusions in plagioclase from Sample D9-1. Symbols; 1- average composition of inclusions homogenised, at the indicated temperature, in a vertical quench furnace by Nielsen et al. (1995); 2 - average composition of homogenised high-An, An_{90}-An_{92}, hosted inclusions from this study. The fields of Central Gorda Ridge pillow-rim glasses and all homogenised melt inclusions in high-An plagioclase from this study are shown for comparison. See text for discussion.

analysed here. Poor quenching has the opposite effect to analytical overlap, further enriching the inclusions in MgO and depleting them in Al_2O_3.

If, however, the true trapping temperature is 1215-1227°C, then the melt inclusions from Nielsen et al. (1995) would have been overheated, and some of their host plagioclase melted, thereby enriching the melt inclusions in Al_2O_3 and depleting them in MgO. The removal of some plagioclase component is then required to produce consistent melt inclusion compositions. Poor quenching, resulting in the crystallisation of plagioclase on the walls of the melt inclusions, is a mechanism that would remove this plagioclase component. A calculation using the compositions shown in Figure 6.10 suggests that crystallisation of approximately 5 wt.% plagioclase is sufficient to produce the average 1230°C composition from the 1250°C composition. Quench modification is also suggested by low calculated plagioclase saturation temperatures, relative to run temperature (Fig. 6.5B).

Quench modification is therefore interpreted to have affected the majority of homogenised plagioclase-hosted melt inclusions analysed by K. Johnson et al. (1995) and Nielsen et al. (1995). This suggests there may be a problem with the efficiency of quenching of vertical furnace experiments, despite the short quench times claimed for

this technique (~0.5-1 sec.; R. Nielsen, pers. comm., 1996). Vertical furnace assemblies were tested and designed to quench liquidus experiments, which generally have high liquid to solid ratios rather than the very low liquid to solid ratios in melt inclusion homogenisation experiments. It therefore needs to be demonstrated that quenching of melt inclusions from a furnace is efficient, and that the quench rate is not significantly affected by factors such as, e.g., the size of the host phenocryst (much larger phenocrysts, up to 4 mm diameter, may be used in the furnace than in the heating stage, which is limited to crystals <1 mm in diameter and 300 μm in thickness).

2. What are the differences in the determination and verification of trapping temperature that lead to the conclusion that the same melt inclusion composition is on the plagioclase-olivine cotectic at different temperatures? Experiments using the heating stage rely on the direct observation of homogenisation, which will equal the trapping temperature if the melt inclusion was homogeneously trapped from a fluid-saturated liquid and the heating rate is suitable, as discussed in Chapter 2. However, the homogenisation process cannot be directly observed in vertical quench furnace experiments, and indirect evidence must be used to establish trapping temperatures. Nielsen and co-workers largely rely on the presence or absence of olivine daughter crystals in plagioclase-hosted melt inclusions; crystallisation is interpreted to have been cotectic, and the temperature at which the olivine daughter crystals melt is the trapping temperature. Further heating will lead to the melting of the host plagioclase and thus a non-cotectic composition. There are two problems with this logic:

A. Non-representative melt inclusion compositions. Clocchiatti and Massare (1985) demonstrated that melt inclusions in plagioclase from continental settings, can be used as 'experimental crystallisation environments', in which the compositions and appearance of daughter phases can be used to interpret the crystallisation history of the trapped liquid.

As an example, daughter olivines formed in many Sample D9-1 melt inclusions during homogenisation experiments. Daughter olivines ($Fo_{88.7}$-$Fo_{89.5}$) were large enough for analysis in only two plagioclase phenocrysts, $An_{91.1}$-$An_{91.4}$ (see Appendix 4.7 for full analyses). Melt inclusions from these experiments, P109 and P118, were underheated, and their compositions are therefore unreliable, however good homogenised inclusions in plagioclase, An_{91}-$An_{91.8}$, from Sample D9-1 have an average Mg' of 71.3 and are in equilibrium (using an olivine-liquid Fe^{2+}-Mg exchange coefficient of 0.3, and a melt Fe^{2+}/Fe^{3+} of 7.9) with olivine of Fo_{89}, i.e., the composition of the daughter olivines. However, the compositions of many plagioclase-hosted melt inclusions may be affected by low-FeO* contents (especially those from Holes 896A and 504B). In these melt inclusions, the daughter olivines will have more forsteritic

compositions than olivine in equilibrium with the trapped liquid and this may have two implications; first, the daughter olivines will not give a reliable estimate of the cotectic olivine composition and second, the non-equilibrium daughter olivines may not melt at the true trapping temperature, and may persist to higher temperatures, as they have higher than equilibrium Fo contents.

B. The kinetics of melting daughter olivine. Coarse, <1-2 μm, olivine daughter crystals formed in some experiments done in the present study (Fig. 6.11). Coarse olivine did not nucleate in the majority of melt inclusions which hosted fine grained aggregates of olivine that melted prior to homogenisation (Fig. 4.18E), and there was no apparent correlation between melt inclusion size and the formation of coarse olivine, except that melt inclusions which leaked during experiments crystallised variable amounts of coarse olivine. The coarse olivine was not easily melted, possibly a result of surface area to volume ratios, and in some experiments did not melt when the melt inclusions were held at T_h for 5-10 min. Overheating appears to be required to melt the coarse olivine daughter crystals, and this may explain the persistence of these crystals at 1240-1250°C, in the vertical quench furnace experiments.

To investigate the persistence of olivine daughter crystals, at temperatures $>T_h$, a series of three experiments were run (at 1250 and 1260°C) using the heating stage. Run conditions were as close as possible to those used by Nielsen and co-workers; the only difference being the rate of initial reheating: Temperature were increased to 1000°C over a period of 3-4 min in the heating stage runs, versus several seconds in the vertical furnace experiments (see section 2.4.2). In the heating stage experiments most small and medium sized melt inclusions (<30-40 μm diameter) were homogeneous by 1235-1240°C (higher than reported in section 4.4.4, a result of the faster heating rate) whereas those large melt inclusions that did not decrepitate, homogenised after ~40 min. at run temperature (1250-1260°C). Coarse olivine daughter crystals were formed during one experiment and were melted after approximately 15 min. at 1250°C. These observations indicate that homogenisation occurred at lower temperatures than 1250°C, but, that overheating, and waiting at this temperature will lead to homogenisation of large melt inclusions and the melting of coarse daughter olivine that was not possible in runs at the true homogenisation temperature (1215-1227°C). These results clearly demonstrate that reliance on the disappearance of large daughter olivine crystals will lead to incorrect (high) estimated trapping temperatures.

6.3.3 Summary

A detailed comparison of the results of heating stage and vertical quench furnace homogenisation experiments on samples from Hole 504B and the Gorda Ridge, indicate

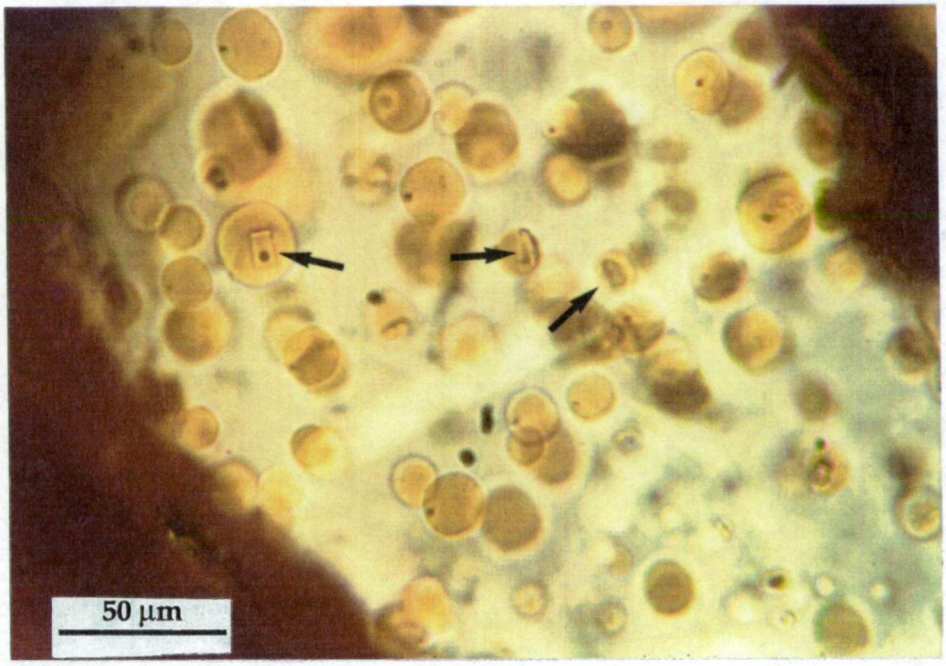

Figure 6.11: Photomicrograph of melt inclusions with coarse daughter olivines (indicated by arrows). The coarse daughter olivines did not crystallise in all melt inclusions, but, when formed the olivines did not melt, even after some time at T_h. Plane light; experiment P118 at 1200°C (considered to be the homogenisation for this experiment).

that significantly different interpreted trapping temperatures and trapped liquid compositions may result. Differences in the inferred trapping temperatures result from the inability to observe phase changes in melt inclusions during reheating in vertical quench furnace experiments, and the lack of consideration of the kinetics of melting daughter olivine in melt inclusions. A result is that trapping temperatures are inferred to be higher for vertical quench furnace experiments than the heating stage experiments, and that the melt inclusions were overheated, most obviously those in plagioclase from Hole 504B and the single olivine from the Gorda Ridge. Overheating was also a problem for melt inclusions in heating stage experiments done as part of the present study, a result of the kinetics of melting. However, the smaller amount of overheating (generally 5-10°C rather than the 20-30°C of vertical quench furnace experiments) and the ability to quench an experiment as soon as homogenisation was observed, prevented the significant melting of the host mineral and re-equilibration, interpreted to occur in the vertical furnace experiments. Problems associated with temperature control of experiments, and in particular, modification of inclusion compositions during quenching, have also contributed to differences in experimental results.

6.4 Summary

The results of detailed studies, including homogenisation experiments, of melt inclusions in plagioclase and olivine phenocrysts from MORB samples indicate that the melt inclusions can provide information on trapped liquid compositions, and crystallisation temperatures.

It has been demonstrated that if the trapped liquids were fluid saturated and due attention is paid to the kinetics of reheating, then trapping, i.e., crystallisation, temperatures can be reliably estimated for plagioclase- and olivine-hosted melt inclusions.

Homogenised melt inclusions in plagioclase phenocrysts are interpreted to recover trapped liquid compositions in terms of Al_2O_3, MgO, CaO, Na_2O and generally K_2O abundances; whereas homogenised or recalculated naturally quenched melt inclusions in olivine recover TiO_2, Al_2O_3, MgO, CaO, Na_2O and K_2O abundances, and naturally quenched melt inclusions in spinel recover TiO_2, CaO, Na_2O and K_2O abundances.

Low TiO_2 and FeO* and high SiO_2 contents in plagioclase-hosted melt inclusions, from all studied suites, are not related to trapped liquid composition, but are most likely a result of re-equilibration processes, although this is not proven. The majority of Sample D9-1 olivine-hosted melt inclusion, and one inclusion from Hole 896A, compositions were affected by variable, typically high, FeO* contents that have not previously been reported in detailed studies of olivine from MORB (e.g., Sobolev et al., 1989). The origin of high-FeO* contents in these melt inclusions is not understood, but spinels included in olivine from Sample D9-1 also show atypical compositional variations. Naturally quenched melt inclusions in spinel may have variable Al_2O_3, FeO*, SiO_2 and(or) MgO contents, possibly a result of re-equilibration. Some of the spinel inclusions were also heterogeneously trapped, with plagioclase crystals, and this suggests that care should be taken when homogenising opaque phases, to avoid the effects of melting such crystals.

On the basis of results from the three suites, I would suggest that the best approach to using melt inclusions is to examine inclusions from all cotectic phases, in combination with detailed petrography and mineral chemistry, to determine the relationships between individual phenocryst phases, and between the phenocrysts and their host pillow-rim glasses. This approach should allow the identification of irregularities in melt inclusion composition and homogenisation behaviour that are related to trapping effects, but, which may be interpreted as primary liquid variations if melt inclusions in only one phenocryst phase are studied.

The differences in trapping temperatures and homogenised melt inclusion compositions between experiments using the vertical quench furnace and the visual heating stage techniques, are interpreted to be a result of the experimental methods used. Overheating of melt inclusions in vertical quench furnaces results from the inability to observe the moment of homogenisation and a lack of consideration of kinetic processes in the melting of daughter phases, in particular olivine. Additional factors include modification of melt inclusion compositions during quenching.

Chapter 7

The Petrogenesis of Hole 896A/504B and Central Gorda Ridge MORB

7.1 Introduction

In this chapter I address the third aim of the present study, i.e., to use the petrological information obtained from primitive phenocrysts, and the melt inclusions that they host, to recover primary MORB melt compositions, and to assess the conditions of melt generation and segregation in the mantle. Data from both the Costa Rica Rift (Holes 896A and 504B) and the Gorda Ridge (Sample D9-1) will be considered. The nature of liquids that crystallise the high-An (An_{88}-An_{94}) plagioclase characteristic of the samples used in the present study, are also discussed and comments made on the failure of some experimental studies to reproduce plagioclase of this composition.

7.2 Primary melt compositions and mantle melting

The compositions of melt inclusions in primitive olivine (>Fo_{88}), plagioclase (>An_{88}) and Cr-Al spinel from all three studied suites provide no evidence for the presence of liquids that could be individual melt fractions produced by polybaric melting in the ascending mantle. The liquids trapped to form the melt inclusions may therefore be aggregated, i.e., mixed, polybaric melts or the fractionation products of isobaric batch melts.

As discussed in section 1.1.1, isobaric batch melts are true primary melts, i.e., they are liquids that were in equilibrium with their residual mantle assemblage at the depth of segregation (Hess, 1992). The compositions of isobaric batch melts can be used to infer the temperature, depth and extent of melting for a given mantle composition by comparison with experimental melting studies (e.g., Jaques and Green, 1980; Falloon and Green, 1988).

Aggregated liquids produced during polybaric melting, either by fractional-continuous or equilibrium melting processes, are not true primary melts, but, their compositions can be inverted to obtain estimates of the extent and initial and final depths of melting. Parameterisations include those of Niu and Batiza (1991b), based on

the equilibrium melting experiments of Jaques and Green (1980), and the exchange coefficient based parameterisation of Langmuir et al (1992), with the additional constraints outlined by Shen and Forsyth (1995). A practical disadvantage of these parameterisations is that they require recalculation of liquid compositions to 8.0 wt.% MgO, to account for the effects of fractionation; problems with this procedure have been discussed by Albarede (1992), Shen and Forsyth (1995) and Bedard and Hebert (1996).

The nature of isobaric batch and polybaric fractional-continuous and equilibrium melts, and implications for melting and segregation conditions, for samples from the Costa Rica Rift (Holes 896A and 504B) and the Gorda Ridge (Sample D9-1) are discussed in the following sections.

7.2.1 Batch melting

Holes 896A and 504B

As discussed in sections 3.5.1 and 5.7.3, the compositions of melt inclusions suggest that plagioclase An_{94} crystallised from liquids with major element compositions similar to the most magnesian pillow-rim glasses. These glasses were in equilibrium with olivine, Fo_{86}-Fo_{87} suggesting (especially as olivines of up to $Fo_{89.5}$ were found in all Hole 896A glass groups) that the plagioclase crystallised from relatively evolved liquids. A period of olivine-only crystallisation therefore preceded cotectic plagioclase-olivine crystallisation.

Heating stage experiments with melt inclusions in olivine, ~Fo_{88}, have been shown to be unreliable due to underheating and magnetite precipitation (section 3.4.4), and these melt inclusions cannot be used to characterise melt compositions in the olivine-only field. However, compositions of primary melts can be estimated by calculations of the reverse of olivine crystallisation from the composition that corresponds to the start of cotectic crystallisation (i.e., the most primitive pillow-rim glasses from groups 1 and 3).

As discussed above, the primary melts for each glass suite can be defined as those melts in equilibrium with the most magnesian olivine sampled. Although olivine of $Fo_{91.6}$ was found in Hole 896A glass group 2 samples only, the similarity of mineralogical features between all glass groups, from Holes 896A and 504B, suggests that this is probably a sampling effect, related to the small number of olivine phenocrysts recovered, and all glass groups are interpreted to have been derived from melts in equilibrium with olivine of this composition.

Compositions of primary melts for groups 1 and 3 were calculated from the

compositions of the most primitive glasses from these groups. Using the Petrolog program (Danyushevsky et al., 1990), olivine was added to the glass compositions until they were in equilibrium with olivine $Fo_{91.6}$ (the most primitive olivine sampled). Melt Fe^{2+}/Fe^{3+}, required for this calculation, was assumed to be 7.9 from calculations described in section 3.3.3. Approximately 15 wt.% olivine addition was required by these calculations and the resultant parental melt compositions are given in Table 7.1. The range of CaO/Na_2O values displayed by melt inclusions from glass groups 1 and 3, being independent of variations in other elements, should reflect variations in CaO/Na_2O values of primary melts for each group. For group 1, this range is 6.0 to 9.8, for group 3 it is 7.0 to 8.4. However, apart from lower H_2O in group 3 pillow-rim glasses, there is no evidence to suggest that other elements varied significantly in primary melts for these two groups.

Some pillow-rim glasses from the group 2+ 2*+3* trend (composed of pillow-rim glass samples from both Holes 896A and 504B), have compositions that are similar, in terms of MgO (9.46 wt.%), to the most primitive group 1 and 3 glasses. However, it is unclear, based on the range in compositions of plagioclase phenocrysts and their melt inclusions from groups 2, 2* and 3* samples, that this most primitive liquid marks the start of cotectic plagioclase-olivine crystallisation and calculations of the primary melt were not attempted. However, as Mg-Fe covariations of these glasses are indistinguishable from those of group 1, it is interpreted that the primary melt for this group had similar MgO to group 1, but lower CaO/Na_2O and CaO/Al_2O_3, and higher TiO_2 and Al_2O_3. These differences may have been produced by lower degrees of melting of the same source as the group 1 melts (Jaques and Green, 1980; Fuji and Scarfe, 1985; Falloon and Green, 1987; Falloon and Green, 1988). A similar source is indicated by trace element (Fig. 3.5), H_2O (Figs. 3.3 and 3.6) and K_2O (Fig. 3.6) contents, which show little variation between glass groups 1, 2, and 4.

Using the data of Jaques and Green (1980), Falloon and Green (1988) and Falloon et al. (1988) the estimated primary melts fall close to the olivine-orthopyroxene-clinopyroxene±spinel cotectic for Tinaquillo lherzolite or MORB Pyrolite-90 (MPY-90) at approximately 18 kb on the CIPW normative basalt tetrahedron (Fig. 7.1). The extent of partial melting is estimated to be ~25%, for both groups 1 and 3, using the parameterisation of Niu and Batiza (1991b), and this estimate is consistent with the projected position of these melts close to the clinopyroxene-out curve (22-30% melting) on Figure 7.1A. The higher CaO/Na_2O values, up to 9.8 (vs, 7.7 from pillow-rim glasses), of some group 1 melt inclusions

Table 7.1. Primary isobaric batch melt compositions, Hole 896A.

[a]Sample	1	2	3
SiO_2	47.84	47.71	48.18
TiO_2	0.57	0.61	0.61
Al_2O_3	13.85	13.95	14.38
Fe_2O_3	1.16	1.03	1.12
FeO	8.24	7.55	7.94
MnO	0.10	0.13	0.10
MgO	15.13	15.36	14.69
CaO	11.59	11.82	11.38
Na_2O	1.40	1.40	1.49
K_2O	0.02	0.06	0.02
P_2O_5	0.03	0.05	0.03
Cr_2O_3	0.07	0.34	0.06
Total	100.00	100.00	100.00
Pressure (kb)		20	
Temperature (°C)	1348	1450	1340

[a]1, estimate calculated from Sample 148-896A-27R-1, Pc.15 (group 3); 2, Run T4107 (T. J. Falloon pers. comm., 1997); 3, estimate calculated from Sample 148-896A-3R-1, Pc.4. (group 1)

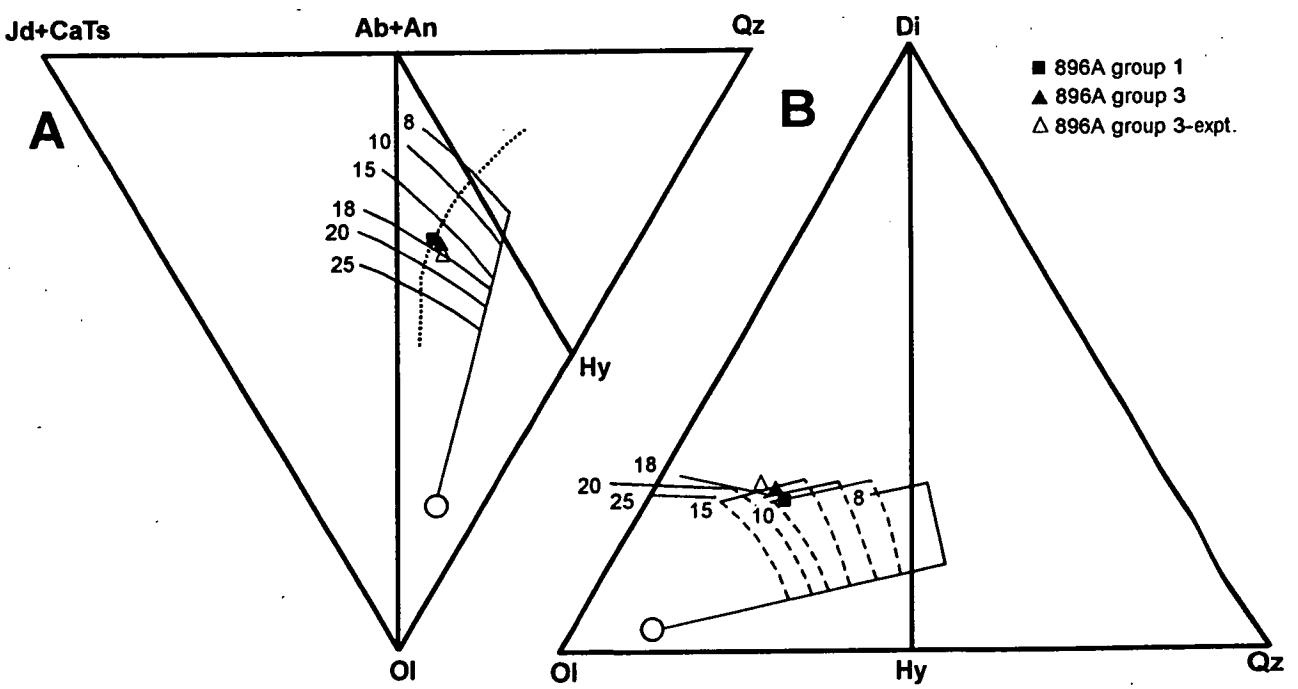

Figure 7.1: Results of olivine addition calculations and basalt-peridotite sandwich experiments (T. J. Falloon pers. comm., 1997) plotted in the CIPW molecular normative basalt tetrahedron. Projections from Diopside (Di) onto the base jadeite+calcium tschermaks molecule (Jd+CaTs)-quartz (Qz)-olivine(Ol) in **A**, and from plagioclase (Ab+An) onto the face Di-Qz-Ol (**B**). Lines shown on projections are cotectics at a range of pressures(8-25 kb) for a MORB Pyrolite-90 (MPY-90; Falloon and Green, 1988) source mantle. The dotted line on A is the approximate location of the clinopyroxene-out reaction for MPY-90(from Falloon et al., 1988). All Hole 896A data are consistent with segregation from a MPY-90 source at approximately 18 kb.

are interpreted to result from higher extents of partial melting of the same source (Jaques and Green, 1980; Fuji and Scarfe, 1985).

The results of basalt-peridotite sandwich experiments (using the primitive liquid calculated from Sample 148-896A-27R-1, Piece 15 and peridotite MM-3, from Baker and Stolper, 1994) indicate that the group 3 primary liquid could be in equilibrium with a lherzolite residue at 20 kb and 1450°C (T. J. Falloon, pers. comm., 1997). Note that the experimental and calculated primary melt compositions plot very close in the normative basalt tetrahedron (Fig. 7.1) despite differences in FeO and MgO contents (Table 7.1). This is a function of the norm recalculation that masks FeO/MgO variations. The differing FeO and MgO contents are partly an artefact of olivine-liquid Fe^{2+}-Mg exchange coefficients that change with pressure (or temperature (Sobolev and Danyushevsky, 1994) and(or) liquid composition (Langmuir et al., 1992)). The calculated group 3 liquid is in equilibrium with $Fo_{91.6}$, at 1 atm using a k_d of 0.3 (Roeder and Emslie, 1970), but, the 20 kb experiment is in equilibrium with $Fo_{91.6}$ at a k_d of 0.34 (consistent with the high-pressure determinations of olivine liquid exchange coefficients of Takahashi and Kushiro (1983) and Ulmer (1989) and the temperature dependant estimate of Sobolev and Danyushevsky (1994)).

Sample KK2-83-NP-D9-1

In contrast to Holes 896A and 504B, mineralogical evidence suggested that cotectic olivine-plagioclase occurred very early in the crystallisation history of Sample D9-1. Plagioclase, ~An_{94} is interpreted to have crystallised with the most primitive olivine sampled, Fo_{90}, a composition that could be in equilibrium with a residual mantle assemblage. However, the compositions of melt inclusions in both primitive olivine and plagioclase are affected by post-trapping modification (Chapter 6) and therefore must be interpreted with care. Two primitive melt inclusions in olivine (recalculated naturally quenched compositions in $Fo_{89.9}$-Fo_{90}; Table 7.2) were selected as candidates for primary melts, on the basis of; higher CaO and Al_2O_3 and lower Na_2O contents than the average high-An plagioclase-hosted melt inclusions, and the lowest FeO* contents of olivine-hosted melt inclusions for their host forsterite content.

When the compositions of the two recalculated naturally quenched melt inclusions in olivine are plotted on projections of the CIPW normative basalt tetrahedron, they lie well above the mantle cotectics, and are therefore not in equilibrium with the mantle at any reasonable (>8 kb) pressure (Fig. 7.2). The high normative diopside (Fig. 7.2) is a function of the high CaO contents of these melt inclusions (13.15-13.69 wt.%) and requires that olivine be added to reach equilibrium with mantle assemblages, an observation consistent with experimental results suggesting

Table 7.2. Compositions of melt inclusions in primitive olivine, Sample D9-1.

Analysis	[a]$Fo_{89.8}$	Fo_{90}	Ave. An_{90}
SiO_2	49.60	48.67	50.34
TiO_2	0.69	0.68	0.31
Al_2O_3	16.58	16.66	16.83
[b]FeO*	7.65	7.80	7.74
MnO	0.12	0.16	0.14
MgO	10.40	10.73	9.64
CaO	13.15	13.72	13.10
Na_2O	1.69	1.45	1.78
K_2O	0.03	0.03	0.03
P_2O_5	0.06	0.03	0.03
Cr_2O_3	0.03	0.07	0.07
Total	100.00	100.00	100.00
CaO/Na_2O	7.8	9.4	7.4

[a] homogenised and recalculated melt inclusions in olivine phenocrysts $Fo_{89.8}$ and Fo_{90}. Average An_{90} is the average of all 'good' homogenised melt inclusions in plagioclase An_{90}-An_{92}.

[b] All Fe as FeO.

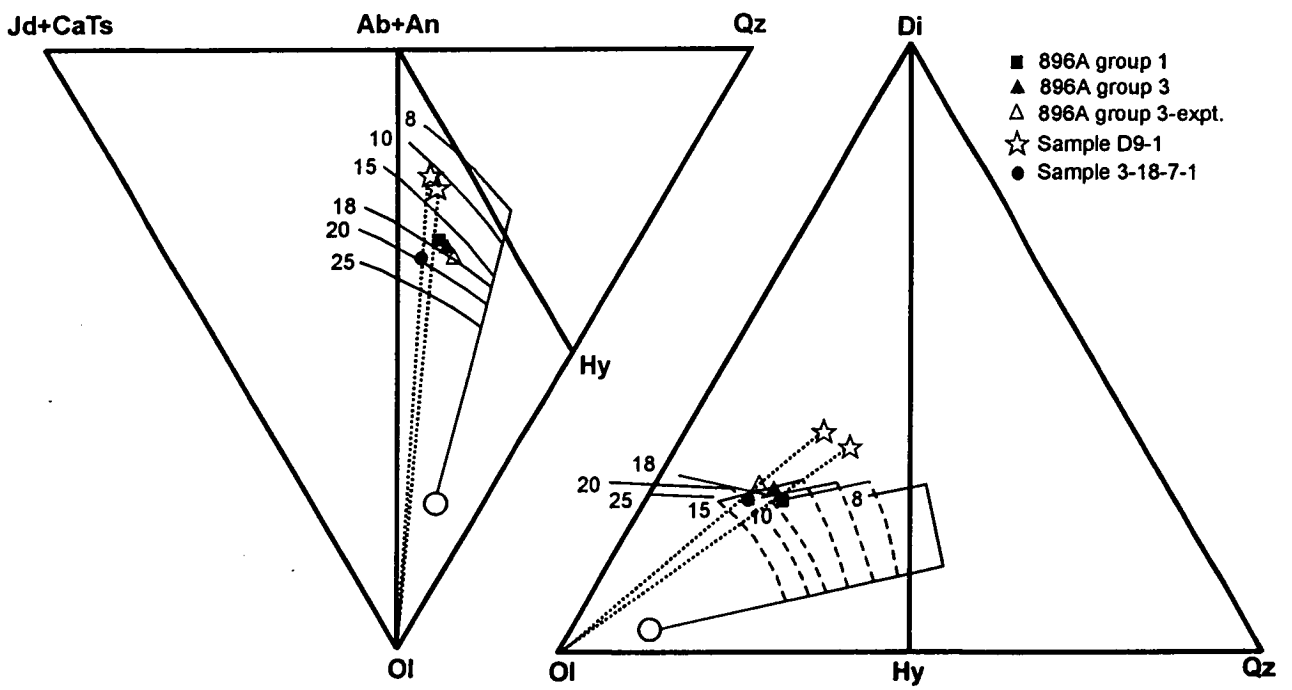

Figure 7.2: Calculated ane experimental primitive liquid compositions from the Costa Rica Rift, melt inclusions in ~Fo_{90} from Gorda Ridge samples and experimental results for Sample DSDP 3-18-7-1+18% olivine (Green et al., 1979) plotted in the CIPW molecular normative basalt tetrahedron in projections from diopside and plagioclase. Dashed lines are olivine control lines linking primitive Sample D9-1 olivine-hosted melt inclusions and possible primary melts. These projections coupled with the olivine projection (Fig. 7.3) indicate that the Sample D9-1 primary liquids may have segregated from a MPY-90 source at 18-20 kb.

that no primitive MORB glasses are in equilibrium with a mantle source (Falloon and Green, 1988; Baker and Stolper, 1994; Kushiro, 1996).

Without olivine more primitive than Fo_{90}, it is unclear how much olivine should be added to the primitive Sample D9-1 liquids; an alternate approach is to examine the melt inclusion compositions in the normative basalt tetrahedron using a projection from olivine, as this projection will minimise the effects of olivine fractionation (Fig. 7.3). When plotted in this projection, the Sample D9-1 melt inclusions lie in similar positions as the Hole 896A calculated and experimental primary liquids, indicating equilibrium with possible mantle sources (MPY-90) at >10 kb. The primary liquids for Sample D9-1 could be estimated by reversing the effects of olivine fractionation until their normative compositions lie on a mantle cotectic in the projection from diopside. However, at this point a second problem arises; the melt inclusions in olivine are affected by higher than predicted FeO* contents (section 4.4.4; Fig. 4.28). This suggests that olivine addition calculations would be unreliable, as was the case with many recalculated melt inclusion compositions in olivine from Sample D9-1. An alternative is to project the Sample D9-1 composition along olivine control lines on both the diopside and plagioclase CIPW-norm projections. Figure 7.2 shows that these olivine control lines pass through the projected position of the Costa Rica Rift (and DSDP 3-18-7-1, as discussed below) primitive liquids, suggesting similar segregation conditions, i.e., 18-20 kb.

Discussion

These results have two major implications:

1. Previous studies of Hole 504B samples have suggested that multi-stage melting, as described by Duncan and Green (1980) and Duncan and Green (1987) , may be an important process in the genesis of Costa Rica Rift basalts (Autio and Rhodes, 1983; Natland et al., 1983; Kempton et al., 1985; Autio et al., 1989). However, the results of olivine addition calculations described above suggest that the majority of erupted basalts may be sourced by variable degrees of melting at a constant pressure and second-stage melting is not required.

2. The similarity of experimental results, indicating melting at ~18-20 kb and 1450°C, for the group 3 liquid and those for glasses DSDP 3-18-7-1 (Mid-Atlantic Ridge; (Green et al., 1979)) and 95-1 (Lau Basin; Falloon et al. (1997)) suggest a common process operating at a range of spreading rates in differing tectonic settings. The nature of this process is not known but the common depth may reflect a point at which the melt is no longer stable in the residuum and separation occurs during adiabatic

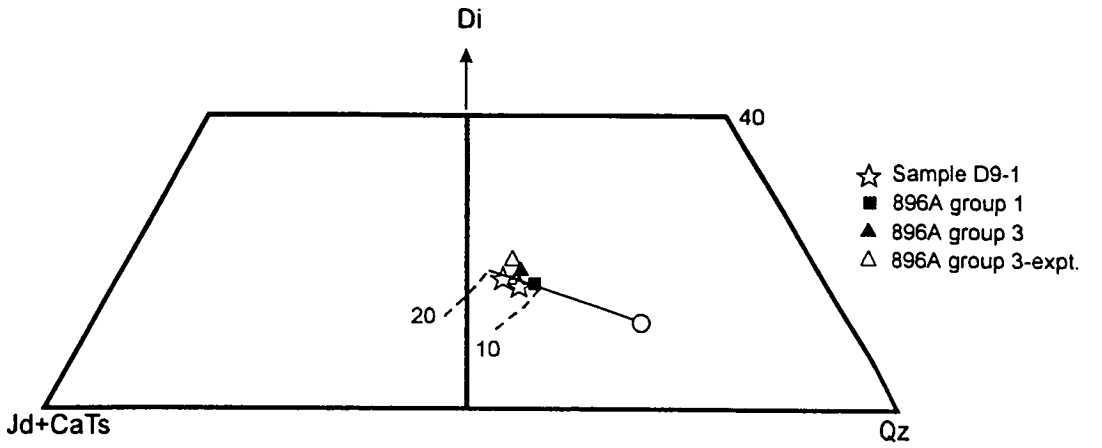

Figure 7.3: Primitive liquid compositions from Costa Rica Rift and Gorda Ridge samples plotted in the CIPW molecular normative basalt tetrahedron. Projection from olivine onto the face Di-Jd+CaTs-Qz. The lines are cotectics at 10 and 20 kb for a MPY-90 source composition (from Falloon et al., 1997). Note that all liquids shown are consistent with melting at 10-20 kb.

ascent commences, a function of the temperature (and thus extent of melting) of the upwelling mantle.

7.2.2 Polybaric melting

Three constraints can be placed on the results of quantitative melting models: 1) The rate of pressure-release melting which is estimated to be 1-2%/kb (Cawthorn, 1975; Ahern and Turcotte, 1979; McKenzie, 1984; McKenzie and Bickle, 1988). 2) The maximum extent of melting (F_{max}), which is largely controlled by the abundance of clinopyroxene in the source peridotite, and is estimated to be 22-30 modal % (Hess, 1992). 3) The depth of initial (P_o) and final (P_f) melting. The depth of initial melting is constrained by trace element data requiring that garnet be one of the stable aluminous phases in the residual mantle (Gast, 1968; Salters and Hart, 1989), i.e., melting commenced in the garnet or garnet+spinel peridotite fields (>20 kb). However, the final depth of melting is not well constrained, but, is considered to be deeper than the base of the crust (Moho) on the basis of seismic evidence suggesting that melting stops at < 10 kb at slow-spreading ridges ((Zhang and Tanimoto, 1993)), phase changes in the ascending mantle (Asimow et al., 1995) , the likelihood of conductive cooling as discussed by Shen and Forsyth (1995) and the presence of excess olivine (implying

crystal fractionation) in many abyssal peridotites (Niu, 1997).

With these constraints in mind, I will evaluate available quantitative polybaric melting models using major element variations of Costa Rica Rift and Gorda Ridge samples (the values of major element oxides for each pillow-rim glass group normalised to 8.0 wt.% MgO and used in these calculations are given in Table 7.3).

1. Niu and Batiza (1991b). This model is based on extrapolation of the batch melting experimental results of Jaques and Green (1980) and assumes near fractional melting (1% melt increments) after an initial period of 5% batch melting, during adiabatic ascent. For Hole 896A and 504B samples, melting both commences and ceases within a narrow depth range, i.e., 23-27 kb and 11 kb respectively. The extent of melting is similar for all groups (Table 7.3) and is consistent with group 3 being the most depleted, with lower $(La/Sm)_n$ than the other two groups (0.29 vs 0.31-0.34).the extent of melting for all groups, 20-25%, is consistent with estimates of modal clinopyroxene abundances, and the melting rate for Costa Rica Rift samples (1.5%/kb) is consistent with thermodynamic estimates. Melting to produce the Costa Rica Rift basalts also commences in the spinel-garnet peridotite transition zone. However, Sample D9-1 has a shallower P_o (20 kb) and a higher melting rate (2.2%/kb).

2. Langmuir et al. (1992). A quantitative model, the" standard model", was developed by combining melting, mixing, and chemistry functions using experimentally determined mineral-liquid exchange coefficients. The standard model assumes melting at 1.2%/kb and aggregated melts were calculated for melting, starting with 2% melting at a given initial depth (from 12-40 kb) and terminating at the base of the Moho (2 kb). Both the fractional and equilibrium end-member melting processes were considered (Fig. 7.4). The Holes 896A and 504B and Sample D9-1 do not appear to be consistent with equilibrium melting, instead falling close to the mantle melt curve for fractional melts with an initial pressure of melting (P_o) of 25-32 kb. These results are therefore consistent with the commencement of melting in the garnet peridotite stability field, however, the model is unrealistic in that it requires melting to continue to the base of the mantle, and thus produces higher maximum extents of melting (30-36%) that are inconsistent with the observed clinopyroxene abundances in peridotites.

The calculated primary melts for Hole 896A groups 1 and 3 (representing possible aggregate liquids at the onset of olivine crystallisation, i.e., at the start of fractionation) do not fall on the pooled fractional melt curve, however, but are closer to the equilibrium melt curve (Fig. 7.5). Additionally, estimates of crustal thickness at the Costa Rica Rift when compared with Na8 are more consistent with equilibrium melting than fractional

Table 7.3. Corrected Oxide values for Holes 896A and 504B and Sample D9-1 accumulated liquids and calculated mantle melt parameters.

Sample	[a]Si8	Ti8	Al8	Fe8	Ca8	Na8	[b]P(0) kb	P(f) kb	F (wt.%)	[c]K_2O/ TiO_2	[d]Na(8,0.1)	Fe(8,0.1)
Group 1	51.01	1.02	14.59	10.24	12.99	1.90	25	11	23	0.022	2.28	9.40
Grp. 2+2*+3*	50.80	0.99	15.07	9.90	13.22	2.02	23	11	22	0.025	2.39	9.09
Group 3	50.65	0.89	14.23	10.58	13.41	1.79	27	11	25	0.030	2.10	9.83
D9-1	50.69	1.25	15.35	9.48	12.09	2.30	20	11	20	0.061	2.50	9.15

[a]Oxide values corrected to 8.0 wt.% MgO to remove the effects of fractionation. Corrections were done by recalculating along lines of best fit for the pillow-rim glass data (in the case of Group 3 where only glasses with > 9.0 wt.% MgO were analysed, it was assumed that the LLD paralleled the Group 1 LLD but offset by the difference in abundance of a given element at 9.4 wt.% MgO).

[b]P(0) = initial melting pressure; P(f) = final melting pressure; F = extent of partial melting. Calculated using the parameterisation of Niu and Batiza (1991b).

[c]Mean K_2O/TiO_2 value for each glass group, or in the case of Sample D9-1, all Central Gorda Ridge glasses.

[d]Na8 and Fe8 values corrected to $K_2O/TiO_2 = 0.1$ using the method described by Shen and Forsyth (1995).

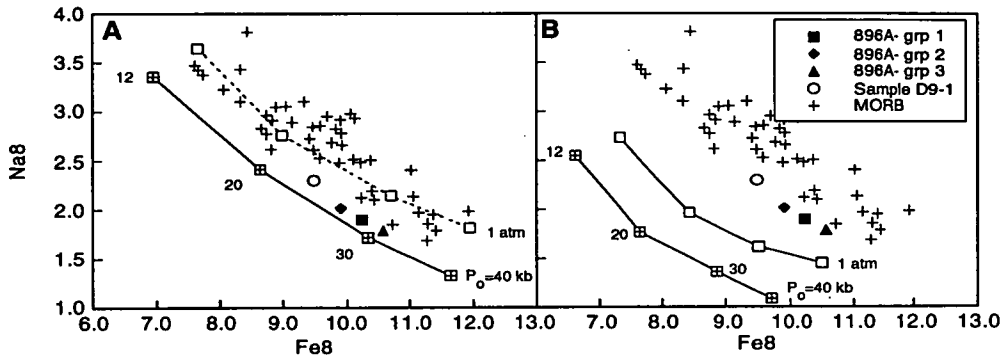

Figure 7.4: The polybaric melting models of Langmuir et al. (1992) for fractional (**A**) and equilibrium (**B**) melting. Values on curves give the initial pressure of melting (P_o) and the curves labelled 1 atm show the effect of fractionating the pooled 8.0 wt.% MgO melts. MORB are the regional averages presented by Langmuir et al. (1992). The Costa Rica Rift pillow-rim glass groups and Gorda Ridge Sample D9-1 have normalised compositions consistent with polybaric fractional melting.

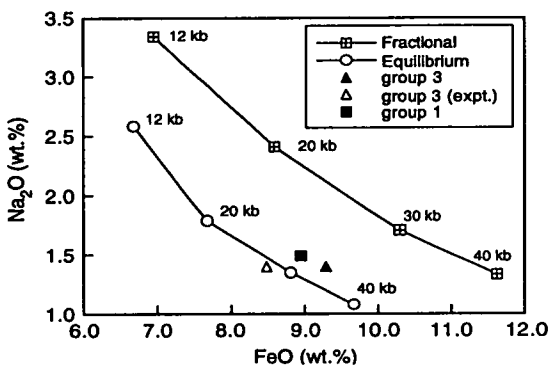

Figure 7.5: 'Primary' Costa Rica Rift melts, from the present study, compared with the standard model pooled polybaric fractional and equilibrium melting curves from Langmuir et al. (1992). Results are consistent with the 'primary' melts being pooled equilibrium melts, rather than fractional melted (as indicated in Fig. 7.4).

melting (Fig. 7.6). Two factors may contribute to this apparent paradox; Firstly P_f should be deeper than the Moho, and secondly there may be problems with the fractionation correction applied to FeO contents and(or) there is an effect on FeO contents from mantle heterogeneity (Shen and Forsyth, 1995). The possible effects of mantle heterogeneity were also recognised by Langmuir et al. (1992)

3. Shen and Forsyth (1995). Quantitative models for fractional and equilibrium melting with passive and dynamic upwelling (Fig. 7.7) are presented and are based on the results of Langmuir et al. (1992) as discussed above. The major difference is that a correction for the enrichment of the mantle source, as indicated by the average K_2O/TiO_2 for a given suite. Results for all Gorda Ridge and Costa Rica Rift samples indicate variable P_o ~20-27 kb and an even more variable final pressure of melting (P_f) of 5-18 kb. However, when an individual group or sample is considered, e.g., group 3, then the model predicts similar P_o (25-27 kb) for all end-members, but variable P_f (5-17 kb). The variable P_f leads to a range in maximum extent of melting (12-24%; assuming melting at 1.2%/kb). The variable P_f contrasts with the fixed P_f at the base of the Moho in the standard model of Langmuir et al. (1992), and the model of Niu and Batiza (1991b) which predicts that, for the studied suites, melting will cease below the Moho, but, at a constant depth.

7.2.3 Discussion

Some recent studies (e.g., McKenzie, 1985a; Johnson et al., 1990) have led to a view that mantle melting is by a near-perfect fractional process, and that therefore mantle porosities are very low < 1%. However, several lines of evidence suggest that near-perfect fractional melting is unlikely: 1) Recent studies of melting olivine (Faul, 1997) and olivine-pyroxene aggregates (Hirth and Kohlstedt, 1995) indicate that mantle melt porosities are in the range 3-5%. 2) Quantitative modelling of abyssal peridotites, the residues of mantle melting, indicate that trends for Na_2O and TiO_2 fit batch, rather than near-perfect fractional melting (Niu, 1997). Current quantitative major element models of polybaric melting, as applied to the Costa Rica Rift and Gorda Ridge samples used in this study, do not provide sufficient evidence to determine if mantle melting proceeds by fractional or equilibrium processes. However, high-pressure experiments indicate that the estimated primitive liquids for Hole 896A can be produced by batch melting and this, coupled with the results discussed above, suggests equilibrium rather than near-perfect fractional melting processes.

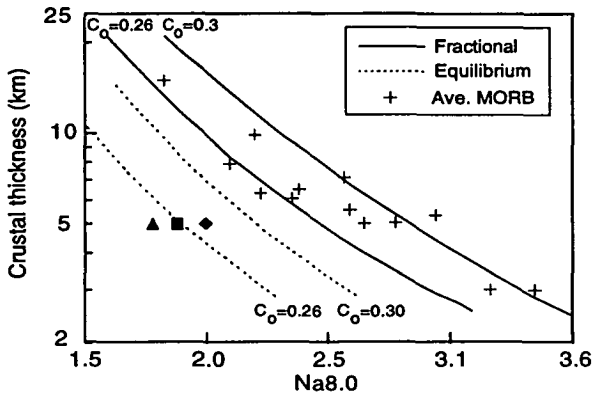

Figure 7.6: Crustal thickness vs Na8.0 for Costa Rica Rift basalts (symbols as for Figure 7.4). Mean fractional and equilibrium melts, calculated by Langmuir et al. (1992) are shown for initial mantle compositions with 0.26 and 0.3 wt.% Na_2O. Average regional MORB are also shown for comparison. the crustal thickness for the Costa Rica Rift is from seismic studies (Brocher et al., 1986; Collins et al., 1989). Note that the Costa Rica Rift primary melts have compositions more consistent with equilibrium than fractional melting (cf. Fig. 7.4).

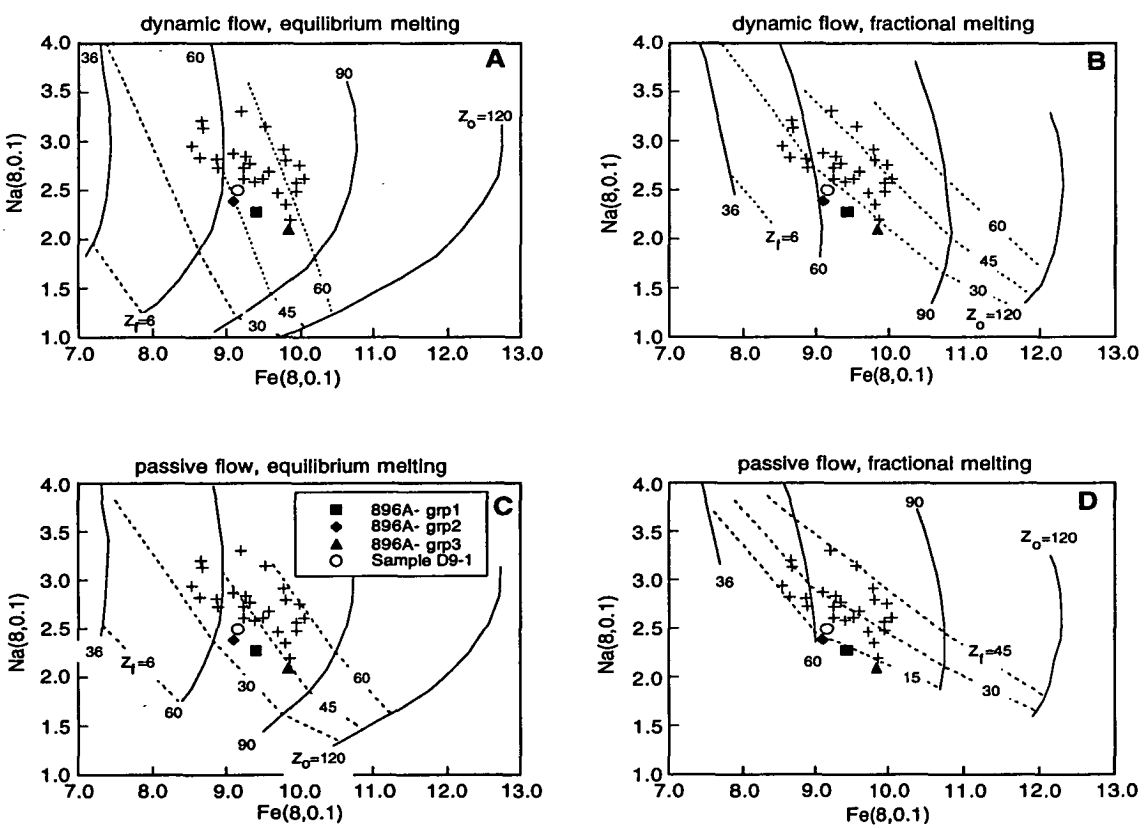

Figure 7.7: Polybaric melting models from Shen and Forsyth (1995). The two end-member melting and upwelling mechanisms are considered by this model which is based on the results of Langmuir et al. (1992). Na8 and Fe8 values have been corrected for mantle heterogeneity to yield Na(8,0.1) and Fe(8,0.1) as outlined in Table 7.3. Costa Rica Rift and Gorda Ridge basalts are plotted and averages for normal ridges (+), from Shen and Forsyth (1995), are included for comparison. P_o and P_f are initial and final depths of melting in km. See text for discussion.

7.3 High anorthite plagioclase in MORB

In addition to the samples described in detail as part of this study, highly anorthitic plagioclase phenocrysts and megacrysts (An_{88}-An_{95}) have been reported from a range of MORB type lavas; from active ridge segments on the Mid-Atlantic Ridge (Donaldson and Brown, 1977; Stakes et al., 1984; Niu and Batiza, 1994), the Central and South East Indian Ridges (Price et al., 1986; Humler and Whitechurch, 1988), the Juan De Fuca Ridge (Karsten et al., 1990; Van Wagoner and Leybourne, 1991), the East Pacific Rise (Natland, 1989); from hotspots, including the Galapagos Platform (Sinton et al., 1993), and Iceland (Hansteen, 1991); from off-axis seamounts, such as the Lamont chain (Allan et al., 1989), and from cumulate gabbros at the Mid-Atlantic Ridge (Hodges and Papike, 1976). The high-An plagioclases are typically associated with megacrysts of Cr-rich magnesian diopside, forsteritic (Fo_{88}-Fo_{91}) olivine, and Cr-Al spinel, and their widespread occurrence implies a common origin from a range of oceanic environments.

Despite this widespread occurrence, high-An plagioclase have been produced in only one published experimental study of erupted MORB compositions from normal ridge segments (Bender et al., 1978). However, high-An plagioclase have been crystallised in 1 atm experiments on liquids from seamounts (Haskell et al., 1993; Sasha Seamount), ocean islands (Yang et al., 1996; RE-46 a primitive depleted Icelandic basalt) and back arc basins (Falloon et al. 1997; a MORB like refractory liquid from the Lau Basin (Sample 95-1; Hawkins and Melchior, 1985).

7.3.1 Controls on plagioclase composition

Magmatic oxidation state, H_2O content, Al_2O_3 content, CaO/Na_2O and, temperature and pressure of crystallisation may all have an effect on plagioclase-melt equilibria (Panjasawatwong et al., 1995). Of these factors, oxidation state has not been investigated. H_2O content may have a major effect in stabilising high An plagioclase, particularly in H_2O-saturated cases (Housh and Luhr, 1991; Sisson and Grove, 1993), but most MORB are considered to be anhydrous and are CO_2 rather than H_2O saturated (Johnson et al., 1994). The effect of pressure has been discussed by Grove et al. (1992), Walter and Presnall (1994), and Fram and Longhi (1992) who concluded that high-an plagioclase in MORB must crystallise at low (<5 kb) pressure, i.e., melts with CaO/Na_2O values >18 at 10 kb and >9 at 5 kb are required to crystallise plagioclase of $>An_{90}$ (Panjasawatwong et al., 1995). Fisk (1984) suggested that, based on the anhydrous 1 atm experimental studies of Drake (1976), melts with CaO/Na_2O >10 are required to crystallise plagioclase with $>An_{90}$. More recently, Walter and Presnall

(1994) found that, in a simplified lherzolite system, liquids with <1 wt.% Na_2O and >52 wt.% SiO_2 would be in equilibrium with plagioclase of >An_{90}, at 7-9 kb. In addition, Panjasawatwong et al. (1995) and Haskell et al. (1993) have shown that at low pressure high Al_2O_3 contents promote the crystallisation of more anorthitic plagioclase, i.e., with an Al_2O_3 content of >18.6 wt.% a liquid with CaO/Na_2O values of 9.5 will crystallise plagioclase with a composition of An_{90}-An_{93}. These experimental studies indicate that crystallisation of high An plagioclase is favoured by high melt CaO/Na_2O (>9-10) and Al_2O_3 (or more strictly Al# (=100 x Al/(Al + Si)); Panjasawatwong et al., 1995), and low pressures.

The CaO/Na_2O and Al_2O_3 content of a magmatic liquid normally decreases as fractionation proceeds along the olivine-plagioclase cotectic, and therefore the An-content of the equilibrium plagioclase should also decrease. This is the case with melt inclusions in plagioclase from Sample D9-1 (Fig. 4.24), however, the correlation is not obvious with melt inclusions from Holes 504B (Fig. 5.15E) and 896A (Fig. 3.23) which may have a range of An-contents at a given MgO content (e.g., An_{86}-An_{91} at 8.7 wt.% MgO for Hole 896A samples). These variations suggest that some factor, as yet unresolved by experimental studies may also have a control on the CaO/Na_2O of a magma, and thus the equilibrium plagioclase composition.

7.3.2 Parental liquids to high-An plagioclase

A survey of primitive MORB glass compositions from the literature (Melson and O'Hearn, 1990; T. J. Falloon pers. comm., 1994) indicates that only one glass (212 from the Indian Ocean; Melson et al., 1976) has the necessary CaO/Na_2O, based on the experiments summarised above, to crystallise plagioclase of ~An_{90}, but not higher. The paucity of erupted magmas with appropriate compositions, in terms of CaO/Na_2O to crystallise >An_{90} has been explained by the presence of low volume refractory (low TiO_2, Na_2O, high Mg#) liquids, which crystallise anorthitic plagioclase but whose compositional signature is lost as a result of pre-eruption processes, including magma mixing, low-pressure fractionation, and magma chamber density filters (Duncan and Green, 1980; Duncan and Green, 1987; Natland, 1989; Grove et al., 1992). The signature of these liquids are, however, preserved in melt inclusions from primitive olivine (Danyushevsky et al., 1988; Sobolev and Shimizu, 1993) and spinels (Donaldson and Brown, 1977) whose compositions are not obviously affected by re-equilibration, as described in Chapter 6.

Such refractory liquids, or second stage melts were thought to be major contributors to erupted liquids from Hole 504B (Autio and Rhodes, 1983; Natland et al., 1983; Kempton et al., 1985). However, the melt inclusions analysed as part of this

study do not have refractory compositions, with CaO/Na_2O contents of largely 6-9, but up to 9.8, in plagioclase of An_{90}-An_{94}, and higher Al_2O_3 contents than the refractory liquids sampled in melt inclusions or, proposed from experimental studies. Anorthitic plagioclase may therefore crystallise from liquids with a range of compositions, and it has been suggested that, based on melt inclusion compositions, high-An plagioclase may also crystallise from a distinct Ca-Al-rich magma type (Sobolev et al., 1989; Sinton et al., 1993).

The interpretation of a range of liquid compositions which crystallise high-An plagioclase is confirmed by systematic differences in the compositions of homogenised melt inclusions, in plagioclase >An_{90}, analysed in this study; CaO/Na_2O values range from 6.6-9.8 and 6.6-8.1, and Al# ranges from 26.1-27.9 and 27.6-29.1 in Hole 896A/504B and Sample D9-1 respectively. High-An plagioclase should therefore crystallise from liquids with a range of compositions, many of which are erupted (Fig. 7.8). Why then have some low-pressure experiments, on basalts with suitable compositions failed to crystallise high-An plagioclase?

Samples 527-1-1 and DSDP 3-18-7-1 revisited

Samples, 527-1-1 and DSDP 3-18-7-1, both primitive glasses from the Mid-Atlantic Ridge, were the subject of experimental studies by Bender et al. (1978) and Green et al. (1979), respectively. The compositions of these two samples, with high CaO/Na_2O, Al# and Al_2O_3 contents (Table 7.4), are comparable with the most magnesian liquids sampled by melt inclusions in olivine and plagioclase (>An_{90}) from Sample D9-1, and may therefore be expected to have crystallised high-An plagioclase (Fig. 7.8). The compositions of experimental (0-10 kb) and natural phenocryst and microphenocryst phases in the two samples are compared in Table 7.3. The 1 atm experiments on DSDP 3-18-7-1 had plagioclase An_{77} as a liquidus phase, consistent with the few analyses of plagioclase microphenocrysts from the cored basalt sample (Frey et al., 1974) and this led Green et al. (1979) to conclude that there was no possibility that liquids like DSDP 3-18-7-1 could crystallise high-An plagioclase and that refractory second stage melts were required to crystallise such plagioclase. However, these results bear closer inspection:

1. As outlined above for a given liquid composition the An-content of the liquidus plagioclase decreases with increasing pressure; this is not the case for the experiments of Green et al., with plagioclase at 1 atm and 5 kb having the same composition. Note that compositions of the calculated (using Panjasawatwong et al., 1995) equilibrium plagioclase and the experimental plagioclase are consistent, within error, for the 5-10 kb experiments for both Samples DSDP 3-18-7-1 and 527-1-1.

Table 7.4. A comparison of experimental results from Green et al. (1979) and Bender et al. (1978)

	Bender et al. (1978)	Green et al. (1979)
SiO_2	48.62	49.68
TiO_2	0.74	0.72
Al_2O_3	16.44	16.39
[a]FeO*	9.00	7.90
MnO	0.25	0.12
MgO	10.79	10.09
CaO	12.10	13.09
Na_2O	1.97	2.00
K_2O	0.09	0.01
P_2O_5	0.00	0.00
Total	100.00	100.00
CaO/Na_2O	6.2	6.6
[b]Al#	28.5	28.1
Phenocryst compositions		
Plag. (An%)	89	79
Olivine (Fo%)	87.7	89.8-89.2
Experimental Results		
[c]0 kb	**89**	**78**
5 kb		77(79)
6 kb	78(77.5)	
8 kb	73(74.4)	
10 kb		73(72)

[a]All Fe as FeO

[b]Al# = 100 x Al/(Al + Si)

[c]Experimental plagioclase (calculated plagioclase); plagioclase compositions in brackets were calculated using Panjasawatwong et al. (1995).

2. Original electron microprobe analyses (obtained courtesy Prof. D. H. Green) of experimental plagioclase from the 1 atm runs on Sample DSDP 3-18-7-1 have high FeO* (1.0-2.9 wt.%) and MgO (1.6-3.3 wt.%) contents when compared with natural MORB plagioclase phenocrysts, the results of Bender et al. (1978) and plagioclase from the 5 kb experiments (Fig. 7.9). The high minor element contents may result from analytical overlap with the host glass. However, recalculating FeO* and MgO contents of the plagioclase to normal MORB values requires the subtraction of ~30 wt.% of the host glass composition, and has only a minimal effect on the plagioclase An-content, that increases by 0.5. Alternatively, and more likely, non-equilibrium crystallisation and kinetic effects during quenching may have caused the high FeO* and MgO contents (e.g., Longhi et al., 1976).

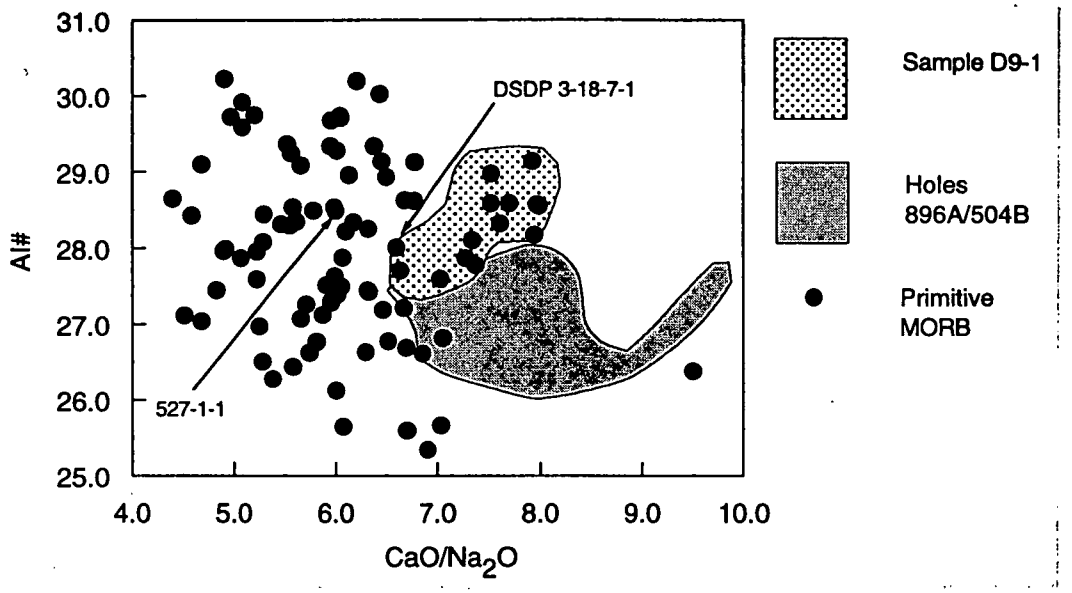

Figure 7.8. Al# (= 100 x Al/(Al + Si)) vs CaO/Na_2O for primitive MORB glasses from all oceanic basins (data from T. J. Falloon, pers. comm., 1997). The fields for homogenised melt inclusions in high-An ($>An_{90}$) plagioclase from Sample D9-1 and samples from Holes 896A and 504B are shown for comparison. The pillow-rim glasses which fall in the field of homogenised melt inclusions have compositions which may be suitable to crystallise high-An plagioclase at low pressures. Experimental studies on the two indicated analyses are discussed in detail in the text.

3. The starting mix used in the Green et al. experiments was a synthetic oxide-mix glass that was devitrified to a mixture of olivine-pyroxene-plagioclase at 1050°C or a mixture of the glass and run product from crystallisation experiments (plagioclase seed crystals were thought to be required as plagioclase nucleation may be sluggish in synthetic glasses). Grove and Bryan (1983) noted that many of the plagioclase crystallised in their 1 atm experiments were compositionally heterogeneous, and suggested that incomplete reaction or re-equilibration of the seed plagioclase occurred in their experiments. Similar problems may also be expected with the experiments of Green et al. (1979) as their run times (2 hours) were much shorter than the >20 hours of Grove and Bryans (1983) experiments, allowing even less time for reaction/re-equilibration.

These observations all suggest that there were problems with the experiments of Green et al. (1979) that led to the crystallisation of non-equilibrium plagioclase. Their conclusion that Sample DSDP 3-18-7-1 type compositions cannot crystallise high-An plagioclase may be flawed, and the conclusion from the present study that by comparison with melt inclusion compositions in high-An plagioclase from Sample D9-1, and experiments on Sample 527-1-1 (Bender et al., 1978), Sample DSDP-3-18-7-1 could have crystallised high-An ($>An_{88}$) at low pressures.

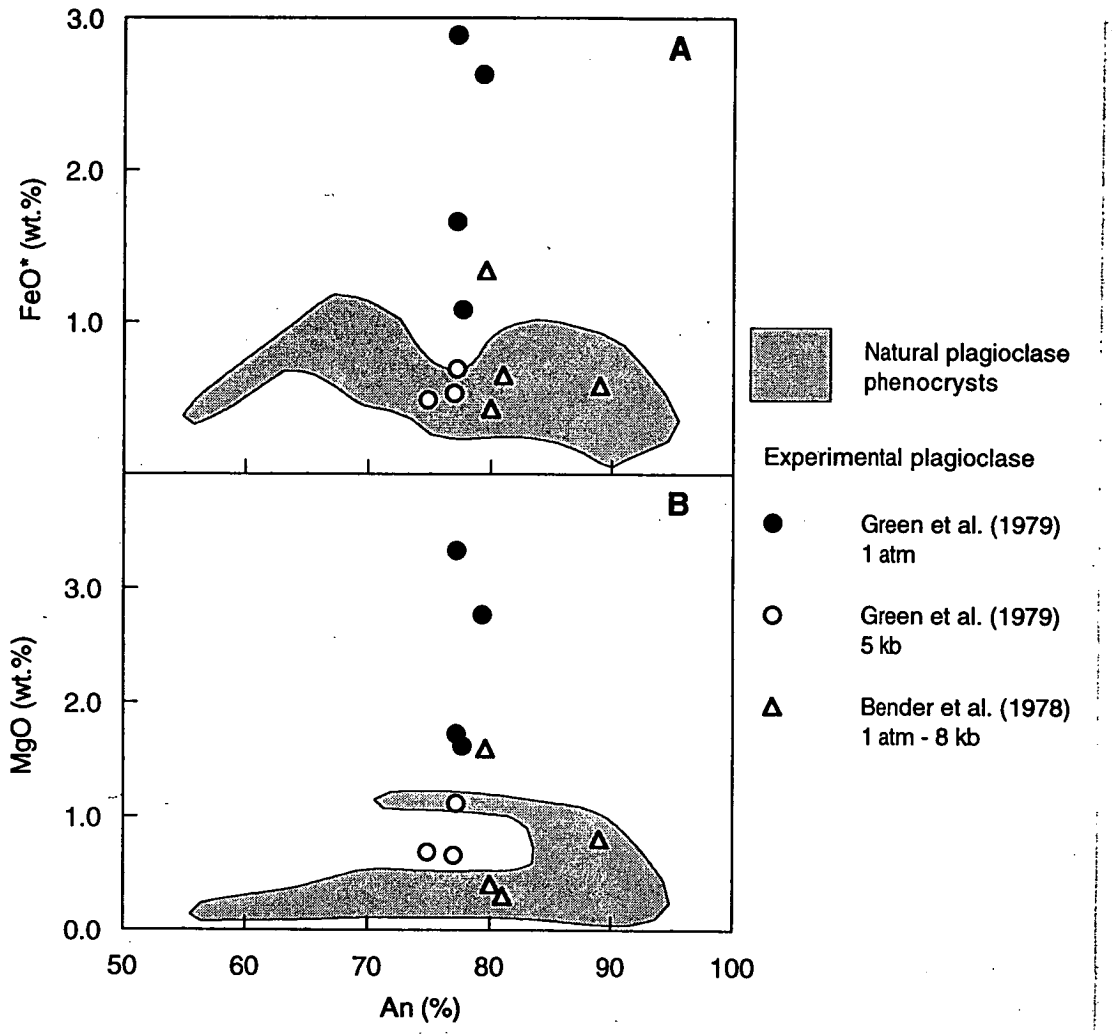

Figure 7.9: FeO* (A) and MgO (B) content vs Anorthite content for natural plagioclase phenocrysts and microphenocrysts (1790 analyses from this study) and plagioclase crystallised in the experiments of Green et al. (1979) and Bender et al. (1978) using the compositions of DSDP 3-18-7-1 and 527-1-1 respectively. The 1 atm analyses of Green et al. (ibid) range to higher MgO and FeO* contents than the other analyses. See text for discussion.

7.4 Summary

The compositions of melt inclusions in primitive olivine (>Fo_{88}), plagioclase (>An_{88}) and Cr-Al spinel from all three studied suites provide no evidence for the presence of liquids that could be individual melt fractions produced by polybaric melting in the ascending mantle. The liquids trapped to form the melt inclusions may therefore be aggregated, i.e., mixed, polybaric melts or the fractionation products of isobaric batch melts.

The results of olivine addition calculations for Hole 896A pillow-rim glass groups 1 and 3 indicate that potential primary liquids, in equilibrium with olivine $Fo_{91.6}$, have 14.7-15.1 wt.% MgO, and are possible isobaric batch melts from a MORB

Pyrolite-90 source at ~18 kb. Initial experimental results suggest that the group 3 liquid is in equilibrium with a mantle source (composition MM-3) at 1450°C and 20 kb (T. J. Falloon, pers. comm., 1997).

The most primitive olivine phenocrysts from Sample D9-1 have compositions, Fo_{90}, that could be in equilibrium with a mantle assemblage. However, when plotted in the CIPW normative basalt tetrahedron, melt inclusions from these phenocrysts have compositions that are too-rich in normative diopside to be in equilibrium with mantle assemblages at any reasonable pressure (i.e., > 8 kb). If the melt inclusion compositions are projected along olivine control lines they intersect the 18 kb mantle cotectic at a similar position to the Hole 896A samples. Similar segregation pressures, i.e., 18 kb, are therefore inferred.

The results of quantitative major element polybaric melting models (e.g., Niu and Batiza, 1991b; Shen and Forsyth, 1995) do not provide consistent results, and suggest that melting may be either equilibrium or fractional. The results presented above suggest that batch melting models currently provide the best results, and are consistent with recent modelling of abyssal peridotite compositions (Niu, 1997) and experimental results indicating significant mantle porosities, 3-5% (Hirth and Kohlstedt, 1995; Faul, 1997) which rule out near-perfect fractional melting.

Experimental data indicate that the crystallisation of high-An ($>An_{88}$) plagioclase is favoured by low pressures and high liquid CaO/Na_2O and Al# values. The results of the present study suggest that highly anorthitic plagioclase can crystallise from primitive anhydrous liquids with compositions that range from a refractory type, similar to the second stage melts of Duncan and Green (1980,1987), to a high Ca-Al type, as proposed by Sobolev et al. (1989) and Sinton et al. (1993). The failure of some experimental studies, e.g., Green et al. (1979), to crystallise high-An plagioclase may be due to the crystallisation of non-equilibrium plagioclase in their 1 atm experiments.

Chapter 8

Synthesis

In this chapter I summarise the results of detailed studies, using the phenocryst mineralogy, and melt inclusion and pillow-rim glass compositions, of MORB samples from DSDP/ODP Holes 896A and 504B and Sample KK2-NP-83-D9-1 from the Costa Rica Rift and Central Gorda Ridge respectively. Results and interpretations are summarised with reference to the aims of the present study:

Aim 1. To investigate in detail, using large numbers of analyses of individual phenocryst phases, the mineralogy of primitive MORB to establish the crystallisation history of each suite, and the relationships of primitive phenocrysts to their host pillow-rim glasses.

Samples from the Costa Rica Rift (Holes 896A and 504B) and the Central Gorda Ridge have phenocryst assemblages dominated by calcic plagioclase (>An_{88}) with lesser olivine (<$Fo_{91.6}$) and Cr-Al spinel. However, in other respects the samples from the two ridge segments are different:

A. The Hole 896A, and the majority of Hole 504B samples, are strongly LREE depleted ($(La/Sm)_n$ values of <0.38) and have lower TiO_2, Na_2O and K_2O contents than the majority of Pacific MORB glasses. In contrast, Sample D9-1, and other Central Gorda Ridge samples, are less depleted ($(La/Sm)_n$=0.4) with Na_2O, TiO_2, and K_2O contents, that are more typical of Pacific MORB and the more "enriched" samples from Hole 504B.

B. Mineralogical evidence for Hole 896A samples indicates that the most abundant plagioclase, in terms of An content, in each sample was in equilibrium with its host liquid, i.e., pillow-rim glass, and that the most calcic plagioclase ($An_{94.5}$) sampled crystallised from liquids with a similar MgO content to the most primitive pillow-rim glass, which was calculated to be in equilibrium with olivine Fo_{87}. As more magnesian olivines, up to $Fo_{91.6}$, occur in these samples, an extensive period of olivine-only crystallisation, prior to cotectic olivine-plagioclase crystallisation, is inferred. In contrast, the most abundant plagioclase phenocrysts from Sample D9-1, An_{91}, are interpreted to have crystallised from liquids more primitive than the host (or any other

Central Gorda Ridge) pillow-rim glass and which were in equilibrium with olivine Fo_{90}, the most primitive olivine sampled. This interpretation suggests that cotectic olivine-plagioclase crystallisation occurred much earlier, i.e., from more magnesian liquids, in the history of Sample D9-1 than for Hole 896A or 504B samples.

At 'high' pressures, >2 kb, olivine-only crystallisation is interpreted to be the major process that affected these samples. There is no compositional evidence from clinopyroxene, spinel or plagioclase phenocrysts to indicate that they crystallised at high pressures. At low pressure (<2 kb), in the crustal magma supply and storage system, cotectic (olivine-plagioclase ±clinopyroxene) crystallisation and magma mixing were the dominant processes, although assimilation of hydrothermally altered crustal material has also been inferred on the basis of decoupled LILE and HFSE for some samples from Hole 896A. Magma mixing is indicated by: 1) variations in phenocryst abundance, morphology and zoning, and particularly, the crystallisation of Cr-rich magnesian diopside during undercooling (Holes 896A and 504B), 2) uphole variations in pillow-rim glass composition (Holes 896A, and 504B), 3) the range of spinel compositions in individual samples, and 4) the 'pyroxene paradox' in Sample D9-1, interpreted to indicate mixing of in-situ and normally fractionated liquids. Mixing is thought to have occurred between primitive and more evolved liquids, the latter produced by normal crystal fractionation or in-situ fractionation in the magma supply system.

Aim 2. Based on the phenocryst data, to investigate in detail, using large datasets, variations in melt inclusion compositions in cotectic phenocryst phases, to resolve the possible problems with interpreting the significance of melt inclusion compositions, and to assess the applicability of these data in interpreting the petrogenesis of MORB.

If the liquids trapped to form melt inclusions were fluid saturated, and account is taken of the kinetics of reheating, then both slowly-cooled crystalline (Hole 504B) and rapidly-quenched glassy (Hole 896A and Sample D9-1) melt inclusions may be successfully homogenised using the visually-controlled heating stage. The similarity of homogenisation temperatures (T_h) for melt inclusions in cotectic plagioclase and olivine, and the calculated liquidus temperatures for pillow-rim glasses, confirm that T_h is equivalent to the trapping (or crystallisation) temperature.

The heating stage experiments yield lower trapping temperatures, by up to 50°C, than published results of vertical quench furnace experiments on melt inclusions in phenocrysts of similar composition from the same suite (Hole 504B) or even the same sample (Sample D9-1). The temperature difference is a result of the inability to

observe homogenisation in the vertical furnace experiments and the reliance on the melting and disappearance of daughter olivine crystals to infer trapping temperatures, a process that is strongly controlled by the kinetics of melting. Homogenised melt inclusions from published vertical furnace experiment studies are overheated, and possibly poorly quenched, and therefore their compositions are generally not representative of the liquids trapped to form melt inclusions.

The present study is, to date, the most detailed comparison of melt inclusion compositions from cotectic phases in several MORB suites. Existing published studies have generally relied, with the exception of Sobolev et al. (1989), on data from one phenocryst phase, be it spinel (Kamenetsky, 1996), olivine (Sobolev and Shimizu, 1993; Shimizu, 1994) or plagioclase (Sinton et al., 1993; Nielsen et al., 1995). A comparison of results from cotectic phases (plagioclase-olivine-spinel) allows the three points discussed in Chapter 1 to be addressed: 1) The compositions of melt inclusions in phenocrysts which crystallised from more evolved liquids (i.e., liquids represented by pillow-rim glasses) must be identical to the compositions of those pillow-rim glasses, and cannot have the unusual incompatible element characteristics found in melt inclusions from more primitive phenocrysts. 2) Melts produced at different depths in the melting column should not only have different trace element contents, but should also have variable major element contents. 3) Melt inclusions in cotectic phases, i.e., in minerals that crystallised together from the same magmatic liquid, should have the same composition.

Plagioclase phenocrysts from Holes 896A and 504B are interpreted to have crystallised from liquids with a range of compositions similar to those of their host pillow-rim glasses. The melt inclusions in these phenocrysts have similar compositions to the glasses in terms of Al_2O_3, MgO, CaO Na_2O and generally K_2O. Rare high K_2O contents are considered to result from the hydrothermal alteration of melt inclusions and are not a primary variation. However, the TiO_2 and FeO* contents of melt inclusions consistently range to lower, and in the case of SiO_2, to higher, abundances than in the pillow-rim glasses at a given MgO content. Variations in these elements are not coupled with obvious trace element variations that are related to sampling of liquids produced by different depths in the melting column, but are the result of re-equilibration processes. Low FeO* and TiO_2 contents are also found in analyses of naturally quenched plagioclase-hosted melt inclusions. This indicates that re-equilibration did not occur during reheating experiments, and that these oxides, generally considered to be incompatible in post-trapping crystallisation of plagioclase, cannot be used for petrogenetic interpretation, as has been done in some published studies (e.g., Sichel and Sigurdsson, 1993).

The high FeO* contents of the majority of Sample D9-1 olivine-hosted melt inclusions, found in only one melt inclusion from Hole 896A, have not previously been reported from MORB samples and are interpreted to result from some form of re-equilibration. The naturally quenched spinel-hosted melt inclusions from Sample D9-1 have variable Al_2O_3, FeO, MgO and SiO_2 contents, suggesting that, in contrast to the conclusions of previous studies (e.g., Kamenetsky, 1996), the compositions of these melt inclusions do not completely recover trapped liquid compositions. More detailed studies, particularly trace element data, are required to resolve the exact nature of the re-equilibration processes in plagioclase-, spinel- and olivine-hosted melt inclusions.

A consequence of the re-equilibration of melt inclusions with their host phenocryst and(or) magmatic liquid is that the compositions of melt inclusions in cotectic phases are not the same, at a similar stage of fractionation, for all major element oxides. However, the CaO, Na_2O and K_2O contents of melt inclusions in cotectic phases are generally consistent and the TiO_2 contents of spinel- and olivine-hosted melt inclusions may be similar.

Identifying problems with melt inclusion results, e.g., the underheating of olivine-hosted melt inclusions in olivine from Hole 896A (the result of fluid-undersaturation) and the low TiO_2 and FeO* contents of plagioclase-hosted inclusions, required a detailed comparison of data from melt inclusions in all cotectic phases in combination with petrography and a comparison of phenocryst, melt inclusion and pillow-rim glass chemistry. The use of melt inclusions in a single phenocryst phase, in isolation from other data, is therefore not recommended and may lead to erroneous conclusions about the petrogenesis of a sample or suite of samples.

Aim 3. To use petrological information obtained from both early formed phenocrysts, and their melt inclusions, to address problems of MORB primary melt compositions, conditions of melt generation and segregation, and models of MORB petrogenesis.

Melt inclusions in primitive plagioclase, olivine and spinel do not preserve evidence for diverse melt fractions that would be expected to be produced by polybaric fractional-continuous melting. Crystallisation must therefore have started after the aggregation of these melt fractions, or alternatively the trapped liquids are the result of the fractionation of primary isobaric batch melts.

Isobaric batch melts in equilibrium with a residual mantle assemblage (i.e., primary melts) were estimated for the studied suites. The Costa Rica Rift samples, interpreted to have undergone extensive olivine fractionation, require addition of ~15%

olivine for equilibrium with a mantle source at 18-20 kb. Although olivine (Fo_{90}) from Sample D9-1 was primitive enough to be in equilibrium with a mantle source, melt inclusions in olivines of this composition have CaO contents that are too high for equilibrium with mantle sources at any reasonable pressure. Addition of olivine was therefore required, and, indicates similar pressures of segregation to the Costa Rica Rift samples.

The depths of segregation obtained in the present study are consistent with experimental results on Samples DSDP 3-18-7-1 (Green et al., 1979) and 95-1 (Falloon et al., 1997) and suggest a common physical process that controls the point at which melt is no longer stable in the residuum for isobaric batch melting.

Melting parameters (P_o, P_f, F) were estimated for the studied suites using polybaric melting models. The major element (FeO* and Na_2O) compositions of aggregate liquids for the studied suites are consistent with both equilibrium and fractional melting and passive or dynamic upwelling, with P_o=20-27 kb, P_f=5-18 kb and F=12-24% (using the parameterisations of Shen and Forsyth (1995) and Niu and Batiza (1991b)).

For the Costa Rica Rift and Gorda Ridge samples available major element melting models cannot differentiate between origins as aggregates of equilibrium or fractional melts, or an origin by fractionation from an isobaric batch melt. However, recent studies (e.g., Hirth and Kohlstedt, 1995; Niu, 1997) do not support near-perfect fractional melting, as has been suggested by some authors, and accumulated equilibrium or isobaric batch melting is more likely.

Melt inclusion compositions indicate that the crystallisation of high-An ($>An_{88}$) plagioclase, characteristic of samples used in the present study, does not require the refractory high CaO/Na_2O (>10), low Al_2O_3 liquids, such as the second stage melts of Duncan and Green (1987). Instead, these plagioclases are considered to have crystallised from liquids with CaO/Na_2O values of 6-8, but up to 9.8, and with higher Al_2O_3, or more strictly higher Al:Si, than the proposed refractory liquids. High-An plagioclase, therefore, may crystallise from a range of liquids, with liquidus plagioclase composition largely a function of CaO/Na_2O and Al_2O_3/SiO_2 at a given pressure, as suggested by Panjasawatwong et al. (1995). The failure of some experimental studies of N-MORB compositions to crystallise high-An plagioclase, e.g., DSDP 3-18-7-1 (Green et al., 1979), may be a function of experimental technique (crystallisation of non-equilibrium plagioclase).

References

Adamson A. C. (1985) Basement lithostratigraphy, Deep Sea Drilling Project Hole 504B. In *Init. Repts. DSDP.*, Vol. 83 (ed. R. N. Anderson, J. Honnorez, K. Becker, et al.), pp. 121-127. U.S. Govt. Printing Office.

Ahern J. L. and Turcotte D. L. (1979) Magma migration beneath an ocean ridge. *Earth Planet. Sci. Lett.* **45**, 115-122.

Albarede F. (1992) How deep do basaltic magmas form and differentiate? *J. Geophys. Res.* **97**, 10997-11009.

Allan J. F. (1992) Cr-spinel as a petrogenetic indicator: deducing magma composition from spinels in highly altered basalts from the Japan Sea, Sites 794, 797. In *Proc. ODP Sci. Results*, Vol. 127/128 Pt.2 (ed. K. Tamaki, K. Suyeiho, and J. F. Allan), pp. 837-847. Ocean Drilling Program.

Allan J. F. (1994) Cr-spinel in depleted basalts from the Lau Basin back-arc: petrogenetic history from Mg-Fe crystal-liquid exchange. In *Proc. ODP Sci. Results*, Vol. 135 (ed. J. Hawkins, L. Parson, and J. F. Allan), pp. 565-583. Ocean Drilling Program.

Allan J. F., Batiza R., Perfit M. R., Fornari D. J., and Sack R. O. (1989) Petrology of lavas from the Lamont seamount chain and adjacent East Pacific Rise, 10°N. *J. Petrol.* **30**, 1245-1298.

Allan J. F., Sack R. O., and Batiza R. (1988) Cr-rich spinels as petrogenetic indicators: MORB-type lavas from the Lamont seamount chain, eastern Pacific. *Am. Mineral.* **73**, 741-753.

Anderson A. T. (1974) Evidence for a picritic, volatile rich magma beneath Mt. Shasta, California. *J. Petrol.* **15**, 243-267.

Arai S. and Matsukage K. (1996) Petrology of the gabbro-troctolite-peridotite complex from Hess Deep, equatorial Pacific: implications for mantle-melt interaction within the ocean lithosphere. In *Proc. ODP Sci. Results*, Vol. 147 (ed. C. Mevel, K. M. Gillis, J. F. Allan, and P. S. Meyer), pp. 135-156. Ocean Drilling Program.

Ariskin A. A. and Barmina G. S. (1990) Plagioclase-melt thermometry for basaltic and andesitic systems. *Geokhimiya* **N3**, 441-446.

Ariskin A. A., Barmina G. S., and Frenkel M. Y. (1986) Computer simulation of basaltic melt crystallisation under controlled fO_2. *Geochimiya* **11**, 1614-1627.

Asimow P. D., Hirschmann M. M., Ghiorso M. S., O'Hara M. J., and Stolper E. (1995) The effect of pressure-induced solid-solid phase transitions on the decompression melting of the mantle. *Geochim. Cosmochim. Acta* **59**, 4489-4506.

Autio L. K. (1984) Compositional diversity of mid-ocean ridge basalts: an experimental and geochemical study with emphasis on the depleted Costa Rica Rift Zone basalts. PhD., Univ. Mass., Amherst.

Autio L. K. and Rhodes J. M. (1983) Costa Rica Rift Zone basalts: geochemical and experimental data from a possible example of multi-stage melting. In *Init. Repts. DSDP.*, Vol. 69 (ed. J. R. Cann, M. G. Langseth, J. Honnorez, R. P. Von Herzen, S. M. White, et al.), pp. 729-745. U.S. Govt. Printing Office.

Autio L. K., Sparks J. W., and Rhodes J. M. (1989) Geochemistry of Leg 111 basalts: intrusive feeders for highly depleted pillows and flows. In *Proc. ODP Sci. Results*, Vol. 111 (ed. K. Becker, H. Sakai, et al.), pp. 3-16. Ocean Drilling Program.

Bach W., Erzinger J., Alt J. C., and Teagle D. A. H. (1996). Chemistry of the lower sheeted dike complex, Hole 504B (Leg 148): Influence of magmatic differentiation and Hydrothermal alteration. In *Proc. ODP Sci. Results*, Vol. 148 (ed. J. C. Alt, H. Kinoshita, L. B. Stokking, and P. J. Michael), pp. 39-55. Ocean Drilling Program.

Baker M. B., Hirschmann M. M., Ghiorso M. S., and Stolper E. M. (1995) Compositions of near-solidus peridotite melts from experiments and thermodynamic calculations. *Nature* **375**, 308-311.

Baker M. B. and Stolper E. M. (1994) Determining the composition of high-pressure mantle melts using diamond aggregates. *Geochim. Cosmochim. Acta* **58**, 2811-2827.

Bakumenko I. T. (1975) Inclusions in minerals of ultrabasic nodules as indicators of their origin. In *Deepseated xenoliths and the upper mantle.* (ed. V. S. Sobolev, N. L. Dobretsov, and N. V. Sobolev), pp. 231-235. (In Russian). Nauka, Siberian Branch.

Ballard R. D., Holcomb R. T., and Van Andel T. H. (1979) The Galapagos Rift at 86°W: 3. Sheet flows, collapse pits and lava lakes in the rift valley. *J. Geophys. Res.* **84**, 5407-5422.

Ballhaus C., Berry R. F., and Green D. H. (1991) High pressure experimental calibration of the olivine-orthopyroxene-spinel oxygen geobarometer: implications for oxidation state of the upper mantle. *Contrib. Mineral. Petrol.* **107**, 27-40.

Basaltic Volcanism Study Project (1981). *Basaltic volcanism on the terrestrial planets*. Pergammon.

Batiza R., Niu Y., Karsten J. L., Boger W., Potts E., Norby L., and Butler R. (1996) Steady and non-steady state magma chambers below the East Pacific Rise. *Geophys. Res. Lett.* **23**, 221-224.

Bedard J. M. (1989) Disequilibrium mantle melting. *Earth Planet. Sci. Lett.* **91**, 359-366.

Bedard J. H. and Hebert R. (1996) The lower crust of the Bay of Islands ophiolite, Canada: petrology, mineralogy, and the importance of syntexis in magmatic differentiation in ophiolites and at ocean ridges. *J. Geophys. Res.* **101**, 25105-25124.

Belkin H. E. and De Vivo B. (1993) Fluid inclusion studies of ejected nodules from plinian eruptions of Mt. Somma-Vesuvius. *J. Volcanol. Geotherm. Res.* **58**, 89-100.

Bender J. F., Hodges F. N., and Bence A. E. (1978) Petrogenesis of basalts from the project FAMOUS area: Experimental study from 0 to 15 kbars. *Earth Planet. Sci. Lett.* **41**, 277-302.

Bloomer S. H., Natland J. H., and Fisher R. L. (1989) Mineral relationships in gabbroic rocks from fracture zones of Indian Ocean ridges: evidence for extensive fractionation, parental diversity and boundary-layer crystallisation. In *Magmatism in the Ocean Basins. Geol. Soc. Spec. Publ.*, Vol. 42 (ed. A. D. Saunders and M. J. Norry), pp. 107-124. Blackwell.

Bonatti E. and Hamlyn P. R. (1981) Oceanic ultramafic rocks. In *The Sea: The Oceanic Lithosphere.* (ed. C. Emiliani), 241p. Wiley.

Bougalt H. and Hekinian R. (1974) Rift valley in the Atlantic ocean near 36 50'N: petrology and geochemistry of basaltic rocks. *Earth Planet. Sci. Lett.* **24**, 249-261.

Brewer T. S., Harvey P. K., and Lovell M. A. (1994) Core-log integration from ODP Hole 896A: re-interpretation of the volcanic stratigraphy. (abstr.). *AGU Fall meeting, Eos* **75**, 315.

Brocher T. M., Geist E. L., Collins J. A., and Mutter J. C. (1986) Seismic structure of the oceanic crust in the vicinity of DSDP Site 504B. *Eos* **67**, 1083.

Brodholt J. P. and Batiza R. (1989) Global systematics of unaveraged mid-ocean ridge basalt compositions: Comment on "Global correlations of ocean ridge basalt chemistry with axial depth and crustal thickness" by E. M. Klein and C. H. Langmuir. *J. Geophys. Res.* **94**, 4231-4239.

Bryan W. B. (1972) Morphology of quench crystals in submarine basalts. *J. Geophys. Res.* **29**, 5812-5819.

Bryan W. B. (1974) Fe-Mg relationships in sector zoned submarine basalt plagioclase. *Earth Planet. Sci. Lett.* **24**, 157-165.

Bryan W. B. (1983) Systematics of modal phenocryst assemblages in submarine basalts: petrologic implications. *Contrib. Mineral. Petrol.* **83**, 62-74.

Bryan W. B., Thompson G., and Michael P. J. (1979) Compositional variation in a compositionally steady-state zoned magma chamber: Mid-Atlantic Ridge at 36° 50'N. *Tectonophys.* **55**, 63-85.

Burnham C. W. (1979) The importance of volatile constituents. In *The evolution of the igneous rocks.* (ed. H. S. J. Yoder), pp. 439-482. Princeton University Press.

Byers C. D., Garcia M. O., and Muenow D. W. (1986) Volatiles in basaltic glasses from the East Pacific Rise at 21°N: implications for MORB sources and submarine lava flow morphology. *Earth Planet. Sci. Lett.* **79**, 9-20.

Byers C. D., Muenow D. W., and Garcia M. O. (1983) Volatiles in basalts and andesites from the Galapagos Spreading Centre, 85°-86°W. *Geochim. Cosmochim. Acta* **47**, 1551-1558.

Campbell I. H. (1978) Some problems with the cumulus theory. *Lithos* **11**, 311-323.

Cawthorn R. G. (1975) Degrees of melting in mantle diapirs and the origin of ultrabasic liquids. *Earth Planet. Sci. Lett.* **27**, 113-120.

Christie D. M., Carmichael I. S. E., and Langmuir C. H. (1986) Oxidation states of mid-ocean ridge basalt glasses. *Earth Planet. Sci. Lett.* **79**, 397-411.

Clocchiatti R. (1975) Glassy inclusions in crystals of quartz; optical, thermo-optical and chemical studies, and geological applications. *Soc. Geol. de France, Memoires, New Series, 54.* **122**, 96.

Clocchiatti R. (1980) Glassy inclusions in plagioclase and pyroxene phenocrysts in the chilled margin of a pillow lava from Hole 417D, Deep Sea Drilling Project. In *Init. Repts. DSDP.*, Vol. 51,52,53 (ed. T. Donnelly, J. Francheteau, W. Bryan, P. Robinson, M. Flower, M. Salisbury, et al.), pp. 1063-1067. U.S. Govt. Printing Office.

Clocchiatti R. and Massare D. (1985) Experimental crystal growth in glass inclusions: the possibilities and limits of the method. *Contrib. Mineral. Petrol.* **89**, 193-204.

Coish R. A. and Taylor L. A. (1979) The effects of cooling rate on texture and pyroxene chemistry in DSDP Leg 34 basalt: a microprobe study. *Earth Planet. Sci. Lett.* **42**, 389-398.

Collins J. A., Brocher T. M., and Purdy G. M. (1989) Seismic reflection structure of the upper oceanic crust: implications from DSDP/ODP Hole 504B, Panama basin. In *Proc. ODP. Sci. Res.*, Vol. 111 (ed. K. Becker, H. Sakai, et al.), pp. 177-191. Ocean Drilling Program.

Corrigan G. M. (1982) Supercooling and the crystallisation of plagioclase, olivine, and clinopyroxene from basaltic melts. *Min. Mag.* **46**, 31-42.

Crane K. (1985) The spacing of rift axis highs: dependance on diapiric processes in the underlying asthenosphere. *Earth Planet. Sci. Lett.* **72**, 405-414.

Cruden A. R. (1990) Flow and fabric development during the diapiric rise of magma. *J. Geol.* **98**, 681-698.

Cullen A., Vicenzi E., and McBirney A. R. (1989) Plagioclase-ultraphyric basalts of the Galapagos archipelago. *J. Volcanol. Geotherm. Res.* **37**, 325-337.

Czabo C. and Bodnar R. J. (1993) Fluid inclusions in olivines and clinopyroxenes of alkali basalts from the Norgard-Gomor volcanic field (north Hungary/ south Slovakia) (Abstr.). *IAVCEI general assembly, Canberra, Australia*, 111.

Danyushevsky L. V., Chizhov S., Kuzmin V., Pugachov R., and Sobolev A. V. (1990) Petrolog. SeLeSoft.

Danyushevsky L. V., Falloon T. J., Sobolev A. V., Crawford A. J., Carroll M., and Price R. C. (1993) The H_2O content of basalt glasses from Southwest Pacific back-arc basins. *Earth Planet. Sci. Lett.* **117**, 347-362.

Danyushevsky L. V. and Sobolev A. V. (1996) Ferric-Ferrous ratio and oxygen fugacity calculations for primitive mantle-derived melts: calibration of an empirical technique. *Mineral. Petrol.* **57**, 229-241.

Danyushevsky L. V., Sobolev A. V., and Dmitriev L. V. (1988) Orthopyroxene-bearing low-Ti tholeiites as a new type of mid-ocean ridge tholeiite. *Trans. USSR Acad. Sci. Earth Sci. Sec.* **292**, 102-105.

Danyushevsky L. V., Sobolev A. V., and Dmitriev L. V. (1996) Estimation of the pressure of crystallization and H_2O content of MORB and BABB glasses: calibration of an empirical technique. *Mineral. Petrol.* **57**, 185-204.

Danyushevsky L. V., Sobolev A. V., and Kononkova N. N. (1992) Methods of studying melt inclusions in minerals during investigations on water-bearing primitive mantle melts (Tonga trench boninites). *Geochem. Int.* **29**, 48-62.

Davis A. S. and Clague D. A. (1987) Geochemistry, mineralogy and petrogenesis of basalt from the Gorda Ridge. *J. Geophys. Res.* **92**, 10467-10483.

Davis A. S. and Clague D. A. (1990) Gabbroic xenoliths from the northern Gorda Ridge, implications for magma chamber processes under slow-spreading ridges. *J. Geophys. Res.* **95**, 10885-10905.

Davis A. S., Clague D. A., and Friesen W. B. (1994) Petrology and mineral chemistry of basalt from the Escanaba Trough. In *Geologic, hydrothermal and biologic studies at Escanaba Trough, Gorda Ridge, offshore N. California. U.S.G.S. Bulletin.*, Vol. 2022 (ed. J. L. Morton, R. A. Zierenberg, and C. A. Reiss), pp. 153-170.

Dick H. J. B. (1989) Abyssal peridotites, very slow spreading ridges and ocean ridge magmatism. In *Magmatism in the ocean basins. Geol. Soc. Spec. Publ.*, Vol. 42 (ed. A. D. Saunders and M. J. Norry), pp. 71-105. Blackwell.

Dick H. J. B. and Bullen T. (1984) Chromium spinel as a petrogenetic indicator in abyssal and alpine-type peridotites and spatially associated lavas. *Contrib. Mineral. Petrol.* **86**, 54-76.

Dick H. J. B. and Johnson K. T. M. (1995) REE and trace element composition of clinopyroxene megacrysts, xenocrysts, and phenocrysts in two diabase dikes from Leg 140, Hole 504B. In *Proc. ODP Sci. Results*, Vol. 137/140 (ed. J. Erzinger, H. J. B. Dick, and L. B. Stokking), pp. 121-130. Ocean Drilling Program.

Dick H. J. B. and Natland J. H. (1996) Late-stage melt evolution and transport in the shallow mantle beneath the East Pacific Rise. In *Proc. ODP Sci. Results*, Vol. 147 (ed. C. Mevel, K. M. Gillis, J. F. Allan, and P. S. Meyer), pp. 103-134. Ocean Drilling Program.

Dick H. J. B., Robinson P. T., and Meyer P. S. (1992) The plutonic foundation of a slow spreading ridge. In *Synthesis of results from scientific drilling in the Indian Ocean. Geophysical Monograph*, Vol. 70 (ed. R. A. Duncan, D. K. Rea, R. B. Kidd, U. von Rad, and J. K. Weissel), pp. 1-39. American Geophysical Union.

Dixon J. E. and Stolper E. M. (1995) An experimental study of water and carbon dioxide solubilities in mid-ocean ridge basaltic liquids. Part II: Applications to degassing. *J. Petrol.* **36**, 1633-1646.

Dixon J. E., Stolper E. M., and Holloway J. R. (1995) An experimental study of water and carbon dioxide solubilities in mid-ocean ridge basaltic liquids. Part I: calibration and solubility models. *J. Petrol.* **36**, 1607-1632.

Dmitriev L. V., Sobolev A. V., Suschevskaya N. M., and Zapunny S. A. (1985) Abyssal glasses, petrologic mapping of the oceanic floor and "geochemical Leg" 82. In *Init. Repts. DSDP*, Vol. 82 (ed. H. Bougalt, S. C. Cande, et al.), pp. 509-518. U.S. Govt. Printing Office.

Dmitriev L. V., Sobolev A. V., Uchanov A. V., Malysheva T. V., and Melson W. G. (1984) Primary differences in oxygen fugacity and depth of melting in the mantle source regions for oceanic basalts. *Earth Planet. Sci. Lett.* **70**, 303-310.

Donaldson C. H. (1979) An experimental investigation of the delay in nucleation of olivine in mafic magmas. *Contrib. Mineral. Petrol.* **69**, 21-32.

Donaldson C. H. and Brown R. Y. (1977) Refractory megacrysts and magnesium-rich melt inclusions within spinel in oceanic tholeiites: indicators of magma mixing and parental magma composition. *Earth Planet. Sci. Lett.* **37**, 81-89.

Dowty E. (1976) Crystal structure and crystal growth, II sector zoning in minerals. *Am. Mineral.* **61**, 460-469.

Drake M. J. (1976) Plagioclase -melt equilibria. *Geochim. Cosmochim. Acta.* **40**, 457-465.

Duncan R. A. and Green D. H. (1980) Role of multistage melting in the formation of oceanic crust. *Geology* **8**, 22-26.

Duncan R. A. and Green D. H. (1987) The genesis of refractory melts in the formation of oceanic crust. *Contrib. Mineral. Petrol.* **96**, 326-342.

Dungan M. A. and Rhodes J. M. (1978) Residual glasses and melt inclusions in basalts from DSDP Legs 45 and 46: evidence for magma mixing. *Contrib. Mineral. Petrol.* **67**, 417-431.

Dunn T. and Sen C. (1993) Mineral/matrix partition coefficients for orthopyroxene, plagioclase and olivine in basaltic to andesitic systems: a combined analytical and experimental study. *Geochim. Cosmochim. Acta* **58**, 717-753.

Eggins S. M., Woodhead J. D., Kinsley L. P. J., Mortimer G. E., Sylvester P., McCullogh M. T., Hergt J. M., and Handler M. R. (1996) A simple method for the precise determination of >40

trace elements in geological samples by ICP-MS using enriched isotope internal standardisation. *Chem. Geol.* **134**, 311-326.

Elthon D. (1984) Plagioclase buoyancy in oceanic basalts: chemical effects. *Geochim. Cosmochim. Acta* **48**, 753-768.

Elthon D. (1987) Petrology of gabbroic rocks from the mid-Cayman Rise spreading centre. *J. Geophys. Res.* **92**, 658-682.

Elthon D. (1990) The petrogenesis of primary mid-ocean ridge basalts. *Rev. Aquatic Sci.* **2**, 27-53.

Elthon D. and Casey J. F. (1985) The very depleted nature of certain primary mid-ocean ridge basalts. *Geochim. Cosmochim. Acta* **49**, 289-298.

Elthon D., Casey J. F., and Komor S. (1982) Mantle chemistry of ultramafic cumulates from the North Arm Mountain Massif of the Bay of Islands ophiolite: evidence for high pressure crystal fractionation of oceanic basalts. *J. Geophys. Res.* **87**, 8717-8734.

Elthon D. and Scarfe C. M. (1984) High-pressure phase equilibria of a high-magnesia basalt and the genesis of a primary oceanic basalt. *Am. Mineral.* **69**, 1-15.

Etoubleau J., Corre O., Joron J. L., Bougalt H., and Treuil M. (1983) Costa Rica Rift: variably depleted basalts in the same hole. In *Init. Repts. DSDP*, Vol. 69 (ed. J. R. Cann, M. G. Langseth, J. Honnorez, R. P. Von Herzen, S. M. White, et al.), pp. 765-773. U.S. Govt. Printing Office.

Falloon T. J. and Green D. H. (1987) Anhydrous partial melting of MORB pyrolite and other peridotite compositions at 10 kbars: implications for the origin of primitive MORB glasses. *Mineral. Petrol.* **37**, 181-219.

Falloon T. J. and Green D. H. (1988) Anhydrous partial melting of a peridotite from 8 to 35 kb and the petrogenesis of MORB. *J. Petrol.*(special Lithosphere issue), 379-414.

Falloon T. J., Green D. H., Hatton C. J., and Harris K. L. (1988) Anhydrous melting of depleted and fertile peridotite from 2 to 30 kb and application to basalt petrogenesis. *J. Petrol.* **29**, 1257-1282.

Falloon T. J., Green D. H., Hawkins J. L., and Jaques, A. L. (1997) Refractory magmas in back-arc basin settings: experimental constraints on the petrogenesis of a Lau Basin example. *J. Petrol.* (submitted).

Fisk M. R. (1984) Depths and temperatures of mid-ocean ridge magma chambers and the composition of their source. In *Ophiolites and oceanic lithosphere. Geol. Soc. Lond. Spec. Publ.*, Vol. 13 (ed. I. G. Gass, S. J. Lippard, and A. W. Shelton), pp. 17-23. Blackwell.

Fisk M. R. and Bence A. E. (1980) Experimental crystallisation of chrome spinel in FAMOUS basalt 527-1-1. *Earth Planet. Sci. Lett.* **48**, 111-123.

Fisk M. R., Johnson K. T. M., and Alt J. C. (1995) Effect of assimilation of altered oceanic crust on magma chemistry: an experimental study. In *Proc. ODP Sci. Results*, Vol. 137/140 (ed. J. Erzinger, K. Becker, H. J. B. Dick, and L. B. Stokking), pp. 43-51. Ocean Drilling Program.

Fisk M. R., McNeill A. W., Teagle D. A., Furnes H., and Bach W. (1996) Major element chemistry of Leg 148, Hole 896A glass: data report. In *Proc. ODP Sci. Results*, Vol. 148 (ed. J. Alt, H. Kinoshita, L. Stokking, and P. J. Michael), pp. 483-487.

Fisk M. R. and Nielsen R. L. (1990) Rare earth elements in partial melts of altered oceanic crust. (Abstr.). *Eos* **71**, 1703.

Flower M. F. J. (1980) Accumulation of calcic plagioclase in ocean ridge tholeiites: An indication of spreading rate. *Nature* **287**, 530-532.

Ford C. E., Russell D. G., Craven J. A., and Fisk M. R. (1983) Olivine-liquid equilibria: temperature, pressure and composition dependence of the crystal/liquid cation partition coefficients for Mg, Ca and Mn. *J. Petrol.* **24**, 256-265.

Forsyth D. W. (1992) Geophysical constraints on mantle flow and melt generation beneath mid-ocean ridges. In *Mantle flow and melt generation at mid-ocean ridges. Geophysical Monograph*, Vol. 71 (ed. J. Phipps Morgan, D. K. Blackman, and J. M. Sinton), pp. 1-65. American Geophysical Union.

Fram M. S. and Longhi J. (1992) Phase equilibria of dykes associated with Proterozoic anorthosite complexes. *Am. Mineral.* **77**, 605-616.

Francheteau J., Armijo R., Cheminee J. L., Hekinian R., Lonsdale P. F., and Blum N. (1990) 1 Ma East Pacific Rise oceanic crust and uppermost mantle exposed by rifting in Hess Deep (equatorial Pacific Ocean). *Earth Planet. Sci. Lett.* **101**, 281-295.

Francis D. (1986) The pyroxene paradox in MORB glasses - a signature of picritic parental magmas? *Nature* **319**, 586-589.

Frey F. A., Bryan W. B., and Thompson G. (1974) Atlantic ocean floor: geochemistry and petrology of basalts from Legs 2 and 3 of the DSDP. *J. Geophys. Res.* **79**, 5507-5527.

Frey F. A., Green D. H., and Roy S. D. (1978) Integrated models of basalt petrogenesis; a study of quartz-tholeiites to olivine melilitites from S.E. Australia utilising geochemical and experimental petrological data. *J. Petrol.* **19**, 463-513.

Früh-Green G. L., Plas A., and Lecuyer C. (1996) Petrologic and stable isotope constraints on hydrothermal alteration and serpentinization of the EPR shallow mantle at Hess Deep (Site 895). In *Proc. ODP Sci. Results*, Vol. 147 (ed. C. Mevel, K. M. Gillis, J. F. Allan, and P. S. Meyer), pp. 255-291. Ocean Drilling Program.

Fuji T. (1989) Genesis of mid-ocean ridge basalts. In *Magmatism in the ocean basins. Geol. Soc. Spec. Publ.*, Vol. 42 (ed. A. D. Saunders and M. J. Norry), pp. 137-146. Blackwell.

Fuji T. and Bougalt H. (1983) Melting relations of a magnesian abyssal tholeiite and the origin of MORBs. *Earth Planet. Sci. Lett.* **62**, 283-295.

Fuji T. and Scarfe C. M. (1985) Composition of liquids coexisting with spinel lherzolite at 10 kb and the genesis of MORBs. *Earth Planet. Sci. Lett.* **90**, 18-28.

Furuta T. and Tokuyama H. (1983) Chromian spinels in Costa Rica Rift basalts, DSDP Site 505: a preliminary interpretation of electron microprobe analyses. In *Init. Repts. DSDP*, Vol. 69 (ed. J. R. Cann, M. G. Langseth, J. Honnorez, R. P. Von Herzen, S. M. White, et al.), pp. 805-810. U.S. Govt. Printing Office.

Gaetani G. A., Grove T. L., and Bryan W. B. (1994) Experimental phase relations of basaltic andesite from hole 839B under hydrous and anhydrous conditions. In *Proc. ODP, Sci. Results*, Vol. 135 (ed. J. W. Hawkins, L. Parson, J. Allan, et al.), pp. 557-565. (Ocean Drilling Program).

Gamble R. P. and Taylor L. A. (1980) Crystal-liquid partitioning in augite: effects of cooling rate. *Earth Planet. Sci. Lett.* **47**, 21-33.

Gast P. W. (1968) Trace element fractionation and the origin of tholeiitic and alkaline magma types. *Geochim. Cosmochim. Acta* **32**, 1057-1086.

Govindaraju K. (1989) 1989 compilation of working values and sample descriptions for 272 geostandards. *Geostandards Newsletter* **13**, 1-113.

Green D. H., Hibberson W. O., and Jaques A. L. (1979) Petrogenesis of mid-ocean ridge basalt. In *The earth: its origin structure and evolution.* (ed. M. W. McElhinney), pp. 265-299. Academic Press.

Green D. H. and Ringwood A. E. (1967) The genesis of basaltic magmas. *Contrib. Mineral. Petrol.* **15**, 103-190.

Grove T. L. and Bryan W. B. (1983) Fractionation of pyroxene-phyric MORB at low pressure: an experimental study. *Contrib. Mineral. Petrol.* **84**, 293-309.

Grove T. L., Gerlach D. C., and Sando T. W. (1982) Origin of calc-alkaline series lavas at Medicine Lake volcano by fractionation, assimilation and mixing. *Contrib. Mineral. Petrol.* **80**, 160-182.

Grove T. L., Kinzler R. J., and Bryan W. B. (1992) Fractionation of mid-ocean ridge basalt (MORB). In *Mantle flow and melt generation at mid-ocean ridges. Geophysical Monograph*, Vol. 71 (ed. J. Phipps-Morgan, D. K. Blackman, and J. M. Sinton), pp. 281-310. American Geophysical Union.

Gu C. and Vanko D. A. (1996) Nature of fluid inclusions in samples of the deep sheeted dykes cored during Leg 148 (Hole 504B). In *Proc. ODP Sci. Results*, Vol. 148 (ed. J. C. Alt, H. Kinoshita, L. B. Stokking, and P. J. Michael), pp. 87-95. Ocean Drilling Program.

Gurenko A. A. and Chaussidon M. (1994) Coexistence of enriched and depleted primitive melts and inclusions in olivine from Reykjanes tholeiites, Iceland (Abstr). *Min. Mag.* **58A**(Goldschmidt Conference, Edinburgh), 356-357.

Gurenko A. A. and Chaussidon M. (1995) Enriched and depleted primitive melts included in olivine from Icelandic tholeiites: Origin by continuous melting of a single magma column. *Geochim. Cosmochim. Acta* **59**, 2905-2917.

Gurenko A. A., Sobolev A. V., and Kononkova N. N. (1991) Petrology of the primary magma of the Reykjanes peninsula rift tholeiites. *Geochem. Int.* **28**, 58-71.

Hansteen T. H. (1991) Multi-stage evolution of the picritic Maelifell rocks, SW Iceland: constraints from mineralogy and inclusions of glass and fluid in olivine. *Contrib. Mineral. Petrol.* **109**, 225-239.

Haskell K., Forsyth L., Nielsen R. L., and Fisk M. R. (1993) Experimental constraints on the parental magma for the high An feldspar bearing Lamont seamount lavas. (Abstr.) *AGU Fall Meeting, San Francisco. Eos.* **74**, 357.

Hawkins J. W. and Melchior J. T. (1985) Petrology of Mariana Trough and Lau Basin basalts. *J. Geophys. Res.* **90**, 11431-11461.

Herbert R., Constantin M., and Robinson P. T. (1991) Primary Mineralogy of Leg 118 Gabbroic Rocks and their Place in the Spectrum of Oceanic Mafic Igneous Rocks. In *Proc. ODP, Sci. Results*, Vol. 118 (ed. R. P. Von Herzen, P. T. Robinson, et al.), pp. 3-20. Ocean Drilling Program.

Herbert R., Serri G., and Hekinian R. (1989) Mineral chemistry of ultramafic tectonites and ultramafic to gabbroic cumulates from the major oceanic basin and the Northern Apennines Ophiolites-a comparison. *Chem. Geol.* **77**, 183-207.

Hekinian R., Moore J. G., and Bryan W. B. (1976) Volcanic rocks and processes of the Mid-Atlantic Ridge Rift Valley near 36 46'N. *Contrib. Mineral. Petrol.* **58**, 83-110.

Hekinian R. and Walker D. (1987) Diversity and spatial zonation of volcanic rocks from East Pacific Rise near 21°N. *Contrib. Mineral. Petrol.* **96**, 265-280.

Hemond C., Arndt N. T., Lichtenstein U., Hofmann A., Oskarsson N., and Steinthorsson S. (1993) The heterogeneous Iceland plume: Nd-Sr-O isotopes and trace element constraints. *J. Geophys. Res.* **98**, 15833-15850.

Hertogen J. and Gijbels R. (1976) Calculation of trace element fractionation during partial melting. *Geochim. Cosmochim. Acta* **40**, 313-322.

Hess P. C. (1992) Phase equilibria constraints on the origin of ocean floor basalts. In *Mantle flow and melt generation at mid-ocean ridges. Geophysical Monograph*, Vol. 71 (ed. J. Phipps Morgan, D. K. Blackman, and J. M. Sinton), pp. 67-102. American Geophysical Union.

Hey R. N. (1977) Tectonic evolution of the Cocos-Nazca spreading centre. *Geol. Soc. Am. Bull.* **88**, 1404-1420.

Hey R. N., Johnson G. L., and Lowrie A. (1977) Recent plate motions in the Galapagos area. *Geol. Soc. Am. Bull.* **88**, 1385-1403.

Hill R. L. and Sack R. O. (1987) Thermodynamic properties of Fe-Mg titanomagnetite spinels. *Can. Mineral.* **25**, 443-464.

Hinton R. W. (1990) Ion microprobe trace element analysis of silicates: measurement of multi-element glasses. *Chem. Geol.* **83**, 11-25.

Hinton R. W. (1995) Ion microprobe analysis in geology. In *Microprobe techniques in the earth sciences.* (ed. P. J. Potts, J. F. W. Bowles, S. J. B. Reed, and M. R. Cave), pp. 235-289. Chapman and Hall.

Hirth G. and Kohlstedt D. L. (1995) Experimental constraints on the dynamics of the partially molten upper mantle: deformation in diffusion creep regime. *J. Geophys. Res.* **100**, 1981-2001.

Hobart M. A., Langseth M. B., and Anderson R. N. (1985) A geothermal and geophysical survey of the south flank of the Cost Rica Rift: Sites 504 and 505. In *Init. Repts. DSDP*, Vol. 83 (ed. R. N. Anderson, J. Honnorez, K. Becker et al.), pp. 379-404. U.S. Govt. Printing Office.

Hodges F. N. and Papike J. J. (1976) DSDP site 334: magmatic cumulates from oceanic layer 3. *J. Geophys. Res.* **81**, 4135-4151.

Housh T. B. and Luhr J. F. (1991) Plagioclase-melt equilibria in hydrous systems. *Am. Mineral.* **76**, 477-492.

Humler E. and Whitechurch H. (1988) Petrology of basalts from the central Indian Ridge (Lat. 25°23'S, Long. 70°04'E):estimates of frequencies and fractional volumes of magma injections in a two-layered reservoir. *Earth Planet. Sci. Lett.* **88**, 169-181.

Ihinger P., Hervig R. L., and McMillan P. F. (1994) Analytical methods for volatiles in glasses. In *Volatiles in magmas. Reviews in Mineralogy*, Vol. 30 (ed. M. R. Carroll and J. R. Holloway), pp. 67-112. Mineralogical Society America.

Ireland T. R. and McDonough W. F. (1993) Insights into the Archaean mantle and komatiite genesis from glass inclusions in olivines (Abstr.). *IAVCEI General assembly, Canberra, Australia,* 52.

Irvine T. N. (1967) Chromian spinel as a petrogenetic indicator: Part 2. Petrological applications. *Can. J. Earth Sci.* **4**, 71-103.

Jaques A. L. and Green D. H. (1980) Anhydrous partial melting of peridotite at 0-15 Kb pressure and the genesis of tholeiitic basalts. *Contrib. Mineral. petrol.* **73**, 287-310.

Jarosewich E. J., Nelen J. A., and Norberg J. A. (1980) Reference samples for electron microprobe analysis. *Geostandards Newsletter* **4**, 43-47.

Johnson J. A., Nielsen R. L., and Fisk M. R. (1995) Plagioclase hosted melt inclusions in the Steens basalt, Southeastern Oregon. (Abstr.) *Spring AGU meeting, Baltimore, Eos,* 76(17), S269.

Johnson K. T. M. and Dick H. J. B. (1992) Open system melting and temporal and spatial variation of peridotite and basalt in the Atlantis II Fracture Zone. *J. Geophys. Res.* **97**, 9219-9241.

Johnson K. T. M., Dick H. J. B., and Shimizu N. (1990) Melting in the oceanic upper mantle: an ion microprobe study of diopsides in abyssal peridotites. *J. Geophys. Res.* **95**, 2661-2678.

Johnson K. T. M., Fisk M. R., and Naslund H. R. (1995) Geochemical characteristics of refractory melt inclusions from Leg 140 basalts. In *Proc. ODP, Sci. Results*, Vol. 137/140 (ed. J. Erzinger, K. Becker, H. B. Dick, and L. Stokking), pp. 112-135. Ocean Drilling Program.

Johnson K. T. M. and Kong L. S. L. (1992) Open system melting at mid-ocean ridges. (Abstr.) *AGU Fall Meeting, San Francisco. Eos* 73(43), 615.

Johnson K. T. M. and Kushiro I. (1992) Segregation of high pressure partial melts from peridotite using aggregates of diamond: a new experimental approach. *Geophys. Res. Lett.* **19**, 1703-1706.

Johnson M. C., Anderson A. T. J., and Rutherford M. J. (1994) Pre-eruptive volatile contents of magmas. In *Volatiles in magmas. Reviews in Mineralogy*, Vol. 30 (ed. M. R. Carroll and J. R. Holloway), pp. 281-330. Mineralogical Society America.

Kamenetsky V. S. (1996) Methodology for the study of melt inclusions in Cr-spinel and implications for parental melts of MORB from FAMOUS area. *Earth Planet. Sci. Lett.* **142**, 479-486.

Karsten J. L., Delaney J. R., Rhodes J. M., and Liias R. A. (1990) Spatial and temporal evolution of magmatic systems beneath the Endeavour segment, Juan de Fuca Ridge: tectonic and petrologic constraints. *J. Geophys. Res.* **95**, 19235-19256.

Keen J. K. and Elthon D. (1996) Anatomy of a Mid-Cayman Rise gabbro (Abstr.). V. M. Goldschmidt Conference, Heidelberg. *J. Conf. Abstr.* **1**, 393.

Kelemen P. B. (1990) Reaction between ultramafic rock and fractionating basaltic magma 1. Phase relations, the origin of calc-alkaline magma series, and the formation of discordant dunite. *J. Petrol.* **31**, 51-98.

Kelemen P. B., Dick H. J. B., and Quick J. E. (1992) Formation of harzburgite by pervasive melt/rock reaction in the upper mantle. *Nature* **358**, 635-641.

Kelemen P. B., Shimizu N., and Salters J. M. (1995) Extraction of mid-ocean ridge basalt from the upwelling mantle by focussed flow of melt in dunite channels. *Nature* **375**, 747-753.

Kelley D. S., Vanko D. A., and Gu C. (1995) Fluid evolution in oceanic crustal layer 2: fluid inclusion evidence from the sheeted dyke complex, Hole 504B, Costa Rica Rift. In *Proc. ODP Sci. Results.*, Vol. 137/140 (ed. J. Erzinger, H. J. B. Dick, and L. B. Stokking), pp. 191-198. Ocean Drilling Program.

Kempton P. D. (1985) An interpretation of contrasting nucleation and growth histories from the petrographic analysis of pillow and dike chilled margins, hole 504B, DSDP Leg 83. In *Init. Repts. DSDP*, Vol. 83 (ed. R. N. Anderson, J. Honnorez, K. Becker, et al.), pp. 165-181. U.S. Govt. Printing Office.

Kempton P. D., Autio L. K., Rhodes J. M., Holdaway M. J., Dungan M. A., and Johnson P. (1985) Petrology of basalts from hole 504B, Deep Sea Drilling Project, Leg 83. In *Init. Repts. DSDP*, Vol. 83 (ed. R. N. Anderson J. Honnorez, K. Becker et al.), pp. 129-164. U.S. Govt. Printing Office.

Kepezhinskas P. K., Sorokina N. A., Mamontova A., and Savichev A. T. (1995) Rare earth and large-ion lithophile (Sr and Ba) element geochemistry of diabase dikes, Hole 504B, Costa Rica Rift, Leg 140. In *Proc. ODP Sci. Results*, Vol. 137/140 (ed. J. Erzinger, K. Becker, H. J. B. Dick, and L. B. Stokking), pp. 107-116. Ocean Drilling Program.

Kinzler R. J. and Grove T. L. (1992a) Primary magmas of mid-ocean ridge basalts 1. Experiments and methods. *J. Geophys. Res.* **97**, 6885-6906.

Kinzler R. J. and Grove T. L. (1992b) Primary magmas of mid-ocean ridge basalts 2. Applications. *J. Geophys. Res.* **97**, 6907-6926.

Klein E. M. and Langmuir C. H. (1987) Global correlations of ocean ridge basalt chemistry with axial depth and crustal thickness. *J. Geophys. Res.* **92**, 8089-8115.

Klein E. M. and Langmuir C. H. (1989) Local versus global variations in ocean ridge basalt composition: A reply. *J. Geophys. Res.* **94**, 4241-4252.

Klitgord K. D., Huestis S. D., Mudie J. D., and Parker R. L. (1975) An analysis of near bottom magnetic anomalies, seafloor spreading and the magnetized layer. *Geophys. J. R. Astron. Soc.* **43**, 387-424.

Kohlstedt D. L. (1992) Structure, rheology and permeability of partially molten rocks at low melt fractions. In *Mantle flow and melt generation at mid-ocean ridges. Geophysical Monograph*, Vol. 71 (ed. J. Phipps Morgan, D. K. Blackman, and J. M. Sinton), pp. 103-121. American Geophysical Union.

Komar P. D. (1976) Phenocryst interactions and the velocity profile of magma flowing through dykes or sills. *Geol. Soc. Am. Bull.* **87**, 1336-1342.

Komor S. C., Grove T. L., and Herbert R. (1990) Abyssal Peridotites from ODP Hole 670A (21°10'N, 45°02'W): Residues of Mantle Melting Exposed by Non-constructive Axial Divergence. In *Proc. ODP, Sci. Results.*, Vol. 106/109 (ed. R. Detrick, J. Honnorez, W. B. Bryan, T. Juteau, et al.), pp. 85-101. Ocean Drilling Program.

Kuo L.-C. and Kirkpatrick R. J. (1982) Pre-eruption history of phyric basalts from DSDP Legs 45 and 46: Evidence from morphology and zoning patterns in plagioclase. *Contrib. Mineral. Petrol.* **79**, 13-27.

Kusakabe M., Shibata T., Yamamoto M., Mayeda S., Kagami H., Honma H., Masuda H., and Sakai H. (1989) Petrology and isotope characteristics (H, O, S, Sr and Nd) of basalts from Ocean Drilling Program Hole 504B, Leg 111, Costa Rica Rift. In *Proc. ODP, Sci. Results.*, Vol. 111 (ed. K. Becker, H. Sakai, et al.), pp. 47-60. Ocean Drilling Program.

Kushiro I. (1996) Partial melting of fertile mantle peridotite at high pressures: an experimental study using aggregates of diamond. In *Earth processes: reading the isotopic code. Geophysical Monograph*, Vol. 95 (ed. S. R. Hart and A. Basu), pp. 109-122. American Geophysical Union.

Langmuir C. H. (1989) Geochemical consequences of in situ crystallisation. *Nature* **340**, 199-205.

Langmuir C. H., Klein E. M., and Plank T. (1992) Petrological systematics of mid-ocean ridge basalts: constraints on melt generation beneath ocean ridges. In *Mantle flow and melt generation at mid-ocean ridges. Geophysical Monograph*, Vol. 71 (ed. J. Phipps Morgan, D. K. Blackman, and J. M. Sinton), pp. 183-280. American Geophysical Union.

Langseth M. G., Cann J. R., Natland J. H., and Hobart M. (1983) Geothermal phenomena at the Costa Rica Rift: background and objectives for drilling at DSDP sites 501, 504, and 505. In *Init. Repts. DSDP*, Vol. 69 (ed. J. R. Cann, M. G. Langseth, J. Honnorez, R. P. Von Herzen, S. M. White, et al.), pp. 5-29. U.S. Govt. Printing Office.

Laverne C., Vanko D. A., Tartarotti P., and Alt J. C. (1995) Chemistry and geothermometry of secondary minerals from the deep sheeted dike complex, Hole 504B. In *Proc. ODP Sci. Results*, Vol. 137/140 (ed. J. Erzinger, K. Becker, H. J. B. Dick, and L. B. Stokking), pp. 167-189. Ocean Drilling Program.

Lavrentev Y. G., Pospelova L. N., and Sobolev A. V. (1974) Rock-forming mineral compositions determination by X-ray microanalysis. *Zavodskaya Laboratoria* **40**, 657-666.

Le Maitre R. W. (1982) Numerical petrology: statistical interpretation of geochemical data. *Developments in petrology*, **8**, 281p, Elsevier.

Le Roex A. P., Erlank A. J., and Needham H. D. (1981) Geochemical and mineralogical evidence for the occurrence of at least three distinct magma types in the "Famous" region. *Contrib. Mineral. Petrol.* 77, 24-37.

Le Roex A. P., Frey F. A., and Richardson S. H. (1996) Petrogenesis of lavas from the AMAR valley and Narrowgate region of the FAMOUS Valley, 36-37N on the Mid-Atlantic Ridge. *Contrib. Mineral. Petrol.* **124**, 167-184.

Longhi J., Walker D., and Hays J. F. (1976) Fe and Mg in plagioclase. ***Proc. Lunar Sci. Conf.*** 7, 1281-1300.

Lonsdale P. and Klitgord K. D. (1978) Structure and tectonic history of the Panama basin. *Geol. Soc. Am. Bull.* **89**, 981-999.

Loomis T. P. (1981) An investigation of disequilibrium growth processes of plagioclase in the system anorthite-albite-water by methods of numerical simulation. *Contrib. Mineral. Petrol.* **76**, 196-205.

Lowenstern J. B. (1994) Dissolved volatile concentrations in an ore-forming magma. *Geology* **22**, 893-896.

Lu F., Anderson A. T., and Davis A. M. (1995) Diffusional gradients at the crystal/melt interface and their effect on the composition of melt inclusions. *J. Geol.* **103**, 591-597.

Lundstrom C. C., Gill J., Williams Q., and Perfit M. R. (1995) Mantle melting and basalt extraction by equilibrium porous flow. *Science* **270**, 1958-1961.

Maaloe S. (1982) Geochemical aspects of permeability controlled partial melting and fractional crystallisation. *Geochim. Cosmochim. Acta* **46**, 43-57.

Maaloe S. and Scheie A. (1982) The permeability controlled accumulation of primary magma. *Contrib. Mineral. Petrol.* **81**, 350-357.

Marsh B. D. (1996) Solidification fronts and magmatic evolution. *Min. Mag.* **60**, 5-40.

Marsh B. D. and Maxey. (1985) On the distribution and settling of crystals in a convecting magma. *J. Volcanol. Geotherm. Res.* **24**, 95-150.

Marsh N. G., Tarney J., and Hendry G. L. (1983) Trace element geochemistry of basalts from Hole 504B, Panama Basin, Deep Sea Drilling Project Legs 69 and 70. In *Init. Repts. DSDP*, Vol. 69 (ed. J. R. Cann, M. G. Langseth, J. Honnorez, R. P. Von Herzen, S. M. White, et al.), pp. 747-763. U.S. Govt. Printing Office.

Mathison C. I. (1987) Pyroxene oikocrysts in troctolitic cumulates - evidence for supercooled crystallisation and post-cumulus modification. *Contrib. Mineral. Petrol.* **97**, 228-236.

Maurel C. and Maurel P. (1982) Etude experimentale de l'equilibre Fe^{2+}-Fe^{3+} dans les spinelles chromiferes et les liquides silicates basiques coexistants, a 1 atm. *C. R. Acad. Sci. Paris* **285**, 209-215.

McBirney A. (1995) Mechanisms of differentiation in the Skaergaard intrusion. *J. Geol. Soc. Lond.* **152**, 421-435.

McKenzie D. (1984) The generation and compaction of partially molten rock. *J. Petrol.* **25**, 713-765.

McKenzie D. (1985a) The extraction of magma from the crust and mantle. *Earth Planet. Sci. Lett.* **74**, 81-91.

McKenzie D. (1985b) ^{230}Th-^{238}U dis-equilibrium and the melting process beneath ridge axes. *Earth Planet. Sci. Lett.* **72**, 149-157.

McKenzie D. and Bickle M. J. (1988) The volume and composition of melt generated by extension of the lithosphere. *J. Petrol.* **29**, 625-679.

McKenzie D. and O'Nions R. K. (1991) Partial melt distributions from inversions of REE concentrations. *J. Petrol.* **32**, 1021-1091.

McNeill A. W. (1995) Petrology of chilled dike margins recovered from Hole 504B, Leg 140. In *Proc. ODP Sci. Results*, Vol. 137/140 (ed. J. Erzinger, H. J. B. Dick, and L. B. Stokking), pp. 35-42. Ocean Drilling Program.

Melson W. G., Vallier T. L., Wright T. L., Byerly G., and Nelen J. (1976) Chemical diversity of abyssal volcanic glass erupted along Pacific, Atlantic, and Indian ocean sea-floor spreading centers. In *The geophysics of the Pacific Ocean basin and its margin. A volume in honour of George P. Woolard. Geophysical Monograph*, Vol. 19 (ed. G. H. Sutton, M. Manghnani, and R. Moberly), pp. 351-367. American Geophysical Union.

Meyer P. S., Dick H. J. B., and Thompson G. (1989) Cumulate gabbros from the Southwest Indian Ridge, 54°S-7°16'E: implications for magmatic processes at a slow spreading ridge. *Contrib. Mineral. Petrol.* **103**, 44-63.

Michael P. J. (1988) The concentration, behaviour and storage of H_2O in the suboceanic upper mantle: implications for mantle metasomatism. *Geochim. Cosmochim. Acta* **52**, 555-566.

Michael P. J. and Chase R. L. (1987) The influence of primary magma composition, H_2O and pressure on mid-ocean ridge basalt differentiation. *Contrib. Mineral. Petrol.* **96**, 245-263.

Michael P. J. and Nielsen R. L. (1995) Volatile contents in plagioclase hosted melt inclusions in MORB from the Gorda Ridge (Abstr). *AGU Spring meeting, Baltimore. Eos.* **76**(17), S267.

Michael P. J. and Schilling J.-G. (1989) Chlorine in mid-ocean ridge magmas: evidence for assimilation of seawater influenced components. *Geochim. Cosmochim. Acta* **53**, 3131-3143.

Morgan J. P. (1987) Melt migration beneath mid-ocean ridge spreading centres. *Geophys. Res. Lett.* **83**, 137-152.

Morimoto N. and Subcommittee on pyroxenes. (1989) Nomenclature of pyroxenes. *Can. Mineral.* **27**, 143-156.

Naslund H. R. (1995) Grain-size, morphological, and compositional variations in igneous silicates in medium grained diabase from Hole 504B. In *Proc. ODP Sci. Results*, Vol. 137/140 (ed. J. Erzinger, H. J. B. Dick, and L. B. Stokking), pp. 3-17. Ocean Drilling Program.

Naslund H. R., Sparks J. W., and Fisk M. R. (1995) Computer modelling of major and trace element variations of Hole 504B and diabase. In *Proc. ODP Sci. Results*, Vol. 137/140 (ed. J. Erzinger, K. Becker, H. J. B. Dick, and L. B. Stokking), pp. 53-61. Ocean Drilling Program.

Natland J. H. (1989) Partial melting of a lithologically heterogeneous mantle: inferences from crystallization histories of magnesian abyssal tholeiites from the Siqueiros Fracture Zone. In *Magmatism in the ocean basins Geol. Soc. Lond. Spec. Publ.*, Vol. 42 (ed. A. D. Saunders and M. J. Norry), pp. 41-70.

Natland J. H., Adamson A. C., Laverne C., Melson W. G., and O'Hearn T. A. (1983) Compositionally nearly steady-state magma chamber at the Costa Rica Rift: evidence from basalt glass and mineral data, Deep Sea Drilling Project sites 501, 504 and 505. In *Init. Repts. DSDP*, Vol. 69 (ed. J. R. Cann, M. G. Langseth, J. Honnorez, R. P. Von Herzen, S. M. White, et al.), pp. 811-858. U.S. Govt. Printing Office.

Navon O. and Stolper E. (1987) Geochemical consequences of melt percolation: the upper mantle as a chromatographic column. *J. Geol.* **95**, 285-307.

Newman S., Stolper. E. M., and Epstein S. (1986) Measurement of water in rhyolitic glasses: calibration of an infrared spectroscopic technique. *Am. Mineral.* **71**, 1527-1541.

Nicolas A. (1986) Melt extraction model based on structural studies in mantle peridotites. *J. Petrol.* **27**, 999-1022.

Nielsen R. L. (1990) Simulation of igneous differentiation processes. In *Modern methods of igneous petrology: understanding magmatic processes. Reviews in Mineralogy*, Vol. 24 (ed. J. Nicholls and J. K. Russell), pp. 65-104. Mineralogical Society America.

Nielsen R. L., Christie D. M., and Sprtel F. M. (1995) Anomalous low Na MORB magmas: Evidence for depleted MORB or analytical artefact. *Geochim. Cosmochim. Acta.* **59**, 5023-5026.

Nielsen R. L., Crum J., Bourgeois R., Hascall K., Forsythe D., Christie D. M., and Fisk M. R. (1994) Local diversity of MORB parent magmas: evidence from melt inclusions in high-An feldspar from the Gorda Ridge (Abstr). *Min. Mag.* **58A**(Goldschmidt Conference, Edinburgh.), 651-652.

Nielsen R. L., Crum J., Bourgeois R., Hascall K., Forsythe L. M., Fisk M. R., and Christie D. M. (1995) Melt inclusions in high-An plagioclase from the Gorda Ridge: An example of the local diversity of MORB parent magmas. *Contrib. Mineral. Petrol.* **122**, 34-50.

Nielsen R. L. and De Long S. E. (1992) A numerical approach to boundary layer fractionation; application to differentiation in natural systems. *Contrib. Mineral. Petrol.* **110**, 355-369.

Niu Y. (1997) Mantle melting and melt extraction processes beneath ocean ridges: evidence from abyssal peridotites. *J. Petrol.* **38**, 1047-1074.

Niu Y. and Batiza R. (1991a) DENSCAL: a program for calculating densities of silicate melts and mantle minerals in the melting range. *Comp. Geosci.* **17**, 679-687.

Niu Y. and Batiza R. (1991b) An empirical method for calculating melt compositions produced beneath mid-ocean ridges: applications for axis and off-axis (seamounts) melting. *J. Geophys. Res.* **96**, 21753-21777.

Niu Y. and Batiza R. (1994) Magmatic processes at a slow spreading ridge segment: 26°S Mid-Atlantic Ridge. *J. Geophys. Res.* **99**, 19719-19740.

Niu Y. and Hekinian R. (1997a) Basaltic liquids and harzburgitic residues in the Garrett Transform: a case study at fast-spreading ridges. *Earth Planet. Sci. Lett.* **146**, 243-258.

Niu Y. and Hekinian R. (1997b) Spreading rate dependance of the extent of mantle melting beneath ocean ridges. *Nature* **385**, 326-329.

Norrish K. and Chappell B. W. (1977) X-ray fluorescence spectrometry. In *Physical methods in determinative mineralogy* (ed. J. Zussman), pp. 201-272. Academic Press.

O'Donnell T. H. and Presnall D. C. (1980) Chemical variations of the glass and mineral phases dredged from 25°-30°N along the Mid-Atlantic Ridge. *Am. J. Sci.* **280A**, 845-868.

O'Hara M. J. (1968a) Are ocean floor basalts primary magma? *Nature* **220**, 683-686.

O'Hara M. J. (1968b) The bearing of phase equilibria studies in synthetic and natural systems on the origin and evolution of basic and ultrabasic rocks. *Earth Sci. Rev.* **4**, 69-133.

O'Hara M. J. (1977) Geochemical evolution during fractional crystallisation of a periodically refilled magma chamber. *Nature* **266**, 503-507.

O'Hara M. J. (1985) Importance of the 'shape' of the melting regime during partial melting of the mantle. *Nature* **314**, 58-62.

O'Hara M. J. and Fry N. (1996) Geochemical effects of small packet crystallisation in large magma chambers-further resolution of the highly compatible element paradox. *J. Petrol.* **37**, 891-925.

O'Hara M. J. and Matthews R. E. (1981) Geochemical evolution in an advancing, periodically replenished, periodically tapped, continuously fractionating magma chamber. *J. Geol. Soc. Lond.* **138**, 237-277.

Osland L. C. J. (1985) *Principles and practices of infrared spectroscopy.* Pye Unicam Ltd.

Ozawa K., Meyer P. S., and Bloomer S. H. (1991) Mineralogy and textures of Iron-Titanium Oxide Gabbros and Associated Olivine Gabbros from Hole 735B. In *Proc. ODP, Sci. Results*, Vol. 118 (ed. R. P. Von Herzen, P. T. Robinson, et al.), pp. 41-73. Ocean Drilling Program.

Pallister J. S. and Hopson C. A. (1981) Samail ophiolite plutonic suite: field relations, phase variation and layering and a model of a spreading ridge magma chamber. *J. Geophys. Res.* **86**, 2593-2644.

Panjasawatwong Y., Danyushevsky L. V., Crawford A. J., and Harris K. L. (1995) An experimental study of the effects of melt composition on plagioclase-melt equilibria at 5 and 10 kb: implications for the origin of magmatic high-An plagioclase. *Contrib. Mineral. Petrol.* **118**, 420-432.

Pasteris J. D. and Wanamaker B. J. (1988) Laser-microprobe analysis of experimentally re-equilibrated fluid inclusions in olivine: some implications for mantle fluids. *Am. Mineral.* **73**, 1074-1088.

Perfit M. and Fornari D. J. (1982) Geochemical studies of abyssal lavas recovered by DSRV Alvin from the Eastern Galapagos Rift, Inca Transform, and the Ecuador Rift. 2. Phase chemistry and crystallisation history. *J. Geophys. Res.* **88**, 10530-10550.

Perfit M. R., Fornari D. J., Smith M. C., Bender J. F., Langmuir C. H., and Haymon R. M. (1994) Small-scale spatial and temporal variations in mid-ocean ridge crest magmatic processes. *Geology* **22**, 375-379.

Peters M. T., Shaffer E. E., Burnett D. S., and Kim S. S. (1995) Magnesium and titanium partitioning between anorthite and type B CAI liquid: dependance on oxygen fugacity and liquid compositions. *Geochim. Cosmochim. Acta* **59**, 2785-2796.

Phinney W. C. (1992) Partition coefficients between plagioclase and basalt as a function of oxygen fugacity: implications for Archaean and lunar anorthosites. *Geochim. Cosmochim. Acta* **56**, 1885-1895.

Phinney W. C. and Morrison D. A. (1990) Partition coefficients for calcic plagioclase: implications for Archaean anorthosites. *Geochim. Cosmochim. Acta* **54**, 1639-1654.

Presnall D. C. and Hoover J. D. (1984) Composition and depth of origin of primary mid-ocean ridge basalts. *Contrib. Mineral. Petrol.* **87**, 170-178.

Price R. C., Kennedy A. K., Riggs-Sneeringer M., and Frey F. A. (1986) Geochemistry of basalts from the Indian Ocean triple junction-Implications for the generation and evolution of Indian Ocean Ridge basalts. *Earth. Planet. Sci. Lett.* **78**, 379-396.

Prinz M., Keil K., Green J. A., Reid A. M., Bonatti E., and Honnorez J. (1976) Mineralogy and petrology of some ultramafic and mafic dredge samples from the equatorial Mid-Atlantic Ridge and fracture zones. *J. Geophys. Res.* **81**, 4087-4103.

Qin Z., Lu F., and Anderson A. T. (1992) Diffusive re-equilibration of melt and fluid inclusions. *Am. Mineral.* **77**, 565-576.

Reynolds J. R., Langmuir C. H., Bender J. F., Kastens K. A., and Ryan W. B. F. (1992) Spatial and temporal variability in the geochemistry of basalts from the East Pacific Rise. *Nature* **359**, 493-499.

Rhodes J. M., Dungan M. A., Blanchard D. P., and Long P. E. (1979) Magma mixing at mid-ocean ridges; evidence from basalts drilled near 22°N on the Mid-Atlantic Ridge. *Tectonophys.* **55**, 35-61.

Richardson C. N., Lister J. R., and McKenzie D. (1996) Melt conduits in a viscous porous matrix. *J. Geophys. Res.* **101**, 20423-20432.

Richardson S. H. (1979) Chemical variation induced by flow differentiation in an extensive Karoo dolerite sheet, southern Namibia. *Geochim. Cosmochim. Acta* **43**, 1433-1441.

Richter F. M. (1986) Simple models for trace element fractionation during melt segregation. *Earth Planet. Sci. Lett.* **77**, 333-344.

Richter F. M. and McKenzie D. (1984) Dynamic models for melt segregation from a deformable matrix. *J. Geol.* **92**, 729-740.

Riddihough R. P. (1980) Gorda plate motions from magnetic anomaly analysis. *Earth Planet. Sci. Lett.* **51**, 163-170.

Riley G. N. and Kohlstedt D. L. (1991) Kinetics of melt migration in upper mantle-type rocks. *Earth Planet. Sci. Lett.* **105**, 500-521.

Ringwood A. E. (1975) *Composition and petrology of the earths mantle*. 616p, McGraw Hill.

Robson D. and Cann J. R. (1982) A geochemical model for mid-ocean ridge magma chambers. *Earth Planet. Sci. Lett.* **60**, 93-104.

Roedder E. (1979) Origin and significance of magmatic inclusions. *Bull. Minéral* **102**, 487-510.

Roedder E. (1984) Fluid inclusions. *Reviews in Mineralogy* **12**, 644p, Mineralogical Society America.

Roeder P. L. (1994) Chromite: from the fiery rain of chondrules to the Kilauea Iki lava lake. *Can. Mineral.* **32**, 729-746.

Roeder P. L. and Emslie R. F. (1970) Olivine-liquid equilibrium. *Contrib. Mineral. Petrol.* **29**, 275-289.

Roeder P. L. and Reynolds I. (1991) Crystallisation of chromite and chromium solubility in basaltic melts. *J. Petrol.* **32**, 909-934.

Salters J. V. M. and Hart S. R. (1989) The Hafnium paradox and the role of garnet in the source of mid-ocean ridge basalts. *Nature* **342**, 420-422.

Sato H. (1989) Mg-Fe partitioning between plagioclase and liquid in basalts of Hole 504B, ODP leg 111: a study of melting at 1 atm. In *Proc. ODP. Sci. Results*, Vol. 111 (ed. K. Becker, H. Sakai, et al.), pp. 17-26. Ocean Drilling Program.

Schiano P., Clocchiatti R., and Joron J. L. (1992) Melt and fluid inclusions in basalts and xenoliths from Taha Island, Society archipelago: evidence for a metasomatised upper mantle. *Earth Planet. Sci. Lett* **111**, 69-82.

Schilling J.-G. (1966) Rare earth fractionation in Hawaiian volcanic rocks. PhD., M.I.T.

Schilling J.-G. (1971) Sea-floor evolution: rare earth evidence. *Phil. Trans. Roy. Soc. Lond.* **268A**, 663-706.

Schilling J.-G. (1975) The Azores mantle blob: rare earth evidence. *Earth Planet. Sci. Lett.* **25**, 103-115.

Schilling J.-G., Kingsley R. H., and Devine J. D. (1982) Galapagos hot spot-spreading centre system 1, spatial petrological and geochemical variations (83°-101°W). *J. Geophys. Res.* **87**, 5593-5610.

Schmelling H., Cruden A. R., and Marquardt G. (1988) Finite deformation in and around a fluid sphere moving through a viscous medium; implications for diapiric ascent. *Tectonophys.* **149**, 17-34.

Schweitzer E. L., Papike J. J., and Bence A. E. (1979) Statistical analysis of pyroxenes from deep sea basalts. *Am. Mineral.* **64**, 501-513.

Scott D. C. (1992) Small scale convection and mantle melting beneath mid-ocean ridges. In *Mantle flow and melt generation at mid-ocean ridges. Geophysical Monograph*, Vol. 71 (ed. J. Phipps Morgan, D. K. Blackman, and J. M. Sinton), pp. 327-352. American Geophysical Union.

Scowen P. A. H., Roeder P. L., and Helz R. T. (1991) Re-equilibration of chromite within Kilauea Iki lava lake, Hawaii. *Contrib. Mineral. Petrol.* **107**, 8-20.

Shackelton N. J. and Hall M. A. (1983) Stable isotope record of Hole 504B sediments: High resolution record of the Pleistocene. In *Init. Repts. DSDP*, Vol. 69 (ed. J. R. Cann, M. G. Langseth, J. Honnorez, R. P. Von Herzen, S. M. White, et al.), pp. 431-441. U.S. Govt. Printing Office.

Shaw D. M. (1970) Trace element fractionation during anatexis. *Geochim. Cosmochim. Acta.* **34**, 237-243.

Shen Y. and Forsyth D. W. (1995) Geochemical constraints on initial and final depths of melting beneath mid-ocean ridges. *J. Geophys. Res.* **100**, 2211-2237.

Shibata T. and Thompson G. (1986) Peridotites from the Mid-Atlantic Ridge at 43°N and their petrogenetic relation to abyssal tholeiites. *Contrib. Mineral. Petrol.* **93**, 144-159.

Shimizu H., Mori K., and Masuda A. (1989) REE, Ba, and Sr abundances and Sr, Nd, and Ce isotopic ratios in Hole 504B basalts, ODP Leg 111, Costa Rica Rift. In *Proc. ODP, Sci. Results.*, Vol. 111 (ed. K. Becker, H. Sakai, et al.), pp. 77-83. Ocean Drilling Program.

Shimizu N. (1994) Depths of melting and melt extraction beneath mid-ocean ridges as recorded in melt inclusions (Abstr.). *Min. Mag.* **58A**(Goldschmidt Conference, Edinburgh), 829-830.

Shimizu N. and Hassler D. (1993) Coexistence of enriched- and depleted- MORB melts as olivine hosted inclusions in single FAMOUS lavas. (Abstr.) *AGU Fall Meeting, Eos.* 74(43), 644-645.

Shipboard Scientific Party. (1988a) Site 504. In *Proc. ODP, Init. Repts. (Pt. A)*, Vol. 111 (ed. K. Becker and H. Sakai et al.), pp. 1-251. Ocean Drilling Program.

Shipboard Scientific Party. (1988b) Site 648. In *Proc. ODP Init. Repts. (Pt. A)*, Vol. 106/109 (ed. R. B. Detrick, J. Honnorez, W. B. Bryan, T. Juteau, et al.), pp. 35-134. Ocean Drilling Program.

Shipboard Scientific Party. (1988c) Sites 677 and 678. In *Proc. ODP, Init. Repts. (Pt. A)*, Vol. 111 (ed. K. Becker, H. Sakai, et al.), pp. 253-346. Ocean Drilling Program.

Shipboard Scientific Party. (1992) Site 504. In *Proc. ODP, Init. Repts. (Pt. A).*, Vol. 140 (ed. H. J. B. Dick, J. Erzinger, L. B. Stokking, et al.), pp. 1-399. Ocean Drilling Program.

Shipboard Scientific Party. (1993a) Site 504. In *Proc. ODP, Init. Repts. (Pt. A).*, Vol. 148 (ed. J. C. Alt, H. Kinoshita J., L. B. Stokking, et al.), pp. 27-121. Ocean Drilling Program.

Shipboard Scientific Party. (1993b) Site 896. In *Proc. ODP, Init. Repts. (Pt. A).*, Vol. 148 (ed. J. C. Alt, H. Kinoshita J., L. B. Stokking, et al.), pp. 123-192. Ocean Drilling Program.

Sichel S. E. and Sigurdsson H. (1993) Melt inclusions from South Atlantic ridge basalts (Abstr.). *IAVCEI general assembly, Canberra, Australia*, 99.

Sigurdsson H. (1977) Spinels in Leg 37 basalts and peridotites: Phase chemistry and zoning. In *Init. Repts. DSDP*, Vol. 37 (ed. F. Aumento, W.B. Melson, et al.), pp. 883-891. U.S. Govt. Printing Office.

Sigurdsson H. and Schilling J.-G. (1976) Spinels in Mid-Atlantic ridge basalts: chemistry and occurrence. *Earth Planet. Sci. Lett.* **29**, 7-20.

Sigurdsson I. A. (1994) Primitive magmas in convergent margins and at oceanic spreading ridges: evidence from early formed phenocryst phases and their inclusions. PhD., University of Tasmania, Hobart, Tasmania.

Sinton C. W., Christie D. M., Coombs V. L., Nielsen R. L., and Fisk M. R. (1993) Near-primary melt inclusions in anorthite phenocrysts from the Galapagos Platform. *Earth Planet. Sci. Lett.* **119**, 527-537.

Sinton J. M. and Byerly G. R. (1980) Mineral compositions and crystallisation trends in DSDP Holes 417D and 418A. In *Init. Repts. DSDP*, Vol. 51,52,53 (ed. T. Donnelly, J. Francheteau, W. Bryan, P. Robinson, M. Flower, M. Salisbury, et al.), pp. 1039-1054. U.S. Govt. Printing Office.

Sinton J. M. and Detrick R. S. (1992) Mid-ocean ridge magma chambers. *J. Geophys. Res* **97**, 197-216.

Sisson T. W. and Grove T. L. (1993) Experimental investigations of the role of H_2O in calc-alkaline differentiation and subduction zone magmatism. *Contrib. Mineral. Petrol.* **113**, 143-166.

Sisson T. W. and Layne G. D. (1992) H_2O in basalt and basaltic andesite glass inclusions from four subduction related volcanoes. *Earth. Planet. Sci. Lett.* **117**, 619-635.

Skulski T., Minarik W., and Watson E. B. (1994) High pressure experimental trace element partitioning between clinopyroxene and basaltic melts. *Chem. Geol.* **117**, 127-147.

Sobolev A. V. (1983) Petrology and geochemistry of ultramafic magmas on the examples of meimechites from the northern Siberian platform. PhD., Vernadsky Institute of geochemistry, Moscow, USSR.

Sobolev A. V. and Danyushevsky L. V. (1994) Petrology and geochemistry of boninites from the north termination of the Tonga trench: constraints on the generation conditions of primary high-Ca boninite magmas. *J. Petrol.* **35**, 1181-1211.

Sobolev A. V., Danyushevsky L. V., Dmitriev L. V., and Suschevskaya N. M. (1989) High-alumina magnesian tholeiite as the primary basalt magma at mid ocean ridge. *Geochem. Int.* **26**, 128-133.

Sobolev A. V., Dmitriev L. V., Barsukov V. L., Nevsorov V. N., and Slutsky A. B. (1980) The formation conditions of the high-magnesium olivines from the monomineralic fraction of Luna 24 regolith. *Proc. Lunar Planet. Sci. Conf* **11**, 105-116.

Sobolev A. V., Kamenetsky V. S., Metrich N., Clocchiatti R., Kononkova N. N., Devirts A. L., and Ustinov V. I. (1991) Volatile regime and crystallization conditions in Etna hawaiite lavas. *Geochem. Int.* **28**, 53-65.

Sobolev A. V. and Kostyuk V. P. (1975) *Magmatic crystallisation based on a study of melt inclusions.* Nauka Press.

Sobolev A. V. and Shimizu N. (1992) Ultra-depleted primary melts and permeability of the oceanic mantle. *Doklady. Acad. Sci. Russia* **236**, 354-360.

Sobolev A. V. and Shimizu N. (1993) Ultra-depleted primary melt included in an olivine from the Mid-Atlantic Ridge. *Nature* **363**, 151-154.

Sobolev A. V. and Shimizu N. (1994) The origin of typical NMORB: the evidence from a melt inclusions study (Abstr.). *Min. Mag.* **58A**(Goldschmidt Conference, Edinburgh), 862-863.

Sorby H. C. (1858) On the microscopical structure of crystals, indicating the origin of minerals and rocks. *Geol. Soc. London Quart. J.* **14**, 453-500.

Sparks J. W. (1995) Geochemistry of the lower sheeted dike complex, Hole 504B, Leg 140. In *Proc. ODP Sci. Results*, Vol. 137/140 (ed. J. Erzinger, K. Becker, H. J. B. Dick, and L. B. Stokking), pp. 81-97. Ocean Drilling Program.

Sparks J. W. and Zuleger E. (1995) Data Report: Chemical analyses of the Leg 140 reference sample. In *Proc. ODP, Sci. Results*, Vol. 137/140 (ed. K. Becker, L. Stokking, J. Erzinger, and H. B. Dick), pp. 353-355. Ocean Drilling Program.

Spiegelman M. and McKenzie D. (1987) Simple 2-D models for melt extraction at mid-ocean ridges and island arcs. *Earth Planet. Sci. Lett.* **83**, 137-152.

Stakes D. S., Shervais J. W., and Hopson C. A. (1984) The volcanic-tectonic cycle of the FAMOUS and AMAR valleys, mid-Atlantic Ridge (36°47') - Evidence from basalt glass and phenocryst compositional variations for a steady state magma chamber beneath the valley mid-sections, AMAR3. *J. Geophys. Res.* **89**, 955-966.

Staudigal H. and Bryan W. B. (1981) Contrasted glass-whole rock compositions and phenocryst distributions, IPOD sites 417 and 418. *Contrib. Mineral. Petrol.* **78**, 255-262.

Stolper E. (1980) A phase diagram for a mid-ocean ridge basalts: preliminary results and implications for petrogenesis. *Contrib. Mineral. Petrol.* **74**, 13-27.

Sun S.-s. and McDonough W. F. (1989) Chemical and isotopic systematics of ocean basalts: implications for mantle composition and processes. In *Magmatism in the ocean basins. Geol. Soc. Lond. Spec. Publ.*, Vol. 42 (ed. A. D. Sunders and M. J. Norry), pp. 313-345. Blackwell.

Tait S. (1992) Selective preservation of melt inclusions in igneous phenocrysts. *Am. Mineral.* **77**, 146-155.

Takahashi E. and Kushiro I. (1983) Melting of a peridotite at high pressures and basalt magma genesis. *Am. Mineral.* **68**, 859-879.

Takahashi N. (1992) Evidence for melt segregation towards fractures in the Horoman mantle peridotite complex. *Nature* **359**, 52-55.

Takazawa E., Frey F. A., Shimizu N., Obata M., and Bodinier J. L. (1992) Geochemical evidence for melt migration and reaction in the upper mantle. *Nature* **360**, 55-58.

Tegner C. (1997) Iron in plagioclase as a monitor of the differentiation of the Skaergaard intrusion. *Contrib. Mineral. Petrol.* **128**, 45-51.

Thompson R. N. (1987) Phase-equilibria constraints on the genesis and magmatic evolution of oceanic basalts. *Earth Sci. Rev.* **24**, 161-210.

Tighe S., Detrick R. S., Fox P. J., Langmuir C. H., Mutter J. C., Ryan W. B., and Tyce R. C. (1988) *East Pacific Rise data synthesis final report* Vol. 1. Joint Oceanographic institute, Washington, D.C.

Tormey D. R., Grove T. L., and Bryan W. B. (1987) Experimental petrology of normal MORB near the Kane Fracture Zone, 22°-25°N, mid-Atlantic Ridge. *Contrib. Mineral. Petrol.* **96**, 121-139.

Tual E., Jahn B. M., Bougalt H., and Joron J. L. (1985) Geochemistry of basalts from Hole 504B, Leg 83, Costa Rica Rift. In *Init. Repts. DSDP*, Vol. 83 (ed. R. N. Anderson, J. Honnorez, K. Becker, et al.), pp. 201-214. U.S. Govt. Printing Office.

Ulmer P. (1989) The dependence of the Fe^{2+}-Mg cation partitioning between olivine and basaltic liquid on pressure, temperature and composition: an experimental study to 30 kbars. *Contrib. Mineral. Petrol.* **101**, 261-273.

Usselman T. M. and Hodge D. S. (1978) Thermal control of low-pressure fractionation processes. *J. Volcanol. Geotherm. Res.* **4**, 265-281.

Vaggelli G., Belkin H., De Vivo B., and Trigila R. (1992) Silicate melt inclusions in recent Vesuvius lavas (A. D. 1631-1944): 1. Petrography and microthermometry. *Eur. J. Mineral.* **4**, 1113-1124.

Van Andel T. H. and Ballard R. D. (1979) The Galapagos Rift at 86°W: 2. Volcanism, structure and evolution of the rift valley. *J. Geophys. Res.* **84**, 5390-5406.

Van Wagoner N. A. and Leybourne M. I. (1991) Evidence for magma mixing and a heterogeneous mantle on the west valley segment of the Juan de Fuca Ridge. *J. Geophys. Res.* **96**, 16295-16318.

Waff H. S. and Bulau J. R. (1979) Equilibrium fluid distribution in an ultramafic partial melt under hydrostatic stress conditions. *J. Geophys. Res.* **84**, 6109-6114.

Walker D. A., Shibata T., and DeLong S. E. (1979) Abyssal tholeiites from the Oceanographer Fracture Zone. II Phase equilibria and mixing. *Contrib. Mineral. Petrol.* **70**, 111-125.

Walter M. J. and Presnall D. C. (1994) Melting behaviour of simplified lherzolite in the system CaO-MgO-Al_2O_3-SiO_2-Na_2O from 7 to 35 Kbar. *J. Petrol.* **35**, 329-359.

Watson E. B. (1976) Glass inclusions as samples of early magmatic liquid: determinative method and application to a South Atlantic basalt. *J. Volcanol. Geotherm. Res.* **1**, 73-84.

Weaver J. S. and Langmuir C. H. (1990) Calculation of phase equilibrium in mineral-melt systems. *Comp. Geosci.* **16**, 1-19.

Wilkinson J. F. G. (1982) The genesis of mid-ocean ridge basalt. *Earth Sci. Rev.* **24**, 1-57.

Wilson D. S. (1989) Deformation of the so-called Gorda Plate. *J. Geophys. Res.* **94**, 3065-3075.

Xue S. and Morse S. A. (1994) Chemical characteristics of plagioclase and pyroxene megacrysts and their significance to the petrogenesis of the Nain anorthosites. *Geochim. Cosmochim. Acta* **58**, 4317-4331.

Yang H. J., Kinzler R. J., and Grove T. L. (1996) Experiments and models of anhydrous, basaltic olivine-plagioclase-augite saturated melts from 0.001 to 10 kbar. *Contrib. Mineral. Petrol.* **124**, 1-18.

Zhang Y.-S. and Tanimoto T. (1993) High resolution global upper mantle structure and plate tectonics. *J. Geophys. Res.* **98**, 9793-9823.

Zuleger E., Alt J. C., and Erzinger J. (1995) Primary and secondary variations in major and trace element geochemistry of the lower sheeted dike complex: Hole 504B, Leg 140. In *Proc. ODP*

Sci. Results, Vol. 137/140 (ed. J. Erzinger, K. Becker, H. J. B. Dick, and L. B. Stokking), pp. 65-80. Ocean Drilling Program.

Zuleger E., Alt J. C., and Erzinger J. (1996) Data Report: Trace-element geochemistry of the lower sheeted dike complex, Hole 504B (Leg 140). In *Proc. ODP Sci. Results*, Vol. 148 (ed. J C. Alt, H. Kinoshita, L. B. Stokking, and P. J. Michael), pp. 455-466. Ocean Drilling Program.

Appendix 1

Analytical Techniques

Contents

1.1 Electron Microprobe Analyses

All analyses were done on an automated three-spectrometer Cameca SX-50 microprobe at the University of Tasmania, Central Science Laboratory using Cameca PAP data reduction routines. Standards used were San Carlos Olivine (USNM 111312/444), plagioclase LPL (USNM 115900), Augite KA (USNM 122142) (Jarosewich et al., 1980), spinel UV-126 (Lavrentev et al., 1974), and basaltic glass VG-2 (USNM 111249/52). Analytical conditions and counting times for each analytical label used are given in Table A1.1. Relevant standards were analysed at the start and end of each session, and at approximately four hour intervals during longer sessions. Each reported standard analysis is the average of three analyses; mineral and melt inclusion analyses are averages of two points, and glass analyses averages of four points. Analyses were normalised using the technique described by Melson et al. (1976) to minimise the effects of systematic day to day variations from the ideal standard values. Long term averages of standard analyses, and their standard deviations, for the Glassleo (glass analyses) and LPLG (plagioclase analyses) labels are given in Table A1.2.

The detection limit for K_2O in glass analyses, using the standard conditions shown in Table A1.1, is 0.034 wt.%, at the 95% confidence level. Many of the pillow-rim glasses from Hole 896A (Chapter 3) therefore have K_2O contents that are below detection limit. For this reason a subset of these glasses were re-analysed using counting times of peak /background = 60/60 s, with a beam size of 20 μm, which yields a detection limit of 0.01 wt.%, at the 95% confidence level. In addition, some phenocrysts from Hole 504B samples were analysed using different conditions and for a wider range of elements, see Table A1.3 for analytical conditions, using plagioclase LPL (USNM 115900) and Delegate clinopyroxene as standards.

Inter-laboratory comparisons

Systematic differences between basalt glass analyses collected in different laboratories are well known (Melson et al., 1976; Presnall and Hoover, 1984; Klein and Langmuir, 1987; Langmuir et al., 1992) and can be seen in the complete Hole 896A glass dataset, a compilation of analyses from five laboratories all using Cameca microprobes (Fisk et al., 1996).

Table A1.1. Electron microprobe analytical conditions.

Oxide	Count times(Peak/background; s)[a] Plagioclase (LPLG)	Olivine (SCOL)	Pyroxene (Leopyr)	Spinel (Uvspleo)	Glass (Glassleo)
SiO_2	10/5	10/5	10/5	10/5	10/5
TiO_2			10/5	20/10	10/5
Al_2O_3	10/5		10/5	20/10	10/5
FeO	20/10	20/10	20/10	20/10	20/10
MnO		20/10	20/10	20/10	10/5
MgO	10/5	10/5	10/5	10/5	10/5
CaO	10/5	20/10	10/5		10/5
Na_2O	10/5		10/5		10/5
K_2O	20/10				20/10
P_2O_5					10/5
Cr_2O_3		20/10	20/10	10/5	10/5
NiO		20/10		10/5	
ZnO				10/5	
Voltage (kV)	15	15	15	15	15
Current (nA)	20	20	20	20	20
Beam (μm)	1	1	1	1	5x8

[a]Blank indicates element not analysed.

Table A1.2. Long term average of standard analyses and standard deviations compared with recommended values.

Oxide	[a]LPL	2s	[b]LPL	Oxide	[c]VG-2	2s	[b]VG-2	[d]2s
SiO_2	51.07	0.79	51.25	SiO_2	50.68	0.72	50.81	0.70
Al_2O_3	30.65	0.86	30.91	TiO_2	1.82	0.12	1.85	0.12
FeO	0.40	0.09	0.46	Al_2O_3	14.16	0.20	14.06	0.30
MgO	0.13	0.03	0.14	FeO	11.88	0.36	11.84	0.34
CaO	13.60	0.25	13.64	MnO	0.20	0.14	0.22	
Na_2O	3.53	0.12	3.45	MgO	6.80	0.15	6.71	0.22
K_2O	0.12	0.02	0.18	CaO	11.02	0.23	11.12	0.30
Total	99.50		100.03	Na_2O	2.57	0.15	2.62	0.08
				K_2O	0.20	0.03	0.19	0.04
				P_2O_5	0.18	0.07	0.20	0.04
				Cr_2O_3	0.03	0.06		
				Total	99.56		99.62	

[a]Average of 20 analyses.
[b]Recommended value from Jarosewich et al. (1980).
[c]Average of 30 analyses.
[d]Standard deviation from Melson, et al. (1976).

2s = two standard deviations.

Table A1.3. Electron microprobe analytical conditions.

	Plagioclase	[a]Other
Voltage (kV)	15	15
Current (nA)	10	20
[b]Count times (peak/background; seconds)		
$Si0_2$	10/5	10/5
TiO_2	20/10	20/10
Al_2O_3	10/5	10/5
FeO	30/15	20/10
MgO	30/15	10/5
MnO	20/10	20/10
CaO	10/5	10/5
Na_2O	20/10	20/10
K_2O	20/10	20/10
Cr_2O_3	20/10	20/10
NiO		20/10
SrO	20/10	
BaO	20/10	

[a]Olivine and pyroxene.
[b]Blank indicates element not analysed.

Analyses from this study and those from Oregon State (M. Fisk data) are compared on Figure A1. It can be seen that there are consistent differences in MgO and Al_2O_3 contents and variable differences in SiO_2 and FeO. As analyses from these two laboratories are compared in Chapters 4 and 5 these differences were assessed to determine if they are statistically and(or) petrologically significant.

The Hole 896A dataset includes 16 samples where both laboratories have analysed the same glass sample and this data, normalised to 100%, was used as the basis for a quantitative comparison (Fig. A2). SiO_2, MgO, Al_2O_3, FeO, and CaO contents all show differences between the two datasets. To evaluate if these differences are statistically significant, the datasets were compared using students-t-statistic and a two tail test (Le Maitre, 1982). Results are given in Table A1.4. The null hypothesis (that analyses from both laboratories are from identical populations) is rejected at the 95% confidence limit for the majority of Al_2O_3, MgO and FeO analyses. Analyses that fail this test differ in consistent directions; FeO and Al_2O_3 are higher and MgO lower in analyses from the University of Tasmania. These differences are of variable magnitude, e.g. 0.02-0.5 wt.% for individual FeO analyses, but lines of best fit (Fig. A2) give 'average' differences of +0.20 wt.%, -0.19 wt.%, and -0.23 wt.%, for MgO, FeO and Al_2O_3 respectively.

The reasons for these differences are not obvious but are probably related to the standards used for calibration, Fisk used basalt glass A99 (Jarosewich et al., 1980), the analytical conditions used ie., beam current, counting times and/or beam size, and, in the case of MgO, the position of the background offset (Fisk et al., 1996).

In conclusion, although there are statistical differences in analyses of MgO, FeO, and Al_2O_3, the magnitude of these differences should not affect any petrological conclusions, as on average these differences should yield a variation of approximately 1 Mg# in analyses from both laboratories, and the remainder of the elements analysed are statistically indistinguishable. However, when microprobe glass analyses from the Oregon State laboratory are plotted in this study a correction of ±0.2% has been applied to these elements to make the two datasets more comparable.

Analyses of pillow-rim glass from sample KK2-83-NP-D9-1 are given in Table 5.1. There are substantial differences in the analysis of this sample between this study and that of (Davis and Clague, 1987). These differences may be partially resolved by referring to the average analyses of glass standards given in (Table 2; Davis and Clague, 1987). It can be seen that for individual elements the analyses of Davis and Clague (ibid.) vary by up to 5 rel.%, from the accepted standard values.

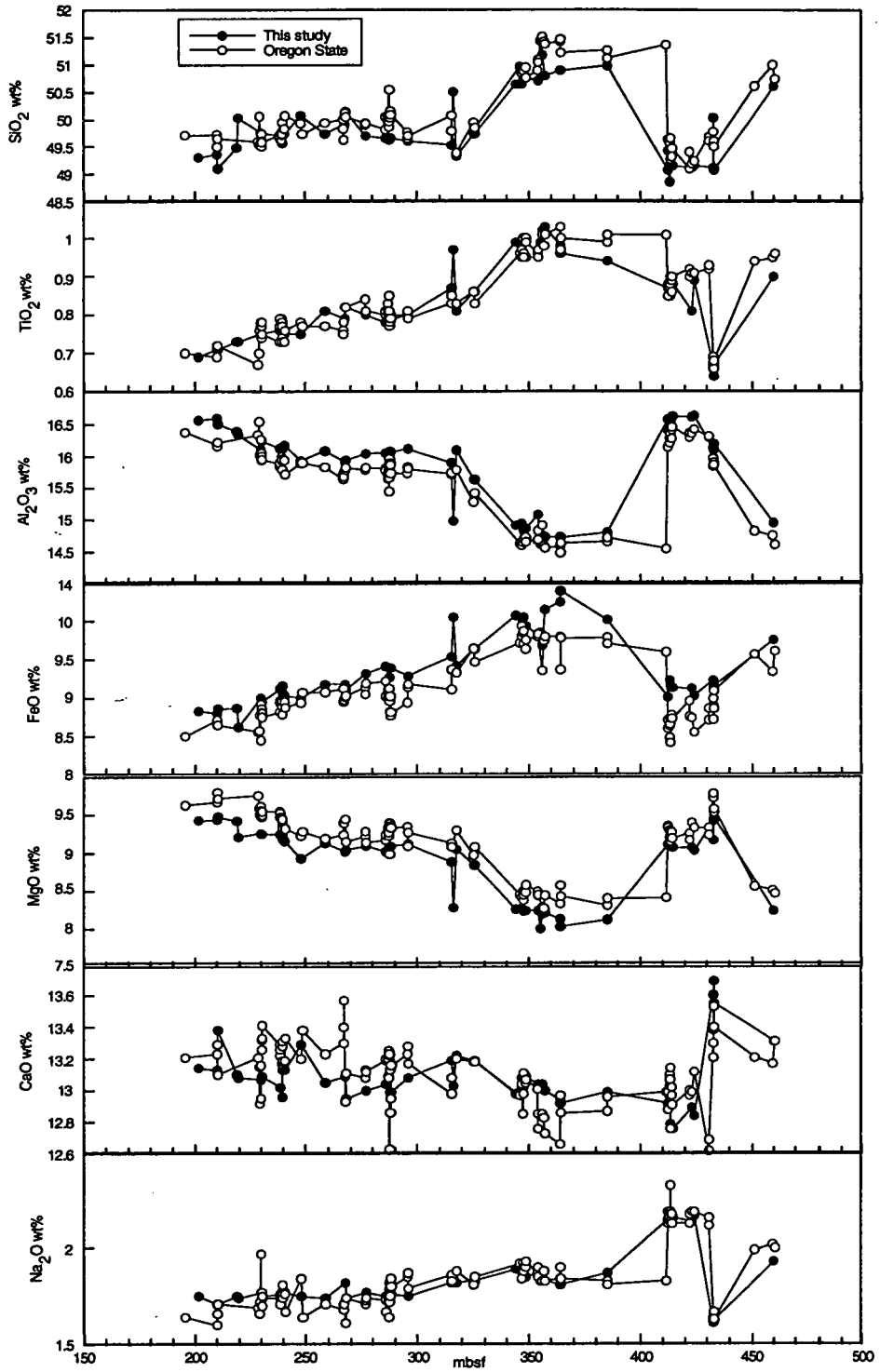

Figure A1: Comparison of electron microprobe pillow-rim glass analyses from Hole 896A. Points labelled as Oregon State are from Fisk et al. (1996). Note the consistent differences in MgO and Al_2O_3 analyses. See text for discussion.

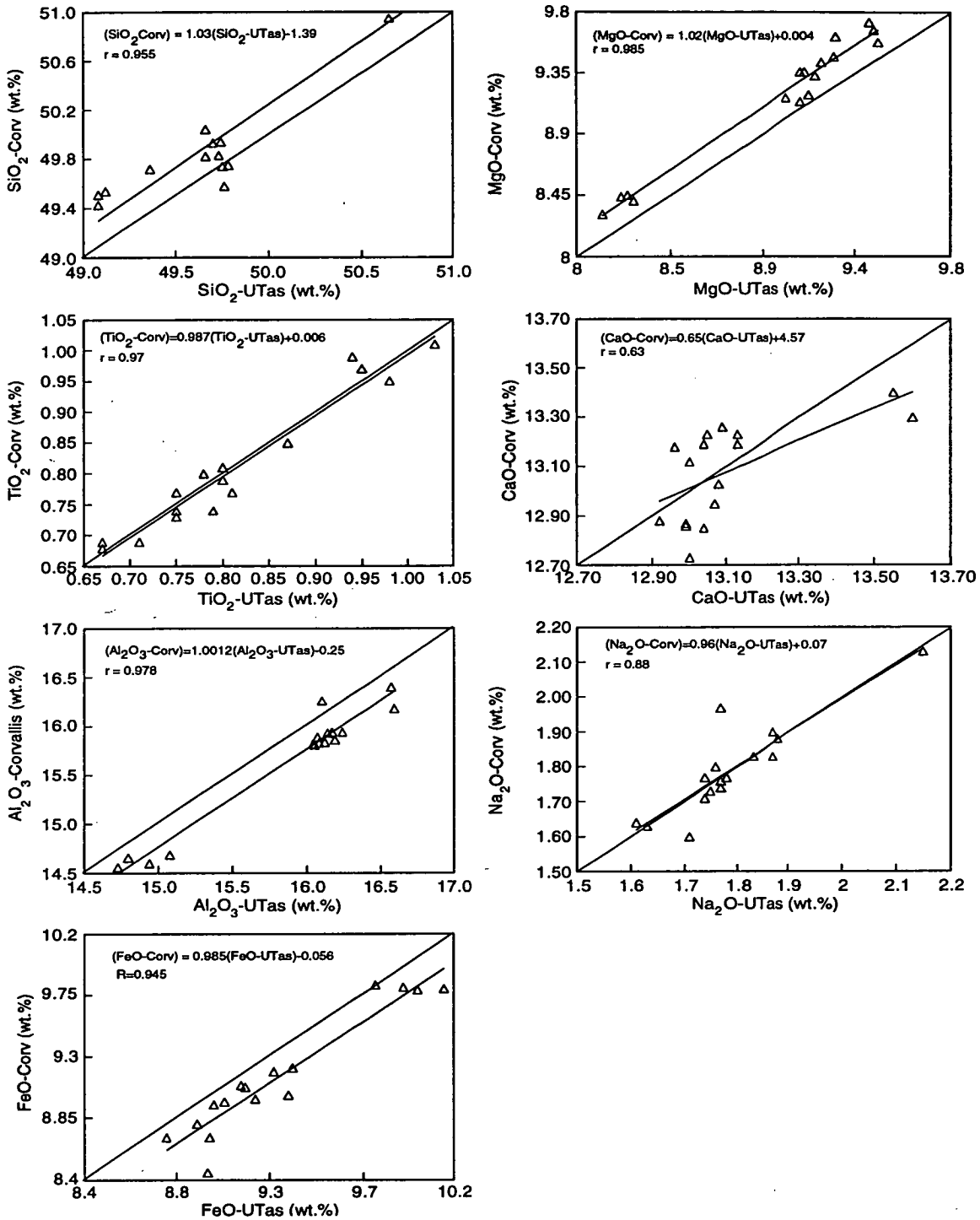

Figure A.2: Comparison of electron microprobe analyses of pillow-rim glass samples, from Hole 896A, that have been analysed both in this study (UTas) and by M. Fisk at Oregon State (Corv; data from Fisk et al. (1996)). Equations are best fit lines from simple linear regression, and r values are correlation coefficients. See text for discussion.

Table A1.4. t-values for pillow-rim glass analyses, Hole 896A.

Sample mbsf	Oxide SiO_2	TiO_2	Al_2O_3	FeO*	MgO	CaO	Na_2O	K_2O	MnO	P_2O_5
210.05	-2.32	0.78	10.14	1.76	-4.55	-1.07	2.66	1.31	-0.39	1.09
229.64	1.16	-0.78	-3.96	10.76	-7.12	1.28	-4.83	-19.64	0.39	-1.63
230.21	0.06	0.39	7.42	2.74	-4.35	-1.82	-0.72	-1.31	0.00	0.54
239.56	0.19	1.96	5.20	2.15	-4.75	-2.35	0.24	1.31	0.39	0.54
240.78	-0.64	0.78	5.69	1.56	-3.36	-0.64	0.24	0.00	-0.39	0.00
258.51	-1.29	1.56	6.19	1.96	-1.19	-1.92	0.72	0.00	0.39	-0.54
276.90	-1.48	-0.39	5.44	2.54	-0.99	-1.28	0.72	1.31	0.39	-0.54
286.00	-1.03	-0.78	5.94	3.72	-2.97	-1.60	0.48	0.00	0.39	-0.54
288.07	-2.45	0.39	4.45	7.24	-5.34	1.39	-0.97	1.31	-0.78	-0.54
346.57	-1.93	1.17	8.41	2.74	-2.77	0.53	0.00	0.00	-0.78	-2.72
354.03	-2.19	-0.78	9.65	-0.39	-4.15	2.03	-0.72	0.00	0.00	0.54
357.15	-3.74	0.78	4.21	6.85	-4.55	2.89	0.00	-1.31	-0.78	0.54
385.33	-3.74	0.78	4.21	6.85	-4.55	2.89	0.00	-1.31	-0.78	0.54
412.19	-2.25	0.78	4.21	5.87	-4.95	0.43	0.48	1.31	1.56	-1.09
433.00	-2.71	-0.78	6.93	4.69	-6.13	3.21	-0.72	1.31	0.78	-2.17
433.31	-2.77	-0.39	8.17	1.37	-2.37	1.60	0.00	0.00	0.00	0.00
Ave. t-value	-1.69	0.34	5.77	3.90	-4.01	0.35	-0.15	-0.98	0.02	-0.37

degrees of freedom: 5

Confidence limits; 99% = 5.89, 95% = 4.02, 90% = 3.37.

The standard Deviations used in these calculations were derived from analyses of sample KK2-NP-83-D9-1 (Table 5.1), which, in the case of the analyses from this study, are consistent with the standard deviations for VG-2 (Table A1.2).

All of Davis and Clague's glass analyses, from Central Gorda Ridge, were therefore normalised to the accepted standard value, as described by (Melson et al., 1976), and these normalised values are used for all comparisons in Chapter 4. After normalisation, some elements, particularly MgO, and Na_2O, have similar abundances to the analysis in this study, however significant differences remain in CaO, Al_2O_3, and TiO_2 contents. The reasons for these variations probably lie in differing experimental conditions, as discussed previously, but as they have little effect on the petrological results of this study, no corrections are required.

1.2 Fourier Transform Infrared Analyses

The H_2O contents of glass samples may be determined by Fourier transform infrared spectroscopy (FTIR) (Ihinger et al., 1994). In this study the H_2O contents of both pillow-rim glasses and melt inclusions were determined using a Bruker IFS 66 spectrometer with attached optical microscope and Bruker Opus/IR data reduction software at the Central Science Laboratory, University of Tasmania. Methods of sample preparation and calibration used in this study were modified from (Danyushevsky et al., 1993), and are described below.

The same glass chips used for electron microprobe analysis were used for FTIR analysis and thin (<200 μm) doubly polished wafers were prepared and glued in position over holes drilled in a glass slide. In contrast samples with melt inclusions were prepared by polishing the host phenocryst until the inclusions were opened from both sides, producing a very thin (50-100 μm) wafers that were stored in a glass vial and positioned in the spectrometer using a fine Cu graticule on a zinc sellenide disc.

Sample thicknesses were measured using two methods; on an optical microscope, as described by (Danyushevsky et al., 1993), and using interference fringe separations on analytical spectra (Osland, 1985). There is an exceptionally good correlation between results from these two techniques (Fig. A3), but measurements from the optical microscope were used in most analyses as interference fringes were not obvious, or easy to measure, on all spectra.

Spectra were collected from 2400-3800 cm^{-1} using 100 scans at 4 cm^{-1} resolution for both background and sample analyses. The microscope attached to the spectrometer was fitted with a set of apertures allowing the area of analysis to be varied, and most analyses were done on areas of 30 or 60μm diameter. Where possible, the data collected were background corrected peak heights at 3500 and 3100 cm^{-1} and the area under the 3500 cm^{-1} peak. The OPUS/IR software was used to both subtract Background spectra, by 'rubber band' correction, and calculate the area under the 3500 cm^{-1} peak using an integration routine over the interval 2493-3766 cm^{-1}. In some cases the 3100 cm^{-1} and/or the area under the 3500 cm^{-1} peak could not be measured due to interference fringes or interference from 'glue' peaks, however where data was collected from all three measurements the calculated water content differed by only 0.01%, with the measurements at 3500 and 3100 cm^{-1} yielding the most consistent results.

Calibration

Calibration curves, prepared using the same standards as Danyushevsky et al. (1993), are shown on Figure A4. Calibrations were done for each measurement type, at varying apertures and with or with out a glass slide between the sample and detector. Best fit lines were forced through zero to produce the relationships between H_2O content and (absorbance/thickness) x 100 given in Table A1.5. Note that as discussed by Newman et al. (1986) and Danyushevsky et al. (1993) the 3500 cm^{-1} peak is poorly suited to analysing H_2O-rich samples, and for this reason calibration curves were prepared for samples with less than 2.15 wt.% H_2O.

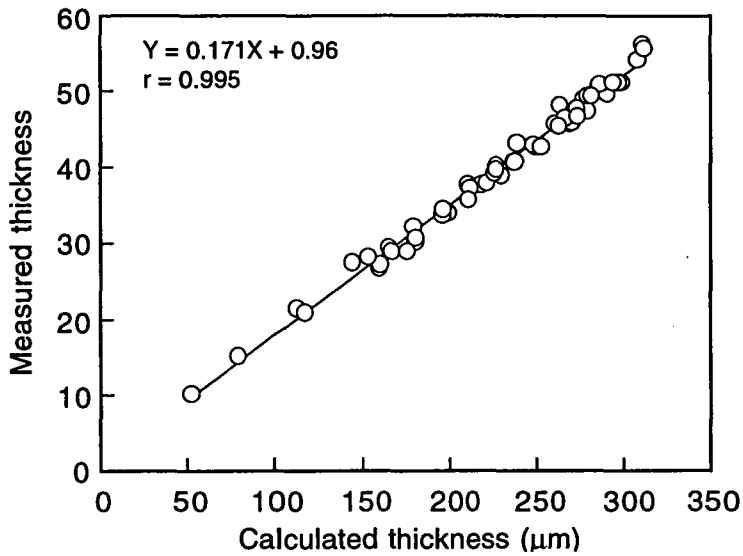

Figure A3: Sample thicknesses for Fourier Transform Infrared Spectroscopy. Measured thicknesses are from measurements made on an optical microscope and are in 'microscope scale units'. Calculated thicknesses are derived from Interference fringes on IR spectra, see text for details.

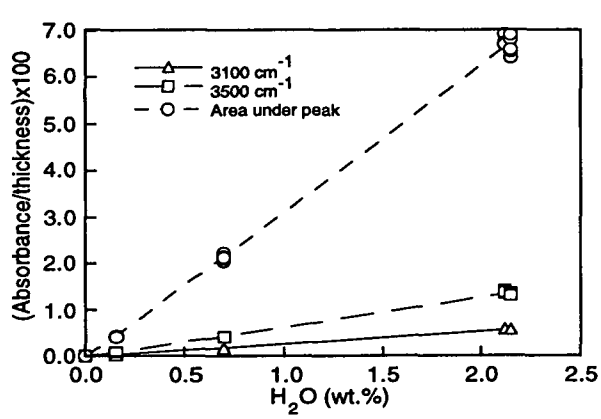

Figure A4: FTIR calibration curves. Standards used are those from Danyushevsky et al. (1993). Thickness is in μm, and was calculated from interference fringes. Aperture for this calibration was 60 μm, and no glass slide was used. Lines of best fit were forced through zero, and correlation coefficients are 0.99 for all three measurement methods.

Table A1.5. FTIR calibration curves used in this study.

[b]Aperture	3500 cm^{-1}	[a]Slope 3100 cm^{-1}	Area under peak
no-slide			
100 μm	0.334	0.728	0.0645
60 μm	0.324	0.720	0.0628
30 μm	0.292	0.666	0.0570
[c]glass slide			
100 μm	0.309	0.697	0.0593
60 μm	0.300	0.680	0.0580
30μm	0.277	0.644	0.0545

[a]Slope of line of best fit forced through zero. Water content is calculated using the relationship; H_2O (wt.%) = Slope x (abs./thickness)x100 where thickness is measured in microscope units.

[b]Diameter of analysis area.

[c]Glass slide present between sample and detector

1.3 Ion-probe (SIMS) Analyses

Trace element analyses of pillow-rim glasses and melt inclusions were done on polished glass chips or phenocrysts mounted in a 25 mm diameter epoxy 'probe mount', by Dr. J.D. Blundy, who provided the following description of the ion-probe method:

Trace element analysis was carried on Au-coated polished mounts at the NERC ion-microprobe facility at the University of Edinburgh using a Cameca IMS-4f with O^- primary beam and 10.69 kV accelerating voltage. A secondary ion accelerating voltage of 4500 V was used with an offset of -74 to -78 V to reduce molecular ion interferences. The beam was focussed at the sample surface to a spot size of 15-60 μm, depending on the size of the inclusion, corresponding to operating currents in the range 2-9 nA. Data were collected in cycles and processed using Charles Evans and Associates software. The following isotopes were counted: ^{7}Li, ^{39}K, ^{47}Ti, ^{85}Rb, ^{88}Sr, ^{89}Y, ^{90}Zr, ^{93}Nb, ^{138}Ba, ^{139}La, ^{140}Ce, ^{141}Pr, ^{143}Nd, ^{149}Sm, ^{153}Eu, ^{139}La, ^{157}Gd, ^{159}Tb, ^{161}Dy, ^{165}Ho, ^{167}Er, ^{172}Yb, and referenced to ^{30}Si. Background was monitored at mass 130.5 and was typically less than 0.08 counts per second (cps). Counting times per cycle for each mass measured and total number of cycles were adjusted so as to give an overall statistical precision for glass analyses of better than ±2% relative for all isotopes except Rb (±3%), Ba and REE (±5%) and Nb (±7%).

Molecular ion interference by FeSi on ^{85}Rb, ZrH on ^{93}Nb, NaO on ^{39}K, BaO on Eu and LREE monoxides on HREE are **not** removed completely at these offsets (e.g. Hinton, 1995). In the case of ^{85}Rb, interference was monitored at mass 84 ($^{56}Fe^{28}Si$) and corrected for accordingly (after removal of ^{84}Sr). This correction reduces Rb

precision to ±35% relative in the most Rb-poor samples. Similarly ZrH was monitored at mass 95, with a resultant Nb precision of ±20% relative in the worst case. In the case of oxide interferences the MO^+/M^+ ratios of Hinton (1990, 1995) were used. These values were confirmed by analysis of secondary standards (see below) and monitored by periodic analysis of ^{151}Eu and ^{153}Eu, from which BaO^+/Ba^+ can be determined by peak-stripping, and ^{156}Gd and ^{157}Gd (for CeO^+/Ce^+). For LREE-depleted MORB glasses these corrections are relatively small (1-20%) and have negligible impact on statistical precision. NaO interference on ^{39}K was corrected for using an NaO^+/Na^+ ratio of 1/1290 (R. W. Hinton, pers. comm. 1995) combined with Na as determined by electron-microprobe. The effect on K precision is negligible.

Count rates were converted to concentration using ion-yields derived from at least three replicate analyses of glass NBS610 made at the beginning of each analytical session. Ion-yields were assumed identical for glass and plagioclase. Hinton (1990) has shown that although ion-yields do depend on matrix composition, calibration on NBS610 produces results to within 10% accuracy on a wide range of minerals and glasses. An independent estimate of the accuracy of the SIMS technique is provided by replicate analyses of secondary glass and mineral standards obtained at Edinburgh by J.D. Blundy (pers. comm., 1996) over a three-year period. For all elements the accuracy is better than 20% relative, despite the very wide range in concentration, with no systematic difference between glass and crystal phases. For most elements the observed/known ratio scatters about unity (Fig. A5), however systematic underestimates for Ti, Rb, Sr, Y and Li may reflect uncertainty in the concentration of these elements in NBS610, for which nominal concentrations of 500 ppm were assumed. A further illustration of this comes from comparison of ion-probe and electron-probe data for Ti (Fig. A6). Ion-probe Ti consistently underestimates the electron-probe value by ~13% for all glasses analysed. This is in excellent agreement with the shortfall observed from secondary standards. In this study all reported analyses are based on the NBS-certified figures for 610. As and when new data for this glass become available the figures can be revised accordingly. For the purposes of plotting the data, and comparing them to data from other laboratories, the following corrections have been introduced: Ti (¥0.87), Rb (¥0.72), Sr (¥0.83), and Y (¥0.81).

Estimates of the overall accuracy of the ion-probe data (after taking into account the above corrections) are: <5% relative (Li, K, Ti, Sr, Y, Nb, Ba), <10% (La, Ce, Pr), <15% (Nd, Sm, Gd, Tb, Dy, Ho, Yb), <20% (Er), <30% (Eu). Accuracy for MREE and HREE in MORB is probably slightly better than quoted due to its LREE- and Ba-depleted nature.

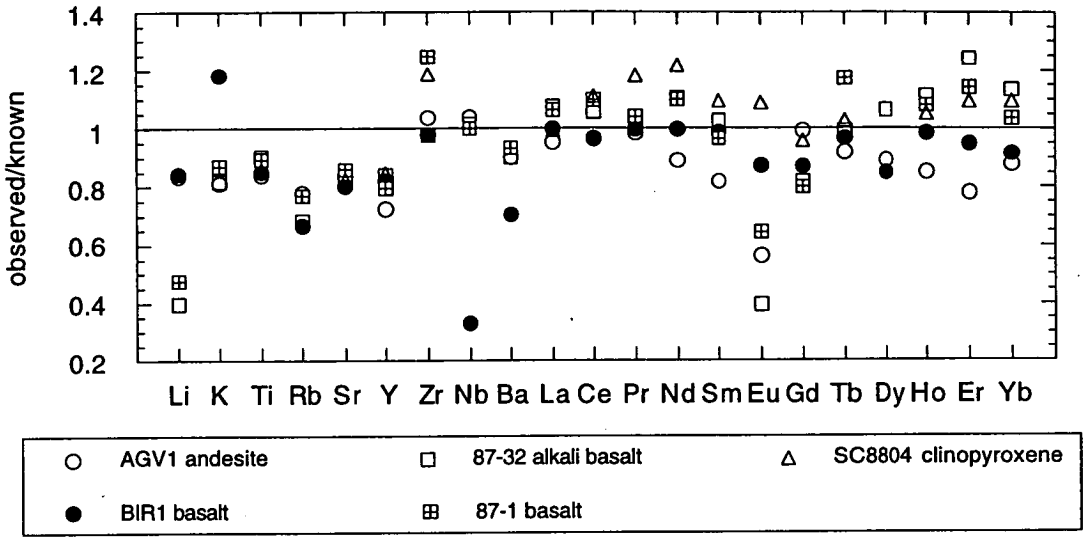

Figure A5: Plot of observed/known ratios for replicate analyses of glass and mineral standards over a three-year period. Note systematic underestimates for Li, Ti, Rb, Sr and Y. Li contents of 87-32 and 87-1 are not thought to be reliable. Nb in BIR1 is very low (~500 ppb) and is therefore not included in our overall estimate of accuracy. Significant underestimates of Eu arise from significant BaO^+ interferences. These are considerably smaller (<2% relative) for low-Ba MORB glasses, with a corresponding improvement in accuracy. Standard data are for AGV1 and BIR1 are taken from Govindaraju (1989), for 87-1 and 87-32 from Dunn and Sen (1993), for SC8804 from Blundy (unpublished data).

1.4 ICP-MS Analyses

Laser ablation ICP-MS analyses were done on polished glass chips in a 25 mm diameter epoxy 'probe mounts', at the Australian National University by Dr. S.M. Eggins, who furnished the following description of the technique:

The laser used was an ArF EXCIMER, which produces 193 nm UV radiation with a light pulse width (duration) of 17 ns. The primary laser beam was masked with an aperture of variable dimension to produce the required/desired spot size. In this case a 4 circular aperture was used and was demagnified ~20 times to a focus point at the sample site which was 200 μm in width. The laser was fired at 5 pulses/second and an energy output of 100 mJ/pulse.

The ejecta/ablation products were swept by a carrier gas flow (99.996% pure Ar) into an ICP operating at 1200W. The ICP-MS instrument is a FISONS PQ2+, which delivers sensitivity of 10,000 counts/second/ppm in the mode specified above, yielding detection limits for most high mass elements (>80 amu) of between 0.1 and 1ppb.

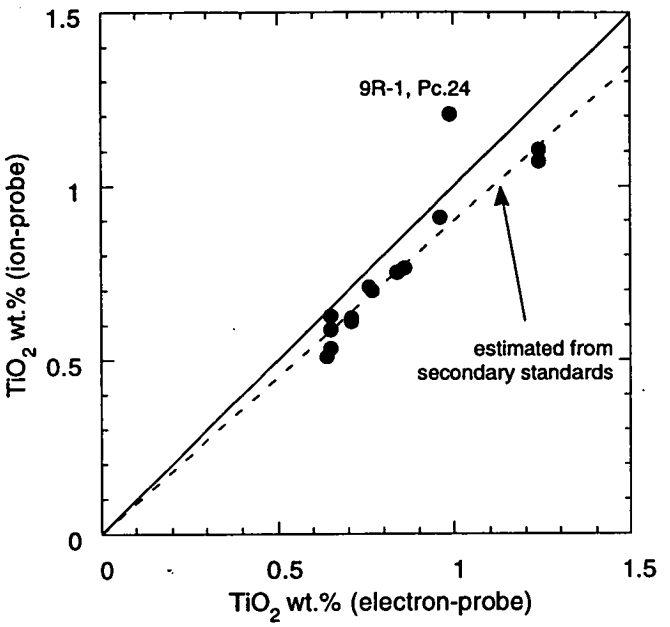

Figure A6: Comparison of TiO_2 contents of glass inclusions as analysed be ion-probe and electron-probe. Note the systematic deviation from the 1:1 line (heavy). The light line shows the effect of the empirical correction factor of 0.87 based on analyses of secondary standards as described in the text. All data points, except one, fall along this line. The high TiO_2 in 9R-1, Pc.24 is interpreted to have resulted from spectrometer drift and this analysis has been removed from the final data set.

As standards with the same composition/matrix as the unknown are not available, data reduction involves knowing the abundance of an element (internal standard) in the sample, Ca as determined by electron microprobe in this case, and in a standard glass (NIST glasses 610 and 612; spiked silicate glasses with nominal trace element concentrations of 500 and 50 ppm respectively). The concentration, C, of an unknown element, i, in the unknown sample, X, is then calculated as follows:

$$C_i = \frac{\left(\frac{C_i \text{ in std}}{C_{Ca} \text{ in std}}\right)}{\left(\frac{Cps_i \text{ in std}}{Cps_{Ca} \text{ in std}}\right)} * \frac{Cps_i \text{ in X}}{Cps_i \text{ in X}} * C_{Ca} \text{ in X} \qquad \text{where } Cps = \frac{\text{counts}}{\text{second}}$$

1.5 Comparison of SIMS and ICP-MS Data

As discussed in Chapter 3 there are significant differences in the results of SIMS and lase-ablation ICP-MS analyses of Hole 896A pillow-rim glasses; variations of 50-100 rel.% for Nb, differences in the range of $(La/Sm)_n$ values (0.29-0.32 and 0.3-0.38 for the same glasses by SIMS and ICP-MS respectively), and more scatter in Ti contents (Fig.

A7). The reasons for these differences are unclear, but possible factors include instrumental drift (particularly common in ICP-MS analyses; Eggins et al. (1996)), differences in standardisation procedures, and inhomogeneity of the sample glass. The laser ablation technique samples an area of 200 μm diameter, versus 15-60 μm, and 5x8 μm for SIMS and electron-microprobe analyses respectively, and may have sampled microlites or other inhomogeneities in the glass samples. Additionally, the ICP-MS and SIMS analyses were done on different chips from the same sample and differences in analyses may therefore result from large scale inhomogeneities in the pillow-rim glasses. The reasons for these differences are unclear. Repeat laser-ablation ICP-MS analyses were being performed but were not available at the time of writing.

1.6 Whole-rock Analyses

Samples were either crushed onboard the JOIDES Resolution, using procedures outlined in Shipboard Scientific Party (1992), or were hand crushed and cleaned in an ultrasonic bath prior to crushing to 325 mesh in a tungsten carbide mill at the University of Tasmania.

Major elements were then analysed on fused glass disks by XRF, using a Phillips PW-1480 spectrometer at the University of Tasmania, and following the methods outlined by Norrish and Chappell (1977). Analytical conditions are given in Table A1.6. Results were checked against two internal standards, analyses of which are included in Sparks and Zuleger (1995). Loss on ignitions (LOI) were determined by firing 0.9-1.1g of pre-dried sample at 1050°C overnight.

Rare earth elements (REE), Hf, Cs, Sc, Th, and Cr were determined by instrumental neutron activation on 0.8-1.1g samples at Becquerel Laboratories, Sydney, Australia (Dr. Helen Waldron analyst). Detection limits are given in Table A1.7.

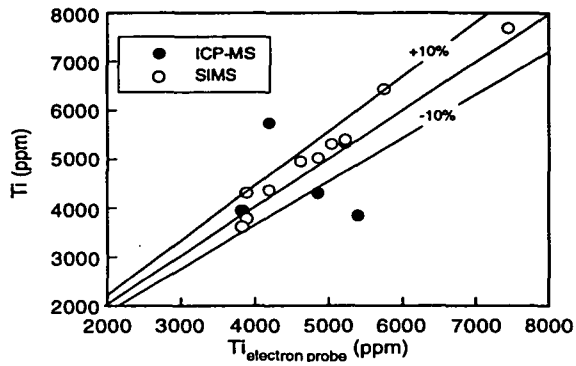

Figure A7: A comparison of the Ti content Hole 896A pillow-rim glasses and melt inclusions determined by electron-microprobe and Ti contents from SIMS and ICP-MS analyses. Note that SIMS analyses have been corrected as discussed above (Figure A6). ICP-MS analyses show considerably more scatter.

Table A1.6. Instrumental conditions for XRF major element analyses.

Oxide	Line	Tube	Crystal	kV/mA	[a]LLD
SiO_2	K alpha	ScMo	PE	40/70	0.002
TiO_2	K alpha	ScMo	LIF200	90/30	0.006
Al_2O_3	K alpha	ScMo	PE	40/70	0.008
Fe_2O_3	K alpha	ScMo	LIF200	90/30	0.0041
MnO	K alpha	ScMo	LIF200	90/30	0.0035
MgO	K alpha	ScMo	TLAP	40/70	0.011
CaO	K alpha	ScMo	LIF200	40/70	0.0009
Na_2O	K alpha	ScMo	TLAP	40/70	0.024
K_2O	K alpha	ScMo	PE	40/70	0.0004
P_2O_5	K alpha	ScMo	GE	40/70	0.0026

[a]Lower limit of detection, 3 sigma (99%) confidence limits, wt.%.

Table A1.7. Detection limits for Neutron Activation analysis.

	Element													
	La	Ce	Nd	Sm	Eu	Tb	Ho	Yb	Lu	Hf	Th	Cs	Sc	Cr
[a]LLD	0.10	1.00	2.00	0.05	0.10	0.20	0.20	0.10	0.05	0.20	0.20	0.50	0.05	2.00

[a]Lower limit of detection, ppm..

Appendix 2

Phenocryst, Pillow-Rim Glass and Melt Inclusion Analyses, Hole 896A

Contents

2.0 Sample Identification

Samples are identified using the standard ODP format; Leg number-site-hole-core number-core type-section, and piece number, e.g. 148-896A-4R-1, Piece 2 is the second piece from the first 1.5 m section of core four (R indicates the core was obtained by rotary coring) of Hole 896A, drilled during Leg 148.

Individual phenocrysts and inclusions are identified as follows; grain mount-Phenocryst type-grain number-inclusion type-inclusion number, e.g. A26-PL15-GL is plagioclase grain 15, from grain mount 26, which hosts an analysed glass inclusion. Phenocryst types are abbreviated as follows; PL, plagioclase; CP, clinopyroxene; OL, olivine; and SP, spinel.

Melt inclusions from homogenisation experiments are identified as follows; host phenocryst-experiment-inclusion, e.g. P115-5 is plagioclase experiment 115, inclusion number five.

Appendix 2.1, Pillow-rim glass analyses.

[a]Sample	[b]Depth (mbsf)	SiO_2	TiO_2	Al_2O_3	[c]FeO	MnO	MgO	CaO	Na_2O	K_2O	P_2O_5	Cr_2O_3	Total	[d]H_2O	CaO/ Na_2O	[e]K_2O	[f]H_2O
2R-1, Piece 14	201.53	48.99	0.69	16.46	8.78	0.16	9.37	13.06	1.74	0.02	0.04	0.07	99.38	0.07	8.0		
3R-1, Piece 4	210.06	48.94	0.70	16.45	8.73	0.12	9.36	13.02	1.70	0.02	0.04	0.07	99.15	0.07	7.7	0.013	0.065
3R-1, Piece 7	210.45	48.65	0.70	16.35	8.78	0.12	9.39	13.26	1.69	0.02	0.05	0.08	99.09	0.07	7.8	0.010	0.061
4R-1, Piece 2	219.00	49.11	0.72	16.27	8.80	0.15	9.35	13.00	1.74	0.03	0.04	0.05	99.26	0.08	7.5	0.012	0.062
5R-2, Piece 1D	229.65	49.46	0.75	16.00	8.95	0.14	9.20	12.99	1.76	0.02	0.04	0.08	99.39	0.07	7.4	0.011	0.067
5R-2, Piece 5	230.31	49.29	0.74	16.09	8.87	0.13	9.16	12.97	1.72	0.01	0.05	0.05	99.08	0.08	7.5	0.013	0.069
6R-1, Piece 9A	238.69	49.41	0.76	16.02	9.07	0.16	9.19	12.94	1.73	0.02	0.04	0.06	99.40	0.08	7.5		
6R-1, Piece 13d	239.28	49.69	0.75	16.11	9.17	0.12	9.28	13.11	1.71	0.02	0.04	0.08	100.08	0.07	7.7	0.012	0.070
6R-2, Piece 2	239.56	49.44	0.78	16.03	9.02	0.15	9.13	12.87	1.77	0.02	0.05	0.05	99.31	0.07	7.3		
6R-2, Piece 5	239.77	49.08	0.77	15.96	9.07	0.12	9.13	13.00	1.76	0.02	0.03	0.09	99.03	0.08	7.4	0.013	0.070
6R-3, Piece 1	244.79	49.36	0.74	16.05	8.96	0.14	9.09	13.03	1.76	0.01	0.04	0.07	99.25	0.08	7.4	0.012	0.065
8R-1, Piece 29	258.51	49.34	0.80	15.95	9.11	0.15	9.06	12.95	1.73	0.01	0.04	0.06	99.20	0.09	7.5		
9R-1, Piece 13	260.70	49.54	0.78	15.79	9.11	0.17	8.95	12.99	1.81	0.02	0.04	0.06	99.26	0.07	7.2		
9R-1, Piece 24	267.48	49.68	0.81	15.79	9.03	0.14	8.96	12.83	1.72	0.01	0.05	0.07	99.09	0.08	7.5	0.012	0.075
10R-1, Piece 7	267.95	49.48	0.80	15.97	9.28	0.15	9.05	12.94	1.76	0.02	0.04	0.07	99.56	0.07	7.4	0.012	0.072
11R-1, Piece 1	276.90	49.38	0.78	15.96	9.36	0.13	8.97	12.97	1.74	0.02	0.06	0.06	99.43	0.08	7.5	0.013	0.071
11R-2, Piece 3	286.00	49.21	0.78	15.88	9.19	0.15	9.00	13.08	1.77	0.01	0.03	0.07	99.17	0.08	7.4	0.013	0.070
11R-2, Piece 8	288.07	49.42	0.80	15.99	9.34	0.10	9.05	12.93	1.75	0.03	0.04	0.07	99.52	0.08	7.4	0.013	0.072
12R-1, Piece 3	295.78	49.16	0.79	15.97	9.21	0.15	9.04	12.96	1.73	0.02	0.03	0.06	99.12	0.09	7.5	0.013	0.073
12R-1, Piece 7	315.36	49.18	0.86	15.79	9.47	0.14	8.82	13.10	1.81	0.01	0.06	0.06	99.30	0.09	7.2	0.014	0.077
14R-2, Piece 1	316.01	50.07	0.96	14.85	9.96	0.21	8.21	12.92	1.82	0.03	0.04	0.06	99.13		7.1	0.015	0.076
14R-3, Piece 1	317.48	49.00	0.80	15.98	9.36	0.14	8.99	13.13	1.81	0.02	0.05	0.06	99.34	0.09	7.3		
15R-1, Piece 17	325.48	49.35	0.85	15.51	9.56	0.14	8.77	13.09	1.82	0.01	0.04	0.07	99.21	0.09	7.2	0.013	0.082
17R-1, Piece 6A	344.05	50.45	0.99	14.85	10.03	0.10	8.23	12.93	1.88	0.02	0.05	0.07	99.60	0.09	6.9	0.018	0.087
17R-3, Piece 1	346.58	50.35	0.97	14.85	9.89	0.16	8.22	13.00	1.87	0.02	0.03	0.04	99.40	0.09	7.0	0.015	0.087
17R-3, Piece 13	347.52	50.47	0.99	14.75	9.99	0.11	8.18	12.95	1.86	0.02	0.06	0.07	99.45	0.10	7.0	0.010	0.091
17R-4, Piece 4B	348.58	50.49	0.94	14.78	9.88	0.14	8.19	13.02	1.84	0.02	0.07	0.07	99.44	0.10	7.1	0.015	0.089
18R-1, Piece 9A	354.02	50.50	0.95	15.02	9.77	0.15	8.21	12.99	1.86	0.02	0.05	0.07	99.59	0.09	7.0	0.016	0.088
19R-1, Piece 2	356.08	50.84	1.01	14.65	9.63	0.14	8.14	12.95	1.83	0.02	0.06	0.07	99.34	0.09	7.1	0.016	0.081
19R-1, Piece 19	357.15	50.87	1.03	14.75	10.16	0.11	8.22	13.02	1.83	0.01	0.06	0.07	100.13	0.09	7.1	0.018	0.082
20R-1, Piece 9	363.87	51.10	0.98	14.79	10.29	0.14	8.16	12.99	1.82	0.02	0.05	0.06	100.40		7.1	0.019	0.086
20R-1, Piece 12	363.98	50.76	0.96	14.68	10.36	0.15	8.01	12.89	1.81	0.02	0.03	0.06	99.73	0.09	7.1	0.015	0.086
22R-2, Piece 17	385.33	51.20	0.94	14.87	10.06	0.13	8.16	13.05	1.88	0.02	0.05	0.08	100.44	0.09	6.9	0.017	0.084
25R-1, Piece 11	412.19	48.96	0.87	16.53	8.99	0.16	9.09	12.89	2.14	0.02	0.03	0.07	99.75	0.09	6.0	0.014	0.082
25R-2, Piece 4	413.12	48.85	0.87	16.54	9.23	0.12	9.15	12.96	2.17	0.01	0.02	0.06	99.98	0.08	6.0	0.012	0.071
25R-2, Piece 11	413.41	49.24	0.85	16.55	9.17	0.15	9.09	12.81	2.16	0.02	0.05	0.05	100.14	0.08	5.9		
25R-3, Piece 2	414.36	49.22	0.88	16.64	9.14	0.11	9.08	12.78	2.16	0.02	0.04	0.07	100.14		5.9	0.012	0.071

Appendix 2.1, continued.

[a]Sample	[b]Depth (mbsf)	SiO_2	TiO_2	Al_2O_3	[c]FeO	MnO	MgO	CaO	Na_2O	K_2O	P_2O_5	Cr_2O_3	Total	[d]H_2O	CaO/Na_2O	[e]K_2O	[f]H_2O
26R-2, Piece 12	423.17	49.25	0.81	16.65	9.14	0.15	9.09	12.92	2.15	0.01	0.04	0.05	100.26	0.08	6.0	0.011	0.067
26R-3, Piece 6	424.32	49.15	0.89	16.63	9.03	0.13	9.03	12.84	2.17	0.01	0.04	0.05	99.97	0.09	5.9	0.012	0.071
27R-1, Piece 13	431.55	49.28	0.67	16.17	9.26	0.13	9.45	13.64	1.62	0.02	0.03	0.05	100.32	0.04	8.4	0.013	0.044
27R-1, Piece 15	431.75	49.03	0.64	16.07	9.12	0.12	9.43	13.66	1.62	0.02	0.03	0.07	99.81	0.05	8.4	0.010	0.039
27R-1, Piece 17	431.86	49.30	0.67	16.26	9.20	0.12	9.50	13.61	1.64	0.02	0.04	0.08	100.44	0.05	8.3	0.011	0.042
30R-1, Piece 8	459.80	50.67	0.90	14.97	9.77	0.15	8.25	13.33	1.93	0.02	0.06	0.07	100.12	0.09	6.9	0.019	0.078

[a]For complete identification sample numbers should be prefixed with "148-896A-".
[b]mbsf = metres below sea floor.
[c]All Fe as FeO.
[d]H_2O determined by Fourier transform infrared spectroscopy.
[e]K2O determined by electron probe but with longer count times (see Appendix 1 for details).
f

Appendix 2.2.1 Plagioclase analyses.

Sample	SiO_2	Al_2O_3	FeO	MgO	CaO	Na_2O	K_2O	Total	An[a]	Sample	SiO_2	Al_2O_3	FeO	MgO	CaO	Na_2O	K_2O	Total	An[a]
148-896A-3R-1, Piece 4																			
PL1	45.49	34.07	0.38	0.28	18.03	1.35	0.02	99.62	88.1	PL34a	46.84	33.56	0.34	0.28	17.63	1.57	0.02	100.24	86.1
PL2	46.09	34.78	0.32	0.22	18.61	1.14	0.00	101.16	90.0	PL35	46.3	33.83	0.3	0.26	18.08	1.33	0.01	100.11	88.3
PL2a	46.76	33.73	0.33	0.27	17.73	1.60	0.02	100.44	86.0	PL36	45.97	34.17	0.41	0.21	18.21	1.26	0.02	100.25	88.9
PL3	45.78	33.97	0.30	0.25	18.29	1.22	0.02	99.83	89.2	PL37	46.38	34.12	0.32	0.26	18.05	1.37	0.01	100.51	87.9
										PL38	46.87	33.88	0.37	0.28	17.8	1.47	0.01	100.68	87.0
PL5	46.57	33.82	0.39	0.28	17.78	1.49	0.04	100.37	86.8	PL39	46.25	33.84	0.35	0.24	18.2	1.36	0.01	100.25	88.1
PL5a	45.77	34.23	0.41	0.24	18.17	1.20	0.01	100.03	89.3	PL39A-GL	46.48	33.62	0.41	0.25	17.8	1.52	0.02	100.1	86.6
PL6	46.04	33.5	0.38	0.23	17.82	1.40	0.03	99.40	87.6	PL40	48.04	32.94	0.45	0.29	17.05	1.91	0.02	100.7	83.1
PL7	48.20	32.34	0.43	0.35	16.67	2.04	0.02	100.05	81.9	PL41	45.31	33.58	1.2	1.01	17.86	0.93	0.15	100.04	91.4
PL8	46.05	33.61	0.35	0.25	18.01	1.40	0.01	99.68	87.7	PL42-SPA	46.24	34.37	0.38	0.27	18.29	1.28	0.01	100.84	88.8
PL9	46.62	33.97	0.34	0.24	17.77	1.41	0.02	100.37	87.4	PL42-SPB	46.24	34.37	0.38	0.27	18.29	1.28	0.01	100.84	88.8
PL10	47.27	33.19	0.31	0.30	17.22	1.83	0.00	100.12	83.9	PL43	45.93	34.52	0.32	0.21	18.42	1.24	0.00	100.64	89.1
PL10a	47.01	33.81	0.46	0.28	17.80	1.51	0.00	100.87	86.7	PL44	46.09	34.28	0.39	0.23	18.3	1.26	0.02	100.57	88.9
PL11	46.34	33.77	0.37	0.28	18.09	1.40	0.01	100.26	87.7	PL45	47.55	33.23	0.42	0.28	17.31	1.8	0.02	100.61	84.2
PL12	45.81	34.24	0.38	0.25	18.46	1.22	0.02	100.38	89.3	PL46	47.01	33.46	0.34	0.28	17.57	1.67	0.01	100.34	85.3
PL13	44.98	34.65	0.26	0.21	18.91	0.95	0.01	99.97	91.7	PL47	47.61	33.28	0.38	0.29	17.26	1.66	0.24	100.72	85.2
PL14	46.60	33.91	0.46	0.29	18.02	1.39	0.02	100.69	87.8	PL48	47.59	33.36	0.37	0.26	17.18	1.84	0.02	100.62	83.8
										PL49	46.97	33.64	0.41	0.27	17.62	1.57	0.02	100.5	86.1
PL16	46.93	33.21	0.40	0.26	17.50	1.58	0.00	99.88	86.0	PL50	46.1	34.11	0.33	0.26	18.3	1.31	0.01	100.42	88.5
PL16a	47.49	32.72	0.33	0.27	17.03	1.87	0.01	99.72	83.4	PL51	46.63	33.8	0.42	0.26	17.94	1.55	0.01	100.61	86.5
PL17	45.78	34.31	0.39	0.22	18.18	1.25	0.01	100.14	88.9	PL52	46.26	33.92	0.38	0.26	17.94	1.45	0.01	100.22	87.2
PL17a	46.54	33.20	0.49	0.29	17.58	1.54	0.01	99.65	86.3	PL53	47.58	33.15	0.41	0.27	17.21	1.79	0.02	100.43	84.2
PL18	45.57	34.54	0.38	0.24	18.55	1.14	0.02	100.44	90.0	PL54	46.48	33.83	0.39	0.23	17.9	1.41	0.01	100.25	87.5
PL19	46.79	33.54	0.30	0.30	17.59	1.59	0.02	100.13	85.9	PL55	46.05	34.36	0.36	0.24	18.19	1.26	0.01	100.47	88.9
PL20	45.59	34.14	0.35	0.26	18.33	1.22	0.03	99.92	89.3	PL57	45.41	34.65	0.28	0.26	18.88	0.99	0.02	100.49	91.3
PL21-GL	46.37	33.96	0.41	0.22	18.07	1.38	0.01	100.42	87.9	PL58	46.34	34.04	0.4	0.22	18.27	1.34	0.01	100.62	88.3
PL22	47.37	33.43	0.35	0.28	17.29	1.69	0.02	100.43	85.0	PL59	45.94	34.31	0.33	0.21	18.19	1.3	0.01	100.29	88.6
PL23	47.67	33.11	0.39	0.30	17.37	1.83	0.01	100.68	84.0	PL60	46.05	34.16	0.36	0.23	18.17	1.34	0.01	100.32	88.2
PL24	46.74	33.72	0.29	0.28	17.68	1.46	0.14	100.31	87.0	PL61-SP	46.4	33.73	0.35	0.28	17.93	1.46	0.01	100.16	87.2
PL25	45.82	34.16	0.34	0.26	18.36	1.21	0.01	100.16	89.3	PL62	46.88	33.72	0.38	0.3	17.66	1.58	0.01	100.53	86.1
PL26-1	47.73	32.64	0.40	0.28	17.14	1.89	0.01	100.09	83.4	PL63	46.53	34.32	0.32	0.26	18.25	1.33	0.01	101.02	88.4
PL26	46.18	34.08	0.32	0.26	18.12	1.29	0.00	100.25	88.6	PL65	46.2	34.16	0.41	0.28	17.91	1.4	0.01	100.37	87.6
PL27	46.11	33.94	0.47	0.29	18.07	1.40	0.01	100.29	87.7	PL65a	47.5	33.37	0.52	0.29	17.36	1.72	0.02	100.78	84.8
PL28	46.17	34.09	0.38	0.22	18.12	1.28	0.01	100.27	88.7	PL66	46.29	34.15	0.38	0.29	18.07	1.33	0.03	100.54	88.3
PL29	47.43	33.18	0.39	0.29	17.18	1.86	0.02	100.35	83.6	PL67	45.81	34.33	0.46	0.23	18.31	1.31	0.02	100.47	88.5
PL30	47.23	33.57	0.43	0.26	17.53	1.60	0.00	100.62	85.8	PL68	45.97	34.27	0.33	0.21	18.43	1.31	0.01	100.53	88.6
PL30a	45.18	34.29	0.36	0.20	18.44	1.15	0.01	99.63	89.9	PL69	45.99	34.53	0.44	0.24	18.4	1.21	0.01	100.82	89.4
PL31	46.09	34.23	0.31	0.28	18.29	1.24	0.02	100.46	89.1	PL70	46.9	33.57	0.33	0.29	17.69	1.56	0.02	100.36	86.2
PL32	46.70	33.79	0.38	0.24	17.94	1.51	0.01	100.57	86.8	PL71	46.04	33.94	0.41	0.23	18.09	1.35	0.02	100.08	88.1
PL33	47.18	33.22	0.43	0.28	17.45	1.67	0.00	100.23	85.2	PL72	46.33	33.97	0.40	0.23	18.21	1.36	0.00	100.50	88.1

Appendix 2.2.1. continued.

Sample	SiO_2	Al_2O_3	FeO	MgO	CaO	Na_2O	K_2O	Total	An[a]	Sample	SiO_2	Al_2O_3	FeO	MgO	CaO	Na_2O	K_2O	Total	An[a]
PL73	46.38	33.80	0.32	0.28	18.07	1.36	0.01	100.22	88.00	PL111	46.41	33.93	0.36	0.25	17.92	1.42	0.01	100.3	87.5
PL74	46.09	34.19	0.52	0.21	18.33	1.30	0.01	100.65	88.6	PL112	46.40	33.99	0.34	0.28	18.00	1.37	0.01	100.39	87.9
PL75	46.00	34.59	0.40	0.21	18.45	1.22	0.01	100.88	89.3	PL113	46.31	34.23	0.38	0.29	18.1	1.39	0.02	100.72	87.8
PL76	46.67	33.83	0.33	0.25	17.98	1.45	0.00	100.51	87.3	PL114	46.34	34.22	0.35	0.21	18.33	1.30	0.01	100.76	88.6
PL77	48.52	32.47	0.44	0.28	16.53	2.10	0.01	100.35	81.3	PL115	45.70	34.80	0.35	0.23	18.82	1.09	0.02	101.01	90.5
PL78	45.99	33.96	0.42	0.24	18.24	1.35	0.01	100.21	88.2	PL116	47.72	32.99	0.51	0.26	17.09	1.88	0.01	100.46	83.4
PL79	45.98	34.37	0.40	0.21	18.34	1.28	0.03	100.61	88.8	PL116a	46.68	33.17	0.37	0.28	17.60	1.60	0.01	99.71	85.9
PL80	45.97	34.30	0.32	0.24	18.35	1.22	0.02	100.42	89.3	PL117	45.84	34.56	0.35	0.22	18.58	1.23	0.01	100.79	89.3
PL81	46.56	33.73	0.36	0.27	18.07	1.45	0.01	100.45	87.3	PL118	46.09	34.09	0.42	0.24	18.04	1.35	0.01	100.24	88.1
PL82	46.69	33.67	0.37	0.30	17.84	1.53	0.01	100.41	86.6	PL119	45.84	34.59	0.40	0.26	18.62	1.12	0.02	100.85	90.2
PL83	46.05	33.98	0.33	0.24	18.10	1.33	0.01	100.04	88.3	PL120	46.57	34.16	0.40	0.28	18.14	1.42	0.00	100.97	87.6
PL84	47.01	33.51	0.40	0.24	17.53	1.64	0.02	100.35	85.5	PL121	46.21	34.42	0.36	0.22	18.29	1.28	0.01	100.79	88.8
PL85	47.17	33.29	0.43	0.26	17.41	1.74	0.03	100.33	84.7	PL122	46.65	34.11	0.40	0.24	17.92	1.43	0.01	100.76	87.4
PL86	45.59	34.38	0.32	0.21	18.67	1.17	0.01	100.35	89.8	PL123	47.51	33.15	0.34	0.29	17.35	1.81	0.02	100.47	84.1
PL87	46.05	34.20	0.31	0.24	18.30	1.28	0.01	100.39	88.8	PL124	46.75	34.09	0.38	0.28	17.91	1.47	0.00	100.88	87.1
PL88	45.68	34.79	0.34	0.21	18.60	1.07	0.02	100.71	90.6	PL125	47.57	33.13	0.43	0.25	17.40	1.75	0.00	100.53	84.6
PL89	45.39	34.88	0.32	0.20	18.72	1.03	0.02	100.56	90.9	PL126	46.19	34.02	0.45	0.20	18.07	1.38	0.02	100.33	87.9
PL90	45.64	34.92	0.38	0.20	18.54	1.08	0.01	100.77	90.5	PL127	45.79	34.45	0.4o	0.18	18.51	1.12	0.01	100.46	90.1
PL91	47.75	32.97	0.38	0.28	17.18	1.82	0.01	100.39	83.9	PL129	46.76	33.69	0.32	0.27	17.89	1.56	0.01	100.5	86.4
PL92	45.78	34.53	0.31	0.25	18.55	1.10	0.02	100.54	90.3	PL130	46.55	33.65	0.34	0.28	17.81	1.50	0.02	100.15	86.8
PL93	47.52	33.12	0.41	0.28	17.30	1.74	0.01	100.38	84.6	PL131	49.54	16.56	8.95	9.25	13.28	1.79	0.01	99.38	80.4
PL94	46.06	34.12	0.36	0.25	18.19	1.34	0.01	100.33	88.2	I2-PL10-GLA	47.15	34.19	0.56	0.26	17.74	1.56	0.01	101.47	86.3
PL95	46.49	33.91	0.40	0.25	18.18	1.37	0.01	100.61	88.0	I2-PL11-GLB	47.07	34.18	0.46	0.22	17.71	1.49	0.02	101.15	86.8
PL96	45.91	34.27	0.39	0.21	18.38	1.25	0.01	100.42	89.0	I2-PL11-GLA	46.68	34.43	0.55	0.22	18.16	1.35	0.02	101.41	88.1
PL97	46.30	34.19	0.35	0.26	18.16	1.36	0.00	100.62	88.1	I2-PL12-GLA	47.18	33.99	0.36	0.27	17.67	1.58	0.01	101.06	86.1
PL98	45.50	34.75	0.31	0.25	18.70	1.04	0.01	100.56	90.9	I2-PL13-GLA	47.29	34.27	0.45	0.27	17.80	1.52	0.02	101.62	86.6
PL99	45.62	34.45	0.45	0.24	18.59	1.17	0.01	100.53	89.8	I2-PL17-GLB	47.36	33.97	0.48	0.39	17.70	1.54	0.01	101.45	86.4
PL100	45.81	34.50	0.35	0.24	18.39	1.25	0.02	100.56	89.1	I2-PL17-GLA	46.68	34.18	0.48	0.23	17.96	1.45	0.03	101.01	87.3
PL101	47.34	33.37	0.42	0.29	17.55	1.74	0.02	100.73	84.8	T-PL1-SP	45.02	33.96	0.43	0.21	18.21	1.01	0.00	98.84	90.9
PL102	46.84	33.66	0.33	0.24	17.91	1.60	0.01	100.59	86.1	T-PL2-SP1	45.87	33.17	0.33	0.27	17.52	1.34	0.07	98.57	87.8
PL103	47.39	33.22	0.38	0.26	17.41	1.72	0.01	100.39	84.8	T-PL2-SP2	46.63	34.54	0.40	0.25	17.73	1.26	0.01	100.82	88.6
PL104	46.66	33.82	0.41	0.29	17.98	1.51	0.01	100.68	86.8	T-PL2-SP3	46.23	33.56	0.39	0.29	17.65	1.43	0.01	99.56	87.2
PL105	46.22	34.31	0.32	0.24	18.16	1.31	0.01	100.57	88.5	T-PL2-SP4	47.27	34.44	0.56	0.46	17.66	1.37	0.01	101.77	87.7
PL106	46.69	34.16	0.35	0.27	18.00	1.45	0.01	100.93	87.3	T-PL3-SP	45.41	34.76	0.38	0.23	18.02	1.08	0.01	99.89	90.2
PL107	46.27	34.21	0.34	0.26	18.20	1.36	0.01	100.65	88.1	T-PL4-SPa	46.02	33.20	0.36	0.27	17.53	1.45	0.03	98.86	87.0
PL108	46.08	34.41	0.32	0.24	18.35	1.27	0.01	100.68	88.9	T-PL4-SPb	46.02	33.20	0.36	0.27	17.53	1.45	0.03	98.86	87.0
PL109	46.82	33.52	0.33	0.30	17.87	1.58	0.01	100.43	86.2	T-PL4-SPc	46.02	33.20	0.36	0.27	17.53	1.45	0.03	98.86	87.0
PL110	47.17	33.40	0.35	0.30	17.40	1.77	0.02	100.41	84.5										

[a]Anorthite content, An = 100 x (Ca/(Ca + Na)).

Appendix 2.2.1, continued.

Sample	SiO_2	Al_2O_3	FeO	MgO	CaO	Na_2O	K_2O	Total	An[a]	Sample	SiO_2	Al_2O_3	FeO	MgO	CaO	Na_2O	K_2O	Total	An[a]
148-896A-4R-1, Piece 2										PL27	46.81	32.87	0.52	0.23	17.08	1.68	0.01	99.20	84.9
PL31	48.29	32.52	0.39	0.35	16.27	2.08	0.01	99.91	81.2	PL28	46.48	32.16	0.42	0.27	16.92	1.80	0.00	98.05	83.9
PL32	46.41	33.49	0.56	0.21	17.19	1.55	0.02	99.43	86.0	PL30	45.56	33.69	0.39	0.27	17.75	1.31	0.01	98.98	88.2
PL56-A	45.77	33.94	0.46	0.46	18.00	1.23	0.01	99.87	89.0	PL32	45.82	33.19	0.39	0.21	17.50	1.47	0.01	98.59	86.8
PL56-B	46.62	33.10	0.49	0.36	17.05	1.67	0.01	99.30	84.9	PL33	46.18	33.80	0.32	0.26	17.34	1.49	0.01	99.40	86.5
PL155	46.46	33.66	0.42	0.24	17.25	1.52	0.02	99.57	86.3	PL34	45.85	33.25	0.40	0.29	17.47	1.55	0.01	98.82	86.2
PL156	45.89	33.78	0.48	0.18	17.42	1.34	0.00	99.09	87.8	PL35	45.52	33.62	0.37	0.26	17.69	1.25	0.01	98.72	88.7
PL157	46.02	33.54	0.41	0.23	17.19	1.48	0.01	98.88	86.5	PL36	45.27	33.69	0.38	0.23	17.87	1.25	0.00	98.69	88.8
PL158	46.23	33.41	0.48	0.32	17.14	1.56	0.01	99.15	85.9	PL37	45.17	33.80	0.35	0.27	17.93	1.31	0.01	98.84	88.3
PL159	46.76	33.15	0.41	0.27	16.85	1.66	0.01	99.11	84.9	PL38	45.53	33.50	0.41	0.32	17.76	1.37	0.01	98.90	87.8
PL160	46.84	32.67	0.43	0.28	16.82	1.80	0.02	98.86	83.8	PL39	45.81	33.83	0.41	0.23	17.95	1.28	0.00	99.51	88.6
PL161	44.58	34.53	0.36	0.21	18.38	0.90	0.00	98.96	91.9	PL40	45.96	33.28	0.30	0.27	17.54	1.53	0.00	98.88	86.4
PL162	47.69	32.13	0.42	0.36	16.15	1.97	0.00	98.72	81.9	PL41	44.93	34.45	0.30	0.20	18.34	1.10	0.01	99.33	90.2
PL163	45.98	33.92	0.36	0.24	17.45	1.36	0.01	99.32	87.6	PL42	45.01	34.35	0.43	0.25	18.46	1.05	0.00	99.55	90.7
PL164-A	45.45	34.21	0.50	0.19	17.81	1.23	0.01	99.40	88.9	PL43	46.50	33.08	0.43	0.27	17.05	1.69	0.01	99.03	84.8
PL164-B	46.26	33.38	0.48	0.24	17.09	1.64	0.00	99.09	85.2	PL44	44.84	34.26	0.34	0.21	18.25	1.09	0.00	98.99	90.3
PL1	45.91	33.47	0.34	0.22	17.95	1.38	0.01	99.28	87.8	PL45	45.80	33.38	0.40	0.24	17.53	1.48	0.01	98.84	86.8
PL2	45.43	34.33	0.34	0.24	18.17	1.18	0.02	99.71	89.5	PL46	45.52	33.76	0.35	0.23	17.93	1.30	0.00	99.09	88.4
PL3	45.95	33.33	0.45	0.23	17.68	1.49	0.01	99.14	86.8	PL47	46.00	33.51	0.30	0.24	17.48	1.46	0.00	98.99	86.9
PL4	46.11	33.69	0.46	0.22	17.69	1.46	0.01	99.64	87.0	PL48	45.88	33.67	0.47	0.21	17.75	1.35	0.02	99.35	87.9
PL5	46.38	32.97	0.46	0.25	17.19	1.70	0.01	98.96	84.8	PL49	44.92	34.50	0.33	0.23	18.37	1.03	0.01	99.39	90.8
PL7	46.36	33.25	0.41	0.22	17.39	1.58	0.03	99.24	85.9	PL50	44.72	34.38	0.33	0.21	18.55	0.99	0.01	99.19	91.2
PL8	45.78	33.39	0.40	0.25	17.57	1.48	0.01	98.88	86.8	PL51	46.69	32.90	0.45	0.26	17.05	1.74	0.01	99.10	84.4
PL9	45.93	33.32	0.33	0.23	17.58	1.45	0.02	98.86	87.0	PL52-A	46.50	33.03	0.35	0.26	17.25	1.73	0.01	99.13	84.6
PL10	46.75	32.38	0.34	0.31	16.71	1.87	0.00	98.36	83.2	PL52	44.64	33.97	0.23	0.24	18.19	1.19	0.01	98.47	89.4
PL11	46.45	32.99	0.49	0.25	17.14	1.65	0.00	98.97	85.2	PL53	46.15	33.31	0.34	0.22	17.48	1.52	0.01	99.03	86.4
PL12	45.49	33.29	0.29	0.23	17.73	1.39	0.01	98.43	87.6	PL54	46.17	33.69	0.41	0.23	17.63	1.47	0.01	99.61	86.9
PL13	46.29	32.52	0.41	0.24	17.40	1.64	0.00	98.50	85.4	PL55	45.45	34.17	0.43	0.25	18.05	1.20	0.03	99.58	89.3
PL14	45.78	33.59	0.49	0.15	17.69	1.43	0.01	99.14	87.2	PL57	45.92	33.46	0.42	0.38	17.67	1.45	0.02	99.32	87.1
PL15	45.97	33.76	0.35	0.26	17.71	1.41	0.01	99.47	87.4	PL58	46.53	33.18	0.38	0.26	17.36	1.62	0.01	99.34	85.6
PL16	46.04	33.46	0.35	0.21	17.73	1.49	0.01	99.29	86.8	PL59	45.78	33.71	0.30	0.24	17.95	1.37	0.00	99.35	87.9
PL17	45.85	33.29	0.33	0.23	17.61	1.50	0.01	98.82	86.6	PL60	46.20	33.25	0.46	0.21	17.56	1.53	0.01	99.22	86.4
PL18	45.31	33.66	0.34	0.27	17.89	1.31	0.01	98.79	88.3	PL61	45.26	34.02	0.28	0.27	18.16	1.20	0.00	99.19	89.3
PL19	45.90	33.40	0.44	0.25	17.70	1.43	0.01	99.13	87.2	PL62	46.80	33.12	0.44	0.23	17.06	1.71	0.01	99.37	84.7
PL20	47.72	31.83	0.47	0.33	16.61	2.06	0.01	99.03	81.7	PL63	44.99	33.92	0.35	0.24	18.25	1.12	0.00	98.87	90.0
PL21	47.71	32.06	0.40	0.35	16.42	2.04	0.01	98.99	81.6	PL64-SP	45.17	34.41	0.28	0.24	18.25	1.09	0.01	99.45	90.3
PL23	46.07	33.18	0.38	0.22	17.53	1.56	0.00	98.94	86.1	PL65	45.48	34.21	0.30	0.23	18.11	1.19	0.01	99.53	89.4
PL24	46.05	33.18	0.46	0.24	17.48	1.52	0.00	98.93	86.4	PL66	46.89	32.85	0.41	0.24	16.95	1.75	0.00	99.09	84.3
PL25	45.20	33.83	0.42	0.42	18.01	1.12	0.01	99.01	89.9	PL67	46.08	33.47	0.48	0.26	17.56	1.49	0.01	99.35	86.7
PL26	46.30	32.70	0.48	0.24	17.16	1.65	0.00	98.53	85.2	PL68	46.49	33.17	0.45	0.27	17.25	1.57	0.07	99.27	85.9
PL27-A	48.24	32.05	0.47	0.34	16.10	2.26	0.02	99.48	79.7	PL69	47.32	32.95	0.42	0.26	16.93	1.85	0.01	99.74	83.5

Appendix 2.2.1, continued.

Sample	SiO_2	Al_2O_3	FeO	MgO	CaO	Na_2O	K_2O	Total	An[a]	Sample	SiO_2	Al_2O_3	FeO	MgO	CaO	Na_2O	K_2O	Total	An[a]
PL70	45.29	33.70	0.26	0.25	18.12	1.30	0.01	98.93	88.5	PL110	45.84	33.55	0.51	0.20	17.73	1.34	0.01	99.18	88.0
PL71	46.21	33.40	0.36	0.29	17.63	1.54	0.00	99.43	86.4	PL111	46.25	33.73	0.40	0.23	17.46	1.46	0.01	99.54	86.9
PL72	46.02	33.76	0.37	0.24	17.72	1.47	0.01	99.59	87.0	PL112	44.91	34.62	0.34	0.21	18.41	0.99	0.02	99.50	91.1
PL73	46.18	33.35	0.44	0.21	17.32	1.60	0.00	99.10	85.7	PL113	46.87	33.08	0.39	0.29	17.19	1.75	0.01	99.58	84.4
PL74	46.10	33.49	0.36	0.23	17.72	1.42	0.01	99.33	87.3	PL114	44.32	35.03	0.34	0.20	18.69	0.80	0.01	99.39	92.8
PL75	45.70	34.14	0.41	0.21	17.95	1.29	0.01	99.71	88.5	PL115	46.20	34.03	0.32	0.24	17.62	1.42	0.02	99.85	87.3
PL76	46.51	33.00	0.37	0.28	17.05	1.69	0.01	98.91	84.8	PL116	45.38	33.87	0.30	0.21	18.18	1.17	0.01	99.12	89.6
PL77	44.91	33.91	0.40	0.42	18.14	1.05	0.01	98.84	90.5	PL117-A	45.92	33.86	0.32	0.27	17.55	1.40	0.00	99.32	87.4
PL78	45.70	33.99	0.35	0.26	18.07	1.23	0.01	99.61	89.0	PL117	45.13	34.67	0.26	0.26	18.29	1.03	0.00	99.64	90.8
PL79-A	45.75	34.02	0.37	0.28	17.75	1.27	0.00	99.44	88.5	PL119	45.57	33.84	0.39	0.26	17.90	1.27	0.01	99.24	88.6
PL79	45.36	33.92	0.24	0.25	18.16	1.10	0.00	99.03	90.1	PL120	45.68	33.63	0.39	0.37	17.62	1.28	0.01	98.98	88.4
PL80	45.96	33.26	0.45	0.20	17.43	1.54	0.01	98.85	86.2	PL121	45.54	33.77	0.38	0.20	17.87	1.32	0.01	99.09	88.2
PL81	46.35	33.49	0.35	0.24	17.47	1.54	0.01	99.45	86.2	PL122	45.88	33.69	0.26	0.27	17.71	1.40	0.01	99.22	87.5
PL82	45.85	33.76	0.29	0.24	17.73	1.32	0.00	99.19	88.1	PL123-A	46.92	32.49	0.48	0.30	16.47	1.81	0.01	98.48	83.4
PL83	46.34	33.11	0.42	0.31	17.39	1.59	0.01	99.17	85.8	PL123	45.61	33.65	0.45	0.34	17.36	1.29	0.06	98.76	88.2
PL84	45.12	34.09	0.35	0.21	17.94	1.25	0.01	98.97	88.8	PL124	46.95	32.79	0.52	0.24	16.74	1.82	0.01	99.07	83.6
PL85	46.56	33.41	0.36	0.25	17.39	1.54	0.00	99.51	86.2	PL125	46.12	33.55	0.43	0.20	17.46	1.52	0.01	99.29	86.4
PL86	45.87	33.59	0.37	0.24	17.59	1.45	0.01	99.12	87.0	PL126	46.17	33.15	0.35	0.28	17.37	1.49	0.01	98.82	86.6
PL87	46.14	33.25	0.43	0.24	17.56	1.48	0.01	99.11	86.8	PL127	45.89	33.58	0.36	0.24	17.48	1.44	0.01	99.00	87.0
PL88	46.21	33.18	0.38	0.26	17.43	1.43	0.18	99.07	87.1	PL128	46.79	33.21	0.43	0.25	17.03	1.73	0.01	99.45	84.5
PL89	46.18	33.07	0.30	0.27	17.34	1.56	0.01	98.73	86.0	PL129	45.95	33.55	0.33	0.27	17.53	1.41	0.01	99.05	87.3
PL90	45.68	34.16	0.27	0.24	18.08	1.23	0.01	99.67	89.0	PL130	45.14	34.15	0.36	0.27	17.96	1.11	0.00	98.99	89.9
PL91	46.91	32.82	0.53	0.42	17.04	1.58	0.01	99.31	85.6	PL131	48.38	32.52	0.42	0.29	16.24	2.09	0.01	99.95	81.1
PL92	45.96	33.76	0.38	0.24	17.80	1.35	0.01	99.50	87.9	PL132	44.98	34.12	0.34	0.24	18.25	1.11	0.01	99.05	90.1
PL93	45.04	34.53	0.33	0.17	18.29	1.05	0.01	99.42	90.6	PL133	45.51	33.87	0.38	0.24	17.82	1.30	0.01	99.13	88.3
PL94	46.36	32.94	0.35	0.36	17.08	1.67	0.02	98.78	85.0	PL134	45.68	33.92	0.38	0.26	17.80	1.31	0.01	99.36	88.3
PL95	46.50	33.46	0.33	0.29	17.41	1.57	0.01	99.57	86.0	PL135	47.44	32.48	0.39	0.30	16.54	1.95	0.00	99.10	82.4
PL96	45.15	34.65	0.31	0.24	18.33	1.06	0.02	99.76	90.5	PL136	45.40	34.20	0.36	0.24	18.09	1.18	0.01	99.48	89.4
PL97	46.47	33.07	0.35	0.28	17.50	1.54	0.03	99.24	86.3	PL137	45.78	34.03	0.32	0.30	17.97	1.26	0.01	99.67	88.7
PL98	46.74	33.81	0.42	0.24	17.00	1.32	0.01	98.54	74.6	PL138	46.35	33.07	0.42	0.24	17.23	1.62	0.01	98.94	85.5
PL100-SP	45.04	34.54	0.29	0.21	18.35	1.03	0.00	99.46	90.8	PL139-A	46.79	33.28	0.38	0.27	16.88	1.74	0.02	99.36	84.3
PL101	46.53	33.18	0.44	0.24	17.12	1.60	0.01	99.12	85.5	PL139	45.82	34.50	0.47	0.20	17.97	1.33	0.00	100.29	88.2
PL102	45.87	33.75	0.48	0.25	17.68	1.36	0.01	99.40	87.8	PL140	45.41	34.26	0.41	0.20	18.19	1.20	0.01	99.68	89.3
PL103	44.78	34.46	0.32	0.21	18.21	1.04	0.00	99.02	90.6	PL141	45.59	33.51	0.40	0.23	17.71	1.36	0.01	98.81	87.8
PL104	46.33	33.40	0.50	0.15	17.16	1.58	0.01	99.13	85.7	PL142	46.84	32.78	0.47	0.27	17.00	1.69	0.01	99.06	84.8
PL105	44.91	34.35	0.29	0.22	18.43	1.01	0.01	99.22	91.0	PL143	46.08	33.69	0.34	0.21	17.67	1.41	0.00	99.40	87.4
PL106	44.81	34.41	0.33	0.20	18.43	1.05	0.01	99.24	90.7	PL144	46.77	33.01	0.45	0.44	16.88	1.60	0.02	99.17	85.4
PL107	45.29	34.74	0.28	0.24	18.41	1.04	0.01	100.01	90.7	PL145	46.15	33.59	0.40	0.23	17.60	1.42	0.01	99.40	87.3
PL108	45.48	34.06	0.34	0.24	17.91	1.29	0.01	99.33	88.5	PL146	45.28	33.73	0.36	0.20	18.00	1.21	0.01	98.79	89.2
PL109	46.31	33.25	0.45	0.31	17.46	1.51	0.01	99.30	86.5	PL147	45.61	34.06	0.40	0.21	18.00	1.21	0.02	99.51	89.2

Appendix 2.2.1, continued.

Sample	SiO_2	Al_2O_3	FeO	MgO	CaO	Na_2O	K_2O	Total	An[a]
PL148	46.35	33.62	0.35	0.22	17.40	1.51	0.02	99.47	86.4
PL149	46.94	33.44	0.35	0.27	17.20	1.67	0.01	99.88	85.1
PL150	46.98	33.28	0.42	0.22	17.00	1.75	0.01	99.66	84.3
PL151	46.49	33.48	0.38	0.24	17.15	1.57	0.01	99.32	85.8
PL152	46.41	33.55	0.39	0.22	17.30	1.60	0.00	99.47	85.7
PL153	45.35	34.24	0.30	0.19	17.98	1.23	0.02	99.31	89.0
PL154	45.55	34.16	0.38	0.26	18.08	1.19	0.00	99.62	89.4
I2-P-11A	45.48	34.08	0.37	0.27	18.29	1.22	0.01	99.72	89.2
I2-P-15A	45.46	34.75	0.29	0.24	18.55	1.10	0.01	100.40	90.3
T-PL1-GL1	44.91	34.90	0.34	0.21	18.68	0.85	0.01	99.90	92.4
T-PL1-GL2	46.06	33.69	0.34	0.27	17.84	1.33	0.01	99.54	88.1
T-PL2-SP1	46.26	33.71	0.43	0.21	17.90	1.42	0.01	99.94	87.5
T-PL2-SP2	46.99	34.00	0.51	0.22	17.56	1.50	0.01	100.79	86.6
T-PL3-SP1	46.34	33.78	0.38	0.24	17.73	1.35	0.01	99.83	87.9
T-PL3-SP3a	45.47	33.36	0.90	0.62	17.71	1.16	0.06	99.28	89.4
T-PL3-SP3b	45.47	33.36	0.90	0.62	17.71	1.16	0.06	99.28	89.4
T-PL3-SP3c	45.47	33.36	0.90	0.62	17.71	1.16	0.06	99.28	89.4
T-PL4-SP1	45.33	34.38	0.41	0.23	18.29	1.05	0.01	99.70	90.6
T-PL5-SP3	45.42	34.49	0.39	0.21	18.40	1.06	0.01	99.98	90.6
T-PL5-SP1	45.72	34.46	0.34	0.28	18.23	1.12	0.01	100.16	90.0
T-PL5-SP2	45.72	34.46	0.34	0.28	18.23	1.12	0.01	100.16	90.0
148-896A-9R-1, Piece 24									
PL1	47.05	33.20	0.01	0.32	17.00	1.68	0.00	99.26	84.8
PL2	46.27	33.42	0.34	0.22	17.55	1.41	0.02	99.23	87.3
PL3	47.88	31.75	0.41	0.34	16.29	2.04	0.01	98.72	81.5
PL4	47.01	32.68	0.36	0.27	16.75	1.78	0.01	98.86	83.9
PL5	46.91	32.98	0.37	0.29	16.89	1.74	0.00	99.18	84.3
PL7	46.83	33.07	0.48	0.27	17.06	1.64	0.02	99.37	85.2
PL8	47.73	32.14	0.44	0.27	16.36	2.07	0.02	99.03	81.4
PL8a	46.86	32.66	0.50	0.25	16.88	1.73	0.01	98.89	84.4
PL9	46.76	32.82	0.41	0.29	16.84	1.74	0.01	98.87	84.3
PL10	46.21	33.02	0.49	0.23	17.27	1.53	0.01	98.76	86.2
PL11	46.99	32.59	0.43	0.31	16.79	1.73	0.01	98.85	84.3
PL12	43.88	35.06	0.27	0.18	18.89	0.62	0.01	98.91	94.4
PL13	46.14	33.74	0.39	0.24	17.68	1.27	0.03	99.49	88.5
PL14	46.35	33.49	0.40	0.24	17.24	1.5	0.02	99.24	86.4
PL15	45.88	33.78	0.35	0.24	17.71	1.32	0.01	99.29	88.1
PL16	46.06	33.33	0.39	0.25	17.32	1.47	0.01	98.83	86.7
PL17	46.73	33.44	0.31	0.25	17.25	1.50	0.01	99.49	86.4
PL18	46.88	33.15	0.43	0.26	17.09	1.59	0.02	99.42	85.6
PL19	46.2	33.22	0.42	0.25	17.53	1.46	0.02	99.1	86.9
PL20	46.54	33.44	0.46	0.26	17.48	1.37	0.01	99.56	87.6
PL21	46.18	33.51	0.47	0.23	17.33	1.51	0.00	99.23	86.4
PL21a	47.71	32.17	0.45	0.31	16.12	2.07	0.02	98.85	81.1
PL23	45.59	33.75	0.34	0.24	17.91	1.24	0.01	99.08	88.9
PL24	45.75	33.68	0.38	0.24	17.64	1.32	0.01	99.02	88.1
PL25	46.22	33.18	0.43	0.21	17.33	1.46	0.00	98.83	86.8
PL26	45.58	33.75	0.36	0.21	17.54	1.32	0.00	98.76	88.0
PL26a	46.56	32.85	0.45	0.24	17.02	1.67	0.02	98.81	84.9
PL28	46.14	33.10	0.38	0.23	17.35	1.5	0.01	98.71	86.5
PL29	45.55	33.69	0.40	0.2	17.9	1.24	0.02	99.00	88.9
PL30	45.45	33.84	0.26	0.23	17.91	1.19	0.00	98.88	89.3
PL31	46.25	32.67	0.7	0.57	17.02	1.48	0.03	98.72	86.4
PL32	46.66	32.21	0.41	0.28	16.68	1.82	0.01	98.07	83.5
PL32a	46.38	33.44	0.41	0.24	17.12	1.45	0.00	99.04	86.7
PL33	46.32	33.18	0.38	0.26	17.14	1.50	0.01	98.79	86.3
PL34	45.34	33.59	0.29	0.27	17.67	1.25	0.01	98.42	88.7
PL35	46.15	33.18	0.41	0.23	17.23	1.50	0.02	98.72	86.4
PL36	46.26	32.90	0.30	0.34	17.18	1.53	0.01	98.52	86.1
PL37	46.23	33.12	0.36	0.26	17.23	1.51	0.00	98.71	86.3
PL38	46.97	32.36	0.37	0.29	16.71	1.74	0.01	98.45	84.1
PL39	46.03	33.23	0.34	0.34	17.38	1.36	0.01	98.69	87.6
PL40	45.80	33.69	0.32	0.28	17.35	1.36	0.00	98.81	87.6
PL41	45.61	33.79	0.42	0.21	18.15	1.26	0.00	99.44	88.8
PL42	45.53	33.82	0.37	0.22	18.10	1.25	0.02	99.31	88.9
PL43	46.32	33.19	0.34	0.27	17.60	1.57	0.01	99.30	86.1
PL44	46.05	32.44	0.69	0.86	17.79	1.30	0.01	99.14	88.3
PL45	45.79	33.45	0.32	0.29	18.12	1.28	0.01	99.26	88.7
PL46	46.38	33.23	0.40	0.22	17.61	1.52	0.01	99.37	86.5
PL47	45.52	34.22	0.33	0.24	18.36	1.14	0.01	99.82	89.9
PL48	46.22	33.31	0.43	0.24	17.94	1.33	0.01	99.48	88.2
PL49-GL	46.26	33.09	0.43	0.54	17.95	1.42	0.02	99.71	87.5
PL50	45.66	33.79	0.39	0.22	18.2	1.29	0.01	99.56	88.6
PL51	46.54	33.18	0.40	0.27	17.57	1.54	0.02	99.52	86.3
PL52	47.25	32.64	0.40	0.38	17.12	1.62	0.05	99.46	85.4
PL53	45.27	34.06	0.26	0.24	18.31	1.12	0.01	99.27	90.0
PL54	46.90	33.16	0.46	0.28	17.32	1.58	0.00	99.70	85.8

Appendix 2.2.1, continued.

Sample	SiO_2	Al_2O_3	FeO	MgO	CaO	Na_2O	K_2O	Total	An[a]
PL54a	47.71	32.31	0.45	0.27	16.6	2.01	0.00	99.35	82.0
PL55	46.52	32.86	0.43	0.26	17.22	1.62	0.02	98.93	85.5
PL56	46.84	32.99	0.45	0.24	17.4	1.61	0.00	99.53	85.7
PL57	46.19	33.62	0.36	0.25	17.68	1.36	0.01	99.47	87.8
PL58	43.92	35.07	0.36	0.16	19.07	0.61	0.01	99.2o	94.5
PL59	46.29	32.95	0.49	0.54	17.69	1.37	0.00	99.33	87.7
PL60	46.53	33.04	0.40	0.24	17.33	1.64	0.01	99.19	85.4
PL61a	44.17	35.26	0.30	0.17	19.31	0.68	0.00	99.89	94.0
PL62	45.84	33.79	0.34	0.21	17.87	1.3	0.01	99.36	88.4
PL63	45.66	33.91	0.35	0.22	18.18	1.23	0.01	99.56	89.1
PL64	45.67	34.19	0.35	0.22	18.35	1.10	0.01	99.89	90.2
PL65	46.40	33.47	0.39	0.26	17.8	1.41	0.01	99.74	87.5
PL66	45.98	33.32	0.62	0.70	17.75	1.14	0.13	99.64	89.6
PL66a	46.62	33.51	0.32	0.25	17.53	1.47	0.02	99.72	86.8
PL67	46.23	33.08	0.41	0.24	17.75	1.48	0.01	99.20	86.9
PL68	45.92	33.50	0.51	0.21	17.93	1.34	0.01	99.42	88.1
PL69	46.41	33.23	0.42	0.28	17.54	1.43	0.01	99.32	87.1
PL70	45.63	34.01	0.38	0.19	18.15	1.23	0.02	99.61	89.1
PL71	48.00	32.00	0.41	0.35	16.32	1.97	0.20	99.25	82.1
PL72	45.84	33.87	0.39	0.23	18.08	1.30	0.01	99.72	88.5
PL72a	45.03	34.42	0.43	0.19	18.75	0.95	0.00	99.77	91.6
PL73	46.63	33.28	0.36	0.31	17.58	1.46	0.01	99.63	86.9
PL74	46.16	33.33	0.39	0.24	17.65	1.47	0.00	99.24	86.9
PL75	46.10	33.10	0.41	0.24	17.45	1.49	0.01	98.80	86.6
PL76	45.88	33.94	0.43	0.21	17.78	1.28	0.01	99.53	88.5
PL77	46.39	33.42	0.37	0.22	17.55	1.44	0.03	99.42	87.1
PL78	45.34	34.06	0.28	0.23	18.14	1.15	0.00	99.20	89.7
PL79	47.09	32.50	0.46	0.26	16.89	1.73	0.17	99.10	84.4
PL80	46.43	33.41	0.36	0.29	17.68	1.42	0.02	99.61	87.3
PL81	45.51	33.73	0.37	0.23	18.07	1.24	0.01	99.16	89.0
PL82	46.77	32.68	0.78	0.70	17.03	1.54	0.01	99.51	85.9
PL83	46.34	33.28	0.47	0.21	17.49	1.53	0.01	99.33	86.3
PL84	46.40	33.63	0.42	0.25	17.49	1.43	0.01	99.63	87.1
PL85	45.19	34.08	0.37	0.19	18.33	1.10	0.00	99.26	90.2
PL87	46.26	33.57	0.38	0.19	17.76	1.32	0.01	99.49	88.1
PL88	47.08	32.84	0.38	0.30	17.23	1.71	0.01	99.55	84.8
PL88a	45.74	34.11	0.45	0.21	18.15	1.14	0.01	99.81	89.8
PL89	44.62	34.82	0.30	0.20	18.97	0.79	0.01	99.71	93.0

Sample	SiO_2	Al_2O_3	FeO	MgO	CaO	Na_2O	K_2O	Total	An[a]
PL90	45.95	33.65	0.46	0.22	17.73	1.35	0.01	99.37	87.9
PL91	46.33	33.53	0.37	0.21	17.72	1.39	0.01	99.56	87.6
PL92	46.57	33.47	0.44	0.21	17.54	1.51	0.02	99.76	86.5
PL93	45.78	33.98	0.34	0.26	18.21	1.19	0.01	99.77	89.4
PL94	46.41	33.53	0.38	0.25	17.73	1.39	0.01	99.70	87.6
PL95	45.49	33.95	0.43	0.18	17.96	1.24	0.01	99.26	88.9
PL96	46.62	33.01	0.38	0.27	17.21	1.61	0.01	99.11	85.5
PL97	46.25	33.26	0.36	0.30	17.61	1.43	0.00	99.21	87.2
PL98	46.02	33.4	0.36	0.23	17.79	1.33	0.01	99.14	88.1
PL99	46.26	33.38	0.46	0.23	17.58	1.46	0.01	99.38	86.9
PL100	45.01	33.85	0.45	0.18	18.03	1.08	0.00	98.60	90.2
PL100a	46.11	33.06	0.38	0.22	17.48	1.43	0.02	98.70	87.1
PL101	46.82	32.78	0.40	0.24	17.10	1.65	0.01	99.00	85.1
PL102	46.62	33.27	0.32	0.27	17.38	1.47	0.02	99.35	86.7
PL103	46.41	33.29	0.35	0.27	17.35	1.48	0.00	99.15	86.6
PL104	46.27	33.21	0.30	0.30	17.76	1.35	0.01	99.2	87.9
PL105	44.97	34.47	0.36	0.15	18.42	0.96	0.00	99.33	91.4
PL106	46.73	33.23	0.36	0.24	17.49	1.51	0.01	99.57	86.5
PL107	47.01	32.77	0.40	0.24	17.18	1.72	0.02	99.34	84.7
PL108	46.59	33.37	0.33	0.26	17.50	1.44	0.10	99.59	87.0
PL109	46.23	33.53	0.33	0.32	17.91	1.31	0.01	99.64	88.3
PL110	45.31	34.30	0.27	0.21	18.40	1.00	0.02	99.51	91.1
PL111	46.01	33.38	0.43	0.21	17.89	1.32	0.01	99.25	88.2
PL112	45.13	34.21	0.32	0.22	18.50	0.97	0.01	99.36	91.3
PL113	44.02	35.06	0.37	0.14	19.3	0.63	0.00	99.52	94.4
PL114	45.43	34.27	0.33	0.23	18.17	1.08	0.01	99.52	90.3
PL115	46.51	33.24	0.31	0.26	17.49	1.46	0.01	99.28	86.9
PL116	47.52	32.38	0.45	0.24	16.89	1.73	0.00	99.21	84.4
PL117	46.74	32.9	0.57	0.15	17.12	1.67	0.00	99.15	85.0
PL118	47.87	32.30	0.39	0.34	16.64	1.91	0.01	99.46	82.8
PL119-GLA	46.23	33.33	0.35	0.26	17.67	1.37	0.01	99.22	87.7
PL119-GLB	46.23	33.33	0.35	0.26	17.67	1.37	0.01	99.22	87.7
PL119-GLC	46.23	33.33	0.35	0.26	17.67	1.37	0.01	99.22	87.7
PL120	46.66	33.29	0.42	0.27	17.62	1.43	0.03	99.72	87.2
PL121	46.84	32.65	0.41	0.24	17.13	1.50	0.01	98.78	86.3
PL121a	48.05	32.27	0.42	0.23	16.57	1.95	0.00	99.49	82.4
PL122	46.66	33.04	0.43	0.26	17.31	1.56	0.01	99.27	86.0
PL123	46.78	33.17	0.41	0.24	17.39	1.51	0.00	99.5	86.4
PL123a	47.85	32.65	0.45	0.27	16.73	1.93	0.01	99.89	82.7
PL124	46.16	33.46	0.47	0.26	17.69	1.37	0.00	99.41	87.7

Appendix 2.2.1, continued.

Sample	SiO_2	Al_2O_3	FeO	MgO	CaO	Na_2O	K_2O	Total	An[a]
PL125	44.80	34.64	0.27	0.21	18.8	0.83	0.01	99.56	92.6
PL126-1	45.17	34.06	0.48	0.18	18.34	1.05	0.01	99.29	90.6
PL126-2	47.01	32.83	0.53	0.24	17.37	1.63	0.01	99.62	85.5
PL127	45.38	34.05	0.30	0.22	18.27	1.1	0.01	99.33	90.2
PL128	46.16	33.57	0.52	0.36	17.83	1.26	0.03	99.73	88.7
PL129	48.53	31.98	0.40	0.37	16.32	2.06	0.02	99.68	81.4
PL130	45.12	34.15	0.41	0.30	18.64	0.91	0.00	99.53	91.9
PL131	45.51	33.95	0.29	0.23	18.33	1.09	0.01	99.41	90.3
PL132	45.95	34.05	0.34	0.23	17.97	1.26	0.01	99.81	88.7
PL133	46.20	33.92	0.41	0.21	18.00	1.27	0.02	100.03	88.7
PL134	46.18	33.68	0.38	0.24	17.72	1.4	0.01	99.61	87.5
PL135	44.18	34.92	0.21	0.17	18.98	0.65	0.01	99.12	94.2
PL135a	45.74	34.06	0.29	0.28	17.76	1.19	0.00	99.32	89.2
PL136	46.48	33.48	0.28	0.27	17.51	1.41	0.02	99.45	87.3
PL137	48.42	31.59	0.60	0.46	16.05	2.16	0.01	99.29	80.4
PL137a	46.84	33.13	0.51	0.27	17.39	1.62	0.01	99.77	85.6
PL138	46.16	33.66	0.41	0.20	17.72	1.43	0.01	99.59	87.3
PL139	45.46	34.10	0.41	0.43	18.31	1.04	0.01	99.76	90.7
PL139a	47.92	31.54	0.73	0.87	16.96	1.69	0.01	99.72	84.7
PL140	45.30	34.46	0.30	0.23	18.69	0.97	0.00	99.95	91.4
PL140a	46.91	33.00	0.35	0.31	17.45	1.52	0.02	99.56	86.4
PL141	46.59	33.26	0.32	0.25	17.36	1.55	0.01	99.34	86.1
PL142	46.30	33.47	0.53	0.2	17.44	1.53	0.01	99.48	86.3
PL143	46.48	33.77	0.35	0.28	17.87	1.44	0.01	100.2	87.3
PL144	46.68	33.37	0.35	0.25	17.67	1.47	0.02	99.81	86.9
PL145	46.69	33.42	0.42	0.26	17.72	1.44	0.03	99.98	87.2
PL146	46.86	33.40	0.35	0.29	17.68	1.44	0.02	100.04	87.2
PL147	46.15	33.66	0.45	0.21	17.72	1.42	0.02	99.63	87.3
PL148	46.25	33.62	0.54	0.29	17.75	1.30	0.07	99.82	88.3
PL149	46.16	33.61	0.33	0.43	18.15	1.31	0.02	100.01	88.5
PL150	46.59	33.52	0.41	0.26	17.65	1.47	0.01	99.91	86.9
PL151	46.64	33.12	0.40	0.26	17.40	1.60	0.01	99.43	85.7
PL152	46.48	33.54	0.44	0.22	17.63	1.49	0.00	99.8	86.7
PL153	46.47	33.67	0.35	0.21	17.70	1.42	0.01	99.83	87.3
PL154	45.72	34.43	0.36	0.21	18.23	1.14	0.01	100.1	89.8
PL155	46.94	33.26	0.44	0.22	17.49	1.59	0.02	99.96	85.9
PL156	45.26	34.41	0.35	0.22	18.38	0.99	0.01	99.62	91.1
PL157	46.62	33.54	0.47	0.23	17.61	1.45	0.01	99.93	87.0
PL158	46.90	33.35	0.42	0.21	17.23	1.48	0.29	99.88	86.6
PL159	47.33	33.13	0.42	0.29	17.18	1.64	0.01	100.00	85.3
PL160	45.88	34.07	0.40	0.21	18.14	1.24	0.00	99.94	89.0
PL161	48.32	32.30	0.46	0.29	16.37	2.12	0.01	99.87	81.0
PL162	45.32	34.58	0.31	0.20	18.70	0.94	0.02	100.07	91.7
I2-PL15-GLA	46.1	34.71	0.32	0.23	18.16	1.34	0.02	100.88	88.2
I2-PL15-GLB	46.16	34.46	0.37	0.27	18.18	1.30	0.01	100.75	88.5
I2-PL18-GLA	47.40	33.72	0.51	0.24	17.61	1.61	0.00	101.09	85.8
A9-PL4	44.43	35.62	0.43	0.15	19.21	0.65	0.01	100.5	94.2
A9-PL16-SP	46.80	33.78	0.47	0.28	17.53	1.44	0.02	100.32	87.1
A9-PL19-SP	46.20	34.08	0.49	0.45	17.57	1.33	0.01	100.13	88.0
A9-PL53-SP	46.44	33.59	0.55	0.45	17.54	1.31	0.03	99.91	88.1
A9-PL4-1	44.33	35.15	0.42	0.15	19.12	0.64	0.01	99.82	94.1
A9-PL4-GL	45.76	34.38	0.58	0.22	17.9	1.19	0.00	100.03	89.3
A9-PL7-GL2	46.21	33.74	0.29	0.28	17.96	1.29	0.00	99.77	88.5
A9-PL7-GL1	44.70	34.84	0.51	0.44	18.68	0.72	0.00	99.90	93.5
A9-PL8-GL1	46.30	33.56	0.38	0.25	17.33	1.45	0.00	99.27	86.9
A9-PL8-GL2	46.28	33.58	0.47	0.25	17.66	1.33	0.00	99.57	88.0
A9-PL10-GL	46.20	33.53	0.34	0.26	17.79	1.33	0.01	99.46	88.1
A9-PL14-GL	46.69	33.49	0.41	0.23	17.47	1.43	0.00	99.72	87.1
A9-PL21-GL	46.38	33.77	0.28	0.31	17.71	1.24	0.00	99.69	88.8
A9-PL54-1	44.58	34.63	0.27	0.20	18.93	0.75	0.00	99.36	93.3
A9-PL54-GL1	45.89	34.16	0.28	0.25	18.09	1.12	0.00	99.79	89.9
A9-PL54-GL2	44.44	35.17	0.28	0.20	19.11	0.68	0.01	99.89	94.0
896A-25R-1, Piece 11									
PL1	45.68	33.74	0.47	0.26	17.61	1.35	0.01	99.12	87.8
PL2	45.99	32.98	0.66	0.57	17.01	1.45	0.06	98.72	86.6
PL3	47.03	32.53	0.38	0.28	16.66	1.83	0.02	98.73	83.4
PL5	46.66	33.22	0.42	0.26	16.95	1.63	0.01	99.15	85.1
PL6	46.87	33.01	0.45	0.26	16.98	1.71	0.01	99.29	84.5
PL7	47.53	32.46	0.46	0.29	16.50	1.96	0.01	99.21	82.3
PL8	46.24	33.67	0.46	0.23	17.29	1.54	0.01	99.44	86.1
PL9	46.21	33.32	0.37	0.27	17.07	1.59	0.01	98.84	85.0
PL10	46.10	33.77	0.40	0.21	17.35	1.43	0.02	99.28	87.0
PL11	45.66	33.48	0.36	0.23	17.49	1.34	0.02	98.58	87.8
PL13	44.93	34.15	0.30	0.23	18.08	1.10	0.00	98.79	90.1
PL14	46.62	32.97	0.46	0.38	16.69	1.66	0.08	98.86	84.8
PL15	46.31	33.28	0.37	0.24	17.07	1.69	0.01	98.97	84.8
PL16	45.90	33.53	0.37	0.23	17.53	1.37	0.00	98.93	87.6
PL17	47.40	32.69	0.38	0.25	16.45	1.94	0.01	99.12	82.4

Appendix 2.2.1, continued.

Sample	SiO_2	Al_2O_3	FeO	MgO	CaO	Na_2O	K_2O	Total	An[a]	Sample	SiO_2	Al_2O_3	FeO	MgO	CaO	Na_2O	K_2O	Total	An[a]
PL19	46.08	33.52	0.41	0.23	17.30	1.49	0.02	99.05	86.5	PL52	47.14	32.48	0.48	0.29	16.56	1.93	0.01	98.89	82.6
PL20	46.63	33.13	0.43	0.26	17.00	1.68	0.01	99.14	84.8	PL53	45.30	34.05	0.40	0.21	18.02	1.18	0.01	99.17	89.4
PL21	47.52	32.44	0.43	0.26	16.23	1.94	0.02	98.84	82.2	PL54	46.76	32.91	0.36	0.23	16.77	1.67	0.18	98.88	84.7
PL21-1	45.99	33.56	0.48	0.21	17.10	1.50	0.01	98.85	86.3	PL55	48.23	31.83	0.36	0.30	16.06	2.26	0.01	99.05	79.7
PL22-A	47.25	32.70	0.39	0.29	16.53	1.91	0.00	99.07	82.7	PL56	46.47	33.09	0.43	0.25	17.00	1.73	0.01	98.98	84.5
PL22-B	46.15	33.50	0.45	0.22	17.44	1.51	0.02	99.29	86.5	PL57	47.68	32.25	0.41	0.32	16.23	2.12	0.01	99.02	80.9
PL23	45.84	33.66	0.39	0.24	17.63	1.45	0.01	99.22	87.0	PL58	46.20	33.62	0.39	0.25	17.64	1.47	0.01	99.58	86.9
PL24	46.01	33.38	0.42	0.21	17.42	1.44	0.01	98.89	87.0	PL59	47.72	32.45	0.41	0.30	16.37	2.07	0.01	99.33	81.4
PL25	46.90	32.94	0.37	0.27	16.74	1.76	0.01	98.99	84.0	PL60-GL	45.91	33.75	0.48	0.24	17.76	1.35	0.02	99.51	87.9
PL26	45.11	34.28	0.32	0.23	18.30	1.08	0.01	99.33	90.4	PL61	46.39	33.49	0.35	0.24	17.44	1.54	0.02	99.47	86.2
PL27	47.48	32.53	0.43	0.26	16.46	1.97	0.01	99.14	82.2	PL62-A	45.64	34.18	0.47	0.20	17.78	1.23	0.02	99.52	88.9
PL28	45.62	33.86	0.46	0.27	17.70	1.29	0.05	99.25	88.4	PL62-B	47.65	32.84	0.36	0.28	16.47	1.96	0.00	99.56	82.3
PL29	45.97	33.53	0.43	0.23	17.45	1.43	0.00	99.04	87.1	PL63	46.69	32.98	0.40	0.28	17.00	1.71	0.02	99.08	84.6
PL30-A	45.41	33.72	0.45	0.24	17.57	1.37	0.01	98.77	87.6	PL64	45.62	33.46	0.41	0.24	17.39	1.43	0.02	98.57	87.1
PL30-B	47.07	32.42	0.45	0.25	16.50	1.92	0.00	98.61	82.6	PL65	47.20	32.81	0.47	0.26	16.59	1.91	0.01	99.25	82.8
PL31	46.61	33.01	0.37	0.23	16.93	1.68	0.01	98.84	84.8	PL66	47.30	32.46	0.41	0.24	16.55	1.97	0.01	98.94	82.3
PL32	45.91	33.39	0.44	0.20	17.34	1.46	0.00	98.74	86.8	PL67	47.25	32.40	0.40	0.28	16.41	1.95	0.01	98.70	82.3
PL33	47.92	32.18	0.43	0.32	16.01	2.15	0.01	99.02	80.5	PL68	45.30	34.11	0.43	0.19	17.91	1.20	0.01	99.15	89.2
PL34	45.61	33.97	0.38	0.22	17.58	1.33	0.01	99.10	88.0	PL69	47.27	32.96	0.53	0.26	16.79	1.84	0.01	99.66	83.5
PL35	46.02	33.62	0.40	0.24	17.51	1.44	0.02	99.25	87.1	PL70	45.77	34.04	0.40	0.21	17.77	1.33	0.01	99.53	88.1
PL36	45.98	33.34	0.39	0.24	17.21	1.49	0.01	98.66	86.5	PL71	46.52	33.34	0.34	0.25	17.03	1.66	0.03	99.17	85.0
PL37	47.16	32.70	0.43	0.26	16.61	1.83	0.02	99.01	83.4	PL72	46.17	33.60	0.41	0.24	17.42	1.48	0.01	99.33	86.7
PL38	45.94	33.90	0.37	0.18	17.33	1.40	0.01	99.13	87.3	PL73	44.95	34.39	0.36	0.22	18.30	1.03	0.01	99.26	90.8
PL39-A	45.53	33.71	0.32	0.20	17.68	1.37	0.01	98.82	87.7	PL74	46.63	31.98	0.91	1.00	16.24	1.74	0.01	98.51	83.8
PL39-B	47.06	32.80	0.38	0.24	16.49	1.85	0.00	98.82	83.1	PL75	46.40	33.34	0.42	0.23	17.09	1.54	0.02	99.04	86.0
PL40	46.11	32.73	0.77	0.62	16.74	1.56	0.06	98.59	85.6	PL76	46.29	33.40	0.35	0.25	17.33	1.56	0.01	99.19	86.0
PL41	46.12	33.38	0.40	0.26	17.26	1.53	0.03	98.98	86.2	PL77	45.73	34.12	0.38	0.26	17.40	1.36	0.01	99.26	87.6
PL41-1	46.48	33.01	0.41	0.25	17.11	1.62	0.02	98.90	85.4	PL78	46.27	33.29	0.42	0.24	17.07	1.63	0.01	98.93	85.3
PL42	45.63	33.49	0.34	0.24	17.59	1.42	0.01	98.72	87.3	PL79	46.40	33.35	0.34	0.26	17.15	1.56	0.01	99.07	85.9
PL43	46.38	33.55	0.38	0.21	17.32	1.57	0.02	99.43	85.9	PL80	45.68	33.92	0.35	0.26	17.71	1.28	0.01	99.21	88.4
PL44-A	45.26	33.99	0.44	0.21	17.87	1.27	0.02	99.06	88.6	PL81	46.15	33.49	0.32	0.24	17.34	1.53	0.01	99.08	86.2
PL44-B	46.65	33.08	0.48	0.25	16.76	1.72	0.01	98.95	84.3	PL82	48.70	31.70	0.39	0.30	15.58	2.48	0.00	99.15	77.6
PL45	46.77	33.17	0.37	0.24	17.04	1.72	0.00	99.31	84.6	PL83	46.46	33.30	0.36	0.22	17.06	1.60	0.01	99.01	85.5
PL46	46.29	33.47	0.40	0.22	17.36	1.57	0.01	99.32	85.9	PL84	47.12	32.73	0.44	0.24	16.63	1.82	0.00	98.98	83.5
PL47	46.87	32.93	0.37	0.26	16.93	1.78	0.00	99.14	84.0	PL85	46.45	33.35	0.43	0.25	17.09	1.66	0.01	99.24	85.1
PL48	46.35	33.46	0.37	0.23	17.50	1.48	0.01	99.40	86.7	PL86	47.77	32.44	0.40	0.27	16.27	2.03	0.02	99.20	81.6
PL49	47.05	33.07	0.40	0.25	16.85	1.84	0.01	99.47	83.5	PL87	46.17	33.49	0.38	0.23	17.32	1.52	0.01	99.12	86.3
PL50	45.96	33.73	0.44	0.24	17.50	1.46	0.00	99.33	86.9	PL88	46.78	32.85	0.51	0.39	16.61	1.73	0.06	98.93	84.1
PL50-1	46.05	32.99	0.58	0.69	16.92	1.50	0.01	98.74	86.2	PL89	45.52	34.14	0.34	0.24	17.65	1.25	0.00	99.14	88.6
PL51	45.84	34.04	0.43	0.23	17.57	1.42	0.00	99.53	87.2	PL90-A	50.99	28.36	1.39	1.13	13.93	3.09	0.01	98.90	71.4

Appendix 2.2.1, continued.

Sample	SiO_2	Al_2O_3	FeO	MgO	CaO	Na_2O	K_2O	Total	An[a]
PL90-B	45.84	34.06	0.36	0.25	17.64	1.38	0.01	99.54	87.6
PL91	46.63	33.42	0.35	0.24	16.90	1.62	0.01	99.17	85.2
PL92	46.33	33.34	0.38	0.24	17.20	1.54	0.01	99.04	86.1
PL93	46.14	33.66	0.31	0.24	17.28	1.51	0.01	99.15	86.4
PL94	47.66	32.44	0.41	0.30	16.15	2.07	0.01	99.04	81.2
PL95	45.19	34.22	0.31	0.20	17.91	1.10	0.01	98.94	90.0
PL96	45.40	34.00	0.42	0.21	17.70	1.23	0.00	98.96	88.8
PL97	45.56	33.69	0.39	0.22	17.83	1.31	0.01	99.01	88.3
PL98	47.54	32.76	0.43	0.28	16.46	1.97	0.01	99.45	82.2
PL99	45.48	34.11	0.37	0.20	17.75	1.22	0.01	99.14	88.9
PL100	47.08	32.80	0.42	0.26	16.74	1.79	0.00	99.09	83.8
PL101	44.78	34.75	0.27	0.23	18.38	0.95	0.00	99.36	91.5
PL102-A	47.12	32.94	0.44	0.26	16.75	1.81	0.00	99.32	83.6
PL102-B	45.79	33.85	0.39	0.25	17.47	1.45	0.02	99.22	86.9
PL103	46.53	33.26	0.39	0.21	17.04	1.59	0.02	99.04	85.6
PL104	47.45	32.77	0.47	0.25	16.57	1.84	0.01	99.36	83.3
PL105	46.26	33.28	0.42	0.28	17.13	1.57	0.01	98.95	85.8
PL106-A	45.23	34.10	0.40	0.23	17.87	1.15	0.00	98.98	89.6
PL106-B	46.11	33.37	0.51	0.23	17.25	1.49	0.01	98.97	86.5
PL107	45.87	33.37	0.42	0.21	17.39	1.42	0.00	98.68	87.1
PL108	46.08	33.46	0.41	0.24	17.21	1.47	0.01	98.88	86.6
PL109	46.56	33.31	0.40	0.22	17.04	1.68	0.01	99.22	84.9
PL110	46.02	33.64	0.38	0.24	17.28	1.42	0.02	99.00	87.1
PL111	46.41	33.43	0.43	0.25	17.11	1.55	0.01	99.19	85.9
PL112	45.83	33.40	0.54	0.33	17.39	1.41	0.02	98.92	87.2
PL113	46.19	33.21	0.38	0.22	17.07	1.52	0.01	98.60	86.1
PL114	46.62	33.31	0.41	0.24	16.99	1.58	0.02	99.17	85.6
PL115	46.80	32.80	0.60	0.49	16.75	1.61	0.04	99.09	85.2
PL116	46.94	32.83	0.46	0.28	16.67	1.87	0.00	99.05	83.1
PL117-A	46.88	33.19	0.42	0.25	16.90	1.74	0.01	99.39	84.3
PL117-B	46.01	33.65	0.35	0.23	17.16	1.43	0.06	98.89	86.9
PL118-A	47.07	32.83	0.42	0.26	16.50	1.85	0.01	98.94	83.1
PL118-B	46.26	33.60	0.42	0.21	17.42	1.44	0.01	99.36	87.0
PL119	46.20	33.21	0.46	0.23	17.01	1.60	0.01	98.72	85.5
PL120	45.86	33.09	0.39	0.25	16.86	1.52	0.00	97.97	86.0
PL122	45.72	33.55	0.41	0.21	17.37	1.40	0.07	98.73	87.3
PL124	45.83	33.47	0.56	0.45	17.26	1.38	0.02	98.97	87.4
PL125	46.91	33.10	0.39	0.24	16.77	1.70	0.02	99.13	84.5
PL126	46.73	33.17	0.43	0.24	16.72	1.70	0.01	99.00	84.5
PL127	47.01	32.88	0.47	0.40	16.70	1.67	0.08	99.21	84.7
PL128	45.70	33.85	0.38	0.22	17.51	1.28	0.01	98.95	88.3
PL129	46.60	33.02	0.36	0.25	16.74	1.66	0.01	98.64	84.8
PL130	47.09	32.39	0.40	0.43	16.22	1.79	0.21	98.53	83.4
PL132	46.02	33.57	0.41	0.27	17.28	1.46	0.02	99.03	86.7
PL133-A	45.49	33.51	0.38	0.22	17.44	1.39	0.00	98.43	87.4
PL133-B	46.53	32.97	0.45	0.22	16.75	1.69	0.01	98.62	84.6
PL134-GLA	46.49	33.25	0.42	0.25	17.01	1.60	0.01	99.03	85.5
PL135	46.22	33.48	0.39	0.22	17.31	1.51	0.01	99.14	86.4
PL136-GLA	45.58	33.94	0.34	0.23	17.69	1.22	0.01	99.01	88.9
PL137	46.38	33.46	0.44	0.24	17.26	1.51	0.02	99.31	86.3
PL138	45.90	33.64	0.41	0.24	17.37	1.46	0.02	99.04	86.8
PL139	45.51	34.36	0.36	0.23	18.09	1.10	0.03	99.68	90.1
PL140	47.06	32.96	0.47	0.27	16.73	1.76	0.02	99.27	84.0
PL141	47.05	32.88	0.42	0.29	16.73	1.83	0.02	99.22	83.5
PL142	46.00	33.78	0.35	0.23	17.39	1.40	0.01	99.16	87.3
PL143-A	48.09	32.07	0.36	0.28	15.97	2.13	0.01	98.91	80.6
PL143-B	46.06	33.49	0.40	0.25	17.25	1.45	0.02	98.92	86.8
PL144	45.97	33.53	0.39	0.23	17.20	1.50	0.01	98.83	86.4
PL145	46.85	33.40	0.36	0.26	16.90	1.65	0.01	99.43	85.0
A8-PL1-SP	46.79	33.35	0.42	0.24	17.15	1.70	0.00	99.65	84.8
T-PL1-SP	46.19	34.10	0.46	0.23	17.59	1.35	0.00	99.92	87.8
T-PL2-SP	45.28	34.37	0.38	0.22	18.34	1.03	0.01	99.63	90.8
148-896A-25R-2, Piece 11									
PL1	47.21	32.34	0.43	0.29	16.68	1.84	0.01	98.80	83.4
PL2	46.34	33.29	0.41	0.21	17.55	1.44	0.01	99.25	87.1
PL3	46.38	33.22	0.39	0.23	17.45	1.50	0.01	99.18	86.5
PL4	46.32	33.02	0.40	0.21	17.31	1.50	0.01	98.77	86.4
PL5	46.25	33.59	0.38	0.22	17.63	1.35	0.01	99.43	87.8
PL6	46.52	33.09	0.44	0.28	17.25	1.60	0.00	99.18	85.6
PL7	46.45	33.27	0.41	0.22	17.33	1.44	0.00	99.12	86.9
PL8	46.27	33.09	0.47	0.24	17.20	1.52	0.01	98.80	86.2
PL9	47.25	32.45	0.42	0.28	16.61	1.88	0.01	98.90	83.0
PL10	48.01	31.67	0.43	0.28	16.18	2.08	0.01	98.66	81.1
PL11	46.49	32.80	0.41	0.23	17.27	1.54	0.01	98.75	86.1
PL12	47.02	32.66	0.45	0.27	17.16	1.73	0.01	99.30	84.6
PL13	45.20	34.02	0.37	0.18	18.18	1.06	0.01	99.02	90.5
PL14	46.20	33.08	0.40	0.25	17.61	1.49	0.03	99.06	86.7
PL15	46.26	33.16	0.48	0.21	17.46	1.52	0.01	99.10	86.4
PL16	46.75	32.90	0.45	0.26	16.91	1.70	0.01	98.98	84.6

Appendix 2.2.1, continued.

Sample	SiO_2	Al_2O_3	FeO	MgO	CaO	Na_2O	K_2O	Total	An[a]	Sample	SiO_2	Al_2O_3	FeO	MgO	CaO	Na_2O	K_2O	Total	An[a]
PL17	45.38	34.06	0.33	0.20	18.18	1.10	0.01	99.26	90.1	PL54-1	45.23	34.07	0.35	0.20	18.09	1.08	0.01	99.03	90.3
PL18	45.95	32.94	0.38	0.21	17.24	1.59	0.01	98.32	85.7	PL55	47.41	32.39	0.42	0.27	16.58	1.85	0.01	98.93	83.2
PL19	46.03	33.17	0.37	0.24	17.50	1.40	0.01	98.72	87.4	PL56	45.39	34.09	0.44	0.16	18.14	1.13	0.01	99.36	89.9
PL20	45.95	33.30	0.35	0.21	17.65	1.38	0.01	98.85	87.6	PL57	46.30	33.07	0.45	0.22	17.31	1.45	0.01	98.81	86.8
PL21	46.25	33.11	0.36	0.22	17.44	1.49	0.01	98.88	86.6	PL59	46.70	33.38	0.43	0.23	17.23	1.47	0.01	99.45	86.6
PL22	47.12	32.36	0.41	0.27	16.74	1.90	0.01	98.81	83.0	PL60	46.30	33.25	0.41	0.23	17.48	1.47	0.01	99.15	86.8
PL23	46.23	33.34	0.41	0.26	17.58	1.44	0.01	99.27	87.1	PL61	46.54	33.08	0.36	0.25	17.18	1.56	0.01	98.98	85.9
PL24	46.27	33.45	0.37	0.20	17.70	1.43	0.01	99.43	87.2	PL62	45.68	33.41	0.34	0.21	17.66	1.33	0.00	98.63	88.0
PL25	46.41	33.44	0.41	0.23	17.54	1.35	0.03	99.41	87.8	PL63	46.25	33.14	0.39	0.26	17.34	1.44	0.01	98.83	86.9
PL26	47.03	32.60	0.47	0.27	17.02	1.74	0.01	99.14	84.4	PL64	46.52	32.90	0.34	0.23	17.01	1.62	0.01	98.63	85.3
PL27	47.47	32.11	0.43	0.29	16.50	1.97	0.01	98.78	82.2	PL65	46.12	33.24	0.42	0.25	17.31	1.51	0.01	98.86	86.4
PL28	46.44	33.17	0.42	0.23	17.27	1.54	0.01	99.08	86.1	PL65-1	45.97	33.56	0.41	0.23	17.39	1.44	0.01	99.01	87.0
PL29	46.53	33.43	0.40	0.24	17.21	1.48	0.01	99.30	86.5	PL66	46.14	33.61	0.35	0.25	17.77	1.31	0.00	99.43	88.2
PL30	46.68	33.05	0.43	0.27	17.12	1.67	0.02	99.24	85.0	PL67	46.88	32.62	0.49	0.26	16.87	1.68	0.01	98.81	84.7
PL31-1	45.58	33.30	0.42	0.22	17.61	1.28	0.02	98.43	88.4	PL68	46.50	33.19	0.40	0.26	17.19	1.56	0.01	99.11	85.9
PL31	46.97	32.78	0.44	0.24	17.11	1.72	0.00	99.26	84.6	PL69	45.94	33.23	0.39	0.23	17.48	1.39	0.00	98.66	87.4
PL32	47.06	32.48	0.42	0.28	16.98	1.78	0.01	99.01	84.1	PL70	46.14	33.34	0.36	0.21	17.82	1.38	0.01	99.26	87.7
PL33	46.37	32.74	0.44	0.25	17.06	1.66	0.01	98.53	85.0	PL71	46.36	33.38	0.36	0.23	17.17	1.53	0.01	99.04	86.1
PL33-1	45.39	32.99	0.39	0.21	17.87	1.17	0.00	98.02	89.4	PL72	47.23	32.75	0.42	0.26	16.70	1.73	0.01	99.10	84.2
PL34	46.58	32.60	0.42	0.24	17.20	1.52	0.01	98.57	86.2	PL73	47.38	32.05	0.47	0.32	16.60	1.88	0.01	98.71	83.0
PL35	47.11	32.19	0.42	0.27	16.48	1.81	0.01	98.29	83.4	PL74	45.81	33.73	0.40	0.18	17.70	1.33	0.01	99.16	88.0
PL36	46.30	33.19	0.38	0.21	17.29	1.46	0.01	98.84	86.7	PL75	44.95	33.80	0.34	0.19	17.98	1.04	0.01	98.31	90.5
PL37	45.92	33.41	0.43	0.23	17.64	1.40	0.01	99.04	87.4	PL76	45.98	33.24	0.38	0.26	17.53	1.35	0.01	98.75	87.8
PL38	47.84	32.20	0.43	0.29	16.45	1.96	0.01	99.18	82.3	PL77	46.42	33.20	0.43	0.32	17.09	1.52	0.02	99.00	86.1
PL39	45.49	33.38	0.39	0.21	17.89	1.35	0.01	98.72	88.0	PL78	45.64	33.73	0.41	0.22	17.69	1.22	0.01	98.92	88.9
PL40	46.82	32.88	0.43	0.26	17.06	1.62	0.01	99.08	85.3	PL79	47.41	32.02	0.43	0.26	16.49	1.91	0.00	98.52	82.7
PL41	46.22	32.67	0.44	0.25	17.06	1.53	0.01	98.18	86.0	PL80	46.47	32.70	0.52	0.51	17.09	1.50	0.04	98.83	86.3
PL42-GL	46.25	33.42	0.43	0.22	17.43	1.42	0.01	99.18	87.2	PL81	46.59	33.16	0.38	0.23	17.19	1.56	0.01	99.12	85.9
PL43	46.60	33.05	0.42	0.25	17.15	1.60	0.01	99.08	85.6	PL83	46.20	33.04	0.43	0.30	17.41	1.46	0.01	98.85	86.8
PL44	46.83	32.73	0.43	0.26	16.86	1.74	0.01	98.86	84.3	PL84	46.64	33.05	0.45	0.23	17.26	1.59	0.01	99.23	85.7
PL45	46.47	32.80	0.42	0.24	16.99	1.54	0.01	98.47	85.9	PL85	45.68	33.65	0.36	0.20	17.80	1.27	0.00	98.96	88.6
PL46	47.05	32.89	0.46	0.23	16.94	1.66	0.05	99.28	84.9	PL86	46.36	32.49	0.95	0.69	16.92	1.48	0.05	98.94	86.3
PL47	46.84	33.20	0.46	0.26	17.23	1.61	0.01	99.61	85.5	PL87	47.66	32.44	0.31	0.26	16.52	1.96	0.03	99.18	82.3
PL48	46.45	33.13	0.51	0.24	17.39	1.55	0.01	99.28	86.1	PL88	47.08	32.65	0.42	0.24	16.66	1.77	0.02	98.84	83.9
PL49	46.87	32.79	0.42	0.23	17.09	1.60	0.01	99.01	85.5	PL89	46.31	33.49	0.45	0.27	17.47	1.42	0.01	99.42	87.2
PL50	46.73	32.56	0.41	0.23	16.75	1.68	0.01	98.37	84.6	PL90-GL	46.89	33.02	0.36	0.30	17.29	1.57	0.01	99.44	85.9
PL51	47.36	32.25	0.35	0.26	16.43	1.88	0.02	98.55	82.9	PL91	47.50	32.50	0.45	0.28	16.59	1.85	0.00	99.17	83.2
PL52	46.36	33.26	0.49	0.20	17.18	1.44	0.01	98.94	86.8	PL92	45.58	33.50	0.35	0.22	17.76	1.36	0.03	98.80	87.8
PL53	48.92	30.91	0.46	0.33	15.25	2.53	0.02	98.42	76.9	PL93	46.18	33.05	0.43	0.23	17.27	1.42	0.08	98.66	87.1
PL54	46.38	33.20	0.42	0.27	17.35	1.49	0.01	99.12	86.6	PL94	46.47	33.11	0.47	0.21	17.18	1.54	0.01	98.99	86.0

Appendix 2.2.1, continued.

Sample	SiO_2	Al_2O_3	FeO	MgO	CaO	Na_2O	K_2O	Total	An[a]
PL95	46.02	33.15	0.36	0.23	17.58	1.38	0.01	98.73	87.6
PL96	46.23	33.07	0.43	0.27	17.27	1.48	0.01	98.76	86.6
PL97	46.36	33.25	0.39	0.25	17.30	1.40	0.01	98.96	87.2
PL98	46.21	33.14	0.32	0.23	17.62	1.37	0.01	98.90	87.7
PL99	47.84	31.93	0.37	0.32	16.13	2.11	0.01	98.71	80.9
PL100	46.68	32.91	0.32	0.25	17.02	1.64	0.01	98.83	85.2
PL101-GL1	45.18	34.23	0.43	0.19	18.25	1.06	0.03	99.37	90.5
PL101-GL2	46.47	33.15	0.41	0.27	17.14	1.53	0.00	98.97	86.1
PL102	46.06	33.48	0.32	0.24	17.49	1.36	0.01	98.96	87.7
PL103	47.29	32.44	0.41	0.27	16.7	1.83	0.01	98.95	83.5
PL104	46.47	33.10	0.46	0.22	17.38	1.51	0.00	99.14	86.4
PL105	46.97	32.61	0.37	0.28	17.19	1.62	0.01	99.05	85.4
PL106	47.88	32.21	0.42	0.27	16.32	2.04	0.04	99.18	81.6
PL107	45.83	33.55	0.42	0.22	17.7	1.24	0.00	98.96	88.8
PL108	45.29	33.92	0.43	0.19	18.19	1.02	0.00	99.04	90.8
PL109	46.74	33.14	0.34	0.23	17.3	1.60	0.01	99.36	85.7
PL110	46.23	33.27	0.37	0.23	17.38	1.47	0.01	98.96	86.7
PL111	46.27	33.34	0.40	0.23	17.55	1.37	0.01	99.17	87.6
PL112	45.24	34.01	0.35	0.23	18.20	1.07	0.01	99.11	90.4
PL113	46.23	33.42	0.38	0.21	17.41	1.40	0.01	99.06	87.3
PL114	46.21	33.35	0.39	0.20	17.66	1.30	0.01	99.12	88.2
PL115	46.34	33.19	0.41	0.24	17.50	1.44	0.00	99.12	87.0
PL116	46.45	33.14	0.37	0.23	17.23	1.55	0.01	98.98	86.0
PL118	45.86	33.36	0.42	0.18	17.56	1.32	0.01	98.71	88.0
PL119-1	45.68	33.94	0.36	0.26	17.76	1.15	0.01	99.16	89.5
PL119	46.40	33.13	0.35	0.28	17.10	1.47	0.00	98.73	86.5
PL120	48.72	31.37	0.53	0.34	15.59	2.37	0.01	98.93	78.4
PL121	46.61	32.89	0.41	0.27	17.28	1.62	0.01	99.09	85.5
PL122	45.52	33.72	0.36	0.21	17.97	1.24	0.00	99.02	88.9
PL123	45.94	33.58	0.31	0.27	17.48	1.36	0.01	98.95	87.7
PL124	47.29	32.71	0.39	0.24	16.67	1.68	0.02	99.00	84.6
PL124-1	45.93	33.60	0.45	0.25	17.40	1.30	0.00	98.93	88.1
PL125	45.98	33.45	0.35	0.23	17.66	1.33	0.01	99.01	88.0
PL126	46.94	32.8	0.41	0.26	17.15	1.66	0.00	99.22	85.1
PL127	50.06	30.39	0.39	0.33	14.73	2.75	0.01	98.66	74.8
PL128	49.08	31.23	0.40	0.30	15.38	2.49	0.01	98.89	77.3
PL129	45.46	33.86	0.36	0.29	18.02	1.19	0.00	99.18	89.3
PL130	46.75	32.76	0.40	0.25	17.06	1.62	0.01	98.85	85.3
PL131	46.31	33.11	0.41	0.24	17.2	1.52	0.01	98.80	86.2
PL132	45.88	33.28	0.40	0.22	17.45	1.33	0.01	98.57	87.9
PL133	45.30	34.01	0.36	0.18	18.12	1.16	0.01	99.14	89.6
PL134	45.76	33.55	0.34	0.22	17.50	1.31	0.01	98.69	88.1
PL135	46.58	32.89	0.42	0.26	17.11	1.55	0.01	98.82	85.9
PL136	46.31	33.30	0.46	0.26	17.46	1.48	0.01	99.28	86.7
PL137	46.57	33.42	0.43	0.26	17.27	1.44	0.02	99.41	86.9
PL141/1	46.56	33.38	0.40	0.23	17.61	1.46	0.01	99.65	87.0
PL141	45.23	33.81	0.34	0.24	17.84	1.14	0.01	98.61	89.6
PL142	46.47	33.18	0.43	0.24	17.28	1.51	0.01	99.12	86.4
PL143-GL	48.33	31.96	0.49	0.31	15.97	2.11	0.01	99.18	80.7
PL143-1	45.68	33.62	0.39	0.23	17.74	1.29	0.00	98.95	88.4
PL144-GL1	45.67	33.70	0.36	0.24	17.77	1.21	0.01	98.96	89.0
PL144-GL2	45.78	33.61	0.34	0.28	17.74	1.24	0.02	99.01	88.8
PL145	46.16	33.29	0.41	0.22	17.37	1.40	0.01	98.86	87.3
PL146	47.31	32.45	0.45	0.31	16.74	1.76	0.04	99.06	84.0
PL147	46.38	32.83	0.64	0.57	17.21	1.40	0.01	99.04	87.2
PL148	46.06	33.45	0.43	0.22	17.45	1.38	0.01	99.00	87.5
PL149	46.12	33.36	0.36	0.25	17.24	1.40	0.01	98.74	87.2
PL150	47.11	33.06	0.41	0.23	17.13	1.66	0.00	99.60	85.1
PL151	46.46	33.07	0.40	0.23	17.15	1.45	0.01	98.77	86.7
PL152	46.61	33.13	0.44	0.26	17.14	1.55	0.01	99.14	85.9
PL153	47.48	31.98	0.50	0.24	16.36	1.88	0.01	98.45	82.8
PL154	45.77	33.59	0.43	0.21	17.61	1.29	0.01	98.91	88.3
148-896A-27R-1, Piece 13									
PL1	46.24	33.68	0.27	0.23	17.93	1.34	0.01	99.70	88.1
PL2	46.68	33.08	0.35	0.30	17.43	1.59	0.01	99.44	85.8
PL3	45.43	34.63	0.30	0.19	18.49	1.02	0.01	100.07	90.9
PL4	45.99	34.00	0.33	0.27	18.00	1.27	0.01	99.87	88.7
PL5	46.16	33.87	0.42	0.23	17.80	1.30	0.05	99.83	88.3
PL6	45.69	34.71	0.29	0.21	18.52	1.03	0.00	100.45	90.9
PL7	45.54	34.58	0.29	0.20	18.30	1.06	0.00	99.97	90.5
PL8	45.63	34.24	0.39	0.21	18.38	1.14	0.01	100.00	89.9
PL9	47.72	32.87	0.42	0.30	17.05	1.78	0.01	100.15	84.1
PL10	45.94	33.62	0.38	0.25	17.91	1.33	0.04	99.47	88.2
PL11	45.22	34.06	0.39	0.34	18.41	1.06	0.01	99.49	90.6
PL12	46.40	34.20	0.32	0.27	17.99	1.30	0.00	100.48	88.4
PL13	47.22	33.35	0.40	0.27	17.48	1.60	0.00	100.32	85.8
PL14	45.26	34.41	0.26	0.22	18.59	1.08	0.01	99.83	90.5
PL15	45.31	34.64	0.29	0.21	18.44	1.00	0.00	99.89	91.1
PL19	45.46	34.56	0.27	0.22	18.59	1.02	0.01	100.13	91.0

Appendix 2.2.1, continued.

Sample	SiO_2	Al_2O_3	FeO	MgO	CaO	Na_2O	K_2O	Total	An[a]	Sample	SiO_2	Al_2O_3	FeO	MgO	CaO	Na_2O	K_2O	Total	An[a]
PL18	45.27	34.54	0.34	0.21	18.62	1.06	0.01	100.05	90.7	PL76B-GL	45.22	34.35	0.36	0.21	18.45	1.02	0.00	99.61	90.9
PL20	45.30	34.57	0.30	0.20	18.55	1.02	0.00	99.94	91.0	PL77	45.62	34.01	0.33	0.22	18.20	1.16	0.00	99.54	89.7
PL21	44.79	34.38	0.30	0.18	18.48	1.01	0.01	99.15	91.0	PL78-SP	45.48	34.63	0.32	0.23	18.38	1.01	0.01	100.06	91.0
PL22	45.45	34.71	0.31	0.22	18.48	1.02	0.01	100.20	90.9	PL79	46.10	33.70	0.38	0.28	17.75	1.38	0.03	99.62	87.7
PL23	45.96	34.82	0.27	0.24	18.44	1.03	0.01	100.77	90.8	PL80A-GL	45.90	33.64	0.39	0.22	17.91	1.33	0.02	99.41	88.2
PL24	45.59	34.60	0.32	0.23	18.62	1.06	0.00	100.42	90.7	PL80B-GL	46.31	33.43	0.43	0.23	17.76	1.42	0.02	99.60	87.4
PL25	45.96	33.99	0.38	0.27	18.16	1.18	0.01	99.95	89.5	PL80C-GL	46.40	33.71	0.48	0.23	17.74	1.40	0.01	99.97	87.5
PL26	46.03	34.07	0.37	0.22	18.07	1.19	0.01	99.96	89.4	PL81	45.79	34.43	0.33	0.21	18.54	1.10	0.06	100.46	90.3
PL28	45.85	34.20	0.37	0.24	18.32	1.17	0.00	100.15	89.6	PL82	45.23	34.68	0.32	0.19	18.50	1.04	0.01	99.97	90.8
PL29	45.21	33.92	0.36	0.18	18.48	1.04	0.01	99.20	90.8	PL84	45.30	34.79	0.23	0.17	18.47	1.00	0.01	99.97	91.1
PL30A-GL	45.17	34.10	0.42	0.24	18.62	1.06	0.01	99.62	90.7	PL85	45.35	34.52	0.29	0.19	18.35	1.08	0.01	99.79	90.4
PL30B-GL	45.19	34.21	0.39	0.24	18.46	1.01	0.01	99.51	91.0	PL86	45.31	34.36	0.31	0.19	18.47	1.01	0.01	99.66	91.0
PL31	45.16	34.31	0.30	0.22	18.59	1.10	0.01	99.69	90.3	PL87	46.68	33.96	0.36	0.28	17.87	1.36	0.01	100.52	87.9
PL32	45.06	34.29	0.32	0.23	18.57	1.00	0.00	99.47	91.1	PL88	45.11	33.95	0.33	0.21	18.31	1.08	0.01	99.00	90.4
PL33	44.80	34.47	0.38	0.20	18.61	0.98	0.00	99.44	91.3	PL89	44.70	34.32	0.42	0.22	18.66	0.95	0.00	99.27	91.6
PL52	49.52	31.29	0.34	0.34	15.75	2.43	0.01	99.68	78.2	PL90	45.29	34.41	0.31	0.24	18.39	1.13	0.01	99.78	90.0
PL48	44.98	34.16	0.35	0.21	18.59	1.01	0.01	99.31	91.1	PL91	45.35	34.52	0.25	0.21	18.51	1.00	0.03	99.87	91.1
PL49	45.80	34.68	0.40	0.25	18.51	1.07	0.00	100.71	90.5	PL92	45.44	34.52	0.34	0.33	18.37	1.04	0.01	100.05	90.7
PL50	44.84	34.28	0.38	0.24	18.80	0.94	0.01	99.49	91.7	PL93	45.02	34.10	0.30	0.22	18.33	1.04	0.00	99.01	90.7
PL51	45.71	34.64	0.37	0.21	18.40	1.11	0.01	100.45	90.2	PL94	45.34	34.54	0.30	0.22	18.50	1.02	0.00	99.92	90.9
PL53-SP-GL	45.34	34.52	0.27	0.23	18.41	1.04	0.01	99.82	90.7	PL95	45.06	34.29	0.28	0.21	18.44	1.04	0.01	99.33	90.7
PL54	45.34	33.88	0.32	0.23	18.22	1.17	0.00	99.16	89.6	PL96	46.77	33.24	0.36	0.28	17.62	1.43	0.01	99.71	87.2
PL57	45.04	34.30	0.29	0.22	18.49	1.03	0.00	99.37	90.8	PL97	44.80	34.13	0.34	0.19	18.54	0.99	0.00	98.99	91.2
PL58	45.47	34.73	0.28	0.21	18.47	1.03	0.01	100.20	90.8	PL99	45.15	34.23	0.26	0.21	18.37	1.04	0.01	99.27	90.7
PL59	47.12	32.97	0.35	0.26	17.34	1.67	0.01	99.72	85.2	PL100	45.60	33.99	0.10	0.22	18.34	1.12	0.01	99.38	90.1
PL60	45.79	33.35	0.46	0.26	17.94	1.38	0.02	99.20	87.8	PL101	45.74	33.71	0.39	0.25	17.70	1.34	0.01	99.14	88.0
PL61	45.26	34.69	0.32	0.20	18.39	1.06	0.01	99.93	90.6	PL103-GL	45.62	34.15	0.39	0.23	18.09	1.13	0.01	99.62	89.8
PL62	45.03	34.29	0.34	0.22	18.56	1.02	0.00	99.46	91.0	PL104	45.40	33.98	0.36	0.19	18.17	1.11	0.01	99.22	90.1
PL63-GL	45.43	34.03	0.34	0.23	18.32	1.13	0.00	99.48	90.0	PL104-1	47.08	33.24	0.31	0.32	17.11	1.70	0.01	99.77	84.8
PL65	45.16	34.29	0.30	0.22	18.54	1.10	0.01	99.62	90.3	PL105	45.48	33.90	0.39	0.24	18.05	1.21	0.01	99.28	89.2
PL66A-GL	45.31	34.13	0.34	0.22	18.39	1.06	0.00	99.45	90.6	A11-PL1	44.76	34.06	0.33	0.20	18.41	1.02	0.00	98.78	90.9
PL66B-GL	45.68	34.06	0.40	0.21	18.41	1.10	0.01	99.87	90.2	A11-PL2	44.64	34.07	0.32	0.20	18.38	0.99	0.01	98.61	91.1
PL67	45.21	34.20	0.35	0.28	18.35	1.12	0.01	99.52	90.1	A11-PL3	44.87	33.99	0.26	0.22	18.25	1.06	0.01	98.66	90.5
PL69	45.54	34.28	0.34	0.23	18.34	1.16	0.01	99.90	89.7	A11-PL4	45.26	34.26	0.29	0.21	18.25	1.06	0.01	99.34	90.5
PL70	46.17	33.24	0.41	0.28	17.62	1.46	0.01	99.19	87.0	A11-PL5	45.09	34.32	0.24	0.19	18.40	1.02	0.01	99.27	90.9
PL71	45.46	34.44	0.38	0.21	18.21	1.12	0.01	99.83	90.0	A11-PL6	45.09	34.67	0.27	0.21	18.61	0.97	0.01	99.83	91.4
PL73	45.16	34.67	0.23	0.23	18.54	0.97	0.01	99.81	91.4	A11-PL7	45.47	34.31	0.30	0.21	18.49	1.06	0.00	99.84	90.6
PL74	46.47	33.20	0.36	0.29	17.47	1.56	0.01	99.36	86.1	A11-PL8	45.23	34.42	0.31	0.21	18.45	1.02	0.01	99.65	90.9
PL75	45.41	34.67	0.28	0.22	18.50	1.06	0.01	100.15	90.6	A11-PL9	45.58	34.20	0.34	0.22	17.96	1.10	0.01	99.41	90.0
PL76A-GL	45.59	33.98	0.35	0.22	18.16	1.21	0.03	99.54	89.2	A11-PL10	45.78	33.98	0.36	0.22	18.11	1.21	0.01	99.67	89.2

Appendix 2.2.1, continued.

Sample	SiO_2	Al_2O_3	FeO	MgO	CaO	Na_2O	K_2O	Total	An[a]
A11-PL11	45.16	34.02	0.31	0.23	18.26	1.10	0.01	99.09	90.17
A11-PL12	45.19	34.27	0.32	0.26	18.20	1.07	0.01	99.32	90.38
A11-PL13	45.80	33.70	0.35	0.24	17.75	1.25	0.01	99.10	88.70
A11-PL14	44.96	34.47	0.31	0.18	18.36	1.05	0.01	99.34	90.62
A11-PL15	45.01	34.55	0.30	0.21	18.40	1.06	0.01	99.54	90.56
A11-PL16	45.34	34.36	0.39	0.21	18.36	1.06	0.01	99.73	90.54
A11-PL17	44.97	33.97	0.34	0.23	18.00	1.06	0.01	98.58	90.37
A11-PL20	45.56	34.24	0.34	0.23	18.18	1.12	0.01	99.68	89.97
A11-PL21	45.27	33.83	0.34	0.23	17.85	1.21	0.00	98.73	89.07
A11-PL22	45.02	34.35	0.32	0.20	18.43	0.98	0.01	99.31	91.22
A11-PL23	44.91	34.14	0.29	0.20	18.41	1.01	0.01	98.97	90.97
A11-PL24	44.81	34.37	0.34	0.20	18.25	1.05	0.00	99.02	90.57
A11-PL25	45.27	33.84	0.33	0.22	18.00	1.11	0.01	98.78	89.96
A11-PL26	44.95	33.94	0.29	0.23	18.37	1.02	0.03	98.83	90.87
A11-PL27	45.25	33.80	0.31	0.23	18.07	1.15	0.02	98.83	89.67
A11-PL28	45.05	34.13	0.30	0.21	18.40	1.04	0.00	99.13	90.72
A11-PL52	44.86	34.01	0.31	0.23	18.21	1.04	0.01	98.67	90.63
A11-PL53	44.94	33.95	0.31	0.23	18.46	1.06	0.01	98.96	90.59
A11-PL54	44.61	34.48	0.27	0.21	18.51	0.97	0.02	99.07	91.34
A11-PL55	44.89	34.23	0.32	0.21	18.23	0.99	0.01	98.88	91.05
A11-PL57	44.91	33.98	0.35	0.20	18.22	1.14	0.00	98.80	89.83
A11-PL20-GL	45.41	34.24	0.35	0.23	18.44	1.15	0.01	99.83	89.86
PL21A-GL	45.38	34.27	0.34	0.24	18.43	1.12	0.01	99.79	90.09
PL21B-GL	45.25	34.33	0.38	0.24	18.36	1.12	0.02	99.70	90.06
A11-OL31-PL	45.16	34.27	0.56	0.23	18.48	1.05	0.01	99.76	90.68
A11-PL51-GL	46.46	33.44	0.38	0.26	17.57	1.42	0.01	99.54	87.24
148-896A-27R-1, Piece 15									
A13-PL1	45.11	34.58	0.34	0.21	18.25	1.03	0.01	99.53	90.73
A13-PL2-1	45.14	34.43	0.28	0.21	18.08	1.05	0.00	99.19	90.49
A13-PL2-2	45.30	34.26	0.33	0.22	18.05	1.08	0.00	99.24	90.23
A13-PL4	46.16	33.58	0.42	0.29	17.45	1.40	0.01	99.31	87.32
A13-PL5	45.21	34.46	0.36	0.23	18.03	1.03	0.01	99.33	90.63
A13-PL5-1	46.52	33.58	0.35	0.27	17.18	1.45	0.00	99.35	86.75
A13-PL7	45.17	34.33	0.36	0.21	18.03	1.02	0.01	99.13	90.71
A13-PL9	45.34	33.51	0.56	0.55	18.12	1.04	0.01	99.13	90.59
A13-PL10	44.85	34.77	0.34	0.21	18.48	0.92	0.01	99.58	91.74
A13-PL12	45.72	33.89	0.38	0.22	17.80	1.26	0.00	99.27	88.64
A13-PL13	46.79	33.24	0.40	0.26	17.13	1.58	0.01	99.41	85.70
A13-PL14	46.32	33.62	0.35	0.28	17.59	1.54	0.00	99.70	86.3
A13-PL14-1	45.34	34.30	0.34	0.23	18.31	1.05	0.00	99.57	90.6
A13-PL15	45.55	33.89	0.38	0.26	17.79	1.22	0.01	99.10	89.0
A13-PL16	45.64	34.06	0.44	0.25	17.99	1.18	0.01	99.57	89.4
A13-PL17	46.48	33.77	0.33	0.28	17.55	1.41	0.01	99.83	87.3
A13-PL18	45.33	34.31	0.34	0.23	18.01	1.12	0.01	99.35	89.9
A13-PL19	45.92	34.10	0.37	0.23	17.84	1.31	0.01	99.78	88.3
A13-PL20	45.19	34.35	0.01	0.24	18.05	1.11	0.01	98.96	90.0
A13-PL21	45.25	34.06	0.27	0.23	17.94	1.13	0.00	98.88	89.8
A13-PL22	45.09	34.36	0.34	0.21	18.02	1.04	0.01	99.07	90.5
A13-PL23	44.79	34.53	0.37	0.33	18.23	0.94	0.03	99.22	91.5
A13-PL24	45.80	33.89	0.40	0.22	17.65	1.28	0.00	99.24	88.4
A13-PL25	45.54	34.10	0.38	0.19	18.01	1.16	0.01	99.39	89.6
A13-PL26	44.98	34.55	0.44	0.24	18.32	0.94	0.03	99.50	91.5
A13-PL29	45.13	34.62	0.36	0.20	18.02	1.03	0.01	99.37	90.6
A13-PL30	44.61	34.88	0.29	0.18	18.79	0.90	0.00	99.65	92.0
A13-PL31	44.70	34.97	0.31	0.17	18.83	0.79	0.01	99.78	92.9
A13-PL32	45.06	34.64	0.39	0.19	18.69	0.97	0.01	99.95	91.4
A13-PL33	45.33	34.45	0.34	0.20	18.44	1.09	0.01	99.86	90.3
A13-PL35	45.57	34.03	0.40	0.23	18.14	1.22	0.01	99.60	89.2
A13-PL36	46.88	33.20	0.41	0.29	17.14	1.63	0.00	99.55	85.3
A13-PL37	45.52	34.61	0.35	0.22	18.45	1.09	0.01	100.25	90.3
A13-PL38	45.71	34.48	0.29	0.23	18.37	1.15	0.01	100.24	89.8
A13-PL39	45.31	34.39	0.29	0.23	18.47	1.05	0.01	99.75	90.7
A13-PL40	45.75	34.08	0.36	0.26	17.99	1.22	0.00	99.66	89.1
A13-PL41	46.48	33.66	0.32	0.28	17.74	1.52	0.01	100.01	86.6
A13-PL41-1	45.82	34.06	0.37	0.26	18.27	1.15	0.01	99.94	89.8
A13-PL42	46.38	33.47	0.38	0.27	17.62	1.48	0.01	99.61	86.8
A13-PL42-1	45.62	34.01	0.36	0.24	18.22	1.19	0.00	99.64	89.4
A13-PL43	45.00	34.70	0.29	0.23	18.55	0.99	0.00	99.76	91.2
A13-PL44	45.70	33.95	0.37	0.24	18.02	1.24	0.01	99.53	88.9
A13-PL45	45.30	34.20	0.26	0.23	18.16	1.10	0.01	99.26	90.1
A13-PL46	45.94	34.03	0.37	0.24	17.98	1.23	0.00	99.79	89.0
A13-PL47	46.20	33.84	0.39	0.24	17.75	1.32	0.01	99.75	88.1
A13-PL48	44.75	34.87	0.32	0.19	18.71	0.91	0.01	99.76	91.9
A13-PL49	45.09	34.52	0.33	0.21	18.46	1.00	0.01	99.62	91.1
A13-PL50	45.55	34.32	0.34	0.21	18.20	1.20	0.00	99.82	89.3
A13-PL51	45.44	34.44	0.28	0.23	18.30	1.10	0.01	99.80	90.2
A13-PL52	45.46	34.42	0.34	0.20	18.23	1.07	0.00	99.72	90.4
A13-PL53	46.81	33.33	0.38	0.28	17.38	1.58	0.01	99.77	85.9

Appendix 2.2.1, continued.

Sample	SiO_2	Al_2O_3	FeO	MgO	CaO	Na_2O	K_2O	Total	An[a]
A13-PL54	45.73	34.16	0.33	0.25	18.01	1.17	0.01	99.66	89.5
A13-PL55	45.17	34.68	0.37	0.17	18.34	1.09	0.01	99.83	90.3
A13-PL57	45.05	34.68	0.31	0.20	18.37	1.05	0.01	99.67	90.6
A13-PL58	45.95	34.00	0.34	0.23	17.91	1.22	0.01	99.66	89.0
A13-PL59	45.34	34.48	0.35	0.22	18.19	1.11	0.01	99.70	90.1
A13-PL60	45.97	33.69	0.42	0.28	17.87	1.40	0.01	99.64	87.6
A13-PL61	45.16	34.39	0.43	0.21	18.19	1.09	0.00	99.47	90.2
A13-PL62	45.50	34.45	0.37	0.21	18.09	1.18	0.01	99.81	89.4
A13-PL63	46.13	33.60	0.38	0.24	17.80	1.39	0.01	99.55	87.6
A13-OL65-PL	44.96	34.85	0.49	0.21	18.41	0.97	0.01	99.90	91.3
A13-OL70-PL	45.41	34.52	0.56	0.24	18.30	1.07	0.01	100.11	90.4
A13-PL80	46.05	34.16	0.29	0.26	17.99	1.28	0.01	100.04	88.6
OL88-PLA	46.37	33.52	0.55	0.25	17.52	1.54	0.00	99.75	86.3
OL88-PLB	44.66	34.70	0.57	0.19	18.65	0.86	0.00	99.63	92.3
A13-PL89-SP	45.30	34.32	0.31	0.22	18.30	1.13	0.01	99.59	90.0
A13-PL92	45.44	34.59	0.36	0.23	18.23	1.10	0.01	99.96	90.2
A13-PL93-1	45.39	34.58	0.32	0.23	18.12	1.09	0.01	99.74	90.2
A13-PL94	45.47	34.49	0.40	0.22	18.05	1.11	0.01	99.75	90.0
A13-PL95	45.25	34.17	0.33	0.21	18.06	1.11	0.01	99.14	90.0
A13-PL97	44.57	34.94	0.33	0.18	18.81	0.91	0.01	99.75	92.0
A13-PL98	45.39	34.58	0.36	0.23	18.38	1.15	0.01	100.10	89.8
A13-PL101	45.25	34.15	0.45	0.33	17.87	1.09	0.09	99.23	90.1
A13-PL103	45.19	34.45	0.28	0.23	18.27	1.08	0.01	99.51	90.3
A13-PL105	45.43	34.57	0.36	0.21	18.21	1.07	0.00	99.85	90.4
A13-PL106	46.46	33.78	0.42	0.26	17.74	1.40	0.01	100.07	87.5
A13-PL108	45.61	34.11	0.47	0.33	18.02	1.13	0.05	99.72	89.8
A13-PL109	44.38	34.38	0.32	0.19	18.68	0.92	0.01	98.88	91.8
A13-PL110-1	45.35	34.25	0.35	0.23	18.33	1.14	0.01	99.66	89.9
A13-PL110	45.91	33.70	0.33	0.29	17.42	1.54	0.00	99.19	86.2
A13-PL111	45.80	34.16	0.40	0.23	18.05	1.17	0.01	99.82	89.5
A13-PL112	45.66	34.37	0.36	0.21	18.28	1.18	0.01	100.07	89.5
A13-PL113	45.30	34.57	0.36	0.21	18.30	1.09	0.01	99.84	90.3
A13-PL115	46.14	33.80	0.39	0.24	17.69	1.35	0.00	99.61	87.9
A13-PL116-1	44.52	34.88	0.35	0.20	18.90	0.82	0.01	99.68	92.7
A13-PL116-2	45.55	34.55	0.30	0.24	18.26	1.15	0.00	100.05	89.8
A13-PL117	45.76	34.26	0.27	0.26	18.00	1.20	0.00	99.75	89.2
A13-PL118	45.41	34.53	0.35	0.22	18.30	1.07	0.00	99.88	90.4
A13-PL119	45.45	34.27	0.33	0.23	18.01	1.22	0.01	99.52	89.1
A13-PL120	45.66	34.31	0.38	0.24	17.96	1.20	0.00	99.75	89.2
A13-PL121	45.53	34.57	0.35	0.23	18.23	1.13	0.01	100.05	89.9
A13-PL122	45.94	33.88	0.34	0.27	17.86	1.34	0.01	99.64	88.1
A13-PL123	45.48	34.29	0.30	0.23	18.18	1.15	0.01	99.64	89.7
A13-PL124	45.02	34.44	0.58	0.55	18.19	0.95	0.03	99.76	91.4
A13-PL125	45.38	34.53	0.34	0.21	17.99	1.13	0.01	99.59	89.8
A13-PL126	45.20	34.48	0.37	0.21	18.44	1.02	0.01	99.73	90.9
A13-PL127	45.34	34.39	0.33	0.23	18.30	1.09	0.01	99.69	90.3
A13-PL128	45.83	34.39	0.34	0.23	18.09	1.22	0.00	100.10	89.1
A13-PL129	45.55	34.22	0.33	0.23	18.10	1.16	0.00	99.59	89.6
A13-PL130	45.62	33.99	0.37	0.24	17.77	1.22	0.01	99.22	89.0
A13-PL131	45.75	34.58	0.33	0.22	18.24	1.18	0.00	100.30	89.5
A13-PL133-1	44.81	35.08	0.30	0.20	19.01	0.89	0.00	100.29	92.2
A13-PL134	45.58	34.19	0.36	0.21	18.34	1.11	0.00	99.79	90.1
A13-PL135	45.22	34.44	0.33	0.23	18.69	1.01	0.01	99.93	91.1
A13-PL4-GL	45.64	33.87	0.38	0.24	18.04	1.22	0.01	99.40	89.1
A13-PL13-GL	46.46	33.63	0.42	0.28	17.49	1.42	0.00	99.70	87.2
A13-PL18-GL	45.52	34.23	0.35	0.23	17.92	1.19	0.01	99.45	89.3
A13-PL19-GL	45.66	34.31	0.35	0.26	18.05	1.23	0.00	99.86	89.0
A13-PL53-GL	46.30	33.59	0.40	0.26	17.51	1.48	0.01	99.55	86.7
PL111-GL	45.79	34.03	0.47	0.27	18.23	1.17	0.01	99.97	89.6
PL115-GL	45.44	33.87	0.41	0.22	17.83	1.22	0.00	98.99	89.0
PL116-GL	44.67	35.08	0.36	0.20	18.79	0.79	0.00	99.89	92.9
PL134-GL	45.56	33.52	0.57	0.45	17.76	1.27	0.06	99.19	88.5
PL133B-SP	45.19	34.29	0.34	0.23	18.20	1.17	0.01	99.43	89.6
PL133A-SP	45.44	34.41	0.48	0.22	18.26	1.12	0.01	99.94	90.0
PL107-SP	45.10	34.55	0.37	0.24	18.44	1.06	0.01	99.77	90.6
PL100-SP	45.23	34.48	0.33	0.23	18.19	1.04	0.04	99.54	90.6
A13-PL93-SP	47.31	32.56	0.53	0.40	16.43	1.80	0.04	99.07	83.5
A13-PL91-SP	45.45	34.41	0.31	0.23	17.95	1.10	0.01	99.46	90.0
A13-PL90-SP	45.42	34.33	0.41	0.24	18.16	1.15	0.01	99.72	89.7
A12-PL3-SP	45.68	34.95	0.36	0.22	18.30	1.07	0.01	100.59	90.4
A12-PL4-SP	45.85	34.72	0.33	0.23	18.14	1.15	0.00	100.42	89.7
A12-PL5-SP	46.37	35.06	0.39	0.25	17.88	1.21	0.01	101.17	89.1
A12-PL9A-SP	46.07	34.40	0.34	0.23	17.89	1.17	0.01	100.11	89.4
PL9B-SPA	45.96	34.28	0.38	0.28	18.06	1.11	0.01	100.08	90.0
PL9B-SPB	45.96	34.28	0.38	0.28	18.06	1.11	0.01	100.08	90.0
A3-OL41-PL1	45.11	34.59	0.72	0.23	18.30	1.02	0.01	99.98	90.8
A3-OL41-PL2	45.19	34.33	0.78	0.23	18.54	0.96	0.01	100.04	91.4
A3-OL41-PL5	46.05	33.82	0.63	0.25	17.85	1.33	0.00	99.93	88.1

Appendix 2.2.1, continued.

Sample	SiO_2	Al_2O_3	FeO	MgO	CaO	Na_2O	K_2O	Total	An[a]	Sample	SiO_2	Al_2O_3	FeO	MgO	CaO	Na_2O	K_2O	Total	An[a]
A3-OL41-PL6	45.92	34.22	0.60	0.27	18.18	1.12	0.01	100.32	90.0	T1-PL2-SP	45.14	34.10	0.34	0.25	17.83	1.09	0.01	98.76	90.0
T-PL1-SP	46.46	34.66	0.53	0.30	18.06	1.19	0.01	101.21	89.4	T1-PL3-SP	45.12	33.93	0.37	0.23	17.76	1.12	0.01	98.54	89.8
T-PL2-SP1	45.77	34.43	0.41	0.24	18.45	1.11	0.01	100.42	90.2	T1-PL4-SP	44.55	34.05	0.37	0.23	18.12	1.13	0.01	98.46	89.9
T-PL2-SP2	45.70	34.14	0.46	0.27	18.31	1.07	0.01	99.96	90.4	T1-PL5-SP	45.95	34.31	0.45	0.42	17.76	1.25	0.00	100.14	88.7
T-PL3-SP	45.77	34.80	0.43	0.22	18.38	1.05	0.01	100.66	90.6	T1-PL6-SP1	44.48	33.89	0.41	0.23	17.93	1.10	0.00	98.04	90.0
T1-PL1-SP	45.28	34.69	0.39	0.20	18.13	1.08	0.00	99.77	90.3	T1-PL6-SP2	45.17	34.28	0.37	0.24	18.19	1.12	0.01	99.38	90.0

[a]An= 100 x (Ca/(Ca +Na)).

Appendix 2.2.2, Olivine analyses.

Sample	SiO_2	FeO	MnO	MgO	CaO	Cr_2O_3	NiO	Total	Fo[a]
148-896A-3R-1, Piece 4									
OL1	39.78	11.24	0.18	47.60	0.32	0.06	0.28	99.46	88.3
OL2	39.91	10.89	0.25	47.70	0.35	0.06	0.25	99.41	88.7
OL3	39.86	10.80	0.19	47.76	0.34	0.06	0.27	99.28	88.7
A14-OL10-GL	40.52	10.63	0.20	47.80	0.30	0.04	0.28	99.77	88.9
A14-OL11	40.04	10.69	0.11	47.65	0.32	0.04	0.26	99.11	88.8
A14-OL12	40.19	10.69	0.11	47.72	0.33	0.06	0.24	99.34	88.8
A14-OL14	40.05	10.76	0.14	47.68	0.32	0.04	0.23	99.22	88.8
A14-OL15	40.07	10.59	0.08	48.00	0.29	0.07	0.24	99.34	89.0
A14-OL16	39.95	11.04	0.15	47.64	0.34	0.07	0.23	99.42	88.5
A14-OL18	39.97	10.81	0.16	47.65	0.32	0.09	0.22	99.22	88.7
A14-OL19	40.26	10.79	0.15	47.69	0.30	0.03	0.24	99.46	88.7
A14-OL26	39.54	10.84	0.13	47.13	0.33	0.07	0.19	98.23	88.6
148-896A-4R-1, Piece 2									
OL1	39.87	10.87	0.20	47.92	0.33	0.06	0.26	99.51	88.7
OL2	40.22	11.10	0.19	47.80	0.37	0.06	0.28	100.02	88.5
148-896A-9R-1, Piece 24									
OL2	39.37	11.49	0.24	46.76	0.39	0.06	0.24	98.55	87.9
OL5	39.60	11.56	0.29	46.84	0.34	0.05	0.21	98.89	87.8
OL1	39.46	12.21	0.24	46.39	0.32	0.04	0.20	98.86	87.1
OL2	39.72	11.54	0.25	46.80	0.34	0.07	0.20	98.92	87.9
OL3	39.98	11.48	0.23	47.14	0.34	0.05	0.23	99.45	88.0
OL4	40.17	11.52	0.24	46.98	0.38	0.06	0.25	99.60	87.9
A9-OL1	40.01	12.14	0.13	47.33	0.34	0.08	0.19	100.22	87.4
A9-OL2	40.11	11.86	0.12	47.79	0.32	0.04	0.23	100.47	87.8
A9-OL3	40.18	11.07	0.15	48.48	0.32	0.06	0.29	100.55	88.7
A9-OL6-SP	40.28	10.59	0.21	48.60	0.32	0.03	0.27	100.30	89.1
A9-OL11-SP	40.12	10.82	0.09	48.52	0.32	0.10	0.27	100.24	88.9
A9-OL13	40.07	10.79	0.15	48.40	0.31	0.08	0.33	100.13	88.9
A9-OL15	39.91	11.15	0.18	48.38	0.33	0.05	0.22	100.22	88.6
A9-OL17	39.63	11.46	0.14	45.97	0.40	0.03	0.27	97.90	87.7
A9-OL20	39.90	11.87	0.16	47.49	0.30	0.08	0.26	100.06	87.7
A9-OL24	39.65	13.48	0.17	45.96	0.33	0.03	0.26	99.88	85.9
A9-OL34	39.67	13.65	0.22	46.06	0.30	0.03	0.21	100.14	85.8
A9-OL40-GL	39.99	11.68	0.17	47.55	0.33	0.07	0.22	100.01	87.9
A9-OL41	40.25	12.07	0.21	47.27	0.46	0.02	0.12	100.40	87.5
A9-OL42	39.63	14.04	0.23	45.64	0.30	0.04	0.23	100.11	85.3
A9-OL43	39.73	13.90	0.26	45.97	0.30	0.04	0.20	100.40	85.5
A9-OL46	40.19	11.27	0.06	48.16	0.34	0.06	0.25	100.33	88.4
A9-OL49	40.10	10.63	0.18	48.76	0.30	0.06	0.33	100.36	89.1
A9-OL50	40.03	11.15	0.06	47.88	0.33	0.07	0.29	99.81	88.5
A9-OL51	39.51	13.97	0.13	45.85	0.30	0.04	0.24	100.04	85.4
A9-OL1	40.17	10.94	0.12	47.70	0.33	0.04	0.26	99.56	88.6
A9-OL9	39.80	12.13	0.18	46.33	0.30	0.03	0.14	98.91	87.2
148-896A-25R-1, Piece 11									
OL12	39.29	12.73		44.97	0.30			97.29	86.3
OL131	39.28	13.78		44.57	0.34			97.97	85.2
I2-OL19-GLA	39.70	13.82		44.80	0.40			98.72	85.3
A8-OL2	39.10	16.76	0.25	43.24	0.34	0.03	0.14	99.86	82.1
A8-OL3	38.77	17.97	0.30	41.94	0.23	0.03	0.17	99.41	80.6
A8-OL4	40.27	12.71	0.18	46.83	0.34	0.03	0.21	100.57	86.8
A8-OL5	40.40	10.13	0.16	48.58	0.34	0.04	0.21	99.86	89.5
A8-OL8	40.71	8.25	0.15	50.16	0.32	0.06	0.26	99.91	91.6
A3-OL1	40.40	11.34	0.13	47.89	0.31	0.10	0.29	100.46	88.3
A3-OL2	39.71	11.36	0.10	47.49	0.36	0.07	0.26	99.35	88.2
A3-OL3	39.73	11.34	0.21	47.38	0.38	0.06	0.22	99.32	88.2
A3-OL4	40.12	11.26	0.13	47.94	0.36	0.06	0.23	100.10	88.4
A3-OL5	39.33	11.18	0.14	46.36	0.36	0.08	0.24	97.69	88.1
T-OL1-SP	40.11	11.04	0.21	47.36	0.32	0.18	0.23	99.45	88.4
T-OL2	40.07	11.37	0.22	47.02	0.33	0.07	0.22	99.30	88.1
T-OL3	39.89	11.49	0.21	47.12	0.29	0.12	0.24	99.36	88.0
148-896A-25R-2, Piece 11									
OL82-SP1	40.04	12.12	0.15	46.84	0.55	0.36	0.20	100.26	87.3
OL82-SP2	39.98	12.09	0.21	46.68	0.52	0.13	0.17	99.78	87.3
OL41	40.20	11.98	0.24	47.09	0.35	0.06	0.21	100.13	87.5
A3-OL1	39.84	11.30	0.17	47.54	0.39	0.09	0.25	99.58	88.2

Appendix 2.2.2, continued

Sample	SiO_2	FeO	MnO	MgO	CaO	Cr_2O_3	NiO	Total	Fo[a]
148-896A-25R-2, Piece 11									
A3-OL2	39.25	11.69	0.20	45.49	0.47	0.04	0.17	97.31	87.4
A3-OL3	40.17	11.65	0.19	47.32	0.30	0.06	0.22	99.91	87.9
A3-OL4	39.81	10.97	0.16	47.75	0.35	0.08	0.29	99.41	88.6
A3-OL5	39.79	11.58	0.17	46.90	0.38	0.09	0.25	99.16	87.8
A3-OL6	39.76	11.62	0.20	47.56	0.42	0.08	0.24	99.88	88.0
A3-OL7	40.19	11.49	0.21	47.21	0.45	0.03	0.24	99.82	88.0
A3-OL8	40.05	11.39	0.15	47.67	0.34	0.07	0.22	99.89	88.2
148-896A-27R-1, Piece 13									
OL11	40.29	11.60	0.12	47.07	0.35	0.11	0.24	99.78	87.9
OL34	40.19	11.21	0.14	47.65	0.33	0.05	0.28	99.85	88.3
OL35	40.19	11.10	0.16	47.41	0.35	0.04	0.26	99.51	88.4
OL36-GL	39.98	11.39	0.16	47.32	0.34	0.04	0.27	99.50	88.1
OL37	40.50	11.21	0.14	47.52	0.33	0.06	0.24	100.00	88.3
OL38	40.54	11.02	0.15	47.58	0.33	0.08	0.26	99.96	88.5
OL39	40.76	11.02	0.18	47.80	0.33	0.07	0.23	100.39	88.6
OL40-GL	40.45	10.96	0.10	47.68	0.32	0.06	0.26	99.83	88.6
OL41	40.19	11.20	0.16	47.44	0.32	0.04	0.24	99.59	88.3
OL42	40.01	10.98	0.15	47.47	0.32	0.07	0.24	99.24	88.5
OL43	40.51	11.21	0.21	47.65	0.36	0.06	0.23	100.23	88.3
OL46	40.22	11.10	0.21	47.51	0.34	0.04	0.28	99.70	88.4
OL47	40.65	11.02	0.15	47.76	0.35	0.06	0.28	100.27	88.5
OL98	40.50	11.37	0.11	47.46	0.32	0.04	0.26	100.06	88.2
A11-OL31-PL	39.79	11.32	0.13	47.39	0.32	0.06	0.26	99.27	88.2
148-896A-27R-1, Piece 15									
A13-OL3	40.03	11.21	0.17	47.59	0.31	0.07	0.27	99.65	88.3
A13-OL5	40.09	11.17	0.17	47.65	0.30	0.03	0.28	99.69	88.4
A13-OL11	40.04	11.34	0.15	47.39	0.35	0.07	0.26	99.60	88.2
A13-OL27	39.99	11.40	0.17	47.53	0.33	0.05	0.23	99.70	88.1
A13-OL64	39.93	11.46	0.12	47.25	0.33	0.07	0.27	99.43	88.0
A13-OL65-PL	40.14	11.00	0.17	47.60	0.31	0.07	0.24	99.53	88.5
A13-OL66	39.98	11.20	0.12	47.41	0.31	0.04	0.23	99.29	88.3
A13-OL68	40.24	10.63	0.20	48.27	0.32	0.04	0.27	99.97	89.0
A13-OL70-PL	40.18	10.73	0.12	47.84	0.33	0.06	0.27	99.53	88.8
A13-OL74	40.10	11.31	0.17	47.57	0.32	0.10	0.25	99.82	88.2
A13-OL75	40.10	11.34	0.14	47.25	0.33	0.03	0.26	99.45	88.1
A13-OL76	39.99	11.64	0.11	47.09	0.32	0.06	0.26	99.47	87.8
A13-OL77	39.20	15.79	0.28	43.71	0.41	0.04	0.16	99.59	83.2
A13-OL78	40.20	10.94	0.14	47.62	0.31	0.07	0.24	99.52	88.6
A13-OL84	40.20	10.97	0.15	47.55	0.32	0.07	0.28	99.54	88.5
A13-OL85	40.10	11.23	0.17	47.32	0.33	0.04	0.24	99.43	88.3
A13-OL81	40.21	10.50	0.13	48.14	0.32	0.06	0.29	99.65	89.1
A13-OL88-PLA	40.23	11.15	0.12	47.55	0.33	0.06	0.26	99.70	88.4
A13-OL88-PLB	40.23	11.15	0.12	47.55	0.33	0.06	0.26	99.70	88.4
A13-OL96	40.35	10.48	0.12	48.32	0.33	0.03	0.27	99.90	89.2
A13-OL99	40.28	10.90	0.20	47.75	0.32	0.03	0.28	99.76	88.7
A13-OL114	40.24	11.01	0.19	47.75	0.33	0.08	0.23	99.83	88.6
A13-OL141-GL	40.15	11.76	0.19	47.31	0.36	0.06	0.17	100.00	87.8
A13-OL88-GL	40.42	11.31	0.16	47.80	0.35	0.08	0.24	100.36	88.3
A13-OL74-GL	40.16	11.18	0.18	47.34	0.34	0.04	0.22	99.46	88.3
A13-OL66-GL	39.95	11.38	0.15	47.73	0.34	0.06	0.26	99.87	88.2
A13-OL64-GL	40.15	11.46	0.14	47.65	0.38	0.05	0.23	100.06	88.1
A12-OL10-1	40.41	11.39	0.19	47.80	0.34	0.03	0.30	100.46	88.2
A12-OL10-2	40.35	11.41	0.21	47.71	0.33	0.06	0.27	100.34	88.2
A12-OL10-3	40.30	10.88	0.14	48.30	0.33	0.08	0.27	100.30	88.8
A12-OL6-1	40.09	11.71	0.20	47.28	0.35	0.10	0.23	99.96	87.8
A12-OL6-2	40.55	11.03	0.10	48.41	0.32	0.05	0.27	100.73	88.7
A12-OL7-1	40.20	11.56	0.07	47.50	0.32	0.07	0.24	99.96	88.0
A12-OL7-2	40.45	11.57	0.12	47.59	0.34	0.07	0.23	100.37	88.0
A12-OL8	40.10	11.06	0.15	47.93	0.32	0.06	0.24	99.86	88.5
A12-OL7-3	40.12	11.92	0.19	46.86	0.34	0.09	0.19	99.71	87.5
A3-OL41-PL1	40.14	11.31	0.11	47.05	0.48	0.06	0.28	99.43	88.1
A3-OL41-PL2	40.17	11.55	0.20	47.73	0.35	0.04	0.26	100.30	88.1
A3-OL41-GL3	40.04	11.60	0.16	47.58	0.32	0.07	0.20	99.97	88.0
A3-OL41-GL4	39.81	11.88	0.17	47.22	0.34	0.05	0.23	99.70	87.6
A3-OL41-PL5	40.02	11.46	0.15	47.58	0.35	0.07	0.26	99.89	88.1

Apppendix 2.2.2, continued.

Sample	SiO_2	FeO	MnO	MgO	CaO	Cr_2O_3	NiO	Total	Fo[a]
148-896A-27R-1, Piece 15									
A3-OL41-PL6	40.12	11.48	0.17	47.33	0.41	0.06	0.25	99.82	88.0
A3-OL1	39.29	11.56	0.15	46.64	0.41	0.08	0.23	98.36	87.8
A3-OL2	40.09	11.69	0.26	47.36	0.35	0.06	0.20	100.01	87.8
A3-OL3	39.90	11.38	0.07	47.46	0.35	0.07	0.23	99.46	88.2
A3-OL4	39.66	11.29	0.12	47.22	0.34	0.05	0.26	98.94	88.2
A3-OL41-GL1	40.14	11.31	0.11	47.05	0.48	0.06	0.28	99.43	88.1
A3-OL41-GL2	40.17	11.55	0.20	47.73	0.35	0.04	0.26	100.30	88.1
A3-OL41-GL5	40.02	11.46	0.15	47.58	0.35	0.07	0.26	99.89	88.1
A3-OL41-GL6	40.12	11.48	0.17	47.33	0.41	0.06	0.25	99.82	88.0
T1-OL7-1	40.18	10.71	0.15	47.27	0.34	0.07	0.28	99.00	88.7
T1-OL7-2	39.99	10.96	0.13	46.85	0.34	0.05	0.28	98.60	88.4

[a]Forsterite content, Fo = 100 x (Mg/(Mg + Fe)).

Appendix 2.2.3, Spinel analyses.

Sample	SiO_2	TiO_2	Al_2O_3	[a]Fe_2O_3	FeO	MnO	MgO	Cr_2O_3	NiO	ZnO	Total
148-896A-3R-1, Piece 4											
PL42-SPA	0.06	0.44	24.72	6.25	11.82	0.23	15.91	41.33	0.22	0.09	101.07
PL42-SPB	0.07	0.44	24.84	5.81	12.26	0.21	15.84	41.96	0.09	0.13	101.65
PL61-SP	0.05	0.35	30.69	7.18	11.14	0.23	17.07	34.88	0.28	0.02	101.89
A14-SP14	0.10	0.33	25.67	6.22	12.4	0.14	15.55	39.86	0.14	0.19	100.60
A14-PL13-SP	0.10	0.36	30.76	6.08	11.38	0.19	16.64	34.2	0.18	0.07	99.96
A14-OL2-SP	0.11	0.21	37.96	5.52	10.28	0.11	18.17	27.74	0.15	0.07	100.32
A14-SP3	0.12	0.30	30.5	6.27	11.45	0.03	16.46	33.74	0.21	0.07	99.15
A14-SP5	0.11	0.25	38.26	5.95	10.54	0.15	18.08	26.98	0.18	0.01	100.51
A14-SP6	0.10	0.35	27.25	5.92	12.24	0.13	15.82	38.17	0.14	0.08	100.20
A14-SP8-1	0.08	0.27	32.09	5.77	11.42	0.12	16.76	33.38	0.18	0.08	100.15
A14-SP8-2	0.08	0.32	32.01	5.82	11.16	0.14	16.85	33.16	0.19	0.11	99.84
T-PL1-SP	0.10	0.34	29.81	5.78	11.62	0.13	16.03	34.04	0.14	0.10	98.09
T-PL2-SP4	0.07	0.38	25.94	5.76	12.08	0.18	15.89	40.5	0.15	0.15	101.11
T-PL2-SP3	0.08	0.44	25.00	5.63	12.08	0.19	15.52	40.11	0.14	0.02	99.20
T-PL2-SP2	0.09	0.44	26.23	5.98	11.83	0.14	16.21	40.02	0.11	0.14	101.19
T-PL2-SP1	0.10	0.36	24.24	5.65	12.18	0.11	15.35	40.98	0.17	0.07	99.21
T-PL3-SP	0.06	0.29	27.38	6.12	11.72	0.13	15.96	37.92	0.12	0.25	99.94
T-PL4-SPa	0.14	0.38	28.22	5.54	12.24	0.12	16.04	37.58	0.15	0.07	100.47
T-PL4-SPb	0.08	0.34	29.83	6.07	11.8	0.12	16.25	35.29	0.22	0.15	100.15
T-PL4-SPc	0.06	0.32	29.77	5.64	11.83	0.15	16.01	34.85	0.19	0.01	98.83
148-896A-4R-1, Piece 2											
SP100	0.39	0.32	27.18	4.83	13.22	0.15	15.16	37.52	0.18	0.00	98.95
PL100-SP	0.06	0.43	23.33	5.83	12.36	0.17	15.14	42.10	0.18	0.21	99.81
PL64-SP	0.05	0.29	25.84	5.52	11.87	0.18	15.82	40.32	0.13	0.02	100.03
SP78	0.11	0.23	37.74	5.92	10.65	0.11	17.88	27.29	0.19	0.02	100.13
T-PL2-SP2	0.07	0.47	26.04	6.86	14.87	0.18	14.30	38.73	0.21	0.01	101.75
T-PL2-SP1	0.08	0.45	25.6	6.77	14.93	0.16	13.91	38.32	0.24	0.09	100.55
T-PL3-SP1	0.06	0.37	24.25	5.46	12.66	0.17	15.22	42.11	0.14	0.18	100.63
T-SP3	0.08	0.34	25.62	5.93	13.06	0.07	15.26	40.00	0.09	0.01	100.46
T-PL3-SP3a	0.09	0.33	30.11	6.02	12.51	0.18	16.05	35.55	0.17	0.08	101.09
T-PL3-SP3b	0.06	0.35	27.57	6.00	13.21	0.10	15.42	38.11	0.12	0.00	100.94
T-PL3-SP3c	0.04	0.32	25.34	5.67	13.17	0.15	15.03	40.58	0.03	0.14	100.47
T-PL4-SP1	0.16	0.36	32.64	6.10	12.11	0.15	16.68	32.99	0.24	0.16	101.59
T-SP4	0.10	0.31	25.25	6.26	12.62	0.17	15.11	39.34	0.20	0.09	99.45
T-PL4-SP3	0.11	0.33	27.95	6.46	12.32	0.10	15.91	37.16	0.12	0.14	100.6
T-PL5-SP1	0.11	0.26	36.46	6.05	11.00	0.14	17.54	28.48	0.19	0.02	100.25
T-PL5-SP2	0.13	0.19	37.22	6.00	10.51	0.05	18.00	28.31	0.24	0.09	100.74
T-PL5-SP3	0.09	0.24	38.60	5.65	10.50	0.13	18.19	27.42	0.22	0.09	101.14
148-896A-9R-1, Piece 24											
SP2	0.14	0.36	22.78	6.04	12.68	0.12	15.05	42.47	0.15	0.06	99.85
SP5-A	0.12	0.27	36.76	6.81	11.14	0.00	17.5	27.42	0.27	0.12	100.41
SP5-D	0.28	0.42	26.58	6.61	12.99	0.14	15.05	35.98	0.12	0.07	98.24
A9-OL6-SP	0.11	0.21	39.73	5.42	10.12	0.14	18.74	27.18	0.23	0.04	101.91
A9-OL11-SP	0.10	0.21	39.12	5.88	10.09	0.12	18.7	27.51	0.23	0.08	102.04
SP5-B	0.15	0.32	34.18	7.26	11.46	0.14	17.15	30.2	0.29	0.12	101.28

Appendix 2.2.3, continued.

Sample	SiO_2	TiO_2	Al_2O_3	$^aFe_2O_3$	FeO	MnO	MgO	Cr_2O_3	NiO	ZnO	Total
148-896A-9R-1, Piece 24											
SP5-C	0.14	0.39	31.67	7.65	12.11	0.12	16.45	31.9	0.28	0.06	100.77
A9-SP12	0.10	0.30	31.65	6.33	12.21	0.14	16.48	33.9	0.17	0.07	101.34
A9-PL16-SP	0.14	0.54	23.48	7.94	15.23	0.18	13.88	39.96	0.14	0.03	101.52
A9-PL19-SP	0.04	0.39	24.00	5.99	12.55	0.15	15.54	42.72	0.16	0.05	101.59
A9-SP21	0.08	0.21	35.51	5.29	10.85	0.17	17.77	31.64	0.16	0.08	101.76
A9-PL53-SP	0.06	0.40	24.51	5.98	12.35	0.19	15.69	41.98	0.12	0.04	101.32
A9-CP25-SP2	0.13	7.07	6.31	50.47	30.09	0.60	5.45	0.66	0.08	0.00	100.87
A9-CP25-SP1	0.14	5.88	5.29	52.79	28.73	0.78	5.11	0.85	0.06	0.12	99.75
148-896A-25R-1, Piece 11											
SP44	0.12	0.36	32.43	7.06	11.48	0.16	16.66	30.96	0.21	0.06	99.50
SP57-GL	0.16	0.57	24.96	6.57	12.42	0.15	15.49	38.8	0.08	0.03	99.23
SP88-A	0.10	0.43	23.25	6.26	11.75	0.08	15.81	42.62	0.21	0.16	100.68
SP88-B	0.11	0.36	31.7	6.27	10.91	0.05	17.35	33.95	0.17	0.08	100.95
A8-PL1-SP	0.07	0.70	22.19	8.28	14.88	0.18	13.69	39.85	0.13	0.04	100.01
T-OL1-SP	0.07	0.58	24.83	6.00	12.53	0.16	15.48	40.4	0.20	0.03	100.27
A3-SP1	0.08	0.32	36.03	5.29	10.94	0.11	17.64	30.03	0.21	0.04	100.68
A3-SP2	0.08	0.3	37.58	5.59	10.57	0.13	18.02	28.3	0.20	0.10	100.87
T-PL1-SP	0.07	0.48	21.35	7.49	14.56	0.16	13.46	41.13	0.16	0.02	98.88
T-PL2-SP	0.09	0.35	24.68	5.88	11.92	0.16	15.6	40.56	0.11	0.06	99.41
148-896A-25R-2, Piece 11											
OL82-SP1	0.03	0.84	14.35	14.08	18.99	0.19	9.99	40.55	0.11	0.12	99.25
OL82-SP2	0.07	0.84	14.91	13.5	18.36	0.29	10.23	39.92	0.14	0.12	98.37
SP83	0.09	0.34	34.19	6.52	10.97	0.16	17.23	30.62	0.24	0.28	100.64
148-896A-27R-1, Piece 13											
PL53-SP-GL	0.04	0.27	31.43	5.83	10.61	0.20	17.30	34.92	0.15	0.07	100.81
PL78-SP	0.08	0.20	35.51	5.76	10.8	0.20	17.65	30.7	0.18	0.04	101.13
148-896A-27R-1, Piece 15											
A13-PL133-SP	0.11	0.17	35.83	5.42	10.14	0.09	17.93	29.97	0.17	0.07	99.90
A13-PL133-SP	0.09	0.21	35.64	5.37	9.96	0.11	17.98	30.27	0.19	0.14	99.96
A13-PL107-SP	0.1o	0.20	35.49	5.9	10.87	0.18	17.54	30.20	0.19	0.04	100.71
13-SP118-GLA	0.09	0.29	30.00	6.45	11.79	0.15	16.4	35.15	0.19	0.04	100.55
13-SP118-GLB	0.09	0.29	30.00	6.47	11.77	0.15	16.4	35.15	0.18	0.08	100.58
A13-PL100-SP	0.18	0.22	35.17	5.23	10.25	0.1	17.78	30.26	0.21	0.02	99.42
A13-SP94	0.09	0.20	35.9	5.28	10.55	0.08	17.65	29.93	0.23	0.09	100.00
A13-PL93-SP	0.07	0.20	34.85	5.64	11.02	0.14	17.08	30.09	0.19	0.06	99.35
A13-PL91-SP	0.08	0.17	35.29	5.32	10.7	0.09	17.42	30.16	0.17	0.01	99.40
A13-PL90-SP	0.09	0.19	35.62	5.38	10.28	0.11	17.84	30.29	0.17	0.05	100.02
A13-PL89-SP	0.05	0.16	39.33	5.53	10.31	0.17	18.08	26.03	0.20	0.01	99.86
A12-SP1	0.08	0.28	23.03	5.87	12.8	0.20	15.07	43.32	0.15	0.03	100.83
A12-SP2	0.08	0.22	35.79	5.61	11.12	0.18	17.70	31.17	0.15	0.07	102.09
A12-PL3-SP	0.06	0.15	38.52	5.51	10.25	0.14	18.47	28.76	0.27	0.06	102.19
A12-PL4-SP	0.09	0.19	35.82	5.45	10.3	0.11	18.05	30.83	0.19	0.06	101.10
A12-PL5-SP	0.07	0.18	35.85	5.55	10.28	0.12	18.21	31.44	0.20	0.06	101.97
A12-PL9A-SP	0.09	0.18	36.2	5.58	10.08	0.12	18.35	30.99	0.22	0.09	101.9
A12-PL9B-SPA	0.08	0.19	35.95	5.29	10.27	0.09	18.07	30.93	0.20	0.12	101.19
A12-PL9B-SPB	0.10	0.17	35.65	5.83	11.16	0.11	17.57	30.65	0.17	0.03	101.43
T-PL1-SP	0.09	0.20	35.67	5.01	10.65	0.06	17.92	31.59	0.20	0.05	101.44
T-PL2-SP1	0.07	0.20	35.71	5.18	10.66	0.12	17.83	31.43	0.23	0.10	101.53
T-PL2-SP2	0.07	0.19	35.57	5.34	11.00	0.15	17.50	31.13	0.22	0.15	101.33
T-PL3-SP	0.06	0.18	35.62	5.34	11.13	0.11	17.52	31.29	0.23	0.08	101.56
T1-PL1-SP	0.05	0.29	26.96	5.92	13.98	0.18	14.24	36.98	0.16	0.09	98.85
T1-PL2-SP	0.06	0.19	35.4	4.96	10.33	0.12	17.47	29.88	0.16	0.05	98.62
T1-SP2	0.10	0.23	34.65	5.71	11.52	0.06	16.70	29.41	0.14	0.06	98.58
T1-PL3-SP	0.07	0.21	35.67	4.75	10.49	0.09	17.50	29.96	0.15	0.07	98.96
T1-PL4-SP	0.08	0.20	36.06	4.88	11.12	0.15	17.19	29.61	0.17	0.09	99.55
T1-PL5-SP	0.09	0.20	36.17	4.95	10.39	0.12	17.85	30.16	0.19	0.04	100.16
T1-PL6-SP1	0.06	0.18	35.93	4.80	10.48	0.11	17.63	30.19	0.18	0.03	99.59
T1-PL6-SP2	0.07	0.20	35.79	4.84	10.73	0.12	17.34	29.84	0.22	0.06	99.22
T1-SP7	0.08	0.07	28.69	4.44	12.18	0.15	15.80	38.54	0.18	0.09	100.21

[a]Fe_2O_3 calculated from stoichiometry.

Appendix 2.2.4, Clinopyroxene analyses.

Sample	SiO_2	TiO_2	Al_2O_3	[a]FeO	MnO	MgO	CaO	Na_2O	Cr_2O_3	Total
148-896A-3R-1, Piece 4										
A14-CP23	47.27	1.17	7.57	8.37	0.04	12.88	21.94	0.32	0.08	99.64
A14-CP24-PL1	46.04	1.42	8.64	8.98	0.16	12.22	21.68	0.37	0.04	99.55
A14-CP24-PL2	46.04	1.42	8.64	8.98	0.16	12.22	21.68	0.37	0.04	99.55
148-896A-9R-1, Piece 24										
A9-CP22	53.03	0.17	2.25	4.72	0.14	17.38	21.74	0.16	0.53	100.12
A9-CP23	50.70	0.57	4.40	6.49	0.10	15.32	22.19	0.25	0.35	100.37
A9-CP25-SP2	51.24	0.47	3.48	6.55	0.29	15.57	21.27	0.29	0.39	99.55
A9-CP25-SP1	51.24	0.47	3.48	6.55	0.29	15.57	21.27	0.29	0.39	99.55
A9-CP26	50.49	0.60	4.74	6.40	0.18	15.18	21.98	0.18	0.21	99.96
A9-CP27	51.73	0.35	3.13	5.09	0.12	15.97	22.68	0.15	0.55	99.77
A9-CP28	49.94	0.65	4.84	6.45	0.19	14.90	21.94	0.21	0.18	99.3
A9-CP29	49.81	0.72	5.03	7.16	0.11	14.54	21.62	0.23	0.22	99.44
A9-CP30	53.97	0.17	1.51	3.19	0.08	17.77	22.89	0.11	0.42	100.11
A9-CP31	52.42	0.21	2.68	5.12	0.20	16.64	21.89	0.15	0.20	99.51
A9-CP32	53.09	0.28	2.64	5.25	0.12	16.63	21.98	0.19	0.45	100.63
A9-CP33	53.36	0.24	2.25	4.05	0.15	16.78	22.70	0.15	0.62	100.3
A9-CP35	50.63	0.54	4.14	6.31	0.07	15.04	22.27	0.21	0.34	99.55
A9-CP36	54.34	0.12	1.03	3.28	0.15	18.04	22.92	0.12	0.56	100.56
A9-CP37	53.05	0.23	1.95	3.89	0.11	17.34	22.71	0.15	0.52	99.95
A9-CP38	50.17	0.62	4.80	7.05	0.07	14.69	21.49	0.28	0.57	99.74
A9-CP39	54.22	0.12	1.21	3.23	0.04	17.90	22.81	0.14	0.59	100.26
A9-CP44	51.11	0.56	4.24	5.37	0.17	15.59	22.54	0.17	0.47	100.22
A9-CP45	50.49	0.48	4.26	5.56	0.14	15.31	22.22	0.17	0.60	99.23
A9-CP47	50.63	0.59	4.92	7.04	0.14	14.91	21.59	0.22	0.15	100.19
A9-CP48	51.35	0.51	4.35	6.05	0.07	15.31	22.21	0.21	0.35	100.41
148-896A-25R-1, Piece 11										
A8-CP9	52.66	0.13	4.29	4.36	0.13	18.55	19.84	0.21	0.48	100.65
A8-CP10	52.43	0.30	2.62	6.87	0.17	16.68	20.42	0.23	0.24	99.96
A8-CP7	48.73	0.90	5.48	9.11	0.24	13.63	21.45	0.28	0.02	99.84
A8-CP6	51.27	0.74	2.88	9.31	0.38	15.54	19.48	0.26	0.02	99.88
148-896A-27R-1, Piece 15										
A13-CP67	51.63	0.30	3.16	4.56	0.08	16.39	22.45	0.17	0.86	99.6
A13-CP73	49.47	0.77	4.78	7.69	0.17	14.47	21.52	0.26	0.05	99.18
A13-CP82	51.27	0.47	3.53	6.63	0.14	15.88	21.38	0.24	0.32	99.86
A13-CP83	50.60	0.56	4.48	6.03	0.15	15.33	22.37	0.22	0.44	100.18
A13-CP86	51.22	0.37	4.02	4.76	0.12	16.06	22.38	0.17	0.94	100.04
A13-CP87	50.18	0.46	4.44	6.07	0.08	15.30	22.20	0.22	0.45	99.4

[a]All Fe as FeO.

Appendix 2.3, Naturally quenched (un-homogenised) melt inclusions.

Sample	SiO_2	TiO_2	Al_2O_3	[a]FeO	MnO	MgO	CaO	Na_2O	K_2O	P_2O_5	Cr_2O_3	Total
148-896A-3R-1, Piece 4												
PL21-GL	51.31	0.70	15.84	8.98	0.16	8.38	12.93	1.81	0.04	0.04	0.08	100.27
PL39A-GL	51.27	0.42	15.56	9.52	0.16	8.77	13.01	1.84	0.03	0.05	0.04	100.67
I2-PL10-GLA	51.13	1.24	15.84	9.09	0.16	8.27	13.12	1.82	0.02	0.04	0.06	100.79
I2-PL11-GLA	51.56	0.65	16.16	9.30	0.19	8.47	13.23	1.91	0.03	0.00	0.06	101.56
I2-PL11-GLB	51.65	0.65	15.14	9.40	0.23	8.74	13.03	1.83	0.01	0.00	0.03	100.71
I2-PL12-GLA	52.39	0.33	16.03	9.09	0.06	8.43	13.03	1.92	0.03	0.00	0.06	101.37
I2-PL13-GLA	50.20	1.34	15.69	9.48	0.20	8.46	13.14	1.69	0.04	0.16	0.01	100.41
I2-PL17-GLA	52.23	0.35	15.71	9.45	0.09	8.62	12.90	1.87	0.03	0.03	0.03	101.31
I2-PL17-GLB	52.62	0.27	16.07	8.98	0.03	8.52	13.05	1.87	0.02	0.00	0.03	101.46
A14-OL10-GL	49.22	0.67	18.41	8.79	0.12	6.62	14.59	1.78	0.01	0.07	0.06	100.34
148-896A-4R-1, Piece 2												
T-PL1-GL1	48.63	0.63	13.22	10.77	0.19	11.63	13.33	0.97	0.01	0.04	0.03	99.45
T-PL1-GL2	48.46	0.99	7.08	12.87	0.33	16.16	12.55	0.42	0.03	0.06	0.06	99.01
148-896A-9R-1, Piece 24												
PL119-GLA	49.24	0.70	15.19	8.51	0.18	9.21	11.70	1.95	0.15	0.02	0.07	96.92
PL119-GLB	50.46	0.78	15.38	7.74	0.14	9.30	12.39	2.04	0.23	0.06	0.06	98.58
PL119-GLC	49.89	0.81	15.03	8.49	0.18	9.35	12.26	2.10	0.20	0.04	0.07	98.42
PL49-GL	50.16	0.38	6.98	10.72	0.20	15.94	13.61	0.48	0.09	0.00	0.12	98.68
I2-PL15-GLA	51.23	0.68	15.88	8.33	0.23	9.54	12.41	2.14	0.20	0.03	0.01	100.68

Appendix 2.3, continued.

Sample	SiO_2	TiO_2	Al_2O_3	[a]FeO	MnO	MgO	CaO	Na_2O	K_2O	P_2O_5	Cr_2O_3	Total
I2-PL15-GLB	50.48	0.77	15.29	8.69	0.27	9.21	12.36	2.25	0.21	0.03	0.04	99.60
I2-PL18-GLA	50.36	0.99	15.36	9.89	0.27	7.92	13.11	1.87	0.04	0.00	0.04	99.85
A9-OL40-GL	51.75	0.96	16.81	8.40	0.20	4.85	14.68	1.89	0.03	0.00	0.06	99.63
A9-PL4-GL	50.00	0.33	11.96	12.14	0.21	11.43	11.95	1.36	0.03	0.07	0.13	99.61
A9-PL7-GL1	50.75	0.15	7.41	10.85	0.21	14.89	13.49	0.80	0.06	0.02	0.16	98.79
A9-PL7-GL2	49.17	0.25	6.71	11.88	0.21	16.10	13.03	0.33	0.05	0.02	0.07	97.82
A9-PL8-GL2	50.81	0.72	14.70	9.86	0.20	8.52	12.62	1.66	0.02	0.03	0.08	99.22
A9-PL8-GL1	50.97	0.71	15.00	9.38	0.16	8.40	12.54	1.88	0.03	0.05	0.04	99.16
A9-PL10-GL	50.50	0.97	8.43	11.93	0.22	13.80	12.36	1.27	0.02	0.05	0.10	99.65
A9-PL14-GL	49.39	0.98	12.71	12.46	0.18	9.80	12.29	1.20	0.01	0.07	0.05	99.14
A9-PL18-GL1	50.63	0.97	15.20	9.39	0.15	8.14	12.49	1.80	0.03	0.08	0.04	98.92
A9-PL18-GL2	51.03	0.73	14.31	9.78	0.19	8.85	12.47	1.60	0.01	0.05	0.02	99.04
A9-PL21-GL	53.19	0.16	9.20	9.34	0.20	13.47	13.88	0.72	0.01	0.01	0.09	100.27
A9-PL54-GL1	50.01	0.15	7.86	12.11	0.19	16.04	12.48	0.55	0.00	0.02	0.10	99.51
A9-PL54-GL2	50.63	0.59	8.71	11.90	0.24	13.59	12.77	1.12	0.01	0.05	0.04	99.65
148-896A-25R-1, Piece 11												
PL134-GL	46.12	0.74	10.56	11.54	0.29	13.31	12.29	0.18	0.11	0.03	0.08	95.25
PL136-GL	46.95	0.98	8.85	11.75	0.21	15.46	12.85	0.23	0.05	0.05	0.10	97.48
PL60-GL	47.41	1.14	6.38	14.14	0.22	14.36	12.28	0.34	0.34	0.06	0.07	96.74
SP57-GL	49.77	0.93	16.39	7.11	0.09	9.98	13.24	1.88	0.02	0.03	0.43	99.87
I2-OL19-GLA	51.14	0.96	14.33	10.81	0.26	7.33	13.49	2.00	0.01	0.08	0.03	100.44
148-896A-25R-2, Piece 11												
PL42-GL	49.73	0.90	15.33	9.76	0.17	9.79	12.18	2.11	0.04	0.05	0.03	100.09
PL90-GL	51.51	0.84	10.68	10.37	0.18	11.58	12.62	1.75	0.03	0.04	0.09	99.69
PL101-GL1	49.48	0.58	14.06	9.10	0.16	8.75	11.46	2.18	0.15	0.02	0.07	96.01
PL101-GL2	51.21	0.55	14.98	8.90	0.21	9.06	12.05	2.38	0.11	0.02	0.08	99.55
PL143-GL	48.77	1.21	5.01	14.79	0.28	14.90	12.61	0.45	0.02	0.09	0.06	98.19
PL144-GL2	47.81	0.67	8.09	12.55	0.24	14.89	13.14	0.26	0.01	0.05	0.09	97.80
PL144-GL1	51.02	0.59	12.78	9.88	0.16	10.71	12.97	1.88	0.02	0.02	0.09	100.12
148-896A-27R-1, Piece 13												
PL30A-GL	49.72	0.68	14.44	9.66	0.14	10.43	13.16	1.33	0.02	0.05	0.05	99.68
PL30B-GL	47.17	0.65	13.89	10.12	0.19	12.76	13.04	0.57	0.11	0.00	0.06	98.56
OL36-GL	50.47	0.79	17.86	8.31	0.26	5.48	15.21	1.83	0.01	0.01	0.07	100.30
OL40-GL	50.61	0.66	18.70	8.01	0.14	3.90	16.26	1.65	0.02	0.06	0.03	100.04
PL53-SP-GL	49.32	0.65	16.17	8.06	0.15	9.51	12.99	1.56	0.01	0.01	0.95	99.38
PL63-GL	49.78	0.41	8.13	12.73	0.26	14.47	11.91	0.53	0.03	0.00	0.09	98.34
PL66A-GL	50.48	0.46	10.99	11.27	0.27	12.51	12.08	1.56	0.04	0.02	0.10	99.78
PL66B-GL	50.80	0.44	10.16	11.99	0.24	13.28	12.19	1.09	0.02	0.00	0.08	100.29
PL76A-GL	50.39	0.50	8.99	12.57	0.18	13.90	12.23	1.15	0.03	0.00	0.10	100.04
PL76B-GL	49.82	0.36	9.59	12.78	0.23	14.14	12.97	0.67	0.03	0.00	0.10	100.69
PL80A-GL	51.08	0.82	13.59	10.71	0.20	9.10	12.77	1.58	0.03	0.04	0.03	99.95
PL80B-GL	51.50	0.89	12.94	11.23	0.19	9.52	12.92	1.34	0.04	0.07	0.05	100.69
PL80C-GL	50.69	0.83	15.20	9.76	0.13	8.26	13.07	1.68	0.01	0.03	0.03	99.69
PL103-GL	49.10	0.75	14.36	10.57	0.13	10.58	12.59	1.59	0.03	0.02	0.11	99.83
A11-PL20-GL	51.14	0.30	15.61	10.15	0.22	9.71	13.37	1.69	0.01	0.03	0.08	102.31
A11-PL21A-GL	49.03	0.59	6.90	14.15	0.26	15.50	11.47	0.36	0.03	0.00	0.08	98.37
A11-PL21B-GL	50.85	0.53	7.56	13.40	0.26	14.95	12.12	0.55	0.01	0.00	0.09	100.32
A11-PL51-GL	50.96	0.48	14.08	10.63	0.14	9.84	12.92	1.53	0.01	0.03	0.01	100.63
148-896A-27R-1, Piece 15												
A13-PL4-GL	50.12	1.07	8.10	13.39	0.25	13.62	12.08	0.62	0.04	0.07	0.06	99.42
A13-PL13-GL	50.74	1.14	8.22	13.90	0.25	12.89	12.36	0.76	0.03	0.08	0.08	100.45
A13-PL18-GL	49.76	0.72	9.17	12.98	0.26	13.28	12.09	0.97	0.07	0.08	0.08	99.46
A13-PL19-GL	49.89	0.95	12.23	11.36	0.23	11.41	12.53	1.47	0.10	0.09	0.06	100.32
A13-PL53-GL	51.67	0.96	9.34	12.86	0.25	12.30	12.52	0.77	0.03	0.08	0.08	100.86
A13-PL111-GL	49.66	0.99	9.12	13.78	0.29	12.39	12.23	1.21	0.12	0.05	0.07	99.91
A13-PL115-GL	49.52	1.17	9.16	13.34	0.27	12.85	12.11	1.07	0.07	0.11	0.07	99.74
A13-PL116-GL	50.12	0.75	12.36	11.04	0.10	12.04	12.73	1.44	0.03	0.06	0.08	100.75
A13-PL134-GL	49.11	1.19	6.32	15.25	0.26	15.25	11.75	0.29	0.07	0.04	0.10	99.63
A13-OL141-GL	50.53	0.66	17.66	8.87	0.08	5.90	14.74	1.71	0.10	0.11	0.14	100.50
A13-SP118-GA	49.79	0.64	15.99	9.27	0.05	9.34	13.40	1.57	0.01	0.05	1.08	101.19
A13-SP118-GB	48.81	0.66	16.08	9.47	0.17	9.32	13.23	1.58	0.01	0.03	1.37	100.73
A13-OL88-GL	50.79	0.72	17.53	9.04	0.18	5.44	15.61	1.68	0.01	0.09	0.07	101.16
A13-OL74-GL	50.86	0.67	18.33	7.96	0.11	3.96	16.49	1.67	0.01	0.08	0.06	100.20
A13-OL66-GL	50.19	0.78	18.24	8.63	0.04	4.87	15.72	1.69	0.02	0.06	0.05	100.29
A13-OL64-GL	49.68	0.63	16.86	8.96	0.15	7.90	13.85	1.63	0.01	0.08	0.04	99.79
A3-OL41-GL1	49.82	0.64	16.15	9.34	0.11	8.38	13.98	1.68	0.01	0.02	0.13	100.26

Appendix 2.3, continued.

Sample	SiO_2	TiO_2	Al_2O_3	[a]FeO	MnO	MgO	CaO	Na_2O	K_2O	P_2O_5	Cr_2O_3	Total
A3-OL41-GL2	49.74	0.70	16.36	9.37	0.10	8.27	14.03	1.52	0.01	0.02	0.10	100.22
A3-OL41-GL3	49.45	0.72	16.07	9.16	0.15	7.82	13.63	1.75	0.04	0.00	0.07	98.86
A3-OL41-GL4	49.98	0.70	16.14	9.31	0.15	8.39	13.82	1.72	0.02	0.01	0.08	100.32
A3-OL41-GL5	49.11	0.78	15.93	8.92	0.12	7.65	12.41	1.88	0.12	0.03	0.14	97.09
A3-OL41-GL6	50.22	0.68	16.05	8.74	0.17	8.70	12.92	1.61	0.05	0.00	0.09	99.23

[a]All Fe as FeO.

Appendix 2.4, Homogenised melt inclusions affected by overheating, analytical overlap or poor quenching (see text for details).

Sample	SiO_2	TiO_2	Al_2O_3	[a]FeO	MnO	MgO	CaO	Na_2O	K_2O	P_2O_5	Cr_2O_3	Total	[b]Host	[c]T_h (°C)
148-896A-3R-1, Piece 4														
I2-P-4B	51.95	0.39	16.34	8.66	0.12	8.01	13.27	1.90	0.03	0.02	0.07	100.86	84.8	1210
I2-P-4C	51.83	0.51	16.76	8.46	0.24	7.63	13.12	1.91	0.04	0.04	0.04	100.68	84.5	1210
I2-P-1A	51.87	0.58	16.94	9.29	0.15	8.37	11.48	1.66	0.36	0.05	0.01	100.87	84.3	1220
I2-P-1B	51.91	0.48	16.57	8.42	0.20	8.13	13.03	1.79	0.37	0.10	0.04	101.14	84.8	1220
148-896A-4R-1, Piece 2														
I2-P-12A	51.8	0.31	15.02	8.99	0.19	9.19	13.72	1.81	0.03	0.05	0.01	101.23	88.0	1200
I2-P-12B	51.52	0.31	15.23	9.07	0.13	9.11	13.85	1.75	0.02	0.02	0.03	101.15	88.2	1200
I2-P-14B	51.2	0.33	14.72	9.28	0.23	8.89	13.5	1.61	0.02	0.00	0.03	99.92	88.0	1200
P71-1	49.68	0.55	15.57	8.59	0.17	10.28	12.76	1.96	0.20	0.05	0.05	99.96	90.7	1200
P72-1	51.19	0.60	15.37	7.97	0.12	9.64	13.45	1.72	0.03	0.05	0.07	100.3	90.7	1197
P72-2	51.25	0.56	15.40	8.15	0.09	9.74	13.39	1.58	0.03	0.00	0.06	100.35	90.6	1197
P73-1	51.01	0.56	15.62	7.98	0.13	9.57	13.53	1.86	0.02	0.05	0.04	100.47	90.4	1205
P73-2	51.17	0.57	15.23	8.00	0.13	9.64	13.60	1.75	0.02	0.02	0.07	100.3	90.3	1205
P73-3	50.98	0.50	15.46	7.88	0.15	9.47	13.45	1.88	0.15	0.00	0.08	100.09	90.9	1205
P73-4	51.09	0.55	15.54	8.15	0.12	10.00	13.36	1.29	0.31	0.01	0.08	100.6	90.6	1205
P75-1	50.75	0.53	15.38	8.12	0.14	9.56	13.60	1.62	0.01	0.09	0.11	100.01	90.6	1210
I2-P-11A	51.11	0.84	15.79	9.39	0.21	7.99	12.96	1.82	0.06	0.09	0.08	100.45	89.2	1225
I2-P-11B	51.77	0.78	16.04	9.11	0.23	8.16	13.07	1.90	0.04	0.08	0.03	101.32	88.1	1225
P71-2	50.88	0.66	15.14	8.34	0.08	9.71	13.51	1.71	0.02	0.09	0.07	100.31	90.8	1200
148-896A-9R-1, Piece 24														
P78-2	50.14	0.47	15.67	9.04	0.15	9.3	13.45	1.44	0.17	0.04	0.04	100.02	94.6	1215
P78-5	50.78	0.54	15.46	8.87	0.17	9.53	13.13	1.41	0.11	0.01	0.08	100.09	93.1	1215
P83-4	48.65	0.27	16.99	10.19	0.22	9.16	12.74	1.63	0.02	0.05	0.2	100.24	94.0	1195
P78-1	50.02	0.52	15.13	9.11	0.14	9.58	13.58	1.43	0.12	0.03	0.07	99.84	93.9	1215
P78-4b	50.24	0.50	15.42	9.06	0.15	9.63	13.46	1.32	0.13	0.04	0.04	100.1	93.7	1215
P79-1	51.69	0.47	14.84	9.75	0.17	7.82	13.04	1.59	0.41	0.04	0.01	99.95	86.0	1205
P79-2	51.16	0.47	14.89	10.01	0.16	7.96	12.90	1.66	0.11	0.06	0.01	99.51	86.3	1205
P79-3	50.76	0.51	14.86	9.91	0.15	7.80	12.80	1.70	0.36	0.02	0.02	99.01	86.1	1205
P81-7	50.57	0.15	15.36	9.48	0.10	9.23	12.74	1.79	0.02	0.04	0.06	99.65	92.5	1195
P82-1a	50.75	0.65	15.30	8.44	0.17	9.78	13.34	1.61	0.01	0.06	0.09	100.3	90.7	1195
P82-2	51.11	0.62	15.37	8.41	0.09	9.40	13.06	1.92	0.03	0.06	0.05	100.22	88.6	1195
P82-5	49.73	0.65	14.77	8.34	0.15	9.48	13.07	1.81	0.02	0.04	0.04	98.2	87.5	1195
P83-1	49.48	0.26	19.00	9.13	0.06	7.49	13.79	1.62	0.01	0.07	0.07	101.09	94.1	1195
P83-6	49.38	0.26	14.80	10.52	0.17	9.58	12.45	1.86	0.03	0.02	0.08	99.27	94.4	1195
P85-2	48.34	0.79	16.07	11.78	0.23	7.96	10.54	2.09	0.79	0.05	0.03	98.81	86.8	1195
P86-2	49.88	0.83	15.89	9.70	0.20	8.03	12.52	2.12	0.24	0.02	0.00	99.55	86.7	1195

Appendix 2.4, continued.

Sample	SiO_2	TiO_2	Al_2O_3	[a]FeO	MnO	MgO	CaO	Na_2O	K_2O	P_2O_5	Cr_2O_3	Total	[b]Host	[c]T_h (°C)
P81-3	50.44	0.14	15.24	9.25	0.16	9.36	12.61	1.8	0.02	0.02	0.1	99.25	93.1	1195
148-896A-25R-1, Piece 11														
I2-P-5A	51.09	0.77	15.53	9.13	0.15	8.69	12.86	1.91	0.01	0	0.1	100.35	85.9	1200
I2-P-6A	52.01	0.42	15.81	7.99	0.16	8.38	13.25	2.61	0.02	0.10	0.08	100.93	86.5	1225
148-896A-27R-1, Piece 13														
P42-8	49.08	0.49	18.12	8.25	0.15	8.52	13.01	1.56	0.04	0.01	0.10	99.43	90.5	1215
P46-2	50.18	0.23	15.50	8.68	0.08	9.35	12.95	1.70	0.01	0.00	0.08	98.86	90.3	1210
P47-2	50.35	0.68	15.36	8.85	0.16	9.69	13.29	1.31	0.15	0.06	0.07	100.07	87.6	1215
P47-3	49.66	0.65	15.40	8.94	0.12	9.51	13.39	1.49	0.01	0.07	0.07	99.42	90.6	1215
P48-6	50.64	0.27	15.31	9.41	0.19	9.15	12.83	1.58	0.27	0.05	0.04	99.85	89.4	1210
P47-1	49.87	0.71	15.39	8.71	0.13	9.55	13.2	1.54	0.01	0.11	0.06	99.38	90.6	1215
148-896A-27R-1, Piece 15														
P58-1	50.29	0.73	15.54	9.75	0.1	8.02	12.52	1.64	0.76	0.04	0.02	99.53	88.7	1215
P58-3	50.3	0.78	15.47	9.75	0.12	8.17	12.8	1.62	0.71	0.02	0.03	99.89	89.3	1215
P58-8	50.06	0.78	15.1	9.79	0.16	8.25	13.03	1.65	0.11	0.01	0.07	99.13	88.8	1215
P66-4	50.77	0.53	15.29	8.94	0.1	9.21	13.16	1.46	0.01	0.03	0.07	99.68	89.3	1200
P56-2	49.98	0.80	15.73	9.11	0.15	7.58	13.61	1.54	0.16	0.03	0.05	98.85	88.6	1195
P56-3	48.21	0.79	17.65	9.07	0.20	8.56	12.29	1.73	0.05	0.01	0.05	98.72	87.1	1195
P58-6	50.94	0.77	15.38	9.62	0.16	8.23	13.14	1.71	0.03	0.05	0.07	100.21	89.0	1215
P58-7	50.92	0.79	15.57	9.67	0.15	8.11	12.79	1.71	0.02	0.08	0.07	100	88.7	1215
P58-8A	50.65	0.71	15.28	9.62	0.17	8.13	13.05	1.74	0.02	0.05	0.05	99.58	88.8	1215
P67-7	51.34	0.46	15.59	8.95	0.10	9.34	12.89	1.74	0.03	0.04	0.05	100.64	89.4	1205
P69-9	50.78	0.73	14.85	9.55	0.17	8.90	12.89	1.72	0.03	0.02	0.05	99.8	89.6	1200
P70-1	51.05	0.76	15.24	9.07	0.15	9.13	12.86	1.73	0.01	0.04	0.07	100.22	90.8	1205
P58-2	50.77	0.71	15.32	9.65	0.18	8.11	12.98	1.73	0.02	0.03	0.06	99.67	88.6	1215

[a]All Fe as FeO.

[b]Anorhtite content of host, An = 100 x (Ca/(Ca + Na)).

[c]Homogenisation temperature.

Appendix 2.5, Homogenised melt inclusions in plagioclase.

Sample	SiO_2	TiO_2	Al_2O_3	[a]FeO	MnO	MgO	CaO	Na_2O	K_2O	P_2O_5	Cr_2O_3	Total	CaO/ Na_2O	[b]Host	[c]T_h (°C)
148-896A-3R-1, piece 4															
I2-P-2A	50.91	0.35	15.53	8.86	0.14	8.13	13.19	1.91	0.01	0.01	0.08	99.12	6.91	85.81	1210
I2-P-4A	51.86	0.36	15.85	9.20	0.14	8.41	12.86	1.74	0.28	0.02	0.05	100.77	7.39	85.05	1210
148-896A-4R-1, Piece 2															
I2-P-10A	52.25	0.54	15.50	9.23	0.10	8.79	12.84	1.92	0.02	0.00	0.05	101.24	6.69	86.76	1200
I2-P-10B	51.90	0.53	15.57	9.29	0.07	8.78	13.19	1.71	0.00	0.00	0.04	101.08	7.71	87.35	1200
I2-P-10C	51.93	0.64	15.50	9.54	0.09	8.96	13.27	1.83	0.03	0.04	0.05	101.88	7.25	86.67	1200
I2-P-14A	49.22	0.30	15.16	10.21	0.17	8.46	13.17	1.86	0.43	0.09	0.05	99.12	7.08	88.00	1200
I2-P-15A	51.68	0.64	15.88	7.92	0.11	9.33	13.65	1.73	0.01	0.04	0.10	101.09	7.89	90.31	1205
I2-P-15B	51.37	0.59	15.65	8.01	0.10	9.14	13.75	1.54	0.02	0.09	0.06	100.32	8.93	90.98	1205
P73-5	51.02	0.53	15.73	8.02	0.15	9.43	13.77	1.64	0.01	0.05	0.07	100.42	8.40	90.66	1205
P76-2	50.57	0.78	14.80	9.42	0.15	8.43	13.19	1.99	0.04	0.08	0.07	99.52	6.63	87.12	1195
P76-3	50.67	0.74	14.70	9.64	0.13	8.27	13.07	1.85	0.01	0.05	0.09	99.22	7.06	0.00	1195
148-896A-9R-1, Piece 24															
P78-4a	49.94	0.44	16.37	9.01	0.12	9.31	13.54	1.38	0.12	0.06	0.04	100.33	9.81	93.68	1215
P81-2	50.59	0.13	15.53	9.37	0.16	9.20	12.90	1.85	0.03	0.01	0.09	99.86	6.97	92.17	1195
P81-8	50.80	0.18	15.21	10.08	0.17	8.85	12.62	1.58	0.27	0.06	0.07	99.89	7.99	92.69	1195
P82-1b	50.14	0.59	16.45	8.22	0.12	9.31	13.39	1.64	0.02	0.12	0.05	100.05	8.16	90.68	1195
P85-1	51.05	0.67	14.86	9.30	0.14	8.20	12.77	1.96	0.01	0.03	0.07	99.06	6.52	85.74	1195
P85-3	49.91	0.69	15.63	9.80	0.21	8.34	11.92	2.00	0.74	0.02	0.03	99.29	5.96	87.91	1195
P86-3	50.86	0.56	14.99	9.24	0.17	8.17	12.77	1.99	0.02	0.03	0.06	98.86	6.42	86.73	1195
P86-5	51.14	0.65	15.08	9.35	0.12	8.29	12.78	2.02	0.04	0.04	0.04	99.55	6.33	87.07	1195
P86-6	51.27	0.64	15.01	9.49	0.12	8.24	13.02	2.03	0.03	0.04	0.05	99.94	6.41	87.06	1195
148-896A-25R-1, Piece 11															
I2-P-5A	51.09	0.77	15.53	9.12	0.15	8.69	12.86	1.91	0.01	0.00	0.10	100.23	6.73	85.94	1200
P61-1	51.31	0.76	15.19	8.60	0.16	8.45	13.19	2.12	0.04	0.03	0.04	99.89	6.22	84.56	1205
P61-2	50.74	0.84	15.12	8.69	0.18	8.41	12.98	2.14	0.04	0.06	0.03	99.23	6.07	84.56	1205
P61-3	50.70	0.78	15.04	8.67	0.11	8.65	12.95	2.05	0.03	0.07	0.08	99.13	6.32	87.33	1205
P61-4	50.96	0.74	15.02	8.83	0.10	8.65	12.97	1.97	0.02	0.06	0.04	99.36	6.58	86.69	1205
P61-6	50.89	0.74	15.09	8.68	0.12	8.56	12.93	2.10	0.03	0.04	0.07	99.25	6.16	83.21	1205
P64-1	50.29	0.87	15.09	9.32	0.14	8.19	13.03	2.20	0.01	0.04	0.05	99.23	5.92	79.62	1205
148-896A-27R-1, Piece 13															
P42-3	50.64	0.20	15.56	8.73	0.16	8.73	13.19	1.69	0.04	0.04	0.08	99.06	7.80	89.69	1215
P42-7	49.97	0.28	15.73	8.69	0.16	9.18	12.94	1.69	0.02	0.03	0.06	98.75	7.66	90.10	1215
P45-1	50.45	0.23	15.87	8.57	0.10	9.14	13.36	1.67	0.02	0.00	0.04	99.45	8.00	89.85	1215
P45-2	50.34	0.20	15.68	8.63	0.16	9.28	12.83	1.71	0.01	0.01	0.05	98.90	7.50	89.38	1215
P45-4	50.36	0.24	15.57	8.41	0.17	9.34	13.03	1.67	0.03	0.01	0.09	98.92	7.80	90.73	1215

Appendix 2.5, continued.

Sample	SiO_2	TiO_2	Al_2O_3	[a]FeO	MnO	MgO	CaO	Na_2O	K_2O	P_2O_5	Cr_2O_3	Total	CaO/ Na_2O	[b]Host	[c]T_h (°C)
P45-5	50.28	0.22	15.98	8.39	0.11	9.31	13.12	1.60	0.01	0.00	0.06	99.08	8.20	90.39	1215
P45-6	50.52	0.19	15.89	8.18	0.15	9.23	13.03	1.55	0.04	0.00	0.06	98.84	8.41	89.77	1215
P45-7A	50.42	0.23	16.09	8.18	0.12	9.27	13.11	1.66	0.01	0.00	0.04	99.13	7.90	90.17	1215
P46-3	50.83	0.21	15.59	8.80	0.16	8.66	13.27	1.73	0.02	0.02	0.07	99.36	7.67	90.21	1210
P46-4	50.18	0.27	16.05	8.78	0.17	9.29	13.21	1.62	0.01	0.02	0.09	99.69	8.15	90.02	1210
P46-5	49.98	0.27	15.88	8.92	0.13	9.27	13.16	1.66	0.01	0.01	0.08	99.37	7.93	90.77	1210
P48-1	50.17	0.26	15.47	9.36	0.13	8.96	12.69	1.61	0.26	0.02	0.06	98.99	7.88	90.52	1210
P48-2	50.15	0.28	15.56	9.50	0.15	9.15	12.74	1.65	0.26	0.03	0.04	99.51	7.72	91.01	1210
P48-3	50.07	0.27	16.15	9.29	0.19	8.96	12.72	1.65	0.28	0.07	0.02	99.67	7.71	90.25	1210
P50-1	50.11	0.53	16.51	7.67	0.11	9.39	13.12	1.66	0.02	0.02	0.09	99.23	7.90	90.88	1215
P51-2	50.84	0.27	16.04	8.72	0.14	8.42	13.50	1.90	0.01	0.00	0.04	99.88	7.11	89.83	1210
P51-6	51.07	0.24	15.68	9.04	0.16	8.74	13.29	1.72	0.03	0.01	0.04	100.02	7.73	90.48	1210
148-896A-27R-1, Piece 15															
P56-4	50.82	0.59	15.70	9.16	0.16	8.87	12.64	1.64	0.03	0.00	0.02	99.63	7.71	88.44	1195
P56-6	51.06	0.65	14.93	8.61	0.16	8.69	12.42	1.61	0.03	0.03	0.01	98.20	7.71	88.52	1195
P57-1	50.45	0.48	15.71	9.50	0.16	8.99	13.03	1.50	0.03	0.00	0.08	99.93	8.69	89.25	1205
P57-2	49.96	0.53	15.19	10.46	0.11	8.25	12.28	1.75	0.30	0.00	0.06	98.89	7.02	89.25	1205
P57-3	49.62	0.51	16.29	8.98	0.17	8.75	12.83	1.46	0.03	0.03	0.06	98.73	8.79	0.00	1205
P65-1	50.51	0.86	15.51	9.27	0.14	8.39	13.10	1.83	0.03	0.08	0.10	99.82	7.16	89.75	1205
P66-2	50.34	0.40	15.48	8.68	0.14	8.99	12.99	1.57	0.02	0.02	0.07	98.70	8.27	89.26	1200
P66-3	50.64	0.42	15.37	8.63	0.15	8.97	13.09	1.62	0.04	0.01	0.04	98.98	8.08	89.13	1200
P66-7	50.19	0.52	15.38	8.75	0.14	8.83	12.79	1.51	0.54	0.00	0.07	98.72	8.47	90.90	1200
P67-1	51.22	0.48	15.62	8.84	0.17	8.96	12.99	1.67	0.03	0.07	0.09	100.14	7.78	89.84	1205
P67-4	51.13	0.51	15.53	8.86	0.10	9.02	13.02	1.81	0.03	0.05	0.04	100.10	7.19	90.02	1205
P67-5	51.05	0.42	16.57	8.52	0.14	8.92	13.28	1.73	0.01	0.03	0.10	100.77	7.68	89.30	1205
P68-1	51.27	0.59	15.30	9.77	0.17	8.08	12.86	1.79	0.01	0.06	0.05	99.95	7.18	88.20	1200
P68-3	51.11	0.57	15.37	9.82	0.17	8.15	13.10	1.81	0.01	0.04	0.08	100.23	7.24	89.30	1200
P68-9	51.52	0.49	15.12	9.63	0.12	8.32	12.88	1.81	0.04	0.01	0.04	99.98	7.12	89.08	1200
P69-14	51.26	0.56	15.03	9.53	0.16	8.68	12.76	1.74	0.01	0.00	0.07	99.80	7.33	89.13	1200
P69-15	51.31	0.57	14.99	9.84	0.17	8.77	12.90	1.75	0.01	0.02	0.09	100.42	7.37	89.00	1200
P69-4	50.64	0.53	15.46	9.40	0.15	8.62	12.76	1.63	0.02	0.01	0.05	99.27	7.83	89.11	1200
P70-2	50.34	0.65	15.98	9.25	0.15	8.84	13.27	1.65	0.02	0.03	0.07	100.25	8.04	90.15	1205

[a]All Fe as FeO.

[b]Host plagioclase composition, An = 100 x (Ca/(Ca + Na)).

[c]Homogenisation temperature.

Appendix 2.6, Homogenised melt inclusions in olivine.

Sample	SiO_2	TiO_2	Al_2O_3	[a]FeO	MnO	MgO	CaO	Na_2O	K_2O	P_2O_5	Cr_2O_3	Total	[b]T_h(°C)	[c]Fo	CaO/ Na_2O
148-896A-27R-1, Piece 13															
OL1-1	48.74	0.59	15.20	11.20	0.12	8.62	12.64	1.54	0.01	0.05	0.05	98.76	1195	88.2	8.2
OL1-2	49.19	0.63	15.77	10.12	0.11	8.60	13.09	1.54	0.03	0.09	0.04	99.21	1195	88.0	8.5
OL2-1	50.09	0.61	16.41	9.75	0.14	8.85	13.20	1.59	0.01	0.06	0.15	100.86	1200	88.3	8.3
OL2-2	49.30	0.59	16.08	10.83	0.14	8.44	13.19	1.52	0.01	0.03	0.12	100.25	1200	88.2	8.7
OL3-1	49.06	0.59	15.98	10.02	0.17	8.43	13.38	1.52	0.03	0.05	0.17	99.40	1195	88.3	8.8
OL4-1	49.58	0.60	16.45	9.80	0.11	8.58	13.51	1.55	0.01	0.08	0.05	100.32	1195	88.3	8.7
148-896A-27R-1, Piece 15															
OL5-1	48.59	0.66	15.99	10.86	0.14	8.27	13.24	1.47	0.01	0.08	0.04	99.35	1190	88.0	9.0
148-896A-9R-1, Piece 24															
OL8-1	49.49	0.69	15.82	9.68	0.14	8.23	12.61	1.89	0.03	0.06	0.03	98.67	1195	88.4	6.7
OL8-2	51.15	0.68	16.45	9.59	0.13	8.77	12.58	1.92	0.01	0.07	0.01	101.36	1195	88.7	6.6

[a]All Fe as FeO.

[b]Homogenisation temperature.

[c]Host forsterite, Fo = 100 x (Mg /(Mg + Fe)).

Appendix 2.7, Trace element compositions; pillow rim-glasses and melt inclusions.

Element (ppm)	Pillow-rim glass				Melt inclusions in plagioclase						inclusion in olivine	Homogenised inclusions	
	1	2	3	4	5	6	7	8	9	10	11	12	13
Rb	0.04		0.19	0.19	0.04		0.24	0.42	0.47	1.61	0.01	0.09	0.09
Ba	0.96	0.90	0.84	0.67	1.25	0.99	0.67	0.9	0.79	5.90	0.45	1.39	0.38
Nb	0.16	0.12	0.22	0.17	0.15	0.34	0.05	0.03	0.04	0.42	0.07	0.25	
K	98	96	110	111	73	61	63	172	142	2398	218	376	116
La	0.94	0.79	0.84	0.85	1.92	1.41	0.66	0.69	0.67	1.45	0.79	1.12	0.40
Ce	3.43	3.51	3.44	3.42	7.25	5.08	2.58	2.3	2.44	5.01	3.32	4.21	1.67
Pr	0.62	0.65	0.65	0.67	1.31	0.96	0.51	0.45	0.46	0.88	0.60	0.86	0.41
Sr	61	62	52	69	74	63	66	69	68	102	57	66	38
Nd	4.00	4.55	4.50	4.63	8.54	6.91	3.12	2.74	2.93	5.06	4.40	5.56	1.95
Sm	1.67	1.70	1.42	1.67	2.61	2.19	1.32	1.08	1.20	1.62	1.54	2.11	0.87
Zr	38.0	37.7	39.1	43.8	74.8	66.1	31.6	39.9	35.8	49.3	46.1	47.4	25.2
Eu	0.70	0.76	0.63	0.79	0.77	0.54	0.49	0.67	0.58	0.65	0.71	0.88	0.23
Ti	4325	4398	5023	5413	7813	7589	4444	4173	4308	4953	6442	5320	3618
Gd	2.05	3.21	2.51	2.86	5.15	3.96	0.63	2.27	2.27	2.20	2.35	3.84	2.14
Tb	0.56	0.51	0.50	0.53	0.97	0.68	0.32	0.35	0.34	0.51	0.43	0.75	0.36
Dy	3.59	4.30	3.52	3.87	6.58	5.23	2.47	2.62	2.54	3.25	3.14	5.03	2.82
Y	25	25	25	24	35.7	33.4	21.9	21.2	22	20	29	30	20
Ho	0.88	0.96	0.82	0.87	1.34	1.16	0.47	0.54	0.51	0.71	0.67	1.08	0.60
Er	3.18	2.97	2.27	2.53	3.96	3.80	1.58	1.71	1.64	2.02	1.88	3.45	1.67
Yb	3.38	3.35	2.35	2.50	4.05	3.14	1.77	2.07	1.92	1.89	2.35	3.70	1.78
H_2O	0.05	0.05			0.06	0.06	0.09	0.09		1.14			

Notes: 1, 148-896A-3R-1, Piece 4. 2, Duplicate of analysis 1. 3, 148-896A-9R-1, Piece 24. 4, 148-896A-25R-1, Piece 11. 5, 148-896A-3R-1, Piece 4 , plagioclase $An_{86.3}$. 6, duplicate of analysis 5. 7, 148-896A-3R-1, Piece 4, plagioclase An_{87}. 8, Duplicate of analysis 7. 9,148-896A-3R-1, Piece 4, plagiolcase An_{88}. 10, 148-896A-9R-1, Piece 24, plagioclase $An_{88.5}$. 11, 148-896A-25R-1, Piece 11, olivine $Fo_{85.3}$. 12, 148-896A-4R-1, Piece 2, experiment 11, T_h=1225°C, host plagioclase An_{88}. 13, 148-896A-4R-1, Piece 2, experiment 15, T_h=1205°C, plagioclase $An_{90.3}$.

[a]Trace elements determined by ion-probe.

[b]H_2O determined by fourier transform infrared spectroscopy.

Appendix 2.8, Trace element composition of pillow-rim glasses, analysed by laser ablation ICP-MS.

Element	Group 1		Group 2	Group3	Group 4
(ppm)	[a]1	2	3	4	5
Ba	0.78	0.98	0.69	0.54	1.13
Th	0.0181	0.0237	0.0185	0.016	0.0252
U	0.006	0.0082	0.0069	0.0052	0.0084
Nb	0.237	0.301	0.258	0.206	0.374
Ta	0.0176	0.0244	0.0214	0.0171	0.0273
La	0.765	0.967	0.898	0.697	0.977
Ce	2.75	3.42	3.37	2.38	3.43
Pb	0.192	0.223	0.246	0.177	0.233
Sr	58.7	60.7	73.3	68.7	60.6
Nd	3.7	4.57	4.76	3.13	4.72
Zr	33.6	41.1	43.3	25.7	42
Sm	1.58	1.97	1.99	1.34	2.04
Hf	1.05	1.341	1.376	0.874	1.367
Eu	0.649	0.777	0.804	0.555	0.809
Ti	5743	4305	5336	3951	3837
Gd	2.51	3.14	3.04	2.09	3.2
Dy	3.57	4.32	3.97	2.86	4.33
Er	2.51	3	2.63	1.9	2.89
Y	22.1	26.1	24	17.2	26.1
Yb	2.54	3.04	2.57	1.85	2.82
Sc	45.3	46.2	41.3	41.2	48.8

[a]Sample; 1 - 3R-1, Piece 24; 2 - 9R-1, Piece 24; 3 - 25R-1, Piece 11; 4 - 27R-1, Piece 15; 5 - 30R-1, Piece 8.

Appendix 3

Whole Rock, Phenocryst, and Melt Inclusion Analyses, Hole 504B

Contents

3.0 Sample identification

Samples are identified using the standard ODP format; Leg number-site-hole-core number-core type-section, and piece number, e.g., 148-504B-249R-1, Piece 2 is the second piece from the first 1.5 m section of core 249 (R indicates the core was obtained by rotary coring) of Hole 504B, drilled during Leg 148.

Individual phenocrysts and inclusions are identified as follows; grain mount-Phenocryst type-grain number-inclusion type-inclusion number, e.g., A26-PL15-GL is plagioclase grain 15, from grain mount 26, which hosts an analysed glass inclusion. Phenocryst types are abbreviated as follows; PL, plagioclase; CP, clinopyroxene; OL, olivine; and SP, spinel. Analyses of phenocrysts from thin sections are identified as follows; Ring-phenocryst type-phenocryst number, e.g., R9-pc1 is ring 9, phenocryst core 1. Abbreviations used are; pc, phenocryst core; pr, phenocryst rim; mp, microphenocrysts and quench crystallites.

Melt inclusions from homogenisation experiments are identified as follows; host phenocryst-experiment-inclusion, e.g., P115-5 is plagioclase experiment 115, inclusion number five.

Appendix 3.1, Major annd trace element compositions of chilled margins.

Sample	203R-1, 4-7 cm	203R-1, 33-36 cm	213R-1, 3-6 cm	219R-1, 7-11 cm	220R-1, 2-6 cm	222R-1, 9-12 cm	249R-1 92-98cm	222R-1, 100-104 cm
Depth(mbsf)	1749.1	1749.4	1812.5	1856.3	1865.5	1884.7	2072.1	1885.6
Major elements (wt.%)								
SiO_2	50.06	49.62	49.82	50.05	50.38	50.34	49.22	50.44
TiO_2	0.83	0.89	1.05	0.84	1.02	0.88	0.74	1.00
Al_2O_3	13.87	14.73	14.17	14.22	14.53	14.92	15.70	14.52
[a]Fe_2O_3	9.82	10.18	10.83	10.67	10.11	9.87	8.77	11.23
MnO	0.17	0.18	0.17	0.19	0.17	0.19	0.14	0.18
MgO	8.40	8.52	8.01	8.49	7.90	7.80	9.15	8.07
CaO	12.69	12.93	12.39	12.58	12.62	13.27	13.21	12.6
Na_2O	2.32	2.05	1.94	1.94	2.27	2.11	1.70	1.92
K_2O	0.02	0.01	0.01	0.01	0.02	0.008	<0.01	0.006
P_2O_5	0.08	0.09	0.10	0.08	0.09	0.06	0.04	0.06
L.O.I.	0.95	0.63	1.25	0.79	0.83	n/a	1.05	n/a
Total	99.21	99.83	99.74	99.86	99.95	99.43	99.72	100.03
[b]H_2O+	1.11	n/a	1.80	1.32	1.30	1.33	1.95	2.46
[b]CO_2	0.04	n/a	0.03	0.04	0.04	0.13	0.05	0.03
[b]Trace elements (ppm)								
Nb	-0.3	n/a	0.4	-0.3	0.6	n/a	<1	-0.3
Zr	44.3	n/a	54.6	38.6	51.8	n/a	46	48.7
Y	24.1	n/a	27.9	23.5	26.8	n/a	20	26.7
Sr	51.3	n/a	52.1	43.5	60.6	n/a	55	50.9
Rb	0.4	n/a	-0.4	-0.4	-0.4	n/a	3	-0.4
Zn	61.7	n/a	36.8	59.4	28.0	n/a	29	43.4
Cu	92.4	n/a	54.4	134.3	21.3	n/a	23	94.4
Ni	95.4	n/a	75.9	83.4	77.7	n/a	144	79.2
V	313	n/a	340	329	343	n/a	217	326
La	1.03	n/a	1.21	0.86	0.98	0.96	n/a	1.08
Ce	2.50	n/a	5.79	3.52	4.55	2.78	n/a	4.69
Nd	4.36	n/a	6.4	4.36	5.81	4.09	n/a	5.9
Sm	2.01	n/a	2.38	1.82	2.20	1.97	n/a	2.18
Eu	0.70	n/a	0.93	0.75	0.8	0.81	n/a	0.84
Tb	0.560	n/a	0.63	0.56	0.56	0.57	n/a	0.59
Ho	0.9	n/a	0.98	0.92	0.85	0.84	n/a	0.95
Yb	2.58	n/a	3.11	2.84	2.72	2.53	n/a	2.82
Lu	0.42	n/a	0.46	0.46	0.45	0.39	n/a	0.42
Cs	-0.50	n/a	0.64	-0.50	-0.50	1.03	n/a	0.70
Cr	356	n/a	155	190	204	248	265	191
Hf	1.55	n/a	1.27	1.15	1.64	1.3	n/a	1.55
Sc	42.3	n/a	40.8	41.1	40.7	39.8	34	41.7
Th	0.34	n/a	-0.2	0.2	0.36	0.48	n/a	-0.2
[c]Mg#	0.65	0.65	0.62	0.64	0.63	0.63	0.07	0.61
CaO/Na_2O	5.47	6.31	6.39	6.48	5.56	6.29	7.77	6.56

n/a = not analysed. -0.3 = below detection limit.

[a] All Fe as Fe_2O_3

[b] Values for H_2O, CO_2, Nb, Zr, Y, Sr, Rb, Zn, Cu, Ni, and V are from Shipboard Scientific Party (1992).

[c] Mg# = (Mg/(Mg + Fe)).

Appendix 3.2.1, Plagioclase analyses.

Sample	SiO_2	TiO_2	Al_2O_3	FeO	MgO	CaO	Na_2O	K_2O	SrO	BaO	Total	^aAn
140-504B-195R-1, Piece 3												
R1-Cp-pl	47.19	0.00	32.81	0.61	0.22	17.16	1.65	0.01	0.19	0.04	99.87	85.0
R1-mp	51.06	0.05	29.59	0.80	0.37	14.54	3.02	0.00	0.15	0.04	99.62	72.6
R2-CP-PL	49.33	0.00	31.45	0.49	0.20	15.52	2.59	0.00	0.15	0.06	99.78	76.7
R2-mp	51.66	0.00	29.22	1.06	0.49	13.76	3.29	0.01	0.20	0.03	99.72	69.8
R2-pc	48.81	0.03	31.31	0.53	0.27	16.03	2.26	0.01	0.19	0.01	99.45	79.6
R2-pr	47.62	0.00	31.82	0.56	0.28	16.29	1.86	0.00	0.16	0.06	98.64	82.8
R3-mp	52.23	0.08	28.26	1.12	0.40	13.56	3.58	0.01	0.18	0.05	99.45	67.6
R3-pc	51.17	0.07	29.62	0.77	0.37	14.35	3.10	0.01	0.15	0.02	99.62	71.9
R6-pc	47.58	0.06	32.08	0.58	0.25	16.68	1.89	0.01	0.16	0.06	99.35	82.9
R6-pc2	47.77	0.00	32.69	0.63	0.24	16.86	1.75	0.00	0.18	0.02	100.13	84.1
R6-pc3	51.00	0.03	29.96	0.86	0.31	14.28	3.06	0.02	0.20	0.04	99.75	72.0
R7-mp	50.80	0.02	29.93	0.81	0.32	14.81	3.02	0.01	0.19	0.00	99.92	73.0
R10-pc	47.29	0.00	32.46	0.52	0.26	17.11	1.73	0.00	0.18	0.06	99.61	84.4
R10-pr	47.23	0.01	32.65	0.50	0.20	17.37	1.64	0.01	0.19	0.05	99.86	85.3
R10-pc2	47.44	0.01	32.71	0.51	0.24	17.41	1.65	0.01	0.17	0.00	100.16	85.3
R10-pr2	47.50	0.00	32.35	0.53	0.22	17.55	1.79	0.00	0.12	0.06	100.13	84.3
R10-pc3	47.70	0.00	32.30	0.60	0.23	17.33	1.76	0.00	0.16	0.04	100.11	84.4
R10-pr3	46.60	0.00	32.78	0.55	0.22	17.54	1.43	0.00	0.19	0.03	99.33	87.1
R10-pc4	47.90	0.00	32.13	0.42	0.25	16.95	1.91	0.02	0.18	0.05	99.81	82.9
R10-pr4	46.64	0.00	32.67	0.54	0.24	17.52	1.56	0.01	0.15	0.06	99.39	86.0
R9-CP-PL	47.47	0.00	32.64	0.58	0.24	17.33	1.71	0.00	0.20	0.00	100.17	84.8
R9-pc	47.27	0.00	32.09	0.62	0.23	16.94	1.94	0.02	0.19	0.04	99.37	82.6
R9-pc2	47.18	0.00	32.40	0.55	0.22	17.29	1.65	0.01	0.17	0.00	99.47	85.2
R9-pr2	48.10	0.00	32.15	0.58	0.26	16.88	2.01	0.01	0.17	0.08	100.24	82.2
R8-mp	51.42	0.05	29.08	0.97	0.48	14.51	3.07	0.01	0.18	0.04	99.81	72.2
R12-pc	48.08	0.00	31.85	0.54	0.24	16.45	2.00	0.01	0.15	0.06	99.37	81.9
R12-mp	50.72	0.00	29.71	0.76	0.38	14.72	2.92	0.02	0.19	0.04	99.46	73.4
140-504B-213R-1, Piece 22												
PL1	46.71		33.59	0.41	0.27	17.38	1.59	0.01			99.97	85.8
PL2	48.64		31.89	0.50	0.32	15.84	2.40	0.01			99.60	78.5
PL3	48.64		31.89	0.45	0.31	15.84	2.47	0.01			99.61	78.0
PL4	47.44		33.18	0.36	0.27	16.80	1.93	0.00			99.98	82.8
PL5	50.13		30.75	0.66	0.33	14.81	2.90	0.03			99.61	73.8
PL6	46.85		33.23	0.48	0.26	17.34	1.74	0.01			99.91	84.6
PL7	48.66		32.32	0.37	0.27	16.00	2.23	0.01			99.87	79.8
PL8	47.30		33.05	0.36	0.25	16.91	1.83	0.02			99.74	83.6
PL9	46.83		33.10	0.45	0.26	17.16	1.70	0.02			99.52	84.8
PL10	46.73		32.94	0.33	0.25	16.87	1.83	0.01			98.96	83.6
PL11	45.87		33.95	0.48	0.22	17.90	1.30	0.00			99.72	88.4
PL12	49.08		31.90	0.40	0.32	15.59	2.47	0.01			99.77	77.7
PL13	45.42		34.11	0.40	0.19	18.23	1.19	0.01			99.54	89.5
PL14	45.37		34.43	0.44	0.43	17.94	1.09	0.00			99.70	90.1
PL15	46.85		32.98	0.47	0.25	17.15	1.78	0.00			99.49	84.2
PL16	51.28		29.60	0.84	0.22	13.45	3.48	0.01			98.87	68.1
PL18	47.77		32.69	0.42	0.29	16.78	1.92	0.02			99.89	82.9
PL19	46.48		33.29	0.30	0.23	17.59	1.55	0.01			99.44	86.3
PL20	45.42		34.30	0.36	0.21	18.30	1.06	0.00			99.64	90.5
PL21	46.19		29.64	0.48	0.24	14.93	2.33	0.01			93.82	78.0
PL22	51.58		29.67	0.88	0.21	13.28	3.71	0.03			99.36	66.4
PL23	46.18		33.43	0.59	0.16	17.35	1.58	0.01			99.30	85.8
PL24	48.70		31.88	0.59	0.24	15.70	2.49	0.02			99.62	77.7
PL25	64.49		22.54	0.02	0.00	3.30	9.07	0.04			99.46	16.8
PL26	54.37		28.67	0.38	0.13	10.92	4.77	0.20			99.43	55.9
PL27	49.89		30.71	0.73	0.24	14.66	3.04	0.01			99.28	72.7
PL28	67.14		21.54	0.05	0.00	2.02	9.67	0.04			100.47	10.4
PL29	46.55		33.42	0.50	0.19	17.13	1.65	0.02			99.46	85.2
PL31	46.49		33.37	0.48	0.25	17.31	1.59	0.01			99.51	85.7
PL32	46.77		33.20	0.47	0.23	17.32	1.68	0.01			99.67	85.1
PL33	47.38		32.74	0.44	0.28	16.83	1.94	0.01			99.62	82.8
PL34	52.64		29.18	0.86	0.21	12.74	4.06	0.02			99.72	63.5
PL35	46.11		33.30	0.45	0.24	17.62	1.45	0.00			99.16	87.1
PL35/1	45.99		33.87	0.40	0.23	17.90	1.33	0.01			99.72	88.1
PL37	45.90		33.98	0.44	0.21	17.96	1.27	0.01			99.76	88.6
PL39	48.37		32.32	0.42	0.22	15.72	2.34	0.02			99.41	78.8
PL40	45.57		34.02	0.33	0.28	18.14	1.25	0.01			99.60	88.9
PL41	47.01		33.39	0.39	0.24	17.09	1.76	0.01			99.89	84.3
PL42	48.87		30.56	0.49	0.12	16.80	2.52	0.01			99.38	78.7
PL43	45.50		34.29	0.37	0.25	18.24	1.15	0.01			99.81	89.8
PL44	48.51		31.74	0.50	0.32	15.79	2.33	0.02			99.21	78.9
PL45	47.73		32.99	0.46	0.21	16.80	1.89	0.01			100.09	83.1
PL46	46.10		34.19	0.43	0.23	17.80	1.36	0.02			100.14	87.9
PL47	48.36		32.36	0.45	0.29	16.27	2.10	0.01			99.84	81.1
PL48	47.40		33.15	0.38	0.24	16.86	1.81	0.02			99.85	83.7
PL49	46.72		33.62	0.45	0.23	17.54	1.44	0.02			100.03	87.0
PL50	48.77		32.20	0.41	0.31	16.10	2.25	0.00			100.04	79.8
PL51	47.32		32.54	0.47	0.29	16.71	1.97	0.01			99.31	82.4
PL52	48.23		32.83	0.39	0.26	16.41	2.04	0.02			100.17	81.6
PL53	46.97		32.80	0.43	0.27	16.96	1.86	0.00			99.30	83.5
PL54	46.83		33.23	0.40	0.25	17.30	1.73	0.01			99.75	84.6
PL55	46.26		33.75	0.57	0.18	17.71	1.51	0.01			99.99	86.7
PL56	46.47		33.32	0.37	0.27	17.35	1.62	0.00			99.40	85.6
PL57	45.66		34.42	0.39	0.31	18.24	1.13	0.00			100.14	90.0
PL58	46.57		33.61	0.48	0.25	17.39	1.54	0.00			99.84	86.2
PL59	45.71		34.15	0.38	0.18	18.02	1.26	0.01			99.71	88.8
PL60	45.28		34.34	0.37	0.20	18.24	1.01	0.01			99.44	90.9
PL61	45.63		34.01	0.44	0.24	17.97	1.21	0.02			99.52	89.1
PL62	47.04		33.18	0.52	0.22	16.95	1.80	0.00			99.71	83.9
PL63	47.15		33.10	0.39	0.22	16.78	1.81	0.01			99.47	83.6
PL64	46.15		33.59	0.33	0.25	17.41	1.57	0.01			99.31	85.9
PL66	46.74		32.86	0.46	0.26	17.00	1.73	0.02			99.08	84.4
PL67	48.84		31.57	0.55	0.32	15.47	2.52	0.01			99.27	77.3
PL68	44.97		34.60	0.30	0.24	18.16	1.02	0.02			99.32	90.8

Appendix 3.2.1, continued

Sample	SiO_2	TiO_2	Al_2O_3	FeO	MgO	CaO	Na_2O	K_2O	SrO	BaO	Total	^aAn
PL69	47.33		33.23	0.41	0.28	16.84	1.83	0.01			99.93	83.6
PL70	47.31		33.07	0.39	0.25	17.13	1.90	0.01			100.06	83.3
PL71	47.88		32.64	0.44	0.27	16.52	2.09	0.02			99.86	81.4
PL72	45.58		34.65	0.47	0.18	18.20	1.16	0.01			100.25	89.6
PL74	45.53		33.91	0.40	0.24	17.86	1.34	0.00			99.28	88.0
PL75	48.35		31.94	0.46	0.31	15.95	2.25	0.01			99.27	79.7
PL76	49.74		30.86	0.64	0.27	14.94	2.87	0.01			99.33	74.2
PL77	48.59		31.45	0.47	0.33	15.70	2.52	0.00			99.06	77.5
PL78	47.23		33.05	0.35	0.24	16.67	1.94	0.02			99.49	82.6
PL79	45.94		33.43	0.54	0.25	17.67	1.54	0.02			99.38	86.4
PL80	48.92		31.92	0.50	0.30	15.86	2.46	0.00			99.96	78.1
PL81	48.04		32.49	0.44	0.32	16.35	2.10	0.00			99.74	81.1
PL82	46.93		32.80	0.36	0.24	16.79	1.86	0.01			98.99	83.3
PL83	45.23		34.34	0.38	0.23	18.14	1.08	0.01			99.41	90.3
PL84	45.29		33.84	0.43	0.21	17.85	1.29	0.00			98.92	88.4
PL87	53.61		2.81	2.79	16.89	20.99	1.53	0.01			98.61	88.4
PL88	45.22		34.69	0.33	0.23	18.30	1.01	0.01			99.79	91.0
PL89	46.07		33.78	0.42	0.25	17.85	1.37	0.00			99.75	87.8
PL90	46.38		33.31	0.34	0.30	17.67	1.47	0.00			99.47	86.9
PL91	47.56		32.75	0.44	0.25	16.50	2.06	0.00			99.56	81.6
PL92	46.57		33.60	0.41	0.31	17.39	1.62	0.01			99.92	85.6
PL94	48.09		32.21	0.45	0.26	16.18	2.16	0.01			99.36	80.5
PL95	46.51		33.50	0.45	0.23	17.46	1.56	0.00			99.70	86.1
PL97	49.27		31.17	0.53	0.31	15.41	2.67	0.02			99.37	76.1
PL98	48.47		32.03	0.53	0.32	15.82	2.40	0.01			99.58	78.4
PL100	46.58		33.24	0.47	0.26	17.05	1.72	0.01			99.32	84.6
PL101	47.81		32.42	0.45	0.28	16.28	2.09	0.02			99.35	81.1
PL102	48.88		31.74	0.49	0.33	15.51	2.53	0.01			99.48	77.2
PL103	46.50		33.38	0.45	0.23	17.28	1.58	0.01			99.43	85.8
PL104	48.78		31.95	0.44	0.33	15.93	2.39	0.00			99.82	78.7
PL105	45.88		33.92	0.38	0.23	17.81	1.37	0.01			99.59	87.8
PL107	45.31		34.38	0.46	0.20	18.32	1.16	0.01			99.84	89.7
PL108	47.43		33.07	0.44	0.29	16.70	1.88	0.00			99.81	83.0
PL109	49.62		31.86	0.52	0.34	15.52	2.58	0.02			100.46	76.9
PL110	48.56		32.39	0.45	0.32	16.15	2.26	0.01			100.13	79.8
PL111	48.86		31.77	0.48	0.31	15.66	2.50	0.01			99.60	77.6
PL112	49.29		31.72	0.56	0.30	15.49	2.55	0.01			99.92	77.1
PL113	45.39		34.34	0.35	0.25	18.22	1.12	0.00			99.66	90.0
PL114	46.35		33.75	0.44	0.23	17.52	1.54	0.01			99.84	86.3
PL115	45.49		34.55	0.39	0.20	18.43	1.17	0.00			100.24	89.7
PL116	50.63		30.47	0.59	0.28	14.35	3.12	0.03			99.46	71.8
PL117	46.58		33.46	0.49	0.23	17.34	1.61	0.01			99.71	85.6
PL118	46.55		33.15	0.35	0.35	17.36	1.56	0.00			99.32	86.0
PL119	45.24		34.12	0.39	0.19	18.13	1.20	0.01			99.28	89.3
PL120	45.72		34.01	0.32	0.23	17.63	1.40	0.01			99.31	87.4
PL121	50.82		30.26	0.78	0.26	14.02	3.33	0.00			99.47	70.0
PL122	45.35		34.18	0.44	0.25	18.13	1.12	0.01			99.49	89.9

Sample	SiO_2	TiO_2	Al_2O_3	FeO	MgO	CaO	Na_2O	K_2O	SrO	BaO	Total	^aAn
PL123	47.31		33.07	0.42	0.28	16.77	1.82	0.02			99.69	83.6
PL124	46.12		33.90	0.38	0.24	17.65	1.46	0.03			99.78	87.0
PL125	46.09		34.17	0.54	0.22	17.89	1.36	0.01			100.27	87.9
PL1-SP	46.48		34.44	0.59	0.17	17.30	1.48	0.00			100.45	86.6
PL64a-SP	46.00		34.04	0.50	0.18	17.81	1.30	0.01			99.84	88.4
PL42-SP	48.06		33.15	0.44	0.26	16.71	1.92	0.00			100.55	82.8
PL4-SP	51.02		30.26	0.80	0.25	14.06	3.33	0.01			99.74	70.0
PL1-SP	51.54		29.25	0.24	0.18	13.95	2.45	0.01			97.62	75.9
PL2-SP	46.64		33.17	0.53	0.27	17.15	1.70	0.01			99.48	84.8
140-504B-222R-1, Piece 1												
PL1	46.34		32.80	0.40	0.23	16.90	1.57	0.00			98.24	85.6
PL2	46.06		33.81	0.44	0.19	17.66	1.31	0.01			99.47	88.2
PL3	46.36		33.02	0.40	0.22	17.30	1.47	0.00			98.77	86.7
PL4	46.81		32.58	0.50	0.23	17.02	1.62	0.00			98.75	85.3
PL5	46.48		33.18	0.44	0.21	17.18	1.56	0.00			99.06	85.9
PL6-SP	45.32		33.40	0.42	0.19	17.81	1.24	0.00			98.38	88.8
PL7	46.46		32.57	0.45	0.23	16.81	1.66	0.00			98.19	84.9
PL8	46.21		32.94	0.48	0.23	17.27	1.56	0.01			98.70	86.0
CP9-PL	46.99		32.77	0.44	0.24	16.90	1.74	0.01			99.10	84.3
PL13	47.95		32.47	0.48	0.25	16.26	2.10	0.00			99.52	81.1
PL13-1	45.25		33.81	0.40	0.18	18.20	1.10	0.00			98.94	90.2
PL16	46.19		33.29	0.41	0.20	17.63	1.39	0.01			99.11	87.5
PL17	45.70		34.19	0.37	0.17	17.69	1.20	0.00			99.31	89.1
PL18	45.34		33.83	0.39	0.18	17.94	1.18	0.01			98.87	89.4
PL19	46.14		33.32	0.44	0.23	17.50	1.43	0.01			99.06	87.1
PL20	45.72		33.73	0.45	0.21	17.79	1.27	0.00			99.16	88.6
PL22	46.02		33.73	0.41	0.21	17.43	1.40	0.00			99.22	87.3
PL23	46.49		32.94	0.44	0.23	17.05	1.51	0.01			98.67	86.2
PL24	45.50		33.81	0.37	0.17	17.81	1.19	0.00			98.84	89.2
PL25	47.38		32.08	0.46	0.28	16.55	1.88	0.01			98.63	82.9
CP28-PL	46.52		32.87	0.53	0.24	16.93	1.64	0.01			98.74	85.1
CP29-PL	47.03		32.86	0.44	0.24	16.88	1.64	0.00			99.09	85.1
CP35-PL	45.68		33.31	0.49	0.21	17.77	1.30	0.00			98.76	88.3
CP36-PL	48.01		32.10	0.50	0.28	16.14	2.02	0.01			99.05	81.5
PL38	47.49		32.67	0.42	0.26	16.60	1.83	0.00			99.26	83.4
PL39	46.11		33.58	0.42	0.22	17.61	1.33	0.00			99.27	88.0
PL40	46.75		33.14	0.48	0.22	17.20	1.57	0.01			99.36	85.8
PL41	46.54		33.35	0.37	0.21	17.53	1.47	0.00			99.48	86.8
PL42	46.00		33.78	0.41	0.21	17.68	1.25	0.01			99.35	88.6
PL43	46.85		32.84	0.47	0.23	16.79	1.62	0.00			98.80	85.2
PL44	48.15		31.38	0.55	0.20	15.81	1.73	0.01			97.84	83.5
PL45	50.23		30.33	0.58	0.24	14.40	2.97	0.00			98.75	72.9
PL47	46.73		33.31	0.46	0.24	17.02	1.59	0.00			99.35	85.6
CP46-PL1	47.12		32.43	0.55	0.27	16.60	1.93	0.00			98.91	82.6
CP46-PL2	47.29		32.45	0.52	0.25	16.40	1.86	0.00			98.77	83.0
PL48	49.51		31.13	0.53	0.25	14.92	2.70	0.00			99.03	75.3

Appendix 3.2.1, Pcontinued

Sample	SiO_2	TiO_2	Al_2O_3	FeO	MgO	CaO	Na_2O	K_2O	SrO	BaO	Total	^aAn
PL49	48.42		31.98	0.42	0.27	15.92	2.08	0.00			99.09	80.9
PL61-SP	45.61		34.34	0.45	0.18	18.16	1.14	0.00			99.88	89.8
PL78-SP	45.81		34.11	0.53	0.22	17.80	1.26	0.00			99.73	88.7
PL60	46.27		33.56	0.47	0.21	17.14	1.37	0.00			99.02	87.4
PL62	46.42		33.43	0.42	0.24	17.11	1.45	0.01			99.08	86.7
PL63	45.86		34.01	0.39	0.21	17.82	1.18	0.01			99.48	89.3
PL64	46.52		33.45	0.42	0.23	17.11	1.48	0.01			99.22	86.5
PL65	46.71		33.72	0.43	0.23	17.24	1.41	0.00			99.74	87.1
PL66	46.91		33.05	0.45	0.24	16.61	1.70	0.01			98.97	84.4
PL67	46.08		34.02	0.40	0.22	17.51	1.28	0.00			99.51	88.3
PL69	46.27		33.73	0.37	0.20	17.43	1.38	0.01			99.39	87.5
PL70	46.49		33.27	0.43	0.23	16.91	1.64	0.01			98.98	85.1
PL71	46.17		33.53	0.39	0.21	17.33	1.44	0.01			99.08	86.9
PL72	46.52		33.09	0.40	0.23	16.95	1.45	0.01			98.65	86.6
PL73	47.00		32.91	0.47	0.24	16.68	1.70	0.01			99.01	84.4
PL74	46.77		33.35	0.42	0.23	16.89	1.57	0.00			99.23	85.6
PL75	50.71		30.70	0.56	0.24	14.18	3.02	0.00			99.41	72.2
PL76	45.86		34.03	0.33	0.20	17.70	1.21	0.01			99.34	89.0
PL77	46.81		33.37	0.41	0.24	16.92	1.51	0.01			99.27	86.1
PL78	45.89		33.91	0.42	0.20	17.61	1.23	0.01			99.27	88.8
PL79	46.24		33.88	0.37	0.21	17.52	1.28	0.00			99.50	88.3
PL80	46.72		33.41	0.39	0.23	17.14	1.50	0.00			99.39	86.3
PL81	45.92		33.33	0.45	0.21	17.34	1.42	0.01			98.68	87.1
PL82	46.72		33.35	0.43	0.23	17.41	1.47	0.00			99.61	86.8
PL83	46.60		33.26	0.45	0.23	17.13	1.60	0.00			99.27	85.5
PL84	45.59		33.36	0.42	0.20	17.66	1.25	0.01			98.49	88.7
PL85	47.81		32.82	0.44	0.25	16.46	1.84	0.00			99.62	83.2
PL86	46.95		32.99	0.46	0.24	17.05	1.61	0.01			99.31	85.4
PL88	47.01		33.14	0.41	0.23	17.02	1.61	0.01			99.43	85.4
PL89	46.20		33.76	0.42	0.21	17.58	1.26	0.01			99.44	88.5
PL92	45.77		33.99	0.42	0.19	17.65	1.27	0.01			99.30	88.5
PL93	45.77		33.81	0.43	0.20	17.68	1.24	0.01			99.14	88.7
PL94	46.32		33.45	0.37	0.22	17.34	1.43	0.01			99.14	87.0
PL96	47.06		33.00	0.41	0.22	16.70	1.65	0.01			99.05	84.8
PL97	45.76		33.59	0.39	0.20	17.59	1.25	0.00			98.78	88.6
PL98	51.55		29.59	0.89	0.13	13.21	3.57	0.02			98.96	67.2
R3-pr	47.65	0.01	32.45	0.48	0.25	16.53	1.74	0.00	0.18	0.02	99.38	83.9
R3-pc	47.07	0.03	32.68	0.51	0.25	17.40	1.54	0.00	0.17	0.02	99.70	86.2
R3-pr2	47.89	0.02	31.78	0.53	0.29	16.62	1.98	0.01	0.19	0.00	99.35	82.2
R3-pc2	46.58	0.03	33.00	0.45	0.22	17.36	1.44	0.01	0.16	0.03	99.30	86.9
R3-pr3	47.88	0.04	32.10	0.59	0.26	16.62	1.81	0.00	0.18	0.02	99.52	83.5
R3 -pc3	47.99	0.02	31.81	0.51	0.25	16.52	1.91	0.02	0.18	0.00	99.24	82.6
R4-pc1	46.78	0.00	32.50	0.42	0.21	17.13	1.59	0.00	0.18	0.06	98.96	85.6
R4-pr1	47.17	0.04	32.70	0.45	0.23	17.11	1.61	0.00	0.19	0.00	99.49	85.4
R4-pc2	46.63	0.00	33.32	0.49	0.17	17.78	1.38	0.01	0.15	0.00	99.94	87.6
R4-pr2	46.86	0.03	32.61	0.52	0.24	16.83	1.60	0.00	0.16	0.00	98.85	85.3
R5-CP-pr1	46.22	0.01	32.78	0.46	0.20	17.67	1.32	0.00	0.14	0.04	98.86	88.0
R5-CP-pc1	46.43	0.02	32.77	0.46	0.19	17.61	1.39	0.01	0.18	0.00	99.13	87.4
R5-CP-pc	48.21	0.02	31.60	0.44	0.25	16.75	2.04	0.00	0.14	0.00	99.46	81.9
R6-CP-pr1	47.03	0.03	32.19	0.54	0.25	17.36	1.74	0.02	0.19	0.00	99.36	84.5
R6-CP-pc1	48.13	0.04	31.45	0.54	0.26	16.58	2.12	0.00	0.18	0.01	99.31	81.2
R7-pr1	46.43	0.02	32.77	0.46	0.19	17.61	1.39	0.01	0.18	0.00	99.13	87.4
R7-pc1	45.75	0.04	33.27	0.43	0.18	17.86	1.24	0.01	0.19	0.00	99.00	88.8
R7-mp	48.21	0.02	31.60	0.44	0.25	16.75	2.04	0.00	0.14	0.00	99.46	81.9
R8-pr1	47.03	0.03	32.19	0.54	0.25	17.36	1.74	0.02	0.19	0.00	99.36	84.5
R8-pc1	48.13	0.04	31.45	0.54	0.26	16.58	2.12	0.00	0.18	0.01	99.31	81.2
R9-pr	49.36	0.03	30.78	0.57	0.28	15.43	2.46	0.01	0.18	0.00	99.08	77.5
R9-pc	47.68	0.02	32.47	0.58	0.24	16.53	1.84	0.01	0.16	0.00	99.56	83.2
R9-pr2	47.93	0.02	32.05	0.42	0.26	16.74	1.95	0.02	0.13	0.04	99.58	82.4
R9pc2	47.69	0.00	32.34	0.49	0.25	16.66	1.86	0.00	0.15	0.02	99.48	83.2
R9-pr3	46.51	0.03	33.03	0.53	0.19	17.30	1.39	0.00	0.17	0.04	99.22	87.3
R9-pc3	47.05	0.05	32.67	0.46	0.21	17.12	1.55	0.00	0.18	0.00	99.33	85.9
R3-mp	50.52	0.02	30.12	0.61	0.31	14.92	3.01	0.00	0.20	0.01	99.75	73.3
R3-mp2	47.76	0.03	31.76	0.59	0.33	17.40	1.89	0.00	0.18	0.01	99.95	83.6
R3-mp3	49.59	0.04	31.18	0.50	0.27	15.73	2.61	0.00	0.21	0.01	100.19	76.9
R3-mp4	49.13	0.04	31.53	0.47	0.22	16.27	2.49	0.02	0.20	0.00	100.37	78.2
R7-mp1	50.67	0.06	29.63	0.79	0.41	14.63	3.09	0.01	0.16	0.00	99.48	72.3
R7-mp2	47.70	0.03	32.15	0.65	0.27	16.84	1.93	0.01	0.16	0.00	99.82	82.8
R7-mp3	47.69	0.05	31.58	0.60	0.22	16.46	2.19	0.02	0.17	0.00	98.98	80.5
R8-mp1	50.66	0.03	30.22	0.72	0.33	14.76	3.08	0.00	0.17	0.02	100.06	72.6
R8-mp2	51.69	0.08	29.27	0.92	0.31	14.00	3.32	0.01	0.16	0.01	99.88	69.9
R8-mp3	47.67	0.03	32.02	0.67	0.26	16.36	2.05	0.01	0.18	0.00	99.32	81.5
R9-CP-pc1	48.03	0.01	31.86	0.45	0.24	16.83	1.91	0.00	0.17	0.03	99.52	83.0
R9-CP-pc2	48.87	0.04	31.45	0.47	0.26	16.12	2.20	0.02	0.15	0.00	99.60	80.1
R9-pc2	46.81	0.00	32.78	0.59	0.27	17.45	1.65	0.00	0.22	0.00	99.83	85.4
R9-pc3	47.13	0.00	32.68	0.65	0.24	17.73	1.67	0.00	0.17	0.00	100.29	85.4
R9-pc4	46.60	0.02	32.80	0.55	0.25	17.98	1.56	0.00			99.77	86.5
R9-mp	50.74	0.06	29.64	0.85	0.41	14.75	3.07	0.00	0.19	0.09	99.81	72.5
R9-mp2	50.50	0.10	27.19	1.58	1.89	14.63	2.85	0.00	0.17	0.00	98.92	73.9
R4-mp	47.47	0.00	29.70	0.66	0.27	15.46	2.64	0.01	0.21	0.04	96.52	76.3
R15-mp	49.92	0.00	28.80	0.77	0.39	14.18	3.16	0.00	0.16	0.00	97.40	71.3
R15-mp2	57.91	0.00	25.88	0.49	0.16	9.09	6.54	0.04	0.21	0.06	100.37	43.3
R15-mp3	48.96	0.02	28.23	0.76	0.35	14.28	2.96	0.00	0.19	0.06	95.81	72.6
R11-OL-pc	45.18	0.00	31.61	0.53	0.22	17.34	1.49	0.01	0.19	0.04	96.63	86.5
R11-OL-pc	45.66	0.00	31.53	0.51	0.23	17.17	1.55	0.02	0.14	0.06	96.88	85.8
R15OL-pc	46.04	0.00	31.59	0.50	0.23	16.39	1.69	0.00	0.19	0.04	96.67	84.3
R15-pc2	45.62	0.00	31.31	0.54	0.23	16.56	1.63	0.00	0.13	0.06	96.09	84.8
PL-R3-SP	47.07	32.68	0.51	0.25	17.40	1.54	0.00	99.45	86.2			
140-504B-249R-1, Piece 28												
R1-pc1	46.10	0.00	33.58	0.38	0.21	17.64	1.43	0.01	0.03	0.10	99.48	87.1
R1-pr1	46.76	0.00	33.53	0.61	0.16	17.58	1.58	0.01	0.25	0.00	100.48	86.0
R1-pc2	48.21	0.07	32.52	0.58	0.28	16.53	2.04	0.02	0.19	0.00	100.44	81.7
R1-pr2	47.20	0.05	32.69	0.73	0.30	16.95	1.80	0.00	0.24	0.02	99.98	83.9
R3-Ol-Pl	47.11	0.03	32.70	0.91	0.75	17.12	1.64	0.02	0.26	0.02	100.56	85.1

Appendix 3.2.1, continued

Sample	SiO_2	TiO_2	Al_2O_3	FeO	MgO	CaO	Na_2O	K_2O	SrO	BaO	Total	^aAn
R2-pc	48.18	0.09	32.44	0.43	0.31	16.44	2.07	0.02	0.17	0.03	100.18	81.4
R2-pr	46.89	0.07	33.48	0.42	0.19	17.49	1.64	0.02	0.15	0.00	100.35	85.4
R2-pc2	48.45	0.00	32.18	0.52	0.26	16.38	2.13	0.00	0.24	0.02	100.18	80.9
R2-pr2	48.06	0.10	31.11	1.58	1.14	16.16	2.33	0.00	0.17	0.06	100.71	79.3
R3-CP-PL	47.88	0.02	32.69	0.48	0.26	16.81	2.08	0.04	0.14	0.00	100.40	81.5
R6-pr	47.91	0.02	32.02	0.58	0.27	16.67	2.12	0.00	0.15	0.08	99.82	81.3
R6-pc	46.42	0.03	34.19	0.61	0.18	17.98	1.39	0.00	0.23	0.00	101.03	87.7
R7-pc	46.77	0.00	33.66	0.47	0.26	17.38	1.67	0.02	0.22	0.01	100.46	85.1
R7-pr	46.58	0.03	34.09	0.62	0.25	17.73	1.60	0.03	0.33	0.00	101.26	85.9
R7-CP-pc	48.08	0.05	32.44	0.55	0.27	16.50	2.16	0.02	0.24	0.00	100.31	80.8
R7-CP-pr	47.39	0.00	33.43	0.46	0.26	17.23	1.75	0.02	0.20	0.01	100.75	84.4
CP-pc10	46.29	0.00	33.65	0.45	0.19	18.06	1.35	0.02	0.14	0.00	100.15	87.9
R7-pc11	47.08	0.00	33.40	0.51	0.21	17.44	1.44	0.04	0.19	0.03	100.34	86.8
R7-pr11	47.22	0.00	33.24	0.62	0.23	17.01	1.83	0.01	0.15	0.15	100.46	83.6
R8-pc	48.35	0.10	32.24	0.53	0.28	16.40	2.17	0.03	0.14	0.00	100.24	80.5
R8-pr	48.41	0.00	31.78	0.88	0.46	16.23	2.16	0.02	0.13	0.12	100.19	80.5
R9-pc	46.26	0.00	34.02	0.63	0.25	17.87	1.32	0.03	0.11	0.03	100.52	88.0
R10-pc	47.37	0.00	33.13	0.38	0.19	16.84	1.80	0.00	0.22	0.17	100.10	83.8
R10-pr	46.82	0.04	33.33	0.62	0.27	17.59	1.54	0.04	0.19	0.00	100.44	86.1
R11-Ol-pc	46.05	0.00	34.48	0.65	0.18	18.37	1.23	0.00	0.15	0.00	101.11	89.2
R11-Ol-pr	46.37	0.01	34.31	0.65	0.14	18.28	1.24	0.01	0.13	0.00	101.14	89.0
148-504B-249R-1, Piece 30												
PL1	45.54		33.91	0.36	0.19	18.00	1.27	0.01			99.27	88.7
PL2	45.48		34.30	0.39	0.23	18.02	1.05	0.00			99.48	90.5
PL3-SP	45.11		34.29	0.37	0.23	18.12	1.10	0.00			99.21	90.1
PL4	46.79		32.68	0.36	0.24	16.80	1.76	0.01			98.63	84.1
PL5	46.62		33.02	0.44	0.23	17.15	1.66	0.00			99.12	85.1
PL6	46.77		32.95	0.42	0.23	17.01	1.66	0.00			99.05	85.0
PL7	46.47		33.15	0.41	0.23	17.23	1.54	0.01			99.05	86.1
PL8-SP	45.60		33.83	0.36	0.20	17.81	1.23	0.00			99.03	88.9
PL9	46.84		32.62	0.37	0.24	16.84	1.78	0.01			98.69	83.9
PL10	48.60		31.24	0.49	0.29	15.67	2.38	0.00			98.67	78.4
PL11	46.46		33.34	0.43	0.24	17.13	1.56	0.01			99.15	85.9
PL12	46.76		33.00	0.46	0.25	17.05	1.66	0.02			99.19	85.0
PL13-SP1	46.27		33.34	0.42	0.23	17.19	1.40	0.00			98.86	87.2
PL13-SP2	45.98		33.39	0.42	0.22	17.67	1.38	0.01			99.07	87.6
PL14	48.33		31.95	0.40	0.30	15.87	2.16	0.00			99.01	80.2
PL15	46.41		32.94	0.44	0.25	17.16	1.57	0.00			98.77	85.8
PL16	46.70		32.93	0.44	0.24	17.01	1.63	0.00			98.96	85.2
PL17	46.24		33.16	0.39	0.26	17.25	1.54	0.00			98.84	86.1
PL18	49.13		31.46	0.43	0.30	15.41	2.48	0.01			99.22	77.5
PL19	45.01		33.89	0.42	0.18	18.12	1.08	0.00			98.70	90.2
PL20	46.44		33.42	0.45	0.19	17.32	1.56	0.00			99.39	86.0
PL21	46.11		33.82	0.38	0.20	17.59	1.38	0.00			99.48	87.6
PL22	45.95		33.52	0.32	0.21	17.54	1.47	0.00			99.02	86.8
PL23	46.83		32.99	0.38	0.23	17.06	1.64	0.00			99.14	85.2
PL24	45.97		33.46	0.39	0.20	17.37	1.39	0.00			98.77	87.4
PL25	46.52		33.30	0.40	0.23	17.32	1.53	0.01			99.31	86.2
PL26	47.11		32.89	0.41	0.27	17.07	1.72	0.01			99.48	84.6
PL27	49.73		31.16	0.48	0.30	15.20	2.66	0.00			99.53	75.9
PL28	47.34		32.68	0.41	0.27	16.52	1.89	0.01			99.12	82.9
PL29	47.36		32.39	0.41	0.25	16.57	1.91	0.00			98.88	82.7
PL30	45.00		34.19	0.41	0.18	18.27	0.99	0.00			99.04	91.1
PL31	47.25		32.63	0.37	0.22	16.44	1.91	0.01			98.82	82.6
PL32	45.79		33.76	0.28	0.19	17.62	1.35	0.00			98.99	87.8
PL33	45.12		34.22	0.34	0.24	18.11	1.06	0.00			99.09	90.4
PL34	46.40		33.32	0.38	0.23	17.31	1.54	0.00			99.17	86.1
PL35	46.26		33.38	0.41	0.22	17.43	1.50	0.01			99.20	86.6
PL36	45.98		33.67	0.31	0.20	17.71	1.40	0.02			99.30	87.5
PL37	47.40		32.59	0.46	0.23	16.52	1.96	0.00			99.17	82.3
PL38	46.21		33.71	0.42	0.23	17.60	1.37	0.01			99.55	87.7
PL39	45.93		34.00	0.42	0.21	17.84	1.31	0.01			99.72	88.3
PL40	45.30		33.94	0.28	0.25	18.20	1.14	0.00			99.10	89.8
PL41	46.00		33.19	0.36	0.21	17.24	1.53	0.00			98.53	86.2
PL42	46.49		33.28	0.38	0.26	17.36	1.55	0.00			99.32	86.1
PL43	46.43		32.90	0.38	0.26	17.23	1.56	0.00			98.76	85.9
PL44	46.35		33.52	0.44	0.23	17.62	1.41	0.00			99.58	87.4
PL45	46.41		33.19	0.40	0.23	17.18	1.59	0.00			98.99	85.7
PL52	46.01		33.11	0.41	0.23	17.34	1.47	0.01			98.57	86.7
PL53	48.25		31.88	0.40	0.38	16.07	2.05	0.00			99.04	81.3
PL54	46.60		33.07	0.37	0.25	17.06	1.57	0.01			98.93	85.8
PL55	45.69		33.60	0.37	0.23	17.57	1.34	0.00			98.80	87.9
PL57	45.52		33.76	0.49	0.20	17.92	1.26	0.01			99.16	88.7
PL59	45.99		32.90	0.56	0.41	17.19	1.45	0.01			98.51	86.7
PL60	46.40		33.50	0.43	0.22	17.41	1.45	0.02			99.43	86.9
PL61	46.12		33.22	0.40	0.25	17.43	1.50	0.01			98.92	86.5
PL62	44.76		34.47	0.40	0.15	18.38	0.91	0.01			99.08	91.8
PL63	45.71		33.80	0.41	0.23	17.66	1.34	0.00			99.15	87.9
PL64	45.89		33.17	0.43	0.23	17.27	1.48	0.01			98.49	86.6
PL66	49.68		30.96	0.50	0.36	15.05	2.72	0.02			99.28	75.4
PL67	46.47		33.51	0.38	0.22	17.27	1.60	0.01			99.45	85.7
PL68	46.11		33.27	0.35	0.23	17.08	1.50	0.01			98.54	86.3
PL69	46.28		33.31	0.45	0.23	17.35	1.53	0.00			99.15	86.3
PL70	46.58		33.07	0.38	0.23	16.88	1.62	0.00			98.76	85.2
PL71	46.99		33.13	0.42	0.25	17.06	1.66	0.00			99.51	85.0
PL72	46.72		33.17	0.42	0.25	16.92	1.72	0.00			99.20	84.4
PL73	46.49		32.93	0.44	0.25	16.62	1.66	0.00			98.39	84.7
PL74	46.87		32.77	0.39	0.24	16.75	1.73	0.02			98.77	84.2
PL75	46.82		32.96	0.42	0.26	16.94	1.71	0.00			99.11	84.6
PL76	47.42		32.61	0.43	0.28	16.83	1.88	0.02			99.47	83.2
PL77	46.80		33.46	0.42	0.26	17.40	1.54	0.00			99.87	86.2
PL78	47.19		33.04	0.42	0.26	16.78	1.78	0.00			99.48	83.9
PL79	46.43		33.50	0.42	0.23	17.57	1.40	0.00			99.56	87.4

Appendix 3.2.1, continued

Sample	SiO_2	TiO_2	Al_2O_3	FeO	MgO	CaO	Na_2O	K_2O	SrO	BaO	Total	^aAn
PL80	45.89		33.14	0.34	0.23	17.37	1.43	0.01			98.40	87.0
CP1-PL	46.82		33.48	0.56	0.25	17.26	1.61	0.02			100.00	85.5
CP2-PL	50.29		31.06	0.69	0.31	14.66	2.92	0.02			99.95	73.5
CP3-PL	48.49		31.92	0.56	0.30	15.88	2.32	0.02			99.48	79.1
CP4-PL	51.14		30.26	1.02	0.18	13.82	3.32	0.03			99.76	69.7
CP5-PL	46.60		33.38	0.52	0.25	17.32	1.58	0.04			99.68	85.8
CP6-PL	47.91		32.74	0.56	0.27	16.56	1.97	0.01			100.02	82.3
CP7-PL	47.01		33.45	0.59	0.24	17.39	1.59	0.02			100.30	85.8
CP8-PL	46.99		32.65	0.59	0.26	17.14	1.73	0.01			99.38	84.6
CP9-PL	51.82		29.28	1.09	0.23	13.44	3.64	0.02			99.52	67.1
CP10-PL	45.98		33.54	0.59	0.21	17.84	1.32	0.01			99.50	88.2
CP11-PL	46.35		33.51	0.46	0.24	17.48	1.41	0.02			99.46	87.2
CP11-PLa	46.81		33.33	0.58	0.22	17.25	1.54	0.01			99.74	86.1
CP12-PL	46.91		33.14	0.55	0.25	17.02	1.66	0.02			99.55	85.0
CP12-PLa	47.28		32.33	0.47	0.22	16.31	2.02	0.02			98.65	81.7
CP13-PL	46.91		33.20	0.56	0.21	17.09	1.62	0.00			99.59	85.4
CP14-PL	46.87		33.66	0.57	0.26	17.34	1.56	0.02			100.28	86.0
CP15-PL	48.03		32.66	0.56	0.26	16.53	1.85	0.03			99.93	83.1
CP16-PL	46.63		33.87	0.63	0.22	17.76	1.43	0.00			100.54	87.3
148-504B-249R-1, Piece 38												
PL1	45.99		33.68	0.36	0.22	17.68	1.41	0.01			99.35	87.4
PL2	46.93		32.93	0.44	0.24	17.14	1.69	0.00			99.37	84.9
PL3	49.81		30.15	0.60	0.29	14.48	3.07	0.02			98.42	72.3
PL4	46.62		32.99	0.41	0.25	17.19	1.59	0.01			99.06	85.7
PL5	46.05		33.28	0.36	0.22	17.56	1.44	0.01			98.91	87.1
PL6	46.08		33.21	0.39	0.23	17.82	1.40	0.00			99.12	87.6
PL7	48.10		31.44	0.45	0.30	15.83	2.23	0.01			98.36	79.7
PL8	46.48		33.00	0.40	0.23	17.12	1.63	0.01			98.87	85.3
PL9	46.01		33.17	0.39	0.25	17.50	1.45	0.00			98.77	87.0
PL10	46.39		32.88	0.36	0.22	16.94	1.68	0.01			98.46	84.8
PL11	46.18		33.26	0.38	0.23	17.36	1.54	0.01			98.95	86.2
PL12	49.18		30.81	0.48	0.36	15.02	2.69	0.01			98.55	75.5
PL11	46.46		33.34	0.43	0.24	17.13	1.56	0.01			99.15	85.9
PL12	46.76		33.00	0.46	0.25	17.05	1.66	0.02			99.19	85.0
PL14	46.09		33.42	0.42	0.24	17.60	1.42	0.00			99.19	87.2
PL15	47.82		32.33	0.37	0.25	16.32	2.05	0.01			99.14	81.5
PL16	45.94		33.28	0.37	0.22	17.31	1.46	0.00			98.59	86.8
PL17	46.01		33.28	0.50	0.26	17.38	1.46	0.01			98.88	86.8
PL18	46.06		33.29	0.37	0.23	17.54	1.45	0.00			98.94	87.0
PL19	48.06		32.52	0.36	0.29	16.43	2.08	0.01			99.75	81.3
PL20	45.99		33.40	0.40	0.23	17.37	1.45	0.00			98.85	86.9
PL21	46.30		33.07	0.47	0.23	17.32	1.54	0.01			98.94	86.1
PL22	46.64		32.79	0.41	0.27	17.15	1.66	0.00			98.92	85.1
PL23	48.10		32.13	0.41	0.30	15.99	2.17	0.01			99.11	80.3
PL24	48.59		31.01	0.38	0.31	15.45	2.38	0.01			98.14	78.2
PL25	47.07		32.36	0.42	0.26	16.77	1.91	0.02			98.81	82.9
PL26	46.56		32.91	0.43	0.24	16.93	1.67	0.01			98.75	84.9
PL27	46.43		33.25	0.36	0.23	17.17	1.54	0.01			98.99	86.1
PL28	45.11		34.37	0.33	0.17	18.29	1.09	0.01			99.37	90.3
PL29	48.78		31.29	0.40	0.29	15.33	2.38	0.02			98.49	78.1
PL30	46.07		33.15	0.41	0.22	17.27	1.55	0.01			98.67	86.1
PL31	48.90		31.21	0.47	0.31	15.32	2.56	0.01			98.77	76.8
PL32	46.97		32.55	0.36	0.26	16.77	1.78	0.00			98.70	83.9
PL33	46.25		33.20	0.41	0.21	17.44	1.51	0.01			99.04	86.4
PL34	46.50		32.87	0.43	0.26	17.28	1.59	0.00			98.92	85.8
PL35	45.95		33.11	0.39	0.22	17.54	1.49	0.00			98.70	86.7
PL36	46.20		32.54	0.41	0.25	17.06	1.65	0.00			98.11	85.1
PL37	46.57		32.54	0.42	0.24	16.87	1.76	0.02			98.42	84.2
PL38	52.24		28.70	0.81	0.15	12.80	3.98	0.01			98.69	64.0
PL39-SP	47.20		32.77	0.48	0.23	16.69	1.88	0.00			99.25	83.1
PL40	47.91		32.04	0.37	0.25	16.19	2.06	0.00			98.82	81.3
PL41	45.78		33.46	0.35	0.20	17.53	1.38	0.00			98.71	87.5
PL42	46.59		32.63	0.44	0.22	16.91	1.77	0.02			98.58	84.1
PL43	46.14		33.10	0.36	0.23	17.34	1.55	0.00			98.72	86.0
PL44	45.56		33.58	0.42	0.21	17.77	1.31	0.00			98.85	88.2
PL46	46.46		32.59	0.41	0.24	17.11	1.60	0.01			98.41	85.6
PL47	46.41		33.09	0.46	0.24	17.17	1.59	0.01			98.96	85.6
PL48	45.68		32.96	0.44	0.20	17.49	1.54	0.00			98.31	86.3
PL49	46.62		31.88	0.39	0.26	16.36	1.93	0.00			97.45	82.4
PL50	46.83		32.48	0.38	0.26	16.76	1.84	0.01			98.56	83.4
PL51	47.27		32.48	0.35	0.27	16.53	1.92	0.01			98.82	82.6
PL52	47.82		32.02	0.41	0.29	16.13	2.12	0.01			98.81	80.8
PL53	51.36		29.60	0.72	0.17	13.46	3.63	0.02			98.97	67.2
PL54	46.58		32.77	0.43	0.26	17.02	1.68	0.00			98.74	84.9
PL55	47.32		32.14	0.42	0.26	16.37	2.01	0.00			98.53	81.8
PL56	49.06		30.98	0.48	0.38	15.37	2.51	0.02			98.80	77.2
PL57	46.27		32.93	0.38	0.24	17.01	1.63	0.02			98.48	85.2
PL58	50.91		29.89	0.46	0.28	13.99	3.32	0.02			98.85	69.9
PL59-SP	47.60		31.92	0.38	0.25	16.09	2.15	0.01			98.40	80.5
PL60	47.63		32.22	0.40	0.28	16.56	1.98	0.02			99.09	82.2
PL61	46.92		32.80	0.41	0.26	16.88	1.77	0.00			99.03	84.1
PL62	50.30		30.46	0.63	0.32	14.21	3.04	0.02			98.97	72.1
PL63	47.62		32.18	0.45	0.29	16.58	1.96	0.01			99.09	82.4
PL64	46.97		32.74	0.39	0.24	16.59	1.84	0.00			98.77	83.3
PL65	47.66		31.99	0.42	0.28	16.18	2.13	0.00			98.67	80.8
PL66	47.67		32.16	0.42	0.27	16.25	1.98	0.01			98.76	81.9
PL67	46.01		33.58	0.40	0.25	17.49	1.48	0.01			99.22	86.7
PL68	47.13		32.72	0.40	0.27	16.85	1.78	0.02			99.16	84.0
PL70	45.91		33.17	0.38	0.23	17.28	1.48	0.02			98.46	86.6
PL71	46.50		32.84	0.38	0.23	16.99	1.55	0.02			98.50	85.8
PL72	46.71		32.26	0.54	0.34	16.49	1.84	0.00			98.19	83.2
PL73	46.00		33.33	0.53	0.31	17.33	1.45	0.02			98.95	86.9
PL74	45.14		33.74	0.40	0.20	17.90	1.21	0.01			98.60	89.1

Appendix 3.2.1, continued.

Sample	SiO_2	TiO_2	Al_2O_3	FeO	MgO	CaO	Na_2O	K_2O	SrO	BaO	Total	^aAn
PL75	46.13		33.37	0.36	0.22	17.53	1.42	0.01			99.04	87.2
PL76	46.88		32.82	0.40	0.26	16.77	1.79	0.02			98.94	83.8
PL77-SP	47.03		32.65	0.48	0.21	16.88	1.85	0.01			99.11	83.4
PL78	46.31		33.11	0.43	0.25	17.33	1.53	0.01			98.97	86.2
PL79	46.78		32.83	0.48	0.24	16.96	1.68	0.01			98.98	84.8
PL80	46.64		33.03	0.42	0.27	17.04	1.63	0.01			99.03	85.3
PL81	46.44		33.37	0.37	0.22	17.33	1.54	0.01			99.26	86.2
PL82	45.86		33.48	0.41	0.20	17.53	1.37	0.00			98.86	87.6
PL83	45.85		33.69	0.36	0.22	17.60	1.35	0.00			99.08	87.8
PL84	46.51		33.24	0.38	0.25	17.06	1.55	0.01			98.99	85.9
PL85	46.24		33.02	0.43	0.23	17.20	1.59	0.00			98.72	85.6

^{a}An = 100 x (Ca/(Ca + Na)).

Appendix 3.2.2, Clinopyroxene analyses.

Sample	SiO_2	TiO_2	Al_2O_3	^aFeO	MnO	MgO	CaO	Na_2O	Cr_2O_3	Total	$^bMg\#$
140-504B-195R-1, Piece 3											
R1-pc	53.14	0.22	2.07	5.65	0.16	18.80	18.59	0.18	0.31	99.11	85.6
R1-pr	52.95	0.24	2.10	5.30	0.23	18.48	19.46	0.16	0.33	99.24	86.1
R1-mp	51.85	0.40	3.46	5.78	0.25	17.37	20.23	0.19	0.46	99.98	84.3
R2-pc	52.40	0.26	2.76	4.65	0.22	17.99	20.62	0.18	0.78	99.86	87.3
R2-pr	53.65	0.22	2.01	5.70	0.15	19.21	18.44	0.16	0.29	99.83	85.7
R2-pc2	52.46	0.33	2.86	5.44	0.18	18.25	19.65	0.17	0.45	99.78	85.7
R2-mp	51.72	0.47	3.46	6.52	0.25	17.85	18.63	0.16	0.45	99.51	83.0
R2-mp	50.69	0.83	4.69	6.62	0.24	16.69	19.96	0.20	0.17	100.07	81.8
R3-pc	53.42	0.26	2.02	5.53	0.15	19.28	18.83	0.18	0.44	100.12	86.1
R3-pr	52.83	0.29	2.61	5.08	0.16	17.91	20.14	0.16	0.49	99.68	86.3
R3-mp	50.97	0.70	4.67	6.53	0.18	17.03	19.40	0.22	0.38	100.09	82.3
R3-mp	52.03	0.55	3.65	6.20	0.15	17.69	18.84	0.15	0.31	99.58	83.6
R4-pc	53.27	0.25	2.37	5.08	0.19	18.62	19.76	0.16	0.39	100.10	86.7
R4-pr	52.75	0.27	2.55	5.07	0.13	18.05	20.28	0.20	0.52	99.83	86.4
R5-pc	53.24	0.23	2.32	5.49	0.17	18.35	19.30	0.18	0.45	99.73	85.6
R5-pr	53.35	0.29	2.41	5.12	0.14	18.26	20.46	0.16	0.41	100.59	86.4
R6-pc	52.77	0.27	2.65	5.02	0.21	18.32	19.81	0.20	0.53	99.78	86.7
R6-pr	52.68	0.29	2.67	5.63	0.15	18.37	19.20	0.18	0.58	99.75	85.3
R6-pc2	52.52	0.28	2.58	5.07	0.20	18.14	198.86	0.17	0.53	278.36	86.4
R6-pr2	52.42	0.43	3.39	7.72	0.33	19.96	15.50	0.13	0.21	100.08	82.2
R6-mp	50.27	0.83	4.57	7.43	0.15	15.88	19.86	0.18	0.11	99.28	79.2
R7-pc	53.15	0.21	2.41	5.67	0.26	19.40	18.03	0.17	0.73	100.03	85.9
R7-pr	52.45	0.33	3.03	5.43	0.22	17.85	19.78	0.18	0.55	99.82	85.4
R7-mp	51.47	0.48	3.87	6.09	0.20	17.10	19.62	0.17	0.37	99.37	83.3
R9-pc	53.15	0.20	2.17	5.20	0.15	18.79	19.19	0.14	0.45	99.44	86.6
R9-pr	52.43	0.29	2.46	5.51	0.12	18.34	19.62	0.15	0.48	99.40	85.6
R8-pc	52.90	0.24	2.32	4.93	0.22	18.12	20.01	0.17	0.48	99.39	86.8
R8-pr	52.69	0.27	2.53	4.91	0.15	17.77	20.43	0.16	0.55	99.47	86.6
R12-pc	52.93	0.32	2.71	5.23	0.15	18.51	20.07	0.18	0.60	100.71	86.3
R12-pr	53.11	0.28	2.52	5.05	0.18	18.28	19.83	0.18	0.62	100.04	86.6
R12-mp	52.16	0.47	3.62	7.45	0.31	19.68	16.15	0.16	0.34	100.35	82.5
R12-mp	50.16	0.87	5.24	9.44	0.25	16.86	16.26	0.20	0.05	99.33	76.1
R12-mp2	51.69	0.48	3.73	6.47	0.23	16.84	19.40	0.21	0.29	99.33	82.3
140-504B-222R-1, Piece 1											
CP7A	51.78	0.24	2.63	4.79	0.09	17.98	19.85	0.19	0.79	98.33	87.0
CP9-PL	51.42	0.28	3.37	4.54	0.12	17.76	19.97	0.20	1.22	98.88	87.5
CP10	51.88	0.25	3.14	5.15	0.14	18.25	19.25	0.19	0.64	98.88	86.3
CP11	51.84	0.28	3.07	4.79	0.12	17.86	19.60	0.21	0.83	98.59	86.9
CP12	51.88	0.28	3.23	4.72	0.05	17.96	19.83	0.18	0.91	99.05	87.1
CP14	51.21	0.27	3.49	4.66	0.15	17.67	19.62	0.22	1.15	98.43	87.1
CP15	52.48	0.23	2.27	4.85	0.13	18.81	19.34	0.17	0.52	98.80	87.4
CP16	51.63	0.21	3.33	4.45	0.11	17.78	20.16	0.20	1.20	99.06	87.7
CP27	51.69	0.32	3.42	4.97	0.10	18.00	19.37	0.19	0.86	98.94	86.6
CP28-PL	51.94	0.28	2.96	4.74	0.15	17.89	19.91	0.21	0.79	98.87	87.1
CP29-PL	51.66	0.24	3.09	4.64	0.11	18.07	19.82	0.18	0.91	98.71	87.4
CP30	51.85	0.25	3.03	4.65	0.16	17.94	19.62	0.21	0.95	98.66	87.3
CP31	52.01	0.24	2.89	4.72	0.22	17.86	19.91	0.22	0.78	98.87	87.1
CP32	51.51	0.27	3.20	4.61	0.07	17.74	19.81	0.21	0.99	98.42	87.3

Appendix 3.2.2, continued

Sample	SiO_2	TiO_2	Al_2O_3	[a]FeO	MnO	MgO	CaO	Na_2O	Cr_2O_3	Total	[b]Mg#
CP33	51.59	0.29	3.33	4.64	0.07	17.72	19.81	0.21	1.04	98.68	87.2
CP34	51.53	0.28	3.38	4.42	0.22	17.63	19.96	0.21	1.23	98.85	87.7
CP35-PL	51.32	0.26	3.37	4.96	0.07	18.25	18.84	0.21	0.98	98.26	86.8
CP36-PL	51.65	0.26	3.42	4.51	0.11	17.63	19.91	0.19	1.17	98.85	87.5
CP37	51.39	0.28	3.41	4.93	0.17	17.91	19.50	0.21	0.86	98.67	86.6
CP45-1	51.80	0.24	2.96	4.53	0.15	17.94	19.78	0.21	0.95	98.56	87.6
CP46-PL	51.75	0.25	2.97	5.57	0.22	19.15	17.93	0.19	0.65	98.69	86.0
R5-pr	52.02	0.35	2.68	4.98	0.21	17.78	20.73	0.22	0.68	99.65	86.4
R5-pc	51.59	0.34	3.24	5.60	0.12	17.37	20.25	0.21	0.83	99.55	84.7
R6-pr	52.37	0.33	2.79	5.02	0.14	18.34	20.01	0.21	0.69	99.91	86.7
R6-pc	52.32	0.30	2.88	5.21	0.23	18.63	19.14	0.19	0.66	99.55	86.4
R8-pr	51.99	0.28	2.99	4.71	0.17	17.74	21.19	0.21	1.04	100.34	87.0
R8-pc	51.91	0.25	2.91	4.65	0.24	18.12	20.20	0.19	1.14	99.61	87.4
R3-pc	52.27	0.25	2.74	4.66	0.20	18.04	21.17	0.21	0.80	100.36	87.3
R3-pc2	51.31	0.50	3.83	6.39	0.18	18.47	17.77	0.17	0.46	99.10	83.7
R3-pr3	52.22	0.26	2.77	4.58	0.15	17.76	20.81	0.19	0.82	99.56	87.4
R3-pc3	51.91	0.28	2.83	4.65	0.19	17.84	20.95	0.21	0.71	99.57	87.2
R4-p1	53.09	0.33	1.89	5.79	0.24	18.14	19.90	0.19	0.32	99.89	84.8
R4-pc	52.34	0.19	2.34	4.92	0.12	18.23	20.14	0.19	0.65	99.12	86.9
R8-pr	51.79	0.23	2.90	4.59	0.15	17.62	21.16	0.18	0.96	99.59	87.3
R8-pc	51.73	0.25	3.06	4.50	0.13	17.57	21.00	0.19	0.99	99.42	87.4
R9-pc	52.79	0.25	2.29	4.85	0.14	18.47	20.25	0.19	0.48	99.72	87.2
R9-pc2	52.63	0.21	2.34	4.73	0.11	18.54	20.20	0.20	0.58	99.55	87.5
pc1	52.13	0.25	2.93	4.47	0.21	17.75	21.20	0.23	0.92	100.09	87.6
pc2	51.23	0.56	4.45	6.22	0.20	17.81	18.38	0.19	0.80	99.84	83.6
R16-pc	52.02	0.29	3.36	4.80	0.15	17.72	20.70	0.22	0.93	100.21	86.8
R16-pr	52.62	0.28	2.75	4.57	0.12	17.52	20.73	0.21	0.84	99.65	87.2
R10-pc	52.25	0.29	3.11	4.56	0.15	17.67	20.83	0.19	1.05	100.13	87.4
R10-pr	52.56	0.23	2.88	4.50	0.16	17.57	21.15	0.21	0.93	100.18	87.4
pc3	52.38	0.29	3.35	4.60	0.11	17.61	20.75	0.23	0.99	100.33	87.2
mp1	53.02	0.41	2.91	6.76	0.18	19.69	16.62	0.19	0.41	100.19	83.9
R1-pc	51.78	0.25	2.74	4.44	0.15	17.07	20.87	0.20	0.81	98.33	87.3
R1-pr	51.53	0.29	2.72	4.88	0.16	17.18	20.90	0.20	0.74	98.62	86.3
R2-pr	51.84	0.27	2.53	4.83	0.13	17.46	20.41	0.18	0.50	98.18	86.6
R3-pc	50.93	0.29	3.14	4.77	0.12	17.20	20.15	0.19	0.82	97.62	86.5
R7-mp	50.68	0.53	3.94	6.47	0.22	17.98	17.62	0.22	0.53	98.20	83.2
R7-mp2	50.33	0.65	4.55	6.48	0.12	17.50	17.77	0.22	0.60	98.23	82.8
R8-pc	51.83	0.23	2.80	4.78	0.18	17.86	20.42	0.22	0.70	99.04	86.9
R8-mp	48.82	0.86	2.45	15.00	0.38	11.98	17.90	0.19	0.00	97.58	58.7
R11-pc	51.48	0.29	2.85	4.53	0.15	17.40	20.66	0.22	0.90	98.49	87.3
R12-mp	51.45	0.63	3.14	6.60	0.20	18.02	18.14	0.18	0.41	98.78	83.0
R13-mp	50.48	0.64	4.14	6.99	0.19	18.42	17.08	0.20	0.38	98.54	82.4
R15-mp	50.35	0.61	4.95	6.54	0.22	16.57	18.39	0.26	0.31	98.22	81.9
R15-mp2	50.42	0.34	3.51	7.43	0.23	18.31	16.22	0.17	0.30	96.97	81.5
140-504B-213R-1, Piece 22											
A21-CP87	53.38	0.21	3.07	2.56	0.00	16.53	20.06	1.63	1.40	98.84	92.0
A21-CP4	51.44	0.42	3.23	6.81	0.17	17.35	19.29	0.19	0.23	99.14	82.0
A21-CP17	51.56	0.41	3.45	5.55	0.14	17.38	20.15	0.18	0.43	99.25	84.8
A21-CP36	50.67	0.43	3.78	5.99	0.26	17.13	19.51	0.20	0.55	98.52	83.6
A21-CP65	52.08	0.35	2.84	6.16	0.22	18.12	19.05	0.20	0.30	99.31	84.0
A21-CP73	50.99	0.48	3.19	7.44	0.27	17.44	18.72	0.18	0.21	98.91	80.7
A21-CP99	50.96	0.42	3.96	5.84	0.17	17.24	19.33	0.22	0.62	98.76	84.0
148-504B-249R-1, Piece 28											
CP-R1-pc	51.96	0.31	3.15	4.36	0.12	17.36	20.87	0.21	1.12	99.46	87.7
CP-R1-pr	50.92	0.29	3.35	4.47	0.17	17.05	21.05	0.20	1.32	98.82	87.2
CP-R2-pc1	52.63	0.24	2.30	5.21	0.21	19.14	18.55	0.18	0.58	99.04	86.8
CP-R2-pc2	52.57	0.19	2.58	5.13	0.24	18.62	19.39	0.17	0.64	99.53	86.6
CP-R2-pc3	51.50	0.28	3.40	5.20	0.21	18.48	19.29	0.21	0.94	99.51	86.4
CP-R2-pc4	51.62	0.30	3.38	4.60	0.12	17.51	20.37	0.20	1.01	99.11	87.2
CP-R2-pr1	52.19	0.24	2.80	4.32	0.22	17.64	21.04	0.18	0.78	99.41	87.9
CP-R2-pr2	52.12	0.25	2.86	4.56	0.15	17.55	21.17	0.21	0.95	99.82	87.3
CP-R2-pr3	51.83	0.21	3.00	4.43	0.14	17.42	21.09	0.19	0.94	99.25	87.5
CP-R3-PL	51.86	0.28	3.35	4.96	0.20	18.30	19.18	0.19	1.00	99.32	86.8
CP-R3-pr1	51.59	0.27	3.32	4.75	0.21	17.33	20.67	0.19	0.90	99.23	86.7
CP-R3-pr2	51.95	0.23	3.01	4.56	0.20	17.98	20.74	0.17	0.88	99.72	87.6
CP-R4	52.45	0.28	2.99	4.50	0.15	17.23	20.87	0.21	0.98	99.66	87.2
CP-R4-pc1	51.66	0.29	3.29	4.58	0.14	17.47	20.76	0.22	1.08	99.49	87.2

Appendix 3.2.2, continued

Sample	SiO_2	TiO_2	Al_2O_3	[a]FeO	MnO	MgO	CaO	Na_2O	Cr_2O_3	Total	[b]Mg#
CP-R4-pc2	51.35	0.31	3.33	4.45	0.06	17.30	21.15	0.18	1.19	99.32	87.4
CP-R4-pc3	51.37	0.29	3.36	4.49	0.13	17.35	21.24	0.19	1.10	99.52	87.3
CP-R4-pr1	51.80	0.24	3.08	4.60	0.07	17.67	21.12	0.20	0.87	99.65	87.3
CP-R5	51.97	0.26	2.43	4.79	0.17	17.84	21.01	0.19	0.52	99.18	86.9
CP-R5-pc1	51.06	0.33	3.64	4.77	0.19	17.52	20.09	0.21	1.01	98.82	86.8
CP-R5-pr1	51.57	0.26	3.08	4.46	0.14	17.34	21.06	0.19	1.11	99.21	87.4
CP-R6-pc1	51.15	0.28	3.68	4.88	0.19	17.77	20.11	0.19	1.17	99.42	86.7
CP-R6-pc2	51.78	0.31	3.44	5.11	0.18	17.35	20.11	0.20	0.79	99.27	85.8
CP-R6-pc3	51.47	0.31	3.08	4.95	0.16	17.22	20.93	0.19	0.67	98.98	86.1
CP-R6-pr1	51.91	0.31	3.00	4.42	0.09	17.53	20.71	0.21	0.99	99.17	87.6
CP-R6-pr2	51.78	0.31	3.09	4.76	0.20	17.70	20.45	0.19	0.80	99.28	86.9
CP-R6-pr3	51.82	0.28	3.10	5.23	0.15	17.98	19.48	0.19	0.73	98.96	86.0
CP-R7-PLpc10	52.25	0.26	2.98	4.47	0.15	17.82	20.90	0.20	0.92	99.95	87.7
CP-R7-PLpc9	51.87	0.31	3.38	4.69	0.14	17.64	20.41	0.20	0.86	99.50	87.0
CP-R7-PLpr10	52.25	0.26	2.98	4.47	0.15	17.82	20.90	0.20	0.92	99.95	87.7
CP-R7-pr1	51.74	0.27	3.31	4.52	0.07	16.97	21.42	0.19	1.06	99.55	87.0
CP-R7-pr2	52.03	0.24	2.99	4.51	0.15	17.84	20.84	0.21	0.80	99.61	87.6
148-504B-249R-1, Piece 30											
A17-CP1-PL	51.99	0.20	3.08	4.38	0.13	17.90	20.11	0.20	1.03	99.03	87.9
A17-CP2-PL	50.77	0.41	4.35	5.27	0.24	17.42	19.34	0.21	0.65	98.67	85.5
A17-CP3-PL	51.96	0.25	3.42	4.47	0.19	17.73	19.98	0.20	1.19	99.38	87.6
A17-CP4-PL	51.60	0.23	3.13	4.40	0.13	17.65	20.23	0.19	0.97	98.53	87.7
A17-CP5-PL	51.43	0.25	3.70	4.69	0.23	17.61	19.41	0.21	1.23	98.74	87.0
A17-CP6-PL	51.36	0.30	3.55	4.79	0.17	17.61	19.61	0.25	1.03	98.65	86.8
A17-CP7-PL	52.53	0.22	2.54	4.58	0.18	18.23	19.86	0.23	0.90	99.28	87.6
A17-CP8-PL	51.41	0.26	3.35	4.32	0.24	17.36	20.21	0.19	1.18	98.53	87.7
A17-CP9-PL	52.41	0.23	2.77	4.87	0.13	18.55	19.04	0.20	0.77	98.96	87.2
A17-CP10-PL	51.65	0.24	3.46	4.45	0.00	17.68	20.02	0.20	1.18	98.87	87.6
A17-CP11-PL	51.44	0.27	3.46	4.79	0.16	18.01	19.28	0.20	1.18	98.78	87.0
A17-CP11-PLa	51.27	0.23	3.28	4.60	0.22	17.83	19.10	0.22	1.06	97.82	87.4
A17-CP12-PL	51.67	0.27	3.14	4.27	0.15	17.84	20.19	0.19	1.07	98.79	88.2
A17-CP12-PLa	51.26	0.25	3.22	4.33	0.15	17.52	20.22	0.23	1.17	98.35	87.8
A17-CP13-PL	52.05	0.22	2.88	4.53	0.13	17.94	20.11	0.19	0.94	98.97	87.6
A17-CP13-PLa	52.15	0.19	2.65	4.54	0.08	18.10	19.99	0.21	0.82	98.73	87.7
A17-CP14-PL	52.34	0.21	2.79	4.34	0.18	18.02	20.22	0.21	0.94	99.25	88.1
A17-CP15-PL	52.14	0.22	2.54	4.44	0.05	17.99	20.13	0.20	0.84	98.55	87.8
A17-CP16-PL	51.67	0.25	3.55	4.68	0.08	18.08	19.61	0.22	1.24	99.37	87.3

[a]All Fe as FeO.

[b]Mg# = 100 x (Mg/(Mg + Fe)).

Appendix 3.2.3, Olivine analyses.

Sample	SiO_2	FeO	MnO	MgO	CaO	NiO	Cr_2O_3	Total	[a]Fo
140-504B-222R-1, Piece 1									
R9-mp	39.34	14.31	0.24	44.38	0.31	0.11	0.04	98.73	84.7
R9-mp2	39.42	14.04	0.24	44.40	0.38	0.14	0.03	98.62	84.9
R6-mp2	39.96	13.97	0.26	44.84	0.35	0.07	0.07	99.45	85.1
R6-mp3	39.52	15.36	0.29	44.10	0.36	0.23	0.02	99.86	83.7
R6-mp1	39.54	15.82	0.37	43.62	0.46	0.10	0.01	99.91	83.1
oR6-mp1	40.05	13.99	0.27	44.61	0.33	0.23	0.05	99.48	85.0
oR6-mp2	39.94	13.83	0.30	44.78	0.35	0.07	0.08	99.27	85.2
R1-pc	39.82	13.49	0.29	45.80	0.31	0.14	0.06	99.85	85.8
R1-pr	39.78	13.56	0.28	45.58	0.36	0.22	0.01	99.78	85.7
R1-pr3	39.94	13.53	0.28	45.70	0.34	0.15	0.03	99.94	85.8
148-504B-249R-1, Piece 28									
R1-pc	39.69	12.99	0.24	45.79	0.31	0.16	0.03	99.21	86.3
R1-pr	39.66	13.93	0.29	44.97	0.31	0.20	0.01	99.37	85.2
R1-pc2	39.79	12.89	0.21	46.17	0.31	0.26	0.03	99.66	86.5
R1-pr2	39.70	12.83	0.28	45.68	0.36	0.19	0.08	99.12	86.4
R1-pc3	39.85	12.83	0.26	46.11	0.33	0.22	0.05	99.65	86.5
R1-pr3	39.90	13.07	0.21	45.73	0.37	0.16	0.12	99.56	86.2
R6-pc1	39.90	13.36	0.18	45.69	0.33	0.14	0.02	99.62	85.9
R6-pr1	39.92	13.33	0.30	45.34	0.33	0.20	0.00	99.42	85.8
R6-pc2	39.51	13.28	0.32	45.35	0.31	0.12	0.05	98.94	85.9
R6-pr2	39.39	14.28	0.26	44.07	0.33	0.20	0.00	98.53	84.6
R7-pc	39.88	12.99	0.23	45.45	0.35	0.22	0.08	99.20	86.2

Appendix 3.2.3, continued

Sample	SiO_2	FeO	MnO	MgO	CaO	NiO	Cr_2O_3	Total	^aFo
R7-pr	39.33	14.68	0.26	43.91	0.35	0.17	0.03	98.73	84.2
R8-mp	39.87	13.60	0.25	44.92	0.32	0.14	0.03	99.13	85.5
R9-pc	40.04	13.07	0.23	45.47	0.33	0.14	0.02	99.30	86.1
R9-pr	39.80	13.31	0.29	45.28	0.34	0.21	0.02	99.25	85.8
R10-pc	39.57	12.79	0.16	46.02	0.32	0.21	0.06	99.13	86.5
R10-pr	40.03	14.09	0.30	45.23	0.34	0.22	0.03	100.24	85.1
R10-pc2	40.24	12.82	0.21	46.25	0.29	0.17	0.00	99.98	86.5
R10-pr2	40.08	13.81	0.19	44.81	0.33	0.17	0.08	99.47	85.3

$^aFo = 100 \times (Mg/Mg + Fe)$.

Appendix 3.2.4, Spinel analyses.

Sample	SiO_2	TiO_2	Al_2O_3	$^aFe_2O_3$	FeO	MnO	MgO	Cr_2O_3	NiO	ZnO	Total
140-504B-213R-1, Piece 22											
PL1-SP	0.13	0.20	40.38	5.81	11.59	0.20	17.57	24.58	0.19	0.07	100.72
PL64-SP	0.16	0.19	39.27	4.33	11.05	0.23	17.39	25.65	0.16	0.04	98.46
PL42-SP	0.07	0.40	27.98	6.45	13.08	0.19	15.34	36.64	0.12	0.10	100.38
A24-PL1-SP	0.23	0.16	26.82	7.65	16.59	0.41	12.96	36.49	0.10	0.25	101.66
140-504B-222R-1, Piece 1											
PL6-SP	0.06	0.33	24.37	6.75	15.01	0.18	13.57	39.26	0.05	0.09	99.67
PL61-SP	0.07	0.30	22.25	7.07	14.72	0.17	13.55	41.53	0.08	0.08	99.82
PL78-SP	0.08	0.62	20.50	7.84	16.34	0.24	12.35	41.15	0.09	0.05	99.27
PL-SP	0.04	0.31	30.30	6.02	13.51	0.25	14.83	33.45	0.05		98.99
148-504B-249R-1, Piece 30											
PL3-SP	0.06	0.35	24.54	5.92	10.71	0.19	16.35	41.21	0.10	0.07	99.50
PL8-SP	0.06	0.37	25.54	6.63	12.58	0.14	15.38	39.12	0.08	0.07	99.97
PL13-SP1	0.10	0.38	24.98	6.24	12.70	0.16	15.25	39.79	0.08	0.02	99.71
PL13-SP2	0.08	0.36	25.13	6.38	12.53	0.17	15.35	39.73	0.08	0.07	99.88
148-504B-249R-1, Piece 38											
PL39-SP	0.06	0.38	25.74	7.66	16.31	0.17	12.74	35.75	0.11	0.02	98.94
PL77-SP	0.06	0.42	25.93	7.94	16.31	0.19	12.90	35.91	0.11	0.13	99.89

$^aFe_2O_3$ calculated from stoichiometry.

Appendix 3.3, Homogenised melt inclusions in plagioclase affected by overheating, analytical overlap or poor quenching (see text for details).

Sample	SiO_2	TiO_2	Al_2O_3	[a]FeO	MnO	MgO	CaO	Na_2O	K_2O	P_2O_5	Cr_2O_3	total	CaO/Na_2O	[b]Host An	[c]T_h (°C)	[d]T_{ol}	[e]T_{pl}	[f]T_{corr}	[g]Comments
140-504B-213R-1, Piece 22																			
P131-2	51.03	0.27	16.20	8.05	0.12	9.42	13.06	2.06	0.04	0.00	0.04	100.30	6.3	89.0	1220	1221	1202	1214	Poorly quenched
P131-8	50.46	0.46	15.68	8.10	0.19	9.17	13.33	2.20	0.03	0.00	0.05	99.68	6.1	90.6	1220	1217	1197	1208	Poorly quenched
P134-1	49.08	0.89	15.01	8.89	0.12	8.58	13.15	2.53	0.02	0.01	0.08	98.36	5.2	83.7	1215	1210	1193	1203	Overheated and poorly quenched
P134-2	51.60	0.62	15.78	8.09	0.13	8.18	12.98	1.80	0.01	0.03	0.06	99.29	7.2	82.4	1215	1185	1197	1201	Overheated and poorly quenched
P137-1	50.65	0.31	15.81	7.66	0.11	9.96	14.09	1.65	0.02	0.00	0.06	100.32	8.6	88.4	1227	1228	1189	1203	Overheated and poorly quenched
P137-6	50.62	0.36	15.65	7.58	0.15	10.08	13.98	1.70	0.02	0.00	0.06	100.21	8.2	89.8	1227	1232	1188	1203	Overheated and poorly quenched
P137-8	50.56	0.41	15.55	7.75	0.14	10.17	14.00	1.62	0.04	0.00	0.05	100.29	8.7	89.7	1227	1233	1185	1200	Overheated and poorly quenched
P138-1	50.40	0.32	15.60	7.98	0.12	9.37	13.25	2.22	0.07	0.05	0.02	99.40	6.0	89.1	1218	1225	1197	1210	Poorly quenched
P138-4	49.76	0.30	15.61	8.26	0.17	9.11	14.29	1.98	0.07	0.02	0.09	99.65	7.2	89.8	1218	1211	1194	1204	Poorly quenched
P140-1	48.00	0.46	17.72	6.27	0.12	8.76	14.86	3.77	0.02	0.00	0.08	100.07	3.9	90.1	1215	1222	1234	1246	Analytical overlap
P140-2	48.43	0.43	16.86	7.52	0.17	7.00	16.42	3.42	0.01	0.00	0.08	100.34	4.8	89.4	1215	1153	1222	1218	Analytical overlap
140-504B-222R-1, Piece 1																			
P150-3	51.68	0.65	15.26	8.71	0.17	8.29	13.10	2.39	0.02	0.00	0.05	100.32	5.5	87.3	1210	1193	1216	1222	Analytical overlap
P150-4	52.12	0.63	15.08	8.65	0.12	8.14	12.89	2.44	0.01	0.00	0.03	100.11	5.3	84.4	1210	1192	1211	1216	Analytical overlap
P151-2	50.96	0.57	16.61	8.08	0.13	7.77	13.24	2.15	0.02	0.05	0.06	99.65	6.1	85.8	1210	1174	1253	1254	Overheated but not equilibrated, analytical overlap
148-504B-249R-1, Piece 30																			
P128-1	50.58	0.69	15.34	9.53	0.17	7.78	12.54	1.91	0.04	0.02	0.05	98.65	6.6	86.8	1209	1179	1194	1196	Overheated and equilibrated, poorly quenched
P128-2	50.74	0.59	15.22	9.62	0.16	7.75	12.79	1.77	0.05	0.00	0.01	98.70	7.2	86.0	1209	1176	1190	1191	Overheated and equilibrated, poorly quenched
P129-1	50.98	0.57	15.91	6.73	0.16	9.57	13.74	1.35	0.02	0.00	0.07	99.10	10.2	90.9	1230	1216	1190	1201	Overheated and equilibrated, poorly quenched
P141-2	51.67	0.74	15.56	8.09	0.21	7.96	13.20	2.27	0.01	0.01	0.03	99.74	5.8	85.3	1208	1183	1198	1201	Overheated but not equilibrated, poorly quenched
P142-1	50.56	0.19	15.36	8.65	0.16	8.01	12.77	2.64	0.05	0.00	0.09	98.49	4.8	89.1	1207	1195	1200	1206	Overheated and poorly quenched
P142-2	49.48	0.22	16.05	8.76	0.14	7.80	13.56	3.48	0.01	0.00	0.05	99.55	3.9	89.2	1207	1194	1210	1216	Overheated and poorly quenched
P145-1	50.83	0.51	15.89	7.03	0.17	9.22	14.17	1.86	0.13	0.04	0.08	99.91	7.6	90.1	1215	1211	1196	1206	Poorly quenched
P146-1	51.09	0.74	16.64	7.47	0.11	7.47	13.21	3.25	0.02	0.01	0.00	100.01	4.1	86.4	1215	1180	1219	1221	Overheated and equilibrated
P146-2	52.84	0.72	15.93	7.71	0.17	7.83	13.03	2.11	0.03	0.04	0.08	100.49	6.2	82.3	1215	1176	1200	1201	Overheated and equilibrated
P146-3	52.47	0.58	15.89	7.90	0.17	7.87	12.43	2.38	0.05	0.01	0.03	99.78	5.2	85.1	1215	1186	1204	1208	Overheated and equilibrated
P146-4	52.32	0.62	15.47	7.68	0.14	7.91	13.00	2.24	0.05	0.02	0.02	99.46	5.8	83.8	1215	1184	1197	1200	Overheated and equilibrated
P149-2	51.06	0.48	15.43	8.40	0.11	9.14	12.74	1.71	0.15	0.02	0.03	99.28	7.5	88.3	1213	1214	1189	1200	Poorly quenched
P149-9	50.95	0.41	16.44	8.18	0.14	8.69	13.15	1.97	0.02	0.00	0.05	100.01	6.7	89.1	1213	1199	1242	1249	Analytical overlap
P152-2	50.13	0.31	16.92	8.70	0.15	9.91	12.24	1.70	0.03	0.00	0.04	100.13	7.2	90.4	1229	1230	1209	1223	?Overheated

Appendix 3.3, continued.

Sample	SiO_2	TiO_2	Al_2O_3	[a]FeO	MnO	MgO	CaO	Na_2O	K_2O	P_2O_5	Cr_2O_3	total	CaO/Na_2O	[b]Host An	[c]T_h (°C)	[d]T_{ol}	[e]T_{pl}	[f]T_{corr}	[g]Comments
148-504B-249R-1, Piece 38																			
P133-1	50.48	0.55	15.25	8.44	0.15	8.85	12.77	2.35	0.02	0.00	0.07	98.93	5.4	85.8	1210	1214	1194	1205	Poorly quenched
P133-3	50.77	0.49	14.84	8.66	0.17	9.00	12.82	2.42	0.10	0.00	0.07	99.32	5.3	86.4	1210	1220	1186	1198	Poorly quenched
P133-5	50.09	0.49	14.73	8.52	0.15	8.69	13.15	3.11	0.56	0.00	0.11	99.61	4.2	86.3	1210	1224	1188	1201	Poorly quenched
P135-1	50.54	0.60	15.91	8.31	0.17	7.85	13.09	2.60	0.02	0.00	0.07	99.15	5.0	86.0	1220	1186	1207	1211	Overheated and poorly quenched
P136-1	51.21	0.51	15.68	8.28	0.14	8.95	13.04	2.24	0.02	0.00	0.03	100.10	5.8	86.4	1216	1212	1197	1207	Poorly quenched
P136-2	51.46	0.56	15.67	8.15	0.16	9.00	12.97	2.32	0.04	0.00	0.00	100.32	5.6	86.4	1216	1214	1197	1208	Poorly quenched
P136-3	50.62	0.47	15.24	8.19	0.14	8.84	13.05	2.56	0.09	0.03	0.02	99.26	5.1	86.4	1216	1216	1195	1206	Poorly quenched

[a]All Fe as FeO.

[b]Host plagioclase composition, An = 100 x (Ca/(Ca + Na)).

[c]Homogenisation temperature.

[d]Calculated temperature using the olivine-melt thermometer of Ford, et al.(1983).

[e]Calculated temperature using the plagioclase-melt thermometer of Weaver and Langmuir(1990).

[f]Calculated plagioclase temperature corrected to obtain a best fit for the MORB olivine-plagioclase cotectic; correction from Danyushevsky, et al.(1996).

[g]Interpretation of inclusion composition based on a comparison of T_h, T_{ol}, T_{pl} and T_{corr}.

Appendix 3.4, Homogenised melt inclusions in plagioclase.

Sample	SiO_2	TiO_2	Al_2O_3	[a]FeO	MnO	MgO	CaO	Na_2O	K_2O	P_2O_5	Cr_2O_3	total	CaO/ Na_2O	[b]Host An	[c]T_h (°C)	[d]T_{ol}	[e]T_{pl}	[f]T_{corr}	[g]Comments
140-504B-213R-1, Piece 22																			
P138-2	50.55	0.36	16.07	7.68	0.20	9.31	13.70	2.07	0.08	0.01	0.05	100.09	6.6	89.8	1218	1217	1201	1212	Good run
140-504B-222R-1, Piece 1																			
P150-1	51.57	0.57	15.21	8.78	0.13	8.17	13.01	2.28	0.02	0.03	0.10	99.88	5.7	87.8	1210	1191	1192	1197	Overheated but not equilibrated
P150-2	50.62	0.64	15.16	8.75	0.12	8.09	13.05	2.56	0.03	0.05	0.09	99.16	5.1	85.3	1210	1193	1195	1201	Overheated but not equilibrated
P151-1	50.90	0.57	15.32	8.67	0.20	8.15	13.12	2.28	0.01	0.01	0.07	99.31	5.8	88.8	1210	1190	1195	1200	Overheated but not equilibrated
148-504B-249R-1, Piece 30																			
P141-3	51.43	0.74	15.25	8.09	0.15	8.01	13.10	2.53	0.02	0.00	0.06	99.38	5.2	84.1	1208	1190	1195	1200	Overheated but not equilibrated
P141-4	51.64	0.65	15.09	7.79	0.17	8.12	13.25	2.10	0.08	0.02	0.05	98.95	6.3	83.3	1208	1188	1190	1194	Overheated but not equilibrated
P145-2	49.48	0.49	17.51	6.68	0.13	9.41	14.03	1.99	0.13	0.05	0.02	99.91	7.1	90.1	1215	1218	1223	1235	Good run
P149-1	51.23	0.46	16.18	8.27	0.15	9.00	12.62	1.72	0.16	0.09	0.06	99.93	7.3	89.0	1213	1207	1200	1209	Good run
P149-10	51.80	0.48	15.31	8.58	0.19	9.42	12.86	1.24	0.02	0.00	0.07	99.97	10.4	88.8	1213	1210	1198	1208	Good run
P149-3	51.31	0.29	15.86	8.11	0.14	8.80	12.53	1.91	0.17	0.09	0.03	99.23	6.6	89.7	1213	1207	1199	1208	Good run
P149-8	51.75	0.49	15.72	8.25	0.14	9.02	12.54	1.75	0.15	0.06	0.03	99.91	7.2	88.9	1213	1209	1214	1223	Good run
P152-1	51.02	0.29	16.41	7.07	0.12	9.19	13.72	2.08	0.02	0.00	0.03	99.95	6.6	90.3	1229	1214	1206	1217	Overheated but not equilibrated
148-504B-249R-1, Piece 38																			
P132-1	50.48	0.61	15.25	9.01	0.15	8.27	12.75	2.04	0.04	0.00	0.03	98.63	6.3	86.8	1210	1195	1193	1199	Overheated but not equilibrated
P132-3	50.26	0.67	15.52	8.46	0.15	8.47	13.04	1.96	0.01	0.00	0.12	98.66	6.7	87.1	1210	1197	1197	1203	Overheated but not equilibrated
P132-4	49.93	0.64	15.19	8.57	0.18	8.31	12.87	2.55	0.00	0.00	0.03	98.27	5.0	86.8	1210	1202	1197	1205	Overheated but not equilibrated
P133-8	51.01	0.52	15.75	8.38	0.11	8.67	13.22	2.24	0.12	0.00	0.08	100.10	5.9	86.0	1210	1204	1199	1207	Good run

[a]All Fe as FeO.

[b]Host plagioclase composition, An = 100 x (Ca/(Ca + Na)).

[c]Homogenisation temperature.

[d]Calculated temperature using the olivine-melt thermometer of Ford, et al.(1983).

[e]Calculated temperature using the plagioclase-melt thermometer of Weaver and Langmuir(1990).

[f]Calculated plagioclase temperature corrected to obtain a best fit for the MORB olivine-plagioclase cotectic; correction from Danyushevsky, et al.(1996).

[g]Interpretation of inclusion composition based on a comparison of T_h, T_{ol}, T_{pl} and T_{corr}.

Appendix 4

Phenocryst and Melt Inclusion Analyses, Gorda Ridge, Sample KK2-83-NP-D9-1

Contents

4.0 Sample Identification

Individual phenocrysts and inclusions are identified as follows; grain mount-Phenocryst type-grain number-inclusion type-inclusion number, e.g., A26-PL15-GL is plagioclase grain 15, from grain mount 26, which hosts an analysed glass inclusion. Phenocryst types are abbreviated as follows; PL, plagioclase; OL, olivine; and SP, spinel.

Melt inclusions from homogenisation experiments are identified as follows; host phenocryst-experiment-inclusion, e.g., P115-5 is plagioclase experiment 115, inclusion number five.

Appendix 4.1, Plagioclase phenocryst analyses.

Sample	SiO_2	Al_2O_3	FeO	MgO	CaO	Na_2O	K_2O	Total	^aAn
PL1-GL1	44.73	33.99	0.38	0.22	18.41	0.92	0.01	98.65	91.7
PL1-GL2	44.75	34.30	0.35	0.20	18.36	0.99	0.01	98.96	91.2
PL1-GL3	45.18	34.37	0.30	0.21	18.40	0.96	0.00	99.42	91.4
PL3-GL1	44.87	34.51	0.30	0.20	18.44	0.95	0.01	99.29	91.5
PL3-GL2	44.83	34.33	0.34	0.22	18.32	0.97	0.00	99.02	91.3
PL4-GL	44.65	34.82	0.30	0.22	18.51	0.83	0.01	99.35	92.5
PL5-GL1	44.82	34.48	0.31	0.22	18.65	0.91	0.01	99.40	91.9
PL5-GL2	44.72	34.25	0.27	0.23	18.34	0.98	0.01	98.80	91.2
PL6-GL1-1	45.17	34.25	0.33	0.21	18.24	1.07	0.01	99.28	90.4
PL6-GL1-2	45.17	34.25	0.33	0.21	18.24	1.07	0.01	99.28	90.4
PL6-GL2	45.07	34.33	0.32	0.21	18.41	1.05	0.02	99.41	90.7
PL6-GL3-1	45.23	34.22	0.32	0.23	18.22	1.09	0.02	99.32	90.3
PL6-GL3-2	45.23	34.22	0.32	0.23	18.22	1.09	0.02	99.32	90.3
PL7-GL1	45.73	33.73	0.31	0.24	17.75	1.20	0.00	98.97	89.1
PL7-GL2	45.64	34.00	0.34	0.25	18.11	1.18	0.00	99.53	89.4
PL7-GL3	45.68	34.20	0.31	0.24	18.18	1.15	0.02	99.77	89.7
PL7-GL4	45.64	33.92	0.29	0.24	17.96	1.24	0.01	99.29	88.9
PL7-GL5	45.54	34.01	0.29	0.24	17.96	1.19	0.00	99.23	89.3
PL8-GL	47.06	33.11	0.45	0.24	16.97	1.70	0.02	99.55	84.7
PL9-GL1	45.18	34.23	0.32	0.27	18.00	1.16	0.01	99.17	89.6
PL9-GL2	45.81	34.04	0.33	0.25	17.91	1.18	0.00	99.51	89.3
PL9-GL3	45.51	34.00	0.30	0.24	18.04	1.21	0.00	99.31	89.2
PL9-GL4	46.00	33.81	0.37	0.34	17.82	1.27	0.00	99.61	88.5
PL9-GL5	45.58	34.01	0.30	0.25	18.13	1.15	0.01	99.41	89.7
PL10-GL1	45.09	34.81	0.29	0.23	18.43	1.03	0.01	99.89	90.8
PL10-GL2	45.09	34.81	0.29	0.23	18.43	1.03	0.01	99.89	90.8
PL11-GL	46.47	33.28	0.45	0.21	17.38	1.63	0.02	99.45	85.5
PL12-GL	46.79	33.19	0.39	0.19	17.08	1.75	0.00	99.40	84.3
PL13-SP1-GL	44.97	34.07	0.34	0.21	18.23	1.02	0.01	98.85	90.8
PL16-GL1	47.20	32.91	0.43	0.21	16.60	1.83	0.02	99.19	83.4
PL16-GL2	47.43	32.85	0.47	0.22	16.78	1.82	0.02	99.59	83.6
PL16-GL3	47.07	32.96	0.41	0.24	16.73	1.84	0.02	99.27	83.4
PL17-GL1	45.24	34.74	0.36	0.21	18.45	1.00	0.02	100.02	91.1
PL17-GL2	45.38	34.73	0.34	0.22	18.34	0.98	0.01	100.00	91.2
PL17-GL3	45.13	34.55	0.32	0.21	18.55	0.95	0.01	99.72	91.5
PL18-GL	46.55	33.30	0.83	0.23	16.78	1.72	0.05	99.47	84.4
PL19-GL1	44.49	35.07	0.35	0.21	18.75	0.90	0.02	99.78	92.0
PL19-GL2	43.56	35.09	0.35	0.22	18.38	0.84	0.02	98.45	92.4
PL19-GL3	44.79	34.87	0.31	0.24	18.38	0.93	0.02	99.53	91.6
PL19-GL4	44.13	35.17	0.30	0.21	18.71	0.83	0.00	99.35	92.6
PL19-GL5	44.39	35.31	0.36	0.19	18.72	0.86	0.01	99.84	92.3
PL20-GL1	46.15	33.56	0.39	0.24	17.27	1.62	0.04	99.27	85.5
PL20-GL2	46.55	33.61	0.37	0.23	17.27	1.60	0.01	99.63	85.6
PL20-GL3	46.30	33.41	0.43	0.26	17.00	1.64	0.03	99.07	85.2
PL21-GL1	44.94	35.18	0.35	0.22	18.64	0.99	0.01	100.32	91.3
PL21-GL2	45.06	34.99	0.37	0.22	18.48	0.92	0.00	100.04	91.7
PL21-GL3	44.69	34.81	0.33	0.22	18.61	0.96	0.01	99.62	91.5
PL21-GL4	44.50	34.84	0.37	0.21	18.49	0.98	0.01	99.41	91.2
PL23-GL1	44.84	34.78	0.36	0.23	18.34	0.97	0.02	99.53	91.3
PL23-GL2	44.35	34.47	0.34	0.21	18.64	0.92	0.01	98.94	91.8
PL23-GL3	44.90	34.40	0.42	0.25	18.14	1.06	0.00	99.16	90.5
PL23-GL4-1	46.54	33.02	0.69	0.57	17.13	1.51	0.00	99.46	86.3
PL23-GL4-2	46.54	33.02	0.69	0.57	17.13	1.51	0.00	99.46	86.3
PL24-GL1	45.04	34.51	0.30	0.24	18.26	1.02	0.01	99.37	90.8
PL29-GL1	44.96	34.73	0.32	0.23	18.21	1.02	0.00	99.48	90.8
PL29-GL2	44.90	34.42	0.33	0.22	18.22	1.07	0.03	99.20	90.4
PL30-GL1	45.19	34.67	0.36	0.23	18.00	1.10	0.01	99.57	90.0
PL30-GL2	45.36	34.70	0.31	0.23	18.08	1.11	0.01	99.80	90.0
PL31-GL1	46.39	33.73	0.42	0.24	17.25	1.50	0.01	99.54	86.4
PL31-GL2	48.02	21.98	6.11	6.39	15.13	1.51	0.03	99.17	84.7
PL31-GL3	46.59	33.92	0.36	0.24	17.40	1.52	0.00	100.02	86.3
PL32-GL	44.70	34.83	0.33	0.21	18.43	1.04	0.01	99.55	90.7
PL33-GL-1	45.67	33.30	0.40	0.22	17.40	1.55	0.01	98.56	86.1
PL33-GL-2	45.67	33.30	0.40	0.22	17.40	1.55	0.01	98.56	86.1
PL34-GL1	45.72	34.26	0.34	0.26	17.91	1.24	0.01	99.74	88.9

Appendix 4.1, continued.

Sample	SiO_2	Al_2O_3	FeO	MgO	CaO	Na_2O	K_2O	Total	^aAn
PL34-GL2	45.55	34.35	0.34	0.28	17.93	1.29	0.02	99.75	88.5
OL57-PL	48.12	33.58	0.95	0.27	16.69	2.02	0.01	101.63	82.0
A27/PL7-SP2-GL	44.33	35.32	0.33	0.16	18.97	0.62	0.01	99.74	94.4
A26-PL1-SP-GL	46.70	33.49	0.43	0.20	17.41	1.57	0.01	99.82	86.0
A26-PL2-SP1	45.54	34.89	0.33	0.22	18.39	0.95	0.02	100.34	91.5
A26-PL2-SP2	44.46	34.82	0.40	0.20	18.92	0.78	0.00	99.59	93.0
A26-PL2-GL1	45.26	34.49	0.31	0.22	18.48	0.97	0.00	99.74	91.3
A26-PL2-GL2	45.36	34.55	0.30	0.22	18.40	0.97	0.00	99.79	91.3
A26-PL2-GL3	45.39	34.27	0.35	0.24	18.49	0.94	0.01	99.69	91.5
A26-PL3-GL	45.34	34.56	0.33	0.21	18.31	1.01	0.01	99.77	90.9
A26-PL4-SP	45.03	34.44	0.32	0.20	18.55	0.96	0.02	99.52	91.4
A26-PL5-GL1	45.54	33.97	0.28	0.23	18.13	1.13	0.01	99.29	89.8
A26-PL5-GL2	45.38	34.54	0.28	0.22	18.29	1.02	0.01	99.74	90.8
A26-PL5-GL3	45.56	34.35	0.35	0.22	18.38	1.02	0.02	99.89	90.9
A26-PL6-SP	44.94	34.82	0.35	0.16	18.60	0.86	0.00	99.73	92.3
A27-PL1-SP	45.39	34.75	0.38	0.19	18.52	0.99	0.02	100.23	91.2
A27-PL2-SP	45.73	34.47	0.50	0.18	18.26	1.08	0.00	100.23	90.3
A27-PL3-SP	45.80	34.65	0.34	0.22	18.20	1.06	0.02	100.28	90.5
A27-PL4-SP	44.90	34.72	0.35	0.18	18.53	0.90	0.01	99.59	91.9
A27-PL5-SP	46.15	34.11	0.62	0.16	17.94	1.25	0.01	100.23	88.8
A27-PL6-SP	44.48	33.39	0.31	0.23	17.90	1.01	0.00	97.33	90.7
A27-PL7-SP1	44.83	35.39	0.30	0.17	18.68	0.72	0.00	100.09	93.5
A27-PL7-SP2-GL	44.51	35.27	0.37	0.16	18.99	0.70	0.00	100.01	93.7
A27-PL7-SP	45.42	34.65	0.31	0.21	18.43	1.00	0.01	100.03	91.1
A27-PL8-SP-GL	46.96	32.05	0.97	0.94	16.86	1.49	0.00	99.27	86.2
A27-PL8-SP-GL2	44.54	35.33	0.34	0.15	18.97	0.71	0.01	100.05	93.7
A27-PL9-SP	46.64	33.83	0.37	0.20	17.06	1.55	0.02	99.66	85.9
A27-PL12-GL1	45.36	34.80	0.41	0.20	18.37	1.00	0.01	100.14	91.0
A27-PL12-GL2	45.34	35.01	0.35	0.19	18.39	0.97	0.02	100.27	91.3
A27-PL12-GL3	45.44	34.89	0.29	0.19	18.25	1.01	0.00	100.07	90.9
A27-PL13-SP-GL	46.04	34.47	0.33	0.23	18.09	1.11	0.00	100.27	90.0
A27-PL13-SP-GL	46.04	34.47	0.33	0.23	18.09	1.11	0.00	100.27	90.0
A27-PL14-SP1-G	46.91	33.54	0.46	0.21	17.54	1.57	0.01	100.24	86.1
A27-PL14-SP1-G	46.91	33.54	0.46	0.21	17.54	1.57	0.01	100.24	86.1
A27-PL14-SP2	46.91	33.54	0.46	0.21	17.54	1.57	0.01	100.24	86.1
A27-PL14-SP3	47.21	33.03	0.44	0.22	17.08	1.82	0.02	99.82	83.9
A30-PL11-GL3	45.66	35.03	0.32	0.24	18.47	1.03	0.01	100.76	90.8
A30-PL11-GL2	45.51	35.08	0.33	0.22	18.33	1.00	0.00	100.48	91.0
A30-PL12-GL1	45.57	34.92	0.30	0.23	18.42	0.96	0.00	100.39	91.4
A30-PL12-GL2	45.44	35.22	0.32	0.24	18.18	1.01	0.01	100.40	90.9
A30-PL13-GL1	47.32	33.74	0.33	0.24	17.17	1.62	0.02	100.43	85.4
A30-PL13-GL2	47.31	33.93	0.39	0.24	17.08	1.62	0.02	100.58	85.3
A30-PL13-GL3	47.31	33.90	0.36	0.24	16.94	1.69	0.02	100.46	84.7
A30-PL10-SP1	45.35	34.88	0.27	0.21	18.11	0.96	0.00	99.79	91.2
A30-PL10-SP2	45.57	35.01	0.44	0.21	18.09	1.04	0.01	100.38	90.6
A30-PL10-SP3	45.42	34.94	0.49	0.22	18.23	1.02	0.01	100.33	90.8
A30-PL10-SP4	45.26	35.01	0.41	0.22	18.18	1.06	0.02	100.15	90.4
A31-PL65-SP2	45.95	35.15	0.37	0.21	18.29	1.05	0.00	101.03	90.6
A31-PL66-SP2	45.43	35.24	0.35	0.21	18.56	0.95	0.02	100.75	91.5
A31-PL66-SP1	45.72	35.00	0.31	0.20	18.07	1.08	0.01	100.39	90.3
A31-PL67-SP1	45.59	34.86	0.28	0.24	18.35	1.05	0.00	100.36	90.6
A31-PL67-SP2	45.36	35.11	0.35	0.23	18.28	1.02	0.00	100.35	90.8
A31-PL68-SP1	45.04	34.96	0.38	0.22	18.52	0.92	0.01	100.05	91.8
A31-PL68-SP2	44.80	34.94	0.37	0.21	18.43	0.93	0.00	99.68	91.7
A31-PL68-SP3	45.38	34.79	0.33	0.24	18.24	0.98	0.00	99.97	91.1
A31-PL68-SP4	44.97	35.38	0.39	0.22	18.55	0.84	0.00	100.34	92.4
A31-PL69-SP2	46.51	34.37	0.35	0.22	17.55	1.50	0.00	100.50	86.6
A31-PL69-GL	46.82	33.46	0.51	0.42	17.08	1.67	0.01	99.96	84.9
A31-PL69-GL2	46.76	33.99	0.39	0.23	17.26	1.57	0.02	100.22	85.9
A31-PL70-SP	45.27	34.99	0.30	0.22	18.57	0.95	0.00	100.30	91.6
A31-PL46-SP	46.16	34.57	0.33	0.19	17.79	1.27	0.01	100.31	88.6
A31-PL47-SP1	45.78	34.61	0.30	0.23	17.98	1.15	0.01	100.05	89.6
A31-PL47-SP2	45.86	34.60	0.35	0.24	18.13	1.19	0.02	100.38	89.4
A31-PL47-SP3	45.41	35.06	0.30	0.23	18.24	0.98	0.01	100.22	91.1
A31-PL50-SP-GL	45.59	35.30	0.29	0.22	18.30	1.01	0.00	100.70	91.0
A31-PL52-SP	46.83	33.80	0.41	0.22	17.35	1.53	0.00	100.15	86.2

Appendix 4.1, continued.

Sample	SiO_2	Al_2O_3	FeO	MgO	CaO	Na_2O	K_2O	Total	[a]An
A31-PL41-SP	46.30	34.66	0.34	0.27	18.02	1.12	0.00	100.71	89.9
A30-PL11-GL1	45.61	35.19	0.34	0.24	18.37	1.01	0.01	100.79	90.9
A31-PL65-SP1	46.32	35.88	0.44	0.22	18.15	1.05	0.01	102.06	90.5
A31-PL66-SP-PL	45.15	34.97	0.51	0.23	18.20	0.99	0.00	100.06	91.0
A31-PL69-SP1	46.74	34.40	0.38	0.22	17.38	1.52	0.00	100.64	86.3
A31-OL/PL42-SP	46.97	34.37	0.47	0.23	17.15	1.58	0.02	100.79	85.7
A29-PL1-GL	46.62	33.09	0.38	0.21	17.23	1.64	0.01	99.19	85.3
A27-PL8-GL1	44.69	34.70	0.30	0.22	18.63	0.93	0.01	99.48	91.7
A27-PL8-GL4	44.77	34.73	0.29	0.21	18.73	0.88	0.01	99.62	92.2
A27-PL8-GL3	44.54	34.70	0.31	0.21	18.69	0.88	0.02	99.35	92..2
A27-PL8-GL6	44.80	35.29	0.32	0.20	19.05	0.85	0.00	100.51	92.5
A27-PL8-GL7	44.19	35.07	0.31	0.18	19.08	0.79	0.02	99.64	93.0
A27-PL8-GL8	44.36	34.77	0.29	0.18	18.79	0.86	0.00	99.25	92.3
A27-PL8-GL9	44.66	34.68	0.36	0.20	18.82	0.91	0.01	99.63	91.9
A27/PL15	45.14	35.25	0.29	0.22	18.68	0.85	0.01	100.44	92.4
A27-PL16	45.37	34.89	0.28	0.24	18.38	1.03	0.00	100.20	90.8
A27-PL17	46.02	34.81	0.26	0.25	18.39	1.11	0.01	100.84	90.1
A27-PL18	45.39	34.79	0.32	0.25	18.28	0.98	0.02	100.04	91.1
A27-PL19	47.32	33.18	0.38	0.26	16.82	1.83	0.00	99.79	83.5
A27-PL20	46.56	33.53	0.35	0.25	17.27	1.66	0.01	99.62	85.2
A27-PL21	45.26	34.73	0.32	0.24	18.33	0.92	0.01	99.80	91.6
A27-PL22	45.32	35.24	0.30	0.25	18.51	0.93	0.00	100.55	91.7
A27-PL23	45.27	34.83	0.27	0.25	18.44	0.99	0.01	100.07	91.2
A27-PL24a	48.70	32.33	0.39	0.30	16.13	2.41	0.02	100.28	78.7
A27-PL24	46.95	34.05	0.43	0.23	17.42	1.56	0.01	100.65	86.1
A27-PL25	45.94	34.47	0.37	0.28	17.98	1.18	0.01	100.23	89.4
A27-PL26	45.40	35.01	0.35	0.24	18.48	0.98	0.02	100.48	91.2
A27-PL27	45.28	34.75	0.29	0.23	18.28	1.01	0.00	99.85	90.9
A27-PL28	45.55	34.76	0.31	0.30	18.27	1.00	0.01	100.19	91.0
A27-PL29	45.33	34.89	0.29	0.25	18.57	0.93	0.00	100.26	91.7
A27-PL30	45.19	34.87	0.30	0.24	18.64	0.91	0.02	100.18	91.87
A27-PL31	47.56	33.82	0.41	0.27	17.20	1.64	0.02	100.92	85.28
A27-PL32	46.18	34.47	0.32	0.26	18.14	1.22	0.01	100.59	89.14
A27-PL33	45.71	35.03	0.30	0.23	18.46	1.02	0.00	100.76	90.94
A27-PL34	46.12	34.43	0.35	0.28	17.97	1.19	0.02	100.36	89.31
A27-PL35	45.40	34.45	0.23	0.27	18.32	1.17	0.00	99.84	89.68
A27-PL36	47.01	33.57	0.33	0.28	17.34	1.67	0.01	100.21	85.20
A27-PL37	47.04	33.47	0.35	0.28	17.23	1.61	0.02	100.01	85.51
A27-PL38	45.76	35.14	0.31	0.24	18.58	1.02	0.01	101.07	91.00
A27-PL39	45.42	34.78	0.33	0.24	18.55	0.96	0.01	100.29	91.44
A27-PL40	47.20	33.49	0.32	0.26	17.20	1.66	0.00	100.13	85.12
A27-PL41	45.33	34.91	0.32	0.24	18.48	0.97	0.01	100.25	91.30
A27-PL42	46.76	34.29	0.34	0.22	17.57	1.49	0.02	100.69	86.72
A27-PL43	48.31	32.82	0.41	0.27	16.29	2.07	0.01	100.18	81.32
A27-PL44	45.48	34.94	0.27	0.24	18.41	0.96	0.01	100.29	91.41
A27-PL45	46.53	34.10	0.33	0.23	17.80	1.37	0.02	100.37	87.76
A27-PL46	46.27	34.68	0.28	0.24	18.13	1.17	0.01	100.78	89.56
A27-PL47	45.51	34.94	0.27	0.22	18.39	0.95	0.00	100.28	91.47
A27-PL48	46.41	34.04	0.31	0.31	17.73	1.34	0.01	100.15	87.97
A27-PL49	47.44	33.66	0.35	0.22	16.88	1.91	0.01	100.47	83.01
A27-PL50	45.58	34.97	0.34	0.23	18.19	1.02	0.03	100.35	90.78
A27-PL51	45.43	34.92	0.27	0.22	18.47	0.96	0.01	100.29	91.41
A27-PL52	46.55	34.31	0.34	0.28	17.90	1.29	0.01	100.68	88.5
A27-PL53	45.29	34.68	0.33	0.26	18.46	0.97	0.01	99.99	91.3
A27-PL54	45.20	35.08	0.34	0.25	18.50	0.99	0.00	100.36	91.2
A27-PL55a	48.56	32.61	0.38	0.27	15.84	2.28	0.02	99.96	79.3
A27-PL55	46.64	34.19	0.33	0.22	17.77	1.38	0.00	100.53	87.7
A27-PL56	45.55	34.88	0.28	0.26	18.29	1.05	0.01	100.32	90.6
A27-PL57	48.64	32.36	0.44	0.28	16.04	2.29	0.00	100.06	79.4
A27-PL59	45.50	35.00	0.33	0.25	18.39	0.97	0.01	100.46	91.3
A27-PL60	45.60	34.33	0.29	0.25	18.02	1.07	0.01	99.56	90.3
A27-PL61	46.07	34.41	0.30	0.31	18.05	1.16	0.02	100.32	89.6
A27-PL62	47.03	33.68	0.35	0.26	17.28	1.62	0.03	100.27	85.5
A27-PL63	46.52	34.18	0.36	0.21	17.64	1.40	0.02	100.32	87.5
A27-PL64	47.41	33.94	0.35	0.26	17.08	1.63	0.01	100.67	85.2
A27-PL65	46.54	33.58	0.42	0.25	17.24	1.61	0.01	99.65	85.6
A27-PL66	46.80	34.09	0.36	0.21	17.43	1.49	0.01	100.40	86.6

Appendix 4.1, continued

Sample	SiO_2	Al_2O_3	FeO	MgO	CaO	Na_2O	K_2O	Total	[a]An
A27-PL67	45.92	34.39	0.31	0.28	17.84	1.22	0.01	99.97	88.9
A27-PL68	45.20	34.81	0.30	0.22	18.23	1.03	0.00	99.78	90.7
A27-PL69	45.72	34.61	0.29	0.25	18.29	1.04	0.00	100.21	90.7
A27-PL70	47.06	33.56	0.38	0.25	17.29	1.67	0.03	100.24	85.2
A27-PL71	45.66	34.86	0.36	0.27	18.08	1.03	0.01	100.28	90.6
A27-PL72	45.84	34.84	0.26	0.31	17.99	1.08	0.02	100.34	90.2
A27-PL73	45.51	35.06	0.24	0.26	18.37	1.00	0.01	100.46	91.0
A27-PL74	45.66	35.05	0.33	0.25	18.65	0.93	0.01	100.88	91.7
A27-PL75	46.43	34.40	0.34	0.29	17.78	1.20	0.01	100.46	89.1
A27-PL76	47.43	33.55	0.35	0.27	16.88	1.80	0.01	100.30	83.8
A27-PL77	45.53	35.10	0.29	0.25	18.39	0.97	0.00	100.52	91.3
A27-PL78	47.28	33.51	0.39	0.24	17.01	1.66	0.01	100.10	85.0
A27-PL80	45.17	35.15	0.29	0.24	18.52	0.91	0.01	100.29	91.8
A27-PL81	46.22	34.78	0.34	0.20	17.88	1.28	0.01	100.70	88.5
A27-PL82	47.36	33.87	0.40	0.24	16.93	1.66	0.01	100.47	84.9
A27-PL83	45.52	35.16	0.31	0.23	18.42	0.98	0.00	100.62	91.2
A27-PL84	45.33	35.10	0.32	0.23	18.65	1.00	0.02	100.65	91.2
A27-PL85	45.44	34.51	0.29	0.24	18.23	1.10	0.01	99.83	90.2
A27-PL86	45.27	34.41	0.42	0.35	18.24	1.00	0.06	99.74	91.0

[a]Anorthite, An = 100 x (Ca/(Ca + Na)).

Appendix 4.2, Olivine analyses.

Sample	SiO_2	FeO	MnO	MgO	CaO	Cr_2O_3	NiO	Total	[a]Fo
OL1	40.26	11.93	0.28	46.73	0.37	0.05	0.16	99.78	87.5
OL2	40.13	12.39	0.17	46.48	0.37	0.07	0.17	99.77	87.0
OL3	39.96	11.48	0.19	47.55	0.37	0.08	0.18	99.80	88.1
OL4-GL1	40.01	12.46	0.23	46.39	0.40	0.06	0.13	99.67	86.9
OL4-SP2	40.44	12.52	0.24	46.68	0.37	0.07	0.10	100.41	86.9
OL6-SP1	40.13	11.57	0.14	46.98	0.38	0.08	0.15	99.44	87.9
OL6-SP2	40.13	11.57	0.14	46.98	0.38	0.08	0.15	99.44	87.9
OL6-SP3-GL	40.13	11.57	0.14	46.98	0.38	0.08	0.15	99.44	87.9
OL5-GL	39.69	12.44	0.19	46.24	0.39	0.05	0.17	99.16	86.9
OL7-GL	39.95	11.85	0.23	46.65	0.37	0.07	0.15	99.27	87.5
OL8	39.79	11.45	0.16	47.28	0.37	0.06	0.22	99.35	88.0
OL9-GL2	39.80	12.43	0.21	46.06	0.35	0.05	0.22	99.11	86.9
OL9-SP1	39.80	12.43	0.21	46.06	0.35	0.05	0.22	99.11	86.9
OL10	39.84	12.01	0.20	46.74	0.38	0.07	0.19	99.43	87.4
OL11	39.83	12.32	0.16	46.51	0.37	0.08	0.20	99.46	87.1
OL12	39.74	12.74	0.16	46.38	0.38	0.09	0.19	99.68	86.6
OL13	39.85	12.32	0.21	46.69	0.37	0.05	0.17	99.66	87.1
OL14	39.82	12.16	0.16	46.61	0.37	0.08	0.20	99.39	87.2
OL15	40.06	12.06	0.18	46.67	0.36	0.08	0.20	99.61	87.3
OL16-GL1	39.65	12.37	0.20	46.29	0.39	0.07	0.20	99.18	87.0
OL16-GL2	39.82	12.38	0.15	46.68	0.36	0.04	0.18	99.61	87.0
OL16-GL3	39.81	12.32	0.17	46.43	0.37	0.05	0.18	99.34	87.0
OL17	40.24	11.91	0.17	46.87	0.36	0.04	0.20	99.79	87.5
OL18-GL1	39.49	12.44	0.21	46.07	0.42	0.04	0.20	98.87	86.8
OL18-SP2	39.80	12.35	0.19	46.26	0.37	0.11	0.13	99.22	87.0
OL19-GL1	39.96	12.06	0.19	47.16	0.34	0.03	0.21	99.94	87.5
OL19-GL2	40.19	11.56	0.26	47.49	0.36	0.06	0.18	100.09	88.0
OL19-GL3	40.41	10.75	0.09	48.14	0.35	0.06	0.22	100.03	88.9
OL20	40.04	12.37	0.22	46.60	0.36	0.04	0.18	99.82	87.0
OL21	39.87	12.25	0.19	46.92	0.35	0.06	0.18	99.83	87.2
OL22	40.25	12.05	0.14	47.38	0.34	0.06	0.14	100.36	87.5
OL23	40.31	10.57	0.11	48.20	0.34	0.08	0.19	99.80	89.1
OL24	39.92	12.43	0.15	46.53	0.40	0.05	0.20	99.67	87.0
OL25	40.10	11.62	0.20	47.25	0.36	0.06	0.19	99.80	87.9
OL26	39.89	11.22	0.17	48.25	0.35	0.06	0.17	100.09	88.5
OL38-GL2	39.74	12.24	0.13	46.66	0.39	0.06	0.13	99.35	87.2
OL29	40.11	12.64	0.13	46.37	0.39	0.06	0.19	99.89	86.7
OL27	39.78	11.95	0.27	47.14	0.37	0.07	0.21	99.79	87.6
OL28-GL	39.89	11.89	0.16	47.18	0.39	0.05	0.17	99.74	87.6
OL38-GL1	39.81	11.92	0.16	46.57	0.36	0.06	0.18	99.06	87.4

Appendix 4.2, continued

Sample	SiO_2	FeO	MnO	MgO	CaO	Cr_2O_3	NiO	Total	[a]Fo
OL30	39.70	13.43	0.21	45.61	0.36	0.02	0.10	99.42	85.8
OL31	40.36	10.51	0.12	48.03	0.34	0.09	0.17	99.62	89.1
OL32	40.03	12.50	0.15	46.81	0.41	0.06	0.14	100.10	87.0
OL33	39.87	12.10	0.21	47.16	0.38	0.05	0.20	99.99	87.4
OL34	39.93	12.19	0.17	46.78	0.37	0.07	0.18	99.68	87.2
OL35	40.10	12.31	0.18	47.08	0.37	0.07	0.18	100.29	87.2
OL36	39.90	11.98	0.19	47.24	0.37	0.05	0.17	99.89	87.5
OL37-SP	40.11	12.59	0.18	46.88	0.39	0.20	0.17	100.51	86.9
OL39-GL	40.00	11.49	0.15	47.44	0.36	0.09	0.25	99.77	88.0
OL40	40.20	10.50	0.21	47.98	0.34	0.07	0.16	99.45	89.1
OL41-SP1	40.00	12.50	0.16	47.08	0.38	0.10	0.17	100.40	87.0
OL41-SP2	40.00	12.50	0.16	47.08	0.38	0.10	0.17	100.40	87.0
OL41-GL3	40.08	12.51	0.21	46.88	0.43	0.08	0.20	100.38	87.0
OL42	40.16	11.96	0.26	47.12	0.38	0.06	0.17	100.11	87.5
OL43	40.04	10.38	0.10	48.46	0.35	0.04	0.17	99.54	89.3
OL46	40.39	10.40	0.17	48.59	0.39	0.07	0.20	100.21	89.3
OL47	40.23	12.26	0.15	47.34	0.37	0.02	0.19	100.56	87.3
OL48-GL	40.29	12.14	0.15	47.26	0.37	0.05	0.18	100.44	87.4
OL49	40.83	10.54	0.16	48.64	0.34	0.07	0.17	100.76	89.2
OL50	40.24	10.84	0.13	47.90	0.40	0.06	0.22	99.79	88.7
OL51-GL	39.83	12.74	0.20	46.71	0.39	0.06	0.13	100.07	86.7
OL52	40.60	10.22	0.11	48.76	0.35	0.06	0.25	100.35	89.5
OL53	40.13	10.34	0.12	48.61	0.34	0.05	0.21	99.80	89.3
OL54	40.46	11.10	0.18	47.67	0.37	0.07	0.15	100.00	88.4
OL55	40.07	12.22	0.22	47.16	0.36	0.06	0.17	100.26	87.3
OL57-PL	40.21	11.76	0.11	47.61	0.36	0.05	0.15	100.25	87.8
OL57-GL2	40.55	11.68	0.16	47.74	0.40	0.06	0.16	100.77	87.9
OL58	40.14	11.07	0.18	47.90	0.34	0.09	0.25	99.96	88.5
OL59-GL1	40.20	12.61	0.21	46.58	0.41	0.05	0.14	100.20	86.8
OL59-GL2	39.83	12.64	0.21	46.34	0.42	0.04	0.17	99.66	86.7
OL60	39.39	14.69	0.22	44.91	0.36	0.03	0.09	99.67	84.5
OL61	40.42	12.02	0.12	47.36	0.35	0.07	0.14	100.47	87.5
OL62	39.76	12.23	0.20	46.96	0.37	0.07	0.15	99.74	87.3
OL63	39.95	12.23	0.20	47.02	0.36	0.07	0.18	100.00	87.3
OL64-SP	40.29	10.49	0.06	48.92	0.35	0.13	0.23	100.47	89.3
OL65	40.26	11.94	0.14	47.43	0.38	0.06	0.17	100.38	87.6
OL66-SP	40.18	12.31	0.16	46.69	0.37	0.22	0.19	100.11	87.1
OL67-SP	39.96	12.71	0.21	46.64	0.39	0.12	0.16	100.21	86.7
OL68-GL	40.27	11.77	0.16	47.53	0.37	0.04	0.18	100.32	87.8
OL69	40.29	11.88	0.10	47.43	0.39	0.05	0.14	100.28	87.7
OL70-GL	40.16	11.78	0.24	47.13	0.39	0.03	0.17	99.90	87.7
OL71-GL1	40.30	11.98	0.17	47.41	0.37	0.06	0.19	100.47	87.6
OL71-SP2	40.05	11.75	0.20	47.05	0.37	0.21	0.20	99.83	87.7
OL71-SP3	40.05	11.75	0.20	47.05	0.37	0.21	0.20	99.83	87.7
OL71-SP4	40.05	11.75	0.20	47.05	0.37	0.21	0.20	99.83	87.7
OL72	40.53	10.69	0.18	48.76	0.36	0.04	0.24	100.80	89.0
OL73-GL1	39.99	12.24	0.20	46.56	0.38	0.06	0.17	99.61	87.1
OL73-SP1	39.99	12.24	0.20	46.56	0.38	0.06	0.17	99.61	87.1
OL73-SP2	39.97	12.47	0.21	47.07	0.39	0.14	0.20	100.45	87.1
OL73-SP3	39.97	12.47	0.21	47.07	0.39	0.14	0.20	100.45	87.1
OL74	39.77	12.91	0.24	46.96	0.37	0.05	0.18	100.47	86.6
OL75	39.93	12.49	0.24	47.28	0.38	0.06	0.21	100.58	87.1
OL76	39.92	12.22	0.12	47.62	0.36	0.07	0.18	100.48	87.4
OL77-GL1	39.76	12.58	0.16	47.00	0.40	0.04	0.17	100.12	86.9
OL80-GL2	39.29	15.79	0.23	43.93	0.30	0.03	0.13	99.70	83.2
OL80-GL1	39.59	15.20	0.22	44.35	0.30	0.00	0.10	99.76	83.9
OL77-SP2	39.78	12.56	0.16	46.64	0.37	0.15	0.18	99.83	86.9
OL78	39.92	12.85	0.21	46.68	0.35	0.04	0.20	100.25	86.6
OL81	39.81	11.77	0.16	47.58	0.36	0.05	0.16	99.90	87.8
OL82-SP	40.10	11.43	0.14	47.81	0.37	0.09	0.22	100.16	88.2
OL83	39.36	12.68	0.20	46.26	0.36	0.06	0.12	99.04	86.7
OL89-GL	40.17	12.09	0.26	47.46	0.38	0.03	0.19	100.58	87.5
OL90-GL1	39.71	11.99	0.15	47.17	0.38	0.04	0.18	99.63	87.5
OL90-GL2	39.78	11.43	0.14	47.57	0.35	0.05	0.22	99.53	88.1
OL96-GL	39.94	10.94	0.19	48.16	0.37	0.04	0.16	99.81	88.7
OL96-1	40.21	11.60	0.21	47.42	0.37	0.05	0.18	100.04	87.9
OL99-SP-GL	40.17	12.11	0.17	47.27	0.37	0.13	0.19	100.42	87.4

Appendix 4.2, continued

Sample	SiO_2	FeO	MnO	MgO	CaO	Cr_2O_3	NiO	Total	[a]Fo
OL101-GL1	39.62	12.80	0.23	46.57	0.40	0.04	0.16	99.82	86.6
OL101-GL3	39.73	13.05	0.24	46.38	0.39	0.02	0.14	99.95	86.4
OL101-GL2	39.66	12.84	0.21	46.50	0.40	0.05	0.15	99.81	86.6
OL102-GL	40.25	11.05	0.15	48.24	0.37	0.04	0.19	100.28	88.6
OL105-GL	39.65	12.83	0.14	46.53	0.41	0.04	0.18	99.77	86.6
OL108-GL	40.01	11.41	0.14	47.53	0.40	0.08	0.21	99.78	88.1
OL112-GL	40.53	10.26	0.12	48.73	0.35	0.10	0.19	100.27	89.4
OL118-GL	39.84	9.59	0.16	48.68	0.34	0.06	0.24	98.91	90.0
OL119	40.21	12.52	0.19	46.71	0.39	0.07	0.13	100.21	86.9
OL56	39.58	11.62	0.18	46.49	0.38	0.06	0.13	98.45	87.7
OL79	39.79	11.97	0.20	46.62	0.35	0.07	0.15	99.14	87.4
OL84	39.98	10.16	0.19	48.59	0.33	0.07	0.18	99.50	89.5
OL85	40.01	10.36	0.20	48.03	0.35	0.08	0.17	99.19	89.2
OL86	39.84	10.29	0.10	48.13	0.36	0.05	0.22	98.99	89.3
OL87	40.17	10.12	0.11	48.21	0.37	0.07	0.21	99.26	89.5
OL91	39.72	11.22	0.17	46.84	0.37	0.04	0.17	98.53	88.2
OL92	39.70	12.21	0.22	46.10	0.34	0.05	0.18	98.80	87.1
OL94	39.96	10.27	0.14	47.75	0.33	0.08	0.19	98.73	89.2
OL95	39.76	10.91	0.15	47.22	0.37	0.04	0.25	98.70	88.5
OL97	39.63	11.98	0.22	46.29	0.38	0.08	0.15	98.73	87.3
OL98	39.83	10.72	0.21	47.66	0.38	0.07	0.21	99.09	88.8
OL100	39.62	12.80	0.16	45.90	0.38	0.06	0.19	99.11	86.5
A30-OL1	40.52	10.10	0.13	48.01	0.29	0.07	0.21	99.33	89.4
A30-OL3	40.68	10.01	0.19	48.59	0.31	0.04	0.23	100.04	89.6
A30-OL4-GL	40.05	11.48	0.18	47.04	0.34	0.07	0.16	99.32	88.0
A30-OL5-GL	40.30	11.63	0.18	47.13	0.32	0.05	0.13	99.73	87.8
A30-OL6-SP	40.20	11.52	0.25	47.13	0.33	0.08	0.15	99.65	87.9
A30-OL7-GL1	40.12	12.44	0.13	46.51	0.33	0.03	0.15	99.70	87.0
A30-OL7-GL2	40.00	12.54	0.18	46.59	0.34	0.08	0.14	99.87	86.9
A30-OL7-GL3	40.09	12.33	0.13	46.25	0.31	0.04	0.13	99.28	87.0
A30-OL8	40.27	10.72	0.18	47.53	0.34	0.07	0.19	99.30	88.8
A30-OL9	40.50	11.93	0.20	46.76	0.34	0.04	0.18	99.95	87.5
A31-0L54-GL	40.01	11.59	0.16	46.84	0.35	0.07	0.14	99.16	87.8
A31-OL56-SP	40.32	11.83	0.16	47.29	0.35	0.07	0.18	100.21	87.7
A31-OL58-GL1	39.92	12.24	0.16	46.36	0.31	0.06	0.19	99.24	87.1
A31-OL58-GL2	40.48	10.35	0.11	47.93	0.32	0.04	0.15	99.37	89.2
A31-OL64-GL1	40.37	11.23	0.20	47.39	0.33	0.05	0.15	99.72	88.3
A31-OL64-GL2	40.09	11.08	0.15	47.17	0.30	0.07	0.19	99.04	88.4
A31-OL42-SP2	40.02	11.90	0.21	46.49	0.33	0.13	0.15	99.23	87.4
A31-OL26-GL	40.14	11.56	0.13	46.96	0.34	0.07	0.14	99.33	87.9
A31-OL20-GL	40.66	9.76	0.12	48.53	0.33	0.08	0.19	99.67	89.9
A31-OL18-SP	40.29	11.36	0.14	47.25	0.31	0.11	0.19	99.65	88.1
A31-OL14-SP	40.06	11.18	0.12	47.21	0.35	0.09	0.19	99.20	88.3
A30-OL2	40.45	10.32	0.17	48.04	0.33	0.04	0.21	99.56	89.2
A31-OL42-SP	40.98	11.62	0.17	47.63	0.35	0.08	0.13	100.96	88.0
A30-OL5	40.02	11.59	0.15	46.50	0.32	0.03	0.16	98.77	87.7
A30-OL7	40.30	11.61	0.19	46.69	0.34	0.07	0.17	99.38	87.8
A30-OL9-GL	40.29	11.34	0.17	46.79	0.30	0.07	0.21	99.17	88.0
A30-OL10-GL2	40.70	10.89	0.15	47.48	0.30	0.05	0.17	99.74	88.6
A30-OL3-GL	40.13	11.31	0.21	46.83	0.35	0.06	0.18	99.07	88.1
A29-OL1A	38.89	12.78	0.19	45.25	0.38	0.05	0.17	97.70	86.3
A29-OL1-GL	39.22	13.36	0.25	45.73	0.38	0.03	0.18	99.15	85.9
A29-OL2	39.24	13.32	0.25	45.17	0.37	0.04	0.17	98.56	85.8
A29-OL3	39.33	13.65	0.15	45.15	0.33	0.09	0.17	98.87	85.5

[a]Forsterite, Fo = 100 X Mg/(Mg + Fe).

Appendix 4.3, Spinel analyses.

Sample	SiO_2	TiO_2	Al_2O_3	[a]Fe_2O_3	FeO	MnO	MgO	Cr_2O_3	NiO	ZnO	Total
OL4-SP2	0.11	0.56	24.82	6.93	14.04	0.18	14.35	38.31	0.16	0.03	99.49
OL6-SP1	0.11	0.49	24.83	6.16	14.15	0.21	14.14	38.95	0.17	0.10	99.31
OL6-SP2	0.11	0.48	24.96	5.70	14.02	0.22	14.35	39.58	0.13	0.05	99.6
OL6-SP3-GL	0.12	0.48	24.95	5.54	13.85	0.18	14.38	39.50	0.21	0.03	99.25
OL9-SP1	0.06	0.49	24.64	6.54	14.16	0.22	13.86	38.08	0.13	0.13	98.32

Appendix 4.3, continued

Sample	SiO_2	TiO_2	Al_2O_3	$^aFe_2O_3$	FeO	MnO	MgO	Cr_2O_3	NiO	ZnO	Total
OL18-SP2	0.12	0.47	27.34	6.85	13.69	0.18	14.69	35.52	0.10	0.13	99.09
OL37-SP	0.05	0.62	24.23	7.49	13.86	0.20	14.40	38.70	0.17	0.09	99.8
OL41-SP1	0.07	0.45	27.40	7.42	13.18	0.18	14.97	35.32	0.18	0.11	99.27
OL41-SP2	0.14	0.45	27.92	7.02	13.51	0.15	15.01	35.30	0.18	0.08	99.75
OL64-SP	0.07	0.31	29.66	5.87	11.35	0.09	16.34	35.02	0.20	0.07	98.98
OL66-SP	0.06	0.53	25.67	6.96	13.99	0.23	14.42	37.70	0.16	0.06	99.78
OL67-SP	0.08	0.43	26.09	6.78	13.53	0.23	14.46	36.66	0.12	0.08	98.46
OL71-SP2	0.06	0.52	23.28	6.39	14.37	0.25	13.85	40.37	0.13	0.00	99.22
OL71-SP3	0.06	0.50	22.80	6.23	14.34	0.23	13.77	41.17	0.13	0.15	99.37
OL71-SP4	0.12	0.46	22.52	6.24	14.66	0.27	13.55	41.20	0.11	0.08	99.22
OL73-SP1	0.07	0.49	24.93	7.31	13.54	0.19	14.50	37.95	0.13	0.16	99.27
OL73-SP2	0.17	0.50	24.82	7.18	13.76	0.17	14.24	37.01	0.17	0.04	98.06
OL73-SP3	0.06	0.50	24.26	6.47	13.59	0.24	14.53	39.97	0.16	0.06	99.84
OL77-SP2	0.06	0.55	23.05	6.99	14.17	0.23	13.92	39.75	0.09	0.01	98.81
OL82-SP	0.10	0.46	25.12	6.06	13.46	0.19	14.71	39.33	0.13	0.10	99.66
OL99-SP	0.20	0.55	24.45	6.19	14.47	0.22	13.94	38.71	0.16	0.09	98.98
PL13-SP1	0.14	0.26	33.27	4.35	10.97	0.09	17.27	33.52	0.15	0.07	100.09
PL13-SP2	0.11	0.27	32.40	4.99	11.85	0.14	16.52	33.42	0.14	0.06	99.9
A26-PL1-SP-GL	0.09	0.68	25.97	6.79	13.54	0.21	14.87	37.32	0.11	0.07	99.65
A26-PL2-SP1	0.09	0.21	38.26	4.11	8.53	0.08	19.08	28.46	0.17	0.08	99.06
A26-PL2-SP2	0.09	0.13	38.53	3.85	8.87	0.06	18.93	28.58	0.17	0.00	99.21
A26-PL3-GL-SP	0.09	0.38	31.97	5.10	10.89	0.13	17.00	33.49	0.15	0.09	99.29
A26-PL4-SP	0.12	0.32	32.25	4.87	10.18	0.10	17.50	33.76	0.13	0.16	99.39
A26-PL6-SP	0.11	0.18	35.45	4.47	9.65	0.10	18.06	30.61	0.04	0.07	98.75
A27-PL1-SP	0.11	0.31	36.14	4.15	10.14	0.11	18.07	30.62	0.15	0.02	99.83
A27-PL2-SP	0.11	0.32	30.54	7.57	14.03	0.15	14.95	32.39	0.18	0.08	100.32
A27-PL3-SP	0.09	0.32	29.98	5.39	10.71	0.18	17.01	35.97	0.10	0.04	99.79
A27-PL4-SP	0.13	0.22	35.57	4.87	9.49	0.08	18.41	30.97	0.16	0.07	99.97
A27-PL5-SP	0.08	0.45	31.07	6.38	12.5	0.13	16.20	33.58	0.05	0.09	100.53
A27-PL7-SP1	0.11	0.14	44.52	4.54	7.94	0.10	20.20	21.87	0.14	0.09	99.65
A27-PL7-SP2-GL	0.11	0.16	44.36	4.18	7.98	0.10	20.17	22.27	0.12	0.07	99.52
A27-PL6-SP	0.09	0.27	32.97	4.4	10.24	0.12	17.63	34.01	0.19	0.02	99.94
A27-PL7-SP	0.12	0.17	37.47	4.45	9.86	0.18	18.29	29.18	0.15	0.00	99.88
A27-PL8-SP-GL1	0.13	0.23	34.98	5.72	9.95	0.13	18.04	30.69	0.16	0.07	100.09
A27-PL8-SP-GL2	0.13	0.27	34.49	5.72	10.02	0.18	17.86	30.62	0.06	0.06	99.40
A27-PL9-SP	0.25	0.60	23.27	7.23	14.07	0.16	14.04	38.45	0.14	0.12	98.33
A27-PL13-SP-G 1	0.11	0.32	29.77	4.75	11.22	0.17	16.70	36.69	0.13	0.01	99.87
A27-PL13-SP-GL	0.65	0.34	29.95	3.95	11.95	0.12	16.85	36.54	0.18	0.05	100.58
A27-PL14-SP1-G	0.10	0.60	24.60	6.78	13.99	0.19	14.48	38.91	0.10	0.01	99.76
A27-PL14-SP1-G	0.10	0.57	24.91	6.77	14.25	0.16	14.48	39.11	0.11	0.03	100.49
A27-PL14-SP2	0.10	0.55	24.67	7.07	13.73	0.19	14.67	39.11	0.09	0.14	100.32
A30-PL10-SP3	0.06	0.33	34.06	4.38	10.91	0.17	17.51	33.28	0.09	0.06	100.86
A30-PL10-SPCR	0.08	0.36	34.08	4.27	11.03	0.20	17.37	33.10	0.23	0.01	100.73
A30-PL10-SPCR	0.10	0.38	34.23	4.27	11.00	0.18	17.56	33.31	0.21	0.03	101.27
A30-PL10-SPCR	0.09	0.35	34.09	4.22	10.88	0.16	17.48	33.04	0.17	0.02	100.50
A30-PL10-SPCR	0.07	0.36	34.15	4.36	10.87	0.20	17.51	33.00	0.06	0.11	100.68
A30-OL6-SP	0.06	0.53	26.69	6.89	13.94	0.22	14.77	37.51	0.19	0.07	100.88
A31-OL56-SP	0.21	0.49	24.10	6.70	14.07	0.21	14.39	39.69	0.20	0.01	100.07
A31-PL65-SP1	0.10	0.28	30.96	4.28	12.49	0.18	16.01	35.68	0.14	0.01	100.13
A31-PL65-SP2	0.11	0.28	32.30	4.54	11.11	0.18	17.09	34.56	0.13	0.03	100.32
A31-PL66-SP1	0.10	0.28	31.92	4.23	10.83	0.19	17.09	34.97	0.15	0.04	99.81
A31-PL66-SP2	0.12	0.26	34.32	4.26	10.60	0.08	17.64	32.85	0.20	0.08	100.41
A31-PL67-SP1	0.11	0.20	34.98	4.32	10.01	0.17	17.94	32.25	0.20	0.12	100.29
A31-PL67-SP2	0.10	0.25	34.74	3.98	10.76	0.12	17.59	32.67	0.16	0.01	100.37
A31-PL68-SP1	0.07	0.18	37.77	4.47	9.71	0.12	18.53	29.52	0.14	0.08	100.60
A31-PL68-SP2	0.09	0.16	37.63	4.33	9.89	0.08	18.36	29.31	0.09	0.04	99.99
A31-PL68-SP3	0.08	0.16	37.96	4.48	9.69	0.07	18.62	29.54	0.24	0.03	100.87
A31-PL68-SP4	0.08	0.18	37.86	4.74	9.62	0.12	18.64	29.40	0.17	0.10	100.91
A31-PL69-SP1	0.06	0.56	24.41	6.18	13.69	0.20	14.64	40.44	0.15	0.13	100.46
A31-PL69-SP2	0.08	0.54	24.55	6.57	13.44	0.19	14.91	40.10	0.11	0.06	100.54
A31-PL70-SP	0.08	0.24	33.76	4.49	10.49	0.13	17.61	33.35	0.18	0.01	100.35
A31-PL46-SP	0.09	0.42	32.73	5.45	12.43	0.19	16.32	32.64	0.18	0.03	100.50
A31-PL47-SP1	0.13	0.17	38.33	4.11	9.84	0.14	18.55	29.23	0.21	0.05	100.74
A31-PL47-SP2	0.10	0.22	33.25	4.49	10.28	0.12	17.83	34.40	0.14	0.03	100.86
A31-PL47-SP3	0.09	0.25	33.24	4.37	10.30	0.09	17.78	34.37	0.15	0.08	100.72
A31-PL50-SP-GL	0.12	0.29	36.45	4.80	9.93	0.13	18.63	31.33	0.13	0.08	101.90
A31-PL52-SP	0.11	0.52	24.96	6.27	13.38	0.24	14.99	39.89	0.10	0.02	100.48

Appendix 4.3, continued

Sample	SiO_2	TiO_2	Al_2O_3	$^aFe_2O_3$	FeO	MnO	MgO	Cr_2O_3	NiO	ZnO	Total
A31-PL41-SPCR	0.07	0.18	33.86	4.60	9.60	0.17	18.13	33.81	0.18	0.16	100.74
A31-PL41-SPCR	0.07	0.18	34.14	4.70	9.68	0.14	18.21	33.49	0.14	0.08	100.83
A31-PL41-SPCR	0.06	0.22	34.07	4.73	9.56	0.11	18.31	33.86	0.37	0.01	101.30
A31-OL42-SP	0.13	0.53	24.42	6.51	13.33	0.28	14.82	39.68	0.08	0.05	99.83
A31-OL42-SP2	0.08	0.60	24.60	7.21	13.63	0.22	14.53	38.72	0.28	0.14	100.01
A31-OL18-SP	0.06	0.47	26.43	5.98	13.32	0.13	15.15	38.92	0.25	0.00	100.70
A31-OL14-SP	0.06	0.53	26.45	6.51	13.24	0.25	15.02	37.85	0.18	0.13	100.22
A30-PL10 -SP4	0.59	0.35	32.79	3.29	12.01	0.19	16.67	32.98	0.26	0.06	99.18
A30-PL10-SP2	0.14	0.36	32.74	4.26	10.98	0.10	17.02	33.19	0.16	0.09	99.04
A31-OL56-SP	0.12	0.52	23.96	7.11	14.13	0.16	14.30	39.66	0.11	0.17	100.25

[a]Calculated from stoichiometry.

Appendix 4.4, Naturally-quenched (un-homogemised) melt inclusions.

Sample	SiO_2	TiO_2	Al_2O_3	^aFeO	MnO	MgO	CaO	Na_2O	K_2O	P_2O_5	Cr_2O_3	Total
Plagioclase												
PL1-GL1	49.63	0.53	12.76	9.67	0.21	12.04	12.32	1.57	0.05	0.00	0.08	98.85
PL1-GL2	49.48	0.41	15.14	8.53	0.17	10.53	12.87	1.72	0.04	0.01	0.06	98.95
PL1-GL3	49.93	0.32	10.87	10.43	0.19	13.20	11.91	1.43	0.05	0.00	0.08	98.41
PL3-GL1	49.72	0.43	14.73	8.80	0.22	10.77	12.52	1.63	0.04	0.00	0.09	98.94
PL3-GL2	49.84	0.38	14.76	8.81	0.11	11.25	12.52	1.57	0.04	0.00	0.08	99.34
PL4-GL	50.51	0.32	14.72	7.63	0.13	11.76	12.91	1.71	0.03	0.00	0.01	99.72
PL5-GL1	50.18	0.30	14.33	7.19	0.12	11.75	13.29	1.70	0.03	0.00	0.11	99.00
PL5-GL2	50.22	0.26	14.15	7.29	0.12	11.93	13.02	1.68	0.02	0.00	0.03	98.72
PL6-GL1-1	49.71	0.65	15.10	8.18	0.14	10.20	12.75	1.84	0.04	0.02	0.07	98.71
PL6-GL1-2	50.06	0.67	14.96	8.13	0.18	10.22	12.93	1.85	0.03	0.02	0.03	99.08
PL6-GL2	50.16	0.63	14.9	8.07	0.15	10.29	13.00	1.78	0.03	0.00	0.08	99.08
PL6-GL3-1	49.82	0.70	15.08	8.18	0.09	10.23	13.10	1.78	0.04	0.00	0.06	99.08
PL6-GL3-2	50.06	0.65	15.40	8.29	0.11	10.21	13.06	1.85	0.03	0.00	0.06	99.71
PL7-GL1	50.12	0.38	15.05	7.98	0.13	10.84	12.78	1.64	0.04	0.00	0.09	99.05
PL7-GL2	50.24	0.49	13.25	8.66	0.12	12.01	12.58	1.46	0.04	0.00	0.06	98.89
PL7-GL3	50.35	0.40	15.56	8.01	0.07	10.74	12.54	1.70	0.03	0.00	0.06	99.47
PL7-GL4	50.52	0.43	14.51	8.34	0.13	11.27	12.54	1.73	0.03	0.00	0.13	99.62
PL7-GL5	50.53	0.51	14.62	8.33	0.19	11.27	13.06	1.54	0.03	0.00	0.04	100.12
PL8-GL	49.94	1.07	13.67	9.88	0.26	9.26	12.93	1.96	0.06	0.04	0.06	99.13
PL9-GL1	51.54	0.25	13.67	8.14	0.26	11.25	12.51	1.72	0.06	0.00	0.07	99.46
PL9-GL2	51.53	0.29	11.43	9.00	0.14	12.48	12.40	1.42	0.04	0.00	0.05	98.79
PL9-GL3	51.62	0.28	13.34	8.30	0.15	11.40	12.15	1.66	0.07	0.00	0.08	99.06
PL9-GL4	51.30	0.34	12.15	9.04	0.20	12.08	12.50	1.52	0.04	0.00	0.04	99.21
PL9-GL5	51.28	0.41	12.14	8.81	0.07	12.13	12.49	1.49	0.06	0.00	0.10	98.98
PL11-GL	50.61	1.30	14.89	8.42	0.16	8.79	12.70	2.21	0.07	0.09	0.06	99.29
PL12-GL	50.38	1.53	14.22	9.27	0.21	8.36	11.98	2.32	0.07	0.04	0.09	98.47
PL16-GL1	47.91	1.32	14.64	9.81	0.18	10.07	11.89	1.90	0.10	0.07	0.07	97.95
PL16-GL2	50.25	1.04	15.38	8.63	0.18	8.55	12.44	2.40	0.06	0.06	0.07	99.06
PL16-GL3	50.25	1.06	14.54	8.89	0.12	9.02	12.29	2.48	0.07	0.08	0.03	98.81
PL17-GL1	50.23	0.34	14.28	9.01	0.19	11.25	12.60	1.67	0.04	0.01	0.06	99.67
PL17-GL2	50.26	0.36	14.98	8.94	0.23	10.81	12.46	1.78	0.04	0.00	0.07	99.93
PL17-GL3	49.83	0.34	13.31	9.36	0.17	11.77	12.30	1.73	0.04	0.00	0.07	98.91
PL18-GL	50.85	1.20	15.18	9.29	0.19	7.78	12.62	2.28	0.06	0.10	0.03	99.58
PL19-GL1	49.95	0.32	14.42	8.20	0.16	11.83	12.56	1.71	0.04	0.00	0.06	99.24
PL19-GL2	50.14	0.35	14.29	8.22	0.15	11.95	12.42	1.66	0.02	0.00	0.04	99.24
PL19-GL3	50.05	0.28	14.42	8.12	0.11	12.07	12.35	1.74	0.04	0.00	0.10	99.29
PL19-GL4	49.92	0.31	14.38	8.12	0.19	12.06	12.19	1.69	0.03	0.00	0.07	98.94
PL19-GL5	49.96	0.41	14.25	8.60	0.27	11.66	12.58	1.75	0.04	0.00	0.02	99.54
PL20-GL1	50.80	0.84	14.43	8.72	0.15	9.26	12.54	2.07	0.06	0.00	0.06	98.93
PL20-GL2	50.79	0.81	14.68	8.62	0.09	8.96	12.83	2.00	0.06	0.00	0.05	98.89
PL20-GL3	50.86	0.80	14.16	8.95	0.16	9.28	12.76	2.08	0.06	0.00	0.05	99.16
PL21-GL1	50.30	0.41	15.14	8.78	0.10	10.19	12.76	1.77	0.03	0.00	0.08	99.56
PL21-GL2	49.93	0.42	15.10	8.64	0.11	10.43	12.7	1.74	0.02	0.00	0.07	99.17
PL21-GL3	50.61	0.32	14.99	8.65	0.14	10.10	12.57	1.74	0.03	0.00	0.02	99.16
PL21-GL4	50.44	0.33	15.07	8.62	0.20	10.20	12.69	1.76	0.02	0.00	0.10	99.42
PL23-GL1	50.79	0.36	13.50	9.41	0.15	11.40	13.03	1.26	0.01	0.00	0.03	99.93
PL23-GL2	49.94	0.51	12.83	9.77	0.23	11.90	12.27	1.58	0.03	0.00	0.08	99.14
PL23-GL3	50.62	0.36	13.50	9.52	0.27	11.49	12.46	1.49	0.02	0.00	0.11	99.84
PL23-GL4-1	50.33	0.46	15.20	8.79	0.14	10.51	12.76	1.64	0.03	0.02	0.09	99.97
PL23-GL4-2	50.25	0.48	14.14	9.42	0.12	11.12	12.82	1.54	0.03	0.00	0.09	100.01

Appendix 4.4, continued

Sample	SiO_2	TiO_2	Al_2O_3	[a]FeO	MnO	MgO	CaO	Na_2O	K_2O	P_2O_5	Cr_2O_3	Total
PL24-GL1	50.61	0.63	14.86	8.59	0.19	10.28	12.55	1.76	0.03	0.00	0.06	99.56
PL29-GL1	50.52	0.43	14.22	8.67	0.22	10.66	13.00	1.79	0.02	0.03	0.04	99.61
PL29-GL2	50.27	0.25	15.23	7.92	0.22	10.09	13.04	1.81	0.03	0.00	0.06	98.92
PL30-GL1	50.71	0.56	15.02	8.62	0.05	10.56	12.31	1.83	0.05	0.00	0.09	99.82
PL30-GL2	50.28	0.51	14.19	8.92	0.19	11.37	12.29	1.75	0.03	0.00	0.05	99.58
PL31-GL1	50.80	0.98	13.87	9.18	0.12	10.00	12.64	2.00	0.06	0.02	0.05	99.72
PL31-GL2	50.63	0.99	13.74	9.07	0.20	10.02	12.71	1.93	0.03	0.01	0.08	99.40
PL31-GL3	50.58	0.95	13.32	9.20	0.17	10.26	12.84	1.91	0.02	0.02	0.05	99.32
PL32-GL	49.93	0.65	13.79	9.30	0.18	10.94	12.37	1.62	0.03	0.00	0.09	98.90
PL33-GL-1	49.99	1.53	14.58	8.86	0.19	8.64	12.60	2.15	0.05	0.09	0.05	98.73
PL33-GL-2	49.40	1.55	14.01	9.12	0.13	8.86	12.64	2.12	0.07	0.07	0.03	98.00
PL34-GL1	50.73	0.65	14.20	8.28	0.25	10.78	12.59	1.70	0.03	0.03	0.09	99.32
PL34-GL2	50.57	0.72	13.72	8.65	0.20	11.26	12.63	1.62	0.03	0.01	0.05	99.46
A26-PL2-GL1	51.05	0.24	12.72	8.60	0.22	12.39	12.62	1.49	0.03	0.01	0.01	99.37
A26-PL2-GL2	50.87	0.26	14.23	8.08	0.17	11.63	12.70	1.61	0.03	0.00	0.05	99.63
A26-PL2-GL3	51.52	0.37	12.34	8.97	0.27	12.41	12.86	1.21	0.03	0.00	0.06	100.04
A26-PL3-GL-SP	49.76	0.96	14.98	8.71	0.16	10.31	12.94	1.82	0.03	0.00	0.04	99.72
A26-PL5-GL1	50.52	0.50	14.78	8.12	0.10	10.6	12.54	1.78	0.05	0.04	0.02	99.05
A26-PL5-GL2	50.94	0.45	14.79	8.29	0.17	10.74	12.67	1.87	0.04	0.00	0.09	100.05
A26-PL5-GL3	50.70	0.46	14.81	8.21	0.12	10.62	12.70	1.78	0.02	0.01	0.05	99.47
A27-PL12-GL1	50.67	0.46	14.76	9.13	0.16	9.88	13.07	1.84	0.03	0.02	0.07	100.09
A27-PL12-GL2	50.82	0.50	14.77	9.01	0.16	9.80	13.09	1.90	0.03	0.07	0.04	100.20
A27-PL12-GL3	50.69	0.45	14.29	9.34	0.11	10.40	12.85	1.83	0.03	0.01	0.08	100.07
A29-PL1-GL	50.53	0.94	14.99	9.09	0.12	8.68	12.44	2.30	0.06	0.06	0.05	99.26
A30-PL11-GL1	50.36	0.38	14.71	8.52	0.18	10.23	12.59	1.78	0.04	0.03	0.05	98.86
A30-PL11-GL2	50.78	0.34	14.84	8.38	0.14	10.34	12.64	1.71	0.04	0.01	0.03	99.27
A30-PL11-GL3	50.91	0.34	14.65	8.44	0.14	10.43	12.61	1.69	0.04	0.02	0.08	99.36
A30-PL12-GL1	49.92	0.47	15.11	8.58	0.15	10.48	12.65	1.73	0.03	0.03	0.06	99.21
A30-PL12-GL2	50.03	0.41	14.98	8.39	0.14	10.42	12.67	1.65	0.02	0.02	0.07	98.80
A30-PL13-GL1	50.54	0.84	15.11	8.46	0.14	8.96	13.03	2.07	0.05	0.04	0.06	99.30
A30-PL13-GL2	50.65	0.77	14.58	8.54	0.18	9.07	12.54	2.09	0.06	0.01	0.05	98.53
A30-PL13-GL3	50.71	0.74	14.88	8.50	0.19	8.98	12.75	2.11	0.06	0.01	0.10	99.02
A31-PL69-GL	50.18	0.95	14.93	8.63	0.18	8.47	12.71	2.11	0.06	0.03	0.11	98.35
A31-PL69-GL2	50.32	0.98	14.97	8.48	0.16	8.56	12.62	2.08	0.05	0.00	0.07	98.28
A25-PL-GL	50.49	1.41	14.23	9.37	0.14	8.42	12.48	2.11	0.05	0.12	0.02	98.83
A27-PL-GL	49.61	0.72	15.01	8.91	0.14	10.88	12.79	1.65	0.03	0.03	0.09	99.85
A27-PL8-GL1	50.80	0.22	14.72	8.02	0.15	12.21	12.71	1.72	0.02	0.00	0.07	100.64
A27-PL8-GL3	50.74	0.24	14.06	8.37	0.16	12.38	12.54	1.66	0.03	0.02	0.04	100.22
A27-PL8-GL4	50.92	0.25	14.16	8.25	0.14	12.44	12.37	1.72	0.04	0.00	0.06	100.34
A27-PL8-GL6	50.62	0.32	13.98	8.53	0.16	12.27	12.50	1.70	0.04	0.03	0.03	100.16
A27-PL8-GL7	50.92	0.34	14.02	8.33	0.17	11.42	12.80	1.81	0.04	0.05	0.12	100.03
A27-PL8-GL8	50.78	0.43	13.48	8.93	0.21	11.96	12.96	1.58	0.02	0.02	0.06	100.43
A27-PL8-GL9	50.84	0.52	13.95	8.67	0.16	11.34	13.10	1.77	0.03	0.01	0.10	100.48
Olivine												
OL4-GL1	49.44	1.14	15.75	9.29	0.11	6.74	13.77	2.18	0.03	0.05	0.03	98.54
OL5-GL	49.81	1.11	16.15	8.70	0.16	5.90	13.75	2.30	0.03	0.01	0.04	97.95
OL7-GL	50.83	1.13	16.32	8.66	0.15	5.14	14.63	1.90	0.03	0.02	0.05	98.87
OL9-GL2	49.48	0.86	16.79	8.10	0.13	5.48	15.17	2.03	0.03	0.22	0.04	98.33
OL16-GL1	49.85	1.17	15.79	9.00	0.13	6.66	13.67	2.18	0.04	0.03	0.04	98.56
OL16-GL2	50.77	1.20	16.82	8.52	0.14	5.37	13.93	2.40	0.04	0.04	0.04	99.27
OL16-GL3	49.76	1.10	15.54	9.17	0.15	7.87	13.09	2.22	0.05	0.05	0.03	99.02
OL18-GL1	49.43	1.02	15.70	9.07	0.14	7.67	13.16	2.21	0.02	0.02	0.01	98.44
OL19-GL1	49.72	1.31	15.81	9.82	0.13	6.97	12.66	2.24	0.06	0.09	0.02	98.84
OL19-GL3	50.38	0.84	16.97	7.94	0.12	7.09	14.04	1.80	0.02	0.06	0.09	99.34
OL28-GL	50.40	1.03	15.55	9.03	0.09	7.03	13.64	2.18	0.05	0.03	0.04	99.08
OL38-GL1	49.46	1.34	15.67	9.85	0.16	6.95	12.75	2.12	0.07	0.06	0.05	98.49
OL38-GL2	49.44	1.26	15.68	9.80	0.19	7.21	12.61	2.23	0.06	0.04	0.08	98.61
OL39-GL	49.94	1.25	15.64	9.66	0.16	7.40	12.68	2.17	0.05	0.05	0.11	99.10
OL41-GL3	50.37	1.02	17.01	8.52	0.08	5.92	13.49	2.60	0.03	0.06	0.08	99.19
OL48-GL	50.02	1.24	15.49	9.69	0.15	7.97	12.30	2.30	0.05	0.08	0.04	99.32
OL51-GL	50.05	1.28	15.87	9.69	0.18	7.47	12.75	2.20	0.07	0.07	0.01	99.63
OL57-GL1	50.16	1.22	16.24	8.74	0.18	6.31	14.60	2.11	0.03	0.36	0.05	99.99
OL68-GL	50.43	1.05	16.42	8.92	0.16	7.59	12.74	2.28	0.05	0.04	0.03	99.70
OL70-GL	50.28	0.96	16.00	8.56	0.11	7.22	13.42	2.23	0.05	0.07	0.07	98.97
OL71-GL1	50.07	1.14	16.37	8.67	0.13	5.70	14.89	2.11	0.04	0.37	0.04	99.52
OL73-GL1	49.34	0.90	16.13	9.28	0.14	7.08	13.38	2.36	0.06	0.07	0.22	98.94
OL77-GL1	50.65	1.23	17.12	8.29	0.14	4.92	13.92	2.64	0.05	0.05	0.12	99.13

Appendix 4.4, continued

Sample	SiO_2	TiO_2	Al_2O_3	[a]FeO	MnO	MgO	CaO	Na_2O	K_2O	P_2O_5	Cr_2O_3	Total
OL80-GL1	49.57	1.34	15.78	9.70	0.18	6.95	12.62	2.34	0.05	0.07	0.05	98.67
OL80-GL2	50.85	2.08	14.51	11.22	0.13	6.56	10.87	2.80	0.09	0.09	0.03	99.24
OL89-GL	51.32	1.07	16.30	8.27	0.13	5.99	14.19	2.21	0.03	0.07	0.07	99.67
OL90-GL1	49.49	1.26	15.71	9.49	0.13	7.76	12.51	2.24	0.06	0.08	0.03	98.76
OL90-GL2	49.79	1.11	16.27	9.08	0.16	7.38	12.77	2.29	0.07	0.05	0.08	99.06
OL96-GL	50.43	0.89	16.3	8.19	0.14	7.45	14.08	1.84	0.02	0.02	0.10	99.48
OL101-GL1	49.99	1.09	16.03	9.30	0.17	7.22	13.17	2.36	0.05	0.06	0.08	99.50
OL101-GL2	49.50	1.11	15.99	9.38	0.15	7.13	13.35	2.32	0.04	0.00	0.08	99.04
OL101-GL3	49.47	1.07	15.97	9.36	0.14	7.20	13.31	2.33	0.05	0.03	0.03	98.95
OL102-GL	49.92	0.77	16.42	8.13	0.06	8.34	13.75	1.80	0.05	0.04	0.03	99.31
OL105-GL	49.66	1.03	15.52	9.44	0.14	7.34	13.46	2.38	0.05	0.04	0.10	99.16
OL108-GL	49.43	0.79	16.33	8.66	0.15	6.99	14.64	1.96	0.03	0.22	0.05	99.25
OL112-GL	50.01	0.72	17.03	7.82	0.22	8.41	13.98	1.66	0.04	0.05	0.10	100.03
OL118-GL	49.11	0.74	18.20	7.36	0.18	6.92	15.00	1.59	0.03	0.00	0.08	99.21
A29-OL1-GL	50.92	1.33	16.57	9.54	0.13	6.18	13.19	2.37	0.05	0.09	0.09	100.45
A30-OL4-GL	51.39	1.02	16.41	8.40	0.13	4.96	14.53	1.96	0.03	0.04	0.08	98.96
A30-OL5-GL	50.65	1.04	15.29	8.64	0.15	7.61	13.03	1.97	0.06	0.02	0.06	98.52
A30-OL7-GL1	50.15	1.06	15.97	9.01	0.21	7.14	12.77	2.40	0.05	0.05	0.08	98.89
A30-OL7-GL2	49.94	1.07	15.96	9.19	0.14	6.90	13.06	2.34	0.04	0.06	0.09	98.77
A30-OL7-GL3	50.13	1.05	15.81	8.95	0.15	7.21	12.78	2.23	0.06	0.07	0.04	98.47
A31-OL54-GL	50.51	0.91	15.50	8.63	0.19	6.91	13.97	1.95	0.03	0.02	0.11	98.72
A31-OL58-GL1	49.83	1.23	15.35	9.73	0.17	7.54	12.43	2.15	0.06	0.09	0.09	98.68
A31-OL58-GL2	49.65	0.67	17.63	7.87	0.14	6.45	14.21	1.77	0.02	0.04	0.10	98.54
A31-OL64-GL1	49.65	1.28	15.52	9.72	0.19	6.75	13.24	2.11	0.06	0.03	0.05	98.59
A31-OL64-GL2	50.49	1.29	17.24	8.90	0.13	4.50	13.45	2.55	0.07	0.07	0.01	98.69
A31-OL26-GL	49.98	0.89	15.36	8.66	0.15	7.76	13.34	2.06	0.01	0.07	0.09	98.37
A31-OL20-GL	49.85	0.73	17.40	7.44	0.13	8.25	13.82	1.78	0.03	0.06	0.03	99.51
A31-OL9-GL	50.25	1.05	16.87	8.88	0.09	6.18	13.13	2.43	0.04	0.06	0.06	99.03
A31-0L10-GL2	50.72	0.83	17.28	7.99	0.17	6.50	14.50	1.96	0.02	0.01	0.04	100.03
A30-OL3-GL	49.93	1.16	15.94	9.40	0.18	7.73	12.59	2.37	0.04	0.05	0.11	99.49
Spinel												
OL6-SP3-GL	49.56	1.21	15.45	9.61	0.16	8.14	12.22	2.26	0.05	0.05	0.22	98.92
PL13-SP1-GL	49.04	0.71	16.93	7.60	0.08	8.86	13.17	1.86	0.03	0.01	0.65	98.95
A6PL8-SP-GL-PL	49.45	0.81	15.47	8.57	0.17	10.3	12.50	1.91	0.03	0.16	0.78	100.15
OL99-SP-GL	48.97	1.31	15.44	9.72	0.12	8.10	11.79	2.19	0.04	0.08	1.60	99.37
A26-PL1-SP-GL	48.62	1.26	17.17	8.70	0.11	7.96	12.67	2.14	0.04	0.06	1.15	99.86
PL8-SP-GL2	48.71	0.73	16.16	7.67	0.12	9.54	13.27	1.55	0.02	0.02	0.78	98.58
A27-PL13-SP-GL	49.08	0.85	16.20	7.72	0.08	9.37	13.03	1.53	0.02	0.06	1.52	99.47
A31-0L66-SP-GL	49.97	0.63	16.44	7.47	0.12	9.35	13.19	1.71	0.02	0.03	0.73	99.66
A31-PL50-SP-GL	48.86	0.66	15.74	7.70	0.17	10.39	13.12	1.66	0.03	0.07	1.13	99.54
A27-PL13-SP-GL	48.77	0.83	16.26	7.92	0.15	9.29	12.86	1.58	0.02	0.01	1.74	99.44
A27-PL14-SP1-G	49.45	1.12	15.83	8.79	0.16	8.05	12.59	2.30	0.05	0.06	1.12	99.53

[a]All Fe as FeO.

Appendix 4.5 Water contents of selected melt inclusions in olivine and plagioclase.

Sample	SiO_2	TiO_2	Al_2O_3	[a]FeO	MnO	MgO	CaO	Na_2O	K_2O	P_2O_5	Cr_2O_3	total	[b]H_2O
A25-PL-GL	50.49	1.41	14.23	9.37	0.14	8.42	12.48	2.11	0.05	0.12	0.02	98.83	0.23
A27-PL-GL	49.61	0.72	15.01	8.91	0.14	10.88	12.79	1.65	0.03	0.03	0.09	99.85	0.11
OL19-GL2	49.94	1.17	16.04	9.29	0.13	7.58	12.51	2.39	0.06	0.04	0.09	99.24	0.12
OL59-GL1	50.12	1.10	15.56	9.60	0.15	7.67	13.15	2.33	0.04	0.07	0.09	99.87	0.22
OL59-GL2	50.25	1.09	15.35	9.58	0.15	7.86	13.20	2.21	0.05	0.08	0.09	99.91	0.23

[a]All Fe as FeO.
[b]H_2O determined by fourier transform infrared spectroscopy.

Appendix 4.6, Analyses of sulfide globules.

Sample	S	Mn	Fe	Co	Cu	Ni	Zn	Se	Cd	Hg	total
OL-90-GL	32.05	0.04	36.67	0.09	23.68	2.85	0.00	0.00	0.00	0.38	95.75
Ol-90-GL	34.81	0.05	50.57	0.21	0.66	12.08	0.00	0.00	0.19	0.00	98.57
OL-48-GL(core)	33.39	0.07	38.71	0.07	25.25	1.07	0.03	0.05	0.10	0.00	98.74
Ol-48-Gl(rim)	34.64	0.06	51.17	0.19	1.77	11.38	0.01	0.00	0.08	0.00	99.30
A25-Pl-GL	31.49		47.82	0.19	8.59	8.30	0.04	0.01			96.43

Appendix 4.7, Olivine daughter crystals in plagioclase hosted melt inclusions.

Sample	SiO_2	FeO	MnO	MgO	CaO	Cr_2O_3	NiO	total	^aFo
P118-OL1	40.06	10.57	0.17	47.47	0.51	0.09	0.11	98.98	88.9
P118-0L2	39.65	9.86	0.16	46.92	0.57	0.09	0.13	97.39	89.5
P109-OL1	39.64	10.26	0.15	45.77	0.92	0.12	0.12	96.98	88.8
P109-OL3	39.90	10.15	0.11	44.67	1.24	0.09	0.11	96.26	88.7

[a]Forsterite content, Fo = 100 x (Mg/(Mg + Fe)).

Appendix 4.8, Homogenised melt inclusions in plagioclase affected by overheating, underheating, analytical overlap or poor quenching (see text for details).

Sample	SiO_2	TiO_2	Al_2O_3	[a]$_{FeO}$	MnO	MgO	CaO	Na_2O	K_2O	P_2O_5	Cr_2O_3	total	CaO/ Na_2O	[b]Host An	[c]T_h (°C)	[d]T_{ol}	[e]T_{pl}	[f]T_{corr}	[g]Comments
P89-1	49.80	0.33	16.42	7.54	0.15	10.91	13.00	1.91	0.03	0.04	0.08	100.21	6.8	91.7	1215	1256	1202	1221	Bad quenching of a slightly underheated run
P89-2	49.24	0.34	17.78	7.01	0.10	10.07	13.34	1.82	0.03	0.00	0.05	99.78	7.3	92.3	1215	1233	1225	1239	Analytical overlap
P89-8	50.07	0.25	15.88	7.52	0.14	11.06	12.88	1.90	0.03	0.00	0.05	99.78	6.8	92.2	1215	1261	1194	1214	Bad quenching of a slightly underheated run
P89-4	49.71	0.28	15.95	7.52	0.15	11.17	12.91	1.88	0.03	0.03	0.02	99.65	6.9	91.9	1215	1265	1195	1216	Bad quenching of a slightly underheated run
P89-10	49.91	0.32	15.70	7.84	0.16	10.78	12.95	1.85	0.02	0.05	0.11	99.69	7.0	92.1	1215	1253	1192	1210	Bad quenching of a slightly underheated run
P89-5	49.71	0.25	15.78	7.59	0.14	10.99	12.95	1.81	0.02	0.02	0.06	99.32	7.2	92.4	1215	1259	1193	1213	Bad quenching of a slightly underheated run
P107-11	49.80	0.87	14.84	9.70	0.18	8.42	12.84	1.79	0.13	0.08	0.02	98.67	7.2	91.2	1210	1194	1184	1188	High-K2O
P107-10	50.26	0.71	14.87	9.27	0.14	8.79	12.91	1.76	0.13	0.08	0.04	98.96	7.3	91.2	1210	1203	1182	1189	High-K2O
P107-8	50.14	0.53	15.21	9.32	0.20	8.92	12.80	1.71	0.14	0.09	0.03	99.09	7.5	90.6	1210	1206	1187	1194	Underheated, poorly quenched
P107-12	50.38	0.78	15.26	9.08	0.07	8.91	12.95	1.70	0.12	0.07	0.03	99.35	7.6	90.7	1210	1205	1187	1194	Underheated, poorly quenched
P107-6	50.43	0.42	15.29	8.47	0.17	9.76	12.93	1.82	0.05	0.01	0.09	99.44	7.1	91.1	1210	1228	1187	1199	Underheated
P107-1	50.81	0.27	16.08	7.92	0.10	9.85	13.17	1.71	0.03	0.05	0.03	100.02	7.7	90.8	1210	1226	1196	1208	Underheated
P107-3	50.52	0.52	15.36	8.20	0.11	9.80	12.96	1.78	0.03	0.05	0.07	99.40	7.3	90.9	1210	1228	1187	1199	Underheated
P106-7	50.25	0.17	15.93	6.72	0.09	11.09	13.21	1.83	0.02	0.00	0.06	99.37	7.2	91.8	1210	1262	1195	1215	Underheated
P106-8	50.13	0.22	15.64	6.73	0.09	10.96	13.24	1.83	0.03	0.00	0.08	98.95	7.2	91.6	1210	1260	1191	1211	Underheated
P106-5	50.62	0.23	15.99	6.98	0.10	11.15	13.12	1.86	0.04	0.06	0.08	100.23	7.1	90.9	1210	1261	1194	1214	Underheated
P106-2	50.66	0.24	15.91	7.12	0.11	11.24	13.16	1.86	0.04	0.02	0.07	100.43	7.1	91.4	1210	1263	1192	1213	Underheated
P106-1	50.89	0.30	15.89	7.00	0.11	11.12	12.99	1.90	0.03	0.04	0.04	100.31	6.8	91.0	1210	1262	1193	1213	Underheated
P106-4	50.64	0.19	16.06	7.13	0.13	11.20	13.18	1.83	0.04	0.04	0.09	100.53	7.2	90.9	1210	1261	1194	1214	Underheated
P105-1	51.56	0.86	17.63	7.59	0.13	7.33	13.06	2.15	0.05	0.02	0.07	100.45	6.1	84.3	1230	1158	1229	1225	Overheated, good quenching
P105-3	50.86	0.71	16.85	7.65	0.10	7.20	13.00	2.49	0.04	0.07	0.03	99.00	5.2	84.1	1230	1162	1223	1220	Overheated, good quenching
P105-2	50.76	0.63	16.79	7.73	0.14	7.14	12.78	2.52	0.04	0.01	0.06	98.60	5.1	82.7	1230	1162	1224	1221	Overheated, good quenching
P105-6	51.08	0.85	16.30	8.09	0.11	7.60	12.64	2.60	0.05	0.03	0.06	99.41	4.9	84.0	1230	1178	1214	1215	Overheated, good quenching
P105-5	51.12	0.66	16.51	7.80	0.10	7.40	12.69	2.49	0.06	0.05	0.11	98.99	5.1	83.4	1230	1171	1218	1217	Overheated and badly quenched
P105-7	50.85	0.80	16.65	7.93	0.14	7.33	12.87	2.54	0.06	0.02	0.04	99.23	5.1	84.2	1230	1167	1220	1218	Overheated, good quenching
P104-3	50.70	0.35	19.17	6.75	0.14	8.50	13.90	1.84	0.03	0.06	0.07	101.51	7.6	91.2	1220	1181	1244	1245	Analytical overlap
P104-10	51.09	0.29	15.96	8.11	0.12	9.97	13.13	1.86	0.03	0.05	0.07	100.68	7.1	91.1	1220	1230	1194	1207	Poor quenching
P103-11	51.75	0.50	16.35	7.90	0.11	10.18	12.94	1.97	0.04	0.00	0.03	101.77	6.6	90.0	1225	1235	1199	1213	Poor quenching
P104-14	50.92	0.24	15.54	7.92	0.06	9.87	12.90	1.90	0.05	0.07	0.03	99.50	6.8	91.3	1220	1232	1191	1204	Poor quenching
P103-14	50.20	0.51	16.45	7.52	0.22	9.99	12.64	1.76	0.02	0.07	0.01	99.40	7.2	89.8	1225	1233	1205	1220	Poor quenching
P103-2	51.29	0.72	16.37	7.78	0.13	10.31	12.75	1.73	0.02	0.07	0.03	101.19	7.4	89.4	1225	1237	1197	1213	Poor quenching
P108-5	50.19	0.33	16.09	8.00	0.19	9.79	13.15	1.86	0.04	0.00	0.07	99.71	7.1	90.4	1234	1229	1199	1213	Overheated and badly quenched
P109-1	50.21	0.30	15.84	7.94	0.18	9.99	13.05	1.76	0.03	0.04	0.04	99.40	7.4	90.9	1220	1234	1195	1210	Badly quenched
P109-2	49.87	0.32	15.88	8.10	0.24	9.78	13.17	1.78	0.05	0.00	0.05	99.25	7.4	91.2	1220	1229	1197	1211	Badly quenched
P109-3	50.14	0.36	16.12	8.17	0.13	9.81	13.29	1.68	0.02	0.01	0.08	99.82	7.9	91.4	1220	1226	1197	1210	Badly quenched
P109-6	50.13	0.36	15.80	8.00	0.22	9.93	13.07	1.84	0.03	0.03	0.05	99.48	7.1	91.2	1220	1233	1195	1210	Badly quenched
P110-1	51.00	0.29	16.92	7.20	0.18	10.64	13.49	1.72	0.02	0.00	0.03	101.50	7.9	90.3	1205	1243	1204	1221	Underheated, good quenching
P110-7	50.25	0.22	16.80	6.92	0.10	10.07	13.58	1.63	0.04	0.04	0.04	99.70	8.3	91.0	1205	1232	1206	1221	Underheated, good quenching

Appendix 4.8, continued.

Sample	SiO_2	TiO_2	Al_2O_3	[a]FeO	MnO	MgO	CaO	Na_2O	K_2O	P_2O_5	Cr_2O_3	total	CaO/ Na_2O	[b]Host An	[c]T_h (°C)	[d]T_{ol}	[e]T_{pl}	[f]T_{corr}	[g]Comments
P110-4	49.58	0.26	16.49	6.75	0.14	9.35	13.53	1.64	0.03	0.02	0.08	97.87	8.2	90.9	1205	1216	1208	1219	Underheated, good quenching
P110-5	50.24	0.25	16.40	6.67	0.16	9.91	13.49	1.73	0.03	0.00	0.06	98.94	7.8	90.8	1205	1231	1204	1219	Underheated, good quenching
P110-3	51.34	0.18	15.99	7.18	0.19	10.55	13.29	1.80	0.03	0.00	0.03	100.59	7.4	90.8	1205	1246	1193	1211	Underheated, good quenching
P113-1	50.85	0.33	16.53	7.97	0.16	9.94	12.90	1.78	0.02	0.00	0.06	100.54	7.3	90.7	1220	1230	1203	1217	Badly quenched
P113-2	50.76	0.35	16.79	7.81	0.11	10.13	12.95	1.53	0.02	0.03	0.07	100.54	8.4	91.0	1220	1231	1203	1218	Badly quenched
P113-4	50.655	0.28	18.78	7.19	0.12	8.71	13.41	1.69	0.02	0.03	0.01	100.90	7.9	91.4	1220	1190	1237	1242	Analytical overlap
P113-3	50.146	0.25	18.67	7.40	0.13	8.99	13.42	1.75	0.03	0.06	0.03	100.88	7.7	91.4	1220	1199	1236	1243	Analytical overlap
P113-7	49.891	0.35	18.81	7.38	0.13	9.09	13.60	1.60	0.01	0.00	0.01	100.88	8.5	91.3	1220	1199	1236	1243	Analytical overlap
P111-5	50.63	0.24	15.98	8.20	0.09	10.40	13.18	1.91	0.02	0.01	0.06	100.73	6.9	91.9	1215	1244	1194	1212	Badly quenched
P111-3	50.75	0.26	16.18	8.01	0.18	10.39	13.14	1.69	0.02	0.00	0.06	100.68	7.8	91.5	1215	1240	1195	1212	Badly quenched
P111-2	50.01	0.27	16.22	7.92	0.12	10.10	13.08	1.53	0.02	0.00	0.09	99.35	8.6	91.8	1215	1233	1197	1212	Badly quenched
P111-1	50.26	0.24	16.36	7.89	0.12	10.14	13.10	1.61	0.02	0.00	0.09	99.83	8.1	91.8	1215	1234	1199	1214	Badly quenched
P111-8	50.68	0.26	15.97	8.19	0.10	10.47	13.12	1.76	0.02	0.03	0.05	100.65	7.5	92.4	1215	1244	1192	1210	Badly quenched
P111-9	50.83	0.26	16.05	8.13	0.13	10.23	13.00	1.85	0.03	0.02	0.09	100.61	7.0	91.6	1215	1239	1195	1212	Badly quenched
P111-6	50.57	0.30	15.90	8.03	0.16	10.51	13.08	1.89	0.02	0.01	0.03	100.49	6.9	92.0	1215	1247	1193	1211	Badly quenched
P116-1	50.09	0.39	16.21	7.94	0.16	9.73	13.32	1.72	0.04	0.03	0.06	99.69	7.7	90.8	1218	1225	1200	1213	Badly quenched
P116-2	50.19	0.47	15.88	7.98	0.14	9.95	13.12	1.86	0.05	0.03	0.09	99.77	7.0	90.9	1218	1233	1196	1211	Badly quenched
P116-3	50.68	0.36	15.59	8.12	0.17	10.11	13.03	1.88	0.04	0.02	0.07	100.06	6.9	90.9	1218	1238	1190	1206	Badly quenched
P116-4	50.46	0.35	15.47	8.23	0.18	9.94	12.97	1.82	0.04	0.01	0.07	99.54	7.1	91.9	1218	1234	1189	1204	Badly quenched
P116-5	50.60	0.37	15.32	8.20	0.24	10.12	12.97	1.89	0.05	0.04	0.04	99.84	6.8	91.1	1218	1239	1186	1203	Badly quenched
P116-6	50.09	0.37	17.73	7.33	0.16	9.14	13.66	1.77	0.03	0.06	0.01	100.36	7.7	91.1	1218	1205	1223	1231	Analytical overlap
P115-6	51.31	0.40	15.69	8.82	0.12	9.44	13.47	1.83	0.15	0.03	0.01	101.28	7.3	90.8	1217	1217	1189	1200	High-K2O
P115-7	51.12	0.40	15.80	8.13	0.20	10.30	12.78	1.91	0.02	0.01	0.02	100.69	6.7	91.0	1217	1242	1192	1209	Badly quenched
P115-9	50.85	0.46	15.70	8.07	0.14	10.23	13.02	1.80	0.02	0.00	0.08	100.40	7.2	90.4	1217	1239	1190	1207	Badly quenched
P115-10	50.98	0.49	15.66	7.83	0.16	10.28	13.10	1.78	0.01	0.04	0.09	100.42	7.4	91.0	1217	1239	1189	1206	Badly quenched
P115-2	50.93	0.38	15.69	8.09	0.11	10.01	13.08	1.98	0.03	0.01	0.07	100.39	6.6	90.8	1217	1236	1192	1208	Badly quenched
P115-1	51.13	0.32	15.78	7.98	0.18	10.25	12.96	1.93	0.03	0.06	0.04	100.65	6.7	90.3	1217	1240	1192	1209	Badly quenched
P114-1	49.69	0.45	15.01	8.10	0.14	9.88	13.08	1.82	0.05	0.04	0.03	98.30	7.2	91.0	1213	1236	1185	1201	Badly quenched
P114-2	49.22	0.48	14.94	8.17	0.16	9.87	13.07	1.58	0.04	0.01	0.11	97.64	8.3	91.1	1213	1233	1182	1197	Badly quenched
P114-3	50.48	0.31	15.53	8.04	0.12	10.01	12.76	1.99	0.04	0.00	0.08	99.36	6.4	91.1	1213	1240	1192	1209	Badly quenched
P114-8	50.92	0.27	15.59	8.24	0.15	10.25	13.05	1.98	0.03	0.00	0.09	100.58	6.6	90.0	1213	1242	1190	1207	Badly quenched
P114-4	49.70	0.38	15.22	8.02	0.10	9.74	13.14	1.76	0.03	0.00	0.04	98.12	7.5	91.3	1213	1232	1188	1203	Badly quenched
P114-6	50.83	0.30	15.77	8.14	0.15	10.26	12.98	1.79	0.03	0.05	0.07	100.36	7.2	90.4	1213	1239	1191	1208	Badly quenched
P114-7	50.36	0.27	15.43	8.63	0.17	9.93	12.97	1.87	0.02	0.04	0.04	99.73	6.9	90.7	1213	1234	1188	1203	Badly quenched
P114-11	50.02	0.54	15.11	8.03	0.13	9.88	13.12	1.89	0.03	0.00	0.08	98.84	7.0	91.2	1213	1235	1186	1202	Badly quenched
P118-2	50.69	0.56	16.58	7.81	0.11	10.32	12.98	1.66	0.03	0.01	0.03	100.78	7.8	91.1	1209	1238	1200	1216	Underheated, good quenching
P118-3	49.96	0.46	15.87	8.18	0.15	10.33	12.77	1.69	0.03	0.00	0.07	99.51	7.6	91.3	1209	1242	1193	1210	Underheated, good quenching
P118-4	50.22	0.35	15.78	7.91	0.13	10.32	12.95	1.68	0.03	0.00	0.06	99.43	7.7	91.1	1209	1242	1192	1209	Underheated, good quenching

Appendix 4.8, continued.

Sample	SiO_2	TiO_2	Al_2O_3	[a]FeO	MnO	MgO	CaO	Na_2O	K_2O	P_2O_5	Cr_2O_3	total	CaO/Na_2O	[b]Host An	[c]T_h (°C)	[d]T_{ol}	[e]T_{pl}	[f]T_{corr}	Comments
P118-6	50.33	0.34	15.67	8.08	0.13	10.28	12.86	1.69	0.03	0.00	0.03	99.44	7.6	91.1	1209	1242	1190	1207	Underheated, good quenching
P118-8	50.01	0.36	16.01	7.91	0.16	9.94	13.02	1.71	0.04	0.00	0.06	99.22	7.6	91.3	1209	1232	1197	1212	Underheated, good quenching
P153-6	50.91	0.78	16.06	7.83	0.06	8.59	13.37	2.23	0.04	0.03	0.08	99.99	6.0	85.4	1220	1199	1204	1211	?Poor quench
P155-1	51.30	0.76	16.83	8.02	0.17	8.28	13.29	2.23	0.05	0.07	0.12	101.11	6.0	85.6	1228	1186	1214	1218	Overheated and equilibrated, slightly poor quer
P155-2	51.11	0.79	16.93	7.57	0.11	8.26	13.44	2.28	0.04	0.03	0.01	100.56	5.9	85.6	1228	1188	1217	1221	Overheated and equilibrated, slightly poor quer
P155-6	51.66	0.77	16.40	7.72	0.15	8.45	13.35	2.28	0.05	0.00	0.04	100.85	5.9	85.4	1228	1193	1207	1213	Overheated and equilibrated, slightly poor quer
P155-4	51.57	0.76	16.50	7.63	0.25	8.34	13.33	2.30	0.06	0.00	0.05	100.80	5.8	85.4	1228	1190	1210	1215	Overheated and equilibrated, slightly poor quer
P155-3	51.02	0.78	16.50	7.75	0.14	8.39	13.37	2.31	0.05	0.02	0.05	100.38	5.8	85.8	1228	1193	1211	1217	Overheated and equilibrated, slightly poor quer
P156-1	50.20	0.80	16.14	7.94	0.12	8.30	13.45	2.15	0.05	0.05	0.04	99.23	6.3	85.2	1223	1191	1207	1212	Overheated not equilibrated, analytical overlap
P157-1	51.18	1.22	17.05	8.08	0.21	7.20	12.32	2.76	0.09	0.06	0.06	100.24	4.5	83.1	1230	1167	1226	1225	Overheated and equilibrated
P158-1	50.84	0.76	16.12	7.81	0.13	8.31	13.17	2.32	0.05	0.04	0.05	99.61	5.7	85.8	1221	1193	1207	1213	Overheated, not equilibrated, analytical overlap
P158-3	50.75	0.82	16.17	7.71	0.14	8.31	13.14	2.32	0.06	0.06	0.12	99.59	5.7	86.0	1221	1193	1208	1214	Overheated, not equilibrated, analytical overlap
P158-5	50.50	0.81	16.55	7.65	0.11	7.73	12.74	2.87	0.14	0.01	0.04	99.15	4.4	85.5	1221	1187	1220	1224	Overheated, not equilibrated, analytical overlap
P159-1	51.52	0.72	16.48	7.72	0.10	8.22	13.23	2.33	0.04	0.06	0.07	100.50	5.7	85.2	1220	1188	1211	1215	Overheated, not equilibrated, analytical overlap
P159-2	51.39	0.73	16.36	7.80	0.14	8.53	13.33	2.32	0.05	0.01	0.06	100.72	5.7	84.8	1220	1197	1207	1213	Overheated, not equilibrated, analytical overlap
P159-3	51.17	0.75	16.47	7.79	0.19	8.50	13.36	2.29	0.05	0.00	0.05	100.62	5.8	85.2	1220	1195	1209	1215	Overheated, not equilibrated, analytical overlap
P160-4	50.97	0.35	15.63	7.78	0.13	9.77	13.08	1.90	0.04	0.00	0.05	99.70	6.9	88.6	1195	1229	1192	1206	Underheated, good quench
P160-2	51.11	0.27	15.51	7.81	0.13	9.70	12.99	1.95	0.03	0.00	0.04	99.53	6.7	89.1	1195	1228	1192	1206	Underheated, good quench
P160-3	50.93	0.23	15.53	7.71	0.17	9.69	12.84	1.99	0.02	0.00	0.03	99.14	6.4	89.1	1195	1230	1193	1207	Underheated, good quench

[a]All Fe as FeO.

[b]Host plagioclase composition, An = 100 x (Ca/(Ca + Na)).

[c]Homogenisation temperature.

[d]Calculated temperature using the olivine-melt thermometer of Ford, et al.(1983).

[e]Calculated temperature using the plagioclase-melt thermometer of Weaver and Langmuir(1990).

[f]Calculated plagioclase temperature corrected to obtain a best fit for the MORB olivine-plagioclase cotectic; correction from Danyushevsky, et al.(1996).

[g]Interpretation of inclusion composition based on a comparison of T_h, T_{ol}, T_{pl} and T_{corr}.

Appendix 4.9, Homogenised melt inclusions in plagioclase.

Sample	SiO_2	TiO_2	Al_2O_3	[a]FeO	MnO	MgO	CaO	Na_2O	K_2O	P_2O_5	Cr_2O_3	total	CaO/ Na_2O	[b]Host An	[c]T_h (°C)	T_{ol}	T_{pl}	T_{corr}	Comments
P104-1	51.16	0.41	16.56	7.75	0.12	9.73	13.07	1.76	0.04	0.07	0.12	100.79	7.4	90.7	1220	1221	1203	1214	Good run
P104-2	51.01	0.38	16.49	7.84	0.16	9.81	13.22	2.01	0.03	0.05	0.06	101.06	6.6	90.7	1220	1226	1204	1216	Good run
P104-8	50.52	0.18	16.40	7.50	0.17	9.78	12.95	1.84	0.03	0.04	0.07	99.48	7.0	91.0	1220	1227	1205	1217	Good run
P104-7	50.22	0.20	16.41	7.37	0.14	9.69	13.14	1.86	0.03	0.06	0.06	99.18	7.1	91.0	1220	1225	1206	1218	Good run
P104-5	50.50	0.26	16.69	7.42	0.16	9.66	13.23	1.92	0.04	0.05	0.10	100.03	6.9	90.3	1220	1223	1209	1220	Good run
P103-15	49.56	0.59	16.97	7.49	0.18	9.59	12.96	1.66	0.04	0.08	0.07	99.18	7.8	90.6	1225	1221	1213	1225	Good run
P108-1	50.07	0.54	17.05	7.62	0.17	9.50	13.16	1.76	0.03	0.05	0.12	100.06	7.5	90.8	1234	1217	1213	1224	Overheated but not equilibrated
P108-3	50.49	0.37	17.06	7.67	0.14	9.60	13.44	1.81	0.03	0.00	0.05	100.66	7.4	91.3	1234	1220	1212	1224	Overheated but not equilibrated
P108-4	49.36	0.33	16.88	7.94	0.17	9.61	13.30	1.76	0.02	0.00	0.05	99.42	7.5	91.5	1234	1222	1212	1224	Overheated but not equilibrated
P108-7	50.45	0.31	16.21	7.95	0.24	9.73	12.91	1.91	0.02	0.00	0.04	99.78	6.8	90.7	1234	1228	1202	1216	Overheated but not equilibrated
P113-5	51.13	0.27	16.71	8.07	0.10	9.81	12.93	1.76	0.02	0.00	0.02	100.82	7.3	91.6	1220	1226	1204	1217	Good run
P113-9	50.66	0.28	16.86	8.16	0.17	9.80	12.99	1.71	0.03	0.00	0.04	100.71	7.6	91.4	1220	1225	1207	1220	Good run
P111-4	50.28	0.27	17.13	7.64	0.10	10.01	13.01	1.74	0.02	0.03	0.10	100.31	7.5	91.7	1215	1231	1212	1227	?good run
P112-R2	50.08	0.22	16.84	7.69	0.11	9.46	13.21	1.68	0.02	0.00	0.09	99.40	7.9	91.2	1232	1217	1210	1221	Overheated but did not equilibrate
P112-R1	49.91	0.19	16.67	7.85	0.13	9.51	13.32	1.73	0.02	0.00	0.04	99.37	7.7	91.5	1232	1220	1208	1220	Overheated but did not equilibrate
P112-R3	50.96	0.22	17.12	7.83	0.05	9.41	12.90	1.66	0.13	0.05	0.03	100.37	7.7	91.0	1232	1216	1212	1223	Overheated but did not equilibrate
P112-7	50.57	0.38	16.81	7.92	0.09	9.68	12.93	1.83	0.03	0.00	0.04	100.27	7.1	91.8	1232	1225	1209	1222	Overheated but did not equilibrate
P112-5	50.68	0.22	17.16	7.86	0.16	9.60	13.48	1.80	0.02	0.02	0.06	101.07	7.5	91.0	1232	1218	1212	1224	Overheated but did not equilibrate
P112-2	50.85	0.30	17.62	7.78	0.10	9.62	13.11	1.80	0.02	0.00	0.08	101.28	7.3	91.6	1232	1218	1218	1230	Overheated but did not equilibrate
P112-1	50.56	0.39	17.61	7.74	0.11	9.53	13.34	1.64	0.02	0.01	0.08	101.04	8.1	91.1	1232	1214	1217	1228	Overheated but did not equilibrate
P153-3	51.15	0.87	15.62	8.28	0.10	8.75	13.35	2.18	0.05	0.00	0.07	100.42	6.1	85.7	1220	1203	1195	1203	Overheated but did not equilibrate
P153-2	50.95	0.86	15.52	7.99	0.12	8.66	13.19	2.23	0.06	0.00	0.02	99.60	5.9	85.8	1220	1204	1196	1204	Overheated but did not equilibrate
P153-1	51.02	0.86	15.63	8.19	0.16	8.67	13.28	2.27	0.04	0.01	0.08	100.20	5.8	86.0	1220	1202	1197	1205	Overheated but did not equilibrate
P156-4	50.69	0.87	15.93	8.04	0.13	8.68	13.36	2.21	0.04	0.05	0.06	100.05	6.0	85.2	1223	1201	1202	1209	Overheated not equilibrated, slightly poor quen
P156-3	50.47	0.88	15.92	7.75	0.12	8.67	13.47	2.19	0.05	0.00	0.04	99.56	6.2	85.3	1223	1202	1202	1210	Overheated not equilibrated, slightly poor quen
P156-6	51.11	0.68	15.88	7.97	0.12	8.70	13.43	2.22	0.04	0.02	0.11	100.27	6.0	85.1	1223	1201	1200	1207	Overheated not equilibrated, slightly poor quen
P156-5	50.67	0.85	15.90	8.04	0.10	8.51	13.46	2.16	0.05	0.07	0.06	99.87	6.2	85.3	1223	1196	1201	1207	Overheated not equilibrated, slightly poor quen
P158-4	50.71	0.79	15.61	7.95	0.12	8.44	13.32	2.21	0.05	0.06	0.04	99.31	6.0	85.6	1221	1197	1199	1205	Overheated but did not equilibrate
P158-6	50.61	0.72	15.67	8.12	0.18	8.50	12.94	2.22	0.04	0.03	0.02	99.04	5.8	85.6	1221	1200	1200	1207	Overheated but did not equilibrate
P158-7	50.78	0.78	15.44	8.10	0.14	8.50	13.02	2.26	0.06	0.01	0.03	99.11	5.8	85.4	1221	1201	1197	1204	Overheated but did not equilibrate
P159-5	51.45	0.69	15.69	8.01	0.14	8.78	12.99	2.08	0.07	0.01	0.07	99.99	6.2	85.7	1220	1204	1197	1205	Overheated but did not equilibrate

[a]All Fe as FeO.

[b]Host plagioclase composition, An = 100 x (Ca/(Ca + Na)).

[c]Homogenisation temperature.

[d]Calculated temperature using the olivine-melt thermometer of Ford, et al.(1983).

[e]Calculated temperature using the plagioclase-melt thermometer of Weaver and Langmuir(1990).

[f]Calculated plagioclase temperature corrected to obtain a best fit for the MORB olivine-plagioclase cotectic; correction from Danyushevsky, et al.(1996).

[g]Interpretation of inclusion composition based on a comparison of T_h, T_{ol}, T_{pl} and T_{corr}.

Appendix 4.10, Homogenised melt inclusions in olivine.

Sample	SiO_2	TiO_2	Al_2O_3	[a]FeO	MnO	MgO	CaO	Na_2O	K_2O	P_2O_5	Cr_2O_3	total	CaO/ Na_2O	[b]Host Fo	[c]T_h (°C)
OL20-1	49.86	0.92	14.14	10.48	0.16	9.47	12.05	2.17	0.04	0.06	0.12	99.46	5.5	87.4	1237
OL20-2	50.46	0.94	14.45	9.16	0.14	9.65	12.33	2.24	0.05	0.07	0.04	99.55	5.5	87.1	1237
OL23-1	48.04	0.89	16.23	7.66	0.12	8.57	13.39	1.97	0.02	0.04	0.10	97.04	6.8	89.3	1215
OL24-1	51.03	0.98	14.37	9.81	0.14	8.43	12.73	2.09	0.03	0.06	0.04	99.70	6.1	86.8	1210
OL24-2	50.73	0.89	14.44	10.16	0.13	7.90	12.70	2.03	0.04	0.09	0.06	99.19	6.3	86.5	1210
OL26-1	51.57	1.04	14.93	9.56	0.13	9.16	12.55	2.06	0.04	0.06	0.06	101.15	6.1	88.1	1210
OL27-1	50.16	0.82	15.67	9.56	0.10	9.00	13.36	1.72	0.03	0.06	0.03	100.50	7.8	88.3	1205
OL28-1	50.76	0.64	16.43	8.01	0.14	8.84	13.51	1.76	0.02	0.00	0.11	100.21	7.7	89.5	1218
OL18-1	49.75	0.74	16.51	7.85	0.08	8.94	13.29	1.68	0.04	0.05	0.03	98.96	7.9	89.6	1217
OL21-2	50.10	1.01	14.94	9.89	0.15	8.63	12.67	2.17	0.04	0.09	0.08	99.76	5.8	87.5	1205
OL22-2	49.95	0.94	14.56	9.79	0.12	9.32	12.20	2.10	0.06	0.16	0.07	99.28	5.8	87.3	1240
OL23-2	49.66	0.84	16.96	7.60	0.06	8.96	13.19	1.99	0.02	0.06	0.09	99.44	6.6	89.4	1215
OL23-3	50.03	0.80	16.66	7.89	0.10	8.63	13.13	2.03	0.04	0.07	0.10	99.48	6.5	89.3	1215
OL23-4	50.36	0.83	16.44	7.89	0.16	8.85	13.23	2.20	0.00	0.06	0.02	100.06	6.0	89.2	1215
OL26-2	50.20	1.01	14.88	9.32	0.14	9.03	12.52	1.99	0.04	0.10	0.03	99.25	6.3	87.6	1210
OL26-3	50.51	1.04	14.68	9.17	0.19	9.06	12.70	2.06	0.05	0.06	0.04	99.56	6.2	87.7	1210
OL27-2	51.06	0.74	15.81	9.21	0.15	9.70	12.85	1.76	0.03	0.03	0.07	101.43	7.3	88.8	1205

[a]All Fe as FeO.

[b]Host olivine composition, Fo = 100 x (Mg/(Mg + Fe)).

[c]Homogenisation temperature.

Appendix 5

Sample Catalogue

Appendix 5, sample catalogue.

UTGD#	Sample Number	Rock description	Longitude	Latitude	Depth	Preparations
132431	KK2-83-NP-D9-1	plag-ol-phyirc basalt	127°04.6'W	42°14.9'N	3048m bsl	CR,MS
132432	140-504B-195R-1,7-10 cm (3)	plag-cpx-ol-phyric chilled dyke margin	83°43.818'W	1°13.611'N	1695.1 mbsf	PS
132433	140-504B-201R-1,14-17cm (4)	plag-phyric microdyke	83°43.818'W	1°13.611'N	1728.98 mbsf	R,PS
132434	140-504B-203R-1, 5-7cm (2)	plag±cpx-phyric chilled dyke material	83°43.818'W	1°13.611'N	1749.1 mbsf	R,PS,PD
132435	140-504B-203R-1,34-35cm (10)	plag-phyric chilled dyke margin	83°43.818'W	1°13.611'N	1749.4 mbsf	CR,PD,PS
132436	140-504B-208R-1,30-33cm (17)	plag-phyric chilled dyke margin	83°43.818'W	1°13.611'N	1779.1 mbsf	PS
132437	140-504B-213R-1,3-6cm (2)	plag±cpx-phyric chilled dyke material	83°43.818'W	1°13.611'N	1812.5 mbsf	PD
132438	140-504B-213R-1,26-28cm (9)	plag±cpx-phyric chilled dyke material	83°43.818'W	1°13.611'N	1812.7 mbsf	R,PS
132439	140-504B-213R-1,32-34cm (11)	plag-phyric microdyke	83°43.818'W	1°13.611'N	1812.8 mbsf	R,PS
132440	140-504B-213R-1,85-90cm (22)	plag±cpx-phyric chilled dyke material	83°43.818'W	1°13.611'N	1813.3 mbsf	CR,MS
132441	140-504B-216R-1,32-34cm (8)	plag±cpx-phyric chilled dyke material	83°43.818'W	1°13.611'N	1830.9 mbsf	R,PS
132442	140-504B-219R-1,8-12cm (3)	plag-cpx-phyric chilled dyke margin	83°43.818'W	1°13.611'N	1856.3 mbsf	R,PS,PD
132443	140-504B-220R-1,2-6cm (1)	plag±cpx-phyric chilled dyke material	83°43.818'W	1°13.611'N	1865.5 mbsf	PD
132444	140-504B-222R-1,0-4cm (1)	plag-cpx-ol-phyric chilled dyke margin	83°43.818'W	1°13.611'N	1884.7 mbsf	PS,CR,PD,MS
132445	140-504B-222R-1,76-79cm (13)	plag-cpx-phyric chilled dyke margin	83°43.818'W	1°13.611'N	1885.4 mbsf	R,PS
132446	140-504B-222R-1,89-93cm (16)	plag-cpx-phyric chilled dyke margin	83°43.818'W	1°13.611'N	1885.5 mbsf	R,PS
132447	140-504B-222R-1,104-107cm (19)	plag±cpx-phyric chilled dyke material	83°43.818'W	1°13.611'N	1885.6 mbsf	R,PS,PD
132448	140-504B-224R-1,76-78cm (18)	plag±cpx-phyric chilled dyke material	83°43.818'W	1°13.611'N	1904.4 mbsf	PS
132449	140-504B-231R-1,4-5cm (2)	plag-phyric chilled dyke margin	83°43.818'W	1°13.611'N	1953.6 mbsf	R,PS
132450	148-504B-249R-1,92-98cm (28)	plag-cpx-ol-phyric chilled dyke margin	83°43.818'W	1°13.611'N	2072.1 mbsf	R
132451	148-504B-249R-1,103-106cm (30)	plag-cpx-ol-phyric holocrystalline dyke	83°43.818'W	1°13.611'N	2072.3 mbsf	CR,MS
132452	148-504B-249R-1,131-134(38)	plag-cpx-ol-phyric holocrystalline dyke	83°43.818'W	1°13.611'N	2072.5 mbsf	CR,MS
132453	148-896A-2R-1,63-66cm (14)	plag-ol-phyric pillow-rim	83°43.392'W	1°13.006'N	201.53 mbsf	R
132454	148-896A-3R-1,16-18cm (4)	plag-ol-phyric pillow-rim	83°43.392'W	1°13.006'N	210.06 mbsf	CR,MS
132455	148-896A-3R-1,55-57cm (7)	plag-ol-phyric pillow-rim	83°43.392'W	1°13.006'N	210.45 mbsf	R
132456	148-896A-4R-1,10-13cm (2)	plag-ol-phyric pillow-rim	83°43.392'W	1°13.006'N	219.00 mbsf	CR,MS
132457	148-896A-5R-2,89-93cm (5)	plag-ol-phyric pillow-rim	83°43.392'W	1°13.006'N	230.31 mbsf	R
132458	148-896A-6R-1,79-81cm (9a)	plag-ol-phyric pillow-rim	83°43.392'W	1°13.006'N	238.69 mbsf	R
132459	148-896A-6R-1,138-140cm (13)	plag-ol-phyric pillow-rim	83°43.392'W	1°13.006'N	239.28 mbsf	R
132460	148-896A-6R-2,18-21cm (2)	plag-ol-phyric pillow-rim	83°43.392'W	1°13.006'N	239.56 mbsf	R
132461	148-896A-6R-2,39-45cm (5)	plag-ol-phyric pillow-rim	83°43.392'W	1°13.006'N	239.77 mbsf	R

Appendix 5, continued.

UTGD#	Sample Number	Rock description	Longitude	Latitude	Depth	Preparations
132462	148-896A-6R-3,0-5cm (1)	plag-ol-phyric pillow-rim	83°43.392'W	1°13.006'N	244.79 mbsf	R
132463	148-896A-8R-1,141-145cm (29)	plag-ol-phyric pillow-rim	83°43.392'W	1°13.006'N	258.51 mbsf	R
132464	148-896A-9R-1,78-81cm (13)	plag-ol-phyric pillow-rim	83°43.392'W	1°13.006'N	267.48 mbsf	R
132465	148-896A-9R-1,125-130cm (24)	plag-ol-phyric pillow-rim	83°43.392'W	1°13.006'N	267.95 mbsf	CR,MS
132466	148-896A-10R-1,50-57cm (7)	plag-ol-phyric pillow-rim	83°43.392'W	1°13.006'N	276.90 mbsf	R
132467	148-896A-11R-1,0-3cm (1)	plag-ol-phyric pillow-rim	83°43.392'W	1°13.006'N	286.00 mbsf	R
132468	148-896A-11R-1,106-108cm (9)	plag-ol-phyric pillow-rim	83°43.392'W	1°13.006'N	287.06 mbsf	R
132469	148-896A-11R-2,30-40cm (3)	plag-ol-phyric pillow-rim	83°43.392'W	1°13.006'N	287.74 mbsf	R
132470	148-896A-11R-2,63-72cm (8)	plag-ol-phyric pillow-rim	83°43.392'W	1°13.006'N	288.07 mbsf	R
132471	148-896A-11R-3,59-67cm (10)	plag-ol-phyric pillow-rim	83°43.392'W	1°13.006'N	289.51 mbsf	R
132472	148-896A-12R-1,18-22cm (3)	plag-ol-phyric pillow-rim	83°43.392'W	1°13.006'N	295.78 mbsf	R
132473	148-896A-14R-1,76-80cm (7)	plag-ol-phyric pillow-rim	83°43.392'W	1°13.006'N	315.36 mbsf	R
132474	148-896A-14R-2,0-3cm (1)	plag-ol-phyric pillow-rim	83°43.392'W	1°13.006'N	316.01 mbsf	R,CR,MS
132475	148-896A-14R-3,0-5cm (1)	ol-plag-phyric pillow-rim	83°43.392'W	1°13.006'N	317.48 mbsf	R
132476	148-896A-15R-1,118-122cm (17)	plag-ol-phyric pillow-rim	83°43.392'W	1°13.006'N	325.48 mbsf	R
132477	148-896A-17R-1,55-59cm (6a)	plag-ol-phyric pillow-rim	83°43.392'W	1°13.006'N	344.05 mbsf	R
132478	148-896A-17R-3,14-16cm (1)	plag-ol-phyric pillow-rim	83°43.392'W	1°13.006'N	346.58 mbsf	R
132479	148-896A-17R-3,108-110cm (13)	ol-plag-phyric pillow-rim	83°43.392'W	1°13.006'N	347.52 mbsf	R
132480	148-896A-17R-4,68-70cm (4b)	ol-plag-phyric pillow-rim	83°43.392'W	1°13.006'N	348.58 mbsf	R
132481	148-896A-18R-1,92-94cm (9a)	plag-ol-cpx-phyric pillow-rim	83°43.392'W	1°13.006'N	354.02 mbsf	R
132482	148-896A-19R-1,8-11cm (2)	plag-ol-cpx-phyric pillow-rim	83°43.392'W	1°13.006'N	356.08 mbsf	R,CR,MS
132483	148-896A-19R-1,115-116cm (19)	plag-ol-cpx-phyric pillow-rim	83°43.392'W	1°13.006'N	357.15 mbsf	R
132484	148-896A-20R-1,37-40cm (9)	plag-ol-cpx-phyric pillow-rim	83°43.392'W	1°13.006'N	363.87 mbsf	R
132485	148-896A-20R-1,48-52cm (12)	plag-ol-cpx-phyric pillow-rim	83°43.392'W	1°13.006'N	363.98 mbsf	R
132486	148-896A-22R-2,124-127cm (17)	plag-ol-cpx-phyric pillow-rim	83°43.392'W	1°13.006'N	385.33 mbsf	R
132487	148-896A-22R-4,35-38cm (5)	plag-ol-cpx-phyric pillow-rim	83°43.392'W	1°13.006'N	387.40 mbsf	R
132488	148-896A-25R-1,89-93cm (11)	plag-ol-phyric pillow-rim	83°43.392'W	1°13.006'N	412.19 mbsf	CR,MS
132489	148-896A-25R-2,32-35cm (4)	plag-ol-phyric pillow-rim	83°43.392'W	1°13.006'N	413.12 mbsf	R
132490	148-896A-25R-2,61-64cm (11)	plag-ol-phyric pillow-rim	83°43.392'W	1°13.006'N	413.41 mbsf	CR,MS
132491	148-896A-25R-3,10-15cm (2)	plag-ol-phyric pillow-rim	83°43.392'W	1°13.006'N	414.36 mbsf	R
132492	148-896A-26R-2,67-69cm (12)	ol-plag-phyric pillow-rim	83°43.392'W	1°13.006'N	423.17 mbsf	R

Appendix 5, continued.

UTGD#	Sample Number	Rock description	Longitude	Latitude	Depth	Preparations
132493	148-896A-26R-3,46-48cm (6)	ol-plag-phyric pillow-rim	83°43.392'W	1°13.006'N	424.32 mbsf	R
132494	148-896A-27R-1,59-63cm (7)	ol-plag-phyric pillow-rim	83°43.392'W	1°13.006'N	431.09 mbsf	R
132495	148-896A-27R-1,105-109cm (13)	ol-plag-phyric pillow-rim	83°43.392'W	1°13.006'N	431.55 mbsf	CR,MS
132496	148-896A-27R-1,124-130cm (15)	ol-plag-phyric pillow-rim	83°43.392'W	1°13.006'N	431.75 mbsf	CR,MS
132497	148-896A-27R-1,136-142cm (17)	ol-plag-phyric pillow-rim	83°43.392'W	1°13.006'N	431.86 mbsf	R
132498	148-896A-30R-1,50-55cm (8)	ol-plag-phyric pillow-rim	83°43.392'W	1°13.006'N	459.80 mbsf	R

UTGD# = catalogue rnumber, University of Tasmania Geology Departmanet.

Sample number follows ODP format; Leg-Hole-Core-section, depth (piece number).

Preparations; R = rock-chip; CR = crushed; MS = mineral separate; PS = polished thin section; PD = powdered sample.

Appendix 6

Publications

Contents